

KONINKLIJKE NEDERLANDSE AKADEMIE  
VAN WETENSCHAPPEN

---

# PROCEEDINGS

SERIES B

PHYSICAL SCIENCES

VOLUME LIX

1956

NORTH-HOLLAND PUBLISHING COMPANY  
(N.V. NOORD-HOLLANDSCHE UITGEVERS MAATSCHAPPIJ)

AMSTERDAM

*The complete Proceedings consist of three Series, viz. :*

SERIES A: MATHEMATICAL SCIENCES

SERIES B: PHYSICAL SCIENCES

SERIES C: BIOLOGICAL AND MEDICAL SCIENCES

*Articles for these Series cannot be accepted unless formally communicated for publication by one of the members of the Royal Neth. Academy of Sciences.*

## GEOLOGY

### A PHASE-TRANSITION LAYER BETWEEN 200 AND 900 KM DEPTH IN THE EARTH?

BY

F. A. VENING MEINESZ

(Communicated at the meeting of October 29, 1955)

There are strong indications for the presence of a transition layer in the earth between the depths of 200 and 900 km. Seismologists as e.g. JEFFREYS, GUTENBERG, BIRCH a.o. agree that over that range the seismic evidence points to a stronger increase of density than that which corresponds to the effect of the increase of pressure. In his study of 1951 BIRCH<sup>1)</sup> reduces all the densities, seismologically derived, to surface temperature and pressure and he thus finds from 900 to 2900 km depth a constant figure of 4.00. From the Mohorovičić discontinuity up to 200 km depth the results are less clear, but probably the results are likewise compatible with a constant figure, viz. with 3.3. In the area in between, no evidence is obtained of a sudden discontinuity separating those two values of 3.3 and 4.0; BIRCH considers this layer as a zone of transition. He leaves it an open question whether this is a transition between two phases of the same substance, probably of an olivine-pyroxene composition, or whether it is also a change of chemical composition.

In this paper the author wants to give arguments in favor of interpreting it purely as a phase-transition zone. The strongest one is found in the probability of convection-currents over the whole depth of the mantle. It is clear that such currents could not take place if there were a chemical difference in composition between the upper and lower layers of the mantle but that a phase-transition is no impediment against them. We shall return to this point.

A first reason to suppose the presence of great current-systems in the mantle is that it is otherwise difficult to account for the crustal deformations in the island-arc areas of Indonesia, of the eastern border of the Asiatic continent and of the West Indies. In Indonesia, e.g., two indications point strongly to the crustal deformations in that area being caused by the relative movement of the whole Indonesian crustal block in a south-southeastward direction with regard to the surrounding area. In the first place the belt of large negative gravity anomalies found over the tectonic

---

<sup>1)</sup> FR. BIRCH, Remarks on the structure of the mantle, and its bearing upon the possibility of convection-currents, Trans. Amer. Geophys. Union, 32, 533-534 (1951).



are gives evidence of strong crustal compression and this compression is much less on the two sides of the arc, i.e. west of Sumatra and east of the Philippine Islands. This indicates that the deformation is not a concentric crustal shortening as would correspond to the contraction hypothesis but a block-movement as mentioned which on the sides mainly brings about a wrench-faulting. This last movement is corroborated by the displacements observed at the surface after earthquakes in the Sumatra and the Philippine Islands areas and by the geology in both areas.

We find similar gravimetric and seismic evidence in other island-arc areas which likewise indicate relative movements of great crustal blocks and no movements of a concentric kind. Wrench-faulting over large distances pointing to such systematic relative movements during long periods of time are, moreover, known in many other parts of the earth's crust as e.g. on the westcoast of America where the San Andreas fault is one of the most spectacular instances.

This pattern of relative movements of great crustal blocks over the earth's surface strongly points to current-systems in the subcrustal layer and the size of the blocks moving in one direction—in Indonesia the movements seem to diverge only slightly over the full breadth of the archipelago of about 3000 km—indicates these currents to have continental dimensions. We thus come to the assumption of current-systems over the whole thickness of the mantle.

A second reason to prefer this supposition for explaining tectonic deformations of the crust to the contraction hypothesis—though contraction is no doubt also present and plays a secondary part—is the size of the crustal shortening in geosynclines as e.g. the Alpine one. For this mountain-range we have HEIM's <sup>2)</sup> figure of 200–300 km, which seems likely to have occurred in about 150 million years and this appears hard to explain by contraction.

A third reason to assume great subcrustal current-systems is provided by the evidence of a wandering of the poles which RUNCORN <sup>3)</sup> and his collaborators have recently derived from the magnetizations of mesozoic and palaeozoic rocks; they show a varying orientation with regard to the rotation-axis of the earth. They are in harmony with the hypothesis that the crust as a whole changed its position with regard to this axis.

Ruling out the practically impossible supposition that a foreign body has come sufficiently near to the earth for disturbing its rotation, we have to attribute it to internal processes which can not affect the position of the axis in space. As we can likewise exclude the possibility of currents in the crust itself, this leads us to two possibilities, viz. great current-systems in the mantle shifting the crust with regard to the poles or great current-systems in the core moving mantle and crust together. It is

<sup>2)</sup> A. HEIM, *Geologie der Schweiz*, II, p. 50.

<sup>3)</sup> S. K. RUNCORN, *Rock Magnetism-Geophysical Aspects*, *Advances in Physics*, 4, 244–291 (London, 1955).



unlikely that these latter currents, which may have velocities of the order of a million times larger than the velocities of a few cm per annum which may be assumed possible in the mantle, could have a sufficiently systematic character over the long time-periods here discussed to bring about the movements required. So we may conclude that mantle-currents are the most probable hypothesis.

The next argument in favor of mantle-currents is likely to have only relation to the first phase of the earth's history and, therefore, to carry less weight than the others. We shall only mention it shortly. Using PREY's development in spherical harmonics of the topography at the earth's surface the author found a remarkable regularity in the distribution of continents and oceans, pointing to this distribution being connected with current-systems in the mantle.<sup>4)</sup>

Adopting the hypothesis of the existence of such currents it is obvious to attribute them to the cooling of the earth and, therefore, to consider them as convection-currents. If we would look for their cause in chemical differences and processes it would be difficult to understand the episodic character of the cycles of tectonic activity which from the beginning of the earth's history, some 4000–5000 million years ago, have repeated themselves about 10 to 15 times.

This episodicity can well be understood by assuming the currents to be caused by the earth's cooling. In 1939 Dr. GRIGGS<sup>5)</sup> has pointed out that if the rocks of the mantle have an elastic limit which must be exceeded before flow is possible, we can explain that a period of rest is needed before, after a tectonic cycle has restored stability by bringing the higher temperature matter to the surface, a sufficient cooling gradient is again present for causing a new cycle. This cycle must have the character of a half turn revolution, bringing again the higher temperature matter to the surface and the lower temperature rocks below. It is not difficult to show that for current velocities of the order of a few cm per annum—such mantle half turn currents thus must last for periods of the order of 50 million years—the temperature conduction is too slow for materially affecting the phenomenon. In view of the small deviations we find from isostatic equilibrium, the elastic limit of the mantle rocks cannot be much more than about  $10^7$  dynes/cm<sup>2</sup>.

As BROOKS<sup>6)</sup> has remarked, the period of rest of a few hundred million years is not sufficient for allowing the downward temperature gradient to develop again after the cycle has destroyed it, if at least this had to come about by temperature conduction alone. We can, however, safely

---

<sup>4)</sup> F. A. VENING MEINESZ, Convection-currents in the Earth and the origin of the continents, *Proc. Kon. Ned. Akad. v. Wet.*, **55**, 527–553 (1952).

<sup>5)</sup> D. A. GRIGGS, Theory of mountain building, *Amer. Journ. o. Sc.*, **237**, 611–650 (1939).

<sup>6)</sup> H. BROOKS, Cyclic convection-currents, *Trans. Amer. Geophys. Union*, **2**, 548–551 (1941).

assume that this is not the case. At both boundaries of the mantle the previous cycle must have left strong temperature gradients; at the upper surface the higher temperature mantle matter must cause an increased outward conduction and radiation and at the lower boundary the lower temperature matter of the mantle is brought into contact with the high temperature of the core. This must soon lead to convection-cells of smaller dimensions at the upper and lower boundaries of the mantle and at the surface of the core.

We shall not here pursue the phenomenon in the core but it is worth while to remark that thus mantle currents may provide the causes for the core-currents which recent studies of ELSASSER, BULLARD, VESTINE, RUNCORN a.o. on geomagnetism and its correlation with the irregularities of the earth's rotation have rendered highly probable.

For the presence in recent geological periods—perhaps even now—of a small type of convection-currents at the surface of the mantle much evidence may be found. As the author has elsewhere pointed out <sup>7)</sup>, the subsidence of deep basins inside island-arcs and the deep focus earthquakes often accompanying these features may well be explained in this way. Moreover, the concentration by the tectonic crustal compression in these arcs of sialic matter gives an increase of radio-active constituents, causing the temperature difference in a horizontal sense, which can provide the trigger effect for setting these convection-currents going. This is important because the supposed elastic limit of the mantle matter must stabilize it in case we have a purely vertical downward temperature gradient. A trigger-effect, e.g. in the shape of a horizontal gradient, is required to set it going and thus starting the convection-current. If our conclusion about the cause of these deep basins is right, the horizontal dimensions of these cells must be of the order of 400–600 km.

Such smaller convection-cells must not only bring about a strong increase of cooling in deeper mantle layers but also differences of temperature in a horizontal sense which, together, must lead to bigger convection-cells. This same process may be supposed to work in the lower half of the mantle and eventually the effect of the phenomena on both sides of the mantle must in a much shorter period than conduction could achieve, lead to convection-currents throughout the whole mantle.

We have thus given the reasons for adopting the hypothesis of convection-currents in the mantle. Before drawing the conclusion that this implies the presence over the lower 2000 km of a denser modification of the same matter as is present in the upper 200 km and of a transition-layer in between, we have to examine one other possibility which has been suggested for explaining the facts, viz. great convection-cells in the lower

---

<sup>7)</sup> F. A. VENING MEINESZ, Gravity expeditions at sea, Vol. II (1934), and Vol. IV (1948), (Delftsche Uitg. Mij., Delft); Deep focus and intermediate earthquakes in the East Indies, Proc. Kon. Ned. Akad. v. Wet., 49, 855–864 (1948); Indonesian Archipelago, Bull. Geol. Soc. o. Amer., 143–164 (1954).



2000 km and some mechanism in the upper 900 km of another substance for transmitting the drag to the crust. We can probably rule this out. In the first place we must assume that such a situation would unavoidably lead to a sharp discontinuity surface—possibly wavy—between both substances and this has not been seismologically found. In the second place such a mechanism could hardly also explain the effects on the crust of the above mentioned smaller convection-cells and the presence of the deep earthquakes.

Adopting our hypothesis we shall find some more facts in favor of it. We may first mention that as early as 1936 BERNAL<sup>8)</sup> suggested the probability of a cubic modification of olivine at extremely high pressures. He remarked<sup>9)</sup> “that most of the space in silicate lattices is taken up by oxygen; the silicon ions, being comparatively small, are placed in holes between them. Compression of the lattice would have qualitatively the same effect as substitution of a larger ion for silicon. GOLDSCHMIDT has studied magnesium germanate,  $\text{Mg}_2\text{GeO}_4$ , and finds that it has two stable modifications, one isomorphic with olivine, and another one cubic. The density of the latter is larger by 9 per cent than that of the orthorhombic variety. This makes it possible to assume the existence of a cubic modification of olivine at extremely high pressures”.

We shall consecutively discuss four questions:

- 1<sup>0</sup>. Is a transition-layer between two phases acceptable?
- 2<sup>0</sup>. Can we explain how such a layer comes into existence?
- 3<sup>0</sup>. What effects may we expect from loading or unloading of the crust?
- 4<sup>0</sup>. What effects may we expect from a subcrustal convection-current breaking through the transition-layer?

If over the whole layer between 200 and 900 km depth the two phases exist side by side we must assume that over that whole height the temperature-depth curve in the earth corresponds to this phase-equilibrium. This is represented by fig. 1 where the full line gives an acceptable temperature-depth curve for the upper 1200 km of the earth (see e.g. fig. 8 on page 162 of “The cooling of the earth and the temperature in its interior” in “Internal constitution of the earth”, 2nd Ed., by GUTENBERG, 1951) and the broken line a temperature-depth relation corresponding to a possible phase-equilibrium curve.

We may assume that the change from the denser to the lighter phase requires a certain heat of transition and that for the reverse transition it is set free again. This energy stabilizes the existing together of the two phases. If somewhere some crystals of the lighter phase change into the denser one, heat is set free which raises the temperature and thus causes a transition of so much of the denser phase in the lighter one that

<sup>8)</sup> J. D. BERNAL, Observatory, 59, 268 (1936).

<sup>9)</sup> Citation from W. M. ELSASSER, The Earth's Interior and Geomagnetism, Rev. o. Mod. Physics, 22, no. 1, 11 (1950).



the consumption of heat brings back the temperature to the original value corresponding to the transition-curve. The reverse phenomenon occurs for a deviation in the opposite sense. We may conclude that the situation is stable for incidental changes.

This is not the case for the heat flow connected with the earth's cooling. This corresponds to the convex shape of the temperature-depth curve as shown by fig. 1; each particle receives less heat from below than it

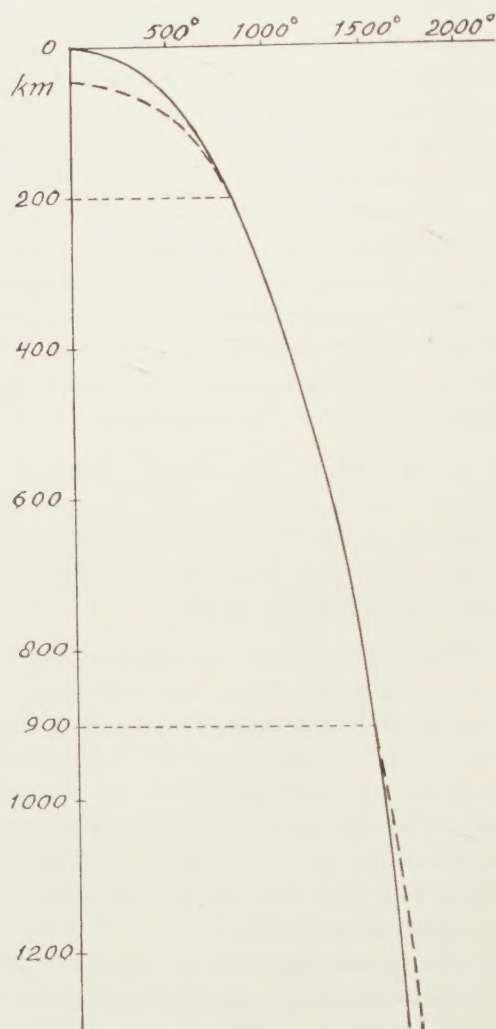


Fig. 1. *Drawn curve*: supposed temperature in the earth,  
*hatched curve* (coinciding from 200–900 km depth): supposed equilibrium-curve of  
the two phases of olivine.

transmits in upward sense. This must cause a slight increase of the denser phase over the whole transition-layer which thus must be supposed to

creep slowly upwards, possibly changing its thickness. Its present position may, therefore, be assumed to be determined by the past developments. As the increase of the denser phase sets free heat, the upward shift of the transition-layer must slow down the earth's cooling.

Examining the second question about the coming into being over such large height of a transition-layer, we may start from the higher temperature of the whole upper part of the mantle which, according to our views, must have been left behind by the previous orogenic cycle, the Hercynian one. The temperature-depth curve must then have been located above the present one; it has probably intersected the transition-curve at great depth. As a consequence of the transition-heat this contact owing to the cooling must have been shifted upwards and grown into a zone over which both phases have existed together. This zone must slowly have travelled to its present position.

The present height of it is a function of the initial situation as well as of the values at different depths of a number of physical constants as e.g. the transition-heat, the thermal conductivity  $\lambda$ , the specific heat  $c$ , the density  $\rho$ , the depth-temperature equilibrium value  $\theta_e$ , etc. Nearly all of them are unknown. We can write down the following heat equations. Dividing them by the specific heat and the density we get outside the transition-layer

$$(1a) \quad \mu \frac{\partial^2 \theta}{\partial z^2} - w_0 \frac{\partial \theta}{\partial z} - \frac{\partial \theta}{\partial t} = 0$$

where  $\theta$  is the temperature,  $z$  the depth coordinate, positive downwards,  $w_0$  a possibly present vertical velocity, likewise positive downwards, and  $\mu$  the thermometric conductivity, i.e. the thermal conductivity  $\lambda$  divided by  $c\rho$ .

As inside the transition-layer we assume  $\theta$  to be equal to the transition temperature  $\theta_e$  which we suppose to be known as function of the pressure  $p$ , we now obtain

$$(1b) \quad \mu \left( \frac{\partial p}{\partial z} \right)^2 \frac{\partial^2 \theta_e}{\partial p^2} + \mu \frac{\partial^2 p}{\partial z^2} \frac{\partial \theta_e}{\partial p} - w_0 \frac{\partial p}{\partial z} \frac{\partial \theta_e}{\partial p} - \frac{\partial p}{\partial t} \frac{\partial \theta_e}{\partial p} + \frac{K}{cA} \frac{\partial q}{\partial t} = 0$$

where  $q$  is the percentage of the heavy phase,  $K$  the transition-energy per gram and  $A$  the heat equivalent.

In these equations the quantities  $\mu$  and  $c$  may differ for the two modifications and, as their densities are different, also  $\partial p / \partial z$ . For the transition-layer where both phases are co-existent, these quantities must have intermediate values varying with the percentage  $q$ . Solutions of these equations thus become complicated and difficult.

We may, however, conclude that the hypothesis of a denser phase of olivine in the lower mantle leads unavoidably to the presence of a transition-layer between both phases which owing to the cooling of the earth is slowly travelling upwards. It is difficult to see how a difference of chemical composition could lead to this same result.



We now come to the third point, the question what effect this transition-layer has in case of a loading or unloading of the crust as e.g. the removal of the ice-load in Fennoscandia and elsewhere at the end of the glacial period. The disappearance of this load must up to great depth have caused a pressure release which must have disturbed the phase-equilibrium in the transition-layer and thus have given rise to the change of part of the heavy modification in the lighter one. This must have continued until the transition absorbed enough heat to lower the temperature to the equilibrium value corresponding to the diminished pressure.

We may expect this phenomenon to have taken place in a relatively short period. As it must have been accompanied by a rise at the crust's surface, this may give a satisfactory explanation of the fact that, when studying the problem of the subcrustal pseudo-plastic flow which, combined with the elastic rebound, after the ice-removal must have restored the crust's equilibrium, the rising velocity thus computed for the first one or two thousand years is less than what has actually occurred; the transition-layer reaction must also have contributed to that rise. We can likewise thus account for the observed delay of rising during the latter part of the phenomenon, because then the rising caused by the subcrustal pseudo-viscous flow was not only diminished by the elastic reaction to the gradual increase of pressure in the deeper layers but also by the corresponding effect of the transition-layer. We thus see that the observed facts in Fennoscandia of which the figures may be published and discussed elsewhere, give a satisfactory support to our hypothesis.

Taking up our fourth problem, the effect of the transition-layer on a convection-current breaking through this layer, we shall first examine the rising part of the current. Assuming that the temperature conduction is too slow to affect the phenomenon appreciably, this rising column would carry its heat with it but its pressure diminishes not only according to its vertical displacement but also because of matter flowing off laterally in the upper part. This must disturb the phase-equilibrium in the transition layer part of this column and so part of the heavier modification must change there into the lighter one till the resulting heat-absorption restores the balance. As we shall presently discuss we shall suppose that because of this process this whole part of the column becomes lighter though at each level, because of the pressure reduction, the temperature did not become higher but lower. For the part of the column outside the transition-layer the rising must at each level cause an increase of temperature and, because of the thermal expansion, likewise a decrease of density. The reverse phenomena must take place in the subsiding column of the current; the density increases over the whole column but the temperature must be only diminished over the part of the column outside the transition-layer but increased in this layer.

This state of affairs may well explain why in general the temperature gradient found below the oceans-floors is about the same as that found in



the continents although we may assume the continental crust to be richer in radio-active constituents than the oceanic one and that we, therefore, might expect a higher gradient in the continental areas. As we may suppose that during our present period of tectonic activity convection-currents, rising below the continents and subsiding below the oceans, are present, the above explanation seems acceptable. As those currents are, however, likely not to be present everywhere, we may expect exceptions. We see that here again our hypothesis of a transition-layer can explain observed facts that otherwise are difficult to account for.

The supposition that in the transition-layer the rising column becomes lighter and the subsiding one denser, though the temperature is lowered in the first and raised in the latter, is obviously required for making it possible that a convection-current can break through it; this layer would otherwise act as a stabilizer. This supposition, however, would put an upper limit for the transition-energy  $K$ . The condition may be written down as follows

$$(2) \quad -\frac{\partial q}{\partial z} w_0 + \frac{\partial q}{\partial t} \geq 0.$$

Introducing the value of  $\partial q/\partial t$  as given by (1b) in which we shall neglect the two conductivity terms and, for simplifying, assume that  $p$  at each level is constant, we obtain, after multiplying by  $K/cAw_0$

$$(3a) \quad -\frac{K}{cA} \frac{\partial q}{\partial z} + \frac{\partial \theta_e}{\partial z} \geq 0$$

which integrated over the whole transition-layer, i.e. between the values for the upper and lower boundaries of the equilibrium-temperature,  ${}_u\theta_e$  and  ${}_i\theta_e$ , and of  $q$  of 0 and 1, gives for the mean value of  $K/cA$  over the height of the layer

$$(3b) \quad \left(\frac{K}{cA}\right)_m \leq {}_i\theta_e - {}_u\theta_e.$$

In two ways we can apply this formula. Making a rough estimate for  ${}_i\theta_e - {}_u\theta_e$  of  $500^\circ$  (see fig. 1) and using the value of the specific heat  $c$  of 0.20 (see "Handbook of Physical Constants" by BIRCH, SCHAIERER and SPICER) we obtain for the transition-energy expressed in calories that it is smaller than 100 calories. This condition is acceptable; all values known are smaller, though of the same order of magnitude.

We can also reverse the application of (3b) and start by assuming a value for  $K/A$  of 50 calories. This leads to the conclusion that the difference  ${}_i\theta_e - {}_u\theta_e$  must be larger than about  $250^\circ$ . We thus get a clear indication of a transition-layer of considerable thickness and so our view is confirmed that the assumption of a transition-layer through which a convection-current can pursue its way leads to a layer of a certain thickness.

The increase of density in the whole subsiding column and the decrease

in the rising one must bring about a subsidence of the earth's surface in the first area and a rising in the second. The well known geological evidence, mentioned e.g. in UMBROVE's "The Pulse of the Earth", that during the first period of an orogenic cycle the continents show a regression is in excellent harmony with this conclusion; it must not only be caused by the rising of the continents below which we must suppose the mounting currents, but also by the subsidence of great parts of the ocean-floors below which we may expect the subsiding columns of the mantle-currents; this must lower the water-surface of the oceans. The fact that during the final part of the orogenic cycle the water transgresses again over the continents and continues to do so during the whole period of rest, again agrees to our conclusions.

For the smaller type of convection-currents mentioned before, the geological and geographic evidence is likewise corroborating our conclusions. In the eastern half of the Indonesian archipelago, e.g., for the deep basins inside the island-arcs, as the Banda Sea, the Molucca Sea and the Celebes Sea, the geological evidence points to these areas having existed above sea-level until a few million years ago. As we have discussed, their fairly rapid subsidence may well be attributed to the sinking currents of smaller convection-systems of which the rising currents occurred below the arcs where the concentration of sialic matter caused an excess of radio-active matter and, therefore, of temperature. Besides this differential movement between basins and arcs, there has also taken place, as already long ago MAC GILLAVRY pointed out, a lowering of the mean level over the whole area of 1000-2000 m. We may obviously explain this as the consequence of the acceleration of cooling brought about by the convection system. Besides the thermal effect of this cooling, it must likewise have caused an increase of the heavier phase of which the effect may even have been greater than the thermal one.

Resuming, we may state that the evidence given by the observed facts is in favor of our hypothesis of the existence of a denser phase of olivine in the lower mantle and of a transition-layer between 200 and 900 km depth of this phase and the orthorhombic one present below the crust.

The author wishes here to acknowledge the helpful discussions he had with his colleague, Prof. Dr. W. NIEUWENKAMP, on the thermodynamic problems connected with this hypothesis.

## GEOLOGY

### STUDIES IN COMPARATIVE PETROFABRIC ANALYSIS

#### I. XENO- AND AUTOLITHIC FABRIC

BY

E. DEN TEX

(Communicated at the meeting of November 26, 1955)

#### ABSTRACT

Strongly contrasting microfabrics, obtained from rocks associated with the Kosciusko pluton, have led to a strictly comparative study of the fabric of (i) the average country-rock, (ii) the main body of plutonic rock, and (iii) some of the inclusions of the latter.

A purely structural distinction between xenolithic and autolithic inclusions appears to be possible where mineralogy and texture fail to be sufficiently distinctive.

Other petrogenetic conclusions are drawn from the contrast between granitic and granitized fabrics causing a break in the fabric evolution of the pluton. They involve the origin of the plutonic rock, its mechanism of emplacement and its tectonic history.

#### INTRODUCTION

While studying the structure and petrology of the Kosciusko pluton in the Snowy Mountains of New South Wales, it occurred to the author that microfabric diagrams could be profitably used in a similar manner as is often done with anatomic and tectonic features: by simply comparing and contrasting their geometrical patterns without having recourse to interpretations of a single pattern in terms of physiology, pathology, kinematics or dynamics. Notwithstanding the growing body of experimental work that is beginning to enlighten the relations between stress, strain and geometry of the deformed body, the dynamic and kinematic interpretations of an essentially static arrangement of fabric elements in a rock are still very much the weak links in the chain of thought of the structural petrologist.

The comparative approach to the problems of rock deformation, intrusion, extrusion etc. is not new. BROWNE (1931), UMBGROVE (1947), CLOOS (1923), STILLE (1924), DE SITTER (1954) and many others have arrived at valuable genetic conclusions from comparative studies of geotectonic styles. The present author is of the opinion that a hoard of petroctectonic and petrogenetic information will remain unrevealed until such studies are deliberately applied to the field of petrofabric analysis.

It is the purpose of this series of papers to demonstrate various ways of extracting such fundamental knowledge from microfabric diagrams of selected rock-types in a complex plutonic setting. The present paper is concerned with the fabrics of mica-cleavage-poles and quartz-optic-axes



from certain inclusions of rather similar texture and mineralogy. A second study will be devoted specifically to the evolution of the quartz-fabric in the plutonic sequence as opposed to that in the country-rock. The author will consider his aim achieved if these examples may contribute towards a more selective procedure in structural petrology and to a wider recognition of the use of petrofabric analysis among petrologists and structural geologists.

#### SYNOPSIS OF THE SAMPLE AREA

The area from which samples for comparative petrofabric analysis have been taken was the subject of a previous paper presenting a full petrological and structural analysis of the main rock types (DEN TEX, *in press*). It forms a superficial and, to some extent, marginal part of the Kosciuszko pluton: an elongate body of N.N.E. trend, parallel to the



Fig. 1. Structural sketch map of the Kosciuszko area in the Snowy Mountains of New South Wales, Australia, showing the localities (A, B, C and D) from which petrofabric samples were obtained. For legend and full explanation see text (p. 13).

"grain" of the Ordovician (?) country-rock. The plutonic rocks are chiefly granodiorites, quartz-diorites or tonalites, and quartz-tonalites without clearly defined mutual boundaries. Structurally the pluton is concordant and almost conformable with regard to the country-rocks which occur in a steep and narrow septum forming the Western boundary of the area (see fig. 1). The latter are probably Ordovician metasediments consisting mainly of phyllites, quartz-phyllites and quartzites, nowhere surpassing the greenschist-facies (biotite-zone) of progressive regional metamorphism. They have been isoclinally folded about N.N.E. trending, subhorizontal axes and were subsequently flattened in the bedding-cleavage plane, whereby mechanical lensing of the quartzose beds became a dominant feature both in the field and under the microscope. Steep pitch reversals of the fold-axis on either side of the larger lenses are probably connected with the formation of the latter.

The structural sketch map (fig. 1) shows the generalized strike and dip of the bedding-cleavage in the metasediments (—|—) and of the foliation in the plutonic rocks (—△—). The average dip of both is  $70^{\circ}$  E.S.E. The arrows indicate bearing and plunge of the fold-axes and plutonic lineations: the shorter the shaft the steeper the plunge. Double-headed arrows represent horizontal directions. There is an obvious tendency of the granitic lineations to plunge N.E. (pitching steeply N.N.E. in the foliation plane) as one proceeds in an easterly direction through the area. Near the eastern margin of the map the angle of pitch averages  $70^{\circ}$  N.N.E. and remains uniform for some 10 miles further East. The foliation consists of a planar parallelism of micaceous minerals, lenticular aggregates of dark and light minerals, and platy inclusions. The lineation is visibly contained within the foliation, and is expressed by a linear parallelism of dark and light mineral streaks (representing mica- and quartz aggregates) and of those inclusions which exhibit a triaxial habit (see fig. 3).

Inclusions, other than mineral streaks, lenses and rods of less than a quarter-inch diameter, are isolated features constituting up to ten percent by volume of the Kosciusko granodiorite in the marginal area under consideration. The upper limit of the maximum diameter of these inclusions is in the order of several feet. A few are of lighter colour than the host-rock, consisting mostly of quartz; others are somewhat darker, with a speckled appearance due to feldspar porphyroblasts; while by far the greater number is very dark and fine-grained. On a basis of mineralogy and texture this latter group of inclusions defies classification as either xenoliths or autoliths because of its uniformly granitic character. From a routine study of thin sections two of these inclusions were selected by virtue of slight differences in mineralogy. The localities of these samples are indicated as *B* and *D* on fig. 1. From *A* and *C* representative samples had been collected, of country- and plutonic rock respectively, in the course of the regional investigation. Their petrofabric analysis is here reproduced for the purpose of comparison.

## COMPARATIVE PETROFABRICS

As a background to the inclusion-fabrics: *B* and *D*, the country-rock and plutonic fabrics: *A* and *C*, will be discussed in alphabetical order, whereby strong similarities between *A* and *B*, and between *D* and *C* will become apparent. Summaries of mineralogy and texture are added in as brief a form as clarity will allow.

*A. Country-rock-fabric*

As a fair sample of the materials constituting the country-rock, within the limits of a thin section, a quartz-phyllite from the S.E. extremity of the septum has been chosen for fabric analysis. Its essential minerals are: quartz, chlorite, sericite and biotite, all of which exhibit preferred dimensional orientation. The micaceous minerals, with their planar habit, are oriented for preference in the bedding-cleavage or in any other of the five *s*-planes present in the rock-fabric. They are concentrated in often crumpled, microscopic laminae. Quartz tends to form lenticular or rod-like aggregates, spliced by micaceous strands, whereby both the individual crystals and the lenses exhibit a triaxial habit with the long and median diameters always in the bedding-cleavage ( $s_1$ ) and the long diameter preferably normal to the fold-axis (see Plate I, fig. A).

Three thin sections were cut at right angles to each other and, in order to test the homogeneity of the fabric, 300 mica-cleavage-poles were measured in each of these on the U stage. On finding sufficient similarity of pattern to claim homogeneity of fabric in three dimensions, the 900 poles were plotted on the lower hemisphere of an equal-area projection normal to the fold-axis *B*. This diagram has been provided with density-contours in the conventional manner and serves as fig. 2A (right). It presents a very characteristic pattern showing six point-maxima (one principal and five subordinate) corresponding to the five visible *s* planes and the *ac*-plane. There is also a strong but rather incomplete girdle-maximum around the fold-axis (*B*), and a weaker but complete girdle around the *a*-axis of the fabric. To a first approximation the symmetry of the fabric is orthorhombic, but closer inspection reveals that unequal development of the paired subordinate maxima ( $s_{2,3,4,5}$ ) reduces the symmetry to triclinic. Almost the same considerations apply to the contoured diagram of 300 quartz-optic-axes measured and plotted in the the *ac*-section (fig. 2A, left). It shows a rare four-girdle pattern of strong triclinic symmetry, with each of the girdles (in the correct order of prominence) normal to one of the paired subordinate *s*-planes, and with the stronger girdles containing a maximum that coincides with the corresponding mica-submaximum. Therefore, the fabric is not only homogeneous but also, to a large extent, homotactic. As further interpretation of the fabric will not be attempted for the present purpose, the time-consuming work required by an axial distribution analysis (RAMSAUER, 1941) does not seem justified.



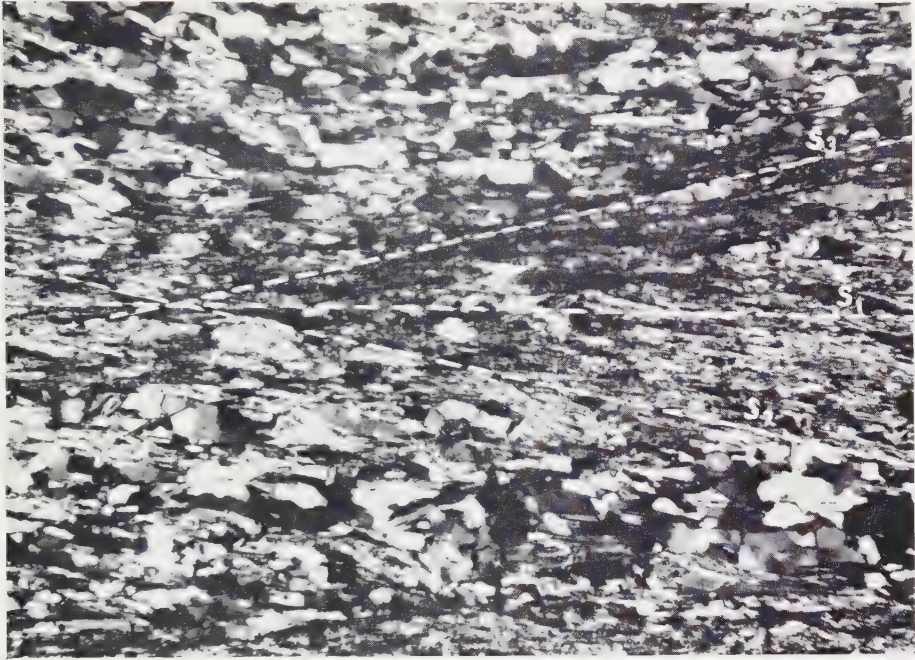


Fig. A. Photomicrograph of quartz-phyllite (A), 58x

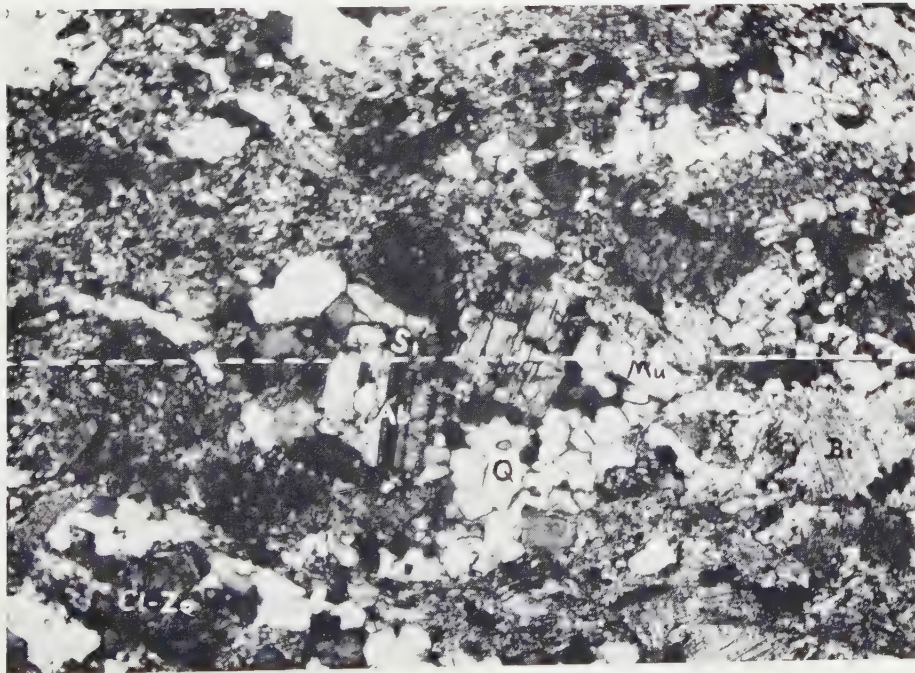


Fig. B. Photomicrograph of xenolith (B), 66x



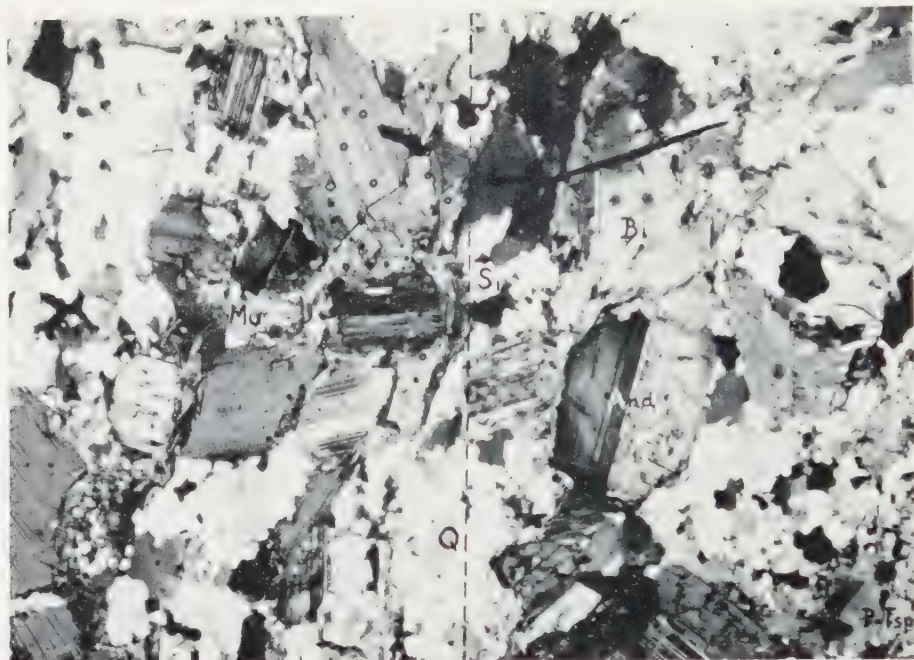


Fig. C. Photomicrograph of quartz diorite (C), 18x

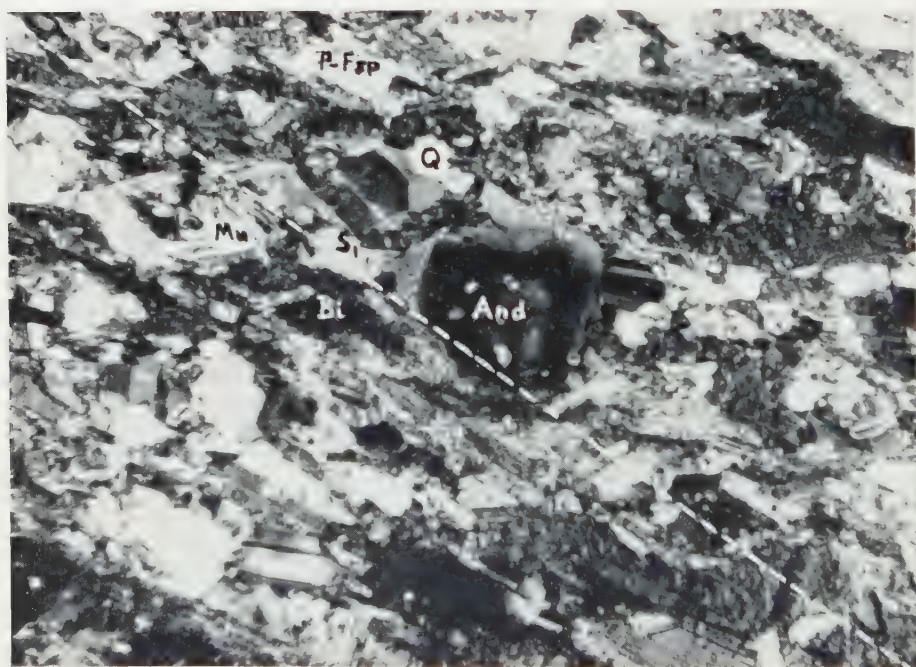


Fig. D. Photomicrograph of autolith (D), 72x

The photomicrograph (Plate I, fig. A) has been taken in the *ac*-section, with crossed nicols, at a linear magnification of  $58\times$ .

### *B. Xenolithic fabric*

Inclusion *B* was found in the granodiorite some 3 miles E. of the septum of country-rock. Being of less fine grain than the latter there is no greater accuracy to be expected from fabric measurements in three sections than from the conventional procedure for micas using two sections at right angles. The essential minerals are: biotite, muscovite, quartz, albite and clinozoisite. There is no visibly expressed, preferred dimensional orientation other than a planar parallelism of micaceous flakes forming an internal foliation, which appears to be parallel to the foliation of the granodiorite (*ab*). Failing an obvious internal lineation the section used for plotting was cut normal to the lineation of the host-rock (i.e. the long axis of the inclusion).

The distribution patterns of 411 mica-cleavage-poles (fig. 2B, right) and 300 quart-axes (fig. 2B, left) are remarkably similar to the corresponding patterns of the country-rock. Although especially the girdles have suffered some loss of density, there can be no doubt that the fabric patterns are sufficiently similar to warrant the claim that inclusion *B* is a granitized fragment of the country-rock, to wit: a xenolith. Yet, granitization-in-situ has been attended by widespread recrystallization and neomineralization, but their combined effects have not succeeded in obliterating the essential features of the fabric with the exception of the dimensional orientation of the quartz grains which has largely, though not completely, disappeared in the xenolith.

Plate I, fig. B, is a photomicrograph of the thin section normal to the lineation (*L*), which was used in the preparation of the fabric diagrams. Nicols crossed. Linear magnification:  $66\times$ .

### *C. Plutonic rock-fabric*

The quartz-diorite or tonalite from locality *C* has previously been proved to yield a representative sample of the fabric of the plutonic rock. In order of prominence the essential minerals are: biotite, normally-zoned andesine, quartz and muscovite, with sporadic potash-felspar. Grain-size is medium. The mica-flakes exhibit a preferred dimensional orientation, visibly expressed by the foliation; but in addition the thin section normal to the lineation reveals that (without concomitant chloritization) the biotite flakes and laminae have been shearfolded on a plane obliquely intersecting the foliation. Quartz occurs typically in elongate lenticular and rod-like aggregates. Individual quartz-crystals present no distinct habit, but the rods and lenticles are strictly oriented according to shape: their long and median diameters in the foliation, and the long diameter parallel to the lineation of the micas. The broad similarities between country- and plutonic rock, as far the texture is concerned, should not distract from the significant differences of detail.



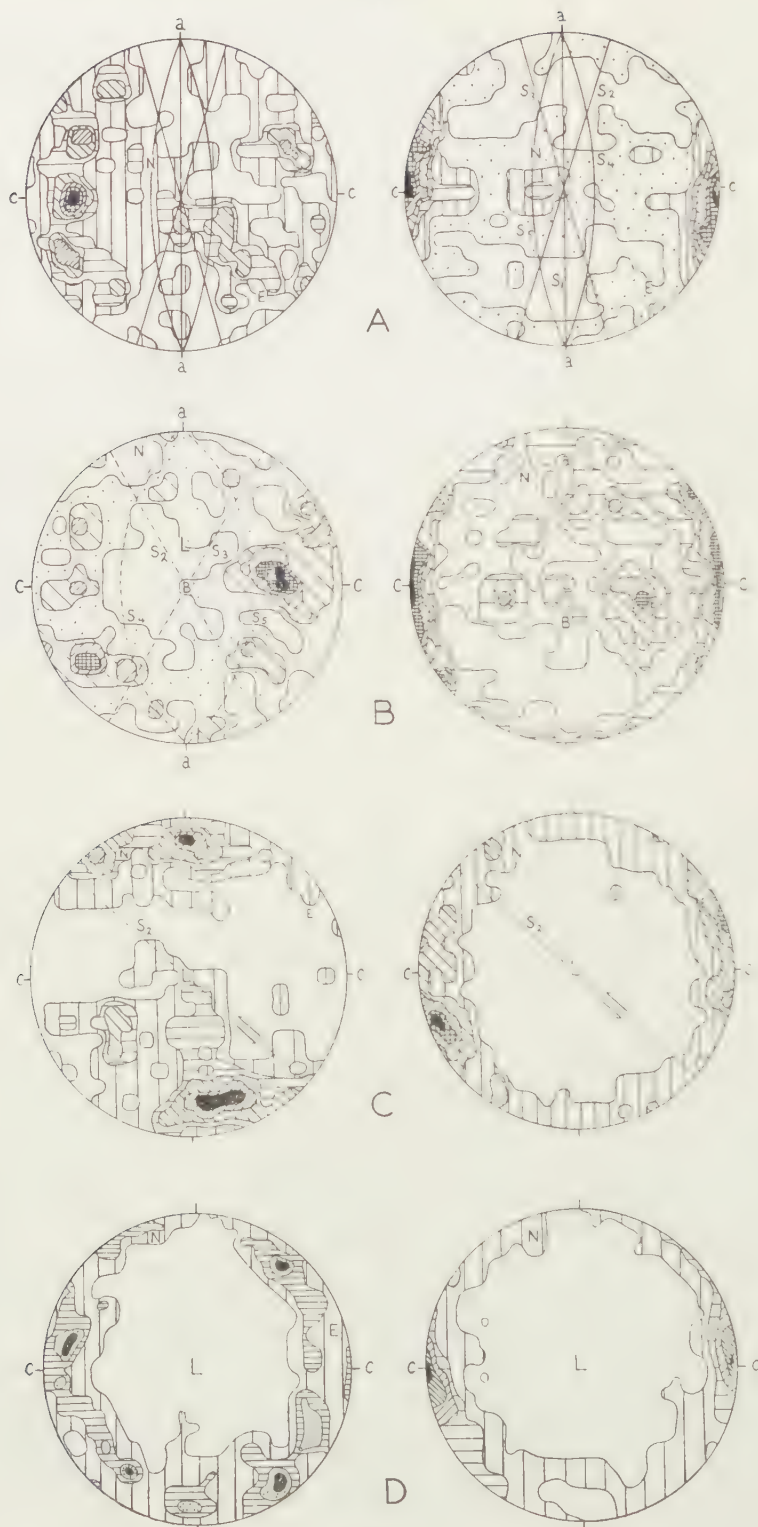


Fig. 2

Microfabric study of specimen *C* has followed along conventional lines. Three hundred mica-flakes and an equal number of quartz-axes have been measured and plotted in the section normal to the lineation (*L*). The contoured diagrams are shown as figs. 2C, right and left, respectively. In the mica-fabric the outstanding feature is a strong and almost complete girdle around the lineation. There is also one principal maximum, contained in the girdle, but inclined to the pole of the megascopic foliation (*c*) at an angle of  $20^\circ$ , reducing the symmetry of the total fabric to monoclinic with the lineation (*L*) as a twofold axis of symmetry. Of the submaxima one is much better developed than the others. Its locus is much nearer *c*, while another submaximum corresponds to the pole of the secondary shearplane (*s*<sub>2</sub>) responsible for the bending and stretching of the micas. This is a clear case of transposition of the foliation.

The quartz-fabric has very little in common with that of the country-rock. Striking features are the double principal maximum at some  $70^\circ$  from *L* in the foliation-plane, and the incomplete cleft-girdle of which it forms part. A strong submaximum close to the movement-direction in *s*<sub>2</sub>, reduces the symmetry of the fabric to monoclinic, while further weak maxima occur in a rather haphazard manner and have a tendency to reduce the symmetry even further.

Plate II, fig. C is a photomicrograph of the section normal to the lineation, taken with crossed nicols, at a linear magnification of  $18\times$ .

Fig. 2. Microfabric samples from the Kosciusko pluton. Lettering corresponds to text and to localities in fig. 1. On the left are quartz-, on the right mica-diagrams.

Schmidt's equal-area net, lower hemisphere projection.

- A* (left) 300 optic axes of quartz from a quartzphyllite near Mt. Kosciusko. Section normal to fold-axis. Contours: 6-5-4-3-2-1-0 % per 1 % area.  
 (right) 900 basal cleavage-poles of chlorite, sericite and biotite from the same sample, but measured equally in three perpendicular thin sections and rotated into the *ac*-section. Contours: 7-6-5-4-3-2-1-0 % per 1 % area.
- B* (left) 300 optic axes of quartz from a dark inclusion in the Kosciusko granodiorite near Mt. Stilwell. Section normal to fold-axis (*B*). Contours: 5-4-3-2-1-0 % per 1 % area.  
 (right) 411 basal cleavage-poles of biotite and muscovite from the same sample, measured in two perpendicular sections and rotated into the section normal to the lineation (*L*) of the granodiorite, which makes an angle of  $15^\circ$  with the fold-axis (*B*). Contours: 4.4-3.6-2.9-2.2-1.5-0.7-0 % per 1 % area.
- C* (left) 300 optic axes of quartz from a quartz-diorite near Mt. Guthrie. Section normal to the lineation (*L*). Contours: 8-6-4-2-0 % per 1 % area.  
 (right) 300 basal cleavage-poles of biotite and muscovite from the same sample, same section. Contours: 10-8-6-4-2-0 % per 1 % area.
- D* (left) 300 optic axes of quartz from a dark inclusion of the Kosciusko granodiorite near the E. margin of the area. Section normal to the lineation (*L*) of the granodiorite. Contours: 4-3-2-1-0 % per 1 % area.  
 (right) 360 basal cleavage-poles of biotite and muscovite from the same sample, measured in two perpendicular sections and rotated into the section normal to *L*. Contours: 7.5-5.8-4.2-2.5-0.8-0 % per 1 % area.

It shows bent biotite, twinned and zoned andesine, and quartz-lenticles with their median and short diameters.

#### *D. Autolithic fabric*

Another representative sample of the dark, fine-grained inclusions in the granodiorite was found at locality *D*. Its essential minerals are, now without exception, those of the host-rock, i.e. biotite, normally-zoned andesine, potash-felspar, muscovite and quartz, in order of prominence. Thus, there is only a difference in relative quantities: less quartz, more potash-felspar and less muscovite than in the quartz-diorite (*C*). In NIGGLI's quantitative mineralogical classification (1931) the rock of this composition is termed a quartz-bearing micro-mela-diorite. In the hand-specimen the texture seems massive, but under the microscope a planar parallelism of the mica-flakes becomes apparent. As for inclusion *B*, the internal foliation is parallel to the plane of long and median diameters and consequently also to the foliation of the host-rock.

Investigation of the micro-fabric has been pursued in exactly the same manner as previously for *B* and *C*. 360 mica-flakes and 300 quartz-axes have been recorded and contoured in figs. 2D, right and left. A first glance at the diagrams leaves the impression that these represent fabrics very different from that of the xenolith and country-rock. The mica-fabric is a single principal point-maximum within a single girdle. Its symmetry is orthorhombic with axial affinities. The girdle has the lineation (*L*) as an axis and the principal maximum is located in *c*, the pole of the megascopic foliation of the host-rock. Except for the coincidence of the main maximum with the pole of the megascopic foliation, and for the absence of submaxima and a visible shearplane ( $s_2$ ), this fabric is a replica of that of the host-rock (*C*).

Again, the quartz-fabric is quite distinct from that of the xenolith or country-rock in having only a single cleft-girdle situated at some  $70^\circ$  radially from the lineation (*L*). This is a feature relics of which are undoubtedly present in the corresponding diagram of the quartz-diorite (fig. 2C, left). However, the three principal maxima spaced at  $120^\circ$  have no counterpart in the host-rock-fabric.

There is every reason then to remove inclusion *D* from the category of xenoliths, while fabric, texture and mineralogy concur in support of the opinion that it is an autolith, i.e. a fragment of an early, chilled phase of the host-rock.

Plate II, fig. D is a photomicrograph of the section normal to *L* showing the relatively untwisted nature of the micas and the lack of dimensional orientation in the quartz grains. It was taken with the nicols crossed, at a linear magnification of  $72\times$ .

#### PETROGENETIC CONCLUSIONS

To illustrate the spatial relations of the various structures and fabrics



referred to above, an isometric block-diagram of the sample area has been constructed and subsequently dissected along those foliation planes which contain the xeno- and autoliths inclusions *B* and *D* so as to expose them in three dimensions. The upper surface of the block-diagram is the somewhat simplified sketch map of fig. 1, the structure in depth has been extrapolated from surface measurements. The inclusions are shown in proper orientation, more or less true to shape, but on a greatly exaggerated scale. Their upper halves have been removed to reveal the internal structure and to accommodate a simplified version of the corresponding fabric diagram. Possible rotations of the xenolith (*B*) are indicated by curved arrows.

Now, having established a clean break between the inclusion-fabrics: one xenolithic, the other autoliths, let us follow up the trails of their development in order to obtain an approach to the granite problem from the vantage point of fabric evolution.

#### *Granitization, mimetic crystallization and fabric revolution*

The fabric comparison of xenolith and country-rock has left no doubt that the former is a product of granitization of the latter. This conservative type of granitization must, of necessity, be a metasomatic process involving no differential movements of crystals, and consequently no fluid motion other than that occurring in an intergranular capillary system. Its recrystallizations are strictly mimetic (e.g. quartz and muscovite), while neomineralizations starting from seed-crystals of comparable structure (biotitization of chlorite) aid in preserving the fabric. Any dimensional orientation, preserved in this manner, is purely incidental to the corresponding lattice-orientation. Thus, the fabric habit of quartz has all but vanished, while the crystal habit of the micas has maintained the original *s*-planes, at least in a statistical sense, throughout the process of granitization of the country-rock.

Now, the portions of country-rock, affected in this way, are isolated fragments in intimate contact with the plutonic host-rock. Furthermore, there is ample evidence that the fabric of the xenolith as a whole has been rotated from its original orientation in the country-rock (see fig. 3). The projection-plane of the xenolithic fabric is obtained by a rotation of that of the country-rock over  $45^\circ$  clockwise in the foliation. A further  $15^\circ$  in the same sense is needed to bring the girdles in exactly similar positions with reference to the geographic and fabric coordinates. A total rotation of  $60^\circ$  clockwise in the foliation plane is therefore implied. But that is not all. When proper account is taken of the order of prominence of the maxima in both diagrams and of the girdles in the quartz-fabric, it appears that the xenolithic fabric is the mirror-image of the country-rock-fabric:  $s_2$  has changed position with  $s_3$ , and  $s_4$  with  $s_5$ . In other words the xenolithic diagrams are country-rock diagrams turned front-to-back. Had they been monoclinic with a symmetry plane in *ac*, then the fabric

would have appeared exactly the same when looked at from the front or from the back. A revolution of the country-rock-fabric seems to have taken place around either the  $a$ - or the  $c$ -axis. Turning the fabric  $180^\circ$  about  $a$  would require the long axis ( $b$ ) of the xenolith to revolve across the foliation plane causing considerable friction. On the other hand, half a revolution about  $c$  could easily be integrated with the already established  $60^\circ$  clockwise rotation about that axis to make the total rotation either  $240^\circ$  clockwise or  $120^\circ$  anti-clockwise.

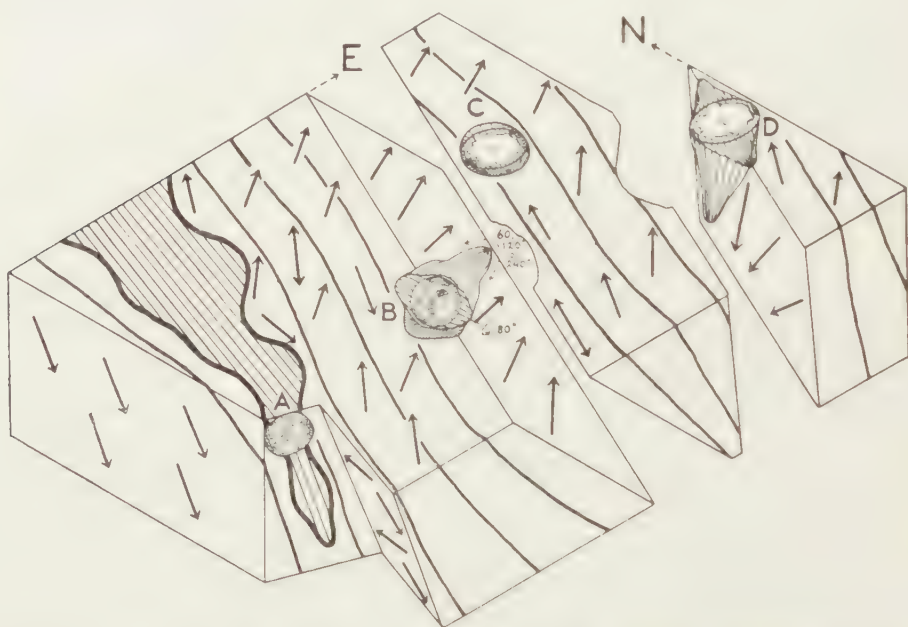


Fig. 3. Isometric block-diagram of the Kosciusko area showing simplified versions of the mica-fabric diagrams in their correct positions and orientations in space. Upper surface is the map of fig. 1. For full explanation see text (p. 19).

A third possibility is mentioned for completeness of record only. Suppose that the xenolith is a slab of country-rock torn from the other limb of the main fold. Then the prominent strain-slip cleavage ( $s_2$ ) would change position with  $s_3$ , but  $s_4$  and  $s_5$  would remain where they are in the other limb. As such the fabric would not stand the test, but half a revolution about  $b$  would now leave  $s_2$  and  $s_3$  as they are and interchange  $s_4$  with  $s_5$ , thus eventually turning the fabric completely front-to-back. This revolution is subject to similar objections as the complex rotation about  $a$  and  $c$ , quite apart from inconsistencies arising from the fabric evolution of the host-rock as discussed below.

#### *The granite problem in the light of fabric evolution*

Having ascertained that the inclusions of type *B* owe their granitic aspect to static metasomatism of semi-pelitic country-rock with little or no evolution of its triclinic fabric, and having shown that, on the

other hand, the monoclinic fabric of the granitic host-rock is most probably a further development of the orthorhombic fabric of the inclusions of type *D*, it follows that the granitic rocks in the Kosciusko area are the results of processes of various trend yielding a distinctly interrupted sequence of fabric evolution.

Evidence of differential or penetrative movements in the granitic host-rock is paramount. Not only are they to be held responsible for dislocation of the country-rock by act of revolution (as shown by the fabric of a xenolith), but the granite also contains oriented autolithic relics of an orthorhombic fabric with axial tendencies. Such a fabric finds no match among the present country-rocks, but its symmetry would be compatible with intrusive flow of a viscous crystal mush. Finally the monoclinic fabric of the quartz-diorite (*C*) provides a record of strong penetrative movement on a single set of shearplanes ( $s_2$ ), which seems to have been overprinted on the orthorhombic fabric as preserved by the autolith (*D*). The lack of swirls around the long axes of the inclusions virtually precludes their revolution about these axes, although they coincide with monoclinic  $b = B$  of the host-rock. Whatever its ultimate source may be, the fabric sequence from autolith to host-rock implies a high but slightly decreasing mobility of the material in the course of evolution.

In the face of similar evidence brought to light by structural scrutiny of an increasing number of granitic plutons, the proponents of wholesale granitization are finding themselves forced to abandon static metasomatism as a major cause of granite in favour of processes of metasomatic mobilization of the country-rock, such as anatexis (SEDERHOLM, 1907), syntexis (LOEWINSON-LESSING, 1911), rheomorphism (BACKLUND, 1938) and fluidization (REYNOLDS, 1954). Now, it is obvious that the concept of mobilization has practical significance only in so far as it may explain a gradual evolution of the *actual* country-rock towards increasingly immobile fractions, each incorporating exclusively fragments of older, less mobile stages. Where sudden changes of mobility mark the onset of an evolutionary trend from a rock-type not representative of the actual environment, mobilization becomes pure hypothesis and, in addition, loses its most attractive claim: the solution of the room problem.

In the case of the Kosciusko granite (*sensu lato*) this restricted notion of mobilization is of no avail. Firstly, there is no indication of a gradual evolution of the country-rock-fabric towards a more mobile phase. Secondly, where evolution of the fabric is evident (as from autolith to host-rock) it is one of *decreasing* symmetry and therefore of *decreasing* original mobility. Lastly, but of no less importance, is the fact that both xenolith and autolith appear to have escaped the penetrative deformation of monoclinic symmetry, which caused micro-shearfolds to develop in the granitic host-rock. This means that both types of inclusion were considerably more rigid than the host-rock during or shortly after emplacement of the latter. Hence, the alternative view that the autolith represents



a final phase of mobilization cannot be supported. It must be part of an early, highly mobile fraction that became chilled before the granitic host-rock arrived in situ.

With these considerations in mind the conclusion seems inevitable that the granitic rocks in the Kosciusko area are of twofold origin. The main body of granodiorite and tonalite is a product of contamination of a dioritic or even more basic magma by semipelitic country-rock, whereas some fragments of the latter (in intimate contact with the magma) have been assimilated or granitized by static metasomatism.

*Department of Geology,  
University of Melbourne, Australia*

#### REFERENCES

- BACKLUND, H. G., The problems of the Rapakivi granites, *Jour. Geol.*, **46**, 390 (1938).  
 BROWNE, W. R., Notes on Bathyliths and some of their implications, *Proc. Roy. Soc. N.S.W.*, **65**, 113-123 (1931).  
 CLOOS, H., Das Batholithenproblem, *Fortschr. Geol. u. Pal.*, **1**, 1-80 (1923).  
 DE SITTER, L. U., Gravitational gliding tectonics. An essay in comparative structural geology, *Amer. Jour. Sci.*, **252**, 321-344 (1954).  
 DEN TEX, E. (in press), Complex and imitation tectonites from the Kosciusko pluton, Snowy Mts., N.S.W., *Jour. Geol. Soc. Aust.*, **3**, for the year 1955.  
 LOEWINSON-LESSING, F., The fundamental problems of petrogenesis, *Geol. Mag.*, **8**, 295 (1911).  
 NIGGLI, P., Die quantitative mineralogische Klassifikation der Eruptivgesteine, *Schweiz. Min. Pet. Mitt.*, **11**, 296-364 (1931).  
 RAMSAUER, H., Achsenverteilungsanalysen an Quarztektoniten, Bibliotheksnummer 304, *Miner. Inst., Universität Innsbruck*, 3-26 (1941).  
 REYNOLDS, D. L., Fluidization as a geological process, and its bearing on the problem of intrusive granites, *Amer. Jour. Sci.*, **252**, 577-613 (1954).  
 SEDERHOLM, J. J., On granite and gneiss, *Bull. Comm. Géol. Finl.*, **V**, **23**, 102 (1907).  
 STILLE, H., *Grundfragen der vergleichenden Tektonik*, 443 pp. (Berlin, Gebr. Borntraeger, 1924.)  
 UMBGROVE, J. H. F., *The Pulse of the Earth*, 358 pp. (Mart. Nijhoff, The Hague, 2nd ed., 1947.)

STARCH ELECTROPHORESIS OF THE BOVINE  
EYE LENS PROTEINS

BY

H. BLOEMENDAL

*(Summary of a contribution published in Series C, 59 of these Proceedings)*

So far the isolation of  $\alpha$ -crystallin, a component of total eye lens extract, was achieved either by precipitating at the isoelectric point or by salting out with ammonium sulphate. The fractions obtained by these methods mostly contain small quantities of one or more other components of the total lens extract. This appeared from electrophoretical and ultracentrifugal studies. Starch electrophoresis opens the possibility of satisfactory separation of eye lens extract in its different fractions without addition of acetic acid, hydrochloric acid-alcohol mixture or saturated solution of inorganic salts. In this way the chance of denaturation of the protein is diminished.

It appeared from our experiments that vertical arrangement of the box containing the supporting medium gave the best results.

Furthermore the level of the buffer solution in the cathode vessel must be higher than that in the anode.

With equal height of buffer solution levels and horizontal arrangement of the starch block, separations were seriously disturbed by electro-osmotic flow towards the cathode.

Traces of the eye lens protein  $\beta$ -crystallin were detected by means of a modification of the well-known nitroprusside reaction.

Details, figures and diagrams are given in Proceedings Series C, Vol. 59 nr. 1 (1956).

A NEW GENERAL THEOREM ON SHAKE-DOWN OF  
ELASTIC-PLASTIC STRUCTURES

BY

W. T. KOITER

(Communicated by Prof. C. B. BIEZENO at the meeting of December 17, 1955)

*Summary*

A new theorem, complementary to MELAN's theorem [ref. 2, 3], is derived on the basis of the concept of an "admissible plastic strain rate cycle". This theorem may be combined with MELAN's theorem in order to obtain upper and lower bounds for the allowable load variations for shake-down. A simplified proof of MELAN's theorem and a refinement of this theorem are also discussed.

1. *Introduction*

Two main types of plastic failure may occur in structures of an ideal elastic-plastic material, i.e. a material with a pronounced yield point and no strain-hardening. The first and simplest type of failure may occur in a single application of loads (if these loads are sufficiently high) by indefinitely increasing plastic deformations under constant loads. This type of failure is described by the term *plastic collapse*, and the corresponding load system is called a collapse load system.

A structure is usually subjected to several loads each of which can vary independently between certain limits. In order to prevent plastic failure it is obviously necessary that no combination of loads within these limits constitutes a collapse load system. However, this requirement is by no means sufficient to prevent plastic failure. Because the independent loads may be repeated in any random sequence the possibility arises that although no single load combination causes collapse, cycles of plastic deformation may occur in the structure for one or more particular load cycles, and these deformation cycles may be repeated each time such a load cycle is applied. Usually the structure will then become unserviceable due to excessive overall deformation. In exceptional cases the cycles of plastic strains may occur in alternating directions in one part of the structure; although no excessive overall deformations will arise in such a case a plastic fatigue failure will result after a comparatively small number of load cycles.

In order to prevent this second type of *failure by cyclic plastic deformations*, the limits on the individual loads will have to satisfy additional requirements. If these requirements are indeed satisfied the structure will,



possibly after a period of initial plastic flow, "shake down" to some state of permanent strain and corresponding residual stress, such that all subsequent load applications will be carried in a purely elastic manner. In other words: plastic deformation will ultimately come to a stop.

The investigation of plastic collapse of a structure, or limit analysis, is greatly facilitated by two complementary theorems. Their general formulation and proof for a three-dimensional continuum are due to DRUCKER, PRAGER and GREENBERG [ref. 1]. In simple structures like continuous beams and frames each of these theorems may be applied to obtain the collapse load rigorously. For more complicated structures the two theorems may be used together to obtain both upper and lower bounds for the collapse load.

On the other hand, only one theorem, due to MELAN [ref. 2], is available for the much more difficult shake-down problem. A complete solution is again possible for continuous beams and frames at the expense of considerable computational effort, and lower bounds for the limits on the external loads, required for shake-down, may be obtained for more complicated structures. However, so far no second, complementary theorem has been available to furnish upper bounds. It is the purpose of the present paper to derive such a second theorem; at the same time a simplified proof of MELAN's theorem and a refinement of this theorem will be given.

## 2. Basic assumptions and material properties

All deformations are assumed to be small, the strain tensor being expressed in the displacements  $u_i$  by the well-known formulae

$$(1) \quad \varepsilon_{ij} = \frac{1}{2} (u_{i,j} + u_{j,i}),$$

where a comma preceding a subscript  $i$  denotes partial differentiation with respect to the Cartesian coordinate  $x_i$ . Changes in geometry due to the deformation are neglected in setting up the equations of equilibrium.

We assume that the external loads are body forces  $X_i$  and surface tractions  $p_i$  on the part of the surface  $S_p$  where the displacements are not prescribed; on the remaining part of the surface  $S_u$  the prescribed displacements are assumed to be zero. The body forces  $X_i$  and surface tractions  $p_i$  can vary arbitrarily and independently between prescribed limits. The loads are assumed to be applied sufficiently slowly in order that dynamic effects can be neglected.

A strain (rate) field  $\varepsilon_{ij}(\dot{\varepsilon}_{ij})$  is called kinematically admissible if it can be derived from a displacement (velocity) field  $u_i(\dot{u}_i)$  by means of (1), where the displacements (velocities)  $u_i(\dot{u}_i)$  vanish on  $S_u$ . The conditions of equilibrium of a stress distribution  $\sigma_{ij}$  with body forces  $X_i$  and surface tractions  $p_i$  on  $S_p$  is expressed by the principle of virtual work

$$(2) \quad \int X_i u_i dv + \int_{S_p} p_i u_i df = \int \sigma_{ij} \varepsilon_{ij} dv,$$

holding for all kinematically admissible strain distributions.

An ideal elastic-plastic material cannot support stresses in excess of a certain fixed limit, the yield limit. A state of stress inside the yield limit will be called safe, a state of stress inside or on the yield limit will be called allowable. In safe states of stress the material behaves in a purely elastic manner. Unloading is said to occur in a state of stress on the yield limit if the stress rates  $\dot{\sigma}_{ij}$  are such that the state of stress returns inside the yield limit.

The strains are the sum of the elastic strains  $\epsilon'_{ij}$ , given by HOOKE'S law, and the plastic strains  $\epsilon''_{ij}$ . An increment of the plastic strains can only occur if the state of stress is on the yield limit and no unloading occurs. Only a single fundamental property of the plastic stress-strain relations is required in the derivation of MELAN'S shake-down theorem and its complementary theorem. If  $\dot{\epsilon}''_{ij}$  is a non-vanishing plastic strain rate, occurring in the state of stress  $\sigma_{ij}$  on the yield limit, and  $\sigma_{ija}$  is a safe state of stress, the required property is (cf. ref. 1]

$$(3) \quad (\sigma_{ij} - \sigma_{ija}) \dot{\epsilon}''_{ij} > 0,$$

where the summation convention has been employed. For an allowable state of stress  $\sigma_{ija}$  it follows immediately from (3)

$$(4) \quad (\sigma_{ij} - \sigma_{ija}) \dot{\epsilon}''_{ij} \geq 0.$$

Moreover the rate of energy dissipation per unit volume

$$(5) \quad \sigma_{ij} \dot{\epsilon}''_{ij} = F(\dot{\epsilon}''_{ij})$$

is a positive and single-valued function of the plastic strain rates.

### 3. Melan's shake-down theorem

At any stage in the loading program the actual stresses may be written as the sum of the "elastic" stresses  $\sigma_{ij}^*$ , which would occur if the structure always behaved elastically no matter how high the stresses would be, and residual stresses  $\rho_{ij}$ , caused by preceding plastic deformation. MELAN'S theorem now asserts that if *any* system of residual stresses can be found such that the sum of residual stresses and "elastic" stresses constitutes a safe state of stress at every point of the structure and for all possible load combinations, then the structure will shake down to *some* distribution of residual stresses (usually depending on the actual loading program) from which all subsequent load applications will be carried in a purely elastic manner. This shake-down criterion is *sufficient*; it is also *necessary* if "a safe state of stress" is replaced by "an allowable state of stress".

SYMONDS [ref. 3] has given a proof of this theorem that is simpler than MELAN'S original argument, although it is based on the same idea. A further simplification, again on similar lines, is contained in the present paragraph.

It is nearly obvious that MELAN'S criterion is a necessary requirement for shake-down. If no distribution of residual stresses exists which satisfies

the condition that the sum of residual stresses and "elastic" stresses is allowable at every point and for all possible load combinations, it is evident that the structure can never find its way to a shake-down state of residual stresses.

In order to prove that the criterion is sufficient we consider the fictitious elastic energy  $A$  corresponding with residual stresses  $\varrho_{ij} - \bar{\varrho}_{ij}$ , where  $\varrho_{ij}$  is the actual residual stress at any stage of the loading program and  $\bar{\varrho}_{ij}$  any system of residual stresses for which the criterion is satisfied. When additional plastic strains occur in the loading program the residual stresses  $\varrho_{ij}$  will change; on the other hand, the residual stresses  $\bar{\varrho}_{ij}$  do not change. Let  $\varepsilon'_{ijr}$  denote the elastic strains, corresponding with the residual stress  $\varrho_{ij}$  by HOOKE's law. The essentially positive fictitious elastic strain energy  $A$  is given by

$$(6) \quad A = \frac{1}{2} \int (\varrho_{ij} - \bar{\varrho}_{ij}) (\varepsilon'_{ijr} - \bar{\varepsilon}'_{ijr}) dv ,$$

where the integral has to be taken over the entire volume of the structure. The derivative of  $A$  with respect to time is given by

$$(7) \quad \dot{A} = \int (\varrho_{ij} - \bar{\varrho}_{ij}) \dot{\varepsilon}'_{ijr} dv .$$

The actual strains at any moment are given by

$$(8) \quad \varepsilon_{ij} = \varepsilon'_{ij} + \varepsilon''_{ij} = \varepsilon^*_{ij} + \varepsilon'_{ijr} + \varepsilon''_{ij} ,$$

where  $\varepsilon^*_{ij}$  are the elastic strains corresponding with the "elastic" stresses, and (7) may be reduced to

$$(9) \quad \dot{A} = \int (\varrho_{ij} - \bar{\varrho}_{ij}) (\dot{\varepsilon}_{ij} - \dot{\varepsilon}^*_{ij} - \dot{\varepsilon}''_{ij}) dv .$$

The system of residual stresses  $\varrho_{ij}$ ,  $\bar{\varrho}_{ij}$  is self-equilibrating and the strain rate  $\dot{\varepsilon}_{ij} - \dot{\varepsilon}^*_{ij}$  is kinematically admissible because it is the difference between two kinematically admissible strain rates. Therefore the volume-integral

$$(10) \quad \int (\varrho_{ij} - \bar{\varrho}_{ij}) (\dot{\varepsilon}_{ij} - \dot{\varepsilon}^*_{ij}) dv = 0$$

on account of the principle of virtual work (2), and we obtain

$$(11) \quad \dot{A} = - \int (\varrho_{ij} - \bar{\varrho}_{ij}) \dot{\varepsilon}''_{ij} dv .$$

We now write again

$$(12) \quad \varrho_{ij} = \sigma_{ij} - \sigma^*_{ij} , \quad \bar{\varrho}_{ij} = \sigma_{ijs} - \sigma^*_{ij} ,$$

where  $\sigma_{ij}$  is the actual stress and  $\sigma_{ijs}$  the safe state of stress which has been assumed to exist. We obtain

$$(13) \quad \dot{A} = - \int (\sigma_{ij} - \sigma_{ijs}) \dot{\varepsilon}''_{ij} dv .$$

On account of (3)  $\dot{A}$  is always negative whenever plastic deformation occurs. Because  $A$  can never become negative, plastic deformation must cease ultimately, i.e. the structure must shake down to some distribution of residual stresses from which all subsequent load applications are carried in a purely elastic manner.

It may be objected that the present proof and earlier proofs do not



say anything about the magnitude of the plastic deformations which may occur before the structure reaches its shake-down state<sup>1)</sup>. In order to meet this objection it would be necessary to establish bounds for these deformations. Unfortunately no such bounds can be given for the local plastic strains. On the other hand, the overall deformation of a structure is quite insensitive to strictly localized high strains. It is suggested that the total amount of plastic work performed on the structure is a suitable criterion to assess the overall plastic deformation. If this point of view is adopted, it may be proved that the overall plastic deformation is bounded, provided that a distribution of residual stresses  $\bar{\sigma}_{ij}$  can be found, such that the sum  $\sigma_{ijs}$  of these residual stresses and the "elastic" stresses remains within a limit that is obtained from the yield limit by multiplication by a number  $k(0 < k < 1)$ . On this assumption we have

$$(14) \quad (\sigma_{ij} - \sigma_{ijs}) \dot{\epsilon}_{ij}'' \geq (1 - k) \sigma_{ij} \dot{\epsilon}_{ij}'';$$

hence

$$(15) \quad \dot{A} \leq -(1 - k) \int \sigma_{ij} \dot{\epsilon}_{ij}'' dv = -(1 - k) \dot{W}_p,$$

where  $W_p$  is the energy dissipated in plastic deformation. By integration with respect to time we obtain

$$(16) \quad W_p \leq \frac{1}{1 - k} A_0 = \frac{1}{1 - k} \int \frac{1}{2} \bar{\sigma}_{ij} \bar{\epsilon}_{ij}' dv.$$

Obviously, a factor  $k$  not much smaller than unity is needed in order to ensure that the overall plastic deformation remains within reasonable bounds.

#### 4. The second shake-down theorem

If the limits between which the independent loads can vary arbitrarily are such that no shake-down occurs, it may be conjectured that one or more particular periodic load cycles entail periodic cycles of plastic strain rates. If this surmise is correct, the residual stresses at the end of such a load cycle must return to their initial values at the beginning of the load cycle; this conjecture is the starting-point of the second theorem.

We introduce the concept of an *admissible plastic strain rate cycle*  $\dot{\epsilon}_{ij0}''(t)$ , characterized by the property that the integrals

$$(17) \quad \Delta \epsilon_{ij0}'' = \int_0^T \dot{\epsilon}_{ij0}''(t) dt$$

for some time interval  $T$  constitute a *kinematically admissible strain field*; hence the strains  $\Delta \epsilon_{ij0}''$  are obtainable from a displacement field  $\Delta u_{i0}$

<sup>1)</sup> The following argument has already been presented in a communication to the 8th International Congress of Applied Mechanics, (Istanbul, 1952). See abstract in the Proceedings of this Congress, I, 220 (1955).

by means of (1), where the displacements  $\Delta u_{i0}$  vanish on  $S_u$ . It may be emphasized that such an admissible strain rate cycle need not occur actually in any loading cycle. A plastic strain rate field  $\dot{\epsilon}_{ij}''$  is accompanied by a *unique* residual stress rate distribution  $\dot{\rho}_{ij}$ , and corresponding elastic strain rates  $\dot{\epsilon}_{ijr}'$ , obtained from the residual stress rates by HOOKE's law; the residual stress rates are zero if the plastic strain rate field is kinematically admissible. The sum of the plastic strain rates and the elastic strain rates obtained from the residual stress rates constitutes a kinematically admissible strain rate field. Let  $\dot{\epsilon}_{ij0}'(t)$  denote the elastic strain rates, computed by HOOKE's law from the residual stress rates  $\dot{\rho}_{ij0}(t)$  which accompany the plastic strain rate cycle  $\dot{\epsilon}_{ij0}''(t)$ , and let  $\dot{u}_{i0}(t)$  denote the velocity field from which the kinematically admissible strain rates

$$(18) \quad \dot{\epsilon}_{ij0}(t) = \dot{\epsilon}_{ij0}''(t) + \dot{\epsilon}_{ij0}'(t)$$

are obtained by means of (1). Obviously, we have

$$(19) \quad \int_0^T \dot{\epsilon}_{ij0}'(t) dt = 0 \quad , \quad \int_0^T \dot{u}_{i0}(t) dt = \Delta u_{i0} ,$$

because the residual stresses at time  $t=T$  have returned to their initial values at time  $t=0$ .

After these preliminaries we can now state our theorem in the following form. *The structure will not shake down, i.e. it will ultimately fail by cyclic plastic deformation, if any admissible plastic strain rate cycle  $\dot{\epsilon}_{ij0}''(t)$  and external loads  $X_i(t)$ ,  $p_i(t)$  within the prescribed limits can be found for which*

$$(20) \quad \int_0^T dt \left\{ \int X_i(t) \dot{u}_{i0}(t) dv + \int_{S_p} p_i(t) \dot{u}_{i0}(t) dS \right\} > \int_0^T dt \int F(\dot{\epsilon}_{ij0}'') dv ,$$

where  $F(\dot{\epsilon}_{ij0}'')$  is the plastic energy dissipation function (5). On the other hand, the structure will shake down if a number  $k < 1$  can be found, such that for all admissible plastic strain rate cycles  $\dot{\epsilon}_{ij0}''(t)$  and external loads  $X_i(t)$ ,  $p_i(t)$  within the prescribed limits

$$(21) \quad \int_0^T dt \left\{ \int X_i(t) \dot{u}_{i0}(t) dv + \int_{S_p} p_i(t) \dot{u}_{i0}(t) dS \right\} \leq k \int_0^T dt \int F(\dot{\epsilon}_{ij0}'') dv .$$

We shall first prove the *first part of our theorem* by showing that the assumption that it were false, leads to a contradiction. If shake-down would indeed occur in spite of (20), it would be possible by MELAN's theorem to find a residual stress distribution  $\bar{\rho}_{ij}$ , independent of time, such that the sum of "elastic" stresses  $\sigma_{ij}^*(t)$  and residual stresses  $\bar{\rho}_{ij}$  would always be allowable

$$(22) \quad \sigma_{ij}^*(t) + \bar{\rho}_{ij} = \sigma_{ija}(t) .$$

Remembering that the strain rates (18) are kinematically admissible, we now obtain from the principle of virtual work (2), applied to the stress

system (22) which is in equilibrium with body forces  $X_i(t)$  and surface tractions  $p_i(t)$  on  $S_p$ ,

$$(23) \quad \int X_i(t) \dot{u}_{i0}(t) dv + \int_{S_p} p_i(t) \dot{u}_{i0}(t) dS = \int \sigma_{ija}(t) \dot{\epsilon}_{ij0}(t) dv.$$

The right-hand member may be rewritten in the form

$$(24) \quad \int \sigma_{ija}(t) \dot{\epsilon}_{ij0}(t) dv = \int \sigma_{ija}(t) \dot{\epsilon}_{ij0}''(t) dv + \int \sigma_{ij}^*(t) \dot{\epsilon}_{ij0}'(t) dv + \int \bar{\varrho}_{ij} \dot{\epsilon}_{ij0}'(t) dv.$$

Denoting the elastic strains corresponding with the "elastic" stresses  $\sigma_{ij}^*(t)$  again by  $\epsilon_{ij}^*(t)$ , and observing that  $\dot{\epsilon}_{ij0}' dt$  are the elastic strains corresponding with the stresses  $\dot{\varrho}_{ij0}(t) dt$ , we obtain from BETTI's reciprocal theorem

$$(25) \quad \sigma_{ij}^*(t) \dot{\epsilon}_{ij0}'(t) = \dot{\varrho}_{ij0}(t) \epsilon_{ij}^*(t).$$

Because  $\dot{\varrho}_{ij0}$  is a self-equilibrating distribution of stress rates and  $\epsilon_{ij}^*$  is a kinematically admissible strain, we now have on account of the principle of virtual work

$$(26) \quad \int \sigma_{ij}^*(t) \dot{\epsilon}_{ij0}'(t) dv = \int \dot{\varrho}_{ij0}(t) \epsilon_{ij}^*(t) dv = 0.$$

Integrating the last term in (24) with respect to time from  $t=0$  to  $t=T$  and remembering that  $\bar{\varrho}_{ij}$  is independent of time, we have (cf. (19))

$$(27) \quad \int_0^T dt \int \bar{\varrho}_{ij} \dot{\epsilon}_{ij0}'(t) dv = \int \bar{\varrho}_{ij} dv \int_0^T \dot{\epsilon}_{ij0}' dt = 0.$$

Therefore we have by integration of (23) from  $t=0$  to  $t=T$

$$(28) \quad \int_0^T dt \left\{ \int X_i(t) \dot{u}_{i0}(t) dv + \int_{S_p} p_i(t) \dot{u}_{i0}(t) dS \right\} = \int_0^T dt \int \sigma_{ija}(t) \dot{\epsilon}_{ij0}''(t) dv,$$

and the contradiction between (20) and (28) is evident on account of (4). Hence, our assumption that shake-down would occur in spite of (20) is untenable, and the first part of our theorem has been proved.

We shall now prove the *second part of our theorem* by showing that the total amount of plastic work is bounded in any loading program within the prescribed limits, if (21) holds for all admissible plastic strain rate cycles. We consider an arbitrary loading program  $X_i(t)$ ,  $p_i(t)$  in the interval of time  $0 < t < t_1$ . Let  $\sigma_{ij}(t)$  denote the actual stresses in this program,  $\sigma_{ij}^*(t)$  the "elastic" stresses and  $\varrho_{ij}(t)$  the residual stresses; we have

$$(29) \quad \sigma_{ij}(t) = \sigma_{ij}^*(t) + \varrho_{ij}(t).$$

Let  $\epsilon_{ij}(t)$  denote the actual strains,  $\epsilon_{ij}''(t)$  the plastic strains,  $\epsilon_{ij}^*(t)$  the "elastic" strains, obtained from the "elastic" stresses by HOOKE's law, and  $\epsilon_{ijr}'(t)$  the elastic strains corresponding with the residual stresses; we have

$$(30) \quad \epsilon_{ij}(t) = \epsilon_{ij}^*(t) + \epsilon_{ij}''(t) + \epsilon_{ijr}'(t).$$

We observe that the actual plastic strain rates  $\dot{\epsilon}_{ij}''(t)$  in the arbitrary



loading program  $X_i(t)$ ,  $p_i(t)$  for  $0 < t < t_1$  will not constitute an admissible cycle by themselves, but we can regard them as the first part of such a cycle. Denoting the increase in residual stresses in the loading program by  $\Delta \varrho_{ij}$ , we complete the cycle by considering the plastic strain rates which would occur if the unloaded structure would be relieved from a state of residual stress distribution  $\Delta \varrho_{ij}$  by a *gradual proportional reduction of the yield limit to zero* in the interval of time  $t_1 < t < T$ . We denote the plastic strain rates in this fictitious "annealing" process by  $\dot{\varepsilon}_{ij}''(t)$ , the accompanying residual stress rates and corresponding elastic strain rates by  $\dot{\varrho}_{ija}(t)$ ,  $\dot{\varepsilon}'_{ija}(t)$ . The plastic strain rates in

$$(31) \quad \begin{cases} \dot{\varepsilon}_{ij0}''(t) = \dot{\varepsilon}_{ij}''(t) & , \quad \dot{\varepsilon}'_{ij0}(t) = \dot{\varepsilon}'_{ijr}(t) & \text{for } 0 < t < t_1, \\ \dot{\varepsilon}_{ij0}''(t) = \dot{\varepsilon}_{ija}''(t) & , \quad \dot{\varepsilon}'_{ij0}(t) = \dot{\varepsilon}'_{ija}(t) & \text{for } t_1 < t < T \end{cases}$$

obviously satisfy our requirement (17) for an admissible cycle because at the end of the cycle the residual stresses will have returned to their initial values.

We shall need the fact that the following integrals are bounded and increase proportionally for a proportional increase of the residual stresses  $\Delta \varrho_{ij}$ :

$$(32) \quad \int_{t_1}^T dt \int F(\dot{\varepsilon}_{ija}'') dv, \quad \int_{t_1}^T dt \int \sigma_{ij} [\dot{\varepsilon}_{ija}''(t) + \dot{\varepsilon}'_{ija}(t)] dv,$$

where  $F(\dot{\varepsilon}_{ija}'')$  is the plastic energy dissipation function (5) and  $\sigma_{ij}$  is an arbitrary distribution of finite stresses, independent of time.

We assume that at time  $t=t_1$  the residual stresses  $\Delta \varrho_{ij}$  at the most critical point are at  $\mu$  times the original yield limit, and we reduce the yield limit in our "annealing" process proportionally with time from  $\mu$  times the original yield limit at  $t=t_1$  to zero at  $t=T$ . Denoting the residual stresses at time  $t$  by  $\varrho_{ija}$ , we have by the principle of virtual work, applied to the residual stresses  $\varrho_{ija}$  and the kinematically admissible strain rates in the "annealing" process

$$(33) \quad \int \varrho_{ija} (\dot{\varepsilon}_{ija}'' + \dot{\varepsilon}'_{ija}) dv = 0.$$

The first integral represents the rate at which energy is dissipated in this process

$$(34) \quad \int \varrho_{ija} \dot{\varepsilon}_{ija}'' dv = \mu \frac{T-t_1}{T-t} \int F(\dot{\varepsilon}_{ija}'') dv.$$

Therefore we obtain from (22)

$$(35) \quad \int F(\dot{\varepsilon}_{ija}'') dv = -\frac{T-t_1}{\mu} \frac{1}{T-t} \int \varrho_{ija} \dot{\varepsilon}'_{ija} dv.$$

Integrating this equation from  $t=t_1$  to  $t=T$  we have

$$(36) \quad \int_{t_1}^T dt \int F(\dot{\varepsilon}_{ija}'') dv = -\frac{T-t_1}{\mu} \int_{t_1}^T \frac{dt}{T-t} \int \varrho_{ija} \dot{\varepsilon}'_{ija} dv,$$

where the integral in the right-hand member converges because the residual

stresses  $\varrho_{ija}$  tend to zero for  $t \rightarrow T$ <sup>2</sup>). Hence the first integral (32) is indeed bounded and the same property follows immediately for the second integral.

Finally, a proportional increase of the residual stresses  $\Delta\varrho_{ij}$ , from which the "annealing" process starts implies multiplication of  $\mu$  by a factor  $c$ . The residual stresses  $\varrho_{ija}$  and strain rates  $\dot{\varepsilon}_{ija}''$  and  $\dot{\varepsilon}_{ija}'$  at time  $t$  are then also multiplied by  $c$ , and the proportional increases of (32) for a proportional increase of the residual stresses  $\Delta\varrho_{ij}$  are evident.

It must be admitted that the foregoing fictitious "annealing" process is a highly artificial device but so far we have been unable to find a simpler method to complete the plastic strain rate cycle, started by the actual arbitrary loading program, which is suitable for our purpose and for all types of yield limit. However, if we assume that the yield limit is *finite* for all types of stress (an assumption that excludes VON MISES' and TRESCA's yield criteria), we may replace the second part of the cycle (31) by

$$(37) \quad \dot{\varepsilon}_{ijo}''(t) = -\dot{\varepsilon}_{ijo}'(t) = \frac{\Delta\varepsilon'_{ijr}}{T-t_1},$$

where  $\Delta\varepsilon'_{ijr}$  are the elastic strains corresponding with the residual stresses  $\Delta\varrho_{ij}$ . The integrals

$$(38) \quad \left\{ \begin{aligned} \int_{t_1}^T dt \int F(\dot{\varepsilon}_{ijo}'') dv &= \int F(\Delta\varepsilon'_{ijr}) dv, \\ \int_{t_1}^T dt \int \sigma_{ij} \dot{\varepsilon}_{ijo}'' dv &= \int \sigma_{ij} \Delta\varepsilon'_{ijr} dv, \end{aligned} \right.$$

which now replace (32), are obviously bounded and increase proportionally for a proportional increase of the residual stresses  $\Delta\varrho_{ij}$ .

The proof of the second part of our theorem is now obtained by applying the principle of virtual work at any time  $t$  in the admissible plastic strain rate cycle (31). During the actual loading program ( $0 < t < t_1$ ) we have (cf. (26))

$$(39) \quad \left\{ \begin{aligned} \int X_i(t) \dot{u}_{io}(t) dv + \int_{S_p} p_i(t) \dot{u}_{io}(t) dS &= \int \sigma_{ij}(t) [\dot{\varepsilon}_{ijo}''(t) + \dot{\varepsilon}_{ijo}'(t)] dv = \\ &= \int \sigma_{ij}(t) \dot{\varepsilon}_{ij}''(t) dt + \int \varrho_{ij}(t) \dot{\varepsilon}_{ijr}'(t) dv, \end{aligned} \right.$$

where the first term in the right-hand member represents the rate at which plastic work is performed in the loading program, i.e.

$$(40) \quad \int \sigma_{ij}(t) \dot{\varepsilon}_{ij}''(t) dv = \int F(\dot{\varepsilon}_{ij}'') dv = \dot{W}_p,$$

and the second term represents the rate of increase of the elastic residual strain energy

$$(41) \quad A = \frac{1}{2} \int \varrho_{ij} \varepsilon'_{ijr} dv.$$

In the second part of the plastic strain rate cycle (31),  $t_1 < t < T$  we take

<sup>2</sup>) We assume that all stresses in the structure vanish for a yield limit zero.

any constant loads  $X_i$ ,  $p_i$  within the prescribed limits. Let  $\sigma_{ij}$  denote a state of stress in equilibrium with these loads. We have

$$(42) \quad \left\{ \begin{aligned} \int X_i \dot{u}_{io}(t) dv + \int_{S_p} p_i \dot{u}_{io}(t) dv &= \int \sigma_{ij} [\dot{\epsilon}_{ij0}''(t) + \dot{\epsilon}_{ij0}'(t)] dv = \\ &= \int \sigma_{ij} \dot{\epsilon}_{ija}''(t) + \int \sigma_{ij} \dot{\epsilon}_{ija}'(t) dv. \end{aligned} \right.$$

Integrating (39) from  $t=0$  to  $t=t_1$  and (42) from  $t=t_1$  to  $t=T$ , we obtain from (21)

$$(43) \quad \left\{ \begin{aligned} \int_0^{t_1} dt \{ \int F(\dot{\epsilon}_{ij}'') dv + \int Q_{ij}(t) \dot{\epsilon}_{ijr}' dv \} + \int_{t_1}^T dt \int \sigma_{ij} [\dot{\epsilon}_{ija}''(t) + \dot{\epsilon}_{ija}'(t)] dv &\leq \\ &\leq k \{ \int_0^{t_1} dt \int F(\dot{\epsilon}_{ij}'') dv + \int_{t_1}^T dt \int F(\dot{\epsilon}_{ija}'') dv \}. \end{aligned} \right.$$

Denoting the total amount of plastic work in the loading program by  $W_p$  and the increase of the residual strain energy (41) in this program by  $\Delta A$ , we have from (43)

$$(44) \quad (1-k) W_p \leq \int_{t_1}^T dt \int \{ k F(\dot{\epsilon}_{ija}'') + \sigma_{ij} [\dot{\epsilon}_{ija}''(t) + \dot{\epsilon}_{ija}'(t)] \} dv - \Delta A.$$

We now remember that the integral in the right-hand member is bounded and increases proportionally for a proportional increase of the residual stresses  $\Delta Q_{ij}$ . On the other hand,  $\Delta A$  has an always positive quadratic part in these residual stresses and it follows that the right-hand member of (44) is bounded. Hence we have completed our proof that the total amount of plastic work, performed in any loading program within the prescribed limits, is bounded if (21) holds for all admissible plastic strain rate cycles.

### 5. Concluding remarks

It is obvious from their formulation that MELAN's theorem and the second shake-down theorem each give both necessary and sufficient conditions for shake-down of an elastic-plastic structure. In principle, each of these theorems is therefore adequate for a complete discussion of shake-down of a particular structure under loads which vary independently and arbitrarily between prescribed limits, and several investigations, based on MELAN's theorem, have been published for trusses, continuous beams and frames. For more complicated structures it will be very difficult to establish exact values for the allowable limits on the individual loads. However, *lower* bounds for the allowable load variations may always be obtained from MELAN's theorem by assuming a suitable residual stress distribution  $\bar{Q}_{ij}$  and calculating the corresponding allowable load variations from the condition that the sum of "elastic" stresses  $\sigma_{ij}^*$  and residual stresses  $\bar{Q}_{ij}$  never exceeds the yield limit. On the other hand, *upper* bounds for the allowable load variations may be established by means of the second, complementary theorem by assuming a suitable plastic strain



rate cycle and suitably varying loads in this cycle. Substitution in (20), where the sign  $>$  is replaced by  $=$  then yields limits for the variable loads under which failure by cyclic plastic deformations is bound to occur. It may therefore be hoped that the second theorem will facilitate shakedown analysis, the more so because it is known from collapse analysis that the "kinematical" type of theorem is often more convenient than the "statical" theorem.

It may be emphasized that no assumption concerning the regularity of the yield limit has been made in our analysis. The only assumptions that have been made are that the yield limit is independent of preceding plastic deformations, i.e. that the material is an ideal elastic-plastic material, and that the stress-strain relations satisfy the basic requirement (3).

Finally, it may be stated without a detailed proof that an extension of the second theorem to discontinuous velocity fields in a plastic strain rate cycle may be obtained along the same lines as in the theory of plastic collapse (cf. ref. 1, para. 6).

*Delft, 15 December 1955.*

#### REFERENCES

1. DRUCKER, D. C., W. PRAGER and H. J. GREENBERG, Extended limit design theorems for continuous media. *Quart. Appl. Math.* **9**, 381 (1951).
2. MELAN, E., Der Spannungszustand eines Hencky-Mises'schen Kontinuums bei veränderlicher Belastung. *Sitz. Ber. Ak. Wiss. Wien* **147**, 73 (1938).
3. SYMONDS, P. S., Shakedown in continuous media. *Journ. Appl. Mech.* **18**, 85 (1951).

## PHYSICS

### SOME PROPERTIES OF LIQUID HELIUM BELOW 1° K. (IV<sub>A</sub>)

BY

H. C. KRAMERS

(Communicated by Prof. C. J. GORTER at the meeting of October 29, 1955)

#### CHAPTER IV: THE HEAT PULSE EXPERIMENTS

In this chapter the results of the experiments concerning the propagation of heat pulses in the liquid are given and discussed. Section 4.1 contains a mere statement of the results. In section 4.2, 4.3, 4.4 and 4.5 they are analysed in more detail for different temperature regions and discussed with respect to experimental and theoretical considerations. Section 4.6 contains the result of a preliminary experiment in which atmospheric helium was used instead of helium from wells. In connection with it the possible influence of extremely small amounts of <sup>3</sup>He is discussed. Section 4.7 is reserved for some final remarks and conclusions.

To avoid confusion the nomenclature used in the description of the results is first given here. The experiment always concerns the behaviour of a heat pulse after travelling through the liquid over a certain distance. The path length is indicated by  $z$ , the diameter of the tube through which propagation takes place is called  $d$ . The zero point of the time of propagation is always put at the start of the transmitting signal. Because in general the pulse changes its shape while passing through the liquid, the time of propagation cannot be defined unambiguously.  $t_1$  indicates the time of arrival of the front of the detected signal,  $t_3$  the time of reaching its half-height and  $t_4$  the time corresponding to its top. The corresponding "velocities", i.e.  $z/t$  are called  $u_1$ ,  $u_3$ ,  $u_4$  respectively. The pulse energy is indicated by  $\varepsilon$  and the pulse width by  $\tau$ .

4.1. *Review of experimental results.* Table 4.1 summarizes the different tubes used in the experiments. An indication of the construction of the heaters and the thermometers is given and lengths and diameters are tabulated. The most reliable measurements were made on tubes 8, 9 and 10; therefore, the main part of the discussion will be devoted to them. Deviating results obtained in experiments with other tubes will be mentioned at the end of this section.

Fig. 4.1 contains eight typical photographs taken from the total amount of a few thousand. In all the pictures the time-scale is shown on the second beam. The distance of the main time markers is 100  $\mu$ sec, in some of the pictures the subdivision of 10  $\mu$ sec markers is also shown. In the upper two photographs the time scale is three times less than that in the

TABLE 4.1.

Measuring tubes				
A. = aquadag on paper				
C.R.S. = commercial resistance strip (carbon)				
Const. = constantan wire				
Ph.br. = phosphorbronze wire				
No.	heater	thermometer	length cm	diameter cm
1	A.	A.	2.99	0.40
2	C.R.S.	C.R.S.	6.02	0.40
3	C.R.S.	C.R.S.	1.53	0.40
6	Const.	Ph.br.	3.0	0.80
7a	Const.	A.	1.60	0.95
7b	Const.	A.	4.72	0.95
8	A.	A.	1.60	0.95
9	A.	A.	3.05	0.95
10	A.	A.	6.4	0.95

remaining ones. The transmitting time is indicated by the pick-up signal at the left on the main beam.

Fig. 4.2 depicts for comparison the shapes of signals for the three main tubes. The fully-drawn lines are direct reproductions from the photographs. The dashed lines were produced in the following way. First the signals from the three tubes at the same temperature were adjusted to equal energies of the input pulse and also as far as possible to the same thermometer-sensitivity. The amplifier correction, mentioned in 2.8.5, was then made. This is an important correction especially in the case of the very long tail signals of the 6 cm tube. The amplitudes obtained in this way should not be taken too seriously, because the thermometers used were not always the same, moreover, their sensitivity is by no means linearly dependent on the direct current. The table underneath figure 4.2 gives the data on the input-pulses.

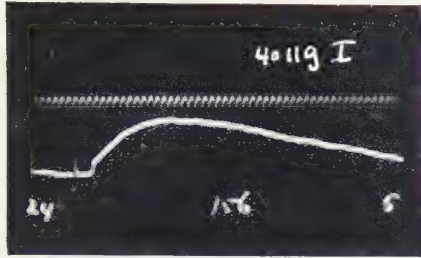
Fig. 4.3 gives the results of the time measurements for the three tubes as a function of temperature. The points plotted are only a part of the total number obtained. To avoid confusion they have been omitted altogether for the 3 cm tube. Because of the poor accuracy the curves for the  $t_4$  values below about  $0.5^\circ \text{K}$  have not been drawn.

All the data summarized in the first part of this section are obtained from pulses with "normal" energies and pulsewidths. Normal means in this respect as small as possible but well defined above the noise level. Of course this depends very much on the temperature and the tube length, thermometer sensitivity, specific heat and pulse-spreading changing within large limits. Table 4.2 contains a review of these "normal" values.

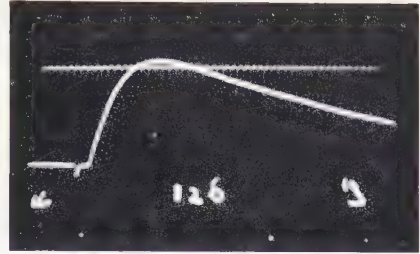
A general survey of the results gives the following picture.

4.1.1.  $T > 1.0^\circ \text{K}$  (region A). This is the region of normal second sound, i.e. the pulses remain well-bunched, apart from some aftereffects

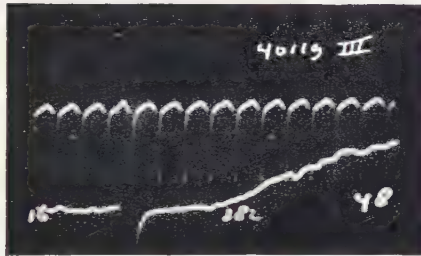




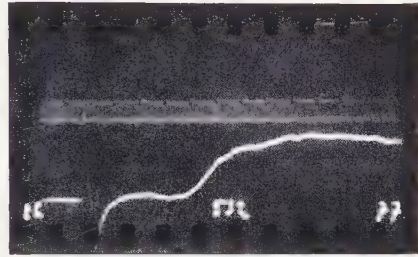
a



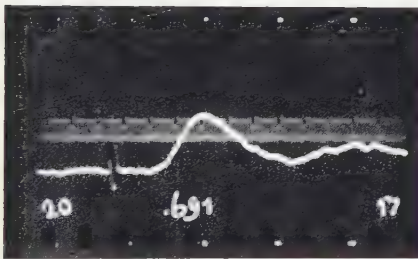
b



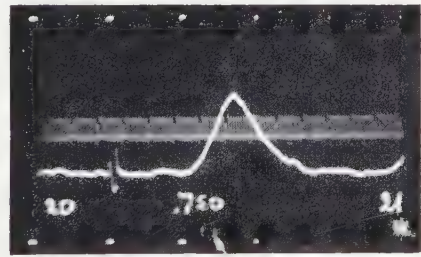
c



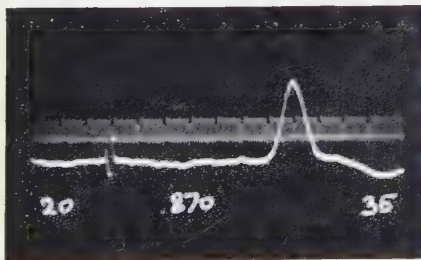
d



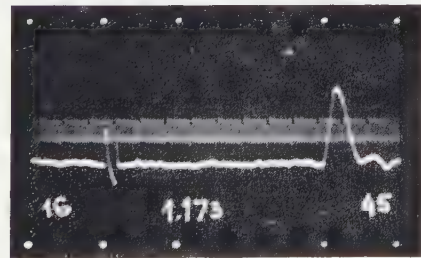
e



f



g



h

Fig. 4.1. Some typical photographs.

a. tube 10 ( $z = 6.4$  cm); note the sharp edge at the start.

b. tube 7b ( $z = 4.72$  cm); constantan heater, no sharp edge.

c. tube 10 ( $z = 6.4$  cm); front of the very flat signal.

d. tube 10 ( $z = 6.4$  cm); typical example of the intermediate region.

e, f, g, h. tube 8 ( $z = 1.60$  cm); the pulse shape in the higher temperature region. The number in the centre of each picture gives the temperature belonging to it in millidegrees Kelvin.



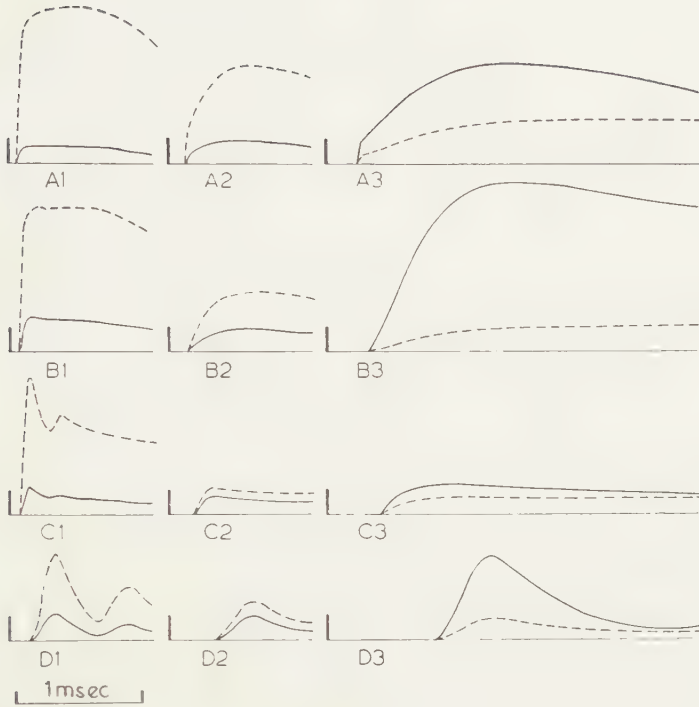


Fig. 4.2. Shape of the detected signal at different temperatures ( $T$ ) and different tube lengths ( $z$ ).

Fully-drawn line: actually observed signal; dotted line: normalized signal (see text).

$\varepsilon$  = energy of actual input pulse.

$\tau$  = width of input pulse.

$\varepsilon_n$  = energy of normalized pulses.

	1			2			3			
	$z = 1.60$ cm			$z = 3.05$ cm			$z = 6.4$ cm			
	$T$ °K	$\varepsilon$ erg	$\tau$ $\mu$ sec	$T$ °K	$\varepsilon$ erg	$\tau$ $\mu$ sec	$T$ °K	$\varepsilon$ erg	$\tau$ $\mu$ sec	$\varepsilon_n$ erg
A	0.172	0.146	20	0.154	0.162	20	0.156	0.88	20	1.2
B	0.402	1.26	20	0.370	9.55	20	0.417	11.5	40	15
C	0.506	1.27	20	0.548	19.3	40	0.532	11.6	40	18
D	0.691	3.34	20	0.674	9.9	20	0.675	11.9	40	30

perhaps due to spurious reflections. No appreciable difference is found between the pulse shapes of the three tubes.

4.1.2.  $1.0^\circ \text{ K} > T > 0.7^\circ \text{ K}$  (region B). Going to lower temperatures one observes firstly a shift of the signal to the left on the oscilloscope screen, i.e. the velocity is increasing as should be expected from other experiments. Moreover the pulsewidth is not preserved, but shows an appreciable spreading (see fig. 4.1. e, f, g, h). There is a marked dependence of the amount of spreading on the tube-length. A good parameter for



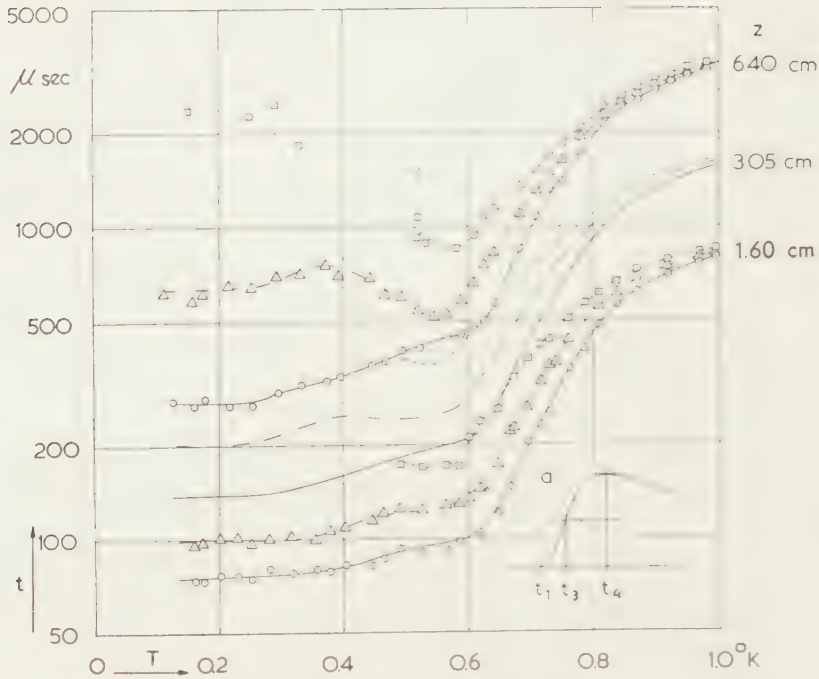


Fig. 4.3. Time-interval measurements for the tubes 10, 9 and 8 ( $z = 6.4$ ,  $3.05$  and  $1.60$  respectively).

○ ——— start of the signal ( $t_1$ )  
 △ ——— half height ( $t_3$ )  
 □ ——— top ( $t_4$ )  
 3a. Review of the measured time points.

TABLE 4.2

Normally used pulse energies ( $\varepsilon$ ) and pulse widths ( $\tau$ )						
$T$ °K	$z = 1.60$ cm		$z = 3.05$ cm		$z = 6.4$ cm	
	$\varepsilon$ erg	$\tau$ $\mu$ sec	$\varepsilon$ erg	$\tau$ $\mu$ sec	$\varepsilon$ erg	$\tau$ $\mu$ sec
0.15	0.15	10 to 20	0.15	20	0.5	20
0.3	0.5	20	1.3	20	3.5	20 to 40
0.5	1.3	20	3.4	20	7.0	40
0.7	3.4	20	3.4	20	18	40
0.9	3.2	20 to 40	6.4	20 to 40	30	40 to (70)
1.1	10	40	19	40	35	40 to (70)

this spreading is the value of  $t_4 - t_3$ ; i.e. the difference of time between top and half-height of the front part of the signal. For constant temperature this time interval is within the limits of accuracy proportional to  $z^{1/2}$  (see fig. 4.6).

In earlier publications [1, 2, 3] the velocity of second sound was supposed to be equal to  $u_1 = z/t_1$ . The value of  $u_1$ , however, appears to be dependent on the length of the tube. This is clearly seen in fig. 4.4;  $u_1$  is plotted as a function of  $T$  for the 6 cm and the 1.6 cm tube. A unique velocity has to be defined in another way (see section 4.2).

4.1.3.  $0.7^\circ \text{ K} > T > 0.5^\circ \text{ K}$ . (region C). In this region a substantial change of shape of the detected signal takes place. Near  $0.7^\circ \text{ K}$  the symmetry is lost and a large tail develops rapidly while passing to the lower temperature. The definition of  $t_4$  becomes very difficult; the top of the signal cannot be defined very well. There is a rather curious effect which is especially well indicated with the longest tube ( $z = 6.4 \text{ cm}$ ). It appears that the front part of the signal, instead of continuing its flattening with decreasing temperature, becomes steeper again. This can be seen clearly by comparing the  $t_3$  and  $t_1$  curves for the long tube in fig. 4.3 (see also fig. 4.1.d). The steepest front is found at a temperature of about  $0.55^\circ \text{ K}$ . Below this the flattening is again increasing with decreasing temperature. The same effect, but less marked, is observed with the 3 cm tube.

The values of  $u_1$  are still increasing with decreasing temperature in this region, appreciably slower, however, between 0.6 and  $0.5^\circ \text{ K}$  than at higher temperatures.

4.1.4.  $T < 0.5^\circ \text{ K}$ . (region D). A very flat signal survives when the temperature is lowered still further. The value of  $t_1$  is not very well defined, because the front of the signal starts in a very concave manner (see fig. 4.1.c). The result is a rather large spreading of the measuring points. In this region the introduction of the amplifier correction is very essential (see fig. 4.2.B3). The 1.6 cm tube is not very suitable for analysis, because the direct signal is probably intermingled with the first *vice versa* reflection (just a trace of a second top can be seen in fig. 4.2.B1). The results of the other two tubes indicate that  $t_4$  is probably proportional to  $z^2$ , although the accuracy is rather poor. The time of the first top of the shortest tube also fits rather well in this assumption.

At about  $0.36^\circ \text{ K}$  with the 3 cm tube and  $0.22^\circ \text{ K}$  with the 6 cm tube a new effect appears. The front of the signal becomes very sharp, so  $t_1$  is again well defined (see fig. 4.1.a). For the 1.6 cm tube no clear demarcation between a sharp edge and the rest of the signal can be observed. The main part of the signal is rather sharp, so that the sharp edge may not easily be distinguishable from it.

The corresponding  $u_1$  values are

$z = 1.60 \text{ cm}$	$u_1 = 215 \text{ m/sec}$
$z = 3.05 \text{ cm}$	$u_1 = 220 \text{ m/sec}$
$z = 6.4 \text{ cm}$	$u_1 = 231 \text{ m/sec}$

It should be noted here that these values are very near to the velocity of first sound.

4.1.5. The influence of large energies. Some experiments have been carried out with larger energy input (between 20 and 200 times larger than the "normal" values). The following deviations from the above mentioned phenomena were observed:

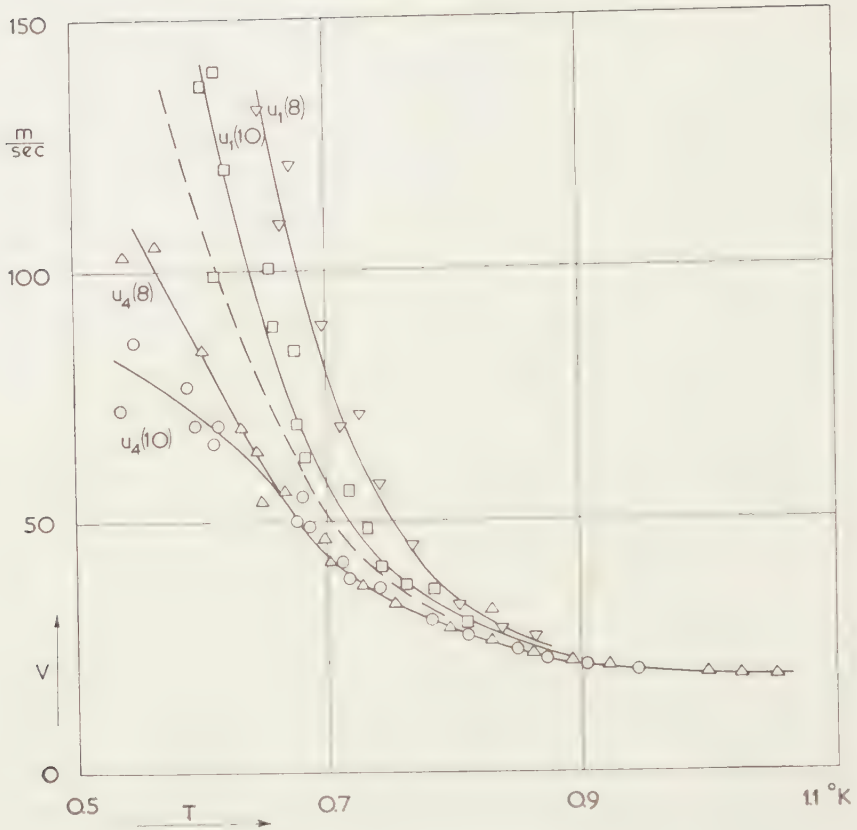


Fig. 4.4. Velocities in the high temperature region.

$\nabla$  tube 8:  $u_1$ .

$\triangle$  tube 8: corrected velocity of the top.

$\square$  tube 10:  $u_1$ .

$\circ$  tube 10: corrected velocity of the top.

Dotted line:  $v_{II}$  according to DE KLERK et al. [3].

- a*: an increase of  $u_1$  with increasing energy for  $T > 0.9^{\circ} K$ .
- b*: the existence of slightly larger  $u_1$ -values below  $0.6^{\circ} K$ , especially between  $0.4^{\circ} K$  and  $0.6^{\circ} K$ .
- c*: the appearance of the sharp edge in region D at somewhat higher temperatures (up to a few hundredths of a degree higher).

Moreover, for very large energies (more than 100 times the "normal" values) were observed:

- d*: an increase of the velocity of the sharp edge nearer to the expected value of  $v_I$  (237 m/sec) (temperature region D).
- e*: an increase of the ratio of the amplitude of the sharp edge to the maximum amplitude of the signal (region D).

*a* is probably a large amplitude effect of the kind also noted by OSBORNE [4]; a detailed discussion is out of the scope of this exposition. It is curious



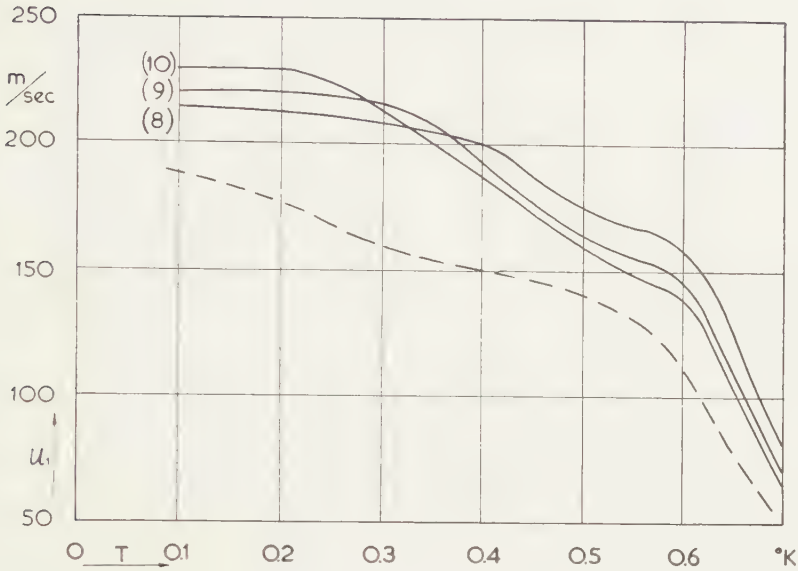


Fig. 4.5. Velocities in the low temperature region.  
Fully-drawn lines:  $u_I$ -values for tubes 8, 9 and 10.  
Dotted line: " $v_{II}$ " according to DE KLERK *et al.* [3].

to note, however, that no such effects appear to occur at lower temperatures.  $b$  and  $c$  can probably be explained by considering the marking effect of the noise. In case  $b$ , because of the concave shape of the signal front, with small input energy (i.e. relatively large noise level) the start of the signal is suppressed by the noise. The same applies to the very small sharp edge signal at its first appearance in case  $c$ .  $e$  is probably due to non-linearity of the amplifier for large input voltages;  $d$  will be discussed in section 4.5.

4.1.6. The other tubes. The first three tubes (no. 1:  $z=3$  cm, no. 2:  $z=6$  cm, no. 3:  $z=1.5$  cm) had about the same lengths as the tubes mentioned above. The diameters were, however, about twice as small. With tubes 2 and 3 the spreading occurring below  $0.5^\circ$  K was observed to be about twice as large as that of the corresponding tubes 10 and 8. The results were, however, not very reliable, probably because of the relatively small sensitivity of the commercial resistance strips used. In the experiments on tube 2 the sharp edge occurred in exactly the same manner as in tube 10. At higher temperatures the results from tube 2 were not very satisfactory. The signals were much more spreaded than in the other tubes and the sensitivity partly for this reason not very good so that pulses of moderate energy did not give adequate results.

Tube 1 was investigated with an amplifier not suitable for low frequency amplification. Therefore, the results from the temperature region with flat signals cannot be considered as reliable. By introducing the amplifier

correction results similar to those later observed with other tubes are found. In this case, however, the correction is so large that these results cannot be used for further analysis. In one respect this tube gave more reliable data than the corresponding tube 9. The appearance of the sharp edge could be analysed much better. The reason for this is the relative smallness of the flat "main body" effect. This is partly due to the reduced amplification of the latter and partly because of the larger spreading probably occurring in narrow tubes. A better differentiation can, therefore, be made between the sharp edge and the main body effect. Actually the results from tube 1 have been used for the estimate of the mean free path (section 4.5).

Tube 6 contained a phosphorbronze thermometer which had a very low sensitivity and also a low resistance ( $2\ \Omega$ ). Because the amplifier was adapted to large input resistance, the results were very meagre, although a step-up transformer was used. The only notable difference with the other tubes was the absence of the sharp edge effect.

This effect was also not observed with the tubes 7a and 7b (home-made thermometers). The sensitivity was again good. No appreciable deviations in other respect were found.

As the common feature of tubes 6, 7a and 7b was the use of a constantan heater, this was probably the cause of the absence of the sharp edge. This question will be discussed in section 4.5.

4.1.7. *The determination of the temperature.* All temperatures given are magnetic temperatures, i.e. no corrections have been introduced for the ellipsoidal shape of the salt or for deviations from the Curie law. The errors thus introduced are small and for the most part either well within the accuracy of the measurements or in a region of practical independence on temperature of the phenomena.

For temperatures above  $0.3^\circ\text{K}$  the correction is less than  $-0.002$  of a degree, at  $0.2^\circ\text{K}$  it is about  $-0.004$  of a degree; only at  $0.1^\circ\text{K}$  it may become of the order of  $-0.01$  of a degree.

4.2. *The temperature range from  $0.7^\circ\text{K}$  to  $1.0^\circ\text{K}$ .* In this region the shape of the original pulse, although spread out substantially, preserves more or less its original character. It will be shown that the experimental results are in agreement with the supposition that second sound still exists but is rather heavily damped. It appears, however, that this absorption is probably still of the kind described in section 1.3, i.e. only relatively small deviations from local equilibrium occur in the gas of excitations and a description using common irreversible processes is adequate. According to equation 1.19 the absorption coefficient in this case is proportional to  $\omega^2$ . The following analysis has first been made by DINGLE [5].

When the original input pulse has approximately the shape of a  $\delta$ -

function, the response can in general be written as a Fourier-integral:

$$(4.1) \quad \psi_\delta(z, t) = (2\pi)^{-1} \int_{-\infty}^{+\infty} \exp \{i\omega(t - z/v(\omega))\} d\omega.$$

The phase velocity  $v$  depends on the frequency in the way indicated by equation 1.18, i.e.

$$(4.2) \quad v^2 = v_{\text{II}}^2 + i\omega\alpha.$$

In this chapter  $v_{\text{II}}$  always indicates the second sound velocity for the limit of zero frequency.

Introducing (4.2) in (4.1) and expanding in rising powers of  $\alpha$  yields:

$$(4.3) \quad \begin{cases} \psi_\delta(z, t) = (v_{\text{II}}^3/2\pi\alpha z)^{1/2} \exp \{-(t - z/v_{\text{II}})^2/(2\alpha z/v_{\text{II}}^3)\} \varphi(z, t) \\ \varphi(z, t) = 1 + \text{terms of the order } (\alpha/zv_{\text{II}})^{1/2}. \end{cases}$$

In first approximation this is a Gaussian curve. The top is determined by

$$(4.4) \quad t_{\text{max}} = zv_{\text{II}}^{-1} \{1 - \text{terms of the order } \alpha/zv_{\text{II}}\}.$$

Returning now to the experiments and identifying the observed symmetric "pulse" with the Gaussian curve of this calculation, the first conclusion which can be drawn concerns the velocity  $v_{\text{II}}$ . As has been pointed out, the velocity  $u_1$ , accepted to be the second sound velocity by earlier investigations [3], actually depends on  $z$ . On the other hand, according to equation 4.4, the proper value of  $v_{\text{II}}$  should be equal to  $z/t_{\text{max}}$ , i.e.  $z/t_4$ . Indeed  $z/t_4$  proved to yield a unique velocity for all tubes down to 0.7° K. Below this temperature the curves for the different tubes deviate (see fig. 4.4).

In view of the very short pulses used, no attempt has been made in this and the next calculation to take into account the finite width of the heating pulse. Merely, the  $t_4$ -values used have been corrected in such a way that the zero point of time lies in the centre instead of at the start of the original pulse.

The  $v_{\text{II}}$  curve from reference [3] is also shown in figure 4.4; it was obtained from the  $u_1$ -values for a 5 cm tube. It is curious that this curve lies below the  $u_1$ -curve for the 6 cm tube in the present investigation. One would expect it to be situated just above but very near the latter. This can perhaps be attributed to a somewhat different definition of the start of the signal or to the characteristics of the amplifier employed.

The second conclusion which can be drawn concerns the value of  $\alpha$  or of  $\beta/\omega^2$ , in which  $\beta$  is the absorption coefficient at frequency  $\omega$ .  $\beta/\omega^2$  is supposed to be independent of the frequency. According to equation 1.19

$$(4.5) \quad \beta/\omega^2 = \frac{1}{2}\alpha/v_{\text{II}}^3.$$

A very simple calculation yields

$$(4.6) \quad (t_4 - t_3)^2/z = 2.8(\beta/\omega^2),$$



$t_4 - t_3$  being the difference of time of the top and the halfheight of the leading part of the signal. Indeed it is found that  $t_4 - t_3$  is, in any case approximately, proportional to  $z^{1/2}$  at constant temperature. Figure 4.6

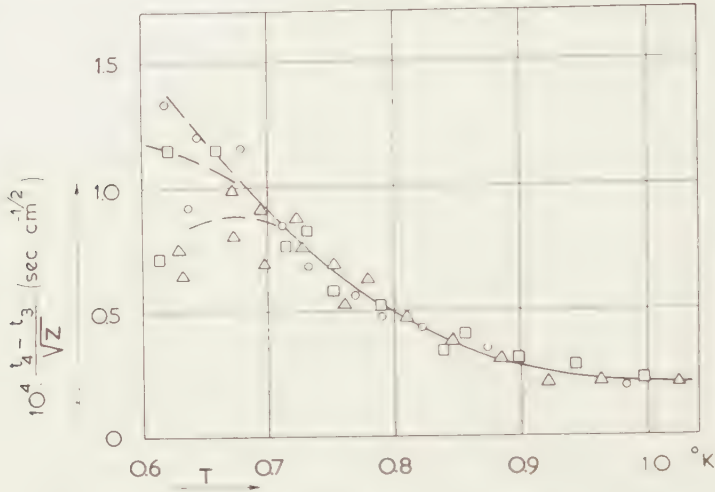


Fig. 4.6. Reduced width of pulses.

- tube 8 ( $z = 1.60$  cm).
- tube 9 ( $z = 3.05$  cm).
- △ tube 10 ( $z = 6.4$  cm).

gives the values of  $(t_4 - t_3)z^{1/2}$  as a function of temperature. The accuracy of this kind of measurements seems to be rather small so that not a very good accuracy can be expected for the resulting data on  $\beta\omega^2$  either. The main cause for the substantial spreading of the points is that the experiments were always performed in such a way that the heating signal and the detected signal appeared both on the oscilloscope screen. For this reason especially with the longest tube the time scale had to be small. In the case of the 1.6 cm tube the time scale was usually three times as large as that employed with the two other tubes. Consequently the largest weight is given to these results. Again, below  $0.7^\circ$  K the values from the different tubes deviate from each other and this calculation has no more any sense.

From figure 4.6 it appears that at the high temperature end the spreading becomes constant. The width of the signal is, however, still much larger than the width of the heating pulse (20 to 40  $\mu$ sec). This spreading may be due to the amplifier characteristics at high frequencies, the transfer of energy from the heater to the liquid and from the liquid to the thermometer or to an extra absorption or reflection by the surface of the walls. Probably all those effects are present but it is not easy to decide which is the most important one. Since also for this constant part the value of  $(t_4 - t_3)^2/z$  appeared to be about the same for the three tubes, this part was just subtracted. The value of  $\beta\omega^2$  was calculated from the corrected data on

$(t_4 - t_3)^2/z$ . In view of this large extra spreading it is of no use to apply a correction for the finite width of the original heating pulse.

The same calculation was made with data from tube 3 (1.5 cm length, 0.4 cm diameter). The accuracy of these early experiments was not very good, but within the experimental limits the same values of  $(t_4 - t_3)z^{-1/2}$  were obtained. One may, therefore, perhaps conclude that, in view of the insensitivity of the spreading to the tube diameter, surface effects do not play an appreciable role.

Figure 4.7 contains the data obtained on  $\beta/\omega^2$ , together with the curve

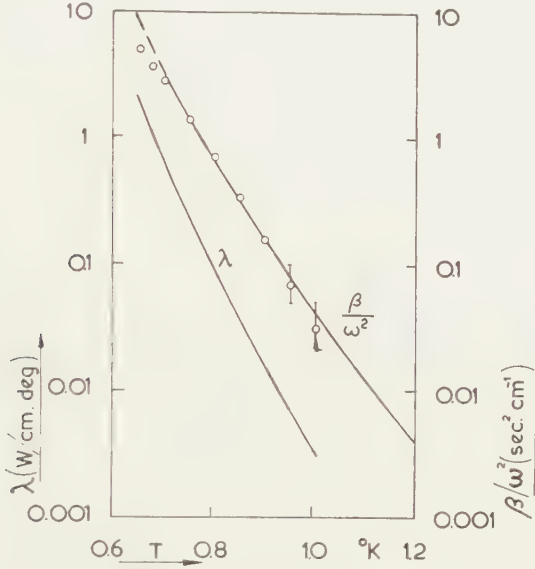


Fig. 4.7.  $\beta/\omega^2$ : reduced absorption coefficient of second sound.  
 $\lambda$ : heat conductivity coefficient (see text).

calculated by KHALATNIKOV [6]. The theory and the experiment appear to be in good agreement. It should be mentioned here that experiments on the absorption of second sound above 1° K performed by ATKINS and HART [7] and by HANSON and PELLAM [8] lead to the same conclusion. The value of  $\alpha$  can be calculated directly from  $\beta/\omega^2$ , using also the data obtained on  $v_{II}$ .

In table 4.3 the smoothed values of  $v_{II}$ ,  $\beta/\omega^2$  and  $\alpha$  are tabulated<sup>1)</sup>.

It is now possible to investigate the validity of neglecting the higher order terms of the equations 4.3 and 4.4.  $\alpha/zv_{II}$  had to be small compared to 1 for the evaluation of  $v_{II}$ . It proves to be equal to 0.02 and 0.07 with the 6 cm and 1.5 cm tubes respectively at  $T = 0.7^\circ$  K. The square root of  $\alpha/zv_{II}$  determines the limit set to the validity of the calculation of  $\beta/\omega^2$  and  $\alpha$ . It is equal to 0.14 and 0.26 in the corresponding cases at  $T = 0.7^\circ$  K.

<sup>1)</sup> In the original publication [9] somewhat different data on  $\alpha$  are given, because the correction just mentioned was not introduced.

TABLE 4.3

(Values in brackets are extrapolated)

$T$ °K	$v_{II}$ m/sec	$\beta/\omega^2 \times 10^9$ sec <sup>2</sup> cm <sup>-1</sup>	$\alpha$ cm <sup>2</sup> sec <sup>-1</sup>	$\alpha_\eta + \alpha_\gamma$ (Khal.) cm <sup>2</sup> sec <sup>-1</sup>	$\alpha_\lambda = \alpha - \alpha_\eta - \alpha_\gamma$ cm <sup>2</sup> sec <sup>-1</sup>	$\lambda = \alpha_\lambda \rho c_p$ watt/cm deg	$\lambda$ (Khal.) watt/cm deg	$l_{ph}$ (exp) cm	$r \times 10^4$
0.65	(61)	(5)	$(2.3 \times 10^3)$	(200)	$(2 \times 10^3)$	(2)	1.3	0.3	1.2
0.67 <sup>5</sup>	53	(3.7)	$(1.1 \times 10^3)$	100	$(1 \times 10^3)$	(1.2)	0.65	0.15	1.75
0.7	42.8	2.9	450	40	410	0.57	0.40	0.06	3.0
0.75	34.1	1.41	112	12	100	0.21	0.20	0.019	5.6
0.8	28.1	0.71	31.4	3.7	28	0.087	0.072	0.0065	10.3
0.85	23.8	0.33	9.1	1.3	7.8	0.038	0.042	0.0023	18.0
0.9	21.1	0.15	2.8	0.5	2.3	0.017	0.018	0.0009	32.7
0.95	19.5	0.067	0.9	0.2	0.7	0.007	0.011	0.0003	50.3
1.0	18.7	(0.03)	(0.4)	0.09	(0.3)	(0.004)	0.0071	(0.0001)	82.5
1.05	18.4						0.0045		112
1.1	18.2						0.0031		161

In view of the accuracy one sees, that the procedure used is just adequate down to 0.7° K (for the evaluation of  $v_{II}$  even somewhat lower). At these temperatures the largest importance was given to the data from the longest tube (smallest high order terms). This does not conflict with the poor accuracy for this tube noted before, since the spreading is very large at  $T = 0.7^\circ$  K.

As has been explained in chapter I,  $\alpha$  is supposed to contain contributions from first and second viscosity and from the heat-conductivity. As neither of these have been measured or even can be measured separately, for the following some conclusions of the theory have to be used. The largest contribution, according to the theory of KHALATNIKOV [6], is that from the heat-conductivity. His calculation gives a contributing term  $\alpha_\eta$  from the first viscosity, which is about 5 % of the contribution from the heat-conductivity term (see equation 1.43). KHALATNIKOV's value of  $\eta$  is a reasonable extrapolation of measurements above 1° K. The second viscosity contribution has been deduced by KHALATNIKOV from the absorption coefficient of normal sound. This is a very complicated calculation which cannot be repeated here. In table 4.3 the total contribution to  $\alpha$  from both the viscosity terms is given according to these calculations. After subtracting it from the experimental value of  $\alpha$  the remaining part  $\alpha_\lambda$  should be due to the heat-conductivity. This procedure has some sense, because the other terms are supposed to be relatively small (together up to 20 %).

One sees from equation 1.21

$$(4.7) \quad \alpha_\lambda = \lambda / \rho c_p$$

so that  $\lambda$  can be evaluated. These data are also given in table 4.3 together



with KHALATNIKOV's values. The agreement is fair. The experimental values of  $\lambda$  are shown in fig. 4.7.

Finally it is possible to get an estimate of the mean free path of the phonons ( $l_{ph}$ ) by using the well-known formula:

$$(4.8) \quad \lambda = \frac{1}{3} \rho c_{vph} l_{ph} v_T;$$

$c_{vph}$  is the phonon part of the specific heat. The data on  $l_{ph}$  are given in fig. 4.11 and in table 4.3.

*(To be continued).*

## SOME PROPERTIES OF LIQUID HELIUM BELOW 1° K. (IVB)

BY

H. C. KRAMERS

(Communicated by Prof. C. J. GORTER at the meeting of October 29, 1955)

4.3. *The low temperature region (main body effect).* The next part of the discussion will be devoted to the region below 0.5° K, the phenomena at intermediate temperatures being postponed until the next section. Also the sharp edge effect is overlooked for the time being.

The main shape of the detected signal shows, at any rate for the longer tubes, a very flat front and a long tail. The time corresponding to the top is roughly proportional to  $z^2$  but, due to the large spreading of the signal, the accuracy of this determination is rather poor. Moreover, as has been pointed out, the amplifier correction has an appreciable influence on  $t_4$ . The quadratic dependence suggests a phenomenon very similar to diffusion or heat conductivity.

As has been discussed in chapter I, it may be expected that the mean free path of the phonons in this region is large compared to the diameter of the measuring tube. In that case the phonons collide mainly with the walls and not with rotons or with one another. As these collisions are probably diffuse (the mean wave length of the phonons is of the order  $5 \times 10^{-6}$  cm), one faces with a problem which is essentially the same as that of the heat conductivity in solid crystal rods at low temperatures, considered by CASIMIR [10]. For a long narrow tube this "random walk" problem can be considered as one-dimensional. The appropriate differential equation is

$$(4.9) \quad \partial T / \partial t = \frac{2}{3} v_1 r \partial^2 T / \partial z^2;$$

$r$  is the radius of the tube (see also [11]). This is indeed a similar equation to that of the normal heat conductivity, only the temperature conduction coefficient  $\lambda/\rho c_v$  is replaced by  $2rv_1/3$ . Incidentally, comparison with equation 4.8 shows that these quantities are identical if the mean free path is taken to be equal to  $2r$ .

With the initial condition of a heat pulse of vanishing length but finite total energy, i.e.  $(\partial T / \partial z)_{z,0} = \delta(z)$  one gets the well-known solution

$$(4.10) \quad T(z, t) = A(z) t^{-1/2} \exp(-3z^2/8rv_1 t).$$

The dependence on  $z$  of the time of the maximum of this long-tailed signal is indeed quadratic:

$$(4.11) \quad t_{\text{top}} = 3z^2/4rv_1.$$

As one sees, the shape of this signal is completely determined by  $r$  and  $v_I$  which are known quantities. Therefore, it is possible to compare the theory with the experimental results.

The condition of a long and narrow tube is, however, not very well fulfilled. The best comparison can be made with the 6 cm tube (no. 10). Figure 4.8 contains the theoretical curve for this tube together with four

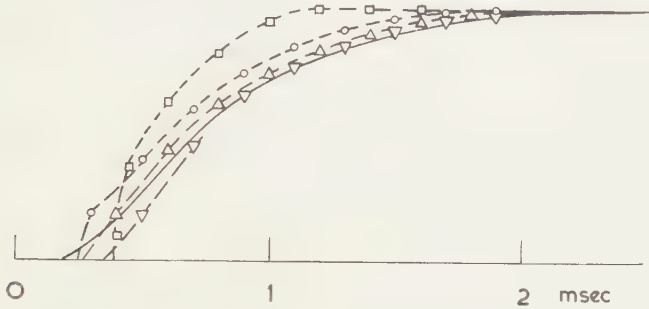


Fig. 4.8. Shape of the signal detected in the long tube ( $z = 6.4$  cm).  
 Fully-drawn line: theoretical curve (formula 4.10).  
 Dotted lines: experimental results.  
 $\bigcirc$   $T = 0.15^\circ \text{ K}$        $\nabla$   $T = 0.40^\circ \text{ K}$ .  
 $\triangle$   $T = 0.25^\circ \text{ K}$        $\square$   $T = 0.55^\circ \text{ K}$ .

experimental curves at different temperatures. Especially around  $0.25^\circ \text{ K}$  the agreement is satisfactory. At lower temperatures the sharp edge disturbs the picture, while at higher temperatures ( $0.4^\circ \text{ K}$ ) the front of the signal has been shifted to a larger time delay. The rear part of the curve, including the top, however, is still in close agreement. The curve at  $T = 0.55^\circ \text{ K}$  shows a quite different character and fits no more with the theoretical curve.

In section 4.5 it will be shown that the mean free path of the phonons is probably not very much larger than the tube diameter. This may perhaps account for the "pushing back" of the front with increasing temperature. It is not unreasonable to suggest that a limited mean free path has indeed a relatively larger influence on the front of the signal. The phonons responsible for building up this part can only have collided a few times with the walls. By passing obliquely with respect to the walls they may easily be diverted by a collision in the liquid itself and so the front may be seriously affected. Similar collisions occur, of course, with the phonons which undergo a larger number of collisions with the wall. The collisions occurring in the liquid with these phonons are even more numerous than with the former ones, because the total path length is longer, but it is not unreasonable to suggest that the relative importance of these collisions is much less. Consequently, only a small change of shape of the rear parts of the signal may occur.

The results from the shorter tubes cannot be used for a similar analysis. Firstly, the condition of a long and narrow tube is by no means fulfilled.



This means a relatively large effect of phonons having collided only once or a few times with the walls and it is no longer a unique problem of one-dimensional "random walk". Secondly, the original signal is reflected by the thermometer and again by the heater and so on. Though these reflections are heavily damped, the detected signal may be built up out of the direct signal together with several of these reflections. Actually a second top can be traced with the 1.6 cm tube (see fig. 2, B1). Thirdly, the "sharp edge" effect is of relatively larger importance with the shorter tubes. For the shorter tubes the only conclusion which can be drawn is that equation 4.11 appears to be satisfied approximately.

Finally one can easily calculate the value of  $\lambda$  which should be found from stationary experiments on thermal conductivity in this temperature region. For a very long and narrow tube with circular cross section, this yields

$$(4.12) \quad \lambda = \frac{2}{3} r v_{\text{I}} \rho c_v = 53 r T^3 \text{ watt/cm deg.}$$

This result is, up to 0.6° K, in approximate agreement as to temperature dependence and order of magnitude with experiments of FAIRBANK and WILKS [12]. They used a capillary of 0.029 cm inner diameter i.e. the condition mentioned above is much better fulfilled than in the present case.  $\lambda$  is of course no real heat-conductivity coefficient, because it depends on the geometry of the measuring vessel. The deviations from formula 4.12 found by these authors may be due to the influence of specular reflections.

**4.4. The intermediate region (0.5–0.7° K).** In this region the change from second sound at the high temperature to the phenomena described in the last section at the low temperature takes place. This is just the region mentioned in section 1.7. When the temperature is decreased, the local equilibrium, characteristic in second sound, is established with increasing difficulty. This can be attributed to the rapid decrease of interaction between the excitations. Finally one may expect, that at low temperatures only some kind of diffusion of phonons is left and all trace of second sound is lost. This picture, however, may be expected to be seriously affected by the influence of the walls, because the mean free path of the phonons becomes at the same time comparable to the diameter of the experimental tube. For this reason it is not easy to give a quantitative analysis of the phenomena in this region.

The most remarkable effect is that of the relatively steep front observed with the longest tube at about 0.55° K (see fig. 4.1.d and fig. 4.8). At that temperature the rear part of the signal has already developed its long tail. The corresponding value of  $u_1$  is about 150 m/sec. Since this is not very different from the hypothetical second sound velocity in the phonon region ( $v_{\text{II}} = v_{\text{I}}/3^{1/2} = 137$  m/sec), it is not unreasonable to suppose that this effect represents the last trace of second sound. Moreover, a pure phonon

diffusion effect without any second sound would give a signal even flatter than that occurring in the lower temperature range.

At first sight the increase of the steepness of the front of the observed signal, when the temperature is lowered from  $0.7^\circ$  to  $0.55^\circ$  K, is very curious. As has been shown, the reverse effect occurring from  $1.0^\circ$  to  $0.7^\circ$  K can be explained by the increase of damping due to irreversible effects. In a more kinetic language this means that, when the temperature is decreased, the excitations diffuse increasingly away from the travelling second sound pulse which, therefore, is spread in the forward as well as in the backward direction. The simple quantitative analysis of section 4.2 can, however, no longer be used, if the second sound velocity becomes of the same order of magnitude as the velocity of the individual phonons ( $v_1$ ) which actually is expected to occur in the region below  $0.6^\circ$  K. It is quite conceivable that in the latter case the front of the pulse cannot travel much faster than the velocity of second sound. This may be an explanation for the observed increase of the steepness below  $0.7^\circ$  K. It should be mentioned, however, that in this region the quantitative analysis of section 4.2 breaks down in any case because of the large magnitude of the spreading effect, which makes the series development inadequate.

It would be very interesting to make observations in this intermediate region without the presence of the walls. When there is time enough for establishment of some kind of local equilibrium, i.e. for large enough  $z$ , one would actually expect a fairly well defined second sound pulse. For short distances no such establishment of equilibrium may be possible, in fact the diffusion effect would predominate. An increased relative sharpness of the second sound pulse with larger values of  $z$  is actually observed in the region above  $0.7^\circ$  K, the spreading being proportional to  $z^{1/2}$  only.

This remark may furnish an explanation for the fact that the steepening of the front at about  $0.55^\circ$  K was well established in the 6 cm tube, but not at all in the 1.5 cm tube. The influence of the walls, however, tends to confuse the whole picture, the observed long tail is probably mainly due to that. More experiments are required for a confirmation or a rejection of the remarks of this section, especially experiments of the kind just mentioned, i.e. care should be taken that the influence of the presence of walls is reduced as well as possible.

**4.5. The sharp edge effect.** This effect, occurring at the lowest temperatures, is especially pronounced for the longest tube. With the 3 cm tube it can just be detected, while the 1.6 cm tube does not show it. As has been pointed out in 4.1.4. it is highly probable that, owing to the pretty sharp front of the main effect in the latter case, it cannot be distinguished from it.

The velocities  $u_1$  are not the same for the three tubes, but all are very near to the expected velocity of first sound (237 m/sec). The difference of

the  $u_1$ -values can be explained by assuming a constant delay of  $8 \pm 2 \mu\text{sec}$ . The corresponding unique velocity is

$$u_1 = 236 \pm 4 \text{ m/sec}$$

and this corresponds indeed to  $v_1$  within the limits of accuracy.

The cause of this constant retardation is not very clear. It is certainly not due to the electronics. Perhaps an explanation would be the combined influence of the KAPITZA thermal resistances at the surfaces of the heater and the thermometer. The heat transfer from the heater to helium is characterised by a quantity having the dimension of time which is the product of this resistance ( $K$ ) and the heat capacity ( $C$ ) of the heater. The same occurs to the heat transfer from helium to the thermometer. If one considers only one of these effects, a time delay can never occur. The result is only a rise of temperature which is not instantaneous but shows a linear ascent. The combination of two such effects (in this case at the heater and the thermometer), however, causes indeed a horizontal tangent at the starting point. An apparent time delay is now found in the experiments, because the noise and the finite line width of the oscilloscope beam prevent the observation of the real starting point of the signal.

By extrapolation of the KAPITZA resistance from the normal helium region, assuming the  $T^{-3}$ -dependence found there [13, 14] to be valid also at low temperatures, one finds at  $0.2^\circ \text{K}$ :  $K \approx 2500 \text{ deg watt}$ . The value of the heat capacity of the carbon resistance corresponding to the noted time delay should be of the order of a few hundredths of an erg per degree, which is not unreasonable.

In section 4.1.5 it was mentioned that with higher pulse-amplitudes  $u_1$  was much nearer to  $v_1$ . This is in agreement with the explanation just given, because the relative influence of the noise is much reduced. Moreover, the temperature of the heater is during the time of the heat transfer almost certainly much higher than the surrounding liquid, so the KAPITZA-resistance much lower than that with small pulses. Because the heat capacity of carbon is proportional to  $T^2$  a smaller time delay should come out. It cannot, however be proved that this is the right explanation. Nothing is actually known about the KAPITZA resistance at low temperatures and the heat capacity of the carbon resistors could not be determined either.

The obvious explanation of the sharp edge effect, being due to thermal phonons (i.e. with  $\omega \approx \kappa T/\hbar$ ) travelling directly from the heater to the thermometer, will be discussed later on in this section. It is, however, first necessary to investigate the other possible explanation ascribing the sharp edge to low-frequency (acoustical) phonons. According to this picture the heater would generate normal sound observable at the thermometer by means of a microphonic effect of the latter.

In an attempt to arrive at a decision between the two possibilities the different kinds of thermometer were used. Unfortunately, however, the



results do not lead to a conclusive answer. If a constantan heater was used, the effect did not occur indeed but, as will be explained now, this is probably due to its large heat capacity. The specific heat of a metal at these low temperatures is almost exclusively due to the electrons and so proportional to  $T$ . Actually for the heater used the heat capacity was of the order of  $10^{-7} \times T$  joule/deg. This means that the “ $KC$ -time”, determining the heat transfer to the liquid is proportional to  $T^{-2}$ , if one assumes the same extrapolation as before of the KAPITZA resistance. The result is  $KC \approx 4 \times 10^{-6} T^{-2}$ , i.e. about 100  $\mu\text{sec}$  at  $0.2^\circ \text{K}$  and even 400  $\mu\text{sec}$  at  $0.1^\circ \text{K}$ . (The magnitude of  $K$  is taken to be twice as large as that in the former case, because the effective area is smaller by a factor 2.) This large  $KC$ -time causes the front of the signal, departing from the heater, to rise only slowly, the tangent at the start being proportional to  $1/KC$ , assuming an original instantaneous rise. So the sharp edge is completely drowned. Moreover, it has been proved that also the overall shape of the signal is seriously affected. It is “rounded off” appreciably, especially with the 1.5 cm tube no. 7a (see also fig. (4.1.b)).

The  $u_1$ -values of these tubes in this region appear to be slightly smaller than those with the tubes no. 8, 9 and 10, but this may be attributed to the combined effect of noise and slow ascent. The conclusion of this discussion is, that the non-existence of the sharp edge in experiments on tubes with constantan heaters is no proof for a sound pulse in the case of carbon heaters. As has been pointed out earlier in this section, no direct evaluation can be made of the heat capacity of the carbon resistors. The amount of carbon and the behaviour of the paper background is unknown but in any case the temperature dependence of the heat capacity is certainly much larger (probably  $\sim T^2$  for the carbon and  $\sim T^3$  for the background paper). The  $KC$ -time is, therefore, only increasing with  $1/T$ , while going to lower temperatures. This points to a much smaller effect in the latter case, compared to that of the constantan heaters.

The observations of the sharp edge with commercially made carbon resistors show exactly the same behaviour as those made with the home-made ones. This is an argument for the phenomenon not to be due to normal sound, because these resistors might be expected to be much less liable to produce sound.

The next part of the discussion will concern the second possibility which attributes the sharp edge to the propagation of thermal phonons. It will be shown, that this hypothesis completely fits into the picture of the liquid at these temperatures.

One has to start with a consideration of the phenomena below about  $0.15^\circ \text{K}$ , where the edge is fully developed. Firstly, the elevation of the sharp edge is roughly proportional to the solid angle looking from the heater to the thermometer (i.e.  $\sim 1/z^2$ ) as should be expected. Secondly, the observed ratio of the height of the sharp edge to the finally reached almost constant value of the corrected signal can be compared with the

computed ratio of the temperature rise due to phonons going the direct way and the final temperature rise reached, if all energy input is used for heating the helium content of the tube. Again only a rough estimate can be given, especially because the height of the tail cannot be measured with much accuracy. In any case the first ratio is found to exceed the second one probably by a factor 3 or 4. This appears at first to be disconcerting. However, phonons which have only once or twice reflected with the walls and pass almost parallel to them, may also contribute to the sharp edge. Moreover, one has to keep in mind that an appreciable amount of heat may escape through the holes in the walls, thus tending to reduce the after-effect. This is in agreement with observations with earlier tubes (no. 1, 2 and 3), where the excess factor was still much larger. The whole surface of the walls of these tubes was perforated with many holes, while in tubes 8, 9 and 10 only four rows of holes were bored.

One must turn now to the curious phenomena of the disappearance of the sharp edge already at about  $0.2^\circ \text{K}$  with the 6 cm tube and at about  $0.34^\circ \text{K}$  with the 3 cm tube. Actually one would expect from an extrapolation of KHALATNIKOV's predictions the mean free path to be much larger than  $z$  in the whole region below about  $0.45^\circ \text{K}$ . If this was true, the sharp edge would exist everywhere below  $0.45^\circ \text{K}$ . Moreover, the increase of the mean free path would be so fast with decreasing temperature, that the appearance of the edge would occur at practically the same temperature for different values of  $z$ . According to KHALATNIKOV  $l_{\text{ph}}$  is proportional to  $T^9$  in this region [18].

The appearance is, therefore, that in reality the mean free path is much more limited than would be expected from KHALATNIKOV's deductions. One can try to calculate the mean free path from the observations in the following way. At extremely low temperatures, i.e. with very large mean free path, all phonons starting from the heater within a certain solid angle will reach the thermometer along the direct way. At higher temperatures only the relative amount  $F = \exp(-z/l_{\text{ph}})$  will accomplish this. For  $F$  equal to 0.5

$$(4.13) \quad l_{\text{ph}} = 1.65 z.$$

As it is not possible to determine the height of the sharp edge in absolute measure, because the thermometer sensitivity changes in an unknown way with temperature, this method could not be used directly. The best procedure appeared to be to calculate the ratio of the height of the sharp edge ( $h_1$ ) and the height of the signal at  $t_2 = 2t_1$  ( $h_2$ ). The result for the tubes 1 and 10 is shown as a function of temperature in fig. 4.9. Tube 1 (the narrow 3 cm tube) was used instead of tube 9, because the sharp edge was much better observable in the former. The reason for that has already been mentioned in 4.1.6. It may be noticed here that the larger spreading occurring with narrower tubes is in complete agreement with what has been said about the main body effect. From equation 4.11 it is

immediately seen, that the signal is much flatter with small  $r$ , because  $t_{\text{top}}$  is inversely proportional to  $r$ .

Equation 4.13 was now taken to be valid at the temperature, where  $h_1/h_2$  was reduced to one half of its value at the lowest temperature. It is clear, that the accuracy is not very good. Moreover, the procedure used

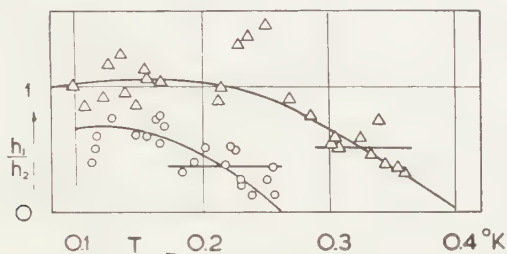


Fig. 4.9. The relative sharp edge effect as a function of temperature.  
 $\triangle$  tube 1 ( $z = 2.99$  cm);  $\circ$  tube 10 ( $z = 6.4$  cm).

here for determining the mean free path is very much open to criticism, because the heat leak through the holes in the wall will also change considerably with temperature (compare equation 4.12). This effect may be supposed to have a much larger influence on  $h_2$  than on  $h_1$ . At any rate it can be expected, that the order of magnitude is right. One finds  $l = 5$  cm at  $T = 0.34^\circ$  K and  $l = 10.5$  cm at  $T = 0.21^\circ$  K.

An explanation for this curious extra-limiting of the mean free path will be discussed in the next section.

**4.6. The influence of very small amounts of  $^3\text{He}$ .** The experimental results of section 4.5 show, that the mean free path of the phonons probably undergoes yet another limitation of its magnitude apart from the processes discussed by KHALATNIKOV. Firstly it may be that KHALATNIKOV has misinterpreted the phonon-phonon interaction processes. His treatment of this part of the theory appears to be not quite satisfactory as has already been mentioned in chapter I. On the other hand in the analogous case of phonons in a crystal one has also concluded to a very large mean free path.

Another possible explanation is that noted in the last part of section 1.7, i.e. a limitation of the mean free path due to interactions with the very small concentration of  $^3\text{He}$  atoms always present in the liquid which is used in the experiment. The concentration of  $^3\text{He}$  in helium from wells is probably about  $1.4 \times 10^{-7}$  [20]. To investigate this influence one experiment was done with atmospheric helium ( $^3\text{He}$  concentration about  $10^{-6}$ ). Unfortunately in this experiment the 3 cm tube 9 was used so that the sharp edge could not be observed properly. An appreciable change was, however, observed in the behaviour of  $u_1$ . Figure 4.10 shows a comparison between the results of both kinds of helium for this tube. With the atmospheric helium  $u_1$  is seen to be practically constant between 0.35

and  $0.6^\circ \text{K}$ . Its magnitude in that case is about  $150 \text{ m/sec}$ . In the liquid with the smaller  $^3\text{He}$  concentration such a constant region perhaps exists between  $0.5^\circ$  and  $0.6^\circ \text{K}$ , but below that temperature  $u_1$  is increasing again. Such an increase occurs with the atmospheric helium only below  $0.35^\circ$ . Moreover, in that case the final  $v_1$  value is reached just below  $0.2^\circ \text{K}$  instead of in the neighbourhood of  $0.3^\circ \text{K}$ . All this points to a considerable decrease of the mean free path. The intermediate zone of section 4.4

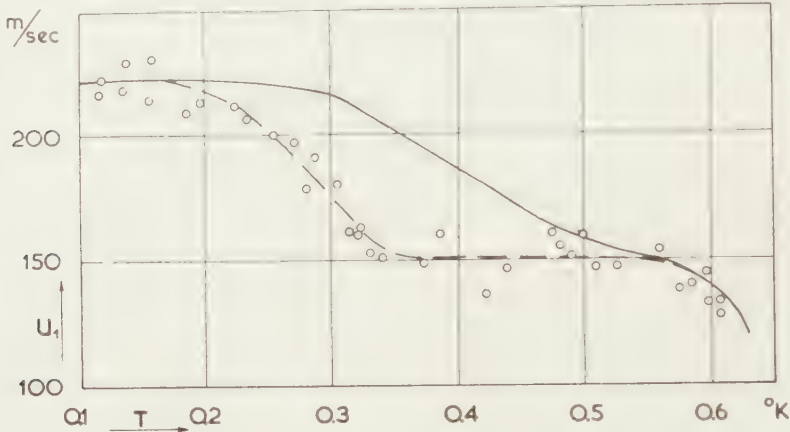


Fig. 4.10. The influence of the  $^3\text{He}$  concentration on  $u_1$ .  
Full line: helium from wells; dotted line and points: atmospheric helium.

appears to be extended down to  $0.35^\circ \text{K}$  and the sharp edge region with  $u_1$ -values very near to  $v_1$  is probably also shifted to lower temperatures. In view of the result of these measurements it is quite plausible, that in the case of a  $^3\text{He}$  concentration which is about 10 times less, i.e. in the normal experimental helium, the mean free path will be limited in the way explained in the last section. In pure  $^4\text{He}$  one may perhaps expect the sharp edge actually to occur already near  $0.45^\circ \text{K}$ .

From a general point of view it is evident, that an interaction of phonons with  $^3\text{He}$  atoms should indeed exist. It is perhaps allowed to compare the latter in this respect with the rotons. Actually the number of rotons and the number of  $^3\text{He}$  atoms in the same volume are of the same order of magnitude at about  $0.5^\circ \text{K}$ . The same applies for  $x_r = \rho_r / \rho$  and the  $^3\text{He}$  concentration at about  $0.45^\circ \text{K}$  (see fig. 4.11), therefore, it is quite feasible, that somewhere near this temperature the  $^3\text{He}$  atoms begin to take over the role of path-limiters from the rotons.

In contrast to that of the rotons the  $^3\text{He}$  concentration is independent of the temperature. Therefore, the dependence of the mean free path on the temperature should indeed be much smaller below the temperature quoted. At first sight one would expect a temperature-dependent factor of  $T^4$  as in the RAYLEIGH type of scattering of phonons by impurities. The experimental values given indicate even a smaller power of  $T$ , but it should be emphasized, that neither the accuracy not the number of experimental



data (two points on the  $l(T)$  curve) is sufficient to draw a definite conclusion.

One may wonder perhaps, if the heat-flush effect does not have a large influence on the actual  $^3\text{He}$  concentration. Due to this effect, as has been observed in the normal helium region, the main part of the  $^3\text{He}$  might be swept by the normal fluid to the coldest spot of the vessel, i.e. the paramagnetic salt. Because of the very small value of  $\varrho_n$  or, in other words, the small amount of excitations at this temperature it is not unreasonable to suppose this effect to be relatively small.

4.7. *Some final remarks and conclusions.* The expositions of the foregoing sections are, in general, well in agreement with the picture proposed in the first chapter. The behaviour of second sound in the region above  $0.7^\circ\text{K}$  finds a reasonable explanation in the theory of elementary excitations combined with KHALATNIKOV's considerations of the interactions. The proposed picture at lower temperatures is a logical extension of the latter and appears to be well in agreement with the experiments. The influence of a very small concentration of  $^3\text{He}$  is probably also established, although more experiments are required to get more exact information.

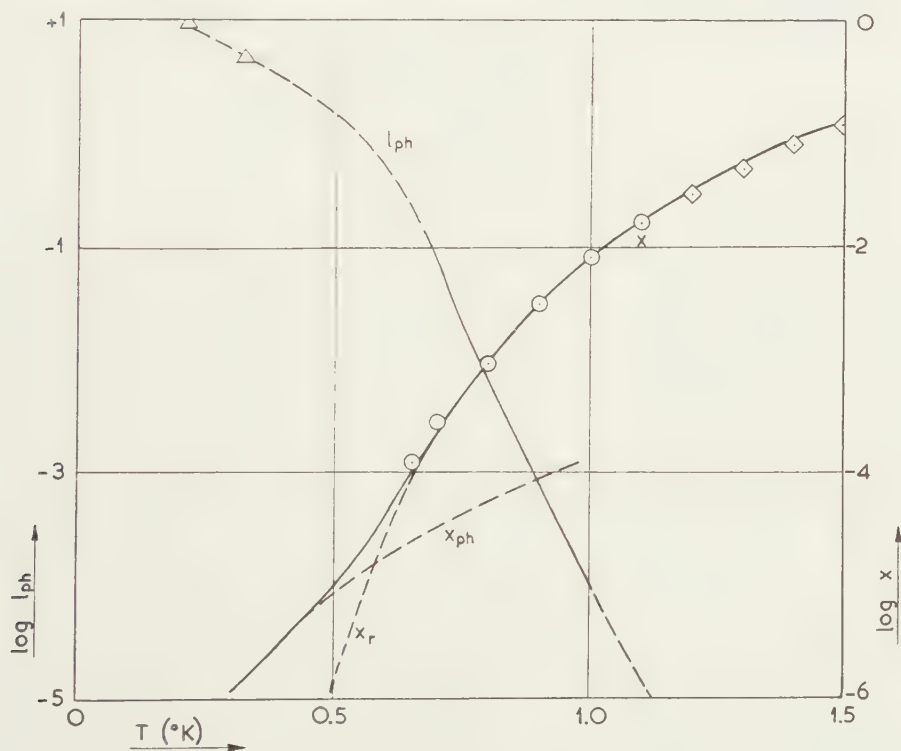


Fig. 4.11.  $x = \varrho_n/\varrho$  and  $l_{ph}$  as a function of temperature.  
 $\bigcirc$  points calculated from the present experiments;  
 $\diamond$  points calculated from PESHKOV's experiments.  
 For further details see the text.

It would give a sufficient explanation of the deviation from KHALATNIKOV's original hypothesis with respect to the mean free path at temperatures below half a degree. There is, therefore, as yet no reason to distrust his deductions for the case of pure  $^4\text{He}$ .

If one accepts equation 1.17 for the velocity of second sound

$$v_{\text{II}}^2 = \frac{\varrho_s}{\varrho_n} \frac{S^2 T}{c_v}$$

$\varrho_n$  or  $x = \varrho_n/\varrho$  can be calculated from the experimental data on  $v_{\text{II}}$  and  $c_v$ . The obtained values can be compared with the theoretical predictions of the theory of excitations.

The latter yields for the phonons

$$(4.14) \quad x_{\text{ph}} = \varrho_{\text{nph}}/\varrho = \frac{1}{3} c_{\text{ph}}/v_{\text{I}}^2 = 14 \times 10^{-5} \times T^4$$

using a value of  $v_{\text{I}}$  equal to 237 m/sec together with the experimental data on the specific heat of chapter III.

One can now compare  $x - x_{\text{ph}}$  with the theoretical formula for  $x_{\text{r}}$  (see equation 1.40). Proceeding in a way analogous to that used for the specific heat one finds:  $\Delta/\kappa = 8.7^\circ \text{K}$  and  $(\mu/m)^{1/2} (p_0/\hbar)^4 = 6.4 \cdot 10^{32}$  c.g.s. units. These values are within a few percent in agreement with the data calculated from the experiments between  $0.8^\circ \text{K}$  and  $1.5^\circ \text{K}$ . For the temperature region above  $1.1^\circ \text{K}$  the data on  $v_{\text{II}}$  of PESHKOV [15, 16] were used. These results can now be combined with those obtained from the specific heat data:  $\Delta/\kappa = 9.1^\circ \text{K}$  and  $(\mu/m)^{1/2} (p_0/\hbar)^2 = 2.4 \times 10^{16}$  c.g.s. units (see section 3.5). The  $\Delta/\kappa$  values are unfortunately not the same. It should, however, be remembered, that especially in the calculation of  $q_{\text{ur}}$  errors of a few percent in the experimental data on  $v_{\text{II}}$  and  $c_v$  may easily be emphasized. On the other hand, the difference appears to be just somewhat too large for such an explanation. This might be attributed to a small complication in the theory. The roton spectrum may contain higher order terms giving a slight correction. Perhaps this can be described by a temperature dependence of one or more of the parameters. The experimental data are, however, not sufficiently accurate to come to a definite conclusion.

The best fit one finds for the parameters of the roton spectrum is

$$(4.15) \quad \Delta/\kappa = 9.0 \pm 0.2^\circ \text{K}, \quad p_0/\hbar = 2.0 \pm 0.1 \text{ \AA}^{-1} \text{ and } \mu/m = 0.3 \pm 0.15$$

$\mu/m$  is only approximately determined, because  $(\mu/m)^{1/2}$  occurs in the equations.

The data given here are in agreement with those of KHALATNIKOV [6]:

$$\Delta/\kappa = 8.9 \pm 0.2^\circ \text{K}, \quad p_0/\hbar = 2.0 \pm 0.05 \text{ \AA}^{-1} \text{ and } \mu/m = 0.32 \pm 0.13.$$

The  $\varrho_n$ -values obtained in this way are too large above  $1.2^\circ \text{K}$ . Perhaps there the values of the parameters proposed by FEYNMAN [17] give a better agreement.

In figure 4.11  $\alpha$ , calculated by means of the equations 4.14 and 1.40, using the data on the rotons 4.15, is plotted as a function of  $T$ . The points shown are calculated from the experiments as explained in this section. In the same figure are also given the data obtained on the phonon mean free path.

The conclusion which can be made from the work of this chapter is that many of the observed phenomena can be explained rather well in a qualitative way by means of the theoretical considerations put forward in chapter I, together with the supposition of the influence of a small  $^3\text{He}$  impurity in the lowest temperature region. Some phenomena have even found a more or less quantitative foundation, but in this respect quite an amount of work remains to be done. Also, more experiments are required on the influence of  $^3\text{He}$ ; these have actually been started in the Kamerlingh Onnes Laboratory <sup>1)</sup>.

#### REFERENCES

1. ATKINS, K. R., D. V. OSBORNE, *Phil. Mag.* (7) **41**, 1078 (1950).
2. MAYPER, V., M. A. HERLIN, *Phys. Rev.* **89**, 523 (1953).
3. DE KLERK, D., R. P. HUDSON, J. R. PELLAM, *Phys. Rev.* **93**, 28 (1954).
4. OSBORNE, D. V., *Proc. Phys. Soc., London*, **A64**, 114 (1951).
5. DINGLE, R. B., *Physica* **18**, 841 (1952).
6. KHALATNIKOV, I. M., *Zh. Eksp. Teor. Fiz.*, **23**, 21 (1952).
7. ATKINS, K. R., K. H. HART, *Phys. Rev.* **89**, 526 (1953).
8. HANSON, W. B., J. R. PELLAM, *Phys. Rev.* **95**, 321 (1954).
9. KRAMERS, H. C., TINEKE VAN PESKI-TINBERGEN, J. WIEBES, F. A. W. VAN DEN BURG, C. J. GORTER, *Comm. Kamerlingh Onnes Lab. Leiden*, No. 296b; *Physica* **20**, 743 (1954).
10. CASIMIR, H. B. G., *Comm. suppl.* No. 85b; *Physica* **5**, 495 (1938).
11. ZIMAN, J. M., *Phil. Mag.* (7) **45**, 360 (1954).
12. FAIRBANK, H. A., J. WILKS, *Phys. Rev.* **95**, 277 (1954).
13. KAPITZA, P. L., *J. Phys. U.S.S.R.*, **4**, 181 (1941).
14. BEENAKKER, J. J. M., K. W. TACONIS, E. A. LYNTON, Z. DOKOUPIL, G. VAN SOEST, *Comm.* 289a; *Physica* **18**, 433 (1952).
15. PESHKOV, V. P., *Zh. Eksp. Teor. Fiz.*, **18**, 951 (1948).
16. ———, *Zh. Eksp. Teor. Fiz.*, **23**, 686 (1952).
17. FEYNMAN, R. P. in *Progress of Low Temperature Physics*, vol. I, chapter 2., North Holland Publ. Comp., Amsterdam, 1955.
18. LANDAU, L. D., I. M. KHALATNIKOV, *Zh. Eksp. Teor. Fiz.*, **19**, 637 and 709 (1949).
19. OSBORNE, D. V., *Conférence de Physique des Basses Températures*, Paris 2-8 septembre 1955, no. 24.
20. ALDRICH, L. T., A. C. NIER, *Phys. Rev.* **70**, 983 (1946).

<sup>1)</sup> Not included in the discussion were the results of the recent experiments by OSBORNE [19] which became available only at the last moment. This author used a continuous wave method for the propagation of second sound. In a qualitative way there is agreement with the results of this chapter, although there seems to be a disagreement with respect to the quantitative data on the mean free path.

## ERRATA

(H. C. KRAMERS: *Some properties of liquid helium below 1° K*)

in article IA (Vol. LVIII, Series B, p. 302).

p. 304 formula (1.04) should be:  $\text{grad } P = \varrho_n S^* \text{grad } T$ .

p. 305 5<sup>th</sup> line should be:  $\text{grad } P / \text{grad } T = \varrho Q / T$ .

p. 306 in formula (1.12) and the formula on the 15<sup>th</sup> line,  $\varrho_n$  should be cancelled in the denominator of the third term.

15<sup>th</sup> line: the + sign before the second term should be a — sign.

17<sup>th</sup> line: the second term should be  $-v \frac{\varrho_n \varrho_s}{\varrho^3} S^* w_0$ .

7<sup>th</sup> line from below:  $16\eta_n^2 \varrho_s^2 \omega^2 / 9\varrho^2 \varrho_n^2$  should be  $16\eta_n^2 \varrho_s \omega^2 / 9\varrho^2 \varrho_n$ .

p. 307 formula (1.21) should run:  $\alpha_{II} = \frac{1}{\varrho} \left( \frac{\varrho_s}{\varrho_n} \left( \cdot \cdot \cdot \right) \right)$

in article IIIA (Vol. LVIII, Series B, p. 386).

p. 392 the first number of the third column of table 3.3 has been omitted; it should be: 17.2.



## CHEMISTRY

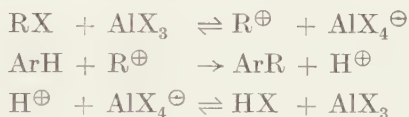
# INVESTIGATIONS OF THE MECHANISM OF THE FRIEDEL-CRAFTS REACTION: THE REACTION OF ETHYL BROMIDE AND ALUMINIUM BROMIDE

BY

F. L. J. SIXMA AND H. HENDRIKS

(Communicated by Prof. J. P. WIBAUT at the meeting of September 24, 1955)

§ 1. For a better understanding of the mechanism of the FRIEDEL-CRAFTS alkylation of aromatic compounds the study of the interaction of alkyl halides with aluminium halides is of considerable importance. The FRIEDEL-CRAFTS reaction shows the typical properties of an electrophilic substitution reaction and several investigators [1] have assumed that in reactions of this type the aromatic nucleus is attacked by carbonium ions which are formed by the interaction of the catalyst with the alkyl halides:



As arguments in favor of this mechanism are given a.o.:

(a) the conductivity shown by solutions of aluminium bromide in alkyl bromides [2];

(b) the results of experiments with alkyl bromides labelled with radioactive bromine, which indicate that a complete exchange takes place between the halogen atoms of the alkyl bromide and the catalyst [3].

However, recent investigations have thrown considerable doubt on the validity of these and other arguments. BROWN and GRAYSON [4] have shown that in the case of the reaction of 3,4-dichlorobenzyl chloride with benzene in nitrobenzene solution third order kinetics is found, the rate of the reaction being proportional to the concentrations of the benzyl halide, the aromatic compound and the catalyst. These authors conclude that their results are consistent with a displacement mechanism involving a nucleophilic attack of the aromatic compound on an alkyl halide-aluminium halide addition compound. The available data on the FRIEDEL-CRAFTS alkylation reaction involving primary alkyl halides seem to be in accordance with such a mechanism. For the reactions of tertiary halides a carbonium ion mechanism is still probable.

At the present moment more experimental information on this point

is very desirable and reinvestigations of several aspects of the FRIEDEL - CRAFTS reaction are in progress in a number of laboratories.

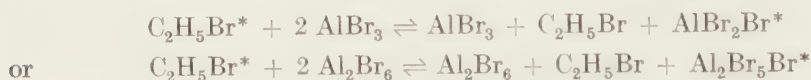
FAIRBROTHER and SCOTT [5] reinvestigated the conductivity of solutions of aluminium bromide in ethyl bromide. It has now been established beyond doubt that these solutions exhibit a small but distinct electrical conductivity which is *not* due to impurities or decomposition products. This conductivity and the results of electrolysis experiments are best explained by the formation of  $\text{AlBr}_4^\ominus$  and  $\text{C}_2\text{H}_5\text{BrAlBr}_2^\oplus$  ions.

Also the second argument which formerly was accepted as favoring the carbonium ion mechanism, viz. the rapid exchange of halogen atoms between alkyl halide and catalyst has been invalidated, as will be shown in this communication.

§ 2. We have investigated the interaction of ethyl bromide and aluminium bromide with the aid of tracer techniques by labelling the ethyl bromide with radio active bromine and with radioactive carbon respectively.

FAIRBROTHER [3] observed a rapid exchange of (radioactive) bromine atoms on mixing alkyl bromides with aluminium bromide at  $15^\circ$ . BREJNEVA, ROGINSKY and SCHILINSKY [6] observed the same reaction in carbon disulfide solution, but they did not determine the kinetics of the reaction.

In collaboration with miss D. HOLTZAPFFEL we have prepared ethyl bromide- $[\text{}^{82}\text{Br}]$  from silver propionate and  $^{82}\text{Br}_2$ . The exchange reaction with aluminium bromide was studied at temperatures between  $0^\circ$  and  $-26^\circ$ . In carbon disulfide solution the reaction velocity appeared to be proportional to the concentration of the ethyl bromide and to the square of the concentration of the aluminium bromide, as would be expected for a net reaction according to:



From the kinetics of the reaction it is impossible to conclude if  $\text{AlBr}_3$  or  $\text{Al}_2\text{Br}_6$  particles are involved. The third order rate constants have been calculated on the assumption that  $\text{AlBr}_3$  is involved, using the formula:

$$k_{\text{III}} = - \frac{6 \times 2.303}{t A_0 (E_0 + 3A_0)} \log \left\{ 1 - \frac{\alpha_t^* (E_0 + 3A_0)}{\epsilon_0^* \cdot E_0} \right\}$$

where:  $t$  = reaction time (sec.);

$A_0$  = concentration of  $\text{AlBr}_3$  (mole/l);

$E_0$  = concentration of ethyl bromide (mole/l);

$\alpha_t^*$  = specific activity of bromine atoms in  $\text{AlBr}_3$  at time  $t$  (counts per minute);

$\epsilon_0^*$  = specific activity of bromine atoms in ethyl bromide at the start of the reaction (counts per minute).

When  $\text{Al}_2\text{Br}_6$  particles should be involved, the values of  $k_{\text{III}}$  should have to be multiplied by 4,  $A_0$  then being the number of moles of  $\text{Al}_2\text{Br}_6$  per litre. The values of  $k_{\text{III}}$  are given in Table I. From these results the value of 11.7 kcal/mole ( $\pm 7\%$ ) is calculated for the energy of activation of this reaction.

The results indicate that from the observation of a rapid exchange reaction it cannot be concluded that carbonium ions must be involved.

TABLE I

Rate of the bromine exchange reaction of ethyl bromide- $^{82}\text{Br}$  with aluminium bromide in carbon disulfide

Temperature (° C)	$k_{\text{III}}$ ( $1^2 \cdot \text{mole}^{-2} \cdot \text{sec}^{-1}$ )		Number of observations
- 26,3	$8,7 \times 10^{-3}$	$\pm 2\%$	38
- 15,1	$19,6 \times 10^{-3}$	$\pm 1\%$	6
+ 0,1	$85 \times 10^{-3}$	$\pm 4\%$	12

§ 3. A preliminary study of the exchange reaction was made in several other solvents, viz. nitromethane, nitrobenzene, ether and acetonitrile. These solvents are known to give complex addition compounds with the aluminium halides. However, nitrobenzene and nitromethane are used extensively as solvents for FRIEDEL-CRAFTS reactions.

In striking contrast with the extremely rapid reaction in carbon disulfide solution it appeared that in these solvents no measurable exchange of bromine atoms occurred up to  $+30^\circ$ . This remarkable difference in reactivity is illustrated by the following figures: in carbon disulfide at  $+0,1^\circ$  50 % of exchange occurred in *10 minutes*, whereas using almost the same concentrations of ethyl bromide and aluminium bromide in nitromethane only 0,3 % of exchange was detected after *18,3 hours* at  $+30^\circ$ .

In one experiment in carbon disulfide solution an amount of nitromethane equivalent to the concentration of aluminium bromide was added; this caused a ten-fold drop of the reaction rate at  $-26,3^\circ$ . Presumably the ethyl bromide has to compete for the aluminium bromide with the nitromethane, which is a much more powerful complexing agent.

Among other things it may be concluded from these experiments that some care should be taken in drawing general conclusions from investigations of the FRIEDEL-CRAFTS reaction in such solvents as nitrobenzene and nitromethane (cf. ref. 4).

§ 4. The isomerisation of alkyl halides by aluminium halides has been noted in many instances. By labelling ethyl bromide with radioactive carbon atoms it was proved that a comparable isomerisation of ethyl bromide takes place under the influence of aluminium bromide:



For the synthesis of the labelled ethyl bromide radioactive barium carbonate was converted into carbon dioxide and treated with 50 % excess of methyl magnesium iodide. The acetic acid was recovered by steam distillation and isolated as potassium acetate (yield 96 %, calculated on barium carbonate). The potassium salt was converted into ethyl acetate by heating with diethyl sulfate at 150° (yield 97 %) and the ester was reduced with lithium aluminium hydride in dry ether (yield 90 %). On heating the alcohol with sulfuric acid and potassium bromide ethyl-[1-<sup>14</sup>C] bromide was obtained (yield 88–94 %).

The distribution of radioactivity over the two carbon atoms in ethyl bromide was determined by conversion into ethanol and subsequent electrochemical oxidation into iodoform and carbon dioxide. Both degradation products were converted into barium carbonate and the activities were determined.

It was checked by a series of independent experiments that during the synthesis and degradation of the ethyl-[1-<sup>14</sup>C] bromide no isomerisations occurred.

The rearrangement reaction was studied by heating solutions of aluminium bromide in ethyl bromide for several hours at temperatures between +25° and +50°. The isomerisation reaction is a rather slow one; after heating a mixture of 50 mmoles of ethyl bromide and 2 mmoles of aluminium bromide for 4,5 hours at +40° only 37,6 (± 0,6) % of rearrangement occurred.

The rate of the reaction was measured at four temperatures using a constant concentration of aluminium bromide. In this way it was possible to measure the apparent energy of activation of the reaction without knowing the dependence of the reaction velocity on the reagent concentrations.

Assuming different reaction mechanisms it turns out that the reaction constant is proportional to

$$k \cdot x = -\frac{1}{2t} \ln \frac{\varepsilon_{1,0}^* - 2\varepsilon_{2,t}^*}{\varepsilon_{1,0}^*}$$

where:  $t$  = reaction time (hrs);

$\varepsilon_{1,0}^*$  = initial specific activity of carbon atom 1 of the ethyl bromide;

$\varepsilon_{2,t}^*$  = specific activity of carbon atom 2 of the ethyl bromide at time  $t$ .

TABLE II  
Isomerisation of ethyl-[1-<sup>14</sup>C] bromide by aluminium bromide

Temperature (° C)		$k \cdot x$ (sec <sup>-1</sup> )	
+ 25.0		$2.83 \times 10^{-6}$	± 4 %
+ 30.0		$4.92 \times 10^{-6}$	± 3 %
+ 40.1		$14.4 \times 10^{-6}$	± 4 %
+ 50.2		$35.3 \times 10^{-6}$	± 4 %



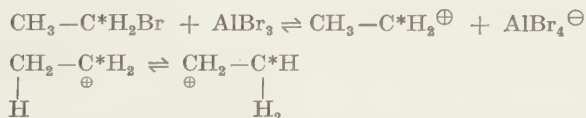
The results are summarized in table II. From these results we have calculated the apparent activation energy of the reaction as: 19,1 kcal/mole ( $\pm 2\%$ ). Without a further knowledge of the reaction mechanism it is not possible to be sure of the exact meaning of this figure. In § 6 we shall return to this point.

§ 5. As aluminium halides catalyse the elimination of hydrogen halides from the alkyl halides and as it is also known that catalysts of this type accelerate the addition of the hydrogen halides to alkenes [7], it was believed for some time that the rearrangement reactions which were frequently observed occurred by elimination and subsequent readdition of hydrogen halide. This hypothesis has been definitely disproved by NASH, TAYLOR and DOERING [8] for the case of the propyl chloride-isopropyl chloride isomerisation. These authors effected the rearrangement of propyl chloride under the influence of aluminium chloride in an atmosphere of deuterium chloride and found that no hydrogen was exchanged for deuterium during the reaction.

In order to exclude this possible mechanism for the rearrangement of ethyl bromide we have studied this reaction in the presence of deuterium bromide (with the collaboration of J. MANASSEN). Deuterium bromide was prepared from deuterium oxide and phosphorus pentabromide. In a sealed tube ethyl bromide, aluminium bromide and deuterium bromide were kept for five hours at  $25^\circ$ . From the results of the rearrangement experiments described in § 4 it was calculated that in this period about 10 % of the ethyl bromide should have been isomerised. The ethyl bromide was isolated, combusted and the combustion water purified and analysed for deuterium. It contained only 0,03<sub>5</sub> ( $\pm 0,01$ ) at. % deuterium in excess.

From this preliminary experiment it is concluded that the rearrangement of ethyl bromide does not occur via elimination and readdition of hydrogen bromide. These experiments are being continued with the collaboration of H. STEINBERG and the final results will be published in the *Recueil des Travaux chimiques des Pays-Bas*.

§ 6. If it is assumed that the isomerisation of ethyl bromide occurs via the formation of ethyl ions which subsequently rearrange by hydride transfer:



then the apparent activation energy of the reaction (19,1 kcal/mole) might have some bearing on the activation energy of the hydride transfer, on the energy necessary for the formation of the carbonium ion or it might even be a function of both quantities. The ultimate exact interpretation will be possible only when a more complete elucidation of the

reaction mechanism has been reached. However, it is of some interest to note that the ethanol formed in the reaction of ethyl-[1- $^{14}\text{C}$ ] amine with nitrous acid contains 1.5 % ( $\pm 0.1$ ) ethanol-[2- $^{14}\text{C}$ ]. This reaction has been studied by ROBERTS and YANCEY [9] and these authors have made it probable that the reaction occurs mainly via the ethyl ion.

In collaboration with Mrs. J. BRACKMAN-BRUGMAN we have reinvestigated this reaction and our results indicate that the ethanol formed contains 1.26 ( $\pm 0.05$ ) % of ethanol-[2- $^{14}\text{C}$ ]. This is in good agreement with the results of ROBERTS and YANCEY.

It is very probable that the half-life time of ethyl ions in aqueous solution is extremely small. From the fact that the hydride ion transfer in the ethyl ion can compete successfully with the very rapid reaction of these ions with water it may be concluded that the rearrangement of the ethyl ion occurs reasonably easy. As on the other hand the isomerisation of ethyl bromide under the influence of aluminium bromide is a rather slow reaction it may be concluded that under these circumstances only a very small amount of ethyl ions is present. If these conclusions are right, the apparent activation energy of this rearrangement reaction may give us some insight into the energy necessary for the formation of the ethyl ion from ethyl bromide and aluminium bromide. Further investigations on the interpretation of our results are in progress.

§ 7. We gratefully acknowledge a grant from the "Van 't Hoff-Fonds" of the Koninklijke Nederlandse Akademie van Wetenschappen, which enabled us to purchase the necessary amount of radioactive barium carbonate and a grant from the "Hoogewerff-fonds" which made available the equipment for the activity determinations.

Radioactive bromine was prepared for us in the cyclotron of the Institute for Nuclear Research (I.K.O.) through the courtesy of Prof. Dr. A. H. W. ATEN Jr, who also kindly put the deuterium oxide at our disposal.

The deuterium analysis was performed in the mass-spectrometer of the Laboratory for Organic Chemistry of the University of Utrecht (Director Prof. Dr. F. KÖGL) through the courtesy of Dr. W. A. J. BORG.

Complete experimental details of this investigation will be published in the *Recueil des Travaux Chimiques des Pays-Bas*.

*Amsterdam, June 1955*

*Laboratory for Organic Chemistry  
of the University of Amsterdam*

#### BIBLIOGRAPHY

1. PRICE, C. C., *Organic Reactions*, Vol. III, 1-82 (John Wiley and Sons, Inc., New York, N.Y., 1947); C. C. PRICE, *Chem. Revs.* **29**, 37 (1941); L. P. HAMMETT, *Physical Organic Chemistry*, p. 309 (Mc. Graw-Hill Book Company, Inc., New York, N.Y., 1940); E. R. ALEXANDER, *Principles of Ionic Organic Reactions*, p. 259 (John Wiley and Sons, Inc., New York, N. Y., 1950).

2. WOHL, A. and E. WERTYPOROCH, Ber. **64**, 1357 (1931); E. WERTYPOROCH, Ber. **64**, 1369 (1931).
3. FAIRBROTHER, F., J. Chem. Soc. **1937**, 503; **1941**, 293.
4. BROWN, H. C. and M. GRAYSON, J. Am. Chem. Soc. **75**, 6285 (1953).
5. FAIRBROTHER, F. and N. SCOTT, J. Chem. Soc. **1955**, 452.
6. BREJNEVA, N., S. ROGINSKY and A. SCHILINSKY, Acta Physicochim. U.R.S.S. **5**, 549 (1936); **7**, 201 (1937); J. Phys. Chem. (U.S.S.R.) **10**, 367 (1937).
7. WIBAUT, J. P. and L. G. BROUWER, Rec. trav. chim. **53**, 1001 (1943); F. R. MAYO and A. A. DOLMICK, J. Am. Chem. Soc. **66**, 985 (1944).
8. NASH, L. M., T. I. TAYLOR and W. VON E. DOERING, J. Am. Chem. Soc. **71**, 1516 (1949).
9. ROBERTS, J. D. and J. A. YANCEY, J. Am. Chem. Soc. **74**, 5943 (1952).

## PALEONTOLOGY

### *MIOGYPSINA* AT PUENTE VIEJO, SPAIN

BY

C. W. DROOGER

(Communicated by Prof. G. H. R. VON KOENIGSWALD at the meeting of Nov. 26, 1955)

*Abstract.* The earlier evidence of nepionic retardation among the *Miogypsinae* of Puente Viejo is contradicted. The assemblages are mainly constituted of drifted elements. With age determinations on larger Foraminifera, care must be taken that the sedimentary environment harmonizes with the life conditions of the organisms. Especially in geosyncline areas, shelled masses of unconsolidated shallow water sediments are frequently intercalated in between *Globigerina* marls.

#### INTRODUCTION

Puente Viejo is an old bridge across the Guadalquivir, and close to the railway station of Jódar on the line from Madrid to Granada. It lies in the area of the former North Betic strait, which connected Atlantic and Mediterranean during part of the Tertiary (COLOM, 1952).

The steeply dressed limestones, intercalated between well-exposed marls, have attracted the attention of several geologists because of their wealth of microfossils. Of these outcrops R. DOUVILLÉ in 1906 gave a detailed discussion with photographs. A number of *Lepidocyclina* species were described or reported from the limestones, first by LEMOINE and R. DOUVILLÉ (1904), later by H. DOUVILLÉ (1925). These authors considered the beds of Aquitanian age because of the similarity of its fauna to that from Saint-Géours in southwestern France, which at that time was (incorrectly) placed in this lowermost Miocene stage.

COSIJN in his thesis (1938) mentioned the limestones of Puente Viejo as an example of transgressive Miocene beds. He found them to contain bipyramidal quartz crystals from the Triassic, *Orbitolina* from the Cretaceous, and *Discocyclina* and *Nummulites* from the Older Tertiary. He added *Miogypsina* to the autochthonous elements of the fauna.

For a statistical analysis of proloculum size COSIJN (1942) used three of the species of larger Foraminifera of Puente Viejo: *Lepidocyclina tournoueri* LEMOINE and DOUVILLÉ, *Miogypsina complanata* SCHLUMBERGER and *Spiroclypeus margaritatus* (SCHLUMBERGER). In this paper he published a sketch of the southern bank of the Guadalquivir, on which he marked the position of his three samples (408-410, 408 being the oldest; our fig. 1).

The *Miogypsinae* of his collections were used for an investigation into the character of the nepionic stage (DROOGER, 1951). In all individuals



the number of nepionic chambers was counted ( $X$ ). COSIJN's material appeared to offer a fine example of nepionic retardation (lengthening of the nepionic spiral in the course of time). This principle was thought to be of restricted application in the evolution of the Miogypsinidae, at least among its older representatives (DROOGER, 1951 and 1952, p. 65).



Fig. 1

Location of COSIJN's samples on the southern bank of the Guadalquivir at Puente Viejo (after COSIJN, 1942).

A grant from the *Molengraaff Foundation* at Delft enabled us to pay a short visit to the locality in 1954. Observations of graded bedding in the limestones proved that the series is not overturned, which is in accordance with the theory of nepionic retardation of the Miogypsinæ. From the limestone breccias of 408 and 410 new samples were taken (408a and 410a respectively). It is unlikely that they were derived from the same layers as COSIJN's samples, but they cannot have been taken at more than a few meters higher or lower. A sample from the accompanying marl (409a) was taken near the level of 409.

The author is gratefully indebted to the *Molengraaff Foundation* at Delft for its financial support which enabled the journey to Spain, and to Mr. P. MEYBOOM (Utrecht) for making the new sections.

#### THE MIOGYPSINÆ

In order to verify the nepionic retardation theory a number of *Miogypsina* specimens was sectioned, both from 408a and from 410a. The results are shown in the next table.

In addition to the previously concluded nepionic retardation in the series 408–409–410, there is a significant decrease in  $M_X$  from 409 to 410a, which suggests nepionic acceleration. Furthermore, there is a very great difference in the  $M_X$  of 410 and 410a, samples that are of nearly the same stratigraphic level.

No	N	R <sub>X</sub>	M <sub>X</sub>	σ <sub>M</sub>	No	N	R <sub>X</sub>	M <sub>X</sub>	σ <sub>M</sub>
410	186	22-9	15.33	0.19	410a	47	19-8	12.4	0.38
409	183	23-7	14.45	0.20					
408	171	19-7	11.58	0.17	408a	28	16-8	12.3	0.42

No = sample number; N = number of individuals; R<sub>X</sub> = observed range of X (= number of nepionic chambers); M<sub>X</sub> = mean of X; σ<sub>M</sub> = standard error of the mean. The stratigraphic order from old to young is given in the table from bottom to top, with the new samples at the level of the corresponding samples in COSIJN's collection.

Evidently, nepionic retardation in the *Miogypsinidae* lost one of its apparently most exact points of evidence.

It is obvious from these confused data that we are not dealing with parts of homogeneous populations. And if regular changes are assumed in any sequence of successive *Miogypsina* populations, the assemblages cannot be autochthonous either. Consequently it is thought very likely that the banks of organic limestone breccia consist of displaced near shore sediments. The separate banks may contain material from unconsolidated earlier sediments of various time levels and in different proportions, as well as from different sources among the original shallow water deposits.

Similar relations were recently found in some Moroccan sections, where organic limestone breccias and conglomerates, both with numerous larger Foraminifera, were found intercalated between marls rich in *Globigerinidae* (DROOGER, 1954). Several other details support the same viewpoint for the Puente Viejo section.

First we have COSIJN's observations on reworked elements from the Triassic, Cretaceous and Older Tertiary. In addition, we found in his collections a few specimens that had been set apart because of their having lateral chambers. As far as could be ascertained these observations were correct, though it was not tried to make further observations on our own material on account of its very moderate state of preservation. In 1951, the meaning of a coexistence of representatives of *Miogypsinoides* and *Miogypsina* s.str. was not yet understood. It has become very likely since that these two subgenera were nowhere contemporaneous in the western Mediterranean area; they succeeded one another. Hence, it is quite probable that all Puente Viejo individuals of *Miogypsina* (*Miogypsinoides*) *complanata* have been reworked.

Yet another observation is favourable to the concept of slided masses. The new samples from the indurated limestones contain several clay slabs, while in the field many hollows were observed in the surface, which might correspond to weathered-out clay lumps just as in the Moroccan beds.

Finally, it must be pointed out that the pseudo-neritic limestones are interstratified with marls, which at least in our sample 409a, is an almost pure fossil *Globigerina* ooze.

The age of the Puente Viejo deposits is difficult to ascertain. In southwestern France *Miogypsina complanata* s.l. and *Lepidocyclus tournoueri* are of pre-Aquitanian, i.e. Late Oligocene age. However, an Early Miocene age of the reworked assemblages is favoured by the presence of *Miogypsina* s.str. individuals. Moreover, the low  $M_x$  values (11.58 in 408) are already partly comparable to those of the Early Aquitanian *M.* (*Miogypsina*) *gunteri* COLE of the *Miogypsina* s.str. series of species.

The planktonic assemblage of 409a gives no opportunity for a choice between Late Oligocene and Early Miocene. The *Globigerina* fauna is composed of numerous specimens of various sizes with maximal diameter of 0.7 mm. The dominant form is *Globigerina dissimilis* CUSHMAN and BERMUDEZ with *G. mayeri* (CUSHMAN and ELLISOR) and *G. cf. bulloides* D'ORBIGNY among the smaller variants, *G. venezuelana* HEDBERG among the larger ones. Some individuals are identical with *G. concinna* REUSS; they are large, five-chambered variants of our *G. cf. bulloides*. This association is considered comparable to that of the *G. dissimilis* zone of Trinidad (BOLLI, 1951, a.o.). According to more recent, unpublished data, this Trinidad zone probably corresponds mainly to the European Early Miocene, but it may range down into the Latest Oligocene.

#### GENERAL COMMENTS

Another, more general conclusion from the Puente Viejo outcrops is concerned with the reliability of larger Foraminifera for age determinations. Many of these organisms are highly valuable index fossils because of their belonging to evolutionary series. However, their sedimentary environment should be carefully considered. Their occurrences, often in abundance, in organic limestones that are interbedded between *Globigerina* marls, are suspicious, even if homogeneous populations seem to be present. The larger Foraminifera point to a shallow-water environment, whereas dominant *Globigerina* faunas occur mainly in the deeper parts of the open ocean.

In order to avoid the assumption of repeated and very great changes of sea level, earlier authors have pointed out that planktonic faunas may occur in relative abundance in neritic environments. This is an exception, however, and it does not account for the frequently observed alternations of both types of sediment. The *Globigerina* beds, as for instance those of Puente Viejo and Morocco, have the character of *Globigerina* oozes with absence or slight percentage of benthonic faunas and of clastic material. They must have been formed in quiet, deeper water with little or no deposition of terrigenous matter.

The sudden and repeated intercalation of limestones with many, usually fragmentary, shallow water organisms points to their secondary character as slid masses of unconsolidated material. If this material was more indurated, we get slip masses and the Wildflysch type of sediment, the importance of which has recently been demonstrated by KUGLER (1953)



for the Tertiary sedimentary series of Trinidad. Slip masses are more easily recognized as such, than the displaced unconsolidated material, which by more or less turbulence during the transport may again have acquired most of the features of homogeneous sediments.

The organisms in the displaced sediments may be contemporaneous, or nearly so, with those in the deeper water beds. So, for instance, the majority of the Puente Viejo larger Foraminifera is probably not much older than the accompanying *Globigerina* fauna. Elsewhere the displaced Foraminifera are much older, such as they are in the limestones of the Moroccan series. The real age of the latter beds could only be ascertained from the few youngest specimens in the extensive collections prepared by BRONNIMANN. Finally the displaced sediments may contain a mixture of organisms from several time levels. In this connection we may recall the opinion of Italian micropaleontologists at the beginning of this century, that larger Foraminifera had but a trifling value as index fossils, since they had been encountered in the Italian peninsula in all kinds of associations in rocks of various Tertiary time levels.

These displacement phenomena are evidently the most common in and near orogenic belts, where repeated movements forced much of the shallow water sediments to slide into deeper parts of the adjoining basins.

#### REFERENCES

- BOLLI, H., Notes on the direction of coiling of rotalid Foraminifera. Contrib. Cushman Found. Foram. Res., **2**, 139-143 (1951).
- COLOM, G., Aquitanian-Burdigalian Diatom deposits of the North Betic strait, Spain. Journ. Pal., **26**, 867-885 (1952).
- COSIJN, A. J., Statistical studies on the phylogeny of some Foraminifera. Acad. thesis Delft (1938).
- , On the phylogeny of the embryonic apparatus of some Foraminifera. Leidsche Geol. Meded., **13**, pt. 1, 140-171 (1942).
- DOUVILLÉ, H., Révision des Lépidocyclines. Mém. Soc. géol. France, new ser., mem. **2**, 1 and 2 (1925).
- DOUVILLÉ, R., Esquisse géologique des Préalpes Subbétiques, partie centrale. Thesis Paris (1906).
- DROOGER, C. W., Notes on some representatives of Miogypsinella. Proc. Kon. Ned. Ak. Wetensch., ser. B, **54**, 357-365 (1951).
- , Study of American Miogypsinidae. Acad. thesis Utrecht (1952).
- , Miogypsina in northwestern Morocco. Proc. Kon. Ned. Ak. Wetensch., ser. B, **57**, 580-591 (1954).
- KUGLER, H. G., Jurassic to recent sedimentary environments in Trinidad. Bull. Ass. Suisse des Géol. et Ing. du Pétrole, **20**, no. 59, 27-60 (1953).
- LEMOINE, P. and R. DOUVILLÉ, Sur le genre *Lepidocyclina* Gümbel. Mém. Soc. géol. France, mem. **32**, 12 (1904).



## CHEMISTRY

### ELECTROCHEMICAL BEHAVIOUR OF ION-EXCHANGING SUBSTANCES

#### XI. ROOT POTENTIALS IN NaCl AND KCl SOLUTIONS

BY

D. MACGILLAVRY

(Communicated by Prof. C. H. MACGILLAVRY at the meeting of September 24, 1955)

#### *Summary*

Potential measurements of Lucerne clover in NaCl and in KCl solutions are discussed further and regression equations for the two media are derived. An interpretation in terms of Donnan potentials is favored.

In a recent publication <sup>1)</sup> on ion-exchanging substances a preliminary investigation of root potentials in NaCl solutions was described. Seedlings of Lucerne clover, Medicago Sativa, were measured first in NaCl and then in a corresponding set of KCl solutions <sup>2)</sup>.

The average potentials for the first series of ten seedlings are given in Table I.

TABLE I  
*Average Root Potentials*

Molarity NaCl				Molarity KCl			
10 <sup>-5</sup>	10 <sup>-4</sup>	10 <sup>-3</sup>	10 <sup>-2</sup>	10 <sup>-5</sup>	10 <sup>-4</sup>	10 <sup>-3</sup>	10 <sup>-2</sup>
- 15.5	- 14.8	+ 4.2	+ 35.8	- 41.3	- 34.4	+ 3.5	+ 40.0

A variance analysis of results showed an effect due to the medium, NaCl or KCl, and an interaction of concentration x medium.

The investigation of potentials in NaCl and KCl solutions has been extended. Conditions were modified from time to time. For one short series of measurements on six seedlings conditions were as follows. The seedlings were grown in nutrient solution. Root potentials were measured first in KCl and then in NaCl solutions <sup>3)</sup>.

Regardless of these and other differences of conditions, it was found

<sup>1)</sup> H. J. C. TENDELOO and D. MACGILLAVRY, Proc. Konink. Ned. Akad. v. Wetenschappen, **57**, 509 (1954) VIII.

<sup>2)</sup> All solutions contained  $5 \times 10^{-5}$  N HCl to get a small but better defined concentration of H-ions.

<sup>3)</sup> An account of these new measurements will be published elsewhere as number X of this series.

regularly that potentials varied less with NaCl concentration than with KCl concentration. This held true even for a somewhat narrower range of concentrations. Thus, it appears appropriate to carry the variance analysis of results presented in publication VIII a step further and to give regression equations for the potentials on concentration in the two media.

*Analysis of the concentration effect. Regression equations*

Data for NaCl and KCl may be analyzed separately. Otherwise, all results of publication VIII can be taken together, since neither pretreatment nor type of electrometer used seemed to influence results. The variance analysis for each medium separately is given in Table II.

TABLE II  
*A. Root potentials in NaCl<sup>2</sup>) solutions*

Source of variation	Sum of squares	Dimension	Variance estimate
concentration . . . . .	17,350.48	3	5,783.49
roots . . . . .	8,125.53	9	902.84
residual . . . . .	823.77	27	30.51
Total	26,299.78	39	

*B. Root potentials in KCl<sup>2</sup>) solutions*

Source of variation	Sum of squares	Dimension	Variance estimate
concentration . . . . .	42,420.9	3	14,140.3
roots . . . . .	3,764.9	9	418.3
residual . . . . .	1,360.1	26	52.3
Total	47,545.9	38	

The analysis of the concentration effects is given in Table III. Since each of the three components has the dimension 1, each corresponding sum of squares at once gives a variance estimate.

TABLE III  
CONCENTRATION EFFECT  
*A. Potentials in NaCl solutions*

Components	Sum of squares and variance	Dimension	Coefficients orthogonal polynomia
linear . . . . .	14,947.2	1	8.6 <sub>4</sub>
quadratic . . . . .	2,387.0	1	7.7 <sub>3</sub>
cubic . . . . .	16.2	1	- 0.2 <sub>0</sub>
Total	17,350.5	3	

*B. Potentials in KCl solutions*

Components	Sum of squares and variance	Dimension	Coefficients orthogonal polynomiala
linear . . . . .	39,705.6	1	14.0 <sub>9</sub>
quadratic . . . . .	2,190.4	1	7.4 <sub>0</sub>
cubic . . . . .	524.9	1	— 1.6 <sub>2</sub>
Total	42,420.9	3	

It is seen that the cubic component for the NaCl solutions is not significant.

On account of a cubic component for KCl solutions, an inflection point can be calculated. It is found at  $\log (M \text{ KCl}) = -3.04$ , in the range of concentrations used. For the KCl solutions without HCl <sup>4)</sup> it was found at  $-2.71$  and  $-2.87$ . The confidence intervals were rather wide. The smaller one had the limits  $x_1 = -3.03$  and  $x_2 = -2.64$ . Hence, in this respect it is doubtful whether the addition of a small concentration HCl had any effect on the inflection point.

The regression equations for potential  $y$  on  $\log (M \text{ NaCl}) = x_1$ , resp.  $\log (M \text{ KCl}) = x_2$  are

$$y = +114 + 38.4 x_1 - 2.25 x_1^2 - 0.95 x_1^3$$

$$y = -20.8 - 107.4 x_2 - 49.30 x_2^2 - 5.40 x_2^3.$$

Cubic components were retained for NaCl as well as for KCl. The coefficients of the regression equation for the KCl–HCl solutions came out larger than those of the corresponding equation for the KCl solutions discussed in IX. This has little influence on the trend of the  $y$ -values in the range of interest. The constant small addition of HCl makes little difference in this respect.

*Discussion*

It was found on several occasions, that in the most dilute solutions stationary potentials might be established at more than one level. One value might fit in the regular pattern, but a less negative potential did not. At this stage it is difficult to tell in how far averages for the more dilute solutions were affected by these peculiarities. These phenomena could well be due to physiological influences.

For the time being it might be best to characterize the different behaviour of potentials in NaCl and in KCl solutions simply by the linear slope between the molarities  $10^{-4}$  and  $10^{-2}$ . All roots were measured at these two concentrations while other concentrations were selected differently.

<sup>4)</sup> See IX, D. MACGILLAVRY and H. J. C. TENDELOO, Proc. Konink. Ned. Akad. v. Wetenschappen, 57, 513 (1954).

For the series of reference VIII the slopes are

$$\begin{aligned} \text{for NaCl } \frac{1}{2} (35.8 + 14.8) &= 24 \text{ mV/log M unit} \\ \text{for KCl } \frac{1}{2} (40.0 + 34.4) &= 37 \text{ mV/log M unit} \end{aligned}$$

and for the series of reference X

$$\begin{aligned} \text{for NaCl } &24 \text{ mV/log M unit} \\ \text{for KCl } &32 \text{ mV/log M unit.} \end{aligned}$$

Whereas the slopes for the two NaCl series differ hardly, there might be a significant difference for the two slopes for KCl. With the long series of VIII the solution above the gelatin contained  $10^{-2}$  M KCl -  $10^{-4}$  M HCl; with the short series of X no HCl was added to the reference solution. Whereas taking measurements was more convenient in the latter case and the spreads for the individual solutions might well be different, no significant difference may be claimed for the two estimates 37 and 32. This was checked with Student's *t*-test and by a variance analysis of the KCl potentials at the molarities  $10^{-4}$  and  $10^{-2}$ . The two tests gave identical results, as it should be.

As some difficulty was experienced in obtaining stationary potentials, the measuring error of individual measurements was estimated for each medium and also for each concentration separately. The respective variance estimates (see Table IV) bring out the greater uncertainty of potential measurements in the more dilute solutions, especially for KCl solutions.

TABLE IV  
*Variance Estimated for Individual Measurements*

Medium	NaCl				KCl			
Variance estimate	42.9				122.2			
Concentration	$10^{-5}$	$10^{-4}$	$10^{-3}$	$10^{-2}$	$10^{-5}$	$10^{-4}$	$10^{-3}$	$10^{-2}$
Variance estimate	77.9	43.0	15.2	33.4	207.7	194.2	33.1	11.7

It was stressed that the dilute KCl solutions appeared to give ambiguous potentials. What seemed to be the better established potentials were selected. The large spread of these potentials, however, seems to indicate that potentials in the dilute solutions of this series somehow vagrate within a fairly wide range.

In the work under discussion a small content of HCl ( $10^{-4}$  M) was added to the reference solution and  $5 \times 10^{-5}$  M HCl was added to all the bathing solutions.

In a forthcoming publication (XII) an investigation of adding increasing amounts of HCl to the external solutions will be discussed. No HCl was added to the reference solution. It was found that residual variance was reduced a great deal. In view of these results it appears that adding at least a small amount of HCl to the bathing solution is beneficial. Adding  $10^{-4}$  M HCl to the reference solution is not desirable, perhaps because



of an irritation effect or of some other physiological interference.

Potential measurements at broad bean roots in several neutral salt solutions were reported by HOPE and STEVENS<sup>5)</sup>. The plot of average potentials in KCl solutions vs. log molarity was considered to be linear. An interpretation in terms of diffusion potentials of KCl diffusing through the membranes was proposed.

The analysis of our own data for Lucerne clover indicates that the concentration effect has at least a second degree component for both salts, KCl and NaCl, and even a third degree component for KCl.

The slopes found by HOPE for broad bean roots are 32 mV/log M unit for KCl and 28 mV/log M unit for NaCl. They are about as steep as found by us for Lucerne clover, but the difference is less marked and might not be significant.

In a recent publication HOPE<sup>6)</sup> investigates the diffusion of KCl into roots on increasing the KCl concentration of the external solution. It was found that after transient diffusion of KCl has subsided stationary states result. Much slower rates of uptake of individual ions persist apparently in accordance with physiological requirements. The stationary states could be explained in terms of changes effected in simple Donnan systems.

In earlier communications by us it was proposed to explain the behaviour of root potentials in terms of Donnan equilibria. An experimental point might be stressed. We found that the times required for establishing steady potentials vary from a few minutes to 20 or 30 minutes. The surges of KCl diffusion also take times of about 20 minutes. It then becomes probable that the two types of phenomena are related and that the interpretation of both in terms of Donnan equilibria is to be preferred.

In a forthcoming publication on potentials in KCl-HCl solutions with varying HCl concentration more definite and direct information about the Donnan equilibria established is presented. Estimates of the pH at the effective isoionic points and also of the buffer capacity of the non-permeating root material are derived. For Lucerne clover an order of magnitude of  $0.6 \times 10^{-2}$  M was estimated for the buffer capacity of the root material.

#### *Acknowledgements*

Thanks are due to Prof. Dr. N. H. KUIPER, Ir. L. C. A. CORSTEN and Mr. F. E. ESSED of the Department of Mathematics for advising about questions of variance analysis.

*Laboratory for Physical and Colloid Chemistry  
Agricultural University, Wageningen, The Netherlands*

---

<sup>5)</sup> A. B. HOPE, Australian J. Sci. Res. B **4**, 265 (1951).

A. B. HOPE and P. G. STEVENS, *ibid.* B **5**, 335 (1952).

<sup>6)</sup> A. B. HOPE, Australian J. Sci. Res. B **6**, 396. (1953).

## PHYSICS

# DEUTERIUM CONTENT OF SOME NATURAL ORGANIC SUBSTANCES <sup>1)</sup>

BY

C. BOKHOVEN AND H. H. J. THEEUWEN

(Communicated by Prof. J. H. DE BOER at the meeting of December 17, 1955)

### 1. *Introduction*

Recent measurements [1] of the deuterium content of natural waters indicate that ocean waters range from 0.0153–0.0156 mole % D. Though fractionation by evaporation and condensation processes may account for local deviations, it seems obvious to assume that at present the abundance ratio on earth amounts to about 1 to 6500.

Up till now, however, there is not much reliable information <sup>2)</sup> about the abundance ratio in natural organic substances such as coal, the hydrogen of which has its origin in some natural water. Therefore, an investigation of the abundance ratio in coal samples of different age might give information about this ratio in water at the time of the formation of the coal.

The object of this investigation was to determine the abundance ratio in coal and other organic substances (wood, petroleum, fatty acids, sugar, ethyl alcohol). However, in connection with the possibility of using hydrogen from coal (coke oven gas) for the production of heavy water, the deuterium content of this hydrogen source was also determined.

### 2. *Experimental* <sup>3)</sup>

The hydrogen-deuterium ratio was always measured on hydrogen gas by means of a Metropolitan Vickers MS 3 type (10 cm, 90°) mass spectrometer.

The organic materials were burnt in dry oxygen (free from hydrogen) after drying at 105° C with nitrogen, after which the water samples were reduced with zinc at about 400° C, according to the method given by FRIEDMAN [1]. Care was taken to ensure that the reduction of the water sample was complete and that all the hydrogen formed was pumped into

---

<sup>1)</sup> The preliminary results of this investigation have already been communicated by Prof. J. H. DE BOER at the "Symposium on production of heavy water" organized by the European Atomic Energy Society at Rome, March 31st–April 2nd, 1955. (See Proceedings of the symposium, p. 89).

<sup>2)</sup> A critical review of the older data, which are all based on density measurements, has been given by M. DOLE, J. Am. Chem. Soc., 58, 580 (1936).

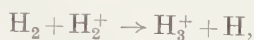
<sup>3)</sup> A more detailed account will be given elsewhere.

the sample bottle. It appeared that no fractionation and memory effects occurred.

As it was found that the mass 3 peak is affected by methane, it was necessary for the analysis of coke oven gas to separate hydrogen from methane. This was performed by oxidation of the hydrogen with CuO at 275° C, after which methane was also burnt to water by means of a hot platinum wire.

The H/D ratio was measured by comparing alternately (by means of the double inlet system) the mass-3 peak of the sample with that of a working standard (Central Laboratory tap water) at equal height of the mass-2 peaks.

In this way the contribution of  $H_3^+$ , according to:



need not be taken into account. Nevertheless, the formation of  $H_3^+$  ions was minimized in the usual way: by applying an ion repeller voltage of about 10 V. by working at the maximum value of the accelerating voltage (2000 V) and at moderate pressures.

By using the recorder (a typical diagram is given in the annexed figure) it was possible to distinguish between samples differing by at least 0.0002 mole % D. The results were brought on an absolute scale by applying the method of CLARKE, DENTON and REYNOLDS [2]. According to this method the deuterium content of our standard amounts to  $0.0150 \pm 0.0004$  mole % D. <sup>4)</sup>

### 3. Results

#### a) Coal samples, mine gas, hydrogen and methane from coke oven gas

Two coal samples of completely different origin and age were taken, a low rank (bituminous coal of State Mine Emma, the Netherlands) and a high rank coal (Donetz anthracite). The hydrogen content of these coals amounted to 4.9 and 2.4 % by weight respectively.

From the results summarized in the annexed table, it appears that the coal is depleted significantly with respect to our standard water of 0.0150 mole % D. The same depletion was also found for a sample of methane of the mine gas drainage of State Mine Hendrik (the Netherlands). On the other hand, however, it appeared that the hydrogen from coke oven gas in all stages of a gas separation plant <sup>5)</sup> is much more

<sup>4)</sup> In some cases a 3/2 ratio versus pressure plot was extrapolated to zero pressure. In this way a value of 0.015<sup>0</sup>–0.015<sup>5</sup> mole % D for our standard was obtained. The relative accuracy of this method amounted to  $\pm 0.0005$  mole % D.

<sup>5)</sup> In a gas separation plant the coke oven gas (60 % H<sub>2</sub>, 25 % CH<sub>4</sub>) is subsequently separated into its constituents i.e. H<sub>2</sub>, CH<sub>4</sub>, CO, C<sub>2</sub>H<sub>4</sub> at several gas separation stages.

depleted (0.0125 mole % D)<sup>6)</sup>, whilst the deuterium content of the methane from this gas amounts to 0.0150 mole % D. With a view to the result on mine gas it is probable, however, that the latter results are caused by the exchange reaction:



which may take place in the manufacture of the coke oven gas.

b) Beech wood, lignin, cellulose, petroleum, fatty acids, beet sugar and ethyl alcohol

In connection with the results on coal samples mentioned above, the question arises whether all coals ranging from peats (through the lignites) to bituminous coals and anthracites are depleted. Therefore we determined the deuterium content of a piece of young beech wood, and of lignin and cellulose both originating from wood. From the table (anex) it appears

#### ANEXE

##### DEUTERIUM CONTENT OF SOME NATURAL ORGANIC SUBSTANCES

	Mole % D *)
Anthracite (Donetz): tertiary . . . . .	0.0141
Bituminous coal (State Mine Emma, the Netherlands): carboniferous . . . . .	0.0141
Beech wood . . . . .	0.0142
Lignin . . . . .	0.0141
Wood-cellulose . . . . .	0.0150
Crude petroleum: permian . . . . .	0.0141
"      "      : hurassic . . . . .	0.0141
"      "      : cretacious . . . . .	0.0140
"      "      : miocene . . . . .	0.0141
Saturated fatty acids from palm oil . . . . .	0.0123
Saturated fatty acids from tallow . . . . .	0.0122
Beet sugar . . . . .	0.0148
Natural (fermentation) alcohol . . . . .	0.0117
Synthetic (from ethylene) alcohol . . . . .	0.0136
Hydrogen of OH group of both natural and synthetic alcohol . . . . .	0.0150

\*) All values were obtained by comparison with our standard (Central Laboratory tap water), with a deuterium content of  $0.0150 \pm 0.0004$  mole % D.

that for wood and lignin the same deuterium content (0.0141 mole % D) was found as for the coal samples. The deuterium content of 0.0150 mole % D of wood cellulose is not a matter for surprise. For it was found by BADGLEY, FRILETTE and MARK [3], that the hydrogen of the primary hydroxyl groups of cellulose (wood pulp) is already easily exchangeable

<sup>6)</sup> It should be remarked that the enrichment of the small amount of hydrogen dissolved in the liquid ethylene-, methane and nitrogenfraction (separation factor 1.2, 1.3 and 1.4 respectively) does not affect this figure appreciably.



at 25° C. Therefore it is conceivable that under the severe conditions of the pulping process the secondary hydroxyl groups or even the non hydroxyl hydrogen will also exchange.

Leaving aside the problem of the fixation of the abundance ratio during the coalification process, the depletion of deuterium in wood and coal might be ascribed to an isotope effect in photo synthesis. This view is supported by the results of old measurements of REITZ and BONHOEFFER [4], who found that certain algae incorporate deuterium to only 30–70 % of its concentration in the nutrient solution, and by the recent measurements of WEINBERGER and PORTER [5] on the incorporation of tritium and deuterium oxide into algae. It seems logical to assume that fractionation of hydrogen and deuterium generally occurs in biological systems<sup>7)</sup>. It should be expected in this connection that all natural organic products from both animal and plant origin are more or less depleted in deuterium. To check this hypothesis we tested samples from:

- a) crude petroleum of different geological origin<sup>8)</sup>
- b) saturated fatty acids obtained from palm oil and tallow respectively<sup>8)</sup>
- c) sucrose (beet sugar)
- d) ethyl alcohol originating both from a fermentation process and from ethylene.

The results of these measurements are also given in the table (anex). In agreement with the results on coal samples the deuterium content of the hydrogen in crude petroleum (0.0141 mole % D) seems also to be independent of the geological age. From this it may be concluded that the hydrogen isotope abundance ratio has been constant for a period of many tens of millions of years.

The results with fatty acids show that both in the plant and in the animal organism the synthesis of fats proceeds with an appreciable isotope effect<sup>9)</sup>.

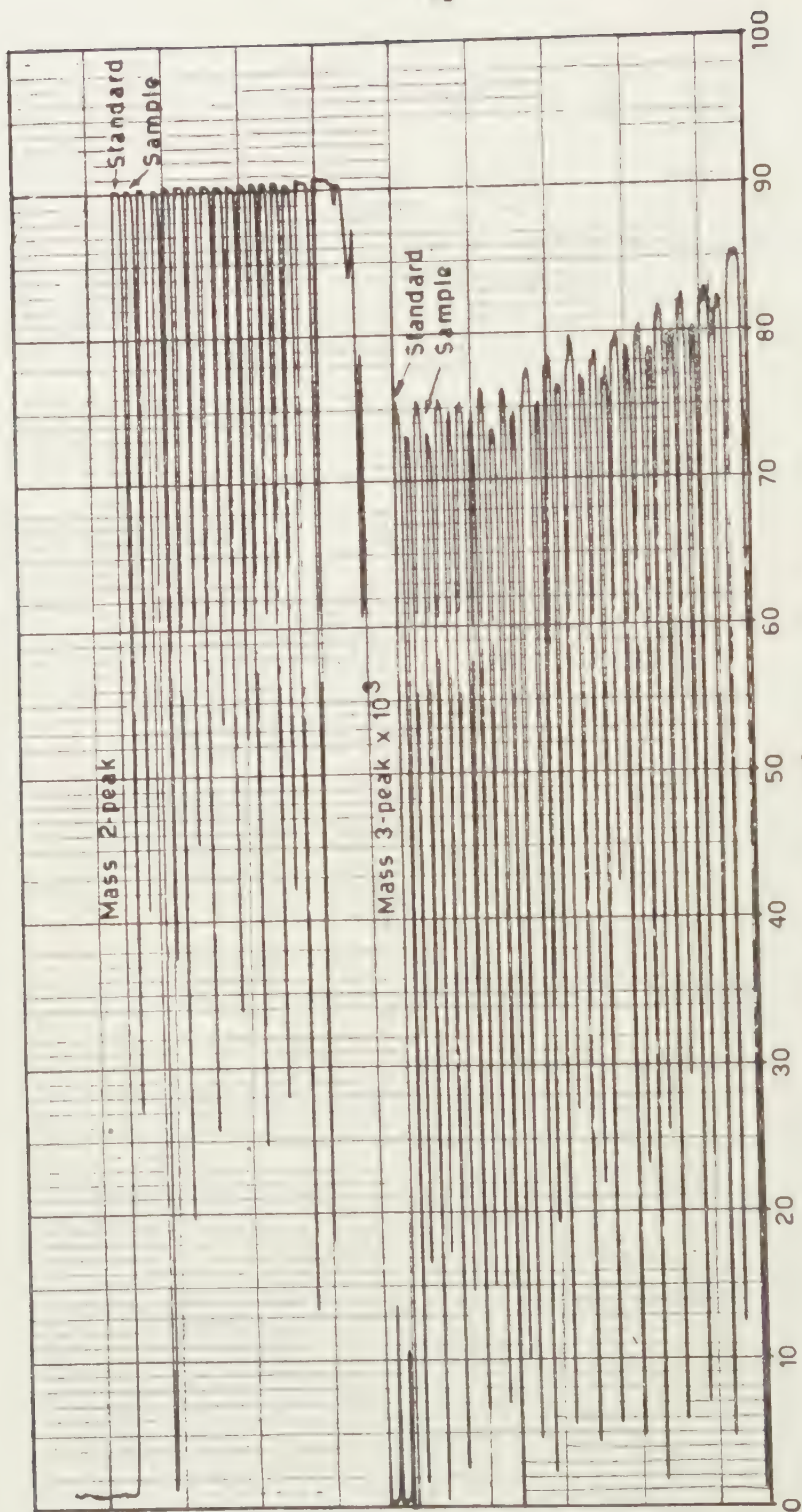
Contrary to the large depletion of the fatty acids, almost the normal abundance ratio was found for the hydrogen in beet sugar (0.0148 mole % D). This figure is probably not comparable with the true deuterium content of sucrose in sugar beets. From exchange experiments with sucrose and D<sub>2</sub>O (99.5 mole % D), it appeared that the hydroxyl hydrogen (8 out of the 22) will certainly exchange during the sugar manufacture.

It is probable that after the processing of natural products the easily exchangeable hydrogen atoms of hydroxyl groups have the normal

<sup>7)</sup> A recent example of D: T fractionation in liver glycogen of rats is given by EIDINOFF *et al.*, J. Am. Chem. Soc., 75, 248 (1953).

<sup>8)</sup> The authors are indebted to the "Unilever Research Laboratorium" at Vlaardingen and the "Koninklijke Shell Laboratorium" at Amsterdam for the samples used in this study.

<sup>9)</sup> It is assumed that during the saponification and successive crystallisation no appreciable exchange occurs on the carbon hydrogen bond.



$$\frac{\Delta \text{Mass 3}}{\text{Mass 2}} = \frac{1.48 \times 10^{-3}}{89.8} = 0.0165 \times 10^{-3}$$

Depletion 0.0008 mole %

Recorder-diagram for a measurement on hydrogen from a coal sample

abundance ratio, and the hydrogen bound to carbon atoms is depleted <sup>10</sup>). This is confirmed by the measurements on fermentation alcohol and on alcohol manufactured from the ethylene fraction of the coke oven gas by means of sulfuric acid and successive saponification with steam. It appears (see the table), that on the one hand fermentation alcohol is more depleted than alcohol from ethylene (deuterium content of the combustion water 0.0117 and 0.0136 mole % D respectively), while on the other hand the hydrogen of the hydroxyl group has in both cases the normal abundance ratio (0.0150 mole % D). This could be proved by quantitative reduction of the alcohol by means of a sodium suspension in water-free xylene.

It will be clear that the difference in the hydrogen abundance ratio in natural and synthetic alcohol is large enough to be used for identification purposes. This method can be extended to other cases, where it is important to distinguish between the natural and the synthetic product.

Summarizing we may say that valuable information may be obtained by determining the hydrogen isotope abundance in organic substances. Though exchange during the processing may have occurred in some cases, the examples given above clearly illustrate that appreciable fractionation effects may take place in different biochemical processes.

*Staatsmijnen in Limburg, Centraal Laboratorium,  
Geleen, The Netherlands*

#### LITERATURE

1. FRIEDMAN, J., *Geochim. Cosmochim. Acta*, **4**, 89 (1953).
2. CLARKE, G. R., W. H. DENTON and P. REYNOLDS, *Nature*, **174**, 469 (1954).
3. BADGLEY, W., V. J. FRILETTE and H. MARK, *Ind. Eng. Chem.*, **37**, 227 (1945).
4. REITZ, O. and K. F. BONHOEFFER, *Z. Phys. Chem.*, **A 172**, 369 (1935).
5. WEINBERGER, D. and J. W. PORTER, *Science*, **117**, 636 (1953); *Arch. Biochem.*, **50**, 160 (1954).

---

<sup>10</sup>) A study of hydrogen exchange reactions of the butanes in sulfuric acid by OTVOS *et al.*, (*J. Am. Chem. Soc.*, **73**, 5741 (1951)) has revealed that neither the primary nor the secondary hydrogens of *n*-butane exchange with 96.2 per cent H<sub>2</sub>SO<sub>4</sub> at 25° C.





BIOLOGICAL PROCESSES IN THE ESTUARINE ENVIRONMENT

III. ELECTROCHEMICAL CONSIDERATIONS REGARDING  
THE SULPHUR CYCLE

BY

L. G. M. BAAS BECKING AND I. R. KAPLAN \*)

(Communicated at the meeting of June 25, 1955)

SUMMARY

1. The applicability of chemical thermodynamics to the metabolism of autotrophic bacteria may be widened by the introduction of hydrogen together with hydrogen ions into the chemical equation, and furthermore by considering as a second parameter the numbers of oxygen molecules per molecule of oxidizable material.

2. The Eh-pH relation tends to boundary conditions, one for  $dE/dpH \rightarrow 0$  or  $\Delta pH = 0^{**}$ ) (pH is indeterminate, Eh is constant) and no hydrogen (or hydroxyl) ions are involved, and one in which  $dE/dpH \rightarrow \infty$  where there is no electron transfer (pH is constant, Eh is indeterminate).

3. A relationship is derived to convert  $E^0$  for acidic conditions into  $E^0$  of the same reaction carried out under alkaline conditions at equilibrium.

4. The generalized equations of a number of reactions are considered.

INTRODUCTION

In a former communication (BAAS BECKING and WOOD, 1955) the environmental characteristics of a number of microbes, algae and sulphur bacteria (*sensu latiore*) were considered. The oxidation-reduction potentials (Eh) and the pH of the environments were shown to be characteristic of specific microbial groups. It seemed tempting to find a theoretical background for these relations.

The authors of this paper cannot share the view of many that certain reactions considered by us are invalid at room temperature and atmospheric pressure, because of their irreversibility, and therefore cannot take place in the living system. The living cells (and in many cases even their enzyme systems), are capable of so many reactions (like nitrogen-fixation) which, in technology, would require high pressures and temperatures, that these objections lose much of their value.

We are aware that we should tread softly on the dangerous road of the rigid application of physical chemistry to vital phenomena. We have

---

\*) Officers of the Division of Fisheries, C.S.I.R.O., Cronulla, Australia.

\*\*)  $\Delta pH$  taken as abbreviation of  $\Delta Eh/\Delta pH$ .

done this with the feeling that, even if a quantitative approach is still unwarranted, there may be enough evidence to indicate some important trends. For instance, the repeated observation by BAAS BECKING and WOOD of an anaerobic "oxidation" of sulphur and of thiosulphate finds its logical explanation in an elementary consideration of the thermodynamics of these reactions. In a similar manner the sharp environmental limits of certain microbes at a fixed pH, or a limit set by a given oxidation-reduction potential over a large pH range, also find their explanation.

At the outset, it may be useful to clarify certain misunderstandings which exist at present in the literature dealing with electrochemical changes, which might lead to unnecessary confusion. This applies in particular to the sign convention used at present. A reaction is considered of the following type.



From the van 't Hoff isotherm it follows,

$$\Delta F = \Delta F^0 + RT \ln \frac{(a'_C)^c (a'_D)^d}{(a'_A)^a (a'_B)^b}$$

$$(1) \quad = \Delta F^0 + RT \ln Q$$

where  $a'$  is the activity of the different entities,  $Q$  the activity quotient and  $\Delta F^0$  is the free energy change in the standard state. This free energy change may be expressed as nett electrical energy;

$$(2) \quad \Delta F = -nE\mathcal{F}$$

where  $\mathcal{F}$  is one faraday, equivalent to 23,060 calories per volt and  $n$  the number of electrons involved. The negative sign indicates useful energy released. Thus from (1) and (2)

$$-nE\mathcal{F} = -nE^0\mathcal{F} + RT \ln Q$$

or

$$(3) \quad E = E^0 - \frac{RT}{n\mathcal{F}} \ln Q$$

As examples the hydrogen- and the oxygen couple are mentioned. The pH-Eh relations for these couples form a lower and an upper boundary for the region in which most biological processes occur<sup>1)</sup>.

$$(4) \quad H_2 \rightleftharpoons 2H^+ + 2e^-, E^0 = 0.000 \text{ volts (by definition)}$$

and

$$(5) \quad H_2O \rightleftharpoons \frac{1}{2}O_2 + 2H^+ + 2e^-, E^0 = -1.23 \text{ volts } ^2)$$

<sup>1)</sup> According to GERSMANN (1955) the theoretical value, calculated for the oxygen couple is rarely, if ever, attained, as agrees with our own observations. At the other hand, under hydrogen pressures or when organic media are used, overvoltages have been frequently recorded beyond the hydrogen boundary.

<sup>2)</sup> LATIMER (1952).

from (4)

$$\begin{aligned}
 E_h &= -0.06 \log \frac{c_{H^+}}{P^{\dagger} H_2} \\
 &= 0.06 \text{ pH} + 0.03 \log PH_2 \\
 (6) \quad &= 0.06 \text{ pH at one atmosphere}
 \end{aligned}$$

from (5)

$$\begin{aligned}
 E_h &= -1.23 - 0.03 \log \frac{[H^+]^2 P^{\dagger} O_2}{H_2O} \\
 &= -1.23 + 0.06 \text{ pH} - 0.015 PO_2 \\
 (7) \quad &= -1.23 + 0.06 \text{ pH at one atmosphere}
 \end{aligned}$$

This refers to a reduction equation with uptake of electrons. In the convention we have used (which has been adopted in Europe, and is the one by which the Jones Electrometer described by BAAS BECKING and WOOD, Part II was calibrated), the signs are reversed. As we have considered only oxidation equations, but still using Latimer's (1952) data, we calculate  $E^0$  using the relationship  $\Delta F^0 = +nE^0 \mathcal{F}$ .

In consequence (6) changes into

$$(8) \quad E_h = -0.06 \text{ pH}$$

and (7) into

$$(9) \quad E_h = 1.23 - 0.06 \text{ pH}$$

or, in general

$$(10) \quad E_h = E^0 + \frac{RT}{n\mathcal{F}} \ln \frac{Ox}{Red}$$

A positive value for a redox potential means that the oxidized form of the couple is a stronger oxidizing agent than hydrogen ions are, and that the reduced form is a weaker reducing agent than gaseous hydrogen. A negative value implies that the oxidized form is a weaker oxidizing agent than hydrogen ions are, and that the reduced form is a stronger reducing agent than gaseous hydrogen.

#### FORMULATION OF OXIDATION-REDUCTION EQUATIONS

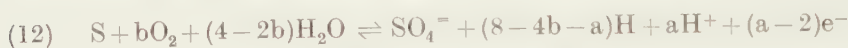
In considering a number of reactions expressing empirical relations the following conditions must be imposed. (a) There should be electron transfer and (b) hydrogen ions or hydroxyl ions should be involved in order to calculate both  $E^0$  from  $\Delta F^0$ , and also to interpret the slope of the Eh-pH curve  $dE/dpH$  (or  $\Delta pH$ ) at equilibrium conditions. In addition to this (in order to make the system biologically acceptable) hydrogen itself should be considered. This hydrogen, the universal fuel of the living cell, which we will call the "Kluyverian" hydrogen, neither represents the molecular nor the atomic states but rather the result of  $H^+ + e^-$ , the combination of a hydrogen ion and an electron. The hydrogen has to be made available in the reaction, or to be generated by the reaction in

order to make it biologically acceptable. In the autotrophic metabolism considered there is (in certain processes) an outside source of hydrogen, e.g.  $\text{Fe} ; 2\text{H}^+ \rightarrow \text{Fe}^{++} + 2\text{H}$ , or (as in certain oxidations) the hydrogen is furnished by the reaction itself. It may be surmised that in photosynthesis hydrogen is formed through an interaction of absorbed radiations of high energy with water. In any equation the extent of the hydrogen production will effect the characteristics of the reaction greatly; e.g.



Here a parameter "a" is introduced which may vary from 3 to 8, the resulting  $E^0$  varying from -0.713 to -0.268 volts, and the  $\Delta\text{pH}$  (decrease of  $E_h$  per pH unit) from 0.180 to 0.080 volts. This consideration may, at first glance, seem superfluous, in as much as, by definition,  $\text{H}^+ + \text{e}^- \rightleftharpoons \text{H}$ . However, if the same reaction at the alkaline side of pH is considered as expressed in equation (18), it appears that here hydrogen *has* to enter in and that the equation cannot be made homogeneous over the entire pH range if hydrogen is not taken into account.

In the aerobic reactions another parameter is of importance — the number of oxygen molecules acting on the oxidizable substance. This should not be confused with the oxygen-tension in the external milieu.



The  $\Delta F$  of this reaction is  $-(113.4b - 49.4)$ , and the

$$E^0 = -\frac{(4.915b - 2.130)}{a-2} \text{ with a } \Delta\text{pH of } \frac{a}{a-2} \times 0.060 \text{ volts.}^1)$$

The reaction will become exergonic for  $b > 0.434$ , while the maximum value for  $b$  will be 2.00. It is thus easy to see that the  $E_h$ -pH relation will change with the amount of oxygen consumed.

For  $(\Delta F/23.06) = \beta$  an anaerobic reaction may be described by

$$(13) \quad \pm E_h = \frac{\beta - .060 a \text{ pH}}{a - \gamma}$$

and for aerobic reactions

$$(14) \quad \pm E_h = \frac{\beta - 4.915b - .060 a \text{ pH}}{a - \gamma}$$

where  $\gamma$  equals the number of electrons minus the number of hydrogen- or hydroxyl-ions involved.

In certain cases the  $E_h$ -pH relations are represented by either  $E_\phi = \text{constant}$  (line parallel to the abscissa) or  $\text{p}\phi = \text{constant}$  (line parallel to the ordinate). In the former case only hydrogen and no hydrogen ions are involved and  $.060a \text{ pH} = 0$ , therefore

$$(15) \quad E_\phi = \frac{\beta - 4.915b}{-\gamma}$$

<sup>1)</sup> At 25° C  $2.303(RT/F) = .0591$  but the value .060 is used in all cases except where stated, as the difference lies well within (our) experimental accuracy.



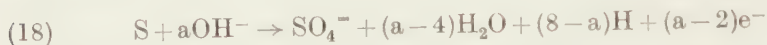


The following data of the free energy of formation in the standard state, which will be used in these communication, are taken from LATIMER (1952).

TABLE 3  
Free energies of formation at standard state  $\Delta F^\circ_{298^\circ}$  in K. cal/mol

OH	aq	+8.53	S <sup>=</sup>	aq	+22.1
OH <sup>-</sup>	aq	-37.595	SO <sub>3</sub> <sup>=</sup>	aq	-116.1
H <sub>2</sub> O	liq	-56.690	SO <sub>4</sub> <sup>=</sup>	aq	-177.34
H <sub>2</sub> O <sub>2</sub>	liq	-27.240	S <sub>2</sub> O <sub>3</sub> <sup>=</sup>	aq	-124.0
H <sub>2</sub> O <sub>2</sub>	aq	-31.470	S <sub>4</sub> O <sub>6</sub> <sup>=</sup>	aq	-244.3
HO <sub>2</sub> <sup>-</sup>	aq	-15.610	HS <sup>-</sup>	aq	+3.01
			H <sub>2</sub> S	aq	-6.54
CO <sub>2</sub>	aq	-92.31	HSO <sub>3</sub> <sup>-</sup>	aq	-126.0
C <sub>6</sub> H <sub>12</sub> O <sub>6</sub>	aq	-217.02	HSO <sub>4</sub> <sup>-</sup>	aq	-179.94
			H <sub>2</sub> SO <sub>3</sub>	aq	-128.59
			H <sub>2</sub> SO <sub>4</sub>	aq	-177.34

Apart from the presence of certain ions at specified pH values there is another point to be considered. Equation (11) showing the "anaerobic oxidation" (better dehydrogenation) of sulphur is only valid on the acid side. On the alkaline side of the neutral point we have to apply the following:



The  $\Delta F$  of this reaction is (49.5-19.1a) K. cal., showing that while reaction (11) (anaerobic oxidation at the acid side) was endergonic with a  $\Delta F = +49.5$  K. cal., the reaction at a higher pH is exergonic if  $a > 2.59$ .

We can now apply formula (10) to equation (11) in the acid range

$$(19) \quad E_h = E^0(ac) + \frac{.06}{a-2} \log_{10} \frac{[H^+]^a [H]^{(8-a)} [SO_4^{=-(a-4)}]}{[S][H_2O]^4}$$

and in the alkaline range

$$(20) \quad E_h = E^0(alk) + \frac{.06}{a-2} \log_{10} \frac{[H]^{(8-a)} [SO_4^{=-(a-4)}]}{[OH^-]^a [S][H_2O]^{(4-a)}}$$

$$[OH^-]^a = \frac{K_w^a}{[H^+]^a} = \frac{10^{-14a}}{[H^+]^a}$$

that is,

$$E_h = E^0(alk) + \frac{.828a}{a-2} + \frac{.060a}{a-2} \log_{10} [H^+] + \frac{.060a}{a-2} \log_{10} \frac{[Ox]}{[Red]}$$

and

$$E_h = E^0(ac) + \frac{.060a}{a-2} \log_{10} [H^+] + \frac{.060}{a-2} \log_{10} \frac{[Ox]}{[Red]}$$

therefore, in general,

$$(21) \quad E^0(ac) = E^0(alk) + \frac{.828a}{a-2}$$

<sup>1)</sup> The figure .828 was calculated on the assumption  $2.303 RT/F = 0.591$ .

This holds for all transitions acid-alkaline if both the reduction and the oxidation stage remain the same over the whole range considered.

In (11)  $\Delta F = +49.5$  and if we make  $a=4$  then  $E^0(\text{ac}) = +1.072$  volts. In (18) if we make  $a=4$  then  $\Delta F = -26.9$  and  $E^0(\text{alk}) = -.584$  volts. Now from (21)

$$E^0(\text{ac}) - E^0(\text{alk}) = \frac{.828a}{a-2}$$

i.e.

$$1.072 - (-.584) = 1.656 = \frac{.828 \times 4}{2}$$

Equation (18) therefore changes into equation (11) and the reaction is called "*homogeneous*" over the whole pH range above pH 2. Below this pH the  $\text{HSO}_4^-$  will enter into the reaction. We can also show this homogeneity over the whole pH range if we use  $\Delta\text{pH}$  for (11) and  $\Delta\text{pOH}^-$  for (18) e.g.

$$(22) \quad E_h(\text{ac}) = \frac{2.13 - .06a \text{ pH}}{a-2}$$

and

$$(23) \quad E_h(\text{alk}) = \frac{2.13 - 0.83a + .06a \text{ pOH}^-}{a-2}$$

Reaction (11) is endergonic, and reaction (18) is exergonic. As can be seen from Figure 1,  $E^0$  is positive in (22) and the  $E_h$  decreases with increasing pH. In (23)  $E^0$  is negative and increases with increasing  $\text{pOH}^-$ . Both reactions represent oxidation of sulphur<sup>1</sup>).

The inverse of (11) and (18) will represent the reduction of sulphate to sulphur. This exergonic at the acid side

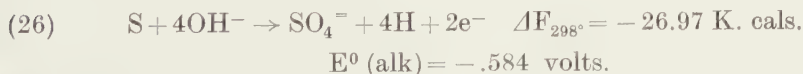
$$(24) \quad E_h(\text{ac}) = \frac{.06a \text{ pH} - 2.13}{a-2}$$

and endergonic at the alkaline side.

$$(25) \quad E_h(\text{alk}) = \frac{.83a - 2.13 - .06a \text{ pOH}^-}{a-2}$$

The two crossing "*homogeneous*" lines will delimit the region in which, under equilibrium conditions  $\text{SO}_4^{=}$  or S will be formed; while the area between these lines indicates the co-existence of these entities.

From equations (11) and (18) it will be seen that, generally, anaerobic oxidations are endergonic and reductions exergonic below pH7, and vice versa on the alkaline side. Thus considering the following:



<sup>1</sup>) A similar "*homogeneity*" is found in the oxidations  $\text{S} \rightarrow \text{S}_2\text{O}_3^{=}$  and  $\text{S}_2\text{O}_3^{=} \rightarrow \text{SO}_4^{=}$ . This conclusion may be due to the lack of data on the dissociations of thio-sulphate. In all other oxidations in the sulphur system, the ionic species concerned appear to be different on the acid and the alkaline sides. However, if the acid and the alkaline reactions show the same electron transfer, the curves representing them will be called "*continuous*".

we can write its counterpart

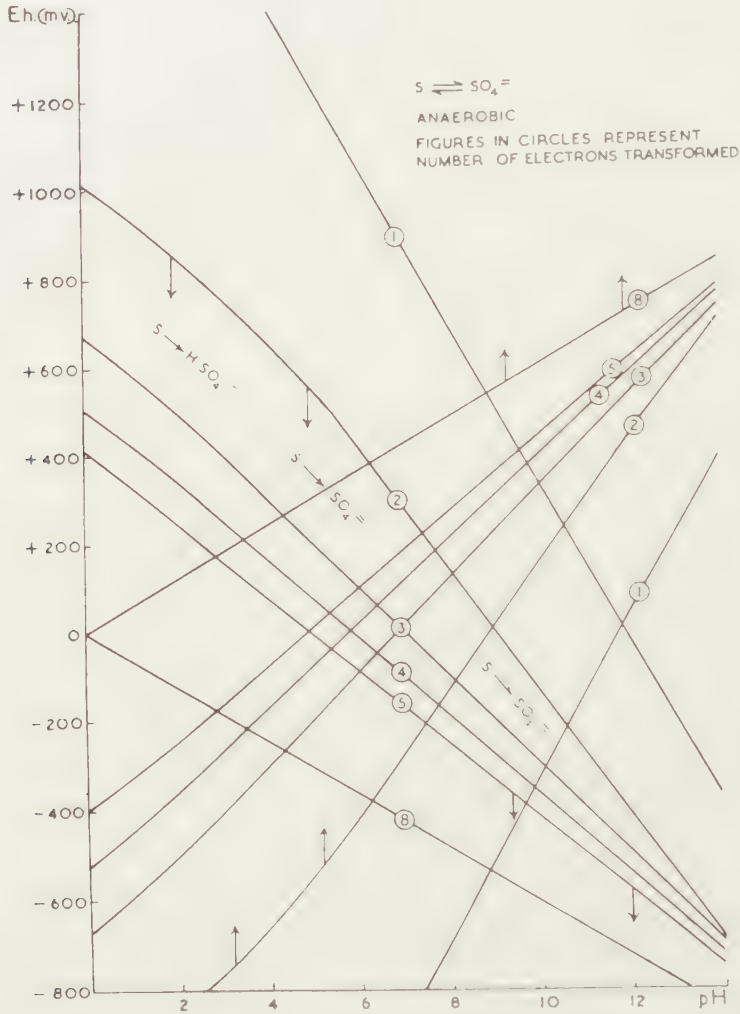
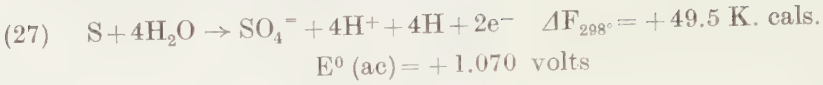


Fig. 1. Anaerobic reaction  $\text{S} \rightarrow \text{SO}_4^{=}$  for various numbers of electrons. Arrows indicate the direction in which the reaction proceeds. It will be seen that sulphur may be stable (at  $\text{pH} < 9$ ) at high electrode potentials

In a pH region where both relationships hold we can write



The  $\Delta F$  of this reaction (limiting condition) will be zero when  $\text{B} = 2.6\text{A}$ , or the proportion  $\frac{[\text{H}^+] \text{ generated}}{[\text{OH}^-] \text{ consumed}}$  will be  $54/26$ , from which we calculate  $\text{pH} = 6.84$ .

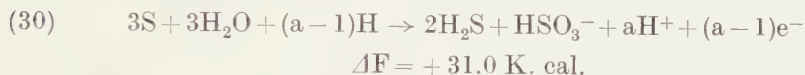


Below this pH the reaction will be endergonic.  
Only the reaction

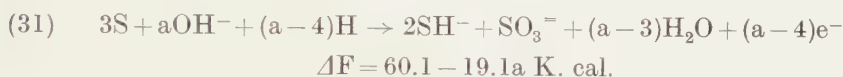


remains exergonic at a lower pH. As there is very little  $\text{SO}_3^=$  below pH6 we would expect this pH to be the logical limit for the reaction.

Gmelins Handbuch (1953) describes the following reaction of sulphur with water  $3\text{S} + 2\text{H}_2\text{O} \rightarrow 2\text{H}_2\text{S} + \text{SO}_2$  and quotes CHERBULIEZ and HERZENSTEIN (1936) and VON DEINES (1934) which workers account for the presence of  $\text{H}_2\text{S}$  in geothermal exhalations (originating at temperatures above  $60^\circ \text{C}$ ) by this reaction. When both hydrogen and hydrogen-ion are considered, this "inorganic Cannizaro reaction" will run as follows:

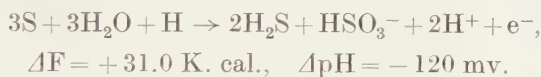


and

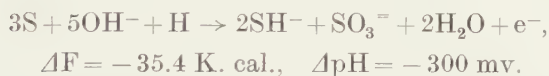


On the whole, the reactions require hydrogen.

The relations are "continuous" for



and



These anaerobic reactions may be the cause of the formation of  $\text{H}_2\text{S}$  during the anaerobic oxidation of sulphur as has been observed by BAAS BECKING and WOOD. They may also play an extremely important role in the metabolism of the purple bacteria, as the breakdown of stored sulphur regenerates  $\text{H}_2\text{S}$ , and the formation of  $\text{HSO}_3^-$  and  $\text{H}^+$  will create a lower pH and higher Eh.

ZILBERMAN (1940, 1941) has described the reverse reaction using both an aqueous solution and gaseous  $\text{H}_2\text{S}$ .



In the presence of an excess of  $\text{H}_2\text{SO}_3$  the reaction proceeds as follows:



together with the formation of polythionates

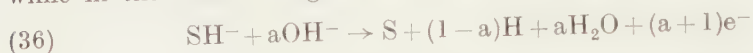


while at higher temperatures sulphates will appear also.

The oxidation of  $\text{H}_2\text{S}$  can be simply represented by the equation



while in the alkaline region only the  $\text{SH}^-$  plays a role.



The rather complicated resulting relation is shown in Figure 2.

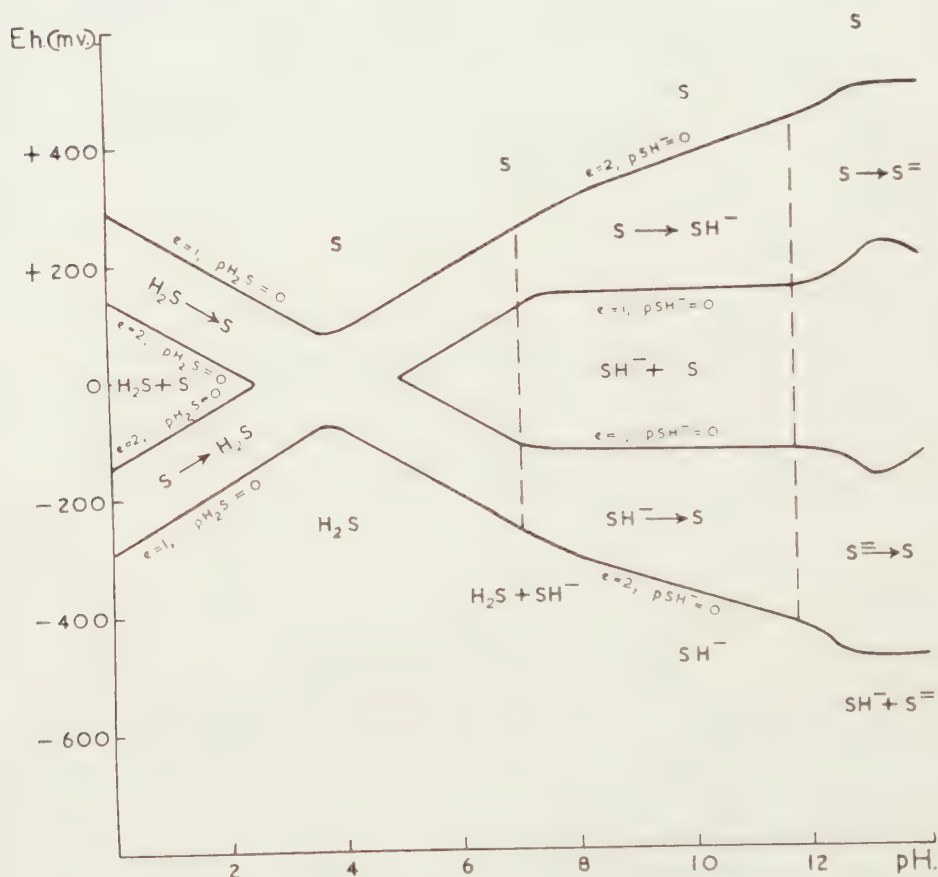
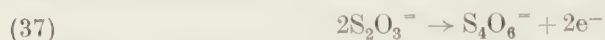


Fig. 2. Anaerobic reaction  $\text{H}_2\text{S} \rightarrow \text{S}$ ,  $\text{SH}^- \rightarrow \text{S}$  and  $\text{S}^{2-} \rightarrow \text{S}$ . Eh is shown for  $e=1$ ,  $\pm 130$  mv. The corresponding pH's are situated at 11.8 and 2.2. Areas indicate presence of ionic species under equilibrium conditions 1 molal. Broken lines indicate pK of  $\text{H}_2\text{S}$  dissociation.

For the sake of completion, mention should be made of the tetrathionate formation from thiosulphate. The reaction



is slightly endergonic,  $\Delta F_{298}^\circ = 3.7$  K. cal. However, traces of oxygen will make the reaction exergonic ("homogeneous" over the whole pH range), if hydrogen is provided, e.g.



whence  $\Delta F = 3.7 - 113.4 b$  K. cal. The lowest value for  $b = .033$ , showing that only one molecule of oxygen per 60 of thiosulphate is necessary to make the reaction proceed spontaneously.

Anaerobically, the reaction may also be exergonic if there is an outside supply of hydrogen, e.g.



where

$$\Delta F = -49.1 \text{ K. cal.}$$

and



where  $\Delta F = -58.2$  K. cal. These reactions are, therefore, most unlikely to support autotrophic bacteria unless hydrogen be generated by other processes. Similar "autotrophs" are known in sulphate reduction. It should be stated that the above examples, where three different oxidation states are involved in one equation may be the rule rather than the exception. This would make our interpretation even more uncertain.

The hydrogen made available, either from an outside source or formed in the substrate itself may be assimilated by carbon dioxide in the almost reversible reaction.



The electrode potential of the internal milieu must be low to enable the cell to perform this reduction. While in Parts I and II of this series, the environment of algae was studied, we will refrain here from interpretation of the data. Oxygen, hydrogen and hydrogen peroxide enter into the picture of photosynthesis, but this picture is clouded through the secretion by various aquatic organisms, of highly reducing substances, which are at least partly sulphonium salts. We intend to revert to this problem later.

We have carried out measurements which relate to conditions in the outer environment, in the "milieu ambiant" and, therefore another element of uncertainty is introduced, as we do not know what conditions occur inside the cell. The above discussion together with Part IV are, therefore, not so much attempts at interpretation of the metabolism in the natural milieu of several autotrophs, as a demonstration that thermodynamics, as far as applicable to our case, gives confirmation and support to the idea that several reactions of an inorganic nature delimit the potential milieu of the organisms studied.

We are grateful for the interest shown in this work by Dr. B. BREYER and Dr. S. HAKOBIAN, of Sydney University.

---

<sup>1)</sup> Here  $\bar{H}\bar{C}\bar{O}\bar{H}$  represents 1/6 molecule of a hexose.

## REFERENCES

1. BAAS BECKING, L. G. M. and E. J. FERGUSON WOOD, Proceedings Kon. Ned. Akad. v. Wet. Amsterdam, **B 58**, 160 (1955).
2. CHERBULIEZ, E. and A. HERZENSTEIN, Helv. chim. Acta **19**, 80 (1936).
3. DEINES, O. VON, Naturwiss. **22**, 129 (1934).
4. GERSMANN, H. R., Chem. Weekbl. **51**, 109 (Dutch, English Summary) (1955).
5. GMELIN's Handbuch der Anorganischen Chemie, (Erich Pietsch *et al.*) 8th ed. Syst. 9. Teil B. Lief. 1. Verlag Chemie (Weinheim, 1953).
6. LATIMER, W. M., The oxidation states of the elements and their potentials in aqueous solutions (Prentice-Hall, N.Y., 1952).
7. MACDOUGALL, F. H., Thermodynamics and chemistry (3d ed., John Wiley & Sons, N.Y., 1939).
8. ZILBERMAN, F. J., J. Gen. Chem. (U.S.S.R.) **10**, 1257 (1940); Chem. Abstr. **35**, 2685 (1941).



## BIOCHEMISTRY

### BIOLOGICAL PROCESSES IN THE ESTUARINE ENVIRONMENT

#### IV. ATTEMPTS AT INTERPRETATION OF OBSERVED Eh-pH RELATIONS OF VARIOUS MEMBERS OF THE SULPHUR CYCLE

BY

L. G. M. BAAS BECKING AND I. R. KAPLAN \*)

(Communicated at the meeting of June 25, 1955)

#### SUMMARY

1. A table is given showing characteristics of 30 reactions in the sulphur cycle, both aerobic and anaerobic.

2. It is shown that, for equilibrium conditions, in many cases two reactions may determine the observed characteristics in the outer environment:



and



3. Several other possibilities are considered as contributory to the observed milieu limits.

4. The uncertainty, introduced by various factors into the calculations prevents a quantitative interpretation of the limits observed.

#### INTRODUCTION

In former papers (Biological Processes in the Estuarine Environment I-II, Proc. Roy. Neth. Ac. Sc. in press) the outer milieu of various microbes living in the estuarine environment was characterized by its electrode potential and pH (BAAS BECKING and WOOD) while, in order to account for the interpretation of the observations, certain conditions were imposed upon the chemical equations, expressing oxido-reductions in the sulphur cycle (BAAS BECKING and KAPLAN, pt. III). In this paper an effort at further interpretation will be made.

Measuring the characteristics of the outer environment, of the "milieu ambiant" may not represent the conditions inside the cell, in the "milieu interne". The purple bacteria are a case in point. At the alkaline side the anaerobic oxidation  $\text{S} \rightarrow \text{SO}_4^{2-}$  is exergonic and no energy would be required for this reaction to take place. However, the intracellular sulphur disappears although it is highly probable that the internal environment is acid. External energy has to be involved in this case. A similar reasoning may be applied to the metabolism of the green bacteria.

---

\*) Division of Fisheries, C.S.I.R.O., Cronulla, Australia.

The reactions in this paper are calculated for standard conditions. When sulphur is present, the solubility of which substance in water is very low indeed, the expression for concentration has not been considered as it is most uncertain. In certain cases, especially where  $\text{H}_2\text{S}$ – $\text{SH}^-$  concentrations were measured, the necessary corrections can be applied. Also corrections for oxygen-tension ( $1.7 \cdot 10^{-3}$  molar in oxygen-saturated seawater at 25 °C) and for sulphate concentration ( $\text{pSO}_4 = 1.77$  in seawater) can be made.

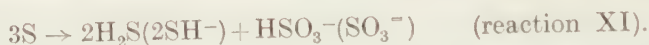
As said in a previous communication, the following remarks are not so much attempts at interpretation of the natural and laboratory milieu of several autotrophs, as a demonstration that thermodynamical consideration give confirmation and support to the idea that several reactions of inorganic nature, in the outer environment, delimit the occurrence of the organisms studied.

TABLE 1

Reactions dealt with in this paper. The numbers refer to reactions in Table 2

$\text{T}_0$	$\text{H}_2\text{S}$	$\text{SH}^-$	$\text{S}$	$\text{S}_2\text{O}_3^{2-}$	$\text{H}_2\text{SO}_3$	$\text{HSO}_3^-$	$\text{SO}_3^{2-}$	$\text{HSO}_4^-$	$\text{SO}_4^{2-}$
From			I	II	III	III		IV	IV
$\text{H}_2\text{S}$			I	II			III		IV
$\text{SH}^-$				V	VI	VI	VI	VII	VII
$\text{S}$					VIII	VIII	VIII	IX	IX
$\text{S}_2\text{O}_3^{2-}$								X	
$\text{H}_2\text{SO}_3$								X	X
$\text{HSO}_3^-$									X
$\text{SO}_3^{2-}$									

We have added to these reactions the well known "inorganic Cannizzaro".



In the physiological range we do not meet with undissociated sulphuric acid nor with sulphide ion.

If we want to interpret a certain relation, e.g. a milieu limit, expressed by a Eh-pH curve, we have to distinguish between aerobic and anaerobic reactions and also consider doubtful cases. We have, as mentioned in the previous communication, for aerobic reactions

$$(1) \quad \pm \text{Eh} = \frac{4.915b - \beta - .059a \text{ pH}}{a - \gamma}$$

and, for anaerobic reactions

$$(2) \quad \pm \text{E}_h = \frac{\beta - .059a \text{ pH}}{a - \gamma}$$

$$\text{If we call } \frac{a}{a - \gamma} = \Delta \text{ we find } a = \frac{\gamma \Delta}{\Delta - 1}, \quad a - \gamma = \frac{\gamma}{\Delta - 1}$$

From this we derive

TABLE 2

The characteristics of 30 reactions, together with their aerobic counterparts. The characteristics of the latter may be obtained by addition of the appropriate coefficients for oxygen, water and hydrogen as given in the last lines of this table

1	2	3	4	5	6	7	8	9	10	11	12	13	14	15	16
		reduced S	$\text{H}_2\text{O}$	$\text{OH}^-$	oxidized S	$\text{H}_2\text{O}$	H	$\text{H}^+$	ne, - (a- $\gamma$ )	$\frac{\text{K, cal}}{\text{mol}}$	$(\text{a}-\gamma) E^0 = \beta$	b lower limit $\beta/4.91$	p $\xi$	$\pm E\xi$	b for p $\xi = 14$ $\bar{y}=0$
		+	+	$\rightleftharpoons$	+	+	+	+	+	+	+	+	+	+	+
I. acid	$\text{H}_2\text{S}$				S		2-a	a	a	6.54	.282	.06			
alk.	$\text{SH}^-$		a		S	a	1-a	a+1	a+1	-3.01	-.130	0	2.20 (11.80)	.130	-
II. acid	$2\text{H}_2\text{S}$	3			$\text{S}_2\text{O}_3^{=}$		7-a	a	a-2	59.2	2.57	.52			.86
alk.	$2\text{SH}^-$		a		$\text{S}_2\text{O}_3^{=}$	a-3	6-a	a	a	40.1	1.74	.35			-
III. acid <sub>1</sub>	$\text{H}_2\text{S}$	3			$\text{H}_2\text{SO}_3$		6-a	a	a	48.0	2.08	.43			-
acid <sub>2</sub>	$\text{H}_2\text{S}$	3			$\text{HSO}_3^-$		7-a	a	a-1	50.6	2.19	.45			.62
alk.	$\text{SH}^-$		a		$\text{SO}_3^{=}$	a-3	6-a	a	a-1	51.0	2.21	.45			.62
IV. acid <sub>1</sub>	$\text{H}_2\text{S}$	4			$\text{HSO}_4^-$		9-a	a	a-1	53.4	2.30	.47			.64
acid <sub>2</sub>	$\text{H}_2\text{S}$	4			$\text{SO}_4^{=}$		10-a	a	a-2	56.0	2.42	.48			.82
alk.	$\text{SH}^-$		a		$\text{SO}_4^{=}$	a-3	9-a	a	a-1	-10.1	-.44	0	7.54 (6.55)	.440	-
V. acid	2S	3			$\text{S}_2\text{O}_3^{=}$		6-a	a	a-2	46.1	2.00	.41			.75
alk.	2S		a		$\text{S}_2\text{O}_3^{=}$	a-3	6-a	a	a-2	46.1	2.00	.41			.75
VI. acid <sub>1</sub>	S	3			$\text{H}_2\text{SO}_3$		4-a	a	a	41.5	1.80	.37			-
acid <sub>2</sub>	S	3			$\text{HSO}_3^-$		5-a	a	a-1	44.1	1.91	.39			.56
alk.	S		a		$\text{SO}_3^{=}$	a-3	6-a	a	a-2	54.0	2.34	.48			.82
VII. acid <sub>1</sub>	S	4			$\text{HSO}_4^-$		7-a	a	a-1	45.9	2.22	.45			.62
acid <sub>2</sub>	S	4			$\text{SO}_4^{=}$		8-a	a	a-2	49.5	2.13	.43			.77
alk.	S		a		$\text{SO}_4^{=}$	a-4	8-a	a	a-2	49.5	2.13	.43			.77
VIII. acid <sub>1</sub>	$\text{S}_2\text{O}_3^{=}$	3			$2\text{H}_2\text{SO}_3$		2-a	a	a+2	36.9	1.60	.33	13.50 (.50)	.800	-
acid <sub>2</sub>	$\text{S}_2\text{O}_3^{=}$	3			$2\text{HSO}_3^-$		4-a	a	a	42.1	1.82	.37			-
alk.	$\text{S}_2\text{O}_3^{=}$		a		$2\text{SO}_3^{=}$	a-3	6-a	a	a-2	61.9	2.67	.54			.88
IX. acid <sub>1</sub>	$\text{S}_2\text{O}_3^{=}$	5			$2\text{HSO}_4^-$		8-a	a	a	47.7	2.07	.42			-
acid <sub>2</sub>	$\text{S}_2\text{O}_3^{=}$	5			$2\text{SO}_4^{=}$		10-a	a	a-2	52.8	2.29	.47			.81
alk.	$\text{S}_2\text{O}_3^{=}$		a		$2\text{SO}_4^{=}$	a-5	10-a	a	a-2	52.8	2.29	.47			.81
X. acid <sub>1</sub>	$\text{H}_2\text{SO}_3$	1			$\text{HSO}_4^-$		3-a	a	a-1	5.35	.23	.05	3.90 (10.10)	.232	.22
acid <sub>2</sub>	$\text{HSO}_3^-$	1			$\text{HSO}_4^-$		2-a	a	a	2.75	.12	.02			-
acid <sub>3</sub>	$\text{HSO}_3^-$	1			$\text{SO}_4^{=}$		3-a	a	a-1	5.35	.23	.05	3.90 (10.10)	.232	.22
alk.	$\text{SO}_3^{=}$		a		$\text{SO}_4^{=}$	a-1	2-a	a	a	-4.55	-.20	0			-
XI. acid	3S	3			$(2\text{H}_2\text{S})$		1-a	a	a-1	-31.9	1.38	.28			.45
alk.	3S		a		$(2\text{SH}^-)$	a-3	4-a	a	a-4	60.0	2.60	.53	10.8 (3.2)	.640	1.21
					$(+\text{SO}_3^{=})$										
ld for aerobic	$\text{bO}_2$	(acid) -2b				(alk) +2b	- -4b			-113.4b	4.91b				

for aerobic reactions

$$(3) \quad \frac{(4.915b - \beta)}{\gamma} = \frac{Eh + .06\Delta pH}{d - 1}$$

which simplifies, for anaerobic reactions, into

$$(4) \quad \frac{\beta}{\gamma} = \pm \frac{Eh + .06\Delta pH}{d - 1}$$

Now, as both pH and Eh are obtained by measurement, and  $\Delta$  can be established from the slope of the line, the values of

$$\frac{4.915b - \beta}{\gamma} \text{ and } \frac{\beta}{\gamma}$$

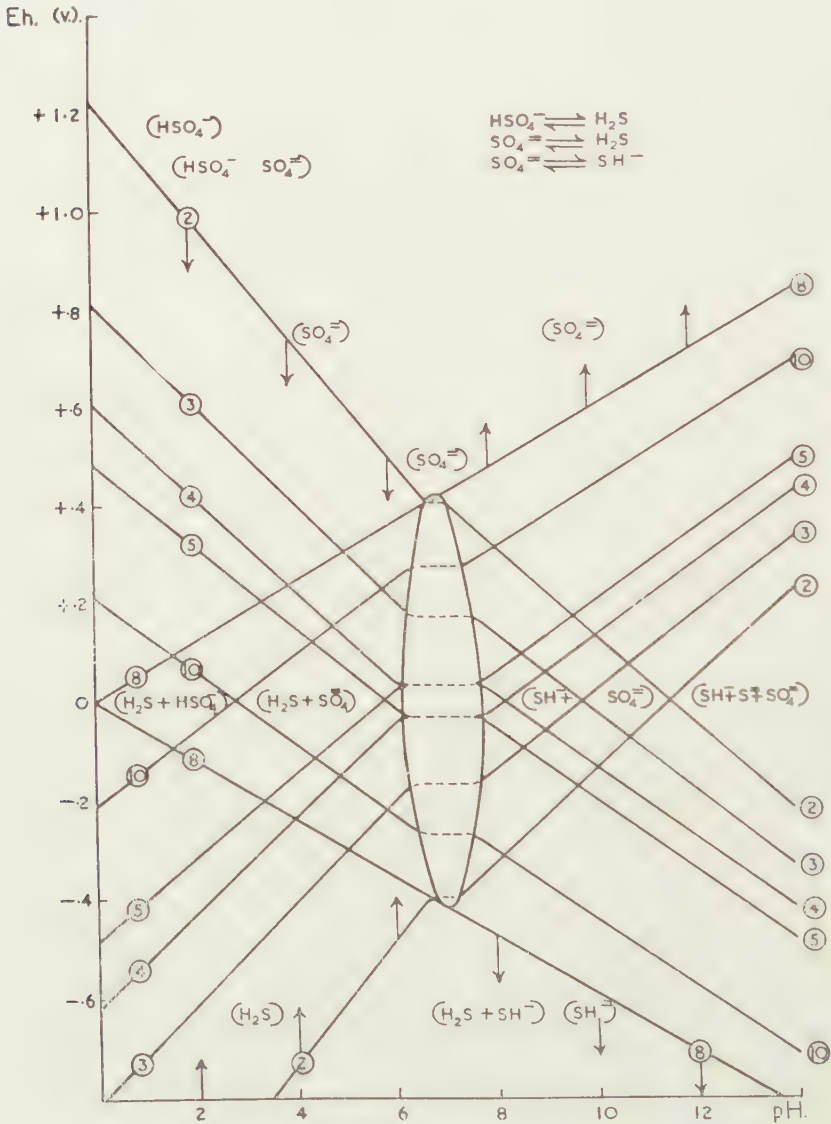


Fig. 1



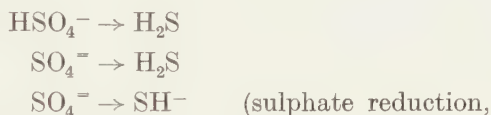
respectively may be calculated. From Table 2 we now test the most likely reactions, using the appropriate values of  $\beta$  and  $\gamma$ . One "master-reaction" may account for several limiting lines, especially in the aerobic range, where two parameters enter into the equations. Of the manifold "three stage reactions" (see BAAS BECKING and KAPLAN pt. III) we will only consider  $3S \rightarrow 2H_2S + SO_3^{2-}$ . We are convinced, however, that many reactions of this type may occur.

We will try to apply the above to indicate (for standard conditions) the most likely reactions concerned in limiting the environment of various members of the sulphur cycle.

As remarked in the preceding communication, the Eh-pH relation shows boundary conditions for Eh = const, and for pH = constant.

Due to the non-homogeneity in the electron transfer of certain reactions over the entire pH-range, there may be regions, in certain reactions, where the Eh remains constant. These regions may represent transfer of undissociated hydrogen. Figure 1 illustrates this point.

The anaerobic reactions



with hydrogen provided) are exergonic on the acid side, and endergonic in the alkaline range. The inverse would hold for the oxidation of the sulphide. The continuous curves for various numbers of electrons (figures in circles) show the characteristics of these reactions. Due to the "non-homogeneity" of these continuous curves a "plateau" appears; a region

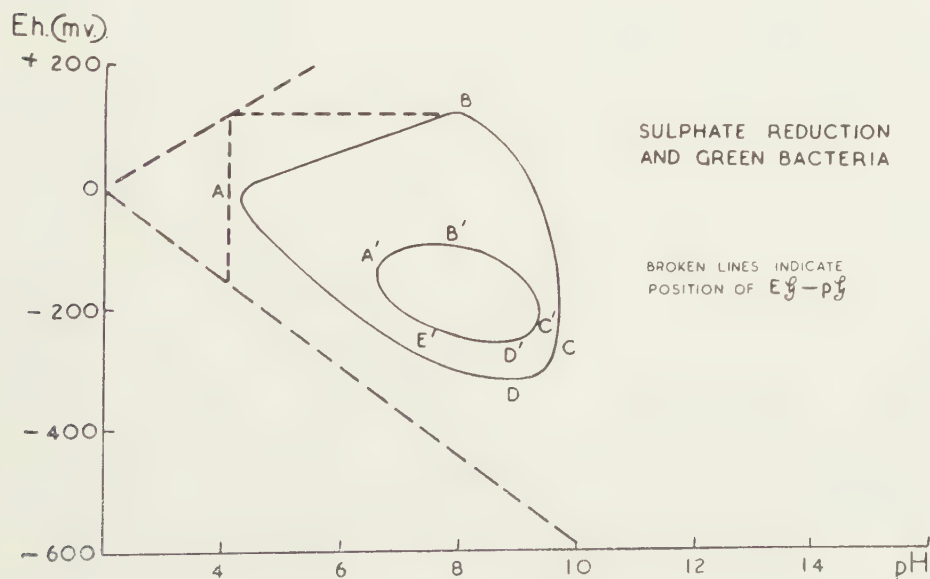


Fig. 2

where Eh remains constant over a certain pH range. This region lies within the milieu limits of the bacterial sulphate reduction for electron transfer values 3-10. The ionic and molecular species present are given in parentheses. The curves represent the reactions between pH 2-12, as neither  $\text{H}_2\text{SO}_4$  nor  $\text{S}^-$  have been considered. The arrows indicate the direction in which the reaction would proceed spontaneously. The ellipsoidal line surrounds the region in which, for a particular reaction,  $\text{Eh} = \text{const.}$

We do not know whether this phenomenon is of influence in the delimitation of a natural milieu. As it is suggestive of such an influence it seemed advisable to include it in our considerations.

The following figures (2-5) show the approximate observed limits for sulphate reducing bacteria, for aerobic and anaerobic-thio bacteria (on sulphur and on thiosulphate media,) for purple bacteria and for green bacteria (see BAAS BECKING and WOOD, 1955). It may be seen at a glance that these limits show a great variation in characteristics, from almost straight lines, in the region between  $\text{pH} = \text{const.}$  to  $\text{Eh} = \text{const.}$ , to curved lines, where a different interpretation is required.

In view of what has been said in this paper and also in the previous communications, due to the great numbers of variables (parameters a and b and departure from equilibrium conditions) interpretation of these limits may seem premature. Certain relations, however, are suggestive.

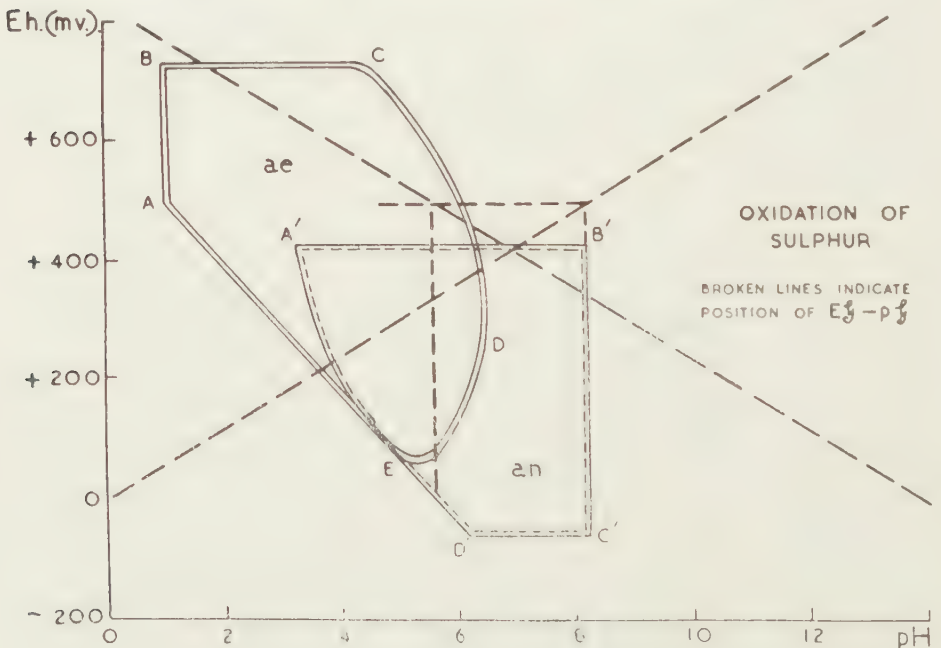


FIG. 3

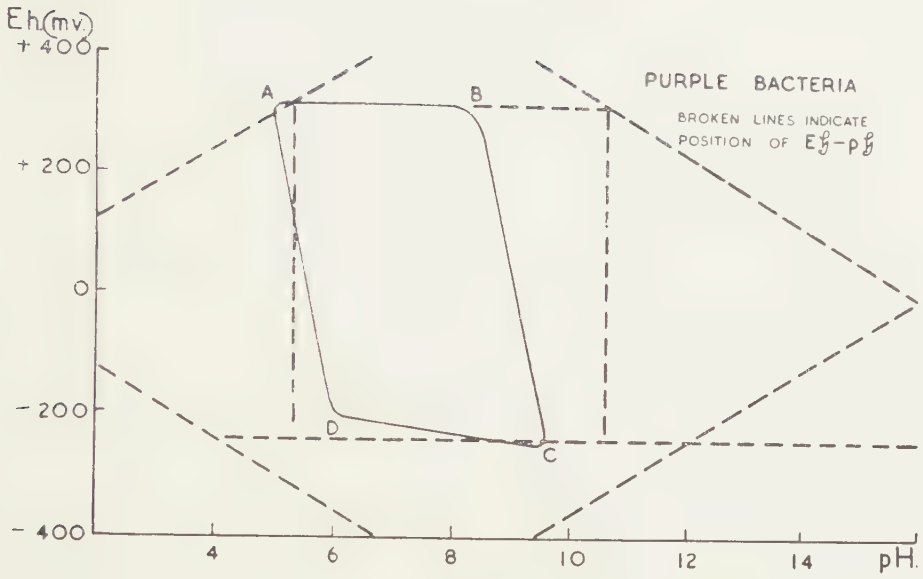


Fig. 4

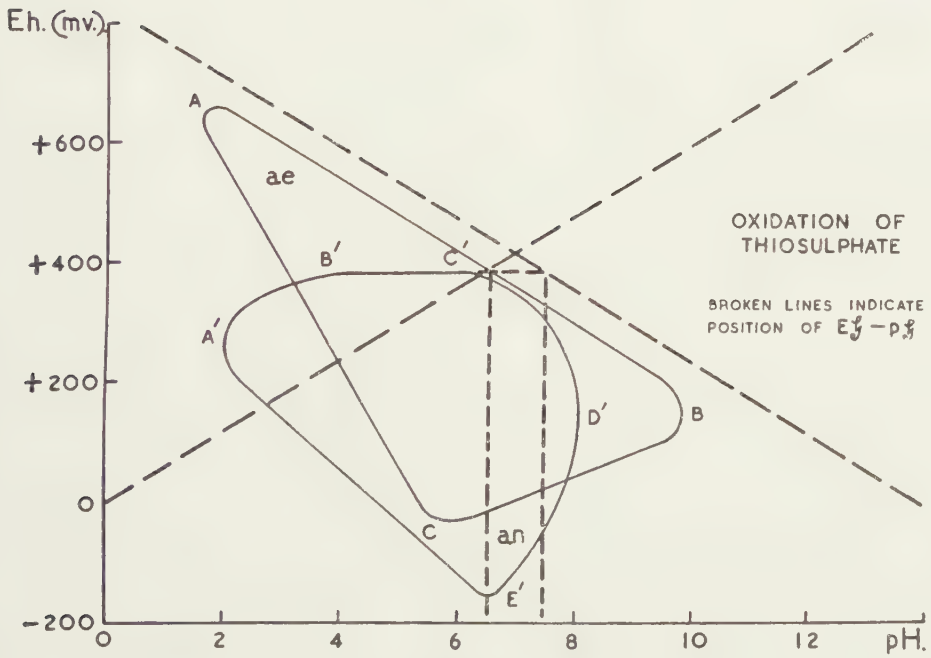


Fig. 5

TABLE 3  
(a) SULPHATE REDUCTION (Figure 2)

	E $\delta$	Figure and Reaction	p $\delta$	Figure and Reaction	E $^0$	pH	Figure and Reaction	E $^0$	$\Delta$ pH	Figure and Reaction	pH <sub>2</sub> S pSH <sup>-</sup>
found	+.110	2B	(9.60)	2C	-.120	.030	2AB	+.141	-.060	2AD	
reaction calcul't	+.130	I alk	—	—	-.115	.030	Xac3		.060	I ac	0
found	(-.300)	2D	(4.20)	2A				+.065	-.030	2AD	
reaction calcul't	—	—	4.05	I alk				+.065	-.030	I alk	0

As seen from the above table, the upper Eh limit, the lower pH limit and the "S.W." and "S" part of the area may be accounted for by the reaction  $\text{H}_2\text{S}(\text{SH}) + \text{S}$ , the "N.W." corner corresponds well with the reaction  $\text{SO}_4^{2-} + \text{H}_2\text{SO}_3$  for  $ae = 2$ . Both the first and the last links in the chain reaction  $\text{SO}_4^{2-} + \text{S}$  are therefore represented by no other equations, listed in Table 2 seem to fit the data.

TABLE 4  
(b) GREEN BACTERIA (Figure 2)

	E $\delta$	Figure and Reaction	p $\delta$	Figure and Reaction	E $^0$	$\Delta$ pH	Figure and Reaction	pSH	$ae^-$
found	(.100)	2B'	(6.55)	2A'	.171	.060	2A E'	1	2
reaction calcul't	—	—	—	—	.171	.060	I ac		
found	(-.270)	2D'	(9.30)	2C'	+.095	-.030	2E'D'		
reaction calcul't	—	—	—	—	+.090	-.030	I alk	1	2
found	—	—	—	—	+.261	-.060	2	4	2
reaction calcul't	—	—	—	—	+.261	-.060	I ac		
found	—	—	—	—	+.185	-.030	2B'C'	4	2
reaction calcul't	—	—	—	—	+.185	-.030	I alk	4	2

The outline of the region may be accounted for entirely by the reaction  $\text{H}_2\text{S}(\text{SH}) + \text{S}$ , the  $\text{H}_2\text{S}(\text{SH})$  tension varying from  $10^{-4}$  mol. to  $10^{-4}$  mol. As the form studied by us proved unable to carry sulphur to a higher oxidation level, reactions I alk. might be expected to dictate the milieu-limits. The lower pH limit at 6.55 might be caused by a toxic effect of undissociated  $\text{H}_2\text{S}$ .



TABLE 5  
(c) PURPLE BACTERIA (Figure 5)

	E $\bar{\phi}$	Figure and Reaction	pH $_2$ S	p $\bar{\phi}$	Figure and Reaction	pH $_2$ S	E $^{\circ}$	$\Delta$ pH	Figure and Reaction	ne-
found	+ .320	5AB		(5.10)	5A		(+2.020)	(- .370)	5AD	
reaction calcul't	+ .130	I alk	6	5.10	I alk		+4.380	-.480	5BC	
found							+4.600	-.480	XI alk	.57
reaction calcul't										

The upper, flat limit (Fig. 5, AB) might represent a limit for hydrogen transfer at a very low SH<sup>-</sup> concentration (pSH<sup>-</sup> = 6). The corresponding p $\bar{\phi}$  (where there is no transfer of hydrogen) at 5.10 corresponds to the "W" limit of the region, while, for the "E" limit, very steep but not vertical, the reaction 3SH<sup>-</sup>  $\rightarrow$  2H $_2$ S + SO $_2$  is invoked, for ne<sup>-</sup> = 5.7, to account for the high  $\Delta$ pH. It may very well be that other "three-component reactions" enter in here. The lower Eh limit may represent the reaction SH<sup>-</sup>  $\rightarrow$  S for pSH = 3. The suggestion that the H $_2$ S would be the limiting factor in the existence of the purple bacteria seems a logical one.

TABLE 6  
(d) SULPHUR. AEROBIC (Figure 3)

	E $\bar{\phi}$	Figure and Reaction	ne-	b	p $\bar{\phi}$	Figure and Reaction	ne-	b
found	+ .730	3BC			1.00	3AB		
reaction calcul't	+ .730	VII ac2	0	.15?	1.00	VII ac1	1	.46
	for $\Delta F = 0$			.43				.45

	-E $^{\circ}$	$\Delta$ pH	Figure and Reaction	ne	b	E $^{\circ}$	$\Delta$ pH	Figure and Reaction	ne-	b
found	-.620	+ .180	3ED			+ .600	-.105	3AE		
reaction calcul't	-.620	+ .180	X ac3	5	.085	+ .600	-.095	VII ac2	3.56	0
	for $\Delta F = 0$				.05					

On the acid side the reaction is endergonic, E $^{\circ}$  is positive. For the region of hydrogen transfer at +.730 volt (Figure 3B $'$ ) we obtain, for the reaction S  $\rightarrow$  SO $_4^{--}$  b = .15. For a  $\Delta F = 0$ , the b for this reaction would be .434 showing that only traces of oxygen are involved. This might indicate that this limit represents the boundary for the opposite reaction, SO $_4^{--}$   $\rightarrow$  S. The p $\bar{\phi}$  at 1.00 would correspond to the reaction S  $\rightarrow$  HSO $_4^-$  for b = .46 which is close to the limit at .45.

The "S - E" boundary might represent actual oxygen consumption in the oxidation of HSO $_3^-$  (Figure 3ED).

TABLE 7  
(e) SULPHUR, ANAEROBIC (Figure 3)

	$E\tilde{\Phi}$	Figure and Reaction	$ne^-$	b	$p\tilde{\Phi}$	Figure and Reaction	$ne^-$	b
found	+ .420	3A'B'			8.25	3B'C'		
reaction calcul't	+ .420	VII ac2	0	.26	8.25	VII alk	2	.24
	for $\Delta F = 0$			.434				.43
found	-.080	D'C'		.44				
reaction calcul't		VII alk	0	lim .434				

Here the upper limit at +.420 volt and the steep boundary at pH 8.25 may both be accounted for by the reaction  $S \rightarrow SO_4^{2-}$  for very low oxygen consumption ( $b = .26$  and  $.24$  respectively) not enough to make the reaction exergonic.  
The evidence points to the presence of air leaks. The lower  $E\tilde{\Phi}$  at -.080 volts would correspond to the reaction  $S \rightarrow SO_4^{2-}$  (alk),  $ne^- = 6$ ,  $b = .44$  (limit for  $\Delta F = 0$ ,  $b = .434$ ).

TABLE 8  
(f) THIOSULPHATE, AEROBIC (Figure 4)

	$E\tilde{\Phi}?$	Figure	$p\tilde{\Phi}?$	Figure	$E^\circ$	$\Delta pH$	Figure and Reaction	$ne^-$	b
found	(-.660)	4A	9.90	4B	.250	.045	4C1		
reaction calcul't					-.286	+.045	IX alk	-8	0
found									
reaction calcul't									
					$E^\circ$	$\Delta pH$		$ne^-$	b
					+.780	-.060	4AB		
					+.780	-.060	VIII ac2	2.33	0
							(does not hold for alk.)		
					+.880	-.172	4AC		
					+.880	-.180	XI ac	.5	.27
									.28

for  $\Delta F = 0$

The "S"  $E^\circ$  boundary represents an exergonic oxidation which fits conditions for IX alk,  $S_2O_3^{2-} \rightarrow 2SO_4^{2-}$ ,  $ne^- = 8$ .  
However, the other limits of the region cannot be accounted for by reaction IX. Figure 4AB is best approximated by reaction VIII acid 2;  
 $S_2O_3^{2-} \rightarrow 2 HSO_3^-$ ,  $ne^- = 2.33$ ,  $b = 0$ . The very steep boundary (Figure 4AC) only fits a more complicated reaction, of which type we only used  $3S + 2 H_2S + SO_2$  (reaction XI ac), for  $ne^- = 5$ ,  $b = .27$ . The latter value is quite close to the value for  $\Delta F = 0$ ,  $b = .28$ .



From the above it appears that the parameter  $b$  (molecules of oxygen consumed per molecule of oxidizable material) sometimes appears in the anaerobic reactions (leaks) and, inversely, many anaerobic reactions may account for boundaries of aerobic regions. Moreover, it should be stressed again that the reactions mentioned in Table 2 only yield an incomplete picture of the actual happenings in the natural environment, not only because of the possibility of more complicated reactions, such as XI, but also because of the interplay between inorganic and organic sulphur compounds.

Only few reactions, mentioned in Table 2, were used to account for the boundaries. Most important are reactions I, VII and XI, while X, the oxidation of sulphite, sometimes enters in. The oxidation of thiosulphate, moreover, requires reactions VIII and IX.

The reactions used are mentioned in the following table.

TABLE 10

Reaction	I	VII	VIII	IX	X	XI	position Ox. sulph.
sulphate reduction . . . . .	+	—	—	—	+	?	East
green bacteria . . . . .	+	—	—	—	—	—	W & E
purple bacteria . . . . .	+	—	—	—	—	+	—
sulphur aerobic . . . . .	—	+	—	—	—	—	W
sulphur anaerobic . . . . .	—	+	—	—	—	—	—
thiosulphate, aerobic . . . . .	—	—	+	+	—	+	—
thiosulphate, anaerobic . . . . .	—	—	?	+	—	+	E
frequency of reaction . . . . .	7	6	1	3	2	3	

While lower and upper Eh limits may be accounted for, in many cases the upper and lower pH limits cannot be derived from the equations considered. This is partly due to the fact that only a limited number of reactions, only concerned with sulphur, have been dealt with.

## CONCLUSIONS

Although the above is a very preliminary approach and may be, at this stage of our knowledge, premature, it seems to us that the method outlined in the last two papers may serve as a basis for further investigation, and not only in the sulphur cycle. The construction of tables like Table 2 in this paper and the correlation of theoretical data with experimental observations might be useful in predicting limiting, as well as other reactions in the external milieu. At present we feel most strongly the lack of data on organo-sulphur compounds, often so preponderant in the anaerobic environment. It may be that a simultaneous determination of the various oxidation-levels of sulphur (e.g. by means of polarography) might bring us nearer to our goal.



BIOLOGICAL PROCESSES IN THE ESTUARINE ENVIRONMENT

VA. THE INFLUENCE OF *ENTEROMORPHA* UPON ITS ENVIRONMENT

BY

L. G. M. BAAS BECKING \* AND MARGARET MACKAY \*\*

(Communicated at the meeting of November 26, 1955)

I. SUMMARY AND CONCLUSIONS

1. The potential environment of *Enteromorpha* is a wide one. Capable of existence in freshwater as well as in concentrations higher than seawater, highly resistant against desiccation, its seasonal disappearance on the New South Wales coast might be ascribed to a combination of high temperature and high light intensities. With *Zostera*, *Enteromorpha* is the chief plant component of many intertidal flats, on which extensive oyster culture occurs in New South Wales. The density of the alga may amount to several kilograms per square metre.

2. The algae secrete highly reducing acidic compounds one of which probably is identical with that described by BYWOOD and CHALLENGER (1953). In the light, some of these compounds are either reabsorbed or destroyed.

Due to this process, as well as to the intensive photosynthesis, the Eh-pH limits of this form are wide; Eh + 600 to - 100 millivolts, pH 4.8-9.5. Due to the production of such sulphonium salts, the environmental characteristics may become fit to support a sulphate reduction in a very short time. It may well be that there is also a direct production of  $H_2S$  by *Enteromorpha*. The influence of these compounds on the total base of the seawater is profound, the carbonate and the bicarbonate almost disappearing. The buffering capacity of the liquid in decomposing *Enteromorpha* might be almost entirely ascribed to the system  $SH^- - H_2S$ . Also free organic acids are formed. Whether metabolism of organic S in the plant or the sulphate reduction is the source of the inorganic sulphide is still an open question.

3. The percentages of dry matter, ash, phosphorus, iron, and silica(tes) are exceptionally variable. This is primarily due to the fact that mineral matter accumulates in the outer, pectin, pellicle. This pellicle sloughs off at the outside and is continuously reformed during the life of the alga.

---

\* Officer of the Division of Fisheries, C.S.I.R.O., Cronulla.

\*\* JOHNSON and FLORENCE STONEY FELLOW, St. Andrews, Scotland. (This work was supported by a grant from the Science and Industry Endowment Fund, C.S.I.R.O.).

Hydroxy-acids, especially uronic acids (present in the pellicle), are known to be powerful chelating agents for phosphates. The presence of particulate phosphate and iron could be demonstrated in the pectin membranes.

4. For this reason it is difficult to measure accumulation rates. Moreover, phosphate is continuously given off by the plant, both in acid-soluble and acid-insoluble form.

When the *Enteromorpha* disappears from the flats, the percentage dry weight of the remaining (young) plants decreases. The particulate phosphate in the surrounding water shows a concomitant increase. The ratio's total  $P_iPO_4$  phosphate given off by the plant, or present in the pellicle, are similar to those observed in the water of the natural environment.

5. Artificially prepared ferric phosphate (strengite) and ferrous phosphate (vivianite) yield FeS (troilite) after treatment with  $H_2S$  or with sulphides. There is a considerable increase of acidity during this process and also a marked release of  $H_2PO_4^-$  and  $HPO_4^{2-}$  ion.

A similar solubilization of calcium orthophosphate with either ferrous hydroxide or hydrated ferric oxide (goethite) could be observed. The release of phosphate, formation of FeS, and increase in acidity are almost instantaneous.

6. *Enteromorpha*, when brought to an environment containing  $H_2S$  or sulphides, will release (probably by a similar mechanism as described under 5) almost instantaneously considerable quantities of both acid soluble and acid insoluble phosphate, in proportions similar to those observed in the natural environment.

7. Apart from its influence on pH, total base, electrode potential, iron and phosphate content of the environment, the metabolism as well as the seasonal decomposition of the algae might contribute many other compounds to the external milieu. The study of some of these compounds will be dealt with in a future publication.

## II. INTRODUCTION

Two species of *Enteromorpha*, *E. intestinalis* L. (Link.) and *E. prolifera* J.G. Ag., dominate, together with several species of *Zostera*, certain parts of the New South Wales estuaries during large part of the year. The association occupies the zone immediately below high water, together with the following organisms, some of which (marked with an asterisk) may temporarily dominate:

*Ulva* (*taeniata* (Setch.) S. & G. *lactuca*, L.) \*, *Monostroma*, *Vaucheria*, *Rhizoclonium*, *Chaetomorpha* (*crassa* \* Kütz a.o.), *Bryopsis plumosa* \* C.L. And. *Cladophora*, *Urospora*, *Ulothrix* (?), *Gracilaria confervoides* \* Farl. *Polysiphonia*, *Erythrioclonium*, *Laurencia* \*, *Mclobesia* \*\*, *Porphyra*, *Endarachne*, *Hypnea* (*musciiformis* ?), *Ectocarpus confervoides* \* (Roth), le Jol. *E. simpliusculus* \*\* Ag., *Scytosiphon*, *Spatoglossum*, and *Catenella*

\*\* epiphytic.

(*ripae* ?), of the diatoms *Mastogloea* \*\*, *Amphora*, *Navicula* spp., *Striatella unipunctata* Ag., *Pleurosigma baltica* Ehr. and *P. angulata* W. Smith, *Licmophora abbreviata* Ag. and *flabellata* Ag. Further various bluegreens, copepods, gammarids, nematodes, barnacles, acariniids, and crabs (chiefly *Myctyrus longicarpus* Latreille), molluscs (chiefly *Bembicium kielmanseggi* Seliber, *Pyrazus ebeneus* Martyn, and *Salinator fragilis* Lamarek. Under the algal mat the euglenoid *Eutreptia viridis* Perty var. *schizochlora* Entz is nearly always found. Of the protozoa we mention *Lionotus*, *Triflagellum*, *Vorticella*, and various foraminifera.

The zone slightly overlaps the *Zostera* association, but *Enteromorpha* extends to higher ground. In order to see how much exposure could be tolerated by the alga we have placed healthy plants of *E. intestinalis* over 8n H<sub>2</sub>SO<sub>4</sub> at 30° C., thus imitating extreme drying (less than 40 per cent. saturation) on a hot summer's day. After seven hours exposure, having lost 42 per cent. of its weight, the alga died. The loss in weight proved to be logarithmic and could be expressed by  $Y = 10 + 53 \log_{10} t$  (t in hours).

In summer, there is a sudden dying off, which may be caused by a sudden rise in temperature, together with a long exposure. In the autumn, the alga resettles the flats. With *Zostera*, and to a lesser extent, with *Posidonia* and *Ecklonia*, *Enteromorpha* dominates the scene in a region where the flats are used for oyster culture. It seemed, therefore, interesting to study its influence upon the environment.

### III. ELECTRODE POTENTIALS

The electrode potentials and the pH of the environment of *Enteromorpha* are given in Figure 1. The alga was observed or grown in both seawater and in synthetic media. The characteristics are distributed as follows:

TABLE 1

Eh	+ .600	+ .500	+ .400	+ .300	+ .200	+ .100	0	-.100
n = 103	10	9	22	24	19	15	4	
av. +.259 volts								
pH	4	5	6	7	8	9	10	
n = 103	2	11	28	33	26	3		
av. 7.27								

There is but little apparent correlation between pH and Eh but the potential milieu is extended, covering part of the region in which sulphate reduction occurs (BAAS BECKING and WOOD 1955).

In artificial seawater (using pyrex-redistilled water and recrystallized salts (HARVEY 1949)) the electrode potentials observed are on the whole higher than those observed in estuarine seawater. This may be due to the absence, in the former, of organic reducing compounds (COOPER 1937).

As compared with other algae, *Enteromorpha* may exist in water of much lower electrode potentials than tolerated by diatoms and unicellular green algae. Only blue greens have a wider milieu, both in electrode potentials and acidities, while diatoms may tolerate a very low pH (1.2 in water from the Rotarua, New Zealand, hot-spring region, BAAS BECKING and KAPLAN 1955).

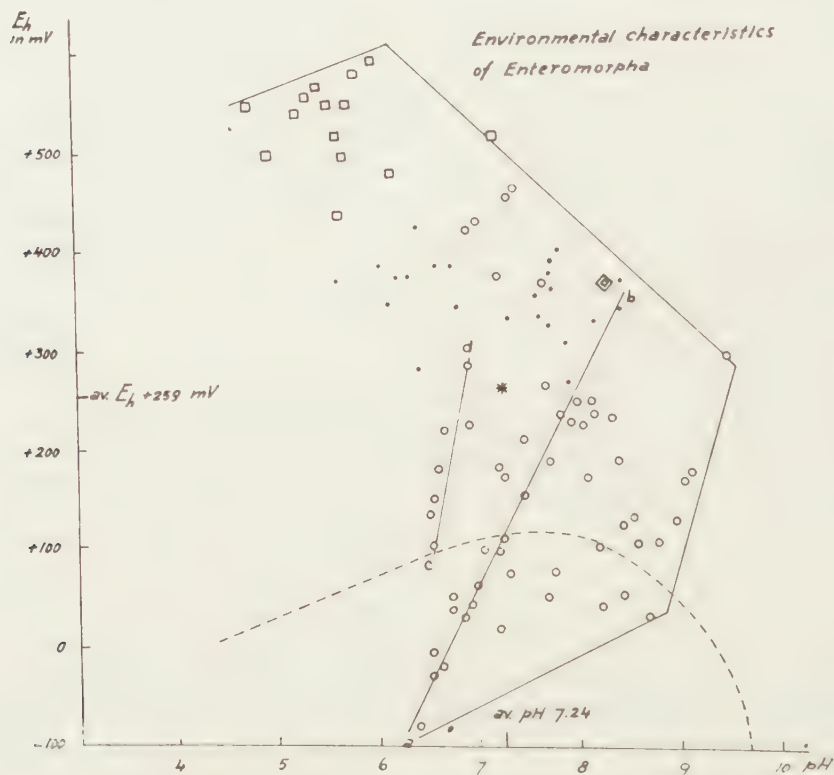


Fig. 1.

- Field observations and observations in seawater
- cultures on artificial media
- do. but with B, Mn, Cu, Co and Mo
- ◻ seawater at Cronulla N.S.W.
- \* average
- limits of sulphate reduction
- a-b, c-d change of characteristics in light and darkness

Most remarkable is the influence exerted by *Enteromorpha* on its environment. In seawater, when illuminated, the pH rises in the usual way to 9.4–9.6 due to the shift in the bicarbonate-carbonate equilibrium brought about by photosynthesis.

However, there appears a steep gradient in both pH and Eh in the algal mat. In a mud flat (Shell Point, George's River, 2.8.54), we found:



TABLE 2

Locality	Eh in volts	pH
Above algal surface . . . . .	+.290	8.68
Pool with algae, surface . . .	+.125	8.98
Pool, 1" deep . . . . .	+.085	7.86
Under algal mat . . . . .	-.045	7.02

If a mass of *Enteromorpha* be freed from debris (which often amounts to more than one-third of the mass) and a small amount of the clean alga is placed in seawater in the dark, in most cases the electrode potential as well as the pH will show a sharp drop, reaching a new level after about 3-4 hours at 20-25° C. Figure 2 shows the results of one experiment which is fairly representative. It will be seen that when light is admitted, there is a steep rise in both electrode potentials and in pH. The pH-Eh relation is linear, and could be represented (from the results of the above experiment) as  $Eh = -1.375 + .205 \text{ pH}$  volts (pH6-8).

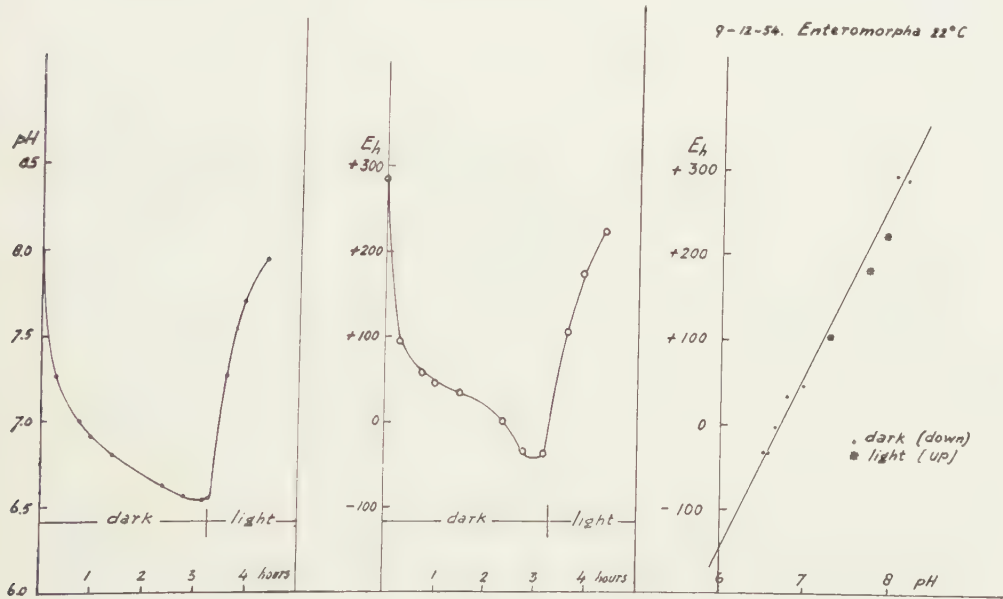


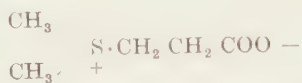
Fig. 2.

It seems that an acid, reducing substance is released into the environment in the dark, which substance is either destroyed or reabsorbed in the light. Because of both the magnitude and the promptness of the effect, it may not be ascribed to respiration and photosynthesis alone. Respiration cannot account for these changes. Bubbling  $\text{CO}_2$  through seawater caused the pH to drop steadily to 4.22, while there appeared no significant change (+406 - +446 mv) in the Eh. It should be remarked that the sudden drop of the electrode potential could always be observed when fresh algae were placed in the dark but that the effect on the pH

either, or both, on darkening and illumination may be less pronounced or even absent. When the acid is formed, titration curves (indicative of a material decrease in excess base) showed a plateau near pH 4.70-4.80, a region corresponding to the pK of many organic acids. It appears that small amounts of *Enteromorpha* may prepare the environment for sulphate-reduction in a short time and a very efficient way to observe the formation of black FeS is to press a mass of *Enteromorpha* between two glass slides, the effect being apparent in eight hours at 20° C.

In order to prove whether the formation of H<sub>2</sub>S is due to the activity of the *Desulphovibrio* or to algal metabolic products, pure cultures of the algae should be prepared; starting with gametes or zoospores. A few preliminary trials have shown that this will be a difficult task. *Zostera*, which behaves in a similar way, will be even more difficult to raise in a pure culture.

BYWOOD and CHALLENGER (1953) have shown that *Enteromorpha* produces dimethyl sulphide, which is apparently a product of a sulphonium salt.



Identical or similar compounds have been shown to be formed by *Polysiphonia* (HAAS 1935), *Fucus*, *Zostera*, and *Posidonia* (WOOD 1954), *Desulphovibrio* and *Thiobacteria* (BAAS BECKING, unpublished data)<sup>1)</sup>. CHALLENGER and collaborators have shown that methionin is their probable precursor. It may well be that sulphonium compounds may be formed by most living cells. Evidence is accumulating to show that sulphide and H<sub>2</sub>S are normal products of protein-metabolism.

As will be seen later, the formation of H<sub>2</sub>S plays a very important part in both the inorganic and the organic cycle of matter in the estuarine environment.

#### IV. CHEMICAL COMPOSITION

Little work has been published on the microchemistry of *Enteromorpha*. We found an outer pectin-pellicle, which is sloughed off continuously (WURDACK 1923) and a very faint indication of cellulose on some inner walls. Further no iodine-blueing starch, and a faint indication of fat or oil in the protoplasm of the young fronds. It could be shown that the outer pellicle is of a variable composition. Sometimes this pellicle is covered, in older plants, with epiphytes (*Mastogloea*, *Ectocarpus*, *Melobesia*), but even the clean spots show a varied picture. Both ferrous and ferric iron are present (acridin, Na<sub>2</sub>S, Fe<sup>++</sup>-Fe<sup>+++</sup> cyanide, NH<sub>4</sub>CNS,

<sup>1)</sup> The peculiar smell of the tidal flats and of algal masses (called "Coogee" by the New South Wales aborigines) is due to these, or similar compounds, together with amines.

dipyridyl) and localized in distinct spots. The same is true of the phosphate ( $\text{NH}_4$  molybdate,  $\text{NH}_4\text{Cl} + \text{MgCl}_2$ ) although the localization is difficult. Sulphide is present (Cd-acetate, Pb-acetate, Hg cyanide, Na nitroprusside) and apparently given off. Manganese could be localized in one case impregnating the outer pellicle (benzidin). Reactions on copper were negative (cupron,  $\text{Na}_2\text{S}$ ). There is evidence that the outer pellicle contains uronic acids (weakly positive reaction with naphthoresorcinol). The epiphytic *Mastogloea*, however, showed strong reactions of uronic acid (also with orcinol, phloroglucinol remained negative). *It seems that Enteromorpha acts like a trap for particulate matter and that this matter is incorporated in the pellicle.* Sooner or later this material returns to the environment. Apart from this there must be a normal 'give and take' of such substances of phosphates and the secretion of the sulphonium salt and the dimethyl sulphide. For the latter we used HAAS' (1935) technique in flushing the water (plus *Enteromorpha*) with  $\text{CO}_2$  and leading the gas through a solution of bromine in carbon tetrachloride. Lemon-yellow glistening crystal plates were formed. In older cultures the presence of several amines could be demonstrated. We could not ascertain whether these substances were actively excreted or whether they originated from dead tissue.

In view of the above findings, we may expect a great variability in the composition of the alga. Table 3 shows the results of several analyses, chiefly performed on *E. intestinalis*.<sup>1)</sup>

Reliable data on *Enteromorpha intestinalis* are given by McPHERSON and YOUNG (1949). While their figures on ash seem a bit low, their averages for iron and phosphate are close to ours. However, this must be accidental, as the variability is very high. We find for this variability:

Dry weight	4 ×
Ash	1.6 ×
Silica(tes)	3.2 ×
Iron	7.0 ×
Phosphate	28.0 ×

Care should be taken to collect the algae under water, as the dry weight will increase with exposure time (see above). Therefore too much importance should not be attached to the figures on dry weight. The ash content seems to be the most conservative, but silica(tes), iron, and phosphates are extremely variable.

In view of the microscopic findings this variability can be accounted for. It is due to the incorporation of particulate matter in and on the pellicle. Due to the sloughing-off of this pellicle, much material is returned to the seawater. Apart from this, we find the excretion of acid and reducing substances.

<sup>1)</sup> We were assisted in these analyses by Messrs. H. JITTS, C. WALKER, and D. IZZARD, all of C.S.I.R.O.

TABLE 3  
Composition in % of dry weight

	Dry weight % air dry	Ash	Silica(tes)	Iron	Phosphate
	7.6	45.6	.511	.140	0.20
	11.4	47.5	.908	.263	.044
	13.0	51.0	1.050	.300	.048
	14.1	53.5	1.055	.316	0.64
	15.6	60.5	1.132	.350	0.72
	16.0	63.0	1.215	.415	0.85
	16.0	66.0	1.227	.461	.087
	17.0	71.0	1.676	.520	.105
	17.0			.525	.114
	17.1			.590	.153
	19.0			.600	.192
	27.2			.660	.200
	28.1			.690	.205
	28.3			.755	.224
				.850	.290
				.870	.355
				.990	.373
					.380
					.420
					.442
					.560
N	14	8	8	17	21
Mean	17.70	57.27	1.079	.545	.193
Range	7.6-28.3	45.6-71.0	.511-1.676	.140-.990	.020-.560
McPHERSON and YOUNG	—	45.4	—	.582	.210

KATAYAMA and TOMIYAMA (1951) have shown that, besides dimethyl sulphide, *Ulva pertusa* contained a great number of aliphatic acids, which KATAYAMA (1953) later specified as acetic, propionic, butyric, valeric, myristic, and linolenic acids. In *Enteromorpha*, similar acids are excreted as electrometric titration of the solution in which *Enteromorpha* had been confined, showed a decided plateau at a pH near 4.80. The pK's of the C<sub>2</sub>-C<sub>4</sub> monobasic acids are all situated in this neighbourhood. The titration-curve of seawater (X base =  $2.45 \times 10^{-4}n$ ) shows a flattening at pH 6.6, corresponding to the pK of the reaction  $H_2CO_3 \rightleftharpoons H^+ + HCO_3^-$ . This plateau disappeared when 10 g *Enteromorpha* (wet weight) were kept in 100 ml seawater for three days. The algae remained in a healthy condition, and the X-base was reduced to .1 of its initial value. Together with the flattening of the curve caused by the organic acids the main region of inflection was situated at pH 7.0, corresponding to the pK of the reaction  $H_2S \rightleftharpoons H^+ + SH^-$ . Titration with .01 n NaOH showed various plateaus apart from NH<sub>4</sub>OH; they may be ascribed to amines.



It is interesting to note that JOHNSTON (1954) described a solvent action on calcium orthophosphate of acetic, butyric and propionic acid, which was twice as strong as that of .01 n HCl. However, the oxyacids, such as lactic, gluconic, and uronic acid, showed a much higher solvent power, as the following table shows:

TABLE 4 (after JOHNSTON, 1954)

mg "P <sub>2</sub> O <sub>5</sub> " in 100 ml filtrate		
HCl	.1n	333
	.01	55
	.001	25
	.0001	25
	acetic	129
	propionic	121
	butyric	123
	lactic	249
	gluconic	225
	galacturonic	241

It will be seen that uronic acid exerts a high solvent power on phosphates. It is also well known that iron enters easily into combination with oxyacids (the "soluble iron phosphate" of the pharmacists is prepared with citric acid). As both lower fatty acids and the uronic acids are apparently continuously formed by *Enteromorpha*, there is reason to assume that both the iron and the phosphate will be in chelate combination. *It may well be that the function of the pectin membrane is to chelate (otherwise insoluble) compounds of the environment.*

(To be continued)

# BIOLOGICAL PROCESSES IN THE ESTUARINE ENVIRONMENT

## VB. THE INFLUENCE OF *ENTEROMORPHA* UPON ITS ENVIRONMENT

BY

L. G. M. BAAS BECKING \* AND MARGARET MACKAY \*\*

(Communicated at the meeting of November 26, 1955)

### V. LIBERATION OF PHOSPHATE

Apart from the chelating action of acids (either secreted or formed by the decomposition of the sloughed off pellicle), *Enteromorpha* possesses another mechanism by which phosphates may be made available. A few simple model experiments led us to the realization of the nature of this process.

Strengite ( $\text{Fe PO}_4 \cdot 2 \text{H}_2\text{O}$ ) was prepared by treating iron powder with 30 per cent. acetic acid. The acetate was neutralized with  $\text{Na}_3\text{PO}_4$  and the precipitate washed. Blueish spots showed the presence of the ferrous phosphate (vivianite). Addition of  $\frac{1}{2}$  vol. 3% soln. of  $\text{H}_2\text{O}_2$  oxidized this ferrous compound completely. When the Fe-acetate and  $\text{Na}_3\text{PO}_4$  are mixed at boiling temperature, chiefly vivianite is obtained.

A suspension of these phosphate treated with  $\text{H}_2\text{S}$ , will react immediately with the formation of  $\text{FeS}$ , with a concomitant decrease in pH. The reaction is completed within 15 minutes at room temperature. There is a

TABLE 5  
Release of P after  $\text{H}_2\text{S}$  treatment  
(determinations by H. JITTS and C. WALKER)

	mg	ml	pH		P in mg/		Time	Temp.
			before	after $\text{H}_2\text{S}$	before	after		
Strengite	100	25	6.57	5.31	4.85	11.63	9'	15° C
						10.16	9'	15° C
	300	100	6.42	3.81	4.12	20.90	20'	15° C
						19.08	20'	15° C
Vivianite	300	100	—	—	2.10	16.20	20'	15° C
$\text{Ca}_3(\text{PO}_4)_2$	2150	100	6.44	6.08	4.40	13.60	30'	17° C
+ $\text{Fe}(\text{OH})_2$	460							
$\text{Ca}_3(\text{PO}_4)_2$	2150	100				10.80	30'	17° C
+ $\text{Fe}^{+2}_{-\text{OH}}$	1000							

\* Officer of the Division of Fisheries, C.S.I.R.O., Cronulla.

\*\* JOHNSON and FLORENCE STONEY FELLOW, St. Andrews, Scotland. (This work was supported by a grant from the Science and Industry Endowment Fund, C.S.I.R.O.)

concomitant increase in soluble phosphate often more than six fold as compared with the control. Calcium orthophosphate may be solubilized in the same way, if either (insoluble) ferrous or ferric oxides be present.

As we have seen, *Enteromorpha* yields phosphate to its environment, especially in the dark. However, the phosphate content of the surrounding seawater may be increased manifold if  $H_2S$  is bubbled for ten minutes through the liquid in which the alga is bathed. Curiously enough the phosphate, not readily soluble in acid ("organic phosphate" of the hydrologist, liberated by K-perchlorate) also increases by the  $H_2S$  treatment (Table 6).

Inasmuch as *Enteromorpha* liberates sulphide it has two mechanisms by which it may solubilize the particulate or chelated phosphate entrapped in its outer, pectin, membrane.

TABLE 6

Yield of phosphorus to the environment in  $\gamma P$ . 2 gr *E. intestinalis* in 200 ml filtered seawater (free of P). T varied between 22–30° C, at 5° C no P was given off

Hours	4				72			
P	H <sub>2</sub> S. 10'				H <sub>2</sub> S. 10'			
	Acid soluble	Total	Acid soluble	Total	Acid soluble	Total	Acid soluble	Total
	0	0	70	100	0	200	330	920
	0	160	140	400	490	520	310	640
					310	—	530	—
					0	0	210	
					20	880		
Av.	0	80	105	250	164	400	346	780
P tot/ac			2.38		2.04		2.27	
Liberated by								
H <sub>2</sub> S			105	170			181	380
P tot/ac			1.62				2.10	

Using the average composition, we find that in 2000 mg air dry weed, 344 mg dry weight, .193 % or 644  $\gamma$  will be, on the average, P. In one case 920  $\gamma P$  was given off in 72 hours at 25° C after  $H_2S$  treatment. If we take the minimum values as expressing the composition of clean, live material, we obtain

dry weight	7.6 %	of air dry
ash	45.6 %	of dry weight
silica(tes)	.511	„
iron	.140	„
P	.020	„

Comparing these values with the analyses of MACPHERSON and YOUNG (1949) for 17 different algae, the above values are all abnormally low, the values for ash and iron excepted, for here the values are abnormally high. The author gives as extreme values

for dry weight <i>Laminaria longicruris</i>	9.5 % of air dry
for ash (highest value) „	34.8 % of dry weight
for P <i>Chondrus crispus</i>	.11 „
for Fe (highest value) <i>Ulva lactuca</i>	.139 „

As MACPHERSON and YOUNG remark, green algae seem to be much higher in iron than the other groups.

Due to this great variability it seems impossible to draw conclusions from the absolute amounts liberated.

In all phosphate excretion into phosphate-free seawater, the quotient Total P/acid soluble P varied between narrow limits: 1.62–2.38, average 2.16.

This means that approximately the same proportion of total P/acid soluble P is released by the algae, but also that the additional P, released by  $H_2S$ , shows the same characteristics.

This may mean that  $H_2S$  not only frees  $HPO_4^-$  ion from iron phosphate or from calcium phosphate plus ferrous or ferric iron, but also from compounds not soluble in acid, which substances only yield phosphate after digestion with perchlorate. More probable seems the explanation that larger aggregates may enter into the outer environment (as suspensions) more readily after some solution has been effected by means of  $H_2S$ , but that these aggregates but slowly yield to  $H_2S$ .

TABLE 7

Average content of acid soluble P (I) and Total P (II)  
in the waters of Shell Point, George's River, 1950–1954

Month	I	II	
1	18	47	2.59
2	24	49	2.02
3	32	78	2.44
4	22	41	1.86
5	10	36	3.60
6	7	16	2.29
7	10	31	3.10
8	12	35	2.91
9	10	19	1.90
10	14	37	2.63
11	14	42	3.00
12	16	57	3.54
Average	15.8	41.5	2.64

Of the water sampled at the jetty near the point where the algae were collected (Shell Point) the hydrology section of our laboratory has kindly supplied us with monthly determinations of both acid soluble and total P, extending over four years. The results are shown in Table 7. It will be seen that the proportions between the two forms of phosphate are similar to (perhaps somewhat higher than) those as excreted by *Enteromorpha*.



In view of the fact that many other organisms contribute to this phosphate (to mention only *Zostera*), the agreement seems more than accidental. As the release of P by *Enteromorpha* might be almost entirely from the

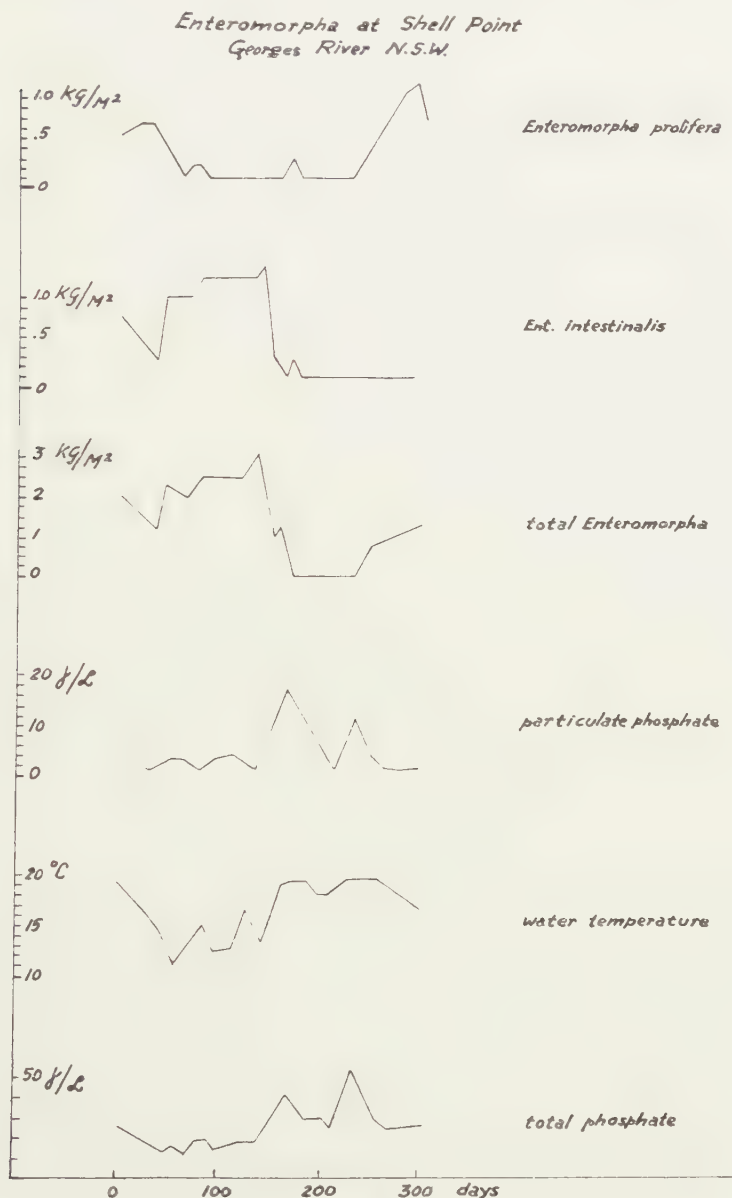


FIG. 3.

pectin pellicle, this alga most likely "catches", by turbulence from the mud-surface as well as by currents, the phosphate from its surroundings, incorporating the aggregates in the outer pectin pellicle and, maybe, partly chelates them. The natural chelates of iron, calcium, phosphates, and uronic acids have never been studied. It would be interesting to

know whether they yield  $\text{PO}_4$  with mineral acid. Fig. 3 shows various characteristics of the water taken at Shell Point, George's River, about 150 yards from the spot where the amount of *Enteromorpha* per square meter was determined regularly.

It will be seen that the dying off was initiated by a sudden jump in the water temperature. While the alga was disappearing, the particulate phosphate showed an increase. This particulate phosphate would later be solubilized.

EINSELE (1938) has called attention to the relation between reducing conditions and the release of phosphate. The reducing conditions in deeper estuarine waters as well as in the surface mud are almost entirely caused by the system  $\text{H}_2\text{S}(\text{SH}^-) \rightleftharpoons \text{S}$  as we hope to elaborate in another paper.

Unfortunately, the hydrologists have not, as yet, determined the sulphide concentration in these deeper waters. If we make the, not unwarranted, assumption that the oxygen deficit of a deeper water is an expression of its sulphide content, we might expect a close relation between available phosphate and oxygen deficit. Such a relation exists. There can be no doubt but that every change in the  $\text{PO}_4$  phosphorus in deeper water (25–30 m deep, S.W. Arm, Port Hacking) corresponds to an inverse change in oxygen saturation of this water. While there is much that is still enigmatical in this matter, the results obtained with *Enteromorpha* at least show a possibility of an explanation. We intend to revert to this problem in a later communication.

We have to thank the Hydrology section of this Division, and more in particular its head, Mr. D. ROCHFORD, for both encouragement and active help. Mr. E. J. F. WOOD has given useful information and criticism.

#### LITERATURE

- BAAS BECKING, L. G. M. and E. J. F. WOOD, Biological processes in the Estuarine Environment I and II. Proc. Kon. Ned. Ak. van Wet. **B 58**, 159 (1955).  
 ——— and I. R. KAPLAN, Biological processes in the Estuarine Environment III and IV. Proc. Kon. Ned. Ak. van Wet. **B 59**, 85 and 97 (1956).  
 BYWOOD, R. and F. CHALLENGER, The evolution of dimethyl-sulphide by *Enteromorpha intestinalis*, isolation of dimethyl-p. carboxyethyl sulphonium chloride from the alga. Biochem. Journal **53**, 4 (1953).  
 COOPER, L. H. N., Oxidation-Reduction Potentials in Seawater. Journ. Marine Biol. Assn. U.K. **22**, 167 (1937).  
 EINSELE, W., Ueber chemische und Kolloidchemische Vorgänge in Eisenphosphat-systemen unter limnochemischen und limnogeologischen Gesichtspunkten. Arch. f. Hydrobiol. u. Planktonkunde **33**, 361 (1938).  
 HAAS, P., The liberation of methyl sulphide by seaweed. Biochem. Journal **29**, 297 (1935).  
 HARVEY, H. W., The supply of iron to diatoms. Journ. Marine Biol. Assn. U.K. **22**, 205 (1937).  
 JACOBSEN, L., Maintenance of iron supply in nutrient solutions by a single addition of ferripotassium ethylenediamine tetra-acetate. Plant. Physiology **26**, 411 (1951).

- JOHNSTON, H. W., The solubilization of "insoluble" phosphate. II. A quantitative and comparative study of the action of selected aliphatic acids on tri-calcium phosphate. New Zealand Journ. of Science and Technology 36, 49 (1954).
- KATAYAMA, T., and TOMIYAMA, Chemical studies on the volatile constituents of seaweed. I. The fractionation of the volatile constituents of *Ulva pertusa* K. Bull. Jap. Soc. Scientif. Fisheries 17, 8 (1951).
- , Chemical studies on the vol. const. of seaweed. II. On volatile acids of *Ulva pertusa* K. Bull. Jap. Soc. Scientif. Fisheries 19, 793 (1953).
- MACPHERSON, M. G. and E. GORDON YOUNG, The chemical composition of marine algae. Canad. Journ. Res. C27, 73 (1949).
- WOOD, E. J. F., Reducing substances in *Zostera*. Nature 172, 916 (1954).
- WURDACK, M. E., Chemical composition of the walls of certain algae. Ohio Journ. Sc. 23, 181 (1923).

CONTRIBUTIONS TO THE COLLOID CHEMISTRY OF  
PHOSPHATIDES. IIIA <sup>1)</sup>

1. *Electrical decompensation of phosphatide micelles by detergents.*
2. *Action of cetyltrimethylammonium bromide on suspensions of egg-phosphatides in the absence and presence of NaCl.*

BY

H. G. BUNGENBERG DE JONG AND A. DE BAKKER

(Communicated at the meeting of December 17, 1955)

1. *Introduction*

In part II of this series the hitherto unknown O-coacervates, elastic-viscous systems and non elastic solutions of phosphatides have been realised from a suspension of the smectic phase of egg-phosphatides by Na-salicylate in increasing concentrations. The action of Na-salicylate has been ascribed to a weakening of the intermicellar interactions as a consequence of decompensation of the original charge ratio 1:1 of the phosphatide by preferential binding of the salicylate ion to the positively charged groups of the phosphatide. The concentrations of Na-salicylate needed to achieve the above transformations are relatively high.

It is conceivable that detergents (anionic as well as cationic) may achieve the same transformations already at low concentrations. This might be expected when:

- a) the detergent becomes strongly bound to the phosphatide,
- b) the detergent ions are taken up in such a manner in the sandwich micelles (of quasi infinite extension and arranged parallel to each other in the smectic phase) of the phosphatide, that their ionized groups are present in the surface of the micelles,
- c) the counter ions of the detergent are not, or not all bound at the same time to the surface of the micelle,
- d) no unforeseen complications occur.

The above is illustrated in the upper row of fig. 1 for the uptake of a detergent cation. With  $Q$  is meant the ratio detergent phosphatide and with  $R$  the ratio negative charges/positive charge. We see that with increase of  $Q$  the decompensation of the charge pattern increases ( $R$  decreases).

We may furthermore expect that in the presence of a salt, higher  $Q$  values will be needed for the transformation into O-coacervates, elastic

<sup>1)</sup> Parts I and II of this series have been published in these Proceedings, Ser. B 58, 238, 251, 257 (1955).



viscous systems and non elastic solutions. This follows from the consideration that as a consequence of binding of that ion of the added salt which is oppositely charged to the detergent ion, the electrical decomposition will be less than in the absence of salt.

Compare lower row in fig. 1 which illustrates the neutralization of decomposition at constant  $Q$  with increased binding of an anion, that is with increased salt concentration.

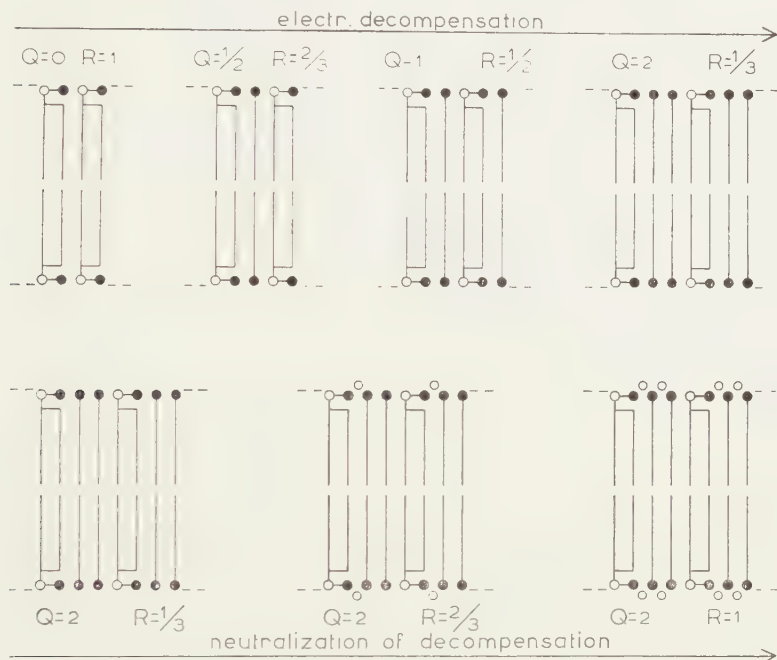


Fig. 1. Electrical decomposition of the phosphatide micelle by a detergent cation (upper row) and its neutralization by salts (lower row)

The present and the next communication (Part IV of this series) deal with the action of cetyltrimethylammonium bromide and of sodium laurylsulphate on suspensions of egg-phosphatides in the absence and presence of salts. The results will show that the above expectations and further consequences of them come true when the salt concentration is higher than a certain minimum value.

## 2. Materials and Methods

### a. Egg-phosphatides

We started from fresh *Eilecthin pur.* from Merck. Two preparations have been used which after arrival were stored in a  $\text{CaCl}_2$ -exsiccator. *Preparation I* (used in Part III), after some months kept at room temperature, was further stored at  $4^\circ \text{C}$ . *Preparation II* (used in Part IV), was at once stored at  $-10^\circ \text{C}$ . The two preparations gave in principle the same results, only the rate of solution in detergent solutions was decidedly slower in preparation II. The preparations contain as main constituents phosphatidylcholine and phosphatidylcolamine in the proportion 4:1. Accordingly we have assumed 751 as mean molecular weight for expressing the

phosphatide concentration. The phosphatide suspensions were prepared according to the detailed description given in Parts I and II of this series, and when not directly used, stored at 4°.

*b. Cetyltrimethylammonium bromide (CTAB)*

Two preparations from Hopkin & Williams have been used. Analysis (precipitation of the solution with excess bichromate and iodometric backtitration of the bichromate in the filtrate) gave for preparation I (used in Part III) a purity of 77 % (calculated as CTAB) and for preparation II (used in Part IV) a purity of 96 %. Whereas preparation I contained  $\text{Na}_2\text{SO}_4$  as impurity, preparation II was ash free.

*c. Sodium laurylsulphate (NaLS)*

We started from Na-Laurylsulphate (NaLS) from the "Amsterdamsche Chinine-fabriek", Amsterdam. It was used in Part IV as such: "preparation I" and after being twice recrystallised from alcohol: "preparation II". Both preparations have been analysed using two methods (precipitation with  $\text{Co}(\text{NH}_3)_6\text{Cl}_3$  and Kjehldal determination of N in the filtrate; hydrolysis with dilute  $\text{H}_2\text{SO}_4$  in a tertiary butanol- $\text{H}_2\text{O}$  mixture—to keep the lauryl alcohol in solution—and measuring the increase of acidity) which gave results which differed no more than 1 % in the calculated purity. The means of the two methods gave for preparation I a purity of 83 % (calculated as NaLS) and for preparation II of 92 %.

*d. Measurement of viscosity and determination of the spinning limit*

In sections 3 and 4 the viscosity of mixtures of phosphatide and CTAB has been measured, using a simple method, which is especially suited for series work <sup>1)</sup>. The viscosimeter is constructed in such a way that the fluid drips off at a low rate into the air. This makes it possible to observe whether the fluid spins a thread or not. This limit indicates the position of the limit elastic/non elastic while the fluid is streaming (dynamic elastic limit).

*e. Determination of the elastic limit*

For observing the presence of static elasticity (elasticity of the fluid at rest) a short rotational impulse is given to the tube containing the fluid + a few suspended air bubbles. Dependent on the damping the bubbles oscillate one or more times to and fro. When the damping is very large only one turning point can be observed. We still regard a fluid as elastic, when after the impulse the bubble comes to a sudden standstill, though a movement in the reverse direction can no longer be observed. The above may suffice to show that the so-called elastic limit is in reality a limit where the damping becomes very large.

*3. Action of CTAB on phosphatide suspensions in the absence of NaCl*

*a. General*

At room temperature (20° C) CTAB at sufficient concentration slowly dissolves the suspension particles and a perfectly clear system may be obtained which is markedly viscous and exhibits elastic properties. At higher CTAB concentrations the viscosity of the clear systems diminishes and elasticity can no longer be observed. Between the very turbid systems

<sup>1)</sup> H. G. BUNGENBERG DE JONG and G. W. H. M. VAN ALPHEN, these Proceedings 50, 849 (1947).

at low CTAB concentrations and the perfectly clear elastic viscous systems no coacervation has been observed with certainty.

Thus instead of the expected series (see Introduction): smectic phase  $\rightarrow$  O-coacervate  $\rightarrow$  elastic viscous system  $\rightarrow$  non elastic solution, we actually obtain:

smectic phase  $\rightarrow$  elastic viscous system  $\rightarrow$  non elastic solution.

The omission of the coacervates in this series of transformations gives rise to the suspicion that the elastic viscous systems are of another kind than those which should be formed as a consequence of an electrical decompensation of the charge pattern of the phosphatide by uptake of CTA-cations. The experiments in this section will settle this question.

#### b. Various limits in dependence on the phosphatide concentration

Starting from an egg-phosphatide suspension containing 46.3 m mol/l phosphatides (preparation I) and a stock solution of CTAB (preparation I) of 42.4 m mol/l, three series of mixtures (A, B and C) were made at 20° C as follows:

A)  $a$  ml CTAB +  $(14-a)$  ml H<sub>2</sub>O + 1 ml phosphatide suspension.

B)  $a$  ml CTAB +  $(9-a)$  ml H<sub>2</sub>O + 1 ml " "

C)  $2a$  ml CTAB +  $(13-2a)$  ml H<sub>2</sub>O + 2 ml " "

in which  $a$  increases with steps of 0.25 ml. After 15 hours standing at 20° it was noted which mixture in the series A, B and C respectively was the first which was perfectly clear. As solution limit is taken the mean of the CTAB concentration of this mixture and the preceding one. See Table I, column 2. In a similar way the lower elastic limit (Table I column 3) and the upper elastic limit (Table I, column 4) are obtained. Between the two latter limits are found the mixtures which clearly show elasticity.

TABLE I

Concentrations of CTAB in m mol/l which correspond to various limits at the indicated times

Series and phosphatide concentr. (m mol/l)	after 15 hours			after 22 hours				maximum viscosity
	clear	elastic limits		thread draw. limit		viscous limit		
	opalesc. (op/cl)	lower (n.e/e)	upper (e/n.e)	lower (n.sp/sp)	upper (sp/n.sp)	lower (n.v/v)	upper (v/n.v)	
A 3.09	7.4	4.4	8.8	4.6	8.8	4.6	11.9	8.3
B 4.63	10.6	7.4	11.7	8.0	11.1	6.6	15.7	12.1
C 6.17	14.8	9.2	16.3	9.2	14.8	8.5	22.2	15.1

In fig. 2 the data of columns 2, 3 and 4 are plotted against the phosphatide concentrations of the series A, B and C. It is seen that the points lie close to three straight lines through the origin. The actual deviations are as a rule not larger than the "error" (0.35; 0.53 and 0.71 m mol/l CTAB, these being half the concentration steps in the series A, B and C respec-

tively). After 22 hours standing at 20° we measured the "viscosity" of the mixtures (20° C). As explained in section 2, the method allowed us to observe whether the fluid is thread drawing or not. Thus we obtained data on the lower and upper limit for thread drawing (spinning) (Table I, columns 5 and 6). They have been plotted in fig. 3 as a function of the

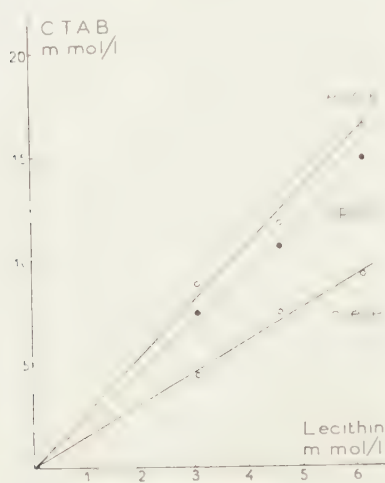


Fig. 2

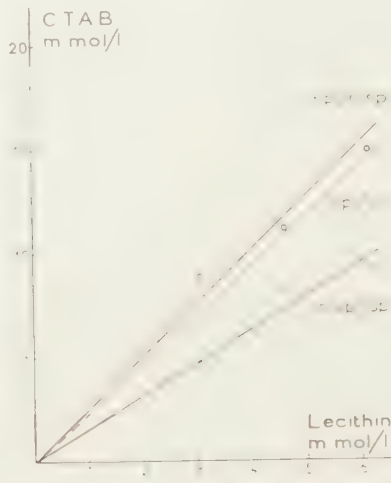


Fig. 3

Figs. 2 and 3. CTAB concentrations corresponding to the limits mentioned in columns 2-6 of Table I in dependence on the phosphatide concentration

phosphatide concentration (n.sp/sp and sp/n.sp). The dotted line gives the limit clear/opalesc. which at 22 hours has the same position as at 15 hours. The results of the viscosity measurements are given in fig. 4<sup>1)</sup>. The CTAB concentration corresponding to the maxima of the three  $t/t_{H_2O}$  curves are given in column 9 of Table I. We have furthermore read from fig. 4 at which CTAB concentrations  $t/t_{H_2O}$  has the value 1.20 for curve A, 1.30 for curve B and 1.40 for curve C. At the above  $t/t_{H_2O}$  values corresponding states as regards viscosity are present, because the phosphatide concentrations in the mixtures A, B and C are in the ratio 2 : 3 : 4<sup>2)</sup>.

In this way we obtain for each curve a lower CTAB concentration at which the viscosity has just begun to increase above its horizontal level, and a higher CTAB concentration at which the high viscosity in between has decreased to the same values (1.20, 1.30 and 1.40 respectively). The above CTAB concentrations have been given in Table I, under the headings

1) The values  $t/t_{H_2O}$  which have been plotted in fig. 4 are the means of the first five successive  $t/t_{H_2O}$  values. It appeared that during these five measurements  $t/t_{H_2O}$  decreases. The effect is appreciable when the viscosity is high and at the same time there is distinct thread drawing. In the reverse cases it is weak. We return to these observations in the next subsection.

2) It is assumed that  $(t - t_{H_2O})/t_{H_2O}$  is approximately proportional to the phosphatide concentration.



"lower viscous limit" (column 7) and "higher viscous limit" (column 8) respectively.

In fig. 5 the data of columns 7, 8 and 9 have been plotted against the phosphatide concentrations of the series A, B and C. The figures 2, 3 and 5 show that at a given observation time (after 15 hours in fig. 2, after 22 hours in fig. 3 and 5) each of the various limits is characterised by a certain CTAB/phosphatide ratio. It seems safe to conclude that in the whole range of ratios between the lowest (about 1.4) and the highest (about 3.6), CTA (or CTAB) is all or nearly all bound to the phosphatide<sup>1)</sup>.

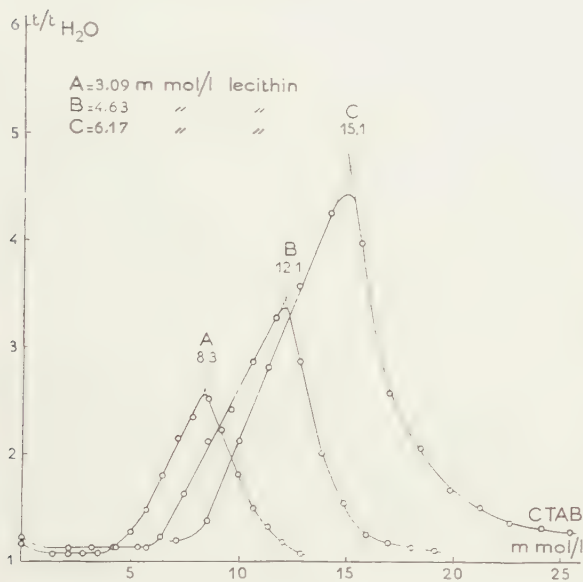


Fig. 4

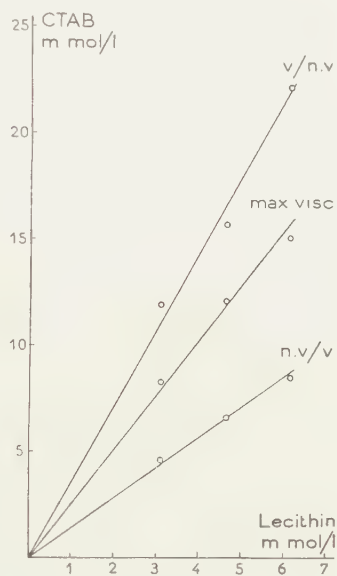


Fig. 5

Fig. 4. Viscosity in dependence on the CTAB concentration at three phosphatide concentrations

Fig. 5. CTAB concentrations corresponding to the limits mentioned in columns 7-9 of Table I in dependence on the phosphatide concentration

### c. The non-equilibrium character of the elastic viscous and non elastic solutions

In the case of series B, we have not only observations after 15 and 22 hours, but also after 2 hours (limit clear/opalesc, lower and upper elastic limits) and after 41 hours (viscosity, compare fig. 6). The various limits have been plotted in fig. 7. It is seen that the distance between the lower and upper elastic limit becomes smaller with time and both limits must have met between 15 and 22 hours, as at 22 hours the mixtures no longer showed (static) elasticity. The shape of the limiting curve

<sup>1)</sup> The errors in the various limits do not allow for the conclusion whether the straight lines in figs. 2, 3 and 5 really go through the origin or whether they cut the CTAB axis at low CTAB concentrations (in the order of 1 or 2 m moles/l.).

enclosing the area of the elastic viscous systems (shaded in fig. 7) has, of course, been drawn tentatively. The same applies for the closed curve giving the thread drawing limit (dynamic elastic limit), for the drawing of which we have only the two limits at 22 hours and the observation that at 41 hours no mixture showed thread drawing any longer.

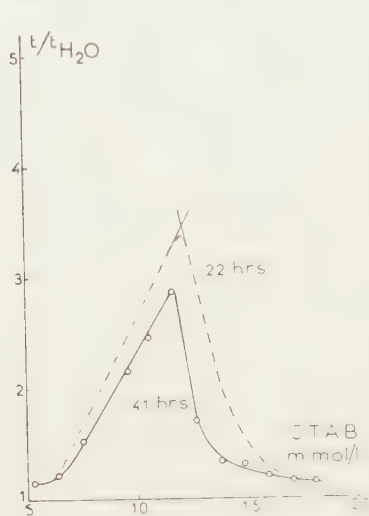


Fig. 6

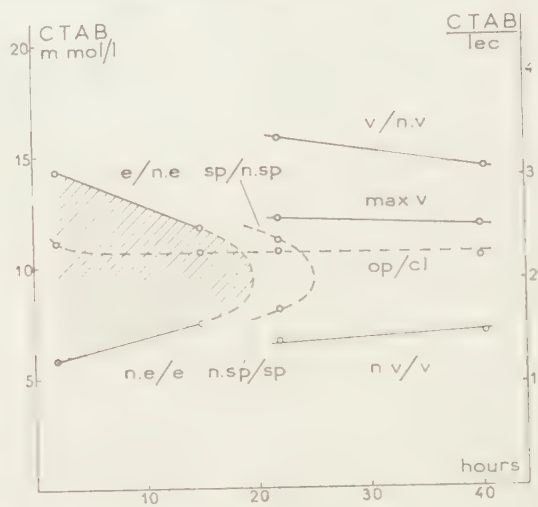


Fig. 7

Fig. 6. Change of viscosity with time for series B

Fig. 7. Change of some limits with time for series B

The fact that the two "viscous limits" lie closer to one another at 41 hours than at 22 hours (combined with the fact that the value  $t/t_{H_2O}$  at the maximum has also decreased, compare fig. 6) suggests that after a sufficiently long time the two viscous limits will meet too.

The above observations allow for the conclusion that no fundamental value can be attached to the proportionality factors which can be calculated from the columns 2-9 of Table I, for they only apply for a given observation time.

The elastic, thread drawing and viscous limits change with time and sooner or later the systems lose their elasticity, thread drawing and presumably their surplus viscosity (reckoned from a certain low level). The only limit which contrasts favourably with the others is the limit clear/opalescent. It soon reaches a value, which thereafter decreases only slightly. It gives the impression that it tends asymptotically to an end value, which expressed in the ratio CTAB/phosphatide has a value of about  $2.2 \pm 0.1$ .

#### d. Nature of the elastic viscous systems

Certain observations (compare note 1 on p. 128) make it probable that the mechanical means applied for measuring viscosity—flow through the capillary—breaks down high viscosity. A similar influence has been observed regarding thread drawing.

When the latter property is vigorous (spinning of thick threads) it usually persists during the five successive passages of the fluid through the capillary. When thinner threads are formed we may meet the case, that thread drawing is only observed during the first four or a lower number of passages of the fluid through the capillary. It seems likely that the vigorous but short rotational impulse given to the tube in order to test the presence of elasticity, will also diminish elasticity (as well as viscosity and thread drawing). It follows that fig. 7 possibly does not give a true representation of the spontaneous changes with time, because each of the mixtures of series B has repeatedly been exposed to mechanical treatments (tests on presence of elasticity after 2, 15, 22 and 41 hours and viscosity measurements after 22 and 41 hours).

The following experiments aim at answering the question whether spontaneous changes with time really exist and whether a weak but continuous mechanical treatment, in itself has influence.

Two identical phosphatide-CTAB mixtures of 100 ml were made in stoppered 500 ml medicine flasks labelled  $A_I$  and  $A_{II}$ , in which the phosphatide concentration was 4.63 m mol/l and the CTAB concentration 10.6 m mol/l. Two further identical mixtures were made at the same time in 500 ml medicine flasks labelled  $B_I$  and  $B_{II}$ , in which the phosphatide concentration was also 4.63 m mol/l, but the CTAB concentration was 12.7 m mol/l. The composition of the mixtures A and B is such that in fig. 4, they would correspond to points high up in the  $t/t_{H_2O}$  curve for series B, at either side of the viscosity maximum. The flasks  $A_I$  and  $B_I$  were left standing (at room temperature, fluctuating around  $20^\circ$ ) while the flasks  $A_{II}$  and  $B_{II}$  were placed horizontally on a rolling device, which gave the flasks about 40 revolutions per minute. After 3.03 days rolling, the flasks  $A_{II}$  and  $B_{II}$  were then left standing at rest.

At appropriate times samples were taken from the flasks, and from these were determined  $t/t_{H_2O}$  (mean of the first five single  $t/t_{H_2O}$  values) and it was observed during how many of the five passages of the fluid through the capillary thread

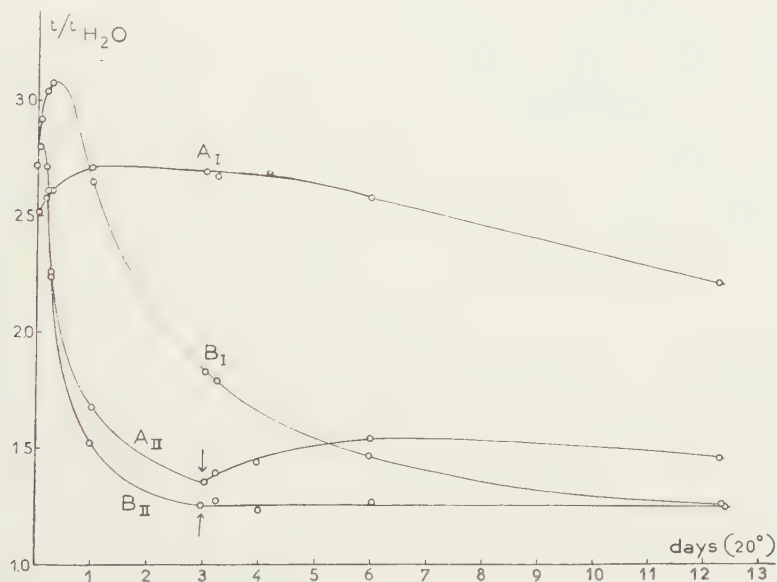


Fig. 8. Loss of the initially developing high viscosity of two phosphatide-CTAB mixtures A and B with time.  $A_I$  and  $B_I$  are kept at rest,  $A_{II}$  and  $B_{II}$  are gently rolled upto the arrow and after this kept at rest (see text)

drawing was present. This number  $n$  attributed to a mixture has as a maximum the value 5 and as a minimum the value zero. After measurement the samples were not returned to the flasks.

The results of the viscosity measurements have been plotted in fig. 8 and the observations regarding thread drawing have been given in fig. 9. From these figures the following facts can be read off.

1. Decrease or loss of high viscosity and loss of thread drawing already takes place spontaneously. Compare curves  $A_I$  and  $B_I$  in the figures 8 and 9.

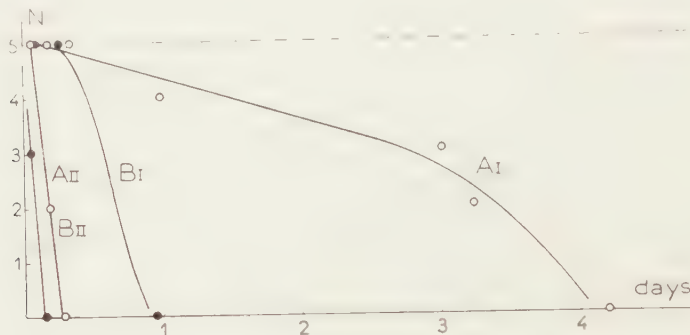


Fig. 9. Loss of the spinning capacity of the mixtures A and B of fig. 8 with time

2. The rate of loss of high viscosity and of thread drawing is strongly increased by constant rolling. Compare the curves  $A_{II}$  with  $A_I$  and similarly  $B_{II}$  with  $B_I$ , both in the figures 8 and 9.

3. The spontaneous loss of high viscosity and thread drawing is much slower in mixtures A (with  $Q = 2.29$ ) than in mixture B (with  $Q = 2.75$ ). Compare curves  $A_I$  with  $B_I$  both in the figures 8 and 9.

4. The influence of rolling is much more accentuated for mixture A, than for mixture B. Compare both in fig. 8 and 9 the shifts of the curves in the direction of the time axis. It is seen that the shift  $A_I \rightarrow A_{II}$  is larger than  $B_I \rightarrow B_{II}$ .

5. When the rolling is stopped there is a slow and imperfect restoration of "high viscosity" in the case of  $A_{II}$ . This restoration is absent in the case of  $B_{II}$ .

The above points can be explained when it is assumed that the initial high viscosity and marked elasticity are due to structures in the clear fluids, consisting of still imperfect solution states of the phosphatide. Hence the structures will diminish, even at rest, with time (explains point 1), which will be markedly accelerated by mechanical motion (explains point 2)<sup>1</sup>). The breakdown of these structures by mechanical means will not or only imperfectly be reversible at subsequent rest (explains point 5). The different behaviour of the mixtures A (with  $Q = 2.29$ ) and B (with  $Q = 2.75$ ) as formulated in the points 3, 4 and 5 are also readily understandable. We recall to mind that the limit clear/opalescent lies at about  $Q = 2.2 \pm 0.1$ , that is practically the  $Q$  value in mixture A. The rate with which structures due to imperfect solution states disappears spontaneously will consequently be small for mixture A, and much larger for mixture B (explains point 3). Two further consequences may be foreseen: 1) the structures in A will be

<sup>1</sup>) The rolling motion applied in the above experiment can still be considered as a gentle disturbing influence. With stronger mechanical means the viscosity can be lowered in a small fraction of the time required by rolling. We had for instance an elastic viscous system with  $t/t_{H_2O} = 2.16$ , which after treatment in a multimix apparatus already showed after only three minutes a  $t/t_{H_2O}$  of 1.16. To obtain this same decrease at least one day rolling would be necessary.



more vulnerable to motion than those in B (explains point 4); 2) the chance of restoration of structures broken down by preceding motion will be greater for mixture A than for mixture B (explains point 5).

e. Conclusion as to the action of CTAB on phosphatide suspension in absence of salts

The results in the preceding subsections allow for the conclusion that the elastic viscous systems which are obtained from the smectic phase of egg phosphatide with CTAB are of a quite different nature than elastic viscous systems which with association colloids lie typically between the O-coacervates and the non-elastic solutions in the series: smectic phase  $\rightarrow$  O-coacervates  $\rightarrow$  elastic viscous systems  $\rightarrow$  non elastic solutions. The latter type of elastic viscous systems have been extensively studied in the case of oleate + KCl<sup>1)</sup> and they appeared to be systems which are typical in internal equilibrium. Their viscous and elastic properties do not change spontaneously, nor are they broken down irreversibly even after severe mechanical treatment<sup>2)</sup>.

The elastic viscous systems which are temporarily formed by the action of CTAB on phosphatide suspensions have only a superficial resemblance to the above systems. They do not represent systems in internal equilibrium. The elastic and viscous properties are due to imperfect solution states of the phosphatide and disappear spontaneously with time, this being accelerated by mechanical means. We furthermore recall to mind that the expected O-coacervates are not formed either. Thus, after a sufficiently long time to allow for the reaching of internal equilibrium, the action of CTAB on egg-phosphatide suspensions will correspond to the simple formulation:

smectic phase  $\rightarrow$  non elastic solution.

This sequence differs from that expected in the introduction in as much as the O-coacervates and true elastic viscous systems have been dropped out. A reason for this omission will be suggested in communication IV section 4 of this series on the colloid chemistry of phosphatides.

<sup>1)</sup> H. G. BUNGENBERG DE JONG and co-workers. See articles in these Proceedings, 51-53 (1948-1950) and Series B 54 (1951).

<sup>2)</sup> It is true that the viscosity of elastic viscous oleate systems is a function of the shearing stress (high viscous Newtonian liquid at low and anomalous low viscous fluid at high shearing stress) but one and only one viscosity belongs to each shearing stress. With variation of the shearing stress the viscosity responds in a reversible way and practically momentarily. The same holds for the elastic properties. When one has measured the shear modulus  $G$  and the damping  $A$  of an elastic viscous system in a spherical vessel and then brings the contents in vigorous rotation relative to the wall of the vessel—whereby the high viscous system changes into a low viscous system—and now puts the vessel down at rest, the circular motion of the contents stops rapidly and directly after the measurement of  $G$  and  $A$  gives exactly the same values as originally found.

#### 4. *Action of CTAB on phosphatide suspensions in the presence of 1.2 N NaCl*

##### *a. General*

When the mixtures of the series A, B, and C were 48 hours old, 3 ml NaCl 4 N were added to 7 ml of each. Before the addition of NaCl to the mixtures, coacervation was nowhere present and the initially formed elastic viscous systems had already completely lost their elasticity. After the addition of NaCl in each series, coacervation occurred in a certain range of CTAB concentrations, and elastic viscous systems were formed in a range of higher CTAB concentrations. The coacervates have been investigated microscopically. None of the peculiarities of P-coacervates are present, so that we have here O-coacervates. In a region of CTAB concentrations lower than those in which O-coacervates are formed, a slowly developing separation into two layers is present. Microscopic investigation showed that here a birefringent liquid phase is present. Between the CTAB concentration zero and that required for the separation of the liquid birefringent phase, with increase of the CTAB concentration the strong turbidity decreases gradually and changes into strong opalescence, the intensity of which decreases further until the limit of the birefringent phase is reached. With increase of the CTAB concentration we find the following sequence in each series:

turbid systems  $\rightarrow$  slightly opalescent systems  $\rightarrow$  birefringent liquid phase + equilibrium liquid  $\rightarrow$  O-coacervate + equilibrium liquid  $\rightarrow$  elastic viscous systems  $\rightarrow$  non elastic solutions.

The limits between the various systems (except between turbid and opalescent systems, which is a gradual change) one day after addition of NaCl are given in Table II. The uncertainty of these limits (mentioned as "error" in column 6) has been taken as equal to half the concentration steps in the series A, B and C.

TABLE II

Series and phosph. conc. (m mol/l)	CTAB concentrations (m mol/l) needed for reaching various limits				
	opal/ birefr.	birefr./ O-coac.	O-coac./ el.visc.	el.visc./ non el.	error
A 2.16	4.7	5.2	6.7	7.7	$\pm 0.25$
B 3.24	7.1	7.8	10.0	11.5	$\pm 0.37$
C 4.32	9.4	10.4	13.4	15.3	$\pm 0.50$
CTAB/phosph. (mean)	2.19	2.41	3.10	3.55	$\pm 0.12$

In fig. 10 the CTAB concentrations of Table II have been plotted against the phosphatide concentrations of the series A, B and C. It appears that for each limit the points from the series A, B and C lie on a straight line

through the origin. This points strongly to a very strong binding of the detergent to the phosphatide, which point will be considered more fully below in subsection *c*.

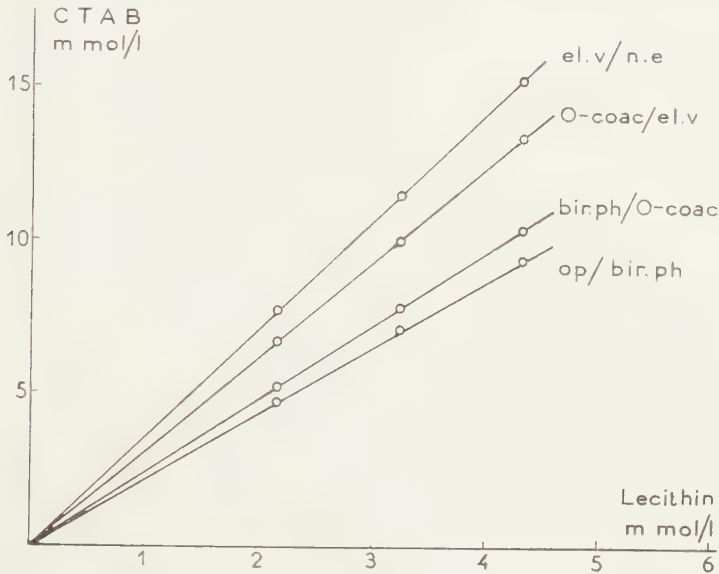


Fig. 10. Position of the boundaries between various regions in a CTAB-phosphatide diagram, at 1.2 N NaCl

*b.* The three systems to the left in the sequence mentioned in sub. *a*

It seems likely that these three systems are not fundamentally different. As a result of the uptake of the detergent the relatively coarse suspension particles of the phosphatide become subdivided into smaller and smaller ones, resulting in the gradual change in appearance of the system (turbid  $\rightarrow$  strong opalescent  $\rightarrow$  weak opalescent). But during this subdivision the smectic phase obviously still retains its quasi solid character, until at a sufficient uptake of the detergent it obtains just enough fluid character to enable confluence into a liquid macrolayer (the liquid birefringent phase). The observation that the separation of this birefringent phase is but a slow process is entirely in accordance with the above. Indeed, there is no very sharp limit opalesc./birefr. liquid, the position shifting very slowly in the direction of lower CTAB concentration.

If we accept the above interpretation, the sequence mentioned in sub *a* may be simplified to:

smectic phase  $\rightarrow$  O-coac.  $\rightarrow$  elast. visc. s.  $\rightarrow$  non elastic s.

This sequence corresponds exactly to the one expected in the introduction.

(To be continued)

CONTRIBUTIONS TO THE COLLOID CHEMISTRY OF  
PHOSPHATIDES. III<sup>B 1)</sup>

1. *Electrical decompensation of phosphatide micelles by detergents.*
2. *Action of cetyltrimethylammonium bromide on suspensions of egg-phosphatides in the absence and presence of NaCl.*

BY

H. G. BUNGENBERG DE JONG AND A. DE BAKKER

(Communicated at the meeting of December 17, 1955)

c. Binding of the detergent to the phosphatide

Above we already concluded (see fig. 10) that there is a strong binding of the detergent to the phosphatide. The same follows from viscosity measurements in the region of the elastic viscous and non elastic solutions. Compare fig. 11, which shows that the maxima lie at higher CTAB concentrations as the phosphatide concentration is higher. The difficulty is, however, to determine the CTAB concentrations which correspond to the maxima. The graphical method used in the case of curve B can only be tentatively applied to the maxima of the curves A and C (which show sufficient experimental points on one of the branches, but only one point on the other). The CTAB concentrations formed in this manner have been plotted in fig. 12 against the phosphatide concentrations of the series A, B and C. Because of the uncertainty of the points corresponding to the maxima of the curves A and C, we need not attach much value to the fact that they do not strictly lie on a straight line through the origin <sup>2)</sup>. In any case, fig. 12 points to a strong binding of the detergent and no indication is present for the existence of a small but distinct CTAB equilibrium concentration.

Much more favourable for our purposes are the results of measurements of the coacervate volumes (compare fig. 13). The latter were measured 24 hours after addition of NaCl, which time sufficed for a complete separation into two clear layers. The coacervate volumes have been expressed in % of the total volumes. We now read off the CTAB concentrations which correspond to coacervate volumina which for the series A, B and C are comparable. As the phosphatide concentrations in the series A, B and C are in the proportion of 2 to 3 to 4, the coacervates are in the same state when the coacervate volumes (expressed in % of the total volume)

<sup>1)</sup> Parts I and II of this series have been published in these Proceedings, Ser. B 58, 238, 251, 257 (1955).

<sup>2)</sup> The slope of the line drawn corresponds to a CTA/phosphatide ratio of 2.85 (which is the mean of the three individual ratios).





Fig. 11

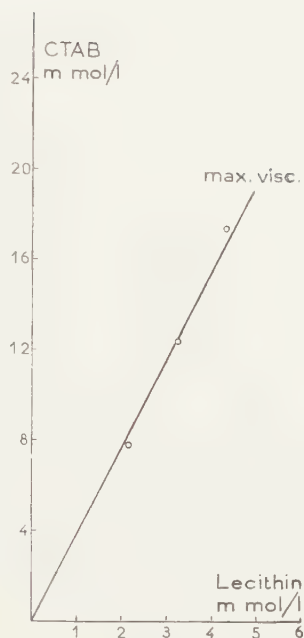


Fig. 12

Fig. 11. Viscosity in dependence on the CTAB concentration at three phosphatide concentrations, in the presence of 1.2 N NaCl

Fig. 12. CTAB concentrations corresponding to the maxima in the viscosity curves of fig. 11, in dependence on the phosphatide concentrations

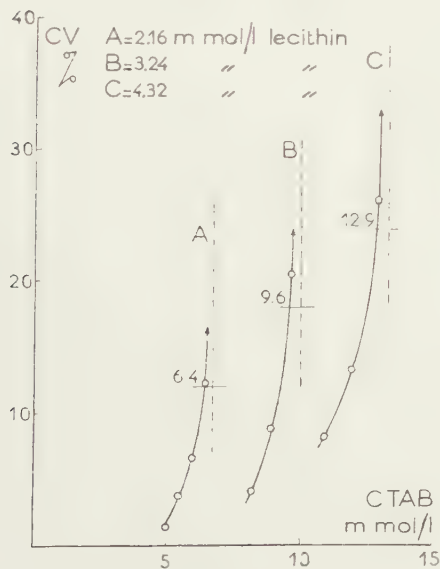


Fig. 13



Fig. 14

Fig. 13. Volume of the coacervate in dependence on the CTAB concentration at three phosphatide concentrations, in the presence of 1.2 N NaCl. The dotted lines indicate the coacervation limits

Fig. 14. CTAB concentrations corresponding to comparable coacervate volumes in fig. 13, in dependence on the phosphatide concentration (see text)

are also in the proportion of 2 to 3 to 4<sup>1)</sup>. We have chosen as comparable coacervate volumes, 12 % for series A, 18 % for series B and 24 % for series C. The CTAB concentrations which correspond to these coacervate volumes and which have been given in fig. 13, have been plotted in fig. 14 against the phosphatide concentration (also given in fig. 13). It appears that the points lie practically on a straight line through the origin and with a slope corresponding to the ratio CTA/phosphatide = 2.97. We think that with this result we have settled the question whether practically all CTA becomes bound to the phosphatide or whether there is a CTAB equilibrium concentration which cannot be neglected in favour of the practically complete binding.

*d. The equilibrium character of the various systems obtained in the presence of 1.2 N NaCl*

The viscosity in the region of the elastic viscous and the non elastic systems has been determined for series A and C, not only 27 hours (fig. 11) after the addition of NaCl, but also after 2 and 117 hours. Within the experimental errors the same viscosity curves were found as for those after 27 hours. It was furthermore observed that the limit elastic viscous non elastic—as a criterion we here choose the limit thread drawing/not thread drawing—remained the same during the period from 2 to 117 hours. Thus already 2 hours after addition of the NaCl the internal equilibrium had been reached, as the viscosity and the limit elastic non elastic does not change with time. This was also the case for the coacervation limit (the limit 0 coacervation elastic viscous systems did not change in the period between 2 and 117 hours).

We furthermore found no indications during the viscosity measurements, that repeated flow through the capillary breaks down high viscosity and thread drawing. Thus there is no systematic decrease of the  $t/t_{H_2O}$  during the five successive passages through the capillary, and when a given mixture is thread drawing, this property never gets lost during the successive passages through the capillary.

We have furthermore made a similar experiment as in section 3d, in which systems of the same composition are compared, one kept at rest, the other being rolled constantly on a rolling device. The compositions of the 100 ml mixtures correspond as to the phosphatide and the NaCl concentration to series B. Two CTAB/phosphatide ratios have been investigated, namely 3.44 (mixtures A<sub>I</sub> and A<sub>II</sub>) and 3.98 (mixtures B<sub>I</sub> and B<sub>II</sub>). The first ratio corresponds to a point to the left of the viscosity maximum which still lies in the region of the elastic viscous systems (3.10–3.55, see Table II). The second ratio corresponds to a point to the right of the viscosity maximum and already lies in the region of non-elastic systems. The flasks A<sub>II</sub> and B<sub>II</sub> were left standing at rest, the flasks A<sub>I</sub> and B<sub>I</sub> were constantly rolled on the rolling device. From time to time samples were taken, measured and

<sup>1)</sup> The method followed here has been worked out in a former investigation: H. G. BUNGENBERG DE JONG and A. RECOURT, these Proceedings, Series B 56, 303, 315, 442 (1953).

rejected. The results—compare fig. 15—clearly show that in the presence of NaCl high viscosity represents the equilibrium state. The same viscosity level is reached when the mixture is left standing at rest or when it is constantly rolled (compare  $A_I$  with  $A_{II}$ , similarly  $B_I$  and  $B_{II}$ ). Constant rolling did not affect the elasticity (thread drawing) of the mixture A either. The contrast with the corresponding experiment in the absence of salts in section 3 (compare fig. 8) is very striking. In the presence of 1.2 N NaCl the elastic viscous and non-elastic solution are typically systems which are in internal equilibrium.

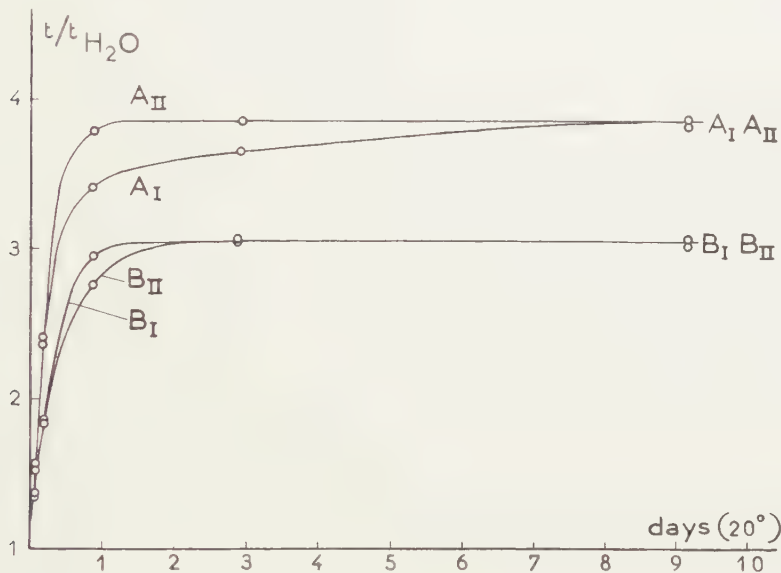


Fig. 15. Development of "high viscosity" with time, of two phosphatide CTAB mixtures A and B, in the presence of 1.2 N NaCl.  $A_I$  and  $B_I$  are gently rolled,  $A_{II}$  and  $B_{II}$  are kept at rest (see text)

We will now discuss some details in fig. 15. In favourable cases ( $A_{II}$  and  $B_I$ ) it took about one day to reach the characteristic levels. This in contrast with the fact that in fig. 11 constant viscosity was already reached two hours after addition of the NaCl to the clear phosphatide CTAB mixtures. This contrast is easily explained by the fact that in the last case we added NaCl to systems in which the phosphatide had already been dissolved, whereas here we start from the massive phosphatide particles in contact with the NaCl containing CTAB solution. A further retardation will presumably result from the fact that at the surface of the suspension particles the systems corresponding to lower phosphatide/CTAB ratios (fluid birefringent phase and O-coacervates) will temporarily be formed which will shield off the particles from the dissolving medium.

One would thus expect that with constant motion the characteristic viscosity level will be reached faster than at rest. This is actually found for the mixtures B. In contradiction to this the constant rolling retards the reaching of the characteristic viscosity level for the mixture A. This, however, is presumably not due to the motion itself but to the very heavy foam formation, which nearly immobilised the contents of the rolling flask  $A_I$ . This foaming made it necessary to let the flasks rest for a few hours before measuring the viscosity. Then only a sufficient quantity of fluid separated at the bottom to take a sample.

*e. Conclusion as to the action of CTAB on phosphatide suspension in the presence of 1.2 N NaCl*

In the presence of 1.2 N NaCl the sequence and kinds of systems arising from the phosphatide suspension at increase of the CTAB concentration:

smectic phase  $\rightarrow$  O-coacervate  $\rightarrow$  elastic viscous S.  $\rightarrow$  non elastic S.

is exactly as expected in the introduction from a progressive electrical decompensation. The elastic viscous systems and the non elastic systems are typical systems which are in internal equilibrium. Their viscous and elastic properties do not change spontaneously, nor are these affected by constant motion. The various limits do not change with time and they are characterized by certain CTAB/phosphatide ratios, which show that the binding of the detergent to the phosphatide is practically complete. As to premise *c*) of the Introduction it must be remarked that at the high NaCl concentration, presumably part of the CTA cations taken up in the micelle will have bound Cl ions. In any case, however, a sufficient fraction of the CTA cations must be taken up without counter ions as otherwise electrical decompensation will not occur.

*5. Position of various regions in a NaCl-Q diagram*

With  $Q$  we will, in the following understand the ratio CTAB bound/phosphatide. As we have seen in the preceding sections CTAB is practically completely bound to the phosphatide;  $Q$  is equal to the ratio CTAB/phosphatide in the mixtures.

For the drawing of a NaCl- $Q$  diagram we already have the  $Q$  values corresponding to various limits at 1.2 N NaCl (lower row in table II). The following experiments serve to obtain more data for this diagram.

The method is as follows. We first make a CTAB-phosphatide mixture ("M") of the composition:  $a$  ml CTAB 44.2 m mol/l +  $(40-a)$  ml  $H_2O$  + 10 ml phosphatide suspension 47.2 m mol/l; keep this mixture overnight in the thermostat at 25° and the following day make a series of mixtures in test tubes of the composition:  $b$  ml NaCl 4 N +  $(6-b)$  ml  $H_2O$  + 2 ml "M", in which in the region where the coacervation limit is situated,  $b$  increases with 0.05 ml (corresponding to an increase of the NaCl concentration of 0.025 N). The series is kept in the thermostat (25°) until the following day and then it is noted at which NaCl concentration coacervation is present for the first time. As coacervation limit we take the mean of this concentration and the concentration in the preceding tube (where no coacervation is present). The results with a number of such "M" mixtures are given in column 2 of Table III.

The head  $M_1$  means that the CTAB-phosphatide mixture is one day old before it is used in determining the coacervation limit. Some of these "M" mixtures were kept at 25° for one or two days longer and the coacervation limit was determined anew.



TABLE III

$Q = \frac{\text{CTAB}}{\text{phosph.}}$	Coacervation limit in N NaCl			Elastic limit in N NaCl
	$M_1$	$M_2$	$M_3$	$M_1$
1.87	0.14	—	—	(0.14)?
2.11	0.16	—	—	0.14
2.34	0.26	0.26	—	0.21
2.57	0.41	—	—	0.34
2.81	0.69	0.69	0.71	0.56
3.04	1.01	1.01	1.01	—
3.28	1.36	—	—	—
3.51	1.71	—	—	—
3.74	2.06	—	—	—

We see from columns 3 and 4 that the two and three days old mixtures ( $M_2$  and  $M_3$ ) gave approximately the same coacervation limits. As the error in such a determination is  $\pm 0.01$  N, the value 0.71 in the fourth row is not significantly higher than 0.69 in the third row.

Now we know from the experiments in section 2 that the M mixtures change continuously with time as regards viscosity and elasticity. On successive days the amount of "structure" in these M mixtures decreases, but just at and somewhat below the limit opalescent/clear the rate of decrease of "structure" is very slow at rest. The fact that we find in the columns 2, 3 and 4 the same coacervation limits, shows that the non equilibrium character plays no role for the coacervation limit itself.

There are indications that the above mentioned non equilibrium character plays a role in the rate of coacervation with NaCl. We know that in general coacervation is practically instantaneous (for instance Oleate + KCl; CTAB + KCNS). The coacervation of the CTAB-phosphatide mixtures generally takes some time. It is fairly rapid at  $Q = 3.5$  and higher but at lower ratios one may observe that after the addition of NaCl during a longer or shorter period, the appearance of turbidity due to coacervation is delayed and then rapidly develops. With still lower ratios ( $Q = 2.5$  and lower) the rate of coacervation becomes extremely slow, as it may take many hours before we can with certainty observe whether in a given tube coacervation takes place or not. This circumstance made it impossible to investigate the coacervation limit at still lower  $Q$ -values than given in the table. It might be reasonable to assume that just at these low ratios relatively persistent structures in the "M" mixtures only yield slowly to the action of the salt and thus delay coacervation.

In figure 16, the coacervation limits in column 2 of the table have been plotted against the CTAB/phosphatide ratio.

In some of the series we had enough tubes with lower NaCl concentrations that we could observe the limit elast. visc. s./non elastic s. See column 5 of Table III.

For drawing the curve representing this limit (curve on the right) we have also used the value 1.20 N NaCl at the ratio CTAB/phosphatide 3.55 of Table II (black dot in fig. 16). The two following black dots in

fig. 16 have also been taken from this table. For drawing the curve liquid birefringent phase O-coacervate in the NaCl- $Q$  diagram, we have insufficient data. We only know that it must proceed through the black point with ordinate 1.20 and abscissa 2.41. We have tentatively drawn this curve (dotted) taking into account that all asterisks in fig. 16 represent O-coacervates and thus the curve must proceed to the left of them, and furthermore assuming that the curve has in principle the same character as the two other curves. The same has been assumed for drawing a small part of the limit opalescent/liquid birefringent phase.

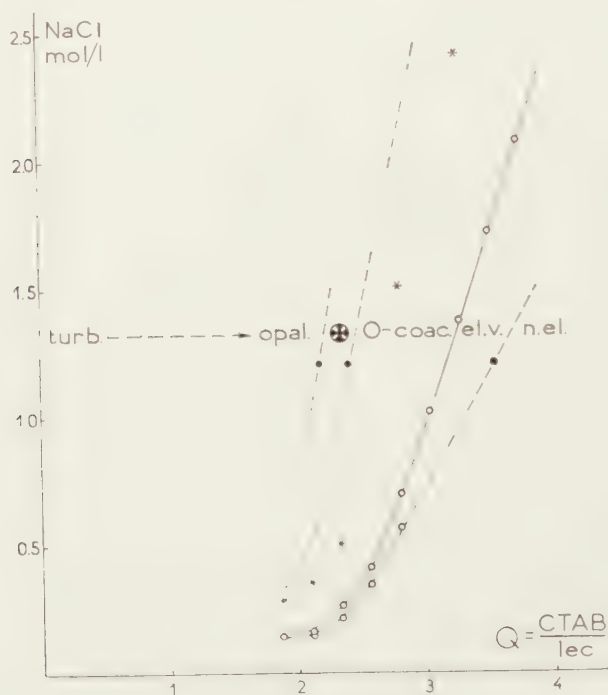


Fig. 16. Position of various regions in a NaCl- $Q$  diagram. The circle with black cross denotes the region in which a liquid birefringent phase is present. (For asterisks see text)

The NaCl- $Q$  diagram obtained in this manner (fig. 16) allows first for the reading off of what happens at constant NaCl concentration and increase of  $Q$ . It appears that from about 0.15 mol/l NaCl up to the highest NaCl concentration investigated the same applies as has been found in section 4 at 1.2 N. As a consequence of a progressive decompensation of the charge ratio on the surface of the micelles (compare in principle fig. 1 upper row) we obtain the sequence:  
smectic phase  $\rightarrow$  O-coacervate  $\rightarrow$  elastic viscous system  $\rightarrow$  non elastic solution.

We may also read off from the NaCl- $Q$  diagram what takes place at

constant  $Q$  and increase of the NaCl concentration. When  $Q$  is taken higher than about 2, we obtain just the reverse sequence:

non elastic solution  $\rightarrow$  elastic viscous system  $\rightarrow$  O-coacervate  $\rightarrow$  smectic phase.

This corresponds to the expectation that at increase of the salt concentration neutralization of the original decompensation may take place as a consequence of binding of that ion of the salt which is oppositely charged to the detergent ion taken up in the phosphatide micelles. Compare Introduction and fig. 1 lower row.

As with higher  $Q$  a larger neutralization of decompensation will be necessary to reach the various limits, we must expect that higher NaCl concentrations will be needed than at lower  $Q$  values. This is confirmed by the experiment. Indeed the curves representing the limits O-coacervate/elastic-viscous and elastic-viscous/non elastic proceed upwards to the right in the NaCl- $Q$  diagram (fig. 16).

This section may be closed with a remark regarding the lower left part of the NaCl- $Q$  diagram.

We recall the results described in section 2, that the expected series of transformations does not occur in the absence of salts, that is along the abscissa of the NaCl- $Q$  diagram. The NaCl- $Q$  diagram now shows that the hindrances to the obtaining of the expected series of transformations at increase of  $Q$  are removed by a relatively small NaCl concentration, although NaCl by itself counteracts the transformations (that is, shifts the limits in the direction of higher  $Q$ ).

Thus it may be stated that NaCl has a dual function, which may be a useful hint for an eventual investigation in the future into the reasons why, in the absence of salt the expected transformations do not occur.

## 6. *Behaviour of drops of the O-coacervate in a direct current field*

In a direct current field drops of the O-coacervate obtained with NaCl from phosphatide + CTAB show remarkable properties (most pronounced on the left half of the coacervate region in the diagram of fig. 16). In a field of 3 Volt/cm nothing in particular happens. A slight vacuolisation occurs and from the movement of these vacuoles it can be concluded that the boundary coacervate/equilibrium liquid moves in the direction of the positive electrode, thus setting up a systematic streaming in the interior of the coacervate. The direction into which the coacervate boundary moves indicates that the interfacial tension coacervate/equilibrium liquid is lowered on the side of the negative electrode and is increased on the side of the positive electrode. In a stronger field the systematic streaming in the interior of the coacervate drop is no longer observed and we see the appearance of a thickening of the wall on the side of the positive electrode (fig. 17,  $a \rightarrow b \rightarrow c$ ). This thick and rather rigid wall shows birefringence with the long axis of the index ellipse

perpendicular to the surface. The radius of curvature of this part of the drop is smaller than that of the right part.

If the electric field is switched off, the thickening disappears in a few minutes. The birefringence too fades away. Thus the phenomenon is completely reversible. If the field is maintained, myelin tubes will suddenly grow out of the surface (fig. 17d). Here too the long axis of the index ellipse stands perpendicular to the surface. A short myelin tube will be retracted when the field is switched off. Under the same conditions a long myelin tube loses its rigid character: if it by chance touches the surface of the coacervate drop, it will fuse with the drop and gradually disappear.

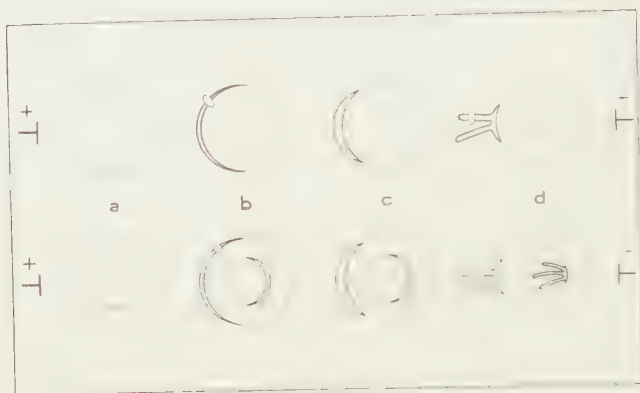


Fig. 17

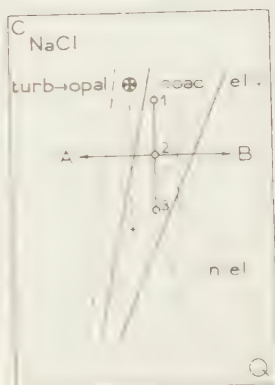


Fig. 18

Fig. 17. Behaviour of drops of the O-coacervate in a direct current field

Fig. 18. Explanation of the phenomena shown by drops of the O-coacervate in a direct current field (see text)

When a vacuole is present, we see in the electric field the same phenomena at the border coacervate/vacuole (fig. 17 lower row). First a thickening of the wall occurs, followed by an outgrowth of myelins.

The explanation of these phenomena must be sought for in the influence of the direct current electric field on the ratio CTA/phosphatide ( $Q$ ). In such a field  $Q$  will decrease in the coacervate on the side of the drop turned to the positive electrode;  $Q$  will increase on the other side. The interfacial tension on the left increases, while that on the right decreases. Thus the coacervate boundary will move from right to left, thus starting the systematic streaming in the interior of the coacervate drop. When, however, the quotient  $Q$  is decreased sufficiently on the left side of the drop, the limit between the O-coacervate and the smectic phase in the NaCl- $Q$  diagram (fig. 16) will be crossed. On the left of the drop this new phase separates out (fig. 17b and c).

When the field is switched off the original ratio CTA/phosphatide is restored throughout the drop and the smectic phase disappears. It remains to explain that at first the smectic phase appears as a birefringent shell



enveloping the left half of the coacervate drop, and that only when the direct current field is maintained sufficiently long, rather rigid myelin tubes grow out suddenly. We think the explanation must start from the fact that in section 4 *a* and *b*, we found that at increase of  $Q$  one observes the existence of a region in which a smectic phase separates out with a distinct liquid character. A small volume of this smectic phase in contact with equilibrium liquid takes a spherical form, though it is a birefringent phase. The internal forces between the parallel layers of oriented molecules are not sufficiently large to impede that the interfacial tension rounds off a small volume of this phase into the shape of a sphere. As this region lies in the NaCl- $Q$  diagram adjacent to the region of the O-coacervate, the shell of birefringent material separating in the direct current field on the side of the positive electrode must consist at first of this distinct fluid birefringent phase. If the field is maintained sufficiently long,  $Q$  in this birefringent phase will decrease still further until we reach a state in which the internal forces between the parallel layers of oriented molecules may be sufficiently great that an external shape deviating from the spherical shape will become possible. The value of  $Q$  must have decreased so far that the limit opalescent/fluid birefringent phase has been passed <sup>1)</sup>.

From now on the situation that a spherical shell of birefringent phase envelops the left half of the coacervate drop will be labile. This labile situation may persist until at an unpredictable time myelin tubes are formed from the cap of birefringent material (aided of course by the pressure of the coacervate boundary, which, as has already been mentioned above, tends to move in the direction of the positive electrode).

Fig. 18 may illustrate the fact that the above described phenomena in a direct current field are most pronounced in the left half of the coacervate region in a NaCl- $Q$  diagram. The points 1, 2 and 3 may represent coacervated systems, obtained at constant CTAB/phosphatide ratio and different NaCl concentrations. Point 1 lies in the left half of the coacervate region, point 2 lying half way and point 3 in the right half of the region.

The original  $Q$  value (represented by the vertical line through 1, 2 and 3) is shifted in a direct current field in the direction A on the side of the coacervate drop directed towards the positive electrode. It will be seen that a same shift of the  $Q$  value—as represented by the dotted vertical line to the left of CD—leads in the case of 1 to a crossing of the boundary O-coacervate/smectic phase, in the case of 2 it has not yet reached this boundary and in the case of 3 the  $Q$  value is still far off from this boundary. Thus the position of point 1—lying in the left half of the coacervate region is most favourable for the formation of a birefringent shell and the subsequent outgrowth of myelin tubes, and the position of

<sup>1)</sup> Compare with the discussion in section 4*b*, in which we ascribed the limit opalescent/liquid birefringent phase to a liquefaction of the smectic phase, which at lower  $Q$  values must have a rather semi solid nature.

point 3—lying in the right half of the coacervate region is least favourable.

We have, up to now, only paid attention to the phenomena occurring on the side of the coacervate drop turned towards the positive electrode. On the other side we may also observe a change—though it bears a much less spectacular character. It consists of a decrease of the visibility of the boundary of the coacervate drop on the side turned towards the negative electrode. The phenomenon is most pronounced in the right half of the coacervate region in the  $\text{NaCl}-Q$  diagram, and here may lead to a fading away of the said boundary. By switching off the field the original optical contrast between coacervate and equilibrium liquid is restored. For an explanation we turn once more to figure 18. On the side of the coacervate drop turned towards the negative electrode the change in the original  $Q$  value will be in the direction B. We know from fig. 13 that at increase of  $Q$  the coacervate volume increases. This will explain that the optical contrast between coacervate and equilibrium diminishes. When the increase of  $Q$  becomes so great that it reaches the boundary O-coacervate-elastic viscous system the coacervate boundary will fade away.

A same shift of the  $Q$  value—as represented by the dotted line to the right of CD—has different effects for the coacervate systems represented by the points 1, 2 and 3. The optical contrast will diminish least in case 1, more in case 2 and a fading of the coacervate boundary will occur in case 3. It is thus clear that the described phenomena are most pronounced in the right half of the coacervate region.

## 7. Summary

1. When detergent ions (anionic or cationic) are taken up in the sandwich micelle of a phosphatide an electrical decompensation will result, provided *a*) the detergent ions are taken in up such a manner that their charged groups lie in the surface of the micelle, and *b*) the counter ions of the detergent are not or only partly bound to the surface of the micelle.

2. Salts will in general have a neutralizing effect on the electrical decompensation, as a consequence of binding of that ion of the salt to the micelle, which is oppositely charged to the detergent ion taken up in the micelle.

3. The electrical decompensation of the phosphatide micelles (which of quasi infinite extension constitute the smectic phase) will lead to a weakening of the intermicellar interactions. It might be expected that detergents acting on a phosphatide suspension in the absence or in the presence of a constant (not too high) salt concentration, will bring about the following transformations with increase of the detergent concentration: smectic phase  $\rightarrow$  O-coacervate  $\rightarrow$  elastic viscous system  $\rightarrow$  non elastic solution.

4. The action of cetyltrimethylammoniumbromide (CTAB) on a sus-

pension of egg-phosphatides has been investigated in the absence and presence of NaCl.

5. In the presence of a constant NaCl concentration higher than about 0.15 N, the full sequence as expected in sub 3) is obtained with increase of the CTAB concentration:

smectic phase  $\rightarrow$  O-coacervate  $\rightarrow$  elastic viscous system  $\rightarrow$  non elastic solution.

The various systems represent systems in internal equilibrium. The CTAB concentrations needed to reach the various limits, or to obtain a comparable coacervate volume or the maximum viscosity are practically proportional to the phosphatide concentrations. This shows that the binding of the detergent to the phosphatide is practically complete.

6. The position of the various regions in a NaCl- $Q$  diagram has been determined,  $Q$  being the ratio CTAB/phosphatide. From this diagram can be read off:

a. with higher constant NaCl concentration the values of  $Q$  characteristic for each of the limits increases.

b. at constant, sufficiently large  $Q$ -value the transformations take place in the reverse order with increase of the NaCl concentration:  
non elastic solution  $\rightarrow$  elastic viscous system  $\rightarrow$  O-coacervate  $\rightarrow$  smectic phase.

Both points a and b follow from the neutralizing effect of salts mentioned in sub 2.

7. In a direct current field the O-coacervate drops develop a birefringent wall on the side of the positive electrode. If the electric field is switched off the thickening and the birefringence soon disappears. If the field is maintained myelin tubes will suddenly grow out of the birefringent wall. When a vacuole is present in the coacervate drop the same phenomena occur at the border coacervate/vacuole.

8. At the side of the negative electrode the boundary of the coacervate drop may become less visible or may even fade away. If the field is switched off the original optical contrast between coacervate and equilibrium liquid is restored.

9. The phenomena mentioned sub 7 and 8 find a simple explanation by considering that the CTA cation is transported within the coacervate in the direction of the negative electrode, thus decreasing  $Q$  locally in the coacervate drop at the side of the positive electrode and increasing  $Q$  in the coacervate drop at the side of the negative electrode.

10. In the absence of salt, the series of transformations expected sub 3 does not take place. No coacervates have been observed and the elastic viscous systems which are initially formed do not represent systems in internal equilibrium. The elastic and high-viscous properties are due to imperfect solution states of the phosphatide and they disappear

spontaneously with time, this being accelerated by mechanical means. After a sufficiently long time to allow for the reaching of internal equilibrium, the action of CTAB corresponds to:

smectic phase  $\rightarrow$  non elastic solution.

that is the series expected sub 3 from which the O-coacervates and true elastic viscous systems have been dropped out. Further experimental work will be required to explain this omission.

*Department of Medical Chemistry,  
University of Leiden.*



CONTRIBUTIONS TO THE COLLOID CHEMISTRY OF  
PHOSPHATIDES. IV <sup>1)</sup>

1. *Sodium laurylsulphate as decompensating agent*
2. *Ion sequences in the neutralization of electrical decompensation*

BY

H. G. BUNGENBERG DE JONG AND A. DE BAKKER

(Communicated at the meeting of December 17, 1955)

1. *Introduction*

The present communication continues the subject of Part III of this series, viz. the electrical decompensation of phosphatide micelles by detergents and its neutralization by salts. For the theoretical considerations, the materials and methods used, we refer to the sections 1 and 2 of the above mentioned communication.

2. *Sodium laurylsulphate as decompensating agent. Comparison with CTAB in a NaCl-Q diagram*

a. *Action in the absence of salts*

In the preceding part (III) we studied the decompensation brought about by cetyltrimethylammonium bromide (CTAB), which is a cationic detergent. The expectations given in the Introduction of part III are also applicable to anionic detergents. Preliminary experiments showed that the action of sodium laurylsulphate (NaLS) on an egg-phosphatide suspension in the absence of salt is similar to that for CTAB in the absence of salts as described in section 3 of part III. With increase of  $Q$  (=ratio detergent/phosphatide), the turbidity decreases and at  $Q$  in the neighbourhood of two, clear solutions are obtained, which are markedly viscous and exhibit elastic properties. The elastic viscous systems quite as those obtained with CTAB in the absence of salts, do not represent systems in internal equilibrium. They lose their high viscosity and elastic properties with time, and are, therefore, not of the kind which should be expected to occur in the series of transformations:

smectic phase  $\rightarrow$  O-coacervate  $\rightarrow$  elastic viscous system  $\rightarrow$  non elastic solution.

As O-coacervates are not formed at lower  $Q$  values, we may conclude that—just as in the case of CTAB—due time being allowed for reaching

---

<sup>1)</sup> Parts I and II of this series have been published in these Proceedings, Series B 58, 238, 251, 257 (1955), Part III in these Proceedings, Series B 59, 124, 136 (1956).

internal equilibrium—the action of NaLS comes to the simple transformation smectic phase  $\rightarrow$  non elastic solution.

*b. The NaCl- $Q$  diagram*

Just as in the case of CTAB the situation is radically altered in the presence of a sufficient NaCl concentration. Starting from a more recent sample of egg-phosphatide (preparation II) and using NaLS (preparation I) we have determined in exactly the same way as in section 4 of part III the NaCl concentration corresponding to the limits O-coacervate elastic viscous s. and elastic viscous s. /non elastic s. for a number of "M" mixtures with different  $Q$  values. The results can be found in Table I (left half) and have been plotted in fig. 1.

TABLE I

NaCl concentrations (moles/l) needed to reach the limits indicated for mixtures of egg-phosphatides with NaLS and CTAB respectively

egg-phosph. + NaLS			egg-phosph. + CTAB		
$Q$	limit non el./el. visc.	limit el.visc./ O-coac.	$Q$	limit el. visc./O-coac.	
				$M_1$	$M_6$
3.13	0.24	(0.24)	1.28	(0.06)?	—
4.18	0.29	0.31	1.71	0.09	—
4.70	0.36	0.39	2.14	0.16	0.16
5.22	0.41	0.49	2.56	0.39	0.39
6.27	0.56	0.66	2.99	0.79	0.76
7.31	0.66	0.79	3.42	1.38	1.36
8.36	0.74	0.91	4.02	2.27	—
9.40	0.84	1.01			
10.8	—	1.11			

A systematic investigation of what happens in the presence of NaCl at lower  $Q$  values has not been undertaken. We have only one series at 0.67 N NaCl, from which it appeared that with increase of  $Q$  the original turbidity decreases and changes into opalescence until a separation of a birefringent liquid phase makes its appearance (at  $Q = 3.86 \pm 0.26$ ). This phase is present until we enter the O-coacervate region (at  $Q = 4.88 \pm 0.26$ ). The above data have also been plotted in fig. 1 (black points), and serve to give an impression where, in the NaCl- $Q$  diagram—we have to seek the curves giving the limits opalescence/liquid birefringent phase and liquid birefringent phase/O-coacervate.

We will assume, as in section 4 in the analogous case of phosphatide + CTAB, that the turbid system, opalescent system and the two-phase system: liquid birefringent phase + equilibrium liquid, only differ as to the degree of subdivision and to the quasi solid or more fluid character of the smectic phase. We may thus read off from the NaCl- $Q$  diagram (fig. 1):

*a.* with increase of  $Q$  at constant (sufficiently high) NaCl concentration the expected series of transformations—in this case as a consequence of decompensation with an anionic detergent—comes to the fore: smectic phase  $\rightarrow$  O-coacervate  $\rightarrow$  elastic viscous systems  $\rightarrow$  non elastic solutions.

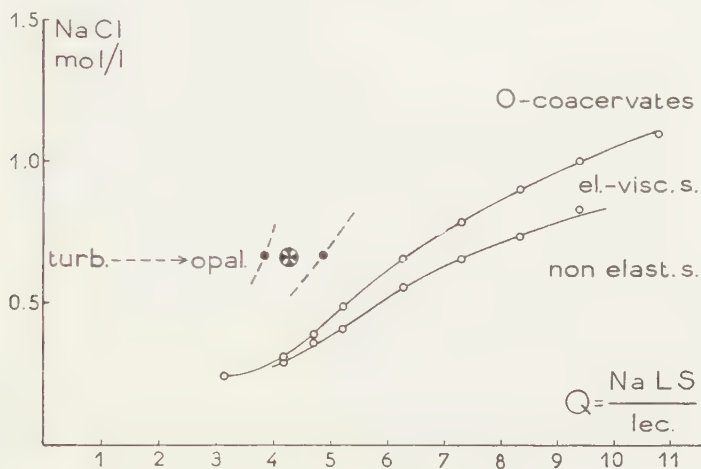


Fig. 1. Position of various regions in a NaCl- $Q$  diagram (see text). The circle with black cross denotes the region in which a liquid birefringent phase is present

*b.* with increase of the NaCl concentration at constant (sufficiently high)  $Q$ , we similarly obtain the series expected from the removal of the original decompensation:

non elastic  $\rightarrow$  elastic viscous  $\rightarrow$  O-coacervate  $\rightarrow$  smectic phase.

*c.* the curves representing the boundaries O-coacervate/elastic viscous systems and elastic viscous systems/non elastic systems show at their lower left end a bend. Here we have the same situation as discussed in Part III, section 5 in the case of phosphatide+CTAB. Because the rate of coacervation becomes extremely small here it is not possible to investigate the further course of the curve to the left.

*d.* it appears that NaCl has a dual function. In the absence of salts hindrances of unknown nature prevent the expected series of transformations (smectic phase  $\rightarrow$  O-coacervate  $\rightarrow$  elastic viscous systems  $\rightarrow$  non elastic solutions) from taking place with increase of  $Q$ . These hindrances are removed by a relatively low NaCl concentration, although NaCl by itself counteracts the transformations (that is, shifts the limits in the direction of higher  $Q$ ).

Taken together there is a close correspondence with the results obtained with phosphatide+CTAB. Compare the NaCl- $Q$  diagram of fig. 16 in Part III.

c. Comparison of the combinations phosphatide+CTAB and phosphatide+NaLS in a NaCl- $Q$  diagram. The bends at the left end of the curves

A comparison of the NaCl- $Q$  diagram of fig. 1 with fig. 16 in Part III will reveal that there are great quantitative differences. To be sure that they are not caused by the fact that different phosphatide preparations have been used, the position of the limit O-coacervate/elastic viscous systems in the combination phosphatide+CTAB has been determined anew, starting with the same phosphatide preparation (II) as was used in the combination phosphatide+NaLS. In this investigation we started from a purer CTAB preparation (II) which we had received in the meantime. The results—compare right half of Table I—have been plotted in fig. 2 (left curve). A comparison with the corresponding curve of fig. 16 in Part III reveals that there are only slight differences. In the same NaCl- $Q$  diagram of fig. 2 we have also drawn the curve representing

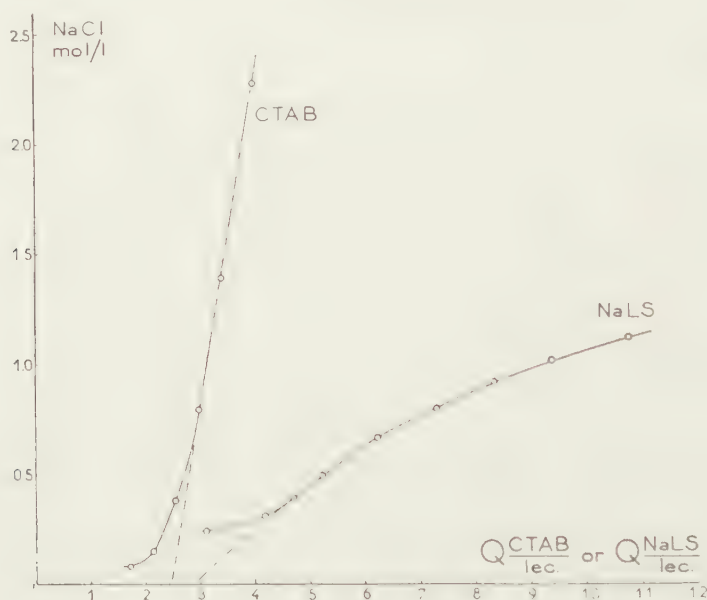


Fig. 2. Position of the elastic viscous s./O-coac. in a NaCl- $Q$  diagram for the combination phosphatide + CTAB and phosphatide + NaLS respectively

the boundary O-coacervate/elastic viscous system for the combination phosphatide+NaLS (from Table I, left half). It is seen that the two curves have a very different position in the NaCl- $Q$  diagram. It might seem that some fundamental conclusion can be drawn from this fact, the salt being the same and only the detergent being different. This is not the case, however, as we have to remember that the agent in the removal of decompensation is not NaCl, but the Cl-ion in the case of CTAB+phosphatide and the Na-ion in the case of NaLS+phosphatide.



Thus the acting salt ion and the detergent being different, a useful conclusion cannot be drawn from the very different positions of the two curves in fig. 2. The figure will be used, however, for discussing the meaning of the bends at the lower left ends of the curves.

In Part III we have already mentioned the fact, that these bends begin to appear when with decreasing  $Q$  the rate of coacervation has become rather small. With further decrease of  $Q$  this rate becomes so extremely slow, that we cannot investigate the further course of the curves to the left.

There is a circumstance not yet mentioned which, when taken into account, leads to the suspicion that experimental points lying on the bends do not represent the true coacervation limits any longer, but lie at too high NaCl concentrations. When at any  $Q$  value (higher than the bend) the coacervation limit is determined by means of a series of mixtures in which the NaCl concentration increases with small steps, it is found that the rate of forming of a coacervate layer is relatively slow when we have just passed the coacervation limit, but increases markedly when the salt concentration increases.

When, at sufficiently lowering  $Q$ , the coacervation rate in general has become extremely small, the above circumstance will lead in practice (after one night at 25°) to too high values for the coacervation limits. Thus the bends at the lower left ends of the curves arise and the true coacervation limits will be lower than given by the bends. The simplest hypothesis is that the true coacervation limits lie on a curve which forms the natural continuation downwards of that part of the experimentally determined curve at higher  $Q$  values, where the points still represent the true coacervation limits. Compare fig. 2, in which the two curves have been extrapolated in the above sense. The further discussion of this hypothesis will be continued in section 4.

#### *d.* A less favourable property of solutions of phosphatide in NaLS solutions

We will close this section with the remark that NaLS proved to be a less ideal detergent for experiments on decompensation of phosphatides than CTAB. It has been mentioned in Part III, that the so-called "M" mixtures give, with NaCl, the same coacervation limits whether they are 1, 2 or 3 days old (compare columns headed with  $M_1$ ,  $M_2$  and  $M_3$  in Table III of Part III). During the experiments in this section we could confirm this, as the coacervation limits with NaCl proved to be practically the same even when 6 days old (stored in the thermostat at 25° C). Compare columns headed with  $M_1$  and  $M_6$  in Table I. This simple behaviour is not found in similar mixtures with NaLS. When stored at 25° they give increasing coacervation limits on successive days. At 40° the increase is more rapid and it is absent when stored at 0°. We have not yet succeeded in tracing the cause of these changes. Growth of micro-organism could be ruled out, as the change was not suppressed in the presence of  $H_2O_2$ . The same coacervation limits were found for M mixtures made with freshly dissolved NaLS and with NaLS solutions stored a couple of days at 25° or 40° and in the absence or presence of  $H_2O_2$ . This proves that NaLS in watery solution is not decomposed (hydrolysis). There seems to be some unknown interaction in play between phosphatide and NaLS in the M mix-

tures, which causes the above shift. This is not present in M mixtures of phosphate + CTAB.

When performing experiments on decompensation with NaLS we must take into account the above "unstability" of the M-mixtures. Both in the experiments in this and the following section we have always prepared the M-mixtures at the end of the day, have kept them overnight in the thermostat at 25° and have used them for estimating the desired limits the next morning. Even for the phosphatide preparation II (the suspension particles of which go much more slowly into solution than those of preparation I) the time in between is sufficient to obtain clear M-mixtures.

### 3. *Ion sequences in the neutralization of decompensation*

The experiments in this section have the aim to control certain consequences of the assumption that the neutralization of decompensation by salts is caused by binding of that ion of the salt which is oppositely charged to the detergent ion.

We begin with the combination (CTAB - phosphatide. Preliminary experiments (phosphatide preparation I and CTAB preparation I) have shown that at constant  $Q$  the coacervation limits are very different with salts (K or Na) with different anions<sup>1</sup>). The concentrations needed increased strongly from left to right in the sequence:



In the following experiments we will investigate such ion sequences at 25° C more systematically. We will not only change the anion at constant cation, but will also investigate the influence of changing the cation at constant anion. We will furthermore not confine ourselves to one  $Q$  value only, but will investigate such sequences at a number of  $Q$  values. We started from the phosphatide preparation II and the much purer CTAB preparation II (ash free), see Part III. The salts which have been used are  $\text{NH}_4\text{Cl}$ ,  $\text{KCl}$ ,  $\text{NaCl}$ ,  $\text{NaBr}$ ,  $\text{NaNO}_3$  and  $\text{Na}_2\text{SO}_4$ . As the rate of coacervation with KCNS and KJ is so extremely small that the coacervation limits cannot be determined with the desired accuracy, we have excluded these salts in the following investigation.

The evening before we made in the usual way at 25° mixtures "M" (of different  $Q$  values), and next day determined the coacervation limits (at 25°) for a number of salts.

<sup>1</sup>) The experiments have been performed at room temperature ( $\pm 19^\circ$ ) and at one  $Q$  value (2.7) only. The salt concentrations needed to obtain coacervation were:

NaCl 0.6 N	NaNO <sub>3</sub> 0.018 N	KCNS 0.003 N
KBr 0.03 N	KJ 0.005 N	

In these determinations it appeared that as the coacervation limit is lower, the rate of coacervation is smaller. In particular with KJ and still more so with KCNS this rate is very small. It lasted for instance three days before with KCNS distinct coacervate drops could be observed with a loupe. As a consequence of this the coacervation limit cannot be determined accurately and the above values for KJ and KCNS are presumably too high.

The results are given in fig. 3. It is observed that salts with the same anion (Cl) but with different cations give curves which in the salt- $Q$  diagram lie close together. In contradistinction to this salts with the same cation (Na) but different anions give a bundle of curves in which the individual curves spread considerably.

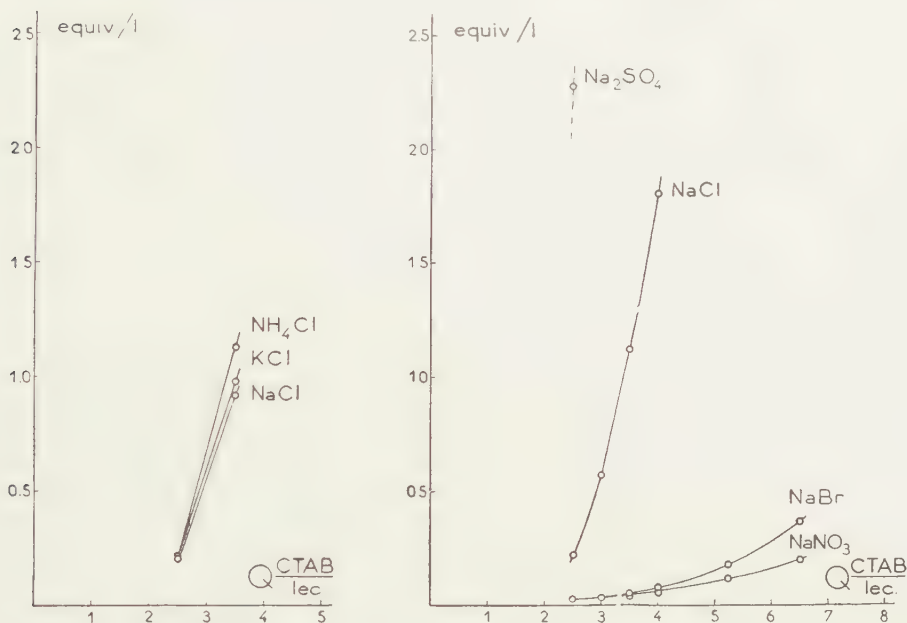


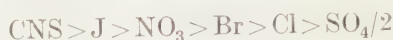
Fig. 3. Cation and anion sequences in the neutralization by salts of the electrical decompensation of the phosphatide by CTAB. The curves give the limits elastic viscous s./O-coac.

The above is exactly what could be expected. The detergent ion used in the decompensation here being a cation, the neutralization of decompensation will be brought about by binding of the anion of the added salt. When we compare NaCl, KCl, NH<sub>4</sub>Cl we should in the ideal case expect the same curve in the salt- $Q$  diagram, or when second order effects resulting from the cations are present a bundle of curves lying close together. This last case obviously applies in fig. 3, left. The nature of the second order effects will not concern us here.

When on the other hand, salts are compared with the same cation and different anions, the neutralization of decompensation will depend on the different affinities of the diverse anions for the quarternary ammonium group of the detergent cation taken up in the phosphatide micelle. When the above mentioned affinities are sufficiently different, this will clearly manifest itself in a different position of the corresponding curves in the salt- $Q$  diagram.

From experiments on the influence of salts on CTAB solutions (coacer-

vation limits, elastic limits) it is known that the affinity of anions strongly decreases (from left to right) in the sequence<sup>1)</sup>:



We may thus expect that in a salt- $Q$  diagram at constant  $Q$  the concentrations needed for salts with the same cation but different anions will increase according to the sequence:



As regards the last four anions this sequence can actually be read off from fig. 3. We may combine this with the results already mentioned at the beginning of this section, as regards the first five anions. Thus we obtain for the concentrations needed to reach the coacervation limit at constant  $Q$ :



which is exactly the same sequence as expected above.

We now turn to the results obtained in the combination NaLS + phosphatide. For this combination we used also the phosphatide preparation II and the twice recrystallized NaLS (preparation II). The coacervation limits obtained with a number of salts have been plotted in fig. 4.

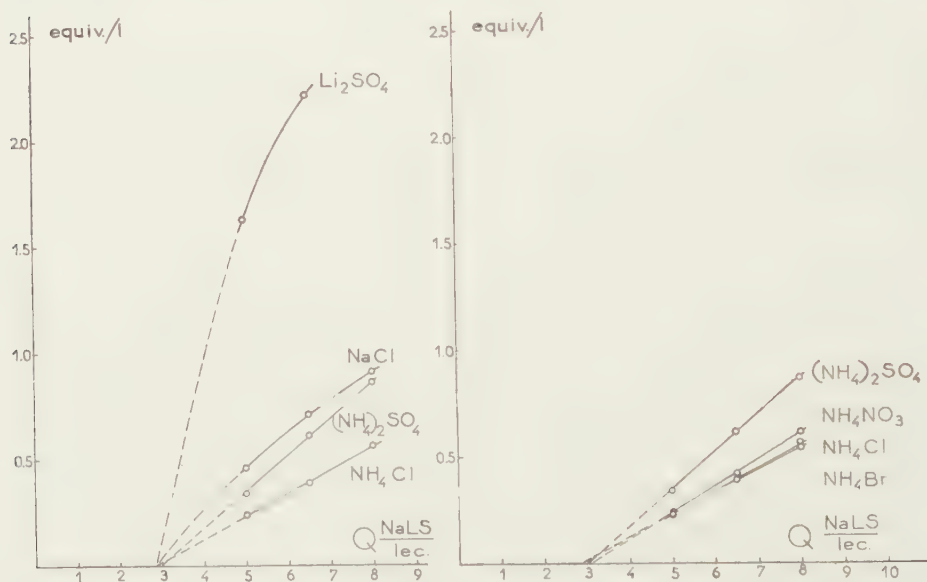


Fig. 4. Cation and anion sequences in the neutralization by salts of the electrical decompensation of the phosphatide by NaLS. The curves give the limits elast.-visc.s./O-coac.

<sup>1)</sup> The sequence  $\text{CNS} > \text{J} > \text{NO}_3, \text{Br} > \text{Cl}$  can be found in: H. G. BUNGENBERG DE JONG and A. RECOURT, these Proceedings, Series B 56, 303, 315, 442 (1953). Later not published observations in this laboratory allowed for  $\text{NO}_3 > \text{Br}$  and the addition of  $\text{SO}_4/2$  at the right end of this sequence.



As the detergent ion now taken up in the phosphatide is an anion, we must expect a) that salts with the same cation but different anions will give a bundle of curves in which second order effects of the anions find expression, and b) that salts with the same anion but different cations will give a bundle of curves, in which the sequence will be predictable from the affinity sequence of the cations for the negatively charged ester sulphate group of Na-laurylsulphate.

There are, however, no data available for the latter affinity sequence, but they are for another sulphate-soap ("Teepol", a sec. alkyl sulphate). Besides this, we also know in this case the second order effects due to different anions. Compare fig. 5, which is reproduced here from a former publication <sup>1)</sup>.

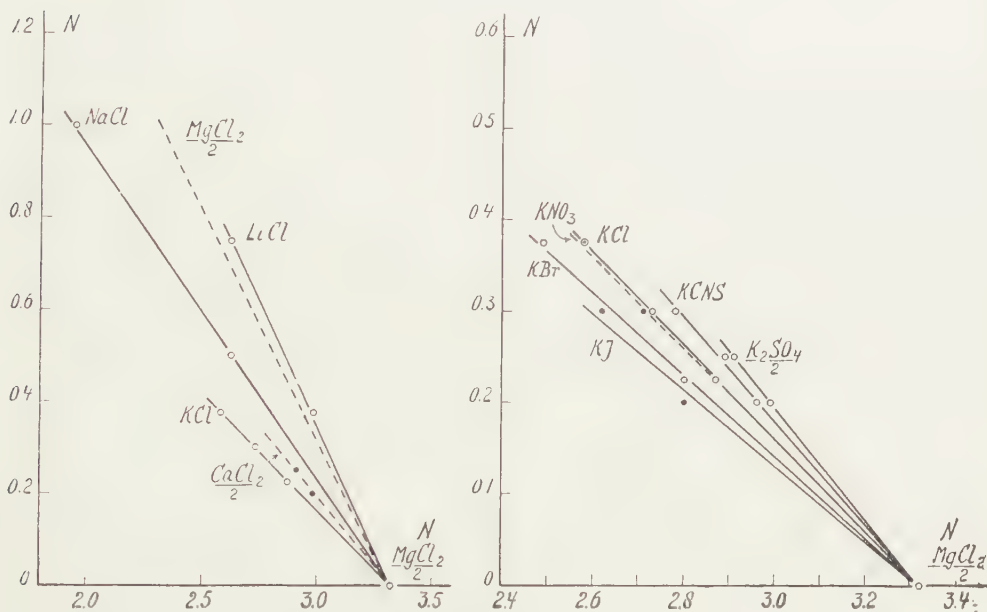


Fig. 5. Determination of the cation (left) and anion (right) sequence for the coacervation of T-pol by means of combining the investigated salts with  $\text{MgCl}_2$

We now turn to fig. 4, right. As here the  $\text{NH}_4$ -ion is the agent which removes the decompensation, the spreading is due to the second order effects of the accompanying anions. The curves for  $\text{NH}_4\text{Br}$ ,  $\text{NH}_4\text{NO}_3$  and  $\text{NH}_4\text{Cl}$  lie close together, but that for  $(\text{NH}_4)_2\text{SO}_4$  lies distinctly higher.

We also see that in fig. 5,  $\text{K}_2\text{SO}_4$  lies distinctly higher than the group of  $\text{KBr}$ ,  $\text{KNO}_3$  and  $\text{KCl}$ . Thus in principle the second order effects of the anions already present in a sulphate soap alone may give at first approximation an explanation of the spreading of the curves in fig. 4, right. To explain the sequence of the curves in fig. 4, left, we must start from

<sup>1)</sup> H. G. BUNGENBERG DE JONG and C. MALLEE, these Proceedings, Series B 55, 360 (1952).

the affinity sequence of the monovalent cations for the sulphate soap, which from fig. 5, appears to be:



In our experiments we could not use K salts, as they already give precipitations with laurylsulphate at low concentration. To have one cation more, we have also plotted in fig. 4, left, the results with  $NH_4Cl$  and  $(NH_4)_2SO_4$ . Thus the question arises which place the  $NH_4$  ion will take in the above affinity sequence. This has not been investigated but we may with certain reserve infer that it will be situated between K and  $Na^1$ ). We thus obtain the affinity sequence:



We may thus expect that in the salt- $Q$  diagram at constant  $Q$  the concentrations needed for reaching the coacervation limit for salts with the same anion but different cations will increase according to the sequence:



In fig. 4, left the curves for  $NH_4Cl$  and  $NaCl$  are directly comparable and give  $NH_4 < Na$ . The curves for  $(NH_4)_2SO_4$  and  $Li_2SO_4$  can also be compared directly which gives  $NH_4 < Li$ . As the distance between  $(NH_4)_2SO_4$  and  $Li_2SO_4$  is very much greater than that between  $NH_4Cl$  and  $NaCl$ , we may conclude, that when  $NH_4$ ,  $Na$  and  $Li$  have been compared combined with the same anion, we should have obtained the following sequence (for increasing concentrations):



which is quite what was expected above.

#### 4. *Some particulars in the salt- $Q$ diagram in connection with the problem of the action of detergents in the absence of salts*

A discussion in section 2 of the bends at the left end of the curves representing in a  $NaCl$ - $Q$  diagram the limit O-coacervate/elastic viscous s. led to the conclusion

<sup>1)</sup> The reversal of charge sequences of macromolecular sulphate colloids show exactly the same particulars as we observe for the sulphate-soap in fig. 5: In both cases we have  $K > Na > Li$  and  $Ca/2 > Mg/2$  and besides the influence of the valency is very much in the background. Thus if for a macromolecular sulphate colloid the position of the  $NH_4$  ion relative to K, Na and Li was known, we could conclude that it would have the same position for a sulphate soap. Unfortunately no such data are available. It has been found that the reversal of charge sequences of  $SiO_2$  particles resemble in all details, those characteristic of macromolecular sulphate colloids. The available  $SiO_2$  data show that  $NH_4$  stands between K and Na, but closer to Na than to K. The affinity series for macromolecular sulphate colloids will therefore presumably be  $K > NH_4 > Na > Li$  and there is no reason why the same sequence should not apply to a sulphate-soap too. Compare H. G. BUNGENBERG DE JONG in H. R. KRUYT, Colloid Science II, (Elsevier, 1949) Chapter IX, see figures 15, 21 and 29.

that the true limits lie at lower NaCl concentration than given by the bends. The hypothesis was put forward, that they lie on the extrapolated curve branches as shown in fig. 2 (dotted lines).

It is seen that these extrapolated curve branches cut the abscissa (in the case of CTAB at about  $Q = 2.5$ , in the case of NaLS at about  $Q = 2.9$ ). This means that in the absence of NaCl, CTAB as well as NaLS should transform the phosphatide suspension with increase of  $Q$  into O-coacervates and elastic viscous systems successively, and that the limit between the latter systems is given by the above intersection points of the extrapolated branches with the  $Q$  axis. Here we seem to come into direct conflict with the results in section 2 of the present communication and section 3 of Part III. It was found that the two detergents acting in the absence of salts give rise neither to O-coacervates nor to true elastic viscous systems. At first sight it seems that we do better to reject the hypothesis from which we started.

Results in the preceding section, however, strongly support this hypothesis. In fig. 4 the experimental points all certainly lie on that part of the curves where they represent true coacervation limits. When the curves are extrapolated downwards to the left (see broken lines) they cut the abscissa at practically the same value of  $Q$  (the actual slight differences in the individual  $Q$  values are presumably due to experimental errors). This is exactly what could be expected from the above hypothesis. The drawn part of the curves (in fig. 4) have different positions in the salt- $Q$  diagram as a result of specific influences of the salt ions. As we proceed downwards to the left along the extrapolated branches the above influences will become smaller and they will have disappeared altogether at the salt concentration zero. Hence the different curves must converge to one and the same point on the  $Q$ -axis, which thus corresponds to the limit O-coacervate/elastic viscous in the absence of salt.

We return to the above signalized contradiction. We have not yet paid sufficient attention to the fact that the rate of coacervation rapidly diminishes as we proceed downwards along the extrapolated curve branch. Here we may discern two cases:

- a. the rate, though becoming extremely small, still remains finite,
- b. the rate already reaches the value zero, before the extrapolated curve branch meets the  $Q$ -axis.

In case a. the contradiction is only an apparent one. The series of transformations: smectic phase  $\rightarrow$  O-coacervate  $\rightarrow$  elastic viscous systems  $\rightarrow$  non elastic solutions will take place in the absence of salt with increase of  $Q$ , but the rate of the transformations is so extremely slow, that in practice the transformations are not observed. This interpretation, however, seems too simplistic. One would expect that in the absence of salt the smectic phase remains practically unaltered when in contact with a detergent solution. But this is not the case (section 2 and in Part III section 3).

For removing the contradiction case b. opens up better possibilities. The attaining of the value zero may mean that further downwards in the salt- $Q$  diagram we enter a region in which O-coacervates and true elastic systems are metastable systems. In this region detergent and smectic phase of the phosphatide still interact with finite rate, but in a different way. Presumably sandwich micelles no longer play a role here, as the transformation of the smectic phase leads at once to non elastic solutions (abstraction made of temporarily formed elastic viscous systems, the nature of which has been investigated in Part III, section 3).

When we accept the above, the crossing point of the extrapolated curves with the  $Q$ -axis has the meaning of the limit between the here metastable O-coacervates and metastable elastic viscous systems.

That the value of  $Q$  at these crossing points is much higher than about 0.5, points

to a not very effective electrical decompensation as a result of the detergent ions taken up in the sandwich micelles at lower  $Q$  values <sup>1</sup>). This will be the case when an appreciable fraction of the counterions is bound to the micelle at the same time.

The above discussions may be of use for a future investigation into the nature of the interaction phosphatide + detergent in the absence of salts. Besides this they provisionally leave open the possibility that examples may be found in which also in the absence of salts with increase of  $Q$ , stable O-coacervates and stable elastic viscous systems are formed.

### 5. Summary

1. The action of NaLS (Na laurylsulphate, anionic detergent) on egg-phosphatide suspensions has been studied in the presence and absence of NaCl. The results are, in principle, the same as obtained in Part III with CTAB (cetyltrimethylammoniumbromide, cationic detergent).

2. In the absence of NaCl the action comes to the transformation  
smectic phase  $\rightarrow$  non elastic solution.

for a complete solution of the phosphatide a value of  $Q$  of about 2 being required, ( $Q$  = ratio NaLS/phosphatide). In a region of  $Q$  values around 2, elastic viscous systems are initially formed, which are systems not in internal equilibrium. Elasticity and high viscosity disappear or tend to disappear with time.

3. In the presence of a certain minimum constant NaCl concentration, with increase of  $Q$ , the transformations are obtained which can be expected from a progressive electrical decompensation of the micelle of the phosphatide (see Part III, Introduction):

smectic phase  $\rightarrow$  O-coacervate  $\rightarrow$  elastic viscous systems  $\rightarrow$  non elastic solution.

4. The position of various regions in a NaCl- $Q$  diagram has been determined, from which can be read off:

a. The  $Q$ -values for each limit shift to higher values as the constant NaCl concentration is higher.

b. At a sufficiently high constant  $Q$  value the reverse sequence is obtained with increase of the NaCl concentration:

non elastic solution  $\rightarrow$  elastic viscous system  $\rightarrow$  O-coacervate  $\rightarrow$  smectic phase.

<sup>1</sup>) With the CTAB preparation II the binding of CNS ions for reaching the limits non elastic/elastic viscous and elastic viscous/O-coacervate has been determined at 45° in the same way as described in H. G. BUNGENBERG DE JONG and A. RECOURT, these Proceedings, Series B 56, 303, 315, 442 (1953). Similar results have been obtained for the first mentioned limit, namely  $37 \pm 3$  % and for the second  $68 \pm 2$  % (expressed in % of the maximal value). When we assume that CTA is taken up in the phosphatide, not accompanied by counterions we might accordingly expect that for the limit O-coacervate/elastic viscous systems a ratio of negative to positive charges of about 2/3 would be found, which will be the case at  $Q = 0.5$  (compare in Part III, fig. 1, upper row).



Both points a and b can be expected from the neutralizing effect of salts on the electrical decompensation (Part III, Introduction).

5. Several salts have been compared as to their neutralizing effect on the electrical decompensation of the phosphatide by CTAB and NaLS respectively.

6. In the case of decompensation by CTAB, large differences are obtained with salts having the same cation but different anions. The latter arrange themselves in the following sequence of decreasing neutralizing effect from left to right:



The neutralizing effect is only slightly different for salts with the same anion but different cations ( $\text{NH}_4$ , K, Na).

7. In the case of decompensation by NaLS, salts having the same anion but different cations differ considerably. The latter arrange themselves in the sequence:



The neutralizing effect is not much affected by changing the anion (Br, Cl,  $\text{NO}_3$ ,  $\text{SO}_4$ ) with constant cation.

8. The results sub 6 and 7 confirm the supposition (Part III, Introduction) that the neutralizing effect of a salt is due to a binding of that salt ion which is oppositely charged to the detergent ion taken up in the phosphatide micelle. Indeed the anion sequence found sub 6 is the affinity sequence of the anions for the CTA cation, and the cation sequence found sub 7 is the affinity sequence for the LS-anion.

9. From certain particulars of the curves in the salt- $Q$  diagrams it is suggested that in the absence of salt the O-coacervates and the true elastic viscous systems are metastable systems.

*Department of Medical Chemistry,  
University of Leiden.*

## THEORY OF LIGHT-SCATTERING BY DETERGENT SOLUTIONS

BY

W. PRINS AND J. J. HERMANS

(Communicated at the meeting of January 28, 1956)

It has become customary to assume that a detergent solution may be treated as ideal provided each micelle is given a charge which is considerably less than the number of monomer ions in it. This amounts to saying that the micelle of a sodium soap, for instance, should be written as  $\text{Na}_{m-p}\text{S}_m$ , where  $m$  is the number of monomer ions  $\text{S}$ , and  $p$  ( $< m$ ) the charge of the micelle. On the basis of this model HUTCHINSON has asserted that the change in the light-scattering micellar weight on addition of salts is only apparent and is caused by charge effects.

In the present paper the general theory of light-scattering by multi-component systems is applied to the above-mentioned model. It is found that Debye's procedure of extrapolating  $(c-c_0)/\tau$  versus  $c$  to the concentration  $c = c_0$  ( $c_0$  = critical micelle concentration,  $\tau$  = turbidity) does not lead to the exact micellar weight  $M_m$  but to a value which will usually differ from  $M_m$  by about 10 %.

An improvement on the model is introduced by taking into account the activity coefficient of the micelles as derived from the volume exclusion principle, assuming that the excluded volume may be derived from a hard sphere approximation (DORY and STEINER), the radius of the sphere being determined by the extension of the electrical double layer. By means of reasonable approximations it is proved that the second virial coefficient in the turbidity equation is the sum of a term resulting from the micellar charge and a term resulting from the excluded volume effect.

Applications of the equations obtained will be given in later work, where it will be shown that the change in the light-scattering micellar weight on addition of salts must be considered as real.

### 1. Introduction

Solutions of ionic detergents show the well-known phenomenon of micellization when the detergent concentration reaches a certain value called critical micelle concentration (CMC). Extensive studies on the equilibrium between monomers and micelles have been made [1-17], and several arguments have been advanced to support the idea that beyond the CMC the monomer concentration remains practically constant on further addition of soap [for example: 1, 6, 8].

The first to indicate the applicability of the light-scattering method to detergent solutions was DEBYE [6], who derived the micellar weight from a plot of  $(c-c_0)/\tau$  versus  $c$ , extrapolated to  $c_0$ . Here  $c$  is the detergent concentration,  $c_0$  the CMC and  $\tau$  the excess turbidity. Complications may arise, however, from non-ideal behaviour and from charge effects.

The effect of the electric charge of colloid particles on their light-scattering in solution has been the subject of many discussions [18-23].

An extreme point of view was assumed by HUTCHINSON [19], who expressed the belief that the change of the light-scattering micellar weight on the addition of salt is only apparent and is due to the suppression of the effective micellar charge. It is the purpose of the present article to investigate this question in some detail. The basis of our discussion will be the general fluctuation theory for multi-component systems as developed by ZERNIKE [24] and later applied by BRINKMAN and HERMANS [25], KIRKWOOD and GOLDBERG [26] and STOCKMAYER [27]: if a system contains  $N_1 N_2 \dots N_s$  solute molecules of type 1, 2 ... s in a volume  $V$ , and the compressibility of the solution is not too different from that of the pure solvent, the excess turbidity of the solution over that of the solvent is

$$(1) \quad \tau = -AVD/\Delta; \quad A = 32\pi^3 kTv^2/3\lambda^4.$$

Here  $v$  is the refractive index of the solution,  $\lambda$  the wavelength of the incident light in vacuo,

$$(2) \quad D = \begin{vmatrix} 0 & v_j \\ v_i & G_{ij} \end{vmatrix}; \quad \Delta = \|G_{ij}\|; \quad i, j = 1, 2 \dots s.$$

$$(3) \quad v_i = (\partial v / \partial N_i)_{p,T}$$

$$(4) \quad G_{ij} = (\partial G_i / \partial N_j)_{p,T} = (\partial^2 G / \partial N_i \partial N_j)_{p,T}$$

$G$  is the Gibbs free energy and  $G_i$  the partial derivative of  $G$  with respect to  $N_i$ . The problem is thus reduced to that of finding the second derivatives of the Gibbs free energy. Now, the thermodynamical properties of an aqueous solution containing detergent monomers, detergent micelles and low molecular weight salt are so complex that it is necessary to introduce simplifying assumptions. It has become customary [5, 8, 14, 17, 19] to assume that the micelles in these solutions show an apparent degree of electric dissociation such that if a micelle contains  $m$  monomer ions, its effective charge is  $p$ , where  $p < m$ . This amounts to saying that  $m - p$  counter ions are bound to the micelle. What one hopes to achieve by this assumption is that activity corrections become much smaller.

A second simplification is introduced by assuming that only one micelle size need be considered. Discussions of the validity of this second assumption can be found in references [2, 6, 8, 11, 16].

One final remark is made to avoid confusion. We will treat monomer and micelle as independent components. One might argue that in reality they are in dissociative equilibrium and that this equilibrium may adjust itself to fluctuations in composition, thus affecting the magnitude of these fluctuations. This, however, is not true. One possible approach is to ignore the equilibrium, i.e., treat monomer and micelle as independent components. An alternative approach is to assume that the equilibrium adjusts itself immediately to fluctuations, but in that case one must take into account that even in the absence of fluctuations in total mass content

there will be fluctuations in the equilibrium itself [28]. If one adds the effect of these fluctuations in the equilibrium to that of the fluctuations in mass content, the final answer is exactly equal to the one obtained by ignoring the equilibrium altogether [29].

## 2. Ideal solutions

In connection with work by previous authors, we first discuss the light-scattering by a soap solution in which activity corrections are negligible. All ions are supposed to be univalent, and the extraneous salt has one ion in common with the soap.

Consider a volume  $V$  containing  $N_0$  water molecules,  $N_1$  monomer ions  $S$ ,  $N_3$  ions of added salt with the same sign of charge as the monomers and  $N_m$  micelles, each with charge  $p$  and containing  $m$  monomers. Then there will be

$$(5) \quad N_2 = N_1 + N_3 + pN_m$$

counter ions, while the total soap content, expressed in monomers, is

$$(6) \quad N = N_1 + mN_m.$$

Assuming ideal behaviour, the Gibbs free energy is given by

$$(7) \quad G/kT = \sum_j N_j (\mu_j^0/kT + \ln x_j); \quad j = 0, 1, 2, 3, m$$

where  $x_j$  represents mole fraction:

$$(8) \quad x_j = N_j/S; \quad S = \sum_j N_j = N_0 + 2N_1 + 2N_3 + (p+1)N_m.$$

As solute components we take the monomer salt, the extraneous salt and the micellar salt, each micellar salt unit being composed of one micelle and  $p$  counter ions. The corresponding variables are  $N_1N_3$  and  $N_m$ . The second derivatives of  $G/kT$  with respect to these variables are found to be

$$(9) \quad \begin{cases} G_{11}/kT = 1/N_2 - 1/N_1 - 4/S & G_{33} = 1/N_2 - 1/N_3 - 4/S \\ G_{13}/kT = 1/N_2 - 4/S & G_{3m} = p/N_2 - 2(p+1)/S \\ G_{1m}/kT = p/N_2 - 2(p+1)/S & G_{mm} = p^2/N_2 + 1/N_m - (p+1)^2/S \end{cases}$$

At all concentrations except very high ones the last term in each of these expressions is small compared with the others and will therefore be omitted. This gives, for the determinants in Eq. 2:

$$(10) \quad \begin{cases} -D \cdot N_1 N_2 N_3 N_m / (kT)^2 = v_1^2 N_1 L_1 + v_3^2 N_3 L_3 + v_m^2 N_m L_m - 2v_1 v_3 N_1 N_3 - \\ \quad - 2v_1 v_m p N_1 N_m - 2v_3 v_m p N_3 N_m \\ \Delta \cdot N_1 N_2 N_3 N_m / (kT)^3 = 2N_1 + 2N_3 + p(p+1)N_m \end{cases}$$

where

$$L_1 = N_1 + 2N_3 - (p^2 + p)N_m; \quad L_3 = 2N_1 + N_3 - (p^2 + p)N_m; \\ L_m = 2N_1 + 2N_3 + pN_m.$$



We now make use of the fact that to a very good approximation

$$(11) \quad v_m = m\nu_1$$

and introduce a factor  $f$  defined by

$$(12) \quad f = \nu_3/\nu_1.$$

With the usual detergents, and NaCl as extraneous salt, the value of  $f$  is about  $1/4$ . Finally, we assume that both  $N_1$  and  $N_3$  are small compared with  $m^2N_m$ . The first of these assumptions is justified as soon as the detergent concentration is slightly higher than the CMC, because  $m$  is of the order of 100. The second assumption implies that the concentration of the extraneous salt is not excessive: since we are interested in the light scattered by the soap we need not consider cases in which that of the added salt is predominant. It is easily verified that as a result of these approximations we may neglect in the expression for  $D$  all terms which do not contain  $N_m$ . Using Eqs. 11 and 12, Eq. 1 becomes

$$(13) \quad \frac{AV\nu_m^2N_m}{\tau kT} = \frac{2N_1+2N_3+p(p+1)N_m}{2b_1N_1+2b_3N_3+pN_m}$$

where

$$(14) \quad b_1 = 1 - \alpha + \alpha^2/2 + \alpha/2m; \quad b_3 = 1 - f\alpha + f^2\alpha^2/2 + f^2\alpha/2m,$$

while

$$(15) \quad \alpha = p/m$$

is the effective degree of dissociation of the micelles. For the sake of simplicity we abbreviate

$$(16) \quad g = \frac{N_1+N_3}{b_1N_1+b_3N_3}.$$

Further, let  $c$  be the detergent concentration in g/ml,  $c_0$  the CMC in g/ml and  $N_A$  Avogadro's number. Since  $c_0$  is practically equal to the monomer concentration we have  $N_m = N_A V(c - c_0)/M_m$  where  $M_m$  is the micellar weight. For  $\nu_m$  we substitute  $\nu_c M_m / VN_A$  where  $\nu_c = (\partial \nu / \partial c)_{p,T}$ . This implies that the soap concentration is sufficiently low to consider  $V$  as a constant in the differentiation of  $c$  with respect to  $N_m$ , a condition which is fulfilled in the range of concentrations studied. If, finally, we introduce the usual symbol

$$(17) \quad H = Av_c^2 RT,$$

we get

$$(18) \quad H \frac{c-c_0}{\tau} = \frac{g}{M_m} \left[ 1 + \frac{c-c_0}{2M_m} \frac{p^2+p-gp}{n_1+n_3} + 0(c-c_0)^2 \right]$$

where  $n_1$  and  $n_3$  are expressed in mole/ml. The series expansion (18) is valid provided  $pN_m < 2(N_1 + N_3)$ . Eq. 18 shows that Debye's extra-

polution procedure does not give the exact micellar weight, but an apparent one

$$(19) \quad M_m^* = M_m/g.$$

It is only when  $\alpha=0$  that  $M_m^* = M_m$ . According to the usual estimates of  $\alpha$  [14, 15], the difference between  $M_m$  and  $M_m^*$  is of the order of 10 % in dilute salt solutions.

It is clear from the formula obtained that in principle it should be possible to calculate both  $m$  and  $p$  if both the intercept and the slope of  $(c-c_0)/\tau$  versus  $c-c_0$  is measured, provided the slope is constant in a sufficiently large concentration interval. Before considering this, however, it will be necessary to discuss the activity correction for the micelles (§3).

In most cases, when the salt content  $N_3$  is appreciable, the CMC is decreased to a low value, so that  $N_1 \ll N_3$ . This means that Eq. 18 is simplified to

$$(20) \quad H \frac{c-c_0}{\tau} = \frac{1}{b_3 M_m} \left[ 1 + \frac{c-c_0}{2n_3 M_m} (p^2 + p - p/b_3) \right].$$

If, on the other hand,  $N_3=0$ , we get

$$(21) \quad H \frac{c-c_0}{\tau} = \frac{1}{b_1 M_m} \left[ 1 + \frac{c-c_0}{2c_0 m} (p^2 + p - p/b_1) \right].$$

This becomes identical with the series expansion of a formula given by PHILLIPS and MYSELS [15] when  $b_1=1$ . HUTCHINSON [19] has derived a formula from the well-known expression

$$(22) \quad \tau \partial \pi / \partial N = V A N v_N^2$$

where  $N$  is the total soap content (Eq. 6) and  $\pi$  the osmotic pressure. In the absence of salt the following formula is applied:

$$\tau = (kT/V)[2N_1 + (p+1)N_m].$$

Using Eq. 6 this leads to

$$(23) \quad \frac{\partial \pi}{\partial N} = \frac{kT}{V} \left[ \frac{p+1}{m} + \left( 2 - \frac{p+1}{m} \right) \frac{\partial N_1}{\partial N} \right].$$

HUTCHINSON supposes that the term with  $\partial N_1 / \partial N$  may be omitted, because it is known that the monomer concentration does not change much with soap content when  $c > c_0$ . Taking this approximation for granted one gets

$$Hc/\tau = (p+1)/M_m.$$

However, it is easy to show that the omission of the second term in the square brackets of Eq. 23 is not permissible. The model used implies the equilibrium condition

$$N_2^{m-p} N_1^p = K N_m$$

in conjunction with:  $N = N_1 + mN_m$  and  $N_2 = N_1 + pN_m$ . From these three equations one derives that

$$F \cdot \partial N_1 / \partial N = 1/N_m + p(m-p)/N_2; \quad F = m^2/N_1 + (m-p)^2/N_2 + 1/N_m.$$

If reasonable values for  $p$  and  $m$  are inserted, for example  $p = 10$ ,  $m = 100$ , and a detergent concentration equal to 3 times the CMC is considered, we have approximately  $N_1 = \text{CMC}$ ;  $N_m = 0.02 N_1$  and  $N_2 = 1.2 N_1$ . This gives a value of about 0.04 for  $\partial N_1 / \partial N$  and leads to the conclusion that the two terms within the square brackets of Eq. 23 are of the same order of magnitude. If Eq. 23, including the term with  $\partial N_1 / \partial N$  is inserted in the turbidity relation 22, one finds the result derived in the present article.

As a final remark it may be observed that the equation for the turbidity becomes

$$Hc/\tau = m/M_m = 1/M_1$$

when  $p$  is set equal to  $m$  in the original Eqs. 10 for  $D$  and  $A$ . This answer must be refuted on experimental grounds. The assumption  $p = m$  would imply that large activity corrections would have to be introduced.

### 3. Activity correction based upon the concept of electric double layer

The effective charge  $p$  of the micelle was introduced as an attempt to treat the system as an ideal solution. There is, of course, no guarantee that the value of  $p$ , thus defined, is independent of soap concentration and (or) salt content. We may hope to improve the description of experimental data by introducing activity corrections. One obvious activity correction is that caused by the restriction in freedom of the micelles as a result of double layer repulsion. This gives the micelles an apparent volume much greater than their own volume. STIGTER [11] has calculated the effective diameter  $D_h$  from the  $\zeta$ -potential of the micelle, by applying the tables of VERWEY and OVERBEEK [30], modified in such a way as to make them valid for rather small spherical particles with a high surface potential [31]. The effective diameter  $D_h$  is determined by the condition that the electrostatic repulsive energy of the double layers equals  $kT$  when the distance between the centres of two particles is  $D_h$ . Following an idea developed by DOTY and STEINER [32] the micelles with their double layer are regarded as hard spheres of diameter  $D_h$ , and the activity coefficient of the micelles in dilute solution is calculated in much the same way as in the derivation of the second virial coefficient for gases. For the entropy of mixing STIGTER writes, just as HUGGINS [33] does:

$$S/k = \sum_i \ln P_i - N_m \ln N_m + N_m$$

where  $P_i = V[1 - (i-1)8v_m]$  is proportional to the number of configurations available to the  $i$ -th micelle. The volume excluded per micelle is

$$8 v_m = 4\pi D_h^3/3.$$

Expansion of the  $(\ln P_i)$ -terms gives

$$S/k = N_m - N_m \ln (N_m/V) - 4 v_m N_m^2/V.$$

We define the activity coefficient  $f_m$  of the micelles by the equation

$$-T(\partial S/\partial N_m)_{p,T} = \text{const.} + kT \ln (f_m x_m)$$

where  $x_m$  is the mole fraction. In this differentiation we set  $\partial V/\partial N_m = v_m$  and obtain to a first approximation:

$$(24) \quad \ln f_m = 6 v_m N_m/V.$$

This holds good when the solute particles actually are hard spheres. One might object that in the present case  $\partial V/\partial N_m$  should be set equal to the real volume of the micelles, which is much smaller than  $v_m$ . This would lead to

$$(25) \quad \ln f_m = 8 v_m N_m/V.$$

STIGTER finds  $4v_m N_m/V$  because he writes, incorrectly,

$$S/k = -N_m \ln (f_m N_m/V).$$

Either Eq. 24 or Eq. 25 may be used. They give the same final result in the light-scattering formula provided in either case the procedure followed is consistent.

To find the effect of activity corrections on light-scattering, we must add to each of the expressions (9) for  $G_{jk}/kT$  a term  $\beta_{jk}$  defined as follows:

$$(26) \quad \beta_{jk} = \partial \ln f_j / \partial N_k.$$

We will not give all the details of the calculations, but merely mention the general procedure and the approximations made. The activity coefficient  $f_m$  depends on the effective diameter  $D_h$  and, therefore, on the  $\zeta$ -potential of the micelle and the ionic strength  $\kappa$  of the solution. In our case

$$(27) \quad \kappa^2 = 8\pi (N_1 + N_3 + pN_m)/\epsilon kTV$$

where  $\epsilon$  is the dielectric constant. It is assumed that the contribution of  $pN_m$  to  $\kappa^2$  may be ignored. This simplifies the computations to a considerable extent and does not affect the order of magnitude of the result obtained. Furthermore, we neglect the effect of changes in  $\zeta$ -potential on  $D_h$ . This is supported by the fact that the  $D_h$  values derived from STIGTER's data do not differ more than a few percentages from the simple estimate:

$$(28) \quad D_h = 2(a + 1/\kappa)$$

where  $a$  is the radius of the micelle. Eq. 28 means that the effective thickness of the double layer may be set equal to  $1/\kappa$ .

Now  $\beta_{1m}$  and  $\beta_{3m}$  follow immediately from Eq. 24 by differentiating  $v_m$  with respect to  $N_1$  and  $N_3$  respectively. Differentiation of  $V$  may be



omitted because this gives higher order virial coefficients. We find  $\beta_{11}$  by integrating  $\beta_{1m}$  with respect to  $N_m$  and subsequently differentiating with respect to  $N_1$ . Similarly, we get  $\beta_{13}$  and  $\beta_{33}$ . This leads to the following results:

$$\begin{aligned}\beta_{11} = \beta_{13} = \beta_{33} &= 3\pi N_m^2 D_h (\partial D_h / \partial N_1)^2 + D_h^2 (\partial^2 D_h / \partial N_1^2); \\ \beta_{1m} = \beta_{3m} &= 3\pi N_m^2 D_h^2 (\partial D_h / \partial N_3); \quad \beta_{mm} = \pi D_h^2 / V.\end{aligned}$$

An estimate of the effect which these activity corrections have on the determinants  $D$  and  $\Delta$  (Eq. 2) is obtained by considering the case of a detergent solution whose concentration is three times the CMC, assuming that  $m=100$  and thus  $N_m=0.02$  times the CMC. For  $N_3$  we take  $10^{-4}$  mole/ml. It is found that of all  $\beta_{jk}$ 's only  $\beta_{mm}$  in the determinant  $\Delta$  needs to be retained. Eq. 13 for the turbidity must now be replaced by

$$(29) \quad \frac{VA v_m^2 N_m}{\tau kT} = \frac{2N_1 + 2N_3 + [p(p+1) + 2(N_1 + N_3)\beta_{mm}]N_m + \beta_{mm}N_m^2}{2b_1N_1 + 2b_3N_3 + pN_m}$$

Expansion in powers of  $N_m$  and introduction of the concentrations  $c$  and  $c_0$  (g/ml),  $n_1$  and  $n_3$  (mole/ml) gives, instead of Eq. 18,

$$(30) \quad H \frac{c-c_0}{\tau} = \frac{g}{M_m} \left[ 1 + \frac{c-c_0}{2M_m} \left( \frac{p^2+p-gp}{n_1+n_3} + 16 v_m N_A \right) \right].$$

We have thus proved rigorously that for our model, taking the approximations made for granted, the Doty-Steiner term which accounts for the repulsion between the double layers around the micelles is simply additive. Applications of Eq. 30 will be discussed in a following article, where it will be shown that the excluded volume term is often of the same order of magnitude as the one due to the charge  $p$ .

Although the procedure is admittedly only approximate, it will be shown that the change in the light-scattering micellar weight on addition of salt is real. If there is, in addition, an apparent change in  $M_m$  as a result of charge effects, this change is small. It is true that our derivation is based on a special model, but the assertion that the change in  $M_m$  is only apparent [19] was based on a less complete treatment of exactly the same model and cannot, therefore, be accepted as reliable.

*Laboratorium voor Anorganische en Fysische Chemie  
Rijks Universiteit, Leiden*

#### REFERENCES

1. GRINDLEY, J. and C. R. BURY, J. Chem. Soc., 679 (1929).
2. MEYER, K. H. and A. VAN DER WIJK, Helv. Chim. Acta 20, 1321 (1937).
3. HARTLEY, G. S., Kolloid Z. 88, 33 (1939).
4. WARD, A. P., Proc. Roy. Soc. London A 176, 412 (1940).
5. CORRIN, M. L., J. Colloid Sci. 3, 333 (1948).
6. DEBYE, P., Ann. N.Y. Acad. Sci. 51, 575 (1949); J. Phys. Coll. Chem. 53, 1 (1949).
7. STAINSBY, G. and A. E. ALEXANDER, Trans. Faraday Soc. 46, 587 (1950).
8. VOLD, M. J., J. Colloid Sci. 5, 506 (1950).

9. HOBBS, M. E., *J. Phys. Coll. Chem.* **55**, 675 (1951).
10. HALSEY, G. D., *J. Phys. Chem.* **57**, 87 (1953).
11. STIGTER, D., *Rec. trav. chim.* **73**, 593, 611 (1954).
12. BOOY, H. L., *Colloid Science II*, Ch. XIV, (Elsevier, Amsterdam, 1949).
13. OOSHIKA, Y., *J. Colloid Sci.* **9**, 254 (1954).
14. PHILLIPS, J. N., *Trans. Faraday Soc.* **51**, 561 (1955).
15. ——— and K. J. MYSELS, *J. Phys. Chem.* **59**, 325 (1955).
16. HERMANS, J. J., *Proc. Kon. Ned. Akademie van Wetensch. Amsterdam B* **58**, 91 (1955).
17. HUTCHINSON, E., A. INABA and L. G. BAILEY, *Z. physik. Chem. N.F.* **5**, 344 (1955).
18. HERMANS, J. J., *Rec. trav. chim.* **68**, 859 (1949).
19. HUTCHINSON, E., *J. Colloid Sci.* **9**, 191 (1954); HUTCHINSON, E. and J. C. MELROSE, *Z. physik. Chem. N.F.* **2**, 363 (1954); M. E. L. MC. BAIN and E. HUTCHINSON, *Solubilisation* (Acad. Press, N.Y., 1955).
20. EDSALL, J. T., H. EDELHOCH, R. LONTIE and P. R. MORRISON, *J. Amer. Chem.-Soc.* **72**, 4641 (1950).
21. MYSELS, K. J., *J. Phys.* **58**, 303 (1954).
22. PRINS, W. and J. J. HERMANS, *J. Phys. Chem.* **59**, 576 (1955).
23. TRAP, H. J. L. and J. J. HERMANS, *Proc. Kon. Ned. Akad. v. Wetensch. Amsterdam B* **58**, 97 (1955).
24. ZERNIKE, F., thesis Amsterdam 1915; *Arch. Néerl. Sci. IIIA*, **4**, 74 (1918).
25. BRINKMAN, H. C. and J. J. HERMANS, *J. Chem. Phys.* **17**, 574 (1949).
26. KIRKWOOD, J. and R. J. GOLDBERG, *J. Chem. Phys.* **18**, 54 (1950).
27. STOCKMAYER, W. H., *J. Chem. Phys.* **18**, 58 (1950).
28. FOWLER, R. H., *Statistical Mechanics*, p. 758-760 (2nd Ed., Cambridge University Press, 1936).
29. PRINS, W., thesis Leiden, 1955.
30. VERWEY, E. J. W. and J. TH. G. OVERBEEK, *Theory Stability Lyophobic Colloids* (Elsevier, Amsterdam, 1948).
31. STIGTER, D. and K. J. MYSELS, *J. Phys. Chem.* **59**, 45 (1955).
32. DOTY, P. and R. F. STEINER, *J. Chem. Phys.* **18**, 1211 (1950); **20**, 25 (1952).
33. HUGGINS, M. L., *J. Phys. Coll. Chem.* **52**, 248 (1948).

## THE ELECTRON MICROSCOPY OF PROTEIN CRYSTALS

BY

LOUIS W. LABAW AND RALPH W. G. WYCKOFF

*(National Institute of Arthritis and Metabolic Diseases,  
National Institutes of Health, Bethesda 14, Maryland)*

(Communicated at the meeting of January 28, 1956)

Improvement in the resolving power of the electron microscope together with better methods of specimen preparation require a renewed examination of the molecular arrangements <sup>1)</sup> in macromolecular crystals. The improvement in method, using evaporated carbon <sup>2)</sup> as substrate and replicating material, yields preparations and electron micrographs of higher quality from the crystals earlier investigated. It has, also, considerably extended the range of crystalline substances accessible to successful study. In principle this new method involves <sup>3)</sup> depositing the crystals for study on a plastic (formvar) substrate, shadowing them with heavy atoms, coating this deposit with a suitably thin layer of evaporated graphite and dissolving away both the initial formvar and the crystals themselves before examination under the electron microscope.

The direct visualization that can thus be obtained of the molecules on the surface of a crystal can establish their three-dimensional arrangement. It can, also, yield information about the mechanism of crystal growth and dissolution. Such information of broad interest to crystallography is best furnished by crystals with very large molecules; those of some of the virus proteins are ideal. Determinations of crystal structure at the molecular level will, however, be especially instructive as applied to proteins with smaller and smaller molecules. With these different goals in mind, we have been examining a series of proteins having molecules of a variety of sizes. The results <sup>4)</sup> <sup>5)</sup>, though incomplete, are commencing to indicate the directions in which further work should proceed.

Thus far, the molecular arrangement has been a cubic closepacking in every instance where the data have been sufficient to establish it. These crystals with the same basic structure have, however, shown a great diversity in external form. It is the purpose of the present communication to illustrate this diversity.

A number of proteins crystallize as octahedra, occasionally modified by other faces. In such instances as edestin (Figure 1) and ferritin these octahedra are commonly well-formed, even under the high magnifications of the electron microscope. Their faces are remarkably smooth, being either molecularly flat or consisting of a few terraces, each a molecule

thick. As can be seen from the figure, the edges between adjacent octahedral faces are often sharp down to molecular dimensions. When other than (111) faces have been seen, these have been, like that on the uppermost crystal of the figure, small molecularly irregular cube faces blunting the apices of the octahedra. Some of these little faces have, however, been good enough to contribute to the spacing measurements required for determinations of molecular arrangement.

Octahedral protein crystals are not always as perfect as the foregoing. Thus the octahedra of the turnip yellows virus protein have always had very rounded edges (Figure 2), and faces on which the underlying order is hidden beneath extraneous deposits and molecules irregularly laid down.

Though the cube faces found on crystals of octahedral habit have always been rather poorly developed, this has not been true when the habit has been cubic. For instance, on the crystal of the necrosis virus protein shown in Figure 3, the dominant cube face with its square net is as perfect and as molecularly flat as the best (111) faces appearing on octahedral crystals. Furthermore, in cubic crystals such as these, the smaller octahedral side faces that are always present are equally good. Both the crystals of octahedral and of cubic habit have been notable for the absence of other forms; the many hundreds examined have rarely exhibited other than [100] and [111] faces.

The southern bean mosaic virus protein provides an example of a cubic crystal which differs remarkably from the foregoing in habit. On its isotropic crystals (110) has always been the principal face. They have, however, never shown a tendency to develop dodecahedra; instead they are lozenge-shaped and bounded on the sides by a number of small faces belonging, not only to [100], [111], and [110], but to the more complicated forms [120] and [113] (Figure 4). A determination of the conditions that favor the production of these complicated faces must inevitably contribute to our understanding of the mechanism of crystal growth.

Such studies will be further aided by our being able to examine forming crystals like the individual shown in Figure 5. These can often be obtained through the controlled crystallization of proteins that crystallize without the addition of salt from aqueous solution. Here the large top face molecularly flat at the right, but shelving off in a succession of terraces to the left, is (111); immediately below it there is a (110) face defined by lines of molecules. The right end of the crystal is terminated by another (111) and by a more or less obscured (100); to the left, the crystal is not yet sufficiently well-developed to exhibit bounding faces. A wide variety of incomplete crystals of this sort can be obtained by altering the conditions of crystallization.

### *Summary*

Recent improvements in techniques of specimen preparation permit an important extension of earlier studies with the electron microscope





Fig. 1. Three minute octahedral crystals of edestin seen at a magnification sufficient to reveal their molecular arrangements. The two lower crystals are twinned. Small cube faces can be seen on each crystal, that on the topmost being exceptionally flat. 61,500  $\times$ .

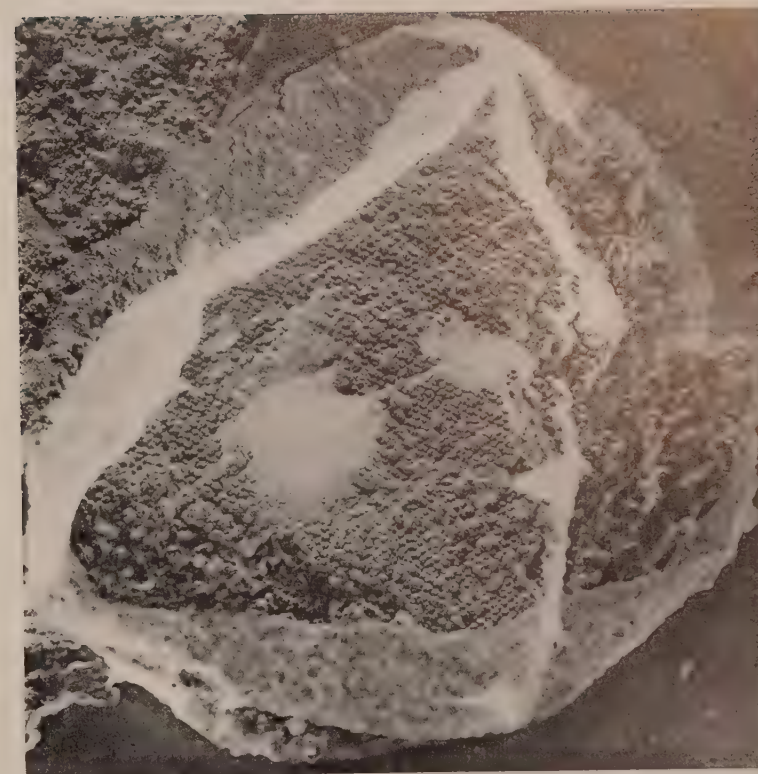


Fig. 2. An octahedral crystal of the turnip yellows virus protein. Note how poorly developed and uneven are its faces compared with those of the octahedra of Figure 1. 28,000  $\times$ .



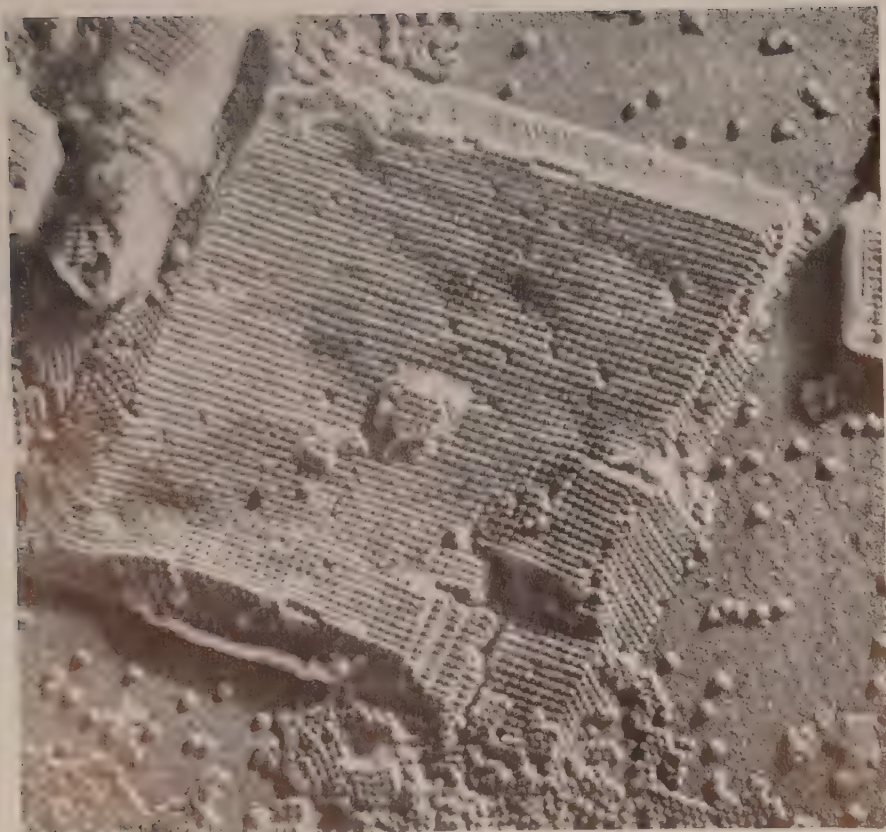


Fig. 3. A crystal of a necrosis virus protein showing its molecularly well-ordered large (100) face and the four equally flat octahedral faces that bevel it. There has been some local dissolution of the crystal in its lower right hand corner. 50,500  $\times$ .



Fig. 4. A corner of a southern bean mosaic virus protein crystal showing the several small faces developed there. The largest face, (110), is separated from another, small, dodecahedral face at the top of the crystal by a rectangular (100) face [characterized by a square molecular net running diagonal to the molecular rows of (110)]. In the upper right corner and bounding the crystal to the left are octahedral faces. Between these and the large (110) are narrow faces of the form [120]. 62,000  $\times$ .



Fig. 5. A partly formed crystal of a tobacco protein having the face development described in the text. The opaque bands obscuring part of the top of the crystal and enveloping its base are of contaminating material that rapidly accumulates under an intense electron beam. 51,500  $\times$ .

of the molecular arrangement in protein crystals. Examples are shown of the different appearances of the crystals of several substances having the same cubic close-packed molecular arrangement; and it is pointed out that these differences provide a novel way of approaching fundamental problems of crystallography.

## BIBLIOGRAPHY

1. See WYCKOFF, R. W. G., *Electron Microscopy*, Chapter X (Interscience Publishers, Inc., New York, 1949).
2. ROBERT, L., J. BUSSOT and J. BUZON, *Compt. rend. 1er Congrès Inter. de Microscopie Électronique*, p. 528 (Paris, 1950).  
BRADLEY, D. E., *Brit. J. Applied Physics*, **5**, 65, 96 (1954).
3. LABAW, L. W. and R. W. G. WYCKOFF, *Experimental Cell Research*, Suppl. 3, 395 (1955).
4. ——— and ———, *Nature*, **176**, 455 (1955).
5. ——— and ———, *Science* (In press).

## ASTRONOMY

# THE EFFECT OF ORIENTATION ON THE THICKNESS OF PROMINENCES

BY

S. G. M. HAUG

*(Circular No. 8 of the Astronomical Institute of the University of Amsterdam)*

*(Communicated by Prof. H. ZANSTRA at the meeting of December 17, 1955)*

### *Summary*

The values for the line of sight thickness of some prominences derived from the intensity of the continuous spectrum and published in the Amsterdam Circulars 5a, 5b and 6, deviate from the mean thickness derived from dark filaments, given by Dr. and Mrs. d'AZAMBUJA (6600 km).

Studying the dark filaments for the prominences in question from the "Cartes Synoptiques de la Chromosphère Solaire" (Meudon) we find an explanation in the orientation of the filaments with respect to the line of sight which during the eclipse are seen as bright prominences.

In earlier publications<sup>1)</sup> determinations were given of the thickness in the line of sight from eclipse spectra for four prominences. Emission data first gave the electron concentration, assuming a reasonable electron temperature, and then the thickness in the line of sight followed from the absolute surface brightness of the general continuous spectrum, assumed to be due to scattering of the photospheric light by the free electrons. The results are gathered in Table 3 of Circular No. 6.

The dimensions of quiescent prominences can be obtained from the  $H_\alpha$  or  $K_3$  spectroheliograms. A prominence at the limb of the sun is seen in emission against the dark sky background. Rotating with the sun the prominence is seen on the following days as a dark filament against the bright solar surface, at various angles with the line of sight. In this manner one can investigate the spatial dimensions of the prominence.

In a general study PETTIT<sup>2)</sup> finds an average length of 200,000 km, height of 50,000 km and thickness of 10,000 km; the prominence thus being a long and thin sheet of gas, nearly perpendicular to the solar surface.

<sup>1)</sup> S. G. M. HAUG, Proc. Kon. Ned. Ak. van Wetenschappen B 55, 517 (1952); D. KOELBLOED, Ibid. B 55, 524 (1952); R. O. REDMAN and H. ZANSTRA, Ibid. B 55, 598 (1952). (Circulars of the Astron. Inst. of the Univ. of Amsterdam, Nos. 5a, 5b and 6). We will refer to this papers as Circulars Nos. 5a, 5b and 6.

<sup>2)</sup> E. PETTIT, Ap. J. 76, 9 (1932).



A real standard work on this matter was published in 1948 by Dr. and Mrs. D'AZAMBUJA <sup>3)</sup>. This work is based on  $H_{\alpha}$  and  $K_3$  spectroheliograms taken from 1919 to 1930 with some supplementary material of later years. In preparation of this study the Observatoire à Meudon has issued solar maps and catalogues of the filaments <sup>4)</sup>. They obtain an average thickness of 6600 km, and there is remarkably little spread about this value. This thickness is meant for the main body of the prominence which corresponds to the portion on which the slit of the spectrograph is set at eclipse observations of bright prominences.

The values for the thickness in the line of sight of the four prominences obtained in the Circulars 5a, 5b and 6, deviate considerably from the above value of 6600 km. In the present study we try to identify our four prominences with dark filaments in the "Cartes Synoptiques" and then to estimate the angle they make with the line of sight at the moment when they appeared as bright prominences during the eclipse. From this we can evaluate the thickness in the line of sight.

From the published eclipse data, and in some cases from reproductions of the photographs, we get the position angle of the prominences and of the sun's axis of rotation. This gives the heliographic latitude of the prominences with sufficient accuracy for identification.

The "Cartes Synoptiques" give the heliographic longitude (according to CARRINGTON) of the central meridian of the sun at the time of the eclipse. Then  $90^\circ$  to the left and to the right we find the longitude of the eastern and western limb meridian of the sun. In this way we get the heliographic latitude  $\varphi$  and longitude  $\mathcal{L}$  of the point where we have to look for the filament that corresponds to the prominence. On the "Cartes Synoptiques" we then read off the angle  $\alpha$  between filament and the sun's equator. Let  $i$  be the inclination of the sun's rotational axis with respect to the plane of the sky at the date of the eclipse <sup>5)</sup>.

The angle  $\gamma$  between filament and line of sight is

$$(1) \quad \gamma = \alpha \pm i$$

since the prominence is then sufficiently close to the limb. The true thickness of the filament being  $d$ , the thickness in the line of sight is

$$(2) \quad L = \frac{d}{\sin \gamma}$$

<sup>3)</sup> M. et Mme L. D'AZAMBUJA, Ann. de l'Obs. de Paris, à Meudon, 6, fasc. VII (1948); referred to as D'AZAMBUJA.

<sup>4)</sup> Années 1919 à 1930: Ibid., 6, fasc. I à VI. Années 1931 à 1944: Cartes Synoptiques de la Chromosphère Solaire (Publ. subventionnée par l' U.A.I.), Meudon (1934 à 1952). This papers will be referred to as Cartes Synoptiques. For 1952 we found analogic maps in the monthly L'Astronomie.

<sup>5)</sup> Greenwich Photoheliographic Results: Positions and Areas of Sunspots and Faculae. For each Day of the Year . . . . (in brackets the heliographic long. and latit. of the disk centre are given).

where  $d=6600$  km according to D'AZAMBUJA. The resulting  $L$  can be compared with its value obtained from eclipse spectra, as outlined in the beginning.

# 1. Prominences of January 14, 1926 (7<sup>h</sup> 36<sup>m</sup> G.M.T.) Sumatra.

The two prominences in this case are called "the low" and "the high" prominence <sup>6)</sup>. From the published data <sup>7)</sup> we derive the latitudes, and from the "Cartes Synoptiques" the longitudes.

Low prom. (east limb)	pos. angle 57°	$\varphi \approx +30^\circ$	$\mathcal{L} \approx 80^\circ$
high (west limb)	250°	$\varphi \approx -17^\circ$	$\mathcal{L} \approx 260^\circ$

The corresponding Rotation No. 967 in the "Cartes Synoptiques" gives filaments at about the same latitudes but at somewhat different longitudes. Since the prominence may be a little in front or behind the limb, we assume these to be our prominences (Figure 1a, 1b).

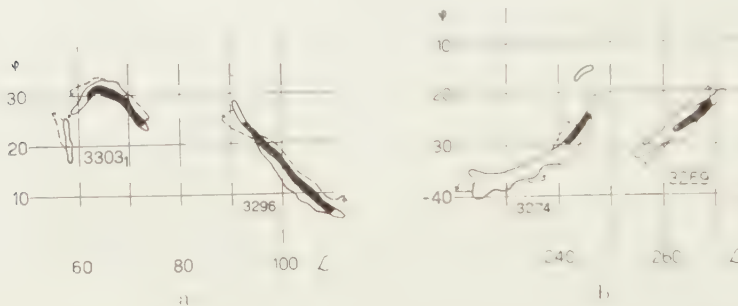


Fig. 1a, 1b. Rotation No. 967 from the "Cartes Synoptiques", January 1926. Filament No. 3303<sub>1</sub> (Low prom.) and No. 3269 (High prom.). The east limb is at about  $\mathcal{L} = 80^\circ$ , the west limb about  $\mathcal{L} = 260^\circ$ . Adjoining filaments No. 3296 and No. 3274 are also shown. For eclipse photograph see Mem. R.A.S. 64, part 4 (1927) The pictures are derived from superposition of the successive images of the same filament at several days of observation. The part that during more than 2/3 of this time was visible is blackened. Small arrows indicate local deformations

The data are the following.

Low prominence: filament No. 3303<sub>1</sub> (during the eclipse 15° behind the eastern limb).

$$\alpha \approx 15^\circ \quad i = 41\frac{1}{2}^\circ \quad \gamma = 20^\circ \quad \text{by formula (1).}$$

Then (2) yields  $L=19,000$  km.

<sup>6)</sup> D. KOELBLOED, Circular No. 5b. Also D. KOELBLOED and W. VELTMAN, Proc. Kon. Ned. Ak. van Wetensch. B 54, 468 (1951). Circular No. 3.

<sup>7)</sup> C. R. DAVIDSON and F. J. M. STRATTON, Mem. R.A.S. 64, part IV, 110, 143 and plate 6 (1927); DAVIDSON, MINNAERT, ORNSTEIN and STRATTON, M.N. 88, 536 (1928).

High prominence: filament No. 3269 ( $10^\circ$  behind the western limb).

$$\alpha \approx 40^\circ \quad i = 4\frac{1}{2}^\circ \quad \gamma = 35^\circ$$

$$L = 11,500 \text{ km.}$$

2. Prominence of June 29, 1927 ( $5^h 46^m$ ) Lapland <sup>8)</sup> <sup>9)</sup>.

On the corona plate of the Greenwich eclipse expedition <sup>10)</sup> the sun's axis is indicated. We get for our prominence  $\varphi \approx +48^\circ$  to  $57^\circ$ , (western limb).

The central meridian is at  $\mathcal{L} = 0^\circ$ , so that the western limb is at  $\mathcal{L} = 90^\circ$ .

Rotation No. 986 of the "Cartes Synoptiques" shows a filament No. 4149 with average coordinates  $\varphi = +52^\circ$  and  $\mathcal{L} = 92^\circ$ .

This must be our prominence. It runs parallel to the equator (Figure 2).

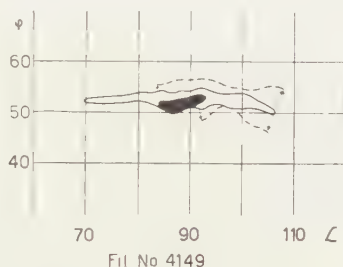


Fig. 2. Rotation No. 986 from the "Cartes Synoptiques". June 1927. Polar filament No. 4149. West limb at about  $\mathcal{L} = 90^\circ$ . For eclipse photograph see M.N. 87, 656 plate 8 (1927)

So during the eclipse we are looking through the filament in its length direction.

There is an uncertainty with regard to the evolution of this particular filament. In the "Cartes Synoptiques" filament No. 4149 is indicated as the 5th and last reappearance of a filament (No. 955) which on March 9 was seen for the first time. D'AZAMBUJA <sup>11)</sup>, however, gives a corrected evolution in which No. 4149 is the 3rd appearance of a filament that is seen during 6 rotations of the sun. In general the re-identification of polar filaments is difficult. During the successive rotations their length, their visibility and the importance of their parts vary highly, much more than those of the equatorial filaments <sup>12)</sup>.

So in our case we can only give a rough value for the thickness in the line of sight:

$$L \approx \text{order of } 100,000 \text{ km.}$$

<sup>8)</sup> A. PANNEKOEK and N. W. DOORN, Verh. Kon. Akad. v. Wetensch., Amsterdam 14, No. 2 (1930).

<sup>9)</sup> S. G. M. HAUG, Circular No. 5a.

<sup>10)</sup> M.N. 87, 656, plate 8 (1927).

<sup>11)</sup> D'AZAMBUJA, p. 274.

<sup>12)</sup> Ibid., p. 101.

### 3. Prominence of February 25, 1952 (11<sup>h</sup> 12<sup>m</sup>), Khartoum <sup>13</sup>).

The value of the position angle was 250° and the value of 270° given in Circular No. 6 should be changed into this.

So it was a prominence on the equator at the western side.

Miss HELEN W. DODSON of the Mc Math Hulbert Observatory of the University of Michigan was so kind to send us two copies of  $H_{\alpha}$  spectroheliograms of February 15 and 19, and a diagram with heliographic coordinates for the latter date (Figure 3). This shows a filament 12° to



Fig. 3. From a diagram by Miss HELEN W. DODSON for 1952 February 19<sup>d</sup> 15<sup>h</sup> 20<sup>m</sup> UT. Composed filament at the equator at about 15° west of the central meridian CM. Note a sunspot at  $\varphi = -10^\circ$ . For eclipse photograph see WALDMAYER, Z. f. Ap. 32, 124 (1953)

24° west of the central meridian with  $\varphi \approx -2^\circ$  to  $+7^\circ$ . During the eclipse it was at and partly behind the limb. The form of this filament looks somewhat like a reversed letter *u*, reaching the equator in two places.

Afterwards we found data given by MARG. D'AZAMBUJA <sup>14</sup>). There rotation No. 1316 shows a filament with  $\varphi \approx -7^\circ$  to  $+7^\circ$  and  $\mathcal{L} \approx 10^\circ$  to  $25^\circ$ , being at the limb during the eclipse. This agrees with the data of Miss DODSON.

Accordingly we estimate the thickness in the line of sight

$$L \approx 2 \times 8000 = 16,000 \text{ km.}$$

The peculiar shape and the quality of the image do not warrant a more accurate estimate.

Table 1 gives the results of the present study.

Electron temperatures of prominences are uncertain. There are indications that they may go up to 15,000°, and this is the reason why for the Khartoum prominence three values were tried. For the other two prominences definite values of  $T_e$  were adopted, but not much weight should be given to them.

There are several factors of uncertainty in our results, so that after all they only have the character of estimates. For that reason we neglected

<sup>13</sup>) R. O. REDMAN and H. ZANSTRA, Circular No. 6.

<sup>14</sup>) L'Astronomie 66, (Avril), 157 (1952).



TABLE 1

Comparison of the line of sight thickness from emission and from filaments

1		2	3	4	5
January 14, 1926					
Sumatra	high	5,000°	— 27° W	10,000 km	11,500 km
	low	5,000°	+ 30° E	20,000 ±	19,000
June 29, 1927					
Lapland		7,000°	+ 52° W	25,000	order 100,000 (polar)
February 25, 1952					
Khartoum		5,000°		38,000	
		10,000°	0° W	12,000	16,000
		15,000°		5,900	

1. Eclipse.
2. Electron temperature  $T_e$  assumed.
3. Heliographic latitude and side of limb.
4. Line of sight thickness from emission data.
5. The same from filaments.

a correction of some per cent due to the mean inclination of the filaments of  $10^\circ$  to the west <sup>15)</sup>.

In the two Sumatra cases there is an uncertainty in the identification. It is not impossible that there was a second filament that contributed.

Another factor is due to the instability and the possibility of abrupt disappearance that have been observed both in filaments <sup>16)</sup> and in prominences <sup>17)</sup>.

As for the determinations of  $L$  from emission data, the absolute photometry was imperfect. On the Sumatra exposures the timing for the calibration spectra was done by ear and the exposition time was much smaller than for the prominence. For the Lapland prominence some data were used of another prominence. In Khartoum the slit width for the calibration spectra may not have been quite the same as for the prominence.

For the Sumatra prominence the line of sight thicknesses  $L$  of column 4 agree well with those of column 5. The same is the case for the Khartoum prominence if an electron temperature of 9000° should be assumed. As was stated, however, those temperatures are uncertain, and a higher temperature might lead to the  $L$  values of column 4 becoming about one third of those of column 5. For the polar prominence of Lapland little can be concluded, since one could only get a very rough estimate. For the other two the results are in agreement with the hypothesis that the prominence material is homogeneous. So it does not seem possible that the main body has a pronounced filamentary or lumpy structure. Even allowing for a higher electron temperature it does not seem likely that

<sup>15)</sup> D'AZAMBUJA, p. 31.

<sup>16)</sup> Ibid., p. 104–115.

<sup>17)</sup> HORN D'ARTURO, Pubbl. Bologna 1, 224 (1929).

one third of the space within the prominence is filled by filaments or condensations of 3 times the mean density, because that would make  $L$  from emission data (column 4) one third of  $L$  from dark filaments (column 5).

I would like to express my gratitude to Miss HELEN W. DODSON for the data she has sent to me, and I also thank Professor H. ZANSTRA for his stimulating discussions.

#### ERRATUM

R. O. REDMAN and H. ZANSTRA, Proc. Kon. Ned. Ak. van Wetensch. Series B, **55**, 598 (1952).

p. 601, line 16: position angle  $270^\circ$  should read  $250^\circ$ .

p. 602, line 16: "lower portion" should read "upper portion".

BIOLOGICAL PROCESSES IN THE ESTUARINE ENVIRONMENT

VI. THE STATE OF THE IRON IN THE ESTUARINE MUD  
IRON SULPHIDES

BY

L. G. M. BAAS BECKING \*)

(Communicated at the meeting of March 24, 1956)

SUMMARY AND CONCLUSIONS

1. The inorganic iron in the mud is present in the ferrous ferroso-ferric, and ferric form. These compounds are usually insoluble. Ferrous ion will occur only in exceptional cases, when the pH drops below 6.8.

2. It is suggested that the following biogenic iron sulphides may occur in the mud:  $\text{Fe}(\text{OH})(\text{SH})$  (hydrotroilite),  $\text{Fe}(\text{SH})_2$  disulphydryl iron),  $\text{Fe}_3\text{S}_2\text{O}_2$  (sulphomagnetite), and  $\text{FeS}_2$  (pyrite). Marcasite is a product of acid freshwater sediments and is absent in estuarine mud. No evidence was found for the presence of either pyrrhotite ( $\text{Fe}_n\text{S}_{n+1}$ ) or of ferric sulphide,  $\text{Fe}_2\text{S}_3$ . It was assumed that neither  $\text{Fe}_3\text{S}_4$  (ferroso-ferric sulphide) nor amorphous  $\text{FeS}_2$  (melnikovite) occurs in nature. Arguments, partly theoretical, are given to substantiate the above statements.

INTRODUCTION

With aluminium, iron is the most obvious metal in the mud. About the biological importance of the iron and its cyclic changes very little is known. In Soil Science, the process of lateritization, and the accumulation of iron in the mineral horizon of podsoles, have drawn attention to the state of this metal in soils. Gas-works chemists, moreover, have extensively studied the bog-iron ores, utilized for the fixation of  $\text{H}_2\text{S}$ . Apart from the above-mentioned sources the literature is old to very old, and very often conflicting.

On the sulphides an outstanding experimental contribution was made by ALLEN, CRENSHAW and JOHNSTON (1912), while JUZA and BILZ (1932) have given a complete physico-chemical analysis of the system  $\text{FeS}_2$ - $\text{FeS}$ -S. The latter contribution materially clarified the picture of the various possible sulphides.

These sulphides are all to be considered biogenic, in so far as their formation presupposes the presence of sulphuretted hydrogen; chiefly a product of sulphate reduction. Due to the very low solubility of the various iron sulphides under natural conditions, they will be formed by

---

\*) Division of Fisheries and Oceanography C.S.I.R.O., Cronulla N.S.W.

the interaction of  $\text{H}_2\text{S}$  with inorganic iron minerals present in the mud. About the action of this gas on organic iron complexes I could find no information. An old hypothesis, according to which  $\text{SO}_4^{2-}$  may be reduced by "organic matter" has to be abandoned.

The iron minerals will be  $\text{FeCO}_3$  (siderite, and, at lower pH, also the bicarbonate),  $\text{Fe}(\text{OH})_2$ , and  $\text{Fe}_2\text{O}_3$  (haematite and "rubinglimmer"), and  $\text{Fe}-\text{O}-\text{OH}$  (goethite and lepidocrocite) and, possibly, higher hydrates,  $\text{Fe}_3\text{O}_4$  (magnetite), phosphate complexes (no strengite or vivianite were found in the alkaline mud), and, of course, the "lattice bound" iron in various silicate minerals.  $\text{Fe}(\text{OH})_3$  apparently does not occur in nature.

Hydrotroilite. — The direct action of  $\text{H}_2\text{S}$  on the above-mentioned compounds in aqueous suspension, whether ferrous, ferric or ferroso-ferric, yields the same substance which we call will hydrotroilite (Doss 1912).

In Figure 1 the inorganic iron compounds mentioned in this paper are gathered. The system  $\text{Fe}-\text{O}-\text{H}-\text{S}$  would require spatial representation

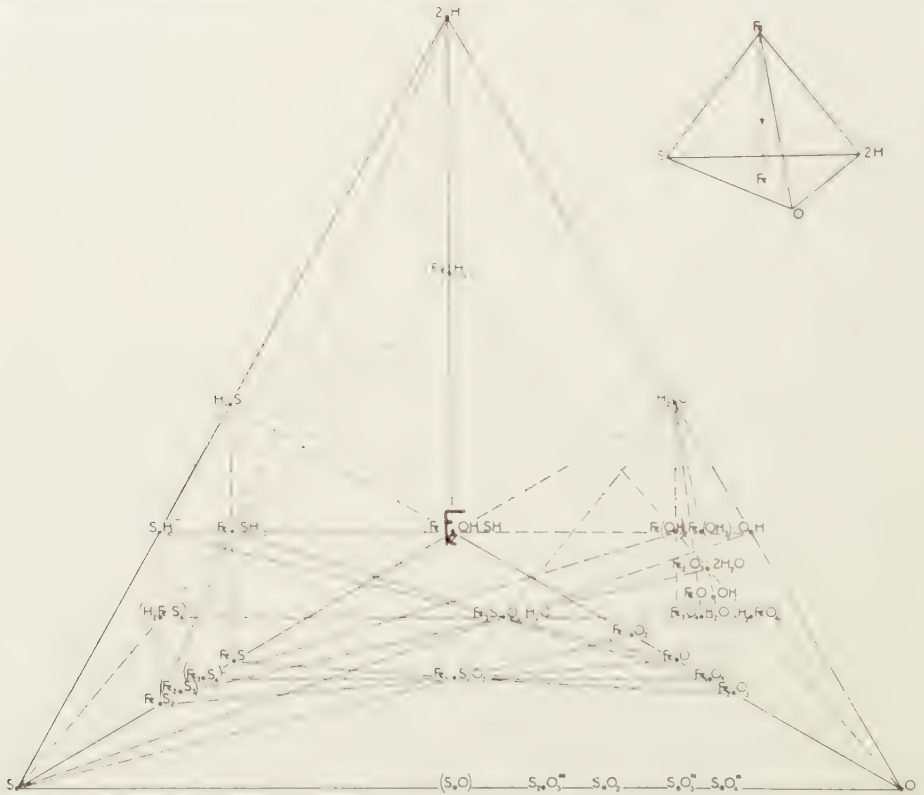


Fig. 1

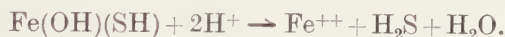
(tetrahedron at upper right in Figure 1). By projecting the Fe corner on the centre of the base plane it becomes possible to represent all possible combinations in one plane (see also BAAS BECKING 1947). The analogy



of the sulphides on one side and of the oxides on the other side is quite apparent. If planes, perpendicular to the paper, are drawn through the point  $\text{H}_2\text{O}$ , a rough idea may be obtained of the free energy of formation of the compounds in this plane, the lowest values (more than  $-100$  K. cal.) being found in the plane  $\text{H}_2\text{O}-\text{Fe}_2\text{O}_3$ , while this value decreases to  $-20$  to  $-30$  K. cal on the line  $\text{H}_2\text{O}-\text{FeS}$  and even becomes positive on the line  $\text{H}_2\text{O}-\text{SH}^-$ . We shall have occasion to revert to this diagram later.

If equivalent amounts of  $\text{H}_2\text{S}$  and of any one of the iron-compounds mentioned are used, a heavy black precipitate is formed, which oxidizes rapidly in air (VERHOOP 1940). This precipitate behaves very much like an  $\text{As}_2\text{S}_3$  sol. If the reaction is slow (as e.g. with metallic iron or with magnetite) a red suspensoid is first formed, the colour changing to dark green while finally a fine black suspension results which will settle with the merest fraction of electrolyte. As JUZA and BILZ (1932) have shown that pyrrhotite is but a mixture of  $\text{FeS}$  and  $\text{S}$  and as, moreover, the troilite of the literature ( $\text{FeS}$ ) is a mineral of different properties, chiefly known from meteorites (ALLEN c. s. 1912). I believe that DOSS (1912) was right to assume the presence of a hydrotroilite, which we should imagine as  $\text{Fe}(\text{OH})(\text{SH})$ . OSTROUMOV (1955) also considers the chief black mineral in the Black Sea to be a hydrated  $\text{FeS}$ .

The compound is highly labile in air, but treatment with absolute alcohol will dehydrate it to  $\text{FeS}$ , which remains unoxidized for an indefinite period in a desiccator. Natural "pyrrhotite" might be  $\text{FeS}$ , at least in part. Free from  $\text{H}_2\text{S}$  it will go into solution at pH 5.8, probably according to:



In air, in unbuffered suspensions, the pH decreases sharply with a concomitant increase of the electrode potential (Fig. 2). In seawater, no such decrease in pH was observed, the electrode potential rising steeply with often little change in pH. As will be seen from the figure, there is no significant difference in the curves for the black substance prepared either from ferrous, ferroso-ferric, or from ferric iron. We will revert to this later in this paper.

If there existed a ferric sulphide in the mud, like the gas technologists claim to have found in the gas-works "ore boxes" (GRIFFITH and MORCOM 1945; WEYMAN 1920), the black substance originating from ferric iron should behave differently to that originating from ferrous hydroxide or from ferrous carbonate. As no such difference was found there is no reason to assume that  $\text{Fe}_2\text{S}_3$  exists in the mud. Moreover, GRIFFITH and MORCOM (1945) give the density of  $\text{Fe}_2\text{S}_3$  as about 3.0, while all other iron sulphides show much higher values, e.g.  $\text{FeS}$  (+S) 4.533–4.769 marcasite 4.887; pyrite 5.027 (ALLEN, C. S. 1912). Even for a mixture of  $2\text{FeS}+\text{S}$  the density will be about 3.6. The existence of  $\text{Fe}_2\text{S}_3$  in nature seems highly problematical.  $\text{Fe}_3\text{S}_4$  (which should have, like magnetite, a spinel-structure)

does not occur in nature. DE JONG and WILLEMS (1927) failed to obtain it experimentally, they always found mixtures of  $\text{FeS}$  and  $\text{FeS}_2$ .

Disulphydryl-iron. It has been known for a long time that "FeS" will be formed, even in acid solutions, if a certain  $\text{H}_2\text{S}$  tension is maintained

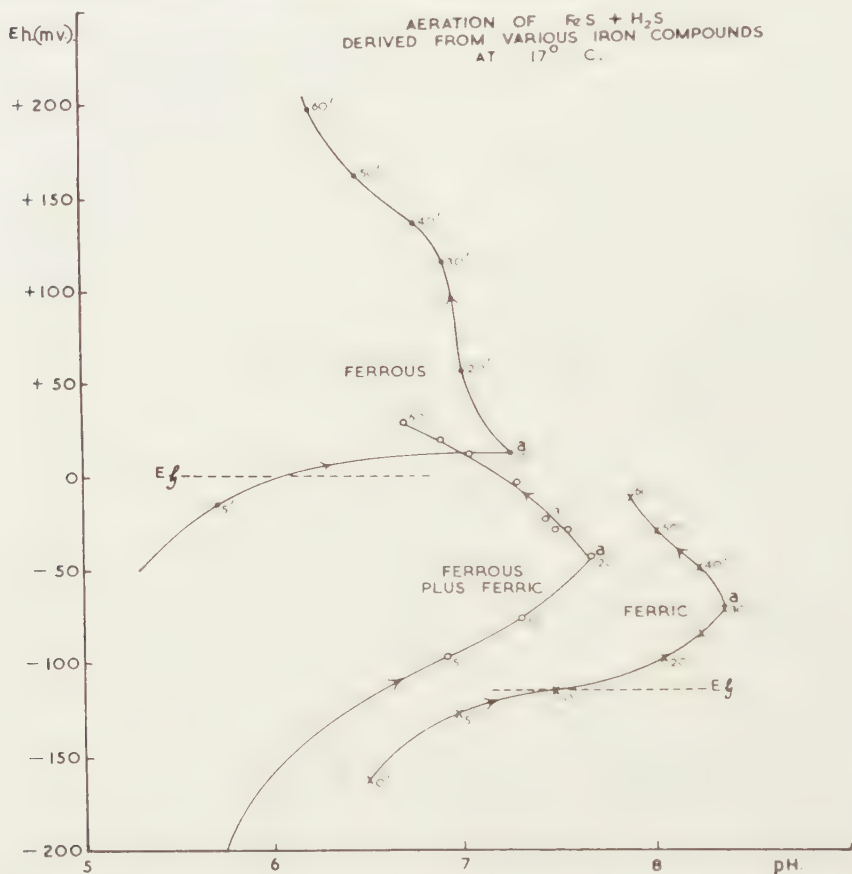


Fig. 2

in the vessel. The hydrotroilite has changed its properties. The labile suspensions of the hydrotroilite may be stabilized by  $\text{H}_2\text{S}$ . Under natural conditions, if the  $\text{H}_2\text{S}$  concentration becomes  $10^{-3}$  n, the hitherto precipitated hydrotroilite becomes peptized, the water will look like ink and by active oxygen absorption may cause a mass death of its inhabitants. This was observed in 1952 at Maianbar, an inlet north of Port Hacking River where a deep pool suddenly showed a black appearance, with a decrease in pH to 6.2. (There was a concomitant increase in soluble phosphate, as could be predicted from the work of BAAS BECKING and MACKAY (1956).

PADOA and CAMBI (1906) have measured the  $\text{H}_2\text{S}$  tension necessary to maintain "FeS" in sulphuric acid. Their results are given in the following table, the values also converted into pH and  $\text{pH}_2\text{S}$ :

$n\text{H}_2\text{SO}_4$	.004	.005	.0067	.01	.02
pH	2.40	2.30	2.13	2.0	1.7
$\text{H}_2\text{S}$ (atm)	.98	2.7	4.0	5.5	9.2
$\text{pH}_2\text{S}$	1.36	.92	.76	.63	.39

Let us assume that there exists an addition-compound  $\text{FeS} + \text{H}_2\text{S}$ , or  $\text{Fe}(\text{SH})_2$ <sup>1)</sup> and that this compound reacts with hydrogen ions as follows:  $-\text{Fe}(\text{SH})_2 + 2\text{H}^+ \rightarrow \text{Fe}^{++} + 2\text{H}_2\text{S}$  we obtain, for  $[\text{Fe}(\text{SH})_2] = [\text{Fe}^{++}]$ ,

$$K = \frac{[\text{H}_2\text{S}]^2}{[\text{H}^+]^2}.$$

When we compare the pK for the reaction with  $\text{FeS}$  and  $\text{Fe}(\text{SH})_2$  respectively, we obtain

pH	2.40	2.30	2.13	2.00	1.70
pK for $\text{FeS}$	3.46	2.68	2.50	2.38	3.01
pK for $\text{Fe}(\text{SH})_2$	2.08	2.86	2.84	2.76	2.74

Apparently  $\text{Fe}(\text{SH})_2$  yields the more constant values.

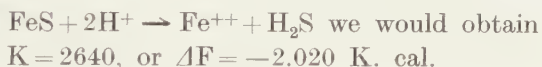
Apart from the values at pH 2.4 this yields, within limits of error,  $K = 575$  or  $\Delta F$  (free energy at  $298^\circ$  absolute)  $= -1.630$  K. cal.

K. cal. $\Delta F$ for $\text{Fe}^{++}$	$= -20.24$ (LATIMER 1952),
for $2\text{H}_2\text{S}$	$= -13.08$
for reaction	$= -1.63$

$-34.95$  K. cal. This would represent the free

energy of formation of the compound  $\text{Fe}(\text{SH})_2$ .

For the reaction



However, from data by LATIMER (1952) we may calculate the free energy of this reaction as  $+23.32 - 20.24 - 6.54 = -3.460$  K. cal. which is too high. There is good evidence to assume that the first reaction represents reality. At pH 5.8 we would have, for  $\text{Fe}(\text{SH})_2$ ,  $\text{pH}_2\text{S} = 4.47$ , and for  $\text{FeS}$ ,  $\text{pH}_2\text{S} = 4.09$ , both plausible values, but with a bias to the lower  $\text{H}_2\text{S}$  concentration: ( $[\text{H}_2\text{S}] = 3.4 \times 10^{-5}$  as against  $6.5 \times 10^{-5}$ ). At pH 4.2 (peat bog, and limit of sulphate reduction) the values would be  $[\text{H}_2\text{S}] = 1.5 \times 10^{-3}$  and  $3.5 \times 10^{-3}$  respectively.

Another argument for the existence of the disulphydryl compound is the formation of coloured sulphides, the sulphoferroates, in the alkaline range;  $\text{Fe}(\text{S Me})_2$  as probably observed by KONSCHIEGG and Malfatti (1906), BECKER (1887), and TERREIL (1870).

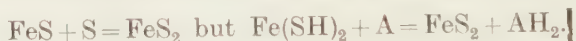
Referring again to Figure 2, which illustrates the changes in pH and Eh during aeration of unbuffered  $\text{FeS}$  suspensions, it may be seen that the oxidation proceeds in three distinct phases (1) a sharp rise in Eh due to

<sup>1)</sup> MIDDLETON and WARD (1935) have shown that when nickel and cobalt sulphides are formed with the exclusion of air, there is evidence to assume the presence of  $\text{Ni}(\text{SH})_2$  and  $\text{Co}(\text{SH})_3$ .

the removal of  $\text{H}_2\text{S}$  from the suspension; (2) a "plateau", pH increasing at a fairly constant Eh. During this period the suspension remains black, and continues to smell of  $\text{H}_2\text{S}$ . It is possible that here the reaction  $\text{Fe}(\text{SH})_2 + \text{H}_2\text{O} \rightarrow \text{Fe}(\text{OH})(\text{SH}) + \text{H}_2\text{S}$  takes place; (3) a sudden change occurs, the solution turns brown and becomes increasingly more acid. As stated above, it is assumed that here the highly labile hydrotroilite, unprotected now by  $\text{H}_2\text{S}$ , starts to oxidize. VERHOOP (1940), VEIL (1928), WEYMAN (1920), SABBATINI (1923), have claimed that oxidation of "FeS" yields ferric (hydr) oxide and sulphur. There are many claims in the literature (also gathered by VERHOOP) that, especially at higher temperatures, sulphate<sup>1)</sup>, magnetite, and hydrogen are formed. From Figure 2 it appears that a similar reaction may take place at room temperature in freshwater suspensions, while this reaction is masked in sea-water.

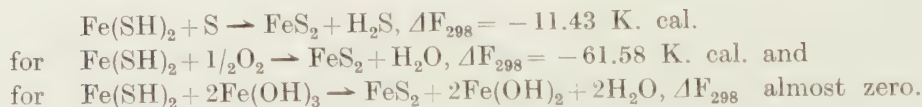
We hope to revert to this matter in a later publication.

Pyrite. — Another argument for the existence of  $\text{Fe}(\text{SH})_2$  may be derived from the various ways pyrite is formed. ALLEN C. S. (1912) and also VERHOOP (1940) have prepared  $\text{FeS}_2$  from FeS plus sulphur, the latter author at room temperature under sterile conditions. This reaction one finds cited throughout the literature. However, GAUTIER (1893) has called attention to the fact that not only in the presence of sulphur, but also in the presence of oxygen this reaction can take place. VON WOLZOGEN KÜHR (1938) observed the formation of pyrite from FeS and ferric hydroxide. In these two cases, there was simply another hydrogen acceptor. Oxygen, sulphur, ferric hydroxide, and organic matter (VAN BEMMELEN 1863) all may act as such. The reaction, therefore, should not read



If the sulphide were present as FeS, no such reaction could take place. The hypothesis of VON DEINES (1933) that pyrite should be formed by an introduction of FeS and  $\text{H}_2\text{S}$  seems unlikely. In Figure 1 the dehydrogenation of  $\text{Fe}(\text{SH})_2$  to  $\text{FeS}_2$  is shown graphically. We hope in the future to obtain additional evidence for the dehydrogenation by using radioactive  $\text{S}^{31}$ , in  $\text{Fe}(\text{S}^{32}\text{H})_2 + \text{S}^{31} = \text{FeS}_2^{32} + \text{H}_2\text{S}^{31}$ .

For the reaction



The evidence for the existence of  $\text{Fe}(\text{SH})_2$  is, therefore, (1) The difference in behaviour of "FeS" in aqueous suspension with and without  $\text{H}_2\text{S}$ : (2) The observations of PADOA and CAMBI (1906) and their physico-chemical consequences: (3) the existence of sulphoferroates: (4) The

<sup>1)</sup> The literature often mentions "sulphuric acid". This would require a pH lower than zero and is, therefore, unlikely.



formation of pyrite by dehydrogenation. (5) The characteristics of the Eh/pH relation on oxidation.

Pyrite is met with in older muds. As already observed by VAN BEMMELEN (1887) whole diatoms, but also spores, cysts, and bluegreen algae may become "pyritized". Pyritized organisms often adhere to quartzite particles. In confirmation of the findings of ALLEN C.S. (1912) in the neutral to alkaline estuarine environment, no marcasite was found. Melnikovite, the amorphous  $\text{FeS}_2$ , assumed by DOSS (1912) has to be considered as microcrystalline pyrite (VAN DER VLERK, in litteris).

Sulphomagnetite. — In order to prepare  $\text{FeS}$  at neutral conditions  $0.84 \text{ n Na}_2\text{S} \cdot 9\text{H}_2\text{O}$  (10 %) was neutralized with  $\text{HCl}$  of equivalent strength. The preparation smelled strongly of  $\text{H}_2\text{S}$  and contained much suspended sulphur. When adding  $1_{10} \text{ vol}/0.1 \text{ n Fe(OH)}_2$  (freshly prepared from  $\text{FeSO}_4$  and  $\text{NaOH}$  and probably containing some  $\text{Fe}^{+++}$ ) an ultramarine-blue precipitate was obtained. The same substance was also obtained when 30 %  $\text{Na}_2\text{S}$  was neutralized by concentrated  $\text{HCl}$  and a few drops of  $\text{FeCl}_3$  were added. The reaction is tricky, and difficult to reproduce. The pH has to be kept in a narrow range, about 6.0. The compound proved to be resistant to high concentrations of acid and alkali, it yielded to three subsequent treatments with potassium perchlorate in sulphuric acid. However, it is readily soluble in 10 per cent.  $\text{KCN}$  with subsequent formation of a brown, acid soluble, precipitate. It is interesting to note that the compound is a pH indicator, with the following characteristics: —

pH 11.0 colourless	pH 8.2 violet-blue
,, 10.0 orange-yellow	,, 7.0 blue
,, 9.4 violet	,, 2.0 blue
,, 8.7 blue-violet	,, 0.0 colourless again.

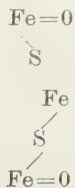
It is highly magnetic, and may be, therefore, related to magnetite. This seems plausible as both  $\text{Fe}^{++}$  and  $\text{Fe}^{+++}$  seem to take part in its formation. A preparation was freed from sulphur and submitted for analysis to the Microanalytical Service, C.S.I.R.O.

It showed 13.91 S, 51.78 % ash (iron oxide) and 12.84 % loss in weight on drying. Assuming the magnetic ash to have been  $\text{Fe}_3\text{O}_4$  we have, for



found 3.00 1.99 3.27

calculated 3.00 2.00 3.00. It may therefore be a sulphomagnetite;



The hydration will yield the free OH groups necessary to account for its indicator qualities. We met this compound before, by chance, while

studying the  $\text{Na}_2\text{S}-\text{FeSO}_4$  system. It adhered so closely to a Büchner funnel and it proved so resistant that we had to discard part of the apparatus.

The compound occurs in nature. After several unsuccessful attempts (mud from Lake Eyre, Gunnamatta Bay, New South Wales, Swan Bay, Port Stephens, New South Wales) Mr. J. MACINTYRE, C.S.I.R.O., submitted a bluish mud from Lake Macquarie (New South Wales) (Chain Valley Bay). This mud had a high organic content, and a high degree of pyritization (blue green algae, diatoms). The shells in the sample (*Maetra* sp.) had recently died. After boiling with 1 n HCl, 1 n NaOH and washing, the sample showed a large number of small (1.5–10  $\mu$ ) intensely blue particles (—200 in one drop). The association with pyrite was unmistakable. The inside of the *Maetra* shell contained many blue particles. A dead *Talina*, from Cockle Creek, Lake Macquarie, showed a blue lining on the margin of the shell. This could not have been vivianite, as both solubility and colour are different. In a similar situation (dying and dead shells) the blue compound appeared in mud from Lake Mallacoota (Vic.). The conditions under which the substance is formed in the laboratory (high  $\text{H}_2\text{S}$ -tension and a low concentration of ferro-ferri iron) were apparently met with here. The reason that this compound has escaped attention so far is that it remains hidden under black sulphide and that only after acid treatment the blue particles become visible. Figure 1 shows the position of the compound (if our surmises are correct) amongst the inorganic iron minerals. It remains puzzling why the substance should disappear at all after it is once formed. Its reaction with complex iron may yield an explanation. Whatever its composition may be, a blue sulphur containing iron compound occurs in the estuarine mud.

#### LITERATURE

- ALLEN, E. T., J. L. CRENSHAW, J. JOHNSTON and E. S. LARSEN, Die mineralischen Eisensulfide. Ztschr. f. Anorg. Chem. **7.6**, 201 (1912).
- BAAS BECKING, L. G. M., On the graphical representation of chemical processes. Proc. Kon. Ned. Akad. v. Wet. Amsterdam, **50**, 1003 (1947).
- and MARGARET MACKAY, Biological processes in the estuarine environment. V. The role of *Enteromorpha*. Proc. Kon. Ned. Akad. v. Wet. Amsterdam, **59**, 109 (1956).
- BECKER, G. F., Natural solutions of cinnabar, gold, and associated sulphides. Am. Journ. Sc. **33**, 199 (1887).
- BEMMELEN, J. M. VAN, Bouwstoffen tot de kennis van de Kleigronden der Provincie Groningen. G. T. Mulder's Scheikundige Verhandelingen **3**, 1 (1863).
- , Bijdragen tot de kennis van den alluvialen bodem in Nederland **3**. Samenstelling en vorming van zure gronden. Verhandelingen Kon. Ned. Akad. v. Wet. Amsterdam, **25**, 33 (1887).
- DEINES, O. VON, Der Stoffwechsel der Schwefelbakterien Naturwiss. **21**, 873 (1933).
- DOSS, B., Ueber die Natur u. Zusammensetzung des in Miocänen Tonen des Gouvernements Samara auftretenden Schwefeleisens. Neues Jahrb. Mineral. Geol. u. Palaeont. **33**, 662 (1912).

- GAUTIER, A., Formation des phosphates naturels d'alumine et de fer. C. R. **116**, 1491 (1893).
- GRIFFITH, R. H. and A. R. MORCOM, The interconversion of iron oxides and sulphides. J. Chem. Soc. **54**, 786 (1945).
- JUZA, R. and W. BILZ, Das Zustandsdiagramm Pyrit, Magnetkies, Troilit u. Schwefeldampf, beurteilt nach Schwefeldampfdrucken, Röntgenbilder, Dichten u. Magnetische Messungen. Ztschr. f. Anorg. u. Allg. Chem. **205**, 273 (1932).
- JONG, W. F. DE and H. M. V. WILLEMS, Die Verbindungen  $\text{Fe}_3\text{S}_4$ ,  $\text{CO}_3\text{S}_4$ ,  $\text{NO}_3\text{S}_4$ . Ztschr. f. Anorg. u. allg. Chem. **161**, 311 (1927).
- KONSCHIEGG, A., und H. Malfatti, Ueber das lösliche Eisensulfid. Ztsch. f. Analyt. Chem. **45**, 747 (1906).
- LATIMER, M. W., Oxidation Potentials (N.Y. Prentice-Hall, 1952).
- MIDDLETON, A. W. and A. M. WARD, The composition and properties of precipitated nickel and cobalt sulphides. Pt. I. Journ. Chem. Soc. London, **2**, 1459 (1935).
- OSTROUMOV, E. A., In Chem. Abstr. **49**, 4346 (1953).
- PADOA, M., and L. CAMBI, Atti. Accad. Lincei (5), **15**, 796 (1906).
- SABBATINI, L., Ricerche farmacologiche sul ferro. I. Sulfuro ferroso colloidale preparato in presenza di gelatina. Att. Accad. Lincei V. (R.C.) **32**, 326 (1923).
- TERREIL, M. A., Réch. Génér. sur les modifications que les minéraux éprouvent par l'action des dissolutions salines (Suite). Bull. Soc. Chim. de Paris N.S. **13**, 113 (1870).
- VEIL, S., Sur l'hydroxyde ferrique jaune, résultat de l'oxydation ménagée du sulfure ferreux en suspension. C.R. **186**, 753 (1928).
- VERHOOP, A., Bijdrage tot de Kennis van de Yzersulfiden in den Bodem. Ph. D. Thesis, Leyden (1940).
- WEYMAN, G., Examination of mixtures of ferrous and ferric sulphides and free sulphur. Gas Journal **149**, 301 (1920).
- WOLZOGEN KÜHR, C. A. VON, De eenheid van het anaerobe en aerobe ijzer corrosieproces in den grond. Water **22**, 33 and 45 (1938).

# EFFECT OF ELECTROLYTE MIXTURES ON THE CRITICAL MICELLE CONCENTRATION IN SOLUTIONS OF DODECYL-1 SULPHATE

BY

W. DORST, W. PRINS AND J. J. HERMANS

(Communicated at the meeting of January 28, 1956)

Experiments show that the critical micelle concentration (CMC) of sodium dodecyl sulphate as measured by the fluorescent dye method is depressed by mixtures of KCl and NaCl in exactly the same way as by NaCl alone. The KCl concentration, however, must be kept small to avoid salting out.

A specific ionic effect of Li as compared to Na could be observed. When the total salt content is kept constant, the CMC of the soap is independent of the Na/Li ratio up to about 60 % Li and then begins to drop fairly rapidly to a considerably lower value.

## 1. Introduction

It is well-known that the critical micelle concentration (CMC) of ionic detergents is lowered on the addition of salts. The equation generally used to describe this phenomenon is

$$(1) \quad \ln c_0 = L - (1 - \alpha) \ln (c_0 + x),$$

where  $c_0$  is the CMC,  $x$  the concentration of extraneous salt, while  $L$  and  $\alpha$  are constants. The soap and the salt are supposed to be uni-univalent electrolytes, and the counter ion of the detergent is identical with one of the ions of the added salt.

Two types of derivation have been given for Eq. 1. The first is based on very simple thermodynamic considerations and was developed by CORRIN [1]. His treatment leads to the result that  $\alpha$  must be considered as the effective degree of dissociation of the micelles. PHILLIPS' discussion [2] starts from similar principles as does CORRIN's and, although his reasoning is not quite the same as CORRIN's, the final result is again Eq. 1.

A different argument has been developed by HOBBS [3], who estimates the electrical free energy of a micelle, taking into account the effect of the electric double layer. From this free energy it is possible to predict the associative equilibrium. To arrive at Eq. 1 HOBBS remarks that those small ions whose charge is opposite to that of the micelle play the predominant role in lowering the CMC. This was used also by CASSIE and PALMER [4]. Furthermore, HOBBS accounts for screening effects by



assuming that only a fraction  $\alpha$  of the micelle charge is effective in determining the electrical energy. The final result is

$$(2) \quad \ln c_0 = L - \alpha \ln (c_0 + x).$$

We are thus faced with the curious situation that two different approaches, both of which make use of quite reasonable assumptions, lead to equations of the same form and are in conformity with experimental results, while the factor  $1 - \alpha$  in Eq. 1 is replaced by  $\alpha$  in Eq. 2. There is one experimental aspect which appears to support Eq. 2 rather than Eq. 1, namely the fact that the slope of  $\ln c_0$  versus  $\ln (c_0 + x)$  increases with decreasing number of carbon atoms in the soap molecule [5]. It is reasonable to expect that the effective degree of dissociation of the micelles will become larger and not smaller when the chain length of the soap molecule decreases.

The effect of kations on the CMC of anionic soaps is more or less specific. GODDARD, HARVA and JONES [6], for example, have found that the CMC of sodium lauryl-sulfate on addition of cations decreases in the order Li, Na, K, Cs. It is therefore of some interest to study the effect of mixtures of counter ions and to follow the course of the CMC with changes in the composition of the salt mixture.

## 2. Experiments

The measurements were made with sodium dodecyl sulfate in the presence of KCl, NaCl and LiCl, using the titration method of CORRIN and HARKINS [7]. To a weighed sample of the detergent in an Erlenmeyer flask, a salt solution containing  $5 \cdot 10^{-5}$  N Rhodamine 6G was added from a burette. Care was taken that the soap dissolved completely before the last few ml of the solution were added. The sudden decrease of the fluorescence of the dye stuff was taken as an indication of the CMC. This could be observed, after some practice, with a reproducibility of 2 % by looking vertically downward through the solution, while holding the Erlenmeyer flask at an angle of  $45^\circ$  to the horizontal. A dark background about 1 meter below the flask was indispensable. Only in this way could the change of greenish fluorescence to a brown-green, more or less translucent colour, be observed reproducibly, even when the end-point of the titration was judged by different persons. All titrations were made at room temperature, at least in triplicate.

The titration method has been questioned as to its reliability for CMC determinations [8, 9]. Although this criticism may be justified with respect to the absolute CMC values, in our case we were interested only in relative values, which could quite well be determined in this way.

Analytical grade salts were used. The soap was prepared from the  $C_{12}$  alcohol according to the procedure of DREGER *et al.* [10], with some slight modifications. While stirring, 0.17 mole dodecylalcohol was added

slowly to a solution of 10 g freshly distilled chlorosulfonic acid (b.p. 148–150°) in 33 g glacial acetic acid, keeping the temperature at 4° C. The reaction produces hydrochloric acid fumes. The mixture was kept at 4° for half an hour after the addition of the alcohol, stirring vigorously all the time; thereupon it was poured on 100 g ice in a two-liter beaker. After the addition of 150 ml n-butanol, neutralization was effected by adding 2N  $\text{Na}_2\text{CO}_3$  solution, while at the same time the water layer was kept saturated with  $\text{NaHCO}_3$ . By means of this the sodium alkyl sulfate was forced into the butanol layer, where it probably formed oleophobic hydromicelles (compare references [11] and [12]). After separation of the layers, the aqueous phase was extracted four times with 150 ml n-butanol. The butanol extracts were distilled until a boiling temperature of 105° C was reached; at this point the salts become insoluble since the water content of the butanol becomes very small. After cooling down to 80° C, the butanol extract was decanted into a beaker. Most of the insoluble inorganic salt adhered to the wall of the distillation vessel. When cooled to room temperature, the soap precipitated; after filtration through a Büchner filter it was washed with water-free butanol. The product was recrystallized from pure butanol and extracted with ether for at least a week in a soxhlet extractor to remove residual alcohol.

TABLE I  
CMC of dodecyl sulfate in mixtures of KCl and NaCl

NaCl mole/l	KCl mole/l	CMC mole/l	$\frac{\text{NaCl} + \text{CMC}}{\text{KCl}}$
0	0	0.0071 <sup>5</sup>	—
0	0	0.0076*	—
0.0061	0	0.0057	—
0.0109	0	0.0050	—
0.0183	0	0.0041	—
0.0321	0	0.0034	—
0.0559	0	0.0030	—
0.0092 <sup>5</sup>	0.0031	0.0051	4.62
0.0113	0.0049	0.0048	4.32
0.0238	0.0024	0.0038	11.4
0.0206	0.0077 <sup>5</sup>	0.0036	3.12
0.0444	0.0032	0.0033	14.8
0.0494	0.0048	0.0029	10.9

\*) Determined conductometrically.

Table I gives the CMC values found in water, in NaCl solutions and in mixtures of KCl and NaCl. The value for water was determined also conductometrically (second row in table I). The logarithm of CMC ( $=c_0$ ) is plotted versus  $\log(b_1 + b_2)$  in fig. 1. Here  $b_1 + b_2$  is the sum  $c_0 + x + y$ , where  $x$  and  $y$  are the concentrations of NaCl and KCl. The straight line

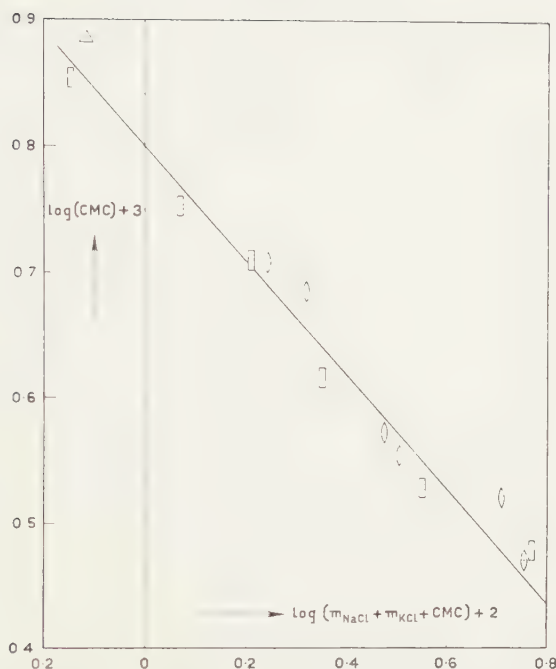


Fig. 1. CMC of dodecyl-1 sulfate as a function of total counter ion concentration, with varying  $\text{Na}^+/\text{K}^+$  ratio. Rectangles: with NaCl only. Triangle: conductometrically determined.

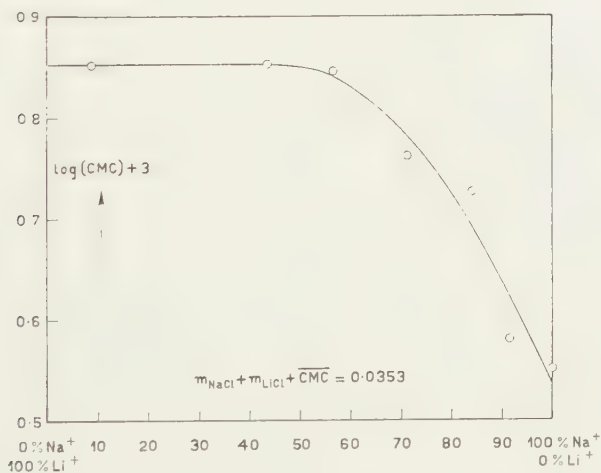


Fig. 2. CMC of dodecyl-1 sulfate in moles/l at constant total counter ion concentration but varying  $\text{Na}^+/\text{Li}^+$  ratio.

indicates that the mixture of electrolytes depresses the CMC in much the same way as NaCl alone, which means that in the concentration range examined the specificity of  $\text{K}^+$  as compared with  $\text{Na}^+$  does not make itself felt. It must of course be borne in mind in this connection that the experimental technique used cannot claim very high accuracy. The slope

of the line in fig. 1 is 0.46, which would mean an effective degree of dissociation of 0.54 according to Eq. 1, but of 0.46 according to Eq. 2.

Since the soap is salted out when the KCl concentration becomes appreciable, a series of measurements at constant counter ion concentration was carried out in a mixture of NaCl and LiCl. The total salt content was 0.030 N; at this rather high value the CMC is small, varying from 0.0035 to 0.0071 N. This means that the total counter ion concentration at the CMC was  $0.035 \pm 0.002$  N, which may be considered as practically constant.

The results are shown in fig. 2, which indicates a pronounced specific ion effect of  $\text{Na}^+$  as compared with  $\text{Li}^+$ . It appears, however, that the role of the Na-ions predominates as long as the lithium-concentration is not too large relative to that of sodium.

*Laboratorium voor Anorganische en Fysische Chemie  
Rijks Universiteit, Leiden*

#### REFERENCES

1. CORRIN, M. L., J. Colloid Sci. **3**, 333 (1948).
2. PHILLIPS, J. N., Trans. Faraday Soc. **51**, 561 (1955).
3. HOBBS, M. E., J. Phys. Coll. Chem. **55**, 675 (1951).
4. CASSIE, A. B. D. and R. R. PALMER, Trans. Faraday Soc. **37**, 156 (1941).
5. TRAP, H. J. L. and J. J. HERMANS, Proc. Kon. Ned. Akad. v. Wetensch. Amsterdam **B 58**, 97 (1955).
6. GODDARD, E. D., O. HARVA and T. G. JONES, Trans. Faraday Soc. **49**, 980 (1953).
7. CORRIN, M. L. and W. D. HARKINS, J. Amer. Chem. Soc. **69**, 683 (1947).
8. KLEVEN, H. B., J. Phys. Chem. **52**, 130 (1948).
9. MUKERJEE, P. and K. J. MYSELS, J. Amer. Chem. Soc. **77**, 2937 (1953).
10. DREGER, E. E., G. I. KEIM, G. D. MILES, L. SHEDLOWSKI and J. ROSS, Ind. Eng. Chem. **36**, 610 (1944).
11. SCHULMAN, J. H. and J. A. FRIEND, J. Colloid Sci. **4**, 497 (1949).
12. WINSOR, P. A., Solvent properties of amphiphilic compounds (Butterworth, London, 1954).



## THERMAL DIFFUSE SCATTERING BY LEAD SINGLE CRYSTALS

BY

W. G. BURGERS, Miss C. L. D. KOOY AND T. J. TIEDEMA <sup>1)</sup>

(Communicated at the meeting of February 25, 1956)

1. *Introduction*

The dependence of the intensity of the thermal diffuse scattering on temperature for long thermal wavelengths is according to a formula given by BORN (1943)

$$(1) \quad I_D \approx T e^{-2M} = T e^{-T/T_h}$$

with

$$(2) \quad T_h = \frac{mka^2\theta^2}{3h^2\Sigma H^2}.$$

In these formulae  $2M$  = Debye temperature factor (see e.g. JAMES (1948) p. 23, 257),  $T$  = absolute temperature,  $\theta$  = Debye characteristic temperature,  $k$  = Boltzmann's constant,  $a$  = lattice constant,  $h$  = Planck's constant,  $\Sigma H^2$  = the sum of the squares of the Miller-indices of the plane from which the diffuse reflexion originates. Formula (1) holds for temperatures well above  $\theta$ . It predicts that  $I_D$  will increase with temperature for  $T < T_h$  and decrease for  $T > T_h$ . As for most materials  $\theta$  is so high that values of  $T_h$ , calculated with (2), lie above the melting-point of the crystal even for high-order reflections [ $\Sigma H^2$  = large], an increase of  $I_D$  with temperature is usually observed. An "unusual" behaviour, however, may be expected for materials for which  $\theta$  is sufficiently low, so that for observable high-order reflections  $T_h$  obtains a value below the melting-point of the material. In the neighbourhood of such reflections  $I_D$  must decrease with temperature in the region  $T > T_h$ . When considering this conclusion it must, however, be put forward that in deriving (1) the assumption is introduced that  $2M < 1$  (so that  $e^{-2M}$  can be replaced by  $1-2M$ ). Application of Born's formula at temperatures above  $T_h$  must, therefore, be considered as tentative.

It was recently shown by CARTZ (1955), following a prediction by LONSDALE (1948), that lead, with a characteristic temperature of circa 80° K and a melting-point of 327° C, shows actually a behaviour predicted by Born's formula. Table 1 gives for this metal the values calculated for  $T_h$  with (1), taking  $\theta = 88^\circ$  K (SMITHELLS, 1955). CARTZ measured  $I_D$  in the range 100 to 600° K for various values of  $\Sigma H^2$  and found a maximum

<sup>1)</sup> Associate worker of the Dutch Foundation for Fundamental Research.

in the diffuse intensity for reflections with  $\Sigma H^2 = 19, 20, 24$  and  $32$ . From her results it can be concluded that Born's formula gives a fairly good approximation of the inversion temperature  $T_h$ .

TABLE I

$hkl$	$\Sigma H^2$	$T_h$ in $^{\circ}\text{K}$	$T_h$ in $^{\circ}\text{C}$	$\frac{T e^{-T/T_h} \text{ at } 573^{\circ}\text{K}}{T e^{-T/T_h} \text{ at } 293^{\circ}\text{K}}$
111	3	2276	2003	1.72
200	4	1707	1434	1.67
220	8	853	580	1.41
311	11	621	348	1.25
222	12	569	296	1.19
400	16	427	154	1.02
331	19	359	86	0.90
420	20	341	68	0.86
422	24	285	12	0.73
511 }	27	253	-20	0.65
333 }				
440	32	213	-60	0.53

In Cartz' work lead single crystals were used in the shape of wires sealed into very thin soda-glass tubes. Monochromatic  $\text{Cu-K}\alpha$  radiation was applied; the scattered X-rays were detected both photographically and by Geiger-counter methods. In the present investigation <sup>1)</sup> we applied a quite different technique using plate-shaped lead single crystals with pre-chosen orientation, from which Laue transmission photographs were taken at two different temperatures, viz.  $20^{\circ}\text{C}$  (room-temperature) and  $300^{\circ}\text{C}$ . In the last column of table I the ratio is given of the diffuse intensities at these two temperatures,  $573^{\circ}\text{K}$  and  $293^{\circ}\text{K}$  respectively, for the values of  $\Sigma H^2$  given in column 2. The table shows that for these two temperatures only diffuse spots corresponding to  $\Sigma H^2 < 16$  must show an increase in the high-temperature photograph, but a decrease for all spots with  $\Sigma H^2 > 19$ . As due to the short wavelengths used (see section 2), Laue photographs could easily be taken showing a large number of diffuse spots with  $\Sigma H^2$  up to at least 59, we thought it worth while to apply this method to test the applicability of Born's formula in the range  $T > T_h$ . Although our work does not reveal new particulars, it gives a directly "visible" illustration of the effect already predicted by LONSDALE.

## 2. Experimental part

The single crystals with pre-determined orientation used for this investigation were prepared after the method described by TIEDEMA and KOOR (1953). As lead is a strong absorber for X-rays, an extra difficulty

<sup>1)</sup> The experimental part of our work was finished when we became aware of Cartz' investigation.

encountered was the necessity to prepare crystals not thicker than about 0.3 mm. For this reason specimens were used of the shape and the dimensions as given in figures 1a and b. It can be seen that the specimen consists of a thicker part (1.7 mm) and a thin part (0.5 mm). When introduced into the furnace the specimen is supported by a sledge with a "step" (c.f. figure 1c). On melting, the step prevents the flow of molten material to the thinner part, which consequently retains its original thickness.

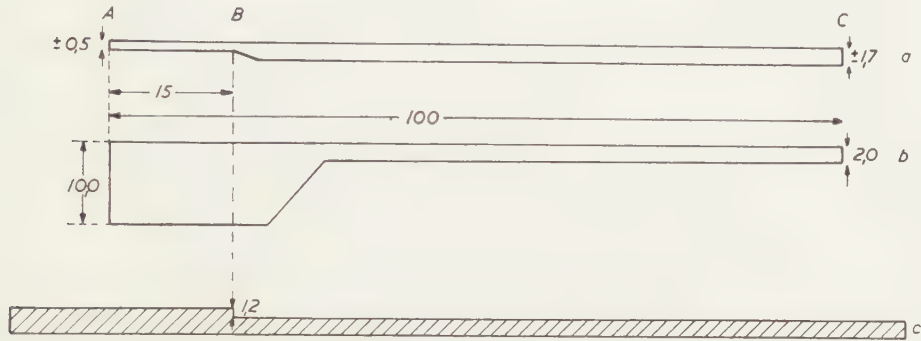


Fig. 1. a) side-view of lead specimen; b) top-view of lead specimen, AB = actual crystal, BC = "tail"; c) sledge on which the specimen is brought into the furnace. Dimensions in mm.

After the crystals were grown the thicker part of the specimen was etched away electrolytically. Finally the thin part was etched down to the thickness of about 0.3 mm. However, even now the characteristic radiation of the X-ray source used (a sealed-off molybdenum-tube) did not pass through the specimen in a sufficient amount. Fortunately, lead chooses its own "monochromatic" radiation from the short wave-lengths present in the X-ray beam. This can be seen in the following way:

For normal incidence the intensity of the transmitted beam is given by

$$(3) \quad I = I_0 e^{-\mu t}$$

in which  $I_0$  = intensity of the incident beam,  $I$  = intensity of the transmitted beam,  $\mu$  = linear coefficient of absorption,  $t$  = specimen thickness.  $\mu$  can be calculated for various wavelengths with the aid of the formula (see f.e. REGLER, 1937):

$$(4) \quad \frac{\mu}{\rho} = C \cdot \lambda^3 \cdot Z^3$$

where:  $\rho$  = density,  $\lambda$  = wavelength of the X-rays considered,  $Z$  = atomic number,  $C$  = constant. Its value can be fixed by inserting in formula (4) the value of  $\mu/\rho$  as given by a table of absorption coefficients for one or more wavelengths in the appropriate region. Knowing  $C$ ,  $\mu/\rho$  was calculated as function of  $\lambda$  for wavelengths above the minimum value given by the tension applied to the X-ray tube (in our case 40 kV, therefore  $\lambda$  minimum is 0.31 Å). Assuming for the dependence of the continuous spectrum of

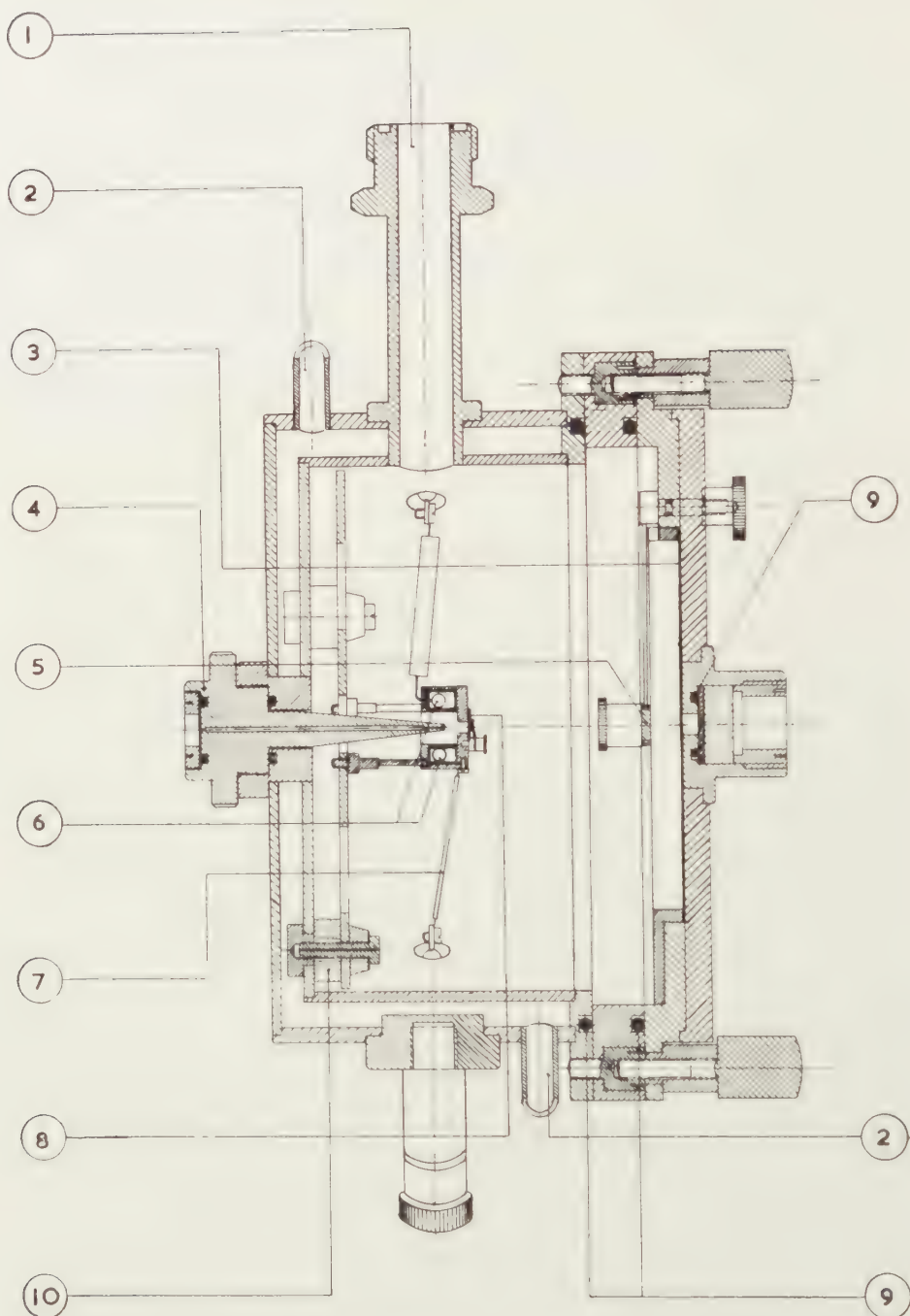


Fig. 2. Cross-section of high temperature vacuum-Laue-camera: 1) to vacuum-pump; 2) water-cooling; 3) film; 4) diaphragm; 5) beam-catcher; 6) heating spiral; 7) thermo-couple; 8) specimen; 9) O-rings; 10) heat-insulating material.



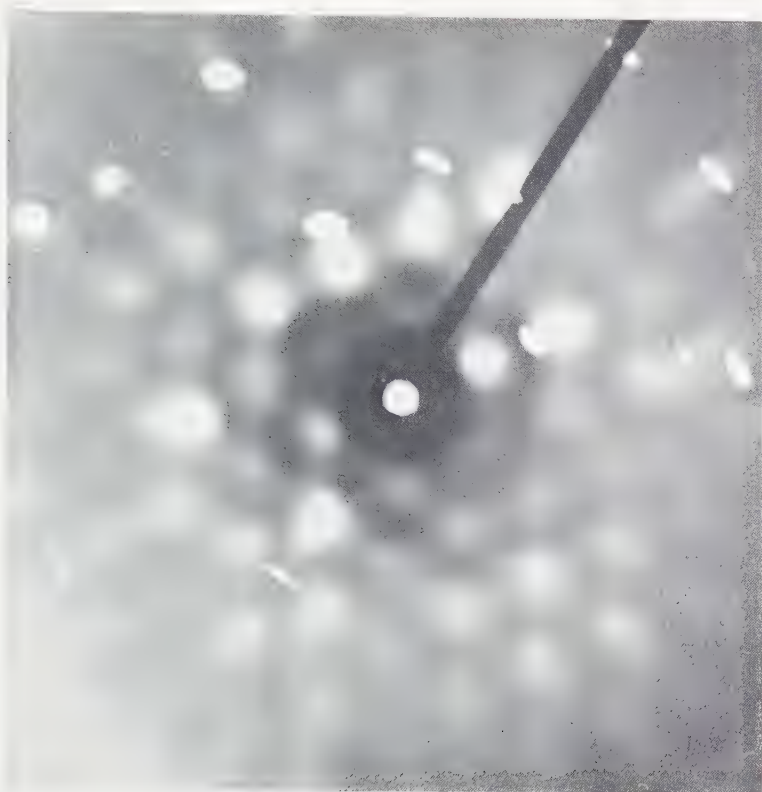


Fig. 3a. Laue-photograph of a lead single crystal with an orientation as given in figure 4, taken at room-temperature.

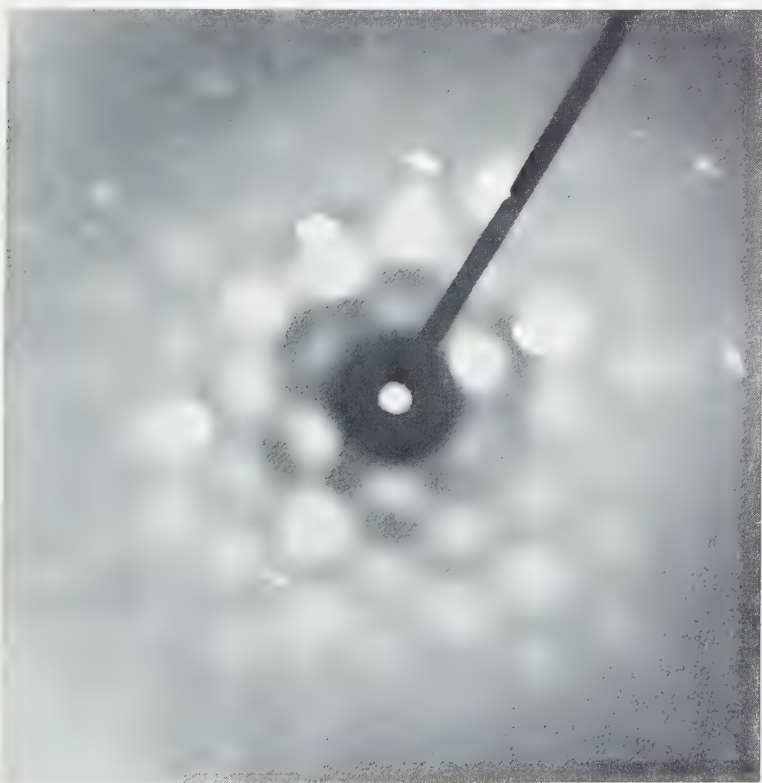


Fig. 3b. Laue-photograph of the same crystal taken at 300° C.



the molybdenum tube on wavelength the same course as given for tungsten (c.f. BRAGG (1939) p. 299), further taking the specimen thickness  $t$  to be 0.32 mm and inserting corresponding values of  $I_0$  and  $\mu$  in formula (3), the transmitted intensity  $I$  could be calculated as a function of wavelength. In this way it was found that the transmitted X-ray beam might be expected to show a not very sharp but clearly pronounced maximum in intensity for a wavelength of about 0.32 Å. Evaluation of the Laue-photographs, as described in section 3, actually showed that the diffuse spots must be caused by radiation of about this wavelength. Both position and intensity of the indexed spots appeared to be in good agreement with it, notwithstanding the approximate character of the above calculation.

The Laue-photographs were taken in a vacuum high-temperature camera after own design, shown in figure 2.

The specimen (8) (the numbers refer to figure 2), which is irradiated perpendicular to its surface, is mounted on a holder containing a small furnace which is heated by a molybdenum spiral (6). The temperature is measured by means of a thermocouple (7), which is fixed on the outside of the furnace close to the specimen. The camera is watercooled (2) and can be evacuated (1) to a pressure of about  $10^{-5}$  mm mercury. Vacuum tight connections are made by means of O-rings. (9).

### 3. Results and discussion

Figures 3a and 3b show two Laue-photographs, taken at room temperature (a) and at 300° C (b), of a lead single crystal. The crystal had an orientation as given in figure 4, a stereographic projection of its {111}-poles. The plane of projection is taken parallel to the specimen-surface and therefore to the photographic film. The orientation is such that a  $[\bar{1}\bar{1}2]$ -direction is vertical on the photograph, whereas a (111)-plane makes an angle of 17° with both specimen-surface and film. In order to be able to index the diffuse spots present on the Laue-photographs, it is necessary to construct a projection of the reciprocal lattice according to the orientation of the crystal used. For the principles of this construction may be referred to JAMES (1948), page 242. For the case described here, this projection is given in figure 5a. The plane of projection (— plane of figure) is taken parallel to the  $(\bar{1}\bar{1}2)$ -plane of the crystal, with the  $[\bar{1}\bar{1}2]$ -direction pointing upwards and the  $[\bar{1}10]$ -direction pointing to the left. This choice fixes the  $[111]$ -direction.

In the  $[\bar{1}\bar{1}2]$ -direction the reciprocal lattice consists of 6 different equidistant layers which repeat themselves with a spacing  $p=1/3a^*\sqrt{6}$  ( $a^*$ =reciprocal lattice constant), the zero-layer lying in the plane of projection. If a certain reciprocal lattice point has the indices  $hkl$ , it is easy to understand that the indices of the next point perpendicular above this point are  $h-2, k-2, l+4$ , whereas the corresponding indices for the next point perpendicular beneath it are  $h+2, k+2, l-4$ . The two- or

three sets of indices of several points in figure 5a are mutually related in this way.

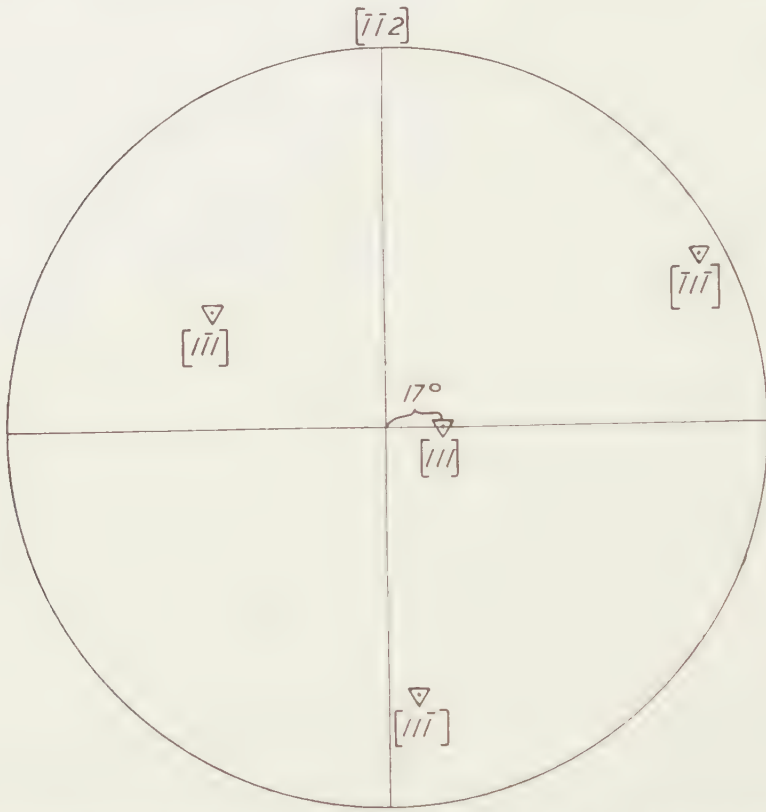


Fig. 4. Stereographic projection (octahedral poles) of the lead single crystal from which the Laue-photographs 3a and 3b were taken.

With the aid of this projection it is possible to index the photographs by means of the normal construction for the reflected beams. Figure 5b shows the traces of the sphere of reflection (radius for a wavelength 0.32 Å and drawn on the same scale as the reciprocal lattice) for perpendicular

Fig. 5a. Reciprocal lattice of lead corresponding to the orientation of the single crystal (c.f. figure 4), the  $[112]$ -direction pointing upwards.

□ = lattice point lying  $p$  below or  $5p$  above plane of projection \*).

▲ = " " "  $2p$  " "  $4p$  " " " " " "

○ = " " "  $3p$  " "  $3p$  " " " " " "

■ = " " "  $4p$  " "  $2p$  " " " " " "

△ = " " "  $5p$  " "  $p$  " " " " " " \*

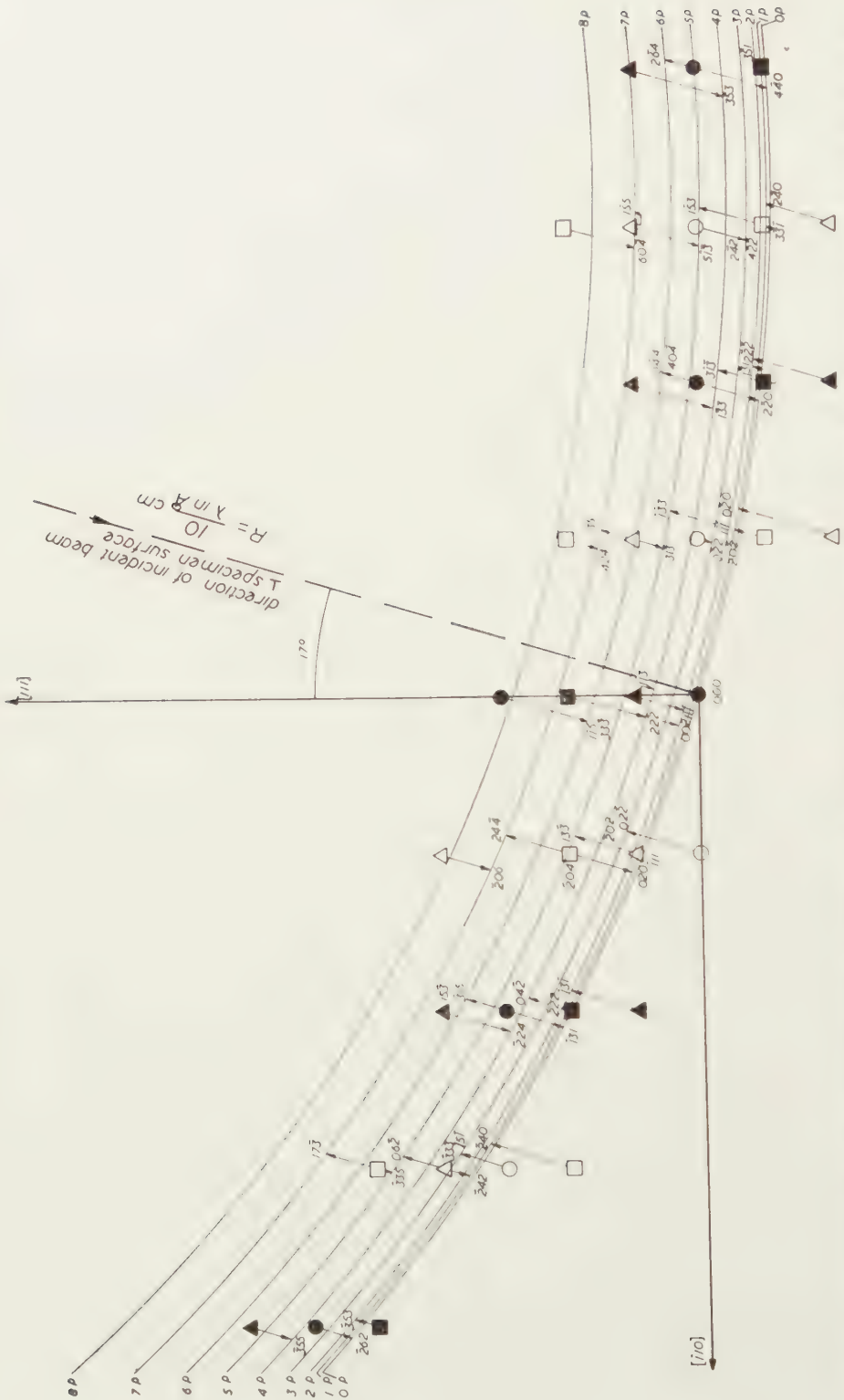
● = " " "  $6p$  " "  $6p$  " " " " " " or in plane of projection.

$p = 1/3 a^* \sqrt{6}$  and  $a^* =$  reciprocal lattice constant  $= \frac{1}{a}$  (in the figure  $\frac{10}{a \text{ in } \text{Å}} \text{ cm}$ ).

\*) The points marked with an asterisk lie  $6p$  further down or up.







incidence of the X-ray beam on the specimen, i.e. (c.f. fig. 4) a direction making  $17^\circ$  with the  $[111]$ -direction. The circles indicated with 0,  $p$ ,  $2p$ , etc., are the projections, parallel to the vertical  $[\bar{1}12]$ -direction, of the intersections of the sphere of reflection with the reciprocal lattice planes at distances respectively 0,  $1/3a^*\sqrt{6}$ ,  $2/3a^*\sqrt{6}$  etc. above or below the plane of projection. The indices of the diffuse spots are found by superimposing figure 5b on figure 5a and correlating the reciprocal spots with circles on the appropriate level passing them at short distance. If now the photographs are viewed in such a way that the direction of the incident beam coincides with the corresponding direction in figure 5b, and if the levels of the reciprocal spots are taken into account, it is not difficult to determine the indices of the diffuse spots on the photographs with the aid of figures 5a and b. They are given in the drawn copy of the Laue-photograph, shown in figure 3c.

To facilitate the comparison of this drawing with the actual photographs we outlined the region containing those spots having indices up to  $\Sigma H^2 = 12$ . The indices of the spots immediately outside this six-sided region, with indices  $\Sigma H^2 = 19$  and  $\Sigma H^2 = 20$  (no spots with  $\Sigma H^2 = 16$  are present on the photographs) have been underlined. The remaining spots, situated more outwardly, with indices up to  $\Sigma H^2 = 59$ , have not been specially indicated. With the aid of figure 3c, a comparison of the photographs 3a and 3b, taken at  $20^\circ\text{C}$  and  $300^\circ\text{C}$  respectively, shows clearly that the "enclosed" spots have all increased in intensity, the underlined ones have practically remained unchanged, whereas spots with higher indices are distinctly weaker on the high temperature photograph. This result is in general agreement with Born's formula and moreover with what might be expected on the basis of table I.

Due to the large number of spots present, it might even be possible by quantitative comparison of the intensity of corresponding spots to fix the temperature  $T_0$  and so the characteristic temperature  $\theta$ . However, the photographs as taken were not suitable for such an evaluation.

#### REFERENCES

- BORN, M., Reports on Progress in Physics **9**, 274 (1943).  
 BRAGG, W. H. and W. L. BRAGG, The Crystalline State, Vol. I (London, Bell, 1939).  
 CARTZ, L., Proc. Phys. Soc. **68**, 951 (1955).  
 JAMES, R. W., The optical principles of diffraction of X-rays (London, Bell, 1948).  
 LONSDALE, K., Crystals and X-rays (London, Bell, 1948).  
 REGLER, F., Grundzüge der Röntgenphysik (Berlin, Urban and Schwarzenberg, 1937).  
 SMITHELLS, C. J., Metals Reference Book, Vol. I, p. 161 (London, Butterworth, 1955).  
 TAYLOR, A., An introduction to X-ray metallography (London, Chapman and Hall, 1949).  
 TIEDEMA, T. J. and C. L. D. KOOP, Ned. Tijdschr. Natuurk. **19**, 170 (1953).

## PALEONTOLOGY

# REMARKS ON THE CORRELATION OF MAMMALIAN FAUNAS OF JAVA AND INDIA AND THE PLIO-PLEISTOCENE BOUNDARY

BY

G. H. R. VON KOENIGSWALD

(Communicated at the meeting of February 25, 1956)

In collaboration with the geologists and palaeontologists of the Geological Survey, in 1935 for the first time we could give the sequence of the fossil mammalian faunas of Java. A correlation with the classical sites in India was—and still is—for lack of larger faunas in the older layers in Java, quite difficult. With certain small corrections, our correlation has been confirmed by E. H. COLBERT, who, working at the extensive collections made by the American Museum of Natural History, in India must be regarded as the leading authority on the fossil faunas of that part of the world.

Since several years Dr. D. A. HOOIJER has been trying to introduce his own correlation, while we have a different view on the position of the Plio-Pleistocene boundary in Java. Both points will be discussed here.

First the correlation of the faunas. Our different views are expressed in the table below. — In this publication the old “oe” in javanese names is changed into “u” according to the modern indonesian orthography.

The correlation of the Narbadas with the Trinil fauna is no problem. Then follows the Boulder Conglomerate. From these layers there is practically no fauna, but DE TERRA and TEILHARD (1936) compare the Lower Narbadas with the Boulder Conglomerate. “The association of advanced *Elephas* with *Hippopotamus* and large *Bos* suggests a stage slightly younger than the older Upper Siwaliks”. The fauna from the Narbadas — no difference is made between upper and lower zones — misses most of the typical genera of the Pinjor. An exception seems to be “*Leptobos fraseri*” RÜTIMEYER, different from the *Leptobos falconeri* from the Pinjor. Most probably the “*Leptobos*” of the Narbada does not belong to that genus. “Dr. TEILHARD who critically examined these specimens in Calcutta, reports that the *Leptobos* of RÜTIMEYER may well be a damaged skull of *Bos*” (DE TERRA and PATERSON, 1939, p. 318). The Boulder Conglomerate and the Narbadas apparently form one unit, separated from the Pinjor: therefore not only the Narbadas, but also the Boulder Conglomerate are the equivalent of the Trinil. There is absolutely no substantial reason to place the Trinil in the Narbadas and the Djetis



— with clear relations to the Pinjor—in the Boulder Conglomerate, as has been done by HOOIJER.

The differences between the Trinil and the Djetis HOOIJER tries to diminish by a comparison with genera alone. “As already remarked in a previous paper (HOOIJER, 1951, p. 278) the faunal distinctions between the Djetis and the Trinil beds are dwindling, the better these faunas

TABLE I  
Correlation of the javanese and indian Faunas

	VON KOENIGSWALD 1940	COLBERT 1942	COLBERT 1943	VON KOENIGSWALD 1950	VON KOENIGSWALD 1955	HOOIJER 1952
TRINIL	NARBADAS					
	BOULDER CONGLOMERATE					
DJETIS	PINJOR					
KALINGGLAH						
DUIDJULANG	TATROT					
					DHOK PATHAN	

become known” (HOOIJER, 1952, p. 441). This must be contradicted. The most typical genera of the Djetis as *Leptobos*, *Nestoritherium* and *Megacyon* do not continue into the Trinil, while most of the species are different. The difference between these faunas is of exactly the same order as between the Villafranchian and the Middle Pleistocene faunas in Europe: practically all of the genera to be found in the latter are already present in the Villafranchian, but the species differ, while typical Villafranchian genera—among them, as in Java, *Leptobos*—are now extinct.

There are, by the way, difficulties in applying the term Middle and Lower Pleistocene. It had been agreed upon at the International Quarternary Conference at Leningrad in 1932, that the Lower Pleistocene should comprise the Günz and Mindel Glaciation with the Interglacial in between. Since, as has been demonstrated by DE TERRA, the Boulder Conglomerate

is the equivalent of the second glaciation, this conglomerate is Lower Pleistocene anyhow.

Coming to the lower part of our sequence, I have been led by a comparison, which is tabulated here.

TABLE II  
Distribution of Genera in Java and India

INDIA:	Dhok Pathan	Tatrot	Pinjor
PLEISTOCENE GUIDEFOSSILS:			
<i>Elephas (planifrons)</i> . . . . .		+	+
<i>Equus</i> . . . . .			+
<i>Bos</i> . . . . .			.
JAVA:			
DJETIS:			
<i>Leptobos</i> . . . . .			.
<i>Nestoritherium</i> . . . . .			+
<i>Hexaprotodon</i> . . . . .	+	+	+
<i>Elephas</i> . . . . .		+	+
KALI GLAGAH:			
<i>Hexaprotodon</i> . . . . .	+	+	+
<i>Trilophodon</i> . . . . .	+		
<i>Stegodon</i> (11+) . . . . .	+	+	
( <i>Elephas</i> ) . . . . .		(+)	
TJIDJULANG:			
<i>Hexaprotodon</i> . . . . .	-		.
<i>Merycopotamus</i> . . . . .	+		+

(Stratigraphy of India, mainly after COLBERT, 1935).

In the Pinjor and the Djetis we find *Nestoritherium* and *Leptobos*; the last molar of the javanese *Stegodon trigonocephalus* from this layer has 13, that of the indian *St. insignis* 11-13 ridges. In India we have together with *Archidiskodon planifrons* the higher developed *Hypsiclephas hysudricus* (M3<sup>18</sup>/<sub>10</sub>) and *Platyclephas platycephalus*; in Java the elephant from these layers has not yet been described, but seems to be close to *H. hysudricus*. HOOLJER describes (1955, pl. XI) some fragments from the Dubois collection from Karang Djati and Tritik has *Archidiskodon planifrons*; these finds most probably come from the Djetis. "VON KOENIGSWALD was fully justified in placing the Djetis fauna fully as late or probably later than the Pinjor assemblage in India" (COLBERT, 1942, p. 1954).

The javanese faunas below the Djetis are not so well known. In the Kali Glagah we have an interesting mastodon, *Trilophodon bumiajuensis* (v. D. MAAREL), lower jaw without tusks, not related to *Mastodon borsoni* or *Anancus*, which continue into the Villafranchian. The hippopotamus — *Hexaprotodon simplex* — is primitive, and with faintly developed cingulum

in the upper molars and a flat roof of the skull comparable and even probably more primitive than the indian *H. sivalensis*.

The *Stegodon trigonocephalus praecursor* has only X 11 X ridges in the last lower molar and, according to the ridge formula, still comparable with *Stegodon bombifrons* with 11 X ridges. Although the eleven-ridged M3 figured by V. D. MAAREL is regarded by VON KOENIGSWALD (1933, p. 104) as belonging to a typical Trinil subspecies *Stegodon trigonocephalus trigonocephalus*, the eleven-ridged M<sub>3</sub> from Boemiajoe (Kali Glagah fauna) is regarded by VON KOENIGSWALD (l.c.) to be subspecifically distinct: *Stegodon trigonecephalus praecursor*" (HOOIJER, 1955, p. 44).

In distinguishing these two subspecies I was mainly influenced by the difference in the folding of the enamel. In V. D. MAAREL's molar from Lepin Alit the ridge formula is X 11 X, that means that there is a talon in front and one behind. Both talons are better developed than in the Bumiaju specimen, and I would not hesitate to count here 13 ridges.

In the excavation in the Kali Glagah (which might be regarded as the type locality) no remains of elephants have been found. The molar from the Tjipangglosoran, described as *Archidiskodon planifrons* by V. D. MAAREL (1932, p. 172), a determination confirmed by HOOIJER (1955, p. 105) comes from a higher level (Geol. Kaart Java, bl. 58, p. 37). From the Tatrot too, the zone from India with which we correlate the Kali Glagah, *Elephas planifrons* has been discovered (LEWIS, 1937, p. 198). It is, however, not known, whether this species occurs in the whole formation or only in the top layers.

In the Tjidjulang we have as characteristic genera *Merycopotamus*, *Hexaprotodon* and *Archidiskodon*. There is nothing against a correlation with the Tatrot. As, however, *Archidiskodon praeplanifrons* (VON KOENIGSWALD, 1951)—by the presence of a very large premolar, still with median sulcus—is more primitive than the typical planifrons, the first species might be older. HOOIJER's argumentation has not convinced me that I am wrong. *Merycopotamus* and *Hexaprotodon* both also occur in the Dhok Pathan, which underlies the Tatrot. As the fauna of marine molluscs from the Tjidjulang Beds contains about 40–45 % extinct species—this is the Tapak series—this fauna is surely of Pliocene age, and, while in a broad sense of Tatrot age, perhaps even partly contemporaneous with part of the Dhok Pathan. This is what I have indicated in my table from 1955.

For the reasons set forth above I cannot accept HOOIJER's correlation.

The second point to be considered is the Plio-Pleistocene Boundary. By the first presence of *Equus* the Villafranchian of Europe—type: Val d'Arno—, the Pinjor of India and the Sanmemian of China are contemporaneous. If we turn to *Leptobos*, another typical guide fossil, we find Europe, Pinjor and Djetis. These faunas mark the beginning of the Pleistocene. As a third guide fossil we find on the list the true elephants *Archidiskodon*, which indeed occur in all of these faunas.

When HAUG (1911) suggested that the beginning of the Pleistocene should be characterized by the first appearance of *Elephas*, *Equus* and *Bos*, he surely had in mind the Villafranchian fauna of southern Europe. The equivalent of the Villafranchian in India is the Pinjor. Neither in the extensive collections of the Indian Geological Survey nor in those of the American Museum of Natural History of New York are *elephas* remains from older levels. It was not before 1937, that LEWIS announced the occurrence of *Archidiskodon* from Tatrot. According to HOOIJER (1955, p. 93) it is a single molar. From where comes this specimen? From the top of the Tatrot formation? The boundaries between the faunas are not always clear cut. Is this single tooth within a fauna, which contains neither *Equus* nor *Leptobos* and has little relation to the typical Villafranchian, sufficient to place now the important border between Pliocene and Pleistocene below the Tatrot?

We furthermore must keep in mind, that *Equus*, originating from North America, has been "released" from that continent and therefore marks a definite level. The elephants have evolved from *Stegodon* in South East Asia, and might very well be older in Asia than in Europe, which they have apparently reached together with *Equus*. *Stegodon* appears with *Stegodon licenti* in the Pontian of China, but reached India not before the Dhok Pathan.

After the discovery of *Archidiskodon* in the Tatrot Lewis directly included this formation in the Pleistocene, and several authors have followed him (DE TERRA, MOVIVUS). Others were more cautious; COLBERT (1942) gives the Tatrot a transitional position, and so do HOOIJER and COLBERT in 1951. To quote from the latter publication: "To the best of our present knowledge the Tatrot zone serves equally well, from the standpoint of the vertebrate palaeontologist, as the beginning of a period as it would do as the end of one. We can only repeat what has already been said by one of us (COLBERT, 1942, p. 1446) that the Tatrot is possibly transitional between the Upper Pliocene and the Lower Pleistocene". Regarding the first sentence, I can only partly agree: for me indeed the Tatrot marks the end of a period; *Equus* the guide fossil for the Pleistocene par excellence, is not yet present. The second sentence is apparently no longer the opinion of HOOIJER.

I am completely willing to accept the Tatrot as "transitional", when there is evidence of a Pleistocene age by other geological or palaeontological observations. This is impossible in India, but possible in Java, where the faunas are intercalated in marine layers of which the molluscan fauna is known and has been studied by specialists as MARTIN and OOSTINGH.

Near Madjenang (sheet 54), where the Tjidjulang fauna has been found intercalated in the Tapak series, these layers contain 65 species of marine molluscs of which only 38 or 39 are recent (58-50 %). In the overlaying Kali Biuk series—which near Bumiaju still underlies the Glagah series with the Kali Glagah fauna—we find 73 species, of which 39 or 40 are



recent (53–55 %). Both series are regarded as belonging to the “Cheribonian” of OOSTINGH.

In the Bumiaju region (sheet 58) we find in the Tapak series 55–58 % recent species (according to MARTIN 60 %). About the younger levels OOSTINGH remarks: “Die Prozentzahlen der K. Glagahschichten (42½–46 oder nach MARTIN 46) und der K. Bioekschichten i.w.S. (42–47 oder 49) sind also vorläufig nicht mit einander vergleichbar und erstere sind lediglich auf Grund ihrer Vertebratenfauna als Jungpliozän zu betrachten, während letztere auf Grund ihrer Prozentzahl dem älteren Pliozän zuzurechnen sind”. (OOSTINGH, 1936, p. 225). From the Kali Glagah layers we have 26 species of freshwater molluscs, of which 11 are still living; it is therefore, that this fauna cannot directly be compared with a marine fauna.

If we turn to the Djetis beds in Eastern Java, the number of marine molluscs is 60, of which 32 % are extinct. MARTIN (1932) has given this fauna an uppermost Pliocene age, and it was on account of the mammals, that these layers were included in the Pleistocene. The mammalian fauna of the Djetis is relatively well known, and therefore such a step was fully justified. But this was the limit, to which such a specialist as OOSTINGH would go.

For Java—and in my opinion also for the Tatrot of India—a shifting of the Plio-Pleistocene boundary to a lower level entirely depends upon the age determination of the “Cheribonian”. Only there is evidence that this assemblage is of Pleistocene age, not by neutralizing it by an “it could be” because of a sole *Archidiskodon* in the Tatrot (where *Equus* and other typical Villafranchian forms are not present) but by a positive comparison between stratigraphically fixed marine faunas, such a step would be justified. In the “Recommendations of the Commission appointed to Advise on the Definition of the Pliocene-Pleistocene Boundary” of the International Geological Congress, London 1948, we read: “The Commission recommends that, in order to eliminate existing ambiguities, the Lower Pleistocene should include as its basal member in the type-area the Calabrian formation (marine) together with its terrestrial (continental) equivalent the Villafranchian” (Rep. Int. Geol. Congr. London, Part IX, p. 6). The type-area for fixing this boundary thus is in Europe, and not in the Indian Siwaliks.

For the reasons discussed above it is not possible for me to accept HOOIJER's view on placing the Plio-Pleistocene boundary in Java below the Tjidjulung. The Djetis fauna of Java is the equivalent of the Indian Pinjor, and both represent the Villafranchian s. str.

A last point to be considered is the correlation of various faunas stage by stage. In India as in Java a fauna is also defined by a certain rock unit, by a certain assemblage of layers, and it is very unlikely, that these units in both regions have exactly the same limits; a correlation is always only possible in a broad sense. In my own correlation tables I have tried

according to my own view, to give certain faunas a somewhat "intermediate" place; I therefore am not in favour of HOOIJER's method, who rigorously correlates stage by stage.

## LITERATURE

- COLBERT, H. E., Siwalik Mammals in the American Museum of Natural History. Trans. Am. Phil. Soc. n.s. **26**, 1-401 (1935).
- , The geologic succession of the Proboscidea. In: Osborn, Proboscidea **2**, 1421-1522 (1942).
- , Pleistocene Vertebrates collected in Burma by the American Southeast Asiatic Expedition. Trans. Am. Phil. Soc. **32**, part III, 395-429 (1943).
- HOOIJER, D. A., Fossil Mammals and the Plio-Pleistocene Boundary in Java. Proc. Kon. Ned. Ak. v. Wetensch. Amsterdam, ser. **B 55**, 436-443 (1952).
- , Fossil Proboscidea from the Malay Archipelago and the Punjab. Zool. Verh. Leiden, nr. **28**, 1-146 (1955).
- and E. H. COLBERT, A Note on the Plio-Pleistocene Boundary in the Siwalik Series of India and Java. Am. J. Sc. **249**, 533-538 (1951).
- KOENIGSWALD, G. H. R. VON, Beitrag zur Kenntnis der fossilen Wirbeltiere Javas. I. Wet. Mededeel. Dienst Mijnb. Ned. Ind. nr. **23**, 1-127 (1933).
- , Die fossilen Säugetierfaunen Javas. Proc. Kon. Akad. v. Wetensch. Amsterdam, **38**, 188-198 (1935).
- , Neue Pithecanthropus-Funde. Wet. Mededeel. Dienst Mijnb. Ned. Ind. nr. **28**, 1-212 (1940).
- , Vertebrate Stratigraphy, in: R. W. van Bemmelen, The Geology of Indonesia, pp. 91-93 (1950).
- , Ein Elephant der planifrons-Gruppe aus dem Pliocaen West-Javas. Eclogae. Geol. Helv. **43**, 268-274 (1951).
- , The Pleistocene of Java and the Plio-Pleistocene Boundary. Congr. Int. Quarternaire (INQUA), Rome 1953, pp. 3-11 (1955).
- LEWIS, E. G., A new Siwalik correlation. Am. J. Sc. **33**, 191-204 (1937).
- MAAREL, F. H. v. D., Contribution to the knowledge of the fossil mammalian fauna of Java. Diss. Utrecht, pp. 1-208 (1932).
- MARTIN, K., De ouderdom der sedimenten van de door Dr. J. Cosijn opgenomen antichinaal in de Residentie Soerabaja. Verh. Geol. Mijnbk. Gen. **9**, 149-151 (1932).
- OOSTINGH, C. H., Die Mollusken des Pliozäns von Boemiajoe (Java). Mededeel. Dienst Mijnb. Ned. Ind. nr. **26**, 1-247 (1936).
- TERRA, H. DE and T. T. PATERSON, Studies on the Ice Age in India and associated Human Cultures—Carnegie Inst. Washington. Publ. nr. **493**, 1-354 (1939).

# NOTE ON THE INFLUENCE OF THE HELIUM AND METAL CONTENT ON THE PRESSURE IN THE SOLAR ATMOSPHERE

BY

H. HUBENET

(Communicated by Prof. M. MINNAERT at the meeting of March 24, 1956)

At this moment the helium content and metal content of stellar atmospheres still form a point of discussion, as possible values the following ones are mentioned (ROSA [1]):

$$A = \frac{N_{\text{H}}}{N_{\text{met}}} = 5000$$

$$B = \frac{N_{\text{He}}}{N_{\text{H}}} = 0.18.$$

Other authors, however, favour different values. As long as this uncertainty exists it seems to be useful to have simple means at hand, in order to convert numerical data obtained for specified values of  $A$  and  $B$  to new data for other values of  $A$  and  $B$ .

We will restrict ourselves to the solar atmosphere and the influence of the composition on the pressures *viz.* total gas pressure  $p$  and the electron pressure  $p_e$ . MINNAERT [2] tabulated mean corrections  $\Delta \log p$  and  $\Delta \log p_e$  as functions of the temperature. The main purpose of this note is to provide some new information and to investigate in how far these corrections may be practically applied.

We start from a temperature distribution  $T(\tau_0)$ , which is assumed to be valid for a standard chemical composition defined by the parameters  $A_1$  and  $B_1$  and we keep to the same function  $T(\tau_0)$  when the composition is modified. This is evidently allowed in the cases where  $T(\tau_0)$  has been obtained from limb darkening measurements; if the relation  $T(\bar{\tau}_0)$  has been obtained from theory, the composition only plays a (minor) role if we want to represent the temperature distribution as a function  $T(\tau_0)$ , which, however, is not necessary for the computation of the pressures. Temperature distributions  $T(\tau_0)$  found from the study of line intensities and profiles may be affected by the assumed composition but even here the influence does not seem to be very important. Therefore we will assume that it is allowed to consider various compositions for one and the same temperature distribution.

Given  $T(\tau_0)$  or  $T(\bar{\tau})$ ,  $A_1$  and  $B_1$  we can compute the pressures  $p$  and  $p_e$  as a function of resp.  $\tau_0$  or  $\bar{\tau}$ , or as a function of  $\vartheta = \frac{5040}{T}$ .

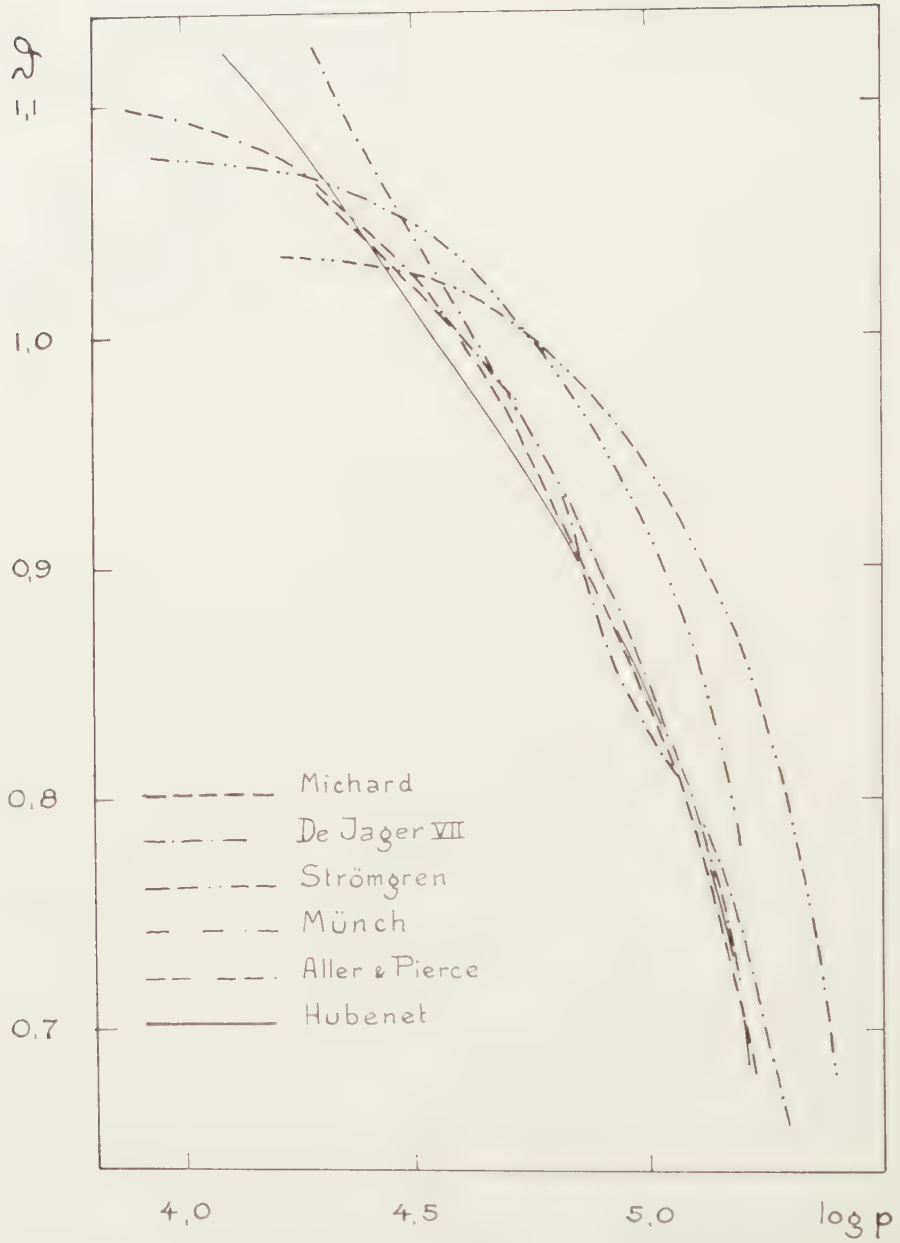


Fig. 1. The solar models used in this investigation. In order to be able to represent the models in a more or less homogeneous way,  $\log p$  instead of  $\tau_0$  is chosen as abscissa. By means of the tables III and IV the pressures have been reduced to pressures for a composition defined by  $\log A = 3.8$  and  $B = 0.2$ .



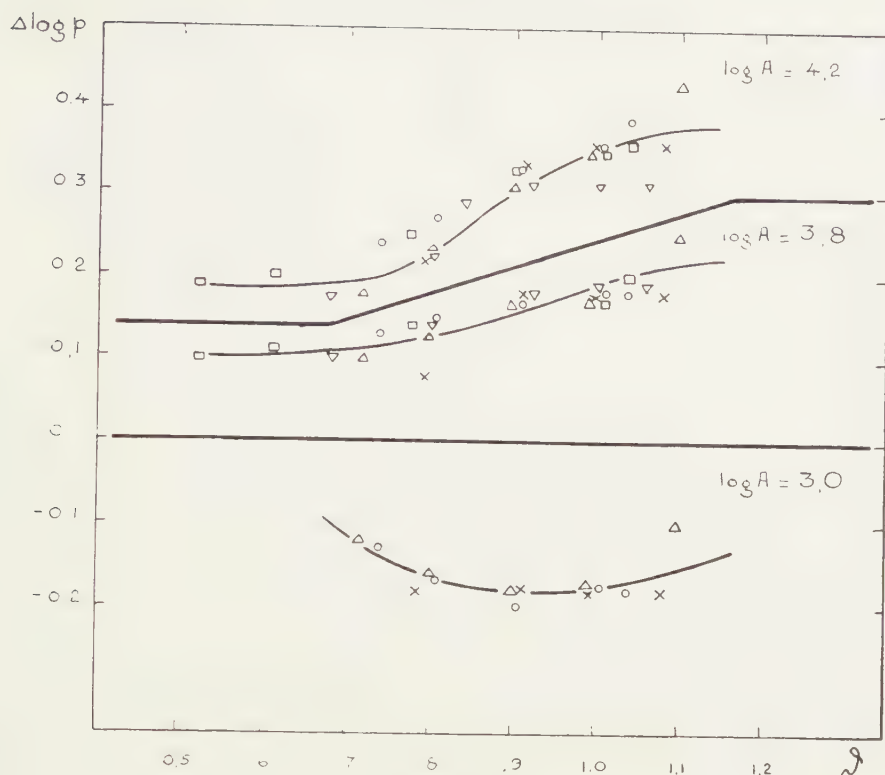


Fig. 2. Differential corrections  $\Delta \log p$  relative to  $\log A = 3.4$

$$\Delta \log p = (\log p)_{\log A} - (\log p)_{\log A = 3.4}$$

△ ALLER and PIERCE [3]

▽ MICHARD [5]

× MÜNCH [6]

○ STRÖMGREN [7]

□ STRÖMGREN-RUDKJØBING [7]

Now when using the same temperature distribution but different composition parameters  $A$  and  $B$  we will find different pressure functions. We can write:

$$\Delta \log p = f(\Delta A, \Delta B, \vartheta)$$

$$\Delta \log p_e = g(\Delta A, \Delta B, \vartheta).$$

Starting from another temperature distribution we might expect different functions  $f$  and  $g$ .

As working hypotheses we assume: 1) the corrections for changes in  $A$  and  $B$  are additive, that means that it is allowed to write:

$$\Delta \log p = f = \varphi_1(\Delta A, \vartheta) + \varphi_2(\Delta B, \vartheta)$$

$$\Delta \log p_e = g = \psi_1(\Delta A, \vartheta) + \psi_2(\Delta B, \vartheta)$$

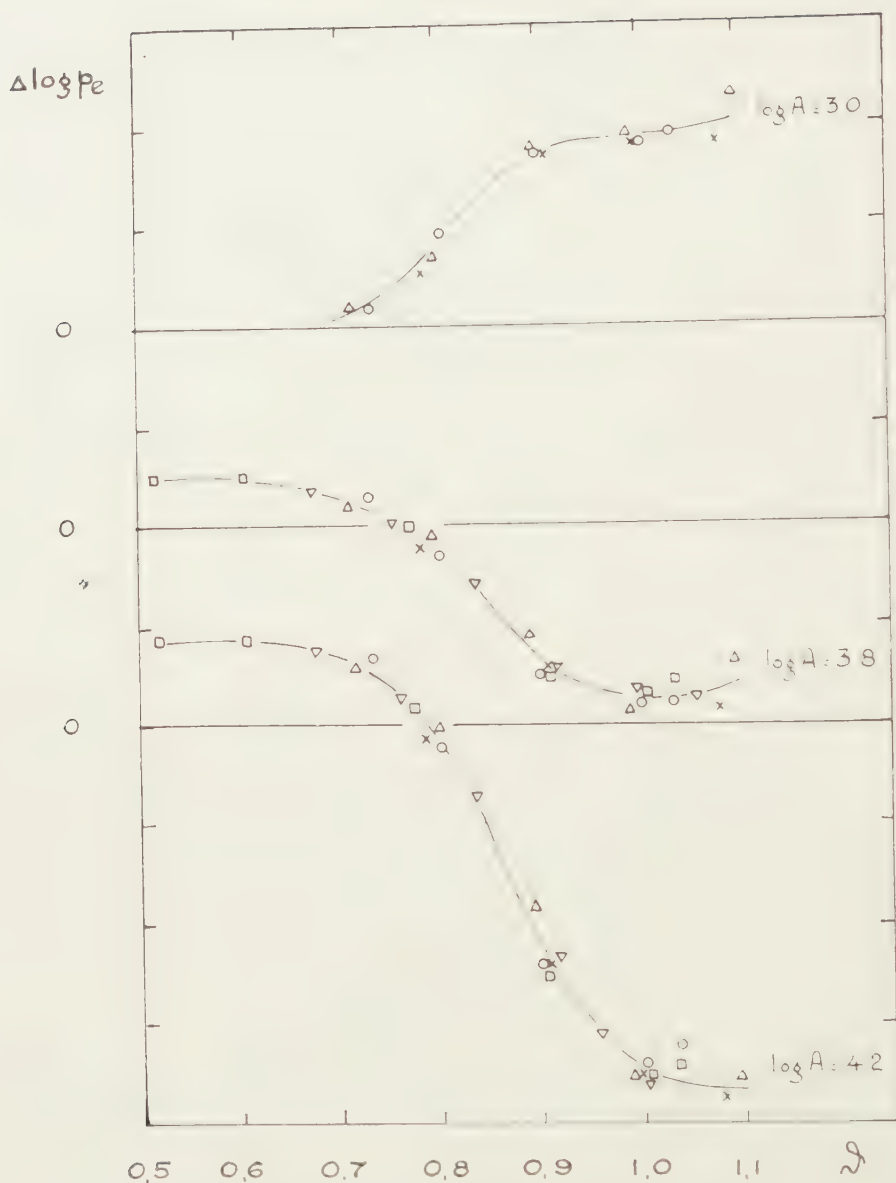


Fig. 3. Differential corrections  $\Delta \log p_e$  relative to  $\log A = 3.4$ . In order to avoid confusion the curves have been shifted, each curve having its own zero line. The axis of the ordinates is intersected in parts of 0.1. For explanation of the symbols see fig. 2.

(so we assume that in the series expansions of  $f$  and  $g$ , the "cross term" coefficients vanish). 2)  $f$  and  $g$  are independent of the temperature distribution.

We shall try to determine in an empirical way the functions  $\varphi_{1,2}$  and  $\psi_{1,2}$ . For this purpose we use the results from computations by various investigators for different temperature distributions and compositions (see

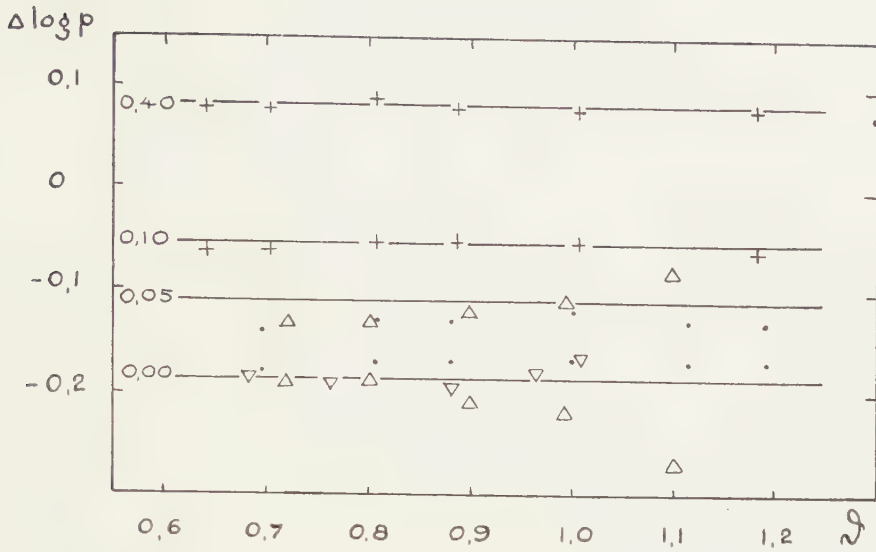


Fig. 4. Differential corrections  $\Delta \log p$  relative to  $B = 0.2$ . Parameter  $B$ . The dots near the curve labeled 0.05 are for  $B = 0.04$ .

- $\triangle$  ALLER and PIERCE [3]
- $\bullet$  HUBENET
- $+$  DE JAGER [4]
- $\nabla$  MICHARD [5]

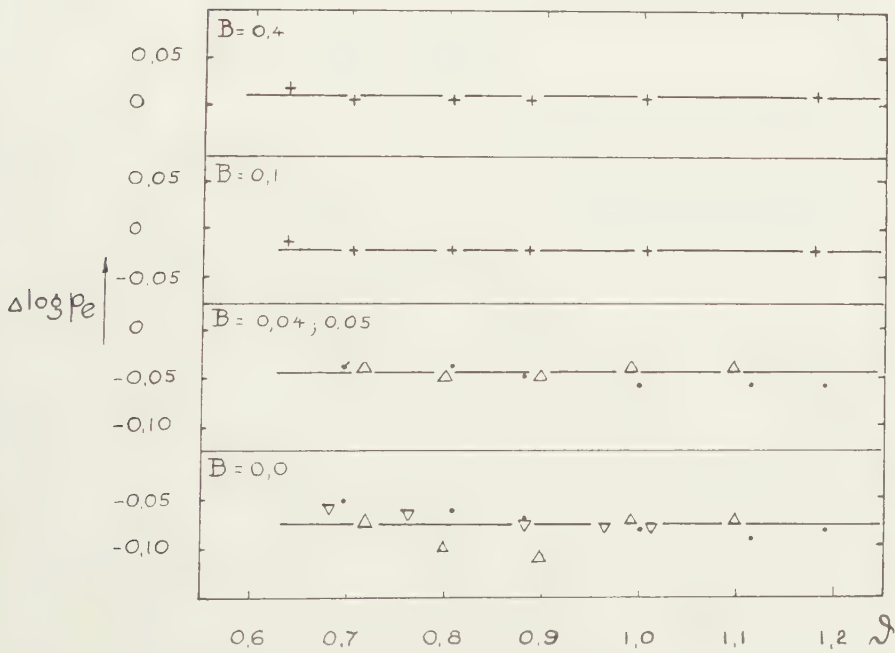


Fig. 5. Differential corrections  $\Delta \log p_e$  relative to  $B = 0.2$ . The curve labeled  $B = 0.04$ ; 0.05 is for  $B = 0.045$ . For explanation of the symbols see fig. 4.

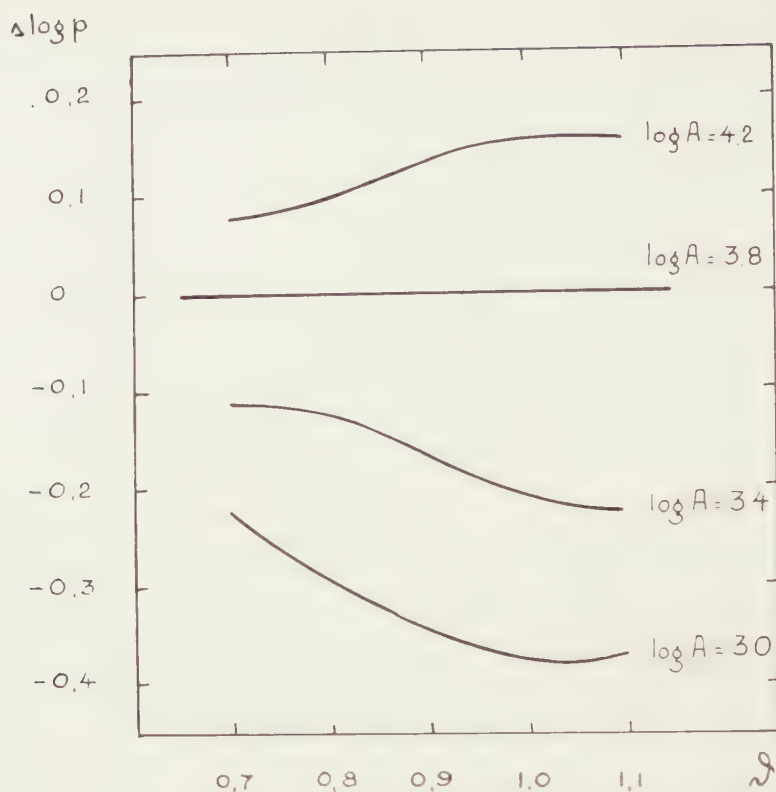


Fig. 6. Differential corrections  $\Delta \log p$  relative to  $\log A = 3.8$ .

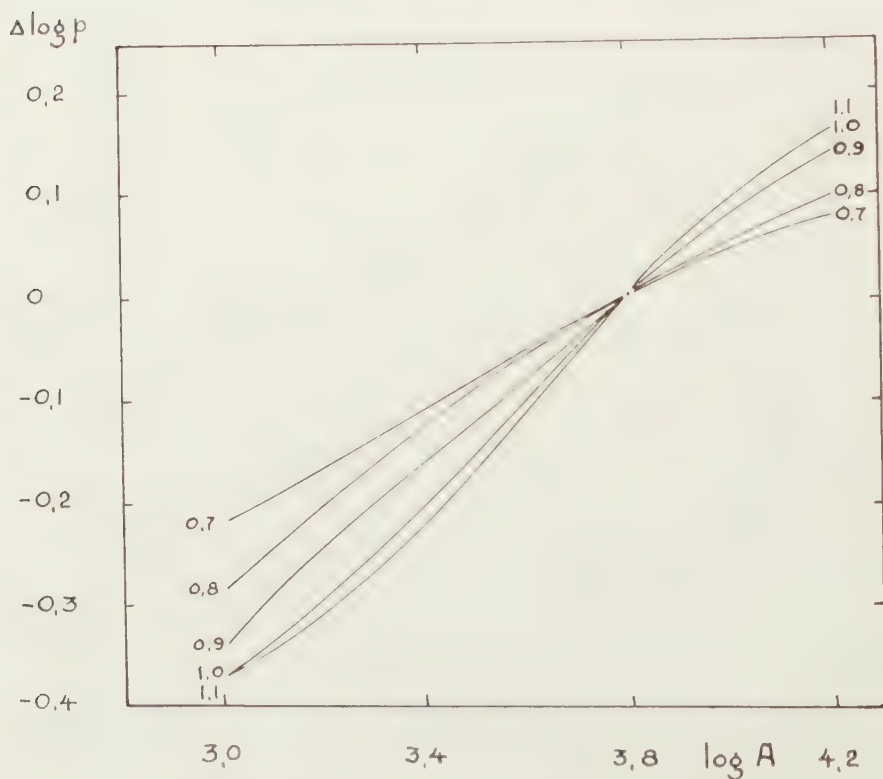


Fig. 7. Differential corrections  $\Delta \log p$  relative to  $\log A = 3.8$ , parameter  $\theta$ .



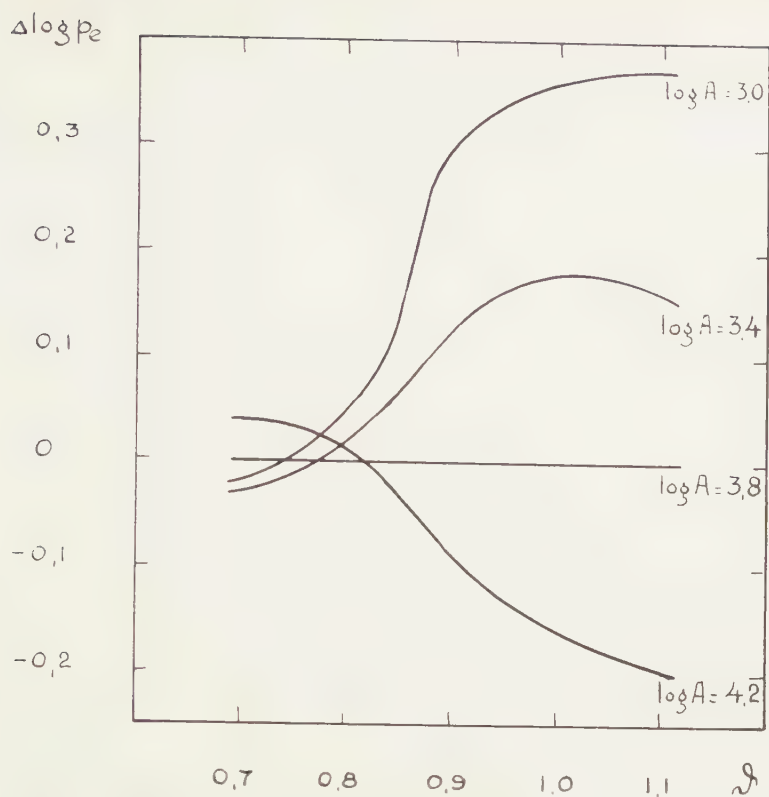


Fig. 8. Differential corrections  $\Delta \log p_e$  relative to  $\log A = 3.8$ .

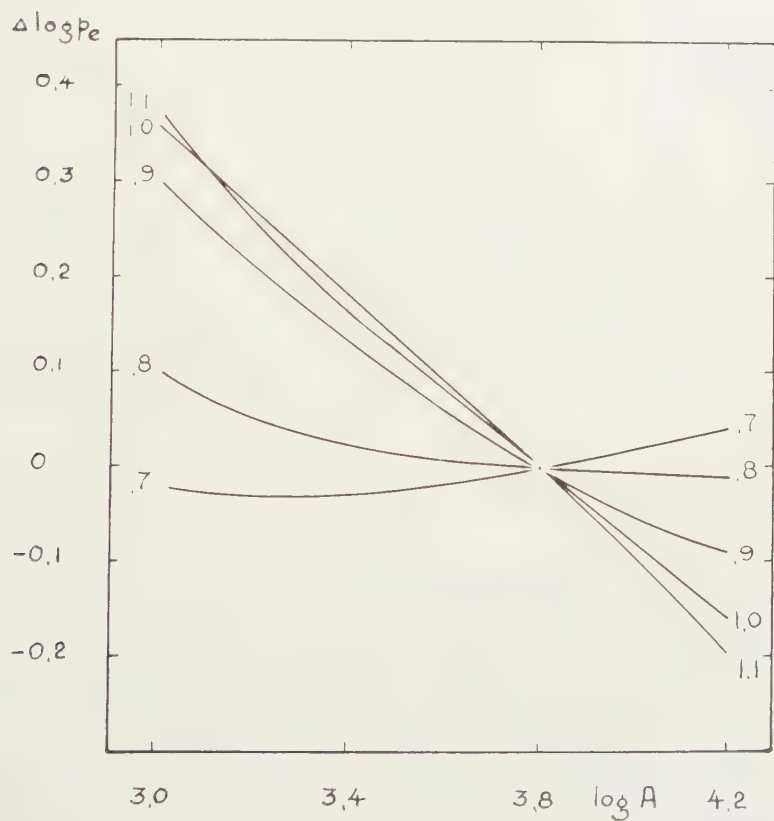


Fig. 9. Differential corrections  $\Delta \log p_e$  relative to  $\log A = 3.8$ , parameter  $\theta$ .

TABLE I

$B \backslash \log A$	3.0	3.4	3.8	3.95	4.2	4.3
0.0	A-P Mü S	A-P Mi Mü S S-R	A-P Mi Mü S S-R	H	A-P Mi Mü S S-R	
0.04				H		H
0.05		A-P				
0.1				J		
0.2		A-P Mi	Mi	H J	Mi	
0.4				J		

Original data used in this investigation:

A-P: ALLER and PIERCE [3] — H: HUBENET — J: DE JAGER [4]

Mi: MICHARD [5] — Mü: MÜNCH [6] — S: STRÖMGREN [7]

S-R: STRÖMGREN-RUDKJØBING [7].

TABLE II

	$B = 0$				$B = 0.2$			
	$\log A$	3.4	$\log A$	4.2	$\log A$	3.4	$\log A$	4.2
$\theta$	$\Delta \log p$	$\Delta \log p_e$	$\Delta \log p$	$\Delta \log p_e$	$\Delta \log p$	$\Delta \log p_e$	$\Delta \log p$	$\Delta \log p_e$
1.06	-0.19	0.18	0.18	-0.18	-0.18	0.18	0.17	-0.18
1.00	-0.19	0.17	0.17	-0.17	-0.19	0.17	0.17	-0.17
0.96	-0.18	0.17	0.17	-0.14	-0.18	0.17	0.17	-0.14
0.92	-0.18	0.14	0.16	-0.10	-0.16	0.15	0.21	-0.07
0.88	-0.16	0.11	0.15	-0.03	-0.17	0.11	0.18	-0.02
0.84	-0.15	0.06	0.13	-0.01	-0.15	0.06	0.15	-0.01
0.80	-0.14	0.01	0.10	0.01	-0.14	0.03	0.13	0.03
0.76	-0.12	-0.01	0.09	0.02	-0.12	0.00	0.11	0.03
0.72	-0.09	-0.03	0.08	0.03	-0.11	-0.03	0.10	0.03
0.68	-0.10	-0.03	0.07	0.04	-0.10	-0.04	0.08	0.04

Differential corrections  $\Delta \log p$  and  $\Delta \log p_e$  relative to  $\log A = 3.8$  for two values of  $B$ .

table I and fig. 1). The same results—except for those obtained by the present author<sup>1)</sup>—are used by MINNAERT.

<sup>1)</sup> These computations were carried through by means of the IBM punched card equipment (CPC) of the Indiana University Research Computing Center. The complete results will be published elsewhere. In the meanwhile the author wants to express his gratitude towards Dr. FRANK K. EDMONDSON, Dr. MARSHAL H. WRUBEL, Mr. ARNOLD M. HEISER of the Astronomy Department of Indiana University for their support and help.

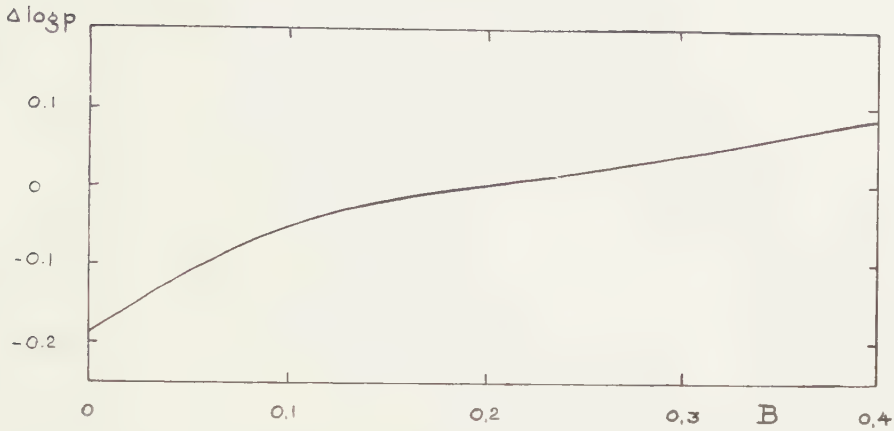


Fig. 10. Differential corrections  $\Delta \log p$  relative to  $B = 0.2$ .

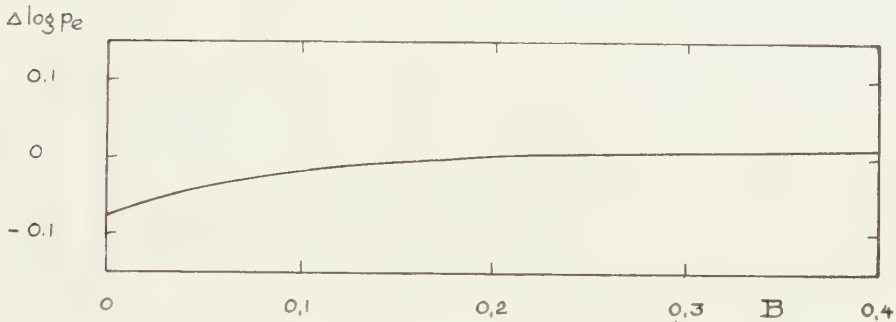


Fig. 11. Differential corrections  $\Delta \log p_e$  relative to  $B = 0.2$ .

Our first working hypothesis can only be checked by means of MICHARD's results, for he computed pressures for all the combinations of  $\log A = 3.4$ ; 3.8; 4.2 and  $B = 0$ ; 0.2. From his data we can derive corrections  $\Delta \log p$  and  $\Delta \log p_e$  relative to  $\log A = 3.8$ . By comparing corresponding corrections for  $B = 0$  and  $B = 0.2$  we can see in how far our hypothesis is correct (table II). The differences generally amount to 0.01 or 0.02 only, the maximum difference turns out to be 0.05 (one has to keep in mind that the round off can introduce spurious differences up to 0.02). For many purposes, these differences may be neglected. Now using our first hypothesis we can check our second one. For this purpose we plotted the corrections  $\Delta \log p$  and  $\Delta \log p_e$  relative to  $\log A = 3.4$  and  $B = 0.2$  as a function of  $\vartheta$  according to the data published by the various authors (fig. 2-5). The curves are obtained by a 2-dimensional smoothing (according to  $\vartheta$  and the composition parameter). The construction of average curves is quite well possible but the deviations of the individual points can amount up to 0.1.

The smoothed differences are tabulated in tables III and IV and plotted in fig. 6-11. Unlike in fig. 2 and 3, the corrections are now relative to  $\log A = 3.8$  since this is a more probable value than  $\log A = 3.4$ . From

TABLE III

$\theta$	Values of $\log A$			
	3.0	3.4	3.8	4.2
1.1	- 0.37	- 0.22	0.00	0.16
	0.37	0.16	0.00	- 0.20
1.0	- 0.37	- 0.20	0.00	0.16
	0.36	0.18	0.00	- 0.16
0.9	- 0.34	- 0.16	0.00	0.14
	0.30	0.13	0.00	- 0.09
0.8	- 0.29	- 0.12	0.00	0.10
	0.10	0.02	0.00	0.01
0.7	- 0.22	- 0.11	0.00	0.08
	- 0.02	- 0.03	0.00	0.04

Differential corrections  $\Delta \log p$  (upper values) and  $\Delta \log p_e$  (lower values).

TABLE IV

	Values of $B$					
	0.00	0.05	0.1	0.2	0.3	0.4
$\Delta \log p$	- 0.19	- 0.11	- 0.05	0.00	0.03	0.08
$\Delta \log p_e$	- 0.08	- 0.04	- 0.02	0.00	0.01	0.01

Differential corrections  $\Delta \log p$  and  $\Delta \log p_e$ .

the figures it is seen that these corrections are dependent on the actual temperature distribution and show slight differences between the individual models and therefore only can be used when a moderate accuracy is sufficient. In order to obtain a higher accuracy it would be useful to investigate in detail the dependence of the corrections on the temperature distribution.

*Utrecht, March, 1956.*

*Sterrenwacht "Sonnenborgh"*

#### REFERENCES

1. ROSA, A., *Z. Astrophysik* **25**, 1 (1948).
2. MINNAERT, M., *The Sun*, ed. G. P. KUIPER (Chicago 1953: The University of Chicago Press), chap. 3.
3. ALLER, L. H. and A. PIERCE, *Astrophysical J.* **116**, 176 (1952).
4. JAGER, C. DE, Thesis, Utrecht 1952 = *Rech. Astronomiques Obs. Utrecht XIII*, Part 1 (1952).
5. MICHARD, R., Thesis, Paris 1953 = *Ann. d'Astrophysique* **16**, 217 (1953).
6. MÜNCH, G., *Astrophysical J.* **106**, 217 (1947).
7. STRÖMGREN, B., *Publ. København Obs. Nr. 138* (1944), tables 14 and 15.



## CHEMISTRY

# THE CRYSTAL STRUCTURE OF LITHIUM-AMMONIUM-TARTRATE-MONOHYDRATE

BY

A. J. J. SPRENKELS

(Communicated by Prof. J. M. BIJVOET at the meeting of January 28, 1956)

### *Introduction*

In a previous communication [1] we gave a preliminary account of the crystal structures of some tartrates. In this paper the detailed X-ray analysis of one of these is described.

$\text{LiNH}_4$ -tartrate monohydrate and the isomorphous  $\text{Li-Tl}$ -salt belong to the group of tartrates which show the phenomenon of ferroelectricity [2]. Since an explanation of these properties will require some knowledge of the crystal structure as detailed as possible, it seemed worthwhile to carry out an investigation with ( $F_0 - F_c$ ) synthesis [3] including estimation of parameters of anisotropic thermal vibration and, if possible, location of hydrogen atoms. Although a series of successive difference syntheses revealed some evidence for the location of the latter, their positions could not be determined with certainty, this because of the small number of reflexions to which the contribution of hydrogen atoms is appreciable.

### *Experimental*

Crystals of  $\text{Li-NH}_4$ -tartrate  $\cdot \text{H}_2\text{O}$  can easily be grown by evaporation of an aqueous solution of tartaric acid, neutralized by the calculated amount of  $\text{NH}_4\text{OH}$  and  $\text{Li}_2\text{CO}_3$ . In an analogous way the isomorphs can be prepared.

The crystals belong to the orthorhombic disphenoidic class, and form prisms elongated along [001]. [4]

The cell dimensions have been determined from rotation photographs with  $\text{CuK}\alpha$  radiation. For the  $\text{Li-NH}_4$ -salt more accurate values were determined from exact measurements of the reflexing angles of a number of high order reflexions and averaging the results by a least squares method.

The values thus obtained are listed in Table I.

In the case of the  $\text{Li-Rb}$ -salt intensity data of the  $hk0$ - and  $0kl$  reflexions were recorded with  $\text{CuK}\alpha$  radiation on zero-level Weissenberg films by the multiple film technique and measured by visual comparison with an intensity scale.

TABLE I

Cell dimensions of Li-NH<sub>4</sub>-Tartrate·H<sub>2</sub>O and isomorphous compounds

	Cell edges			Density		
	<i>a</i>	<i>b</i>	<i>c</i>	<i>U</i>	<i>D<sub>m</sub></i>	<i>D<sub>x</sub></i>
Li-NH <sub>4</sub> -Tartr·H <sub>2</sub> O	7.878	14.642	6.426 Å ± 0.04 %	741.2 Å <sup>3</sup>		
Li-K-	7.83	14.34	6.35	713(0)		
Li-Rb-	7.89	14.65	6.36	735(1)	2.28	2.296g/cm <sup>3</sup>
Li-Tl-	7.88	14.63	6.40	737(8)	3.356	3.353

Systematic absences  $h00$  for  $h$  odd and  $0k0$  for  $k$  odd indicate the space group  $P 2_12_12$ . There are four molecules in the unit cell.

For the Li-NH<sub>4</sub>-salt more accurate Geigercounter measurements were made with monochromized CuK $\alpha$  radiation on crystal specimen shaped to exact cylinders with  $\varnothing = 0.20$  mm.

Absorption can be neglected in this case. Corrections were applied for Lorentz- and polarisation factors.

Throughout the investigation the atomic scattering factors for C, N, O and Li were used as given by HOERNI and IBERS [5]. In the first stages an isotropic correction for the thermal vibration  $e^{-B(\frac{\sin \theta}{\lambda})^2}$  with  $B = 1.7$  was applied to all atoms, obtained by plotting  $|F_0|/|F_c|$  against  $\sin^2 \theta$ .

#### Structure determination

Only projections on (100) and (001) are used in the investigation since the  $b$ -axis is comparatively long.

Patterson projections for the Li-Rb-salt along [001] and [100] show heavy peaks at the positions:

$$\begin{array}{llll}
 u, v : & 0^\circ, 0^\circ & 0^\circ, 180^\circ & 180^\circ, 0^\circ & 180^\circ, 180^\circ \\
 v, w : & 0^\circ, 52^\circ & 0^\circ, \overline{52^\circ} & 180^\circ, 52^\circ & 180^\circ, \overline{52^\circ}
 \end{array}$$

This indicates a distribution of the four Rb-atoms on the two twofold positions, with  $z_1 \cong z_2$ .

In the last stage of Fourier refinement  $z_1$  and  $z_2$  were found to have values of  $\overline{22^\circ}$  and  $\overline{27\frac{1}{2}^\circ}$  respectively.

In the final combination of the two Fourier projections to a spatial model there are two possible ways of combining the Rb-maxima:

$$\begin{array}{ll}
 \text{either} & \text{Rb}_{\text{II}} \text{ in } 2a) 0^\circ 0^\circ z_1 \quad \text{Rb}_{\text{I}} \text{ in } 2b) 0^\circ 180^\circ z_2 \\
 \text{or} & \text{Rb}_{\text{II}} \text{ in } 2a) 0^\circ 0^\circ \overline{z_2} \quad \text{Rb}_{\text{I}} \text{ in } 2b) 0^\circ 180^\circ \overline{z_1}
 \end{array}$$

Only the first appeared to fit in with reasonable distances to the other atoms in the unit cell.

In the (001) projection the Rb-atoms contribute only to the structure factors for which  $h+k=2n$  i.e. one half of the total number.

In the (100) projection the Rb-atoms in principle contribute to all structure factors. However, since  $z_1 \cong z_2$ , their joint contribution is only appreciable for those for which  $k = \text{even}$  i.e. again one half of the total number. The special positions of the Rb-atoms thus prohibit a straightforward application of the heavy atom technique. However, for the (100) projection direct results were obtained from a Patterson shift implying the vector  $0^\circ 0^\circ \rightarrow 180^\circ 52^\circ$  which combines two equivalent Rb-atoms.

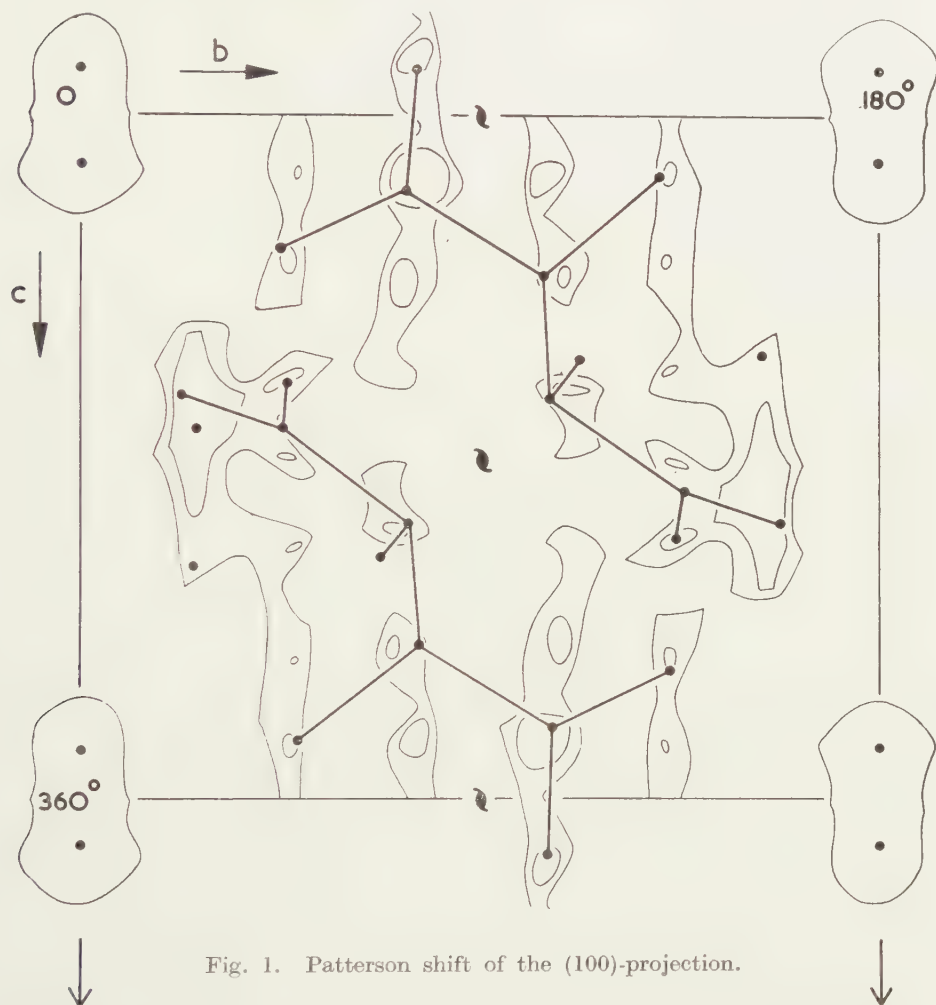


Fig. 1. Patterson shift of the (100)-projection.

In this diagram (fig. 1) it was possible to fit a molecular model, which gave reasonable agreement between calculated and experimental  $0kl$  structure factors.

In the  $x$ -direction the position of the molecule could be estimated with the help of spatial and intensity considerations.

The first refinements of the coordinates of both (100) and (001) projections were carried out for the  $\text{Li-NH}_4\text{-tartrate}\cdot\text{H}_2\text{O}$  with successive Fourier-syntheses and least squares methods.

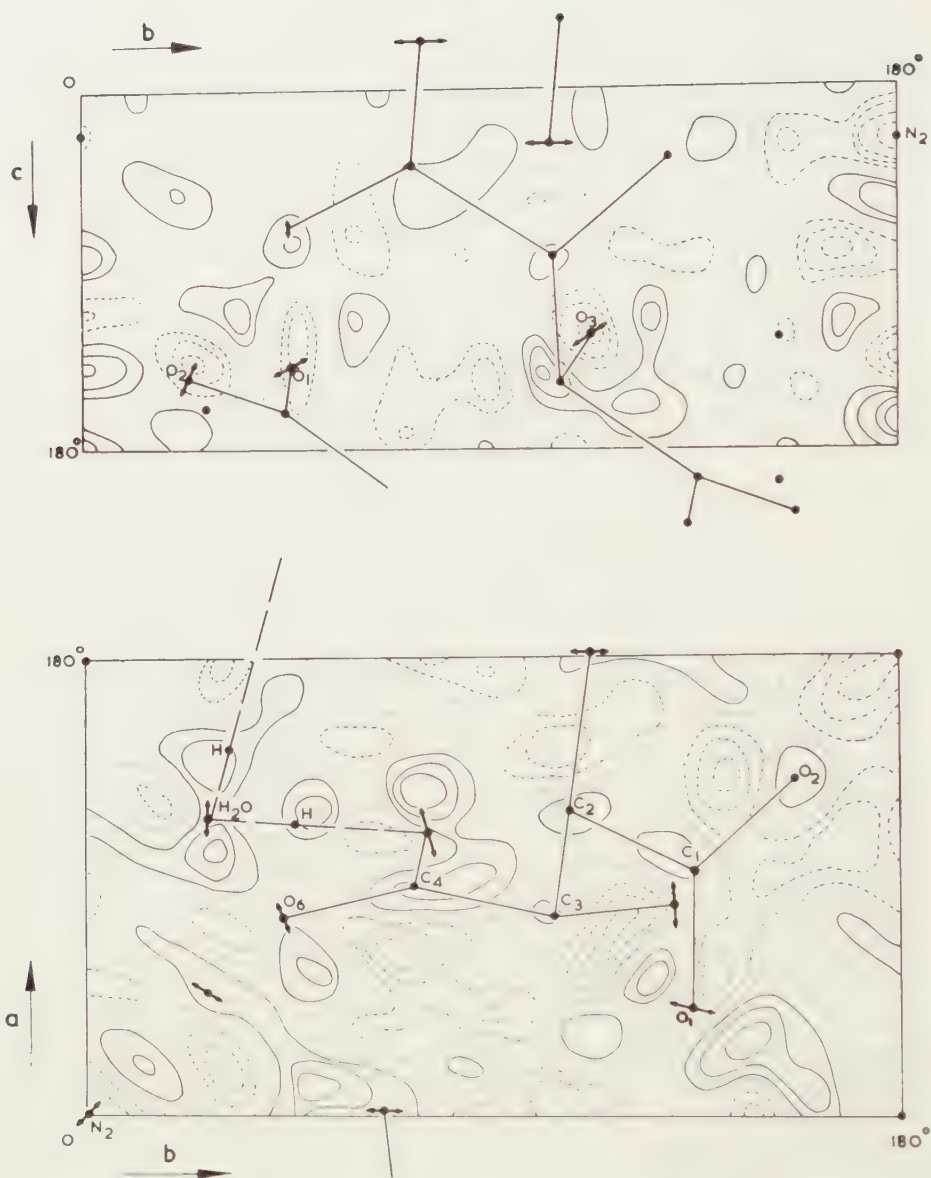


Fig. 2.  $(F_0 - F_c)$  maps of (001) and (100) projections before the introduction of individual heat factors. The anisotropy in heat motion finally arrived at is indicated for the different atoms. The contours are at intervals of  $\frac{1}{4}$  el.  $\text{\AA}^{-2}$ . Negative contours broken.

(Conclusive evidence about the position of the Li-ion could be obtained for the [001] projection from a  $(F_0 - F_c)$  synthesis, using  $F_c$ -values in which the Li-contribution is omitted. The  $z$  coordinate could be fixed initially by spatial considerations.

In these calculations a mean isotropic temperature factor with  $B=1.7$  was applied for all atoms.



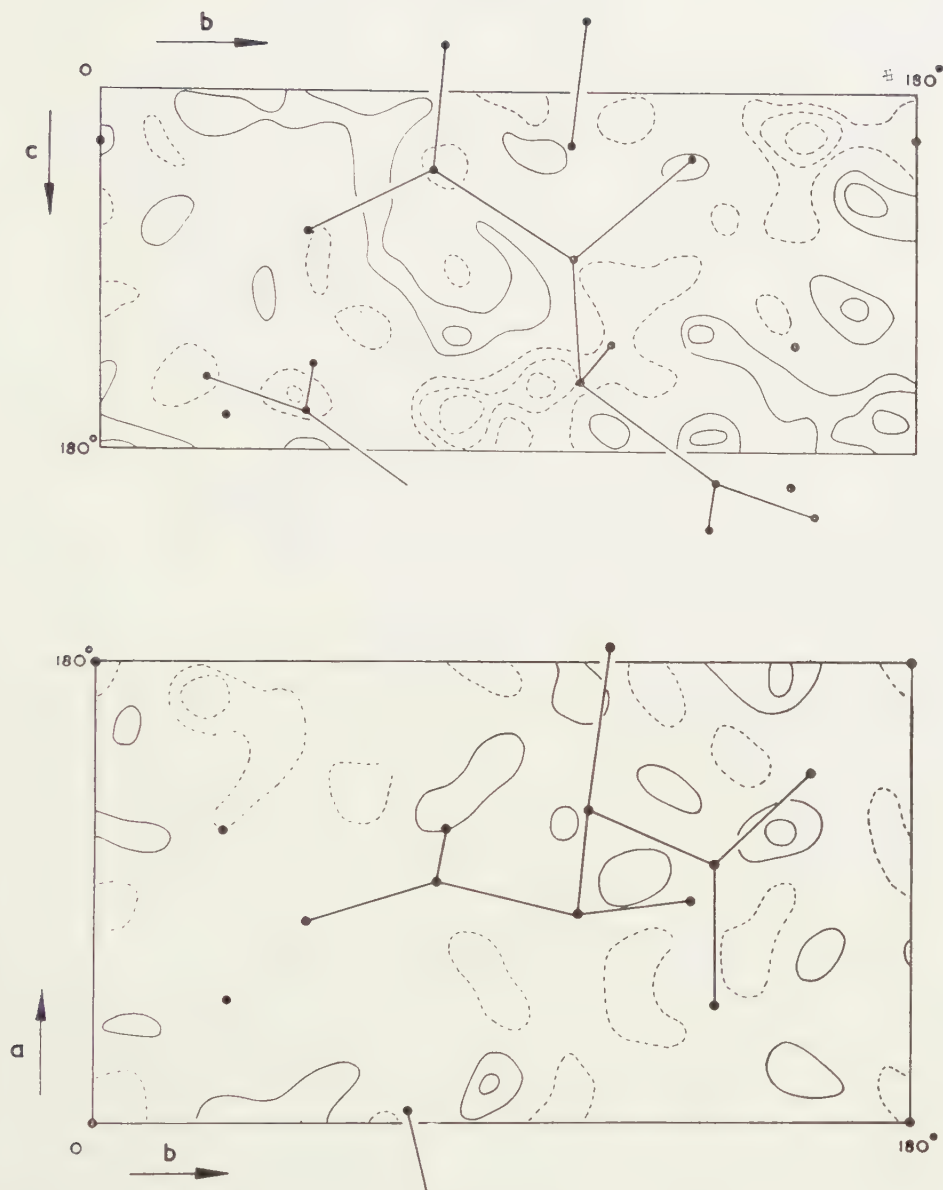


Fig. 3. Final difference-maps. The contours are at intervals of  $\frac{1}{4}$  el.  $\text{\AA}^{-2}$ . Negative contours broken. Zero contour omitted.

The reliability index:

$$R = \frac{\sum ||F_o| - |F_c||}{\sum |F_o|}$$

during this process dropped to 0.15 for the (001) and 0.14 for the (100) projection.

A first difference-synthesis of the (001) projection showed some atomic coordinates not to be correct. Refinement of these coordinates by the

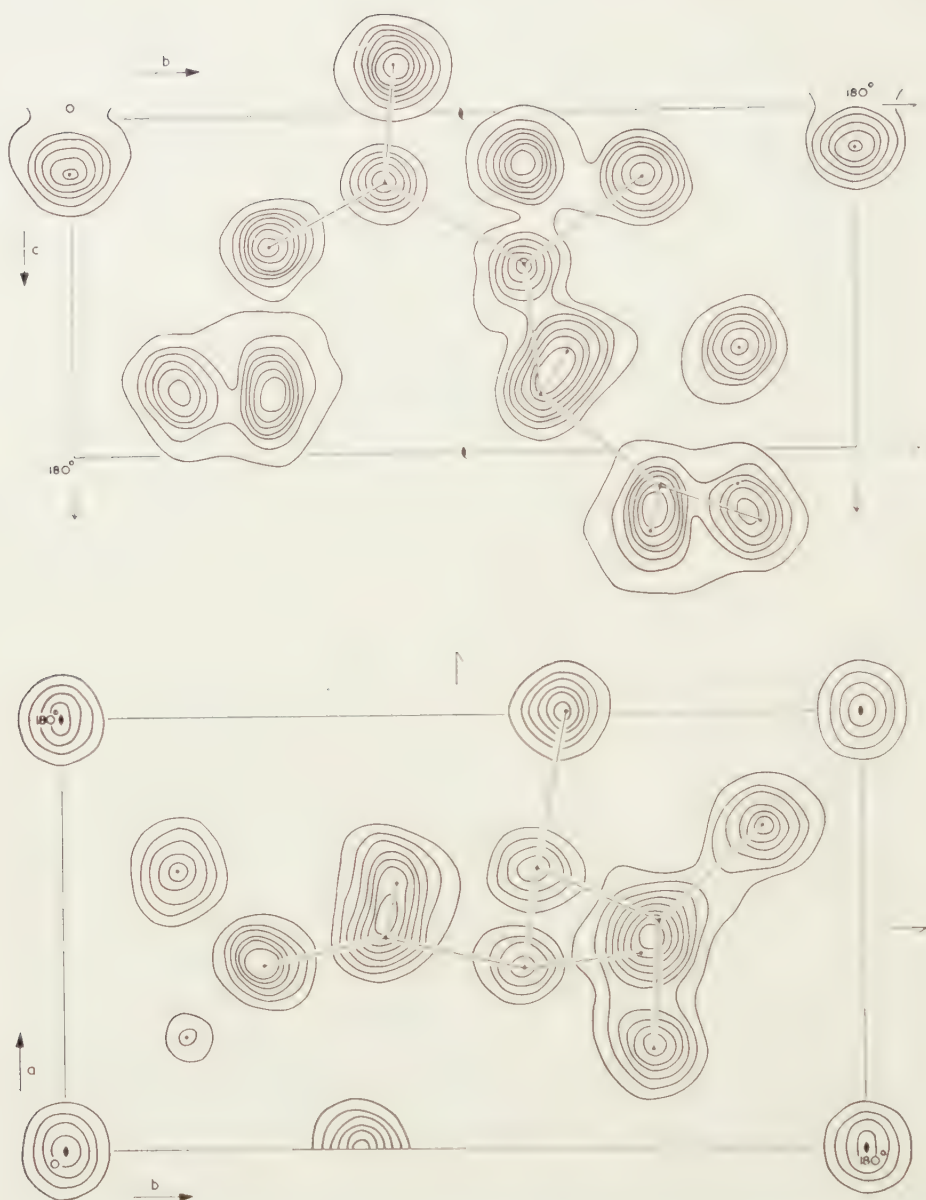


Fig. 4. Electron density of  $\text{Li-NH}_4\text{-Tartrate}\cdot\text{H}_2\text{O}$  projected on (001) and (100).

difference method was carried through until a difference map resulted in which the slopes at atomic centres were nearly zero.

This map also showed certain maxima that could reasonably be ascribed to the presence of hydrogen atoms. Two aliphatic H-atoms were therefore placed at the calculated positions.

The four H-atoms of the  $\text{NH}_4^+$ -groups were assumed to be located in a sphere surrounding the N-atom, though the ordered position with H-atoms

pointing towards neighbouring oxygens could not be rejected with certainty.

For the assumed positions of the hydroxyl-hydrogens from the inner two carbons of the tartrate molecule there is some evidence, though not conclusive.

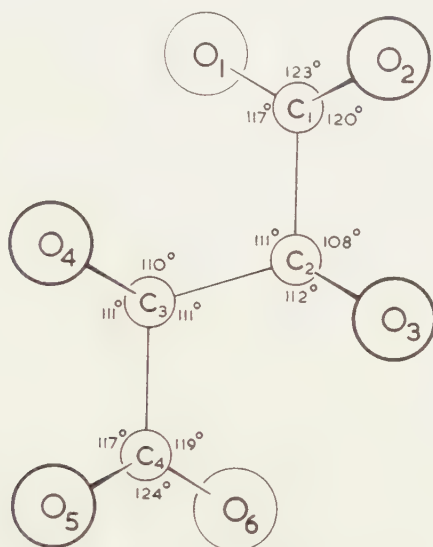


Fig. 5. Tartrate-ion: bond angles.

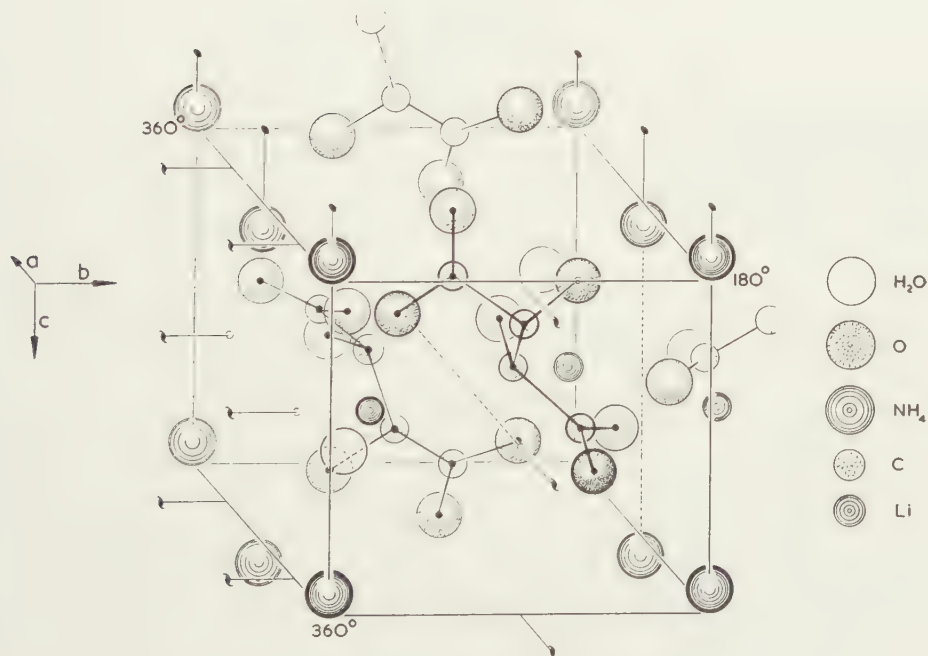


Fig. 6. Structure of  $\text{Li-NH}_4\text{-Tartrate}\cdot\text{H}_2\text{O}$ .

All of these corrections being achieved for both (001) and (100) projections, the  $R$  reduced to 0.11 and 0.13 respectively.

Fig. 2 shows the maps of the  $(F_0 - F_c)$  function at this stage. From these maps it proves to be possible to refine the assumed values of the parameters of thermal vibration of the atoms.

Some atoms e.g. the carbon atoms and  $O_2$  in (001) have a positive maximum at their centre, which points to too great a value of  $B$  used in the calculation of their contribution to the structure factors.

Some other atoms e.g.  $H_2O$ ,  $O_1$ ,  $N_2$  in (001) lie between two opposite maxima and two opposite minima, which indicates an anisotropic vibration with largest amplitude in the direction of the maxima.

TABLE II  
Atomic coordinates

	$x$	$y$	$z$
$C_1$	0.272	0.375	0.444
$C_2$	0.333	0.299	0.414
$C_3$	0.217	0.289	0.226
$C_4$	0.254	0.203	0.106
$O_1$	0.121	0.370	0.379
$O_2$	0.375	0.439	0.392
$O_3$	0.504	0.318	0.356
$O_4$	0.233	0.367	0.099
$O_5$	0.314	0.211	0.074
$O_6$	0.218	0.126	0.192
$H_2O$	0.325	0.074	0.350
Li	0.129	0.078	0.444
$NH_4^I$	0.000	0.500	0.076
$NH_4^{II}$	0.000	0.000	0.061

A superposition of these effects occurs at the atoms  $N_2$   $O_1$   $O_2$   $O_3$  in (100).

In the difference maps of fig. 2 the anisotropic heat motions have been indicated.

The [001] diagram also gives an indication of the position of the two H-atoms of the  $H_2O$ -molecule forming hydrogen bridges with two oxygens of the tartrate molecule, the  $H_2O$  molecule thus turning its electrically negative side to the cations.

The atomic vibrations indicated on the projections are in accordance with an oscillation of the molecule as a whole about the  $C_1$ - $C_4$ -direction i.e. the long axis of the molecule.

In a model this is easily seen.

The effect of these refinements and some succeeding corrections of



TABLE III  
Parameters of thermal vibration of atoms

	(001) projection			(100) projection		
	$\alpha$	$B_{\max.}$	$B_{\min.}$	$\beta$	$B_{\max.}$	$B_{\min.}$
C <sub>1</sub>	113°	1.4	1.2	135°	1.4	1.2
C <sub>2</sub>		1.0	1.0	135°	1.2	1.0
C <sub>3</sub>	23°	1.4	1.2	135°	1.4	1.2
C <sub>4</sub>		1.3	1.3	90°	1.5	1.3
O <sub>1</sub>	113°	3.0	1.5	135°	3.2	1.5
O <sub>2</sub>		1.5	1.5	113°	3.0	1.5
O <sub>3</sub>	90°	2.5	1.1	135°	3.0	2.5
O <sub>4</sub>	0°	3.0	1.5	90°	1.8	1.5
O <sub>5</sub>	23°	3.2	2.6	0°	2.4	1.2
O <sub>6</sub>	23°	2.2	1.2	90°	1.8	1.2
H <sub>2</sub> O	0°	2.8	1.8	90°	3.2	1.8
Li	45°	2.0	1.5		1.7	1.7
NH <sub>4</sub> <sup>I</sup>		1.7	1.7		1.7	1.7
NH <sub>4</sub> <sup>II</sup>	45°	3.0	1.1		2.0	2.0

$\alpha$ : angle between direction of maximum thermal vibration and positive a-axis in the (001) projection.

$\beta$ : angle between direction of maximum thermal vibration and positive b-axis in the (100) projection.

TABLE IV  
Interatomic distances

Intra molecular		Intermolecular			
C <sub>1</sub> — C <sub>2</sub>	1.52 Å	Li — O <sub>6</sub>	1.90 Å	N <sup>I</sup> — O <sub>1</sub>	2.89 Å
C <sub>2</sub> — C <sub>3</sub>	1.52	— O <sub>2</sub>	2.04	— O <sub>4</sub>	2.92
C <sub>3</sub> — C <sub>4</sub>	1.51		2.06	— O <sub>6</sub>	2.98
C <sub>1</sub> — O <sub>1</sub>	1.26	— H <sub>2</sub> O	2.04	— H <sub>2</sub> O	3.25
C <sub>1</sub> — O <sub>2</sub>	1.28	— O <sub>3</sub>	2.22		
C <sub>4</sub> — O <sub>5</sub>	1.26	H <sub>2</sub> O — O <sub>5</sub>	2.68	N <sup>II</sup> — O <sub>4</sub>	2.90
C <sub>4</sub> — O <sub>6</sub>	1.29	— O <sub>1</sub>	3.02	— O <sub>6</sub>	3.00
C <sub>2</sub> — O <sub>3</sub>	1.43	O <sub>1</sub> — O <sub>3</sub> '	2.91	— O <sub>2</sub>	3.20
C <sub>3</sub> — O <sub>4</sub>	1.41	O <sub>2</sub> — O <sub>2</sub> '	2.66	— O <sub>3</sub>	3.27

minor importance, is seen in the final difference maps, given in fig. 3.

The reliability index has now been reduced to 0.08 for the (001) and 0.09 for the (100) projection.

In the (001) projection there is the less serious overlap of atoms.

Table II shows the final atomic coordinates and the parameters of thermal vibration are listed in table III.

Fig. 4 presents the electron densities of Li-NH<sub>4</sub>-tartrate·H<sub>2</sub>O projected on (001) and (100).

The shape of the tartrate molecule is essentially the same as in Rochelle-salt. The values of interatomic distances and bond angles are given in table IV and fig. 5.

Fig. 6 shows the coordinates of atoms in a spatial model.

Full particulars will be given in a forthcoming thesis.

Recently a few results of an X-ray analysis of  $\text{Li} \cdot \text{NH}_4\text{-tartrate} \cdot \text{H}_2\text{O}$  by VERNON and PEPINSKY [6] came to our notice from a very brief account of their investigation [7].

The results of the two investigations seem to agree except for details. A comparison between the two investigations has not yet been made.

*Laboratorium voor Kristalchemie  
der Rijks Universiteit, Utrecht*

#### REFERENCES

1. Proc. Kon. Ned. Akad. Wetenschappen **B 57**, 524-528 (1954).
2. MATTHIAS, B. T. and J. K. HULM, Phys. Rev. **82**, 108 (1951). W. J. MERZ, Phys. Rev. **82**, 562 (1951).
3. COCHRAN, W., Acta Cryst. **4**, 81-92 (1951); **4**, 408-411 (1951).
4. GROTH, P., Chemische Krystallographie III, 331.
5. HOERNI, J. and J. IBERS, Acta Cryst. **7**, 744 (1954).
6. VERNON, R. C. and R. PEPINSKY, "Structure determination of  $\text{LiNH}_4$  Tartrate.  $\text{H}_2\text{O}$ ". Program and Abstracts, American Crystallographic Association, Camp Tamiment, Pa. June 18, 1952. "X-ray Analysis of  $\text{LiNH}_4\text{-Tartrate} \cdot \text{H}_2\text{O}$  and  $\text{LiRb Tartrate} \cdot \text{H}_2\text{O}$ ". Final Report, Contract DA-36-039-SC-21, Signal Corps Engineering Laboratories, January, 1953.
7. SHIRANE, G., F. JONA and R. PEPINSKY, Some Aspects of Ferroelectricity (June 30, 1955).

## BIOCHEMISTRY

### OVER DE INVLOED VAN HETERO-AUXINE OP BIOCHEMISCHE PROCESSEN IN DE KIEMPLANT VAN *AVENA SATIVA*

DOOR

F. KÖGL

(mede namens I. MULDER)

(Communicated at the meeting of February 25, 1956)

Door het pionierswerk van F. W. WENT [1] werd in 1928 de mogelijkheid geschapen, het bij de strekking der plantencellen werkzame stoffelijke principe chemisch te onderzoeken. In de jaren 1931 tot 1934 konden in het Utrechtse [2] laboratorium de groeistoffen auxine-a, auxine-b en hetero-auxine in gekristalliseerde vorm worden geïsoleerd. De laatstgenoemde verbinding bleek identiek te zijn met het synthetisch gemakkelijk te bereiden  $\beta$ -indolyl-azijnzuur en hiermede werden dan ook in het vervolg overal ter wereld de betreffende groeiverschijnselen onderzocht. Aangezien ook vele analoga van het indol-azijnzuur in het laboratorium resp. in de praktijk groeistof-achtige eigenschappen toonden, is als het ware een "*planten-pharmacologie*" ontstaan, wat voor het begrip van de normale *physiologische* verschijnselen niet evenredig van nut bleek.

Het is een algemeen kenmerk van de hedendaagse biochemie, dat men het begrip van de "werkingsmechanismen" als het belangrijkste doel beschouwt. Ofschoon hetero-auxine, het indol-3-azijnzuur, nu bijna een kwart eeuw overal ter wereld als groeistof ter beschikking staat, is het merkwaardig dat ook na deze lange tijd de kardinale vraag, op welke wijze deze groeistof de strekking van de plantencel katalyseert, nog steeds niet algemeen bevredigend kan worden beantwoord. Het is niet mogelijk hier de uitgebreide plantenphysiologische literatuur [3] over dit probleem ook maar enigszins volledig te refereren. Sinds F. W. WENT in 1928 de primaire werking van de groeistof in een verhoging van de plasticiteit van de celmembraan zag, werd uiteraard getracht de groeistofwerking door verhoging van de osmotische waarde of door "anomale osmose" te verklaren, echter zonder positief eindresultaat. Volgens een recente theorie van R. J. GOLDAKRE [4, 3] zou de aan de celstrekking inherente *wateropneming* via de plasma-eiwitten tot stand komen, die zich door bemiddeling van de "groeistof" met water zouden beladen, dat dan door de protoplasmastroming aan de vacuolen zou worden afgestaan. Een zeer concrete bijdrage tot het probleem werd door de fraaie electronen-microscopische onderzoeken van FREY-WYSSLING en MÜHLETHALER [5] geleverd.

Amerikaanse werkgroepen, vooral die van THIMANN [6] en BONNER [7]

hebben op grond van hun experimenten geconcludeerd dat de groeistoffen via de *ademhaling* werken. Tegen hun experimentele techniek werd ingebracht [3] dat de toegepaste concentraties aan indol-azijnzuur 100 tot 1000 maal groter zijn dan het natieve groeistofgehalte van het *Avena-coleoptiel* en dat bovendien het plaatsen van weefselstukjes in groeistofoplossingen heel andere condities schept dan bij de groei van intacte planten optreden.

Een raadsel op zichzelf is het feit dat de groei van de *wortel* geremd wordt bij een auxine-concentratie, die de groei van de *spruit* bevordert. Dit verschijnsel is volgens BOYSEN JENSEN [8] door de grotere gevoeligheid van de wortel te verklaren en inderdaad konden GEIGER-HUBER [9] en BURLET een dienovereenkomstig optimum van de groeistofwerking bij worteltoppen constateren.

Wat na een kwart eeuw groeistofonderzoek opvalt, is het feit dat tot nu toe niet eens bij *Avena*, het gewillige donkere-kamer plantje van de botanici, een systematisch analytisch-chemisch onderzoek van de gehele plant werd verricht. Het leek mogelijk dat onder invloed van auxinen — b.v. in de celwand — chemische veranderingen optreden, welke een nieuw licht op het vraagstuk zouden kunnen werpen.

Het lag voor de hand dat wij met de ons sinds 25 jaar welvertrouwde haverplantjes moesten werken, zoals deze voor de Went'se test worden gebruikt. Ook voor de toediening van de groeistof konden wij aanknopen aan vroegere ervaringen [2]. In 1934 hebben wij voor het eerst haverkorreltjes op zeer verdunde oplossingen van gekristalliseerd auxine-a resp. van hetero-auxine laten kiemen. Hierbij ontstonden planten met korte en verdikte, rijkelijk met haren bezette wortels.

Wij hebben ons tot taak gesteld te onderzoeken of deze wortels, die "te veel van het goede" gekregen hadden, ook *chemisch* verschillen van even oude normale wortels.

*Kweek.* Svalöf's "Siegeshafer" werd gedurende drie dagen in het donker bij 25° op gedestilleerd water gekweekt, dat de volgende zouten bevatte:

CaCl <sub>2</sub>	10 <sup>-3</sup> m	K <sub>2</sub> HPO <sub>4</sub>	6.10 <sup>-4</sup> m
MgSO <sub>4</sub>	2,5.10 <sup>-4</sup> m	KH <sub>2</sub> PO <sub>4</sub>	4.10 <sup>-4</sup> m
KNO <sub>3</sub>	5.10 <sup>-4</sup> m	[p <sub>H</sub> =6,1]	

Bij de "remproeven" bevatte deze oplossing van de voedingszouten bovendien 5.10<sup>-8</sup> g hetero-auxine pro ml. Deze concentratie geeft bij de Went'se test 10° kromming. Zij is dus groeibevorderend bij het coleoptiel, terwijl hiermede bij de wortel reeds een sterke remming optreedt.

In porceleinen bakken waren glazen rekjes met hydrophiel gaas bespannen; hierop lagen de korrels, en wel 500 pro bak. In der loop van het onderzoek werden op deze wijze circa 74.000 haverplantjes gekweekt. Aanvankelijk hadden wij veel teleurstellingen bij de proeven met hetero-auxine. Series met goed geremde wortels wisselden af met series die geen of slechts een geringe remwerking toonden. De oorzaak bleken bacteriële



infecties te zijn. Wij konden uit de betreffende cultures een *Pseudomonas*-soort (*P. dacunhae*?) isoleren, die het indol-azijnzuur van de voedingszout-oplossing reeds na korte tijd vernietigt. Sterilisatie van de voorwerpen etc. mocht niet baten. De moeilijkheid werd eerst verholpen toen wij aan de cultures bovendien  $5.10^{-5}$  g penicilline-G (Na-zout) pro ml toevoegden. Natuurlijk hebben wij ons ervan overtuigd, dat deze penicilline-concentratie noch op de groei van de plantjes noch op de wortelremming door hetero-auxine van invloed is. Overigens dient nog te worden vermeld dat de cultuurvloeistof dagelijks verversst werd.

Na de oogst hebben wij wortel, korrel en spruit gescheiden, alles grondig afgespoeld, het gewicht van het *vers* materiaal en, na volledig drogen en malen, dat van de *droge* producten bepaald. Deze werden dan achtereenvolgens met aether, koud water en heet water geëxtraheerd. Het verenigde waterextract wordt in het vervolg als "oplosbaar gedeelte" aangeduid, het onoplosbare residu kan practisch als *celwand-materiaal* worden beschouwd. Om voor de vergelijkende analyses over gelijkmatig materiaal te kunnen beschikken, werden de betreffende fracties uit 5900 normale resp. 8375 geremde plantjes "gepooled".

#### Gewichten

(Normale gewichten = 100% gesteld)

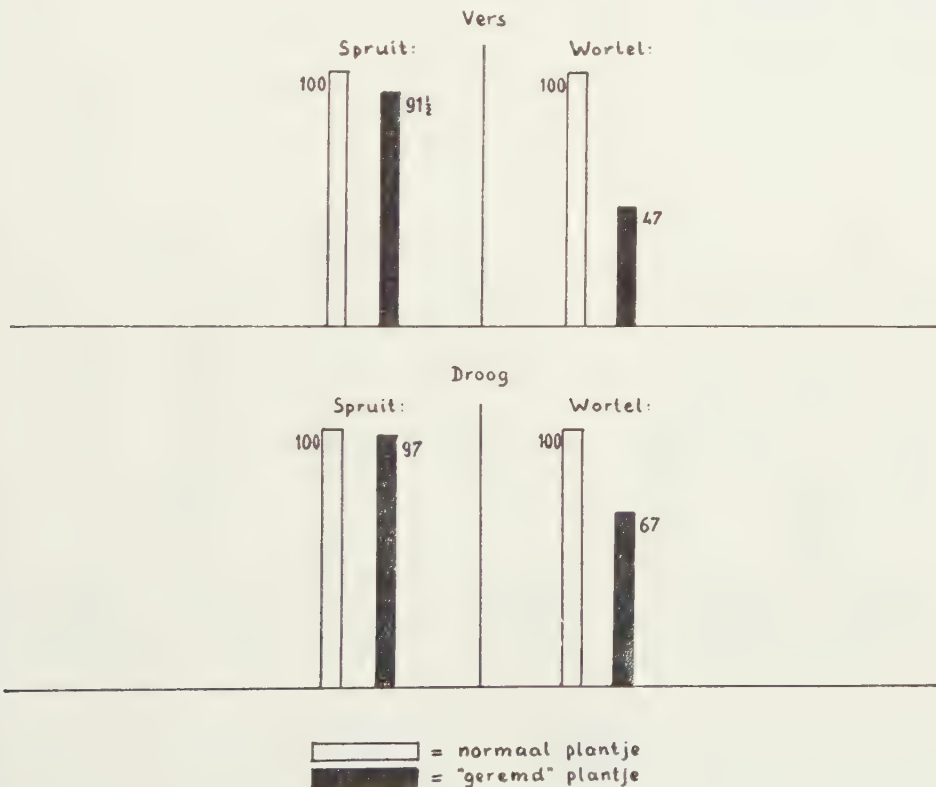


Fig. 1.

*Analytische methoden.* De toegepaste analytische methoden zijn in het volgende overzicht kort vermeld:

a) *Vrije suikers*  
volgens M. SOMOGYI [10].

b) *Polysacchariden*

*Celwand*-materiaal met 2-proc.  $H_2SO_4$  18 uur bij 95° in toegesmolten buisjes gehydrolyseerd. Bouwstenen van *hemicellulosen* (galactose, glucose, arabinose en xylose) papierchromatografisch gescheiden en na elutie van de betr. zônes eveneens volgens SOMOGYI bepaald.

*Cellulose*: Residu van voorgaande hydrolyse na behandeling met 80-proc.  $H_2SO_4$  ( $3\frac{1}{2}$  uur, K.-temp.) tot 8-proc.  $H_2SO_4$  verdund en 100 min. in toegesmolten buisjes op 100° verhit. Glucose-bep. volgens SOMOGYI.

c) *Pectine*

Semi-micro-uronzuur-bepaling, gebaseerd op de methode van TOLLENS en LEFÈVRE [11].

d) *Vrije aminozuren en eiwit*

Kjeldahl-bepalingen en kwalitatieve papierchromatografie voor en na hydrolyse.

#### Celwand

(Totaal = 100%; hiervan koolhydraten:)

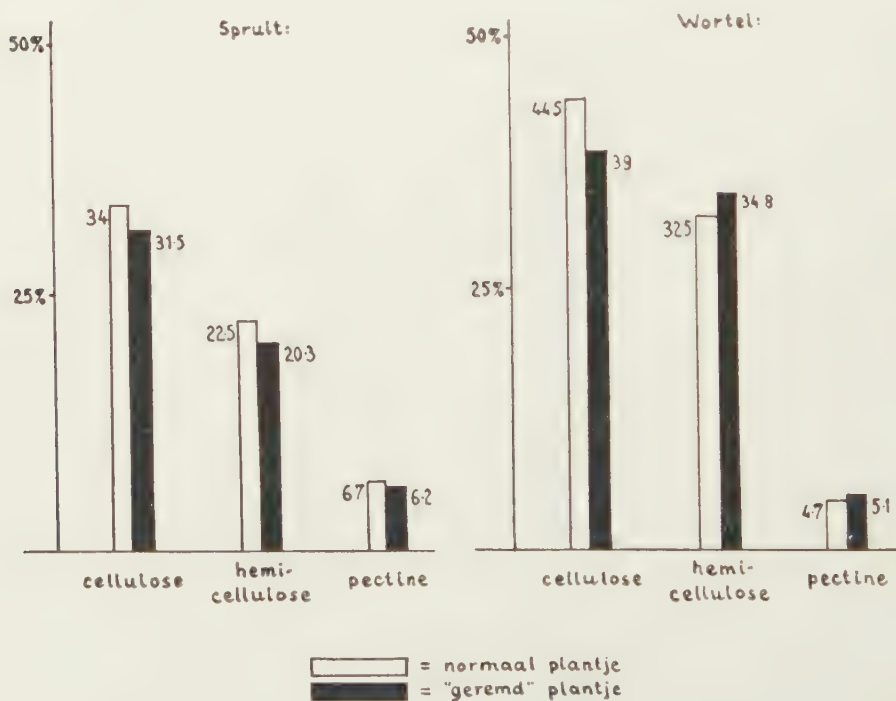


Fig. 2.

Samenstelling hemicellulosen  
(In %)

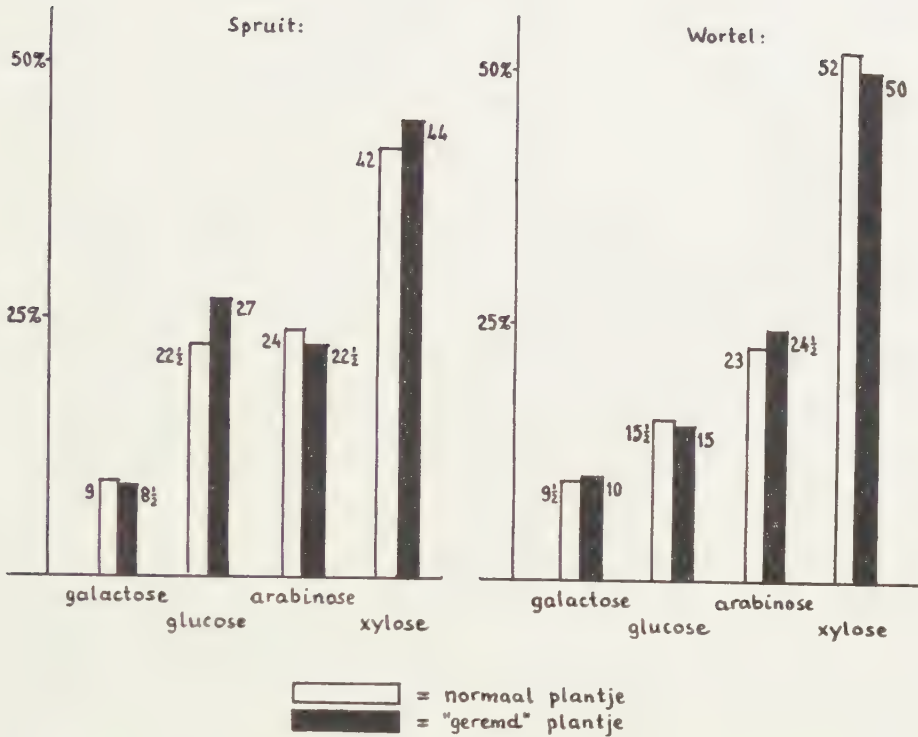


Fig. 3.

e) *Asrest*, *Ca*- en *Mg*-bepaling

Titratie met complexon III, murexide (voor  $\text{Ca}^{++}$ ) resp. eriochroom-zwart T (voor  $\text{Ca}^{++} + \text{Mg}^{++}$ ) als indicatoren [12]; omslagpunt m.b.v. foto-electrische colorimeter bepaald.

*Resultaten.* Uiteraard schuilen de resultaten in een vloed van analyse-getallen. Om er niettemin een overzichtelijke indruk van te geven, zal van graphieken gebruik worden gemaakt. In de regel zijn de waarden bij spruit resp. wortel van de *normale* plant gelijkgesteld aan 100 %.

a) *Watergehalte.* Fig. 1 toont de invloed van hetero-auxine op het watergehalte van spruit en wortel:

Zoals uit een vergelijking van de gewichten van het verse en het gedroogde materiaal blijkt, wordt bij onze proefomstandigheden het watergehalte — vooral bij de wortel — nog sterker gereduceerd dan de droge stof.

b) *Celwand.* Kijken wij nu naar de percentages van de verschillende koolhydraten in de celwand (Fig. 2), dan blijkt ten eerste dat de som van de percentages cellulose, hemicellulose en pectine bij de spruit ca. 60 % bij de wortel ca. 80 % bedraagt. Dit verschil zal natuurlijk met de uiteenlopende biologische functies verband houden. Wat de invloed van hetero-

auxine betreft, treden bij onze proefplanten wel kleine verschillen op. Wij willen echter uit dergelijke geringe veranderingen voorlopig geen conclusie trekken. Vermeld zij hier alleen dat het N-gehalte der celwand van de geremde wortel relatief verhoogd is (120 %); overigens werden t.o.v. aminozuren etc. geen bijzondere verschillen geconstateerd. Voor onze algemene verkenning van het gebied hebben wij bijzondere aandacht besteed aan de samenstelling van de *hemicellulose*- en *pectine*-fracties. Theoretisch was natuurlijk ook bij de biosynthese van de hemicellulosen een groeistofeffect denkbaar.

Fig. 3 geeft een beeld van de kwalitatieve en kwantitatieve samenstelling van de *hemicellulose*-fracties. De onderlinge verhouding van de vier bouwstenen, vooral de dominerende rol van xylose, is wel instructief. Wat de invloed van hetero-auxine betreft willen wij ook hier uit de kleine verschillen geen conclusies trekken.

c) *Pectinen*. Bij de samenstelling van de celwand (Fig. 2) hebben wij ook ten opzichte van *pectine* geen opvallende verschillen gezien. Nu is echter een deel van de pectinen in water oplosbaar; men verkrijgt dit

#### Pectinen

(In % van totaal droog materiaal)

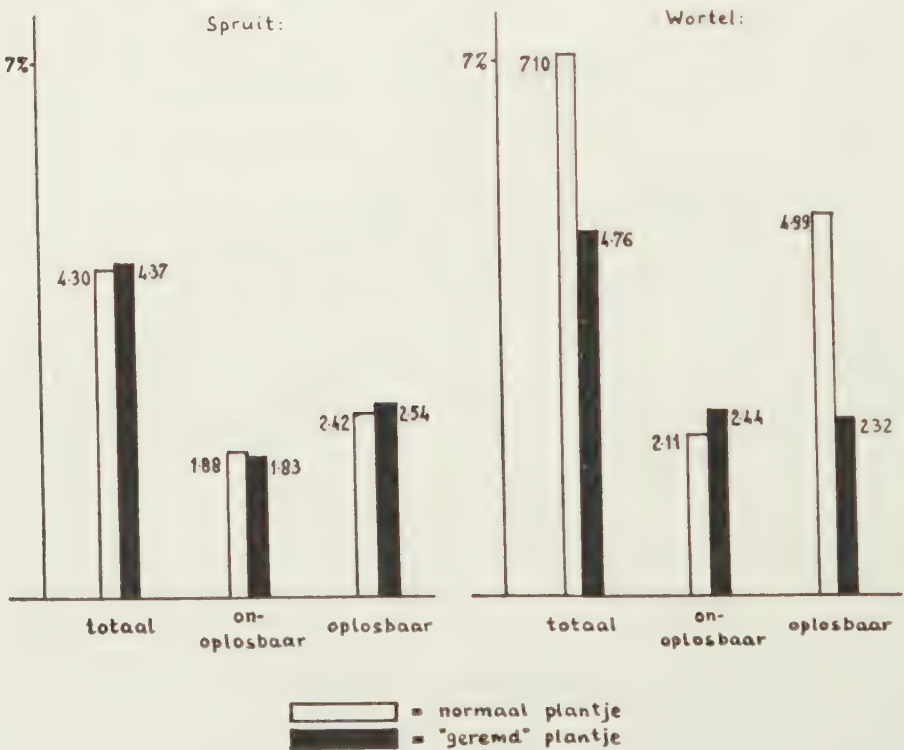


Fig. 4.



## Veranderingen van enige componenten in verband gezien

(Alle normale waarden = 100% gesteld)

## Totale gehalten

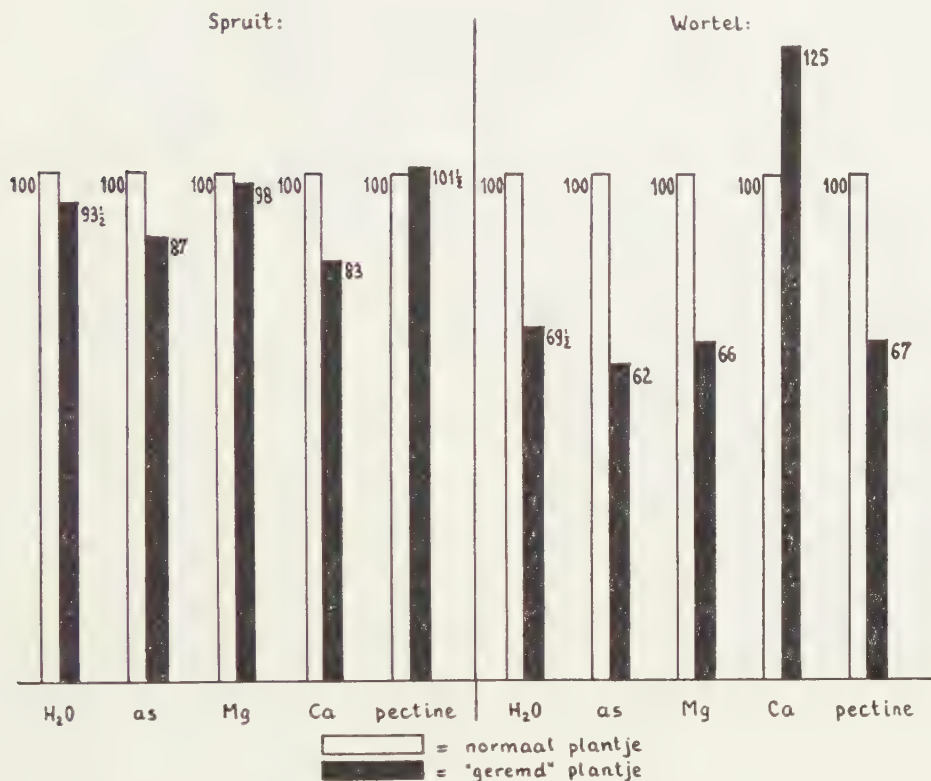


Fig. 5.

percentage door het pectine-gehalte van de "celwand" in mindering te brengen van het pectine-gehalte van het totale droge materiaal.

Uit Fig. 4 blijkt, dat de pectine-waarden van de normale *spruit* en de *spruit* van het geremde plantje praktisch gelijk zijn. Zeer opvallend zijn daarentegen de bij de *wortel* optredende verschillen. Men ziet dat het totale pectine-gehalte bij de geremde *wortel* van 7.1 tot 4.8 % verminderd is en verder, dat deze differentie geheel op rekening van het *oplosbare* pectine van de geremde *wortel* komt! Dit op zichzelf al interessante feit heeft door de nu te bespreken gegevens over het Ca<sup>++</sup>- en het Mg<sup>++</sup>-gehalte van onze proefplanten o.i. nog meer betekenis verkregen.

Zoals Fig. 5 toont, zakt de asrest bij de *spruit* tot 87 % en bij de *wortel* zelfs tot 62 %, indien wij de resp. waarden van de normale plant gelijk 100 % stellen. Het staat natuurlijk op ons programma, de afzonderlijke bestanddelen van de as-monsters quantitatief te bepalen. Tot nu toe hebben wij ons in dat opzicht beperkt tot de bepaling van de calcium- en magnesiumpercentages. Bij deze keuze lieten wij ons vooral leiden door de reeds lang bekende relaties tussen calcium en pectine en verder ook door de

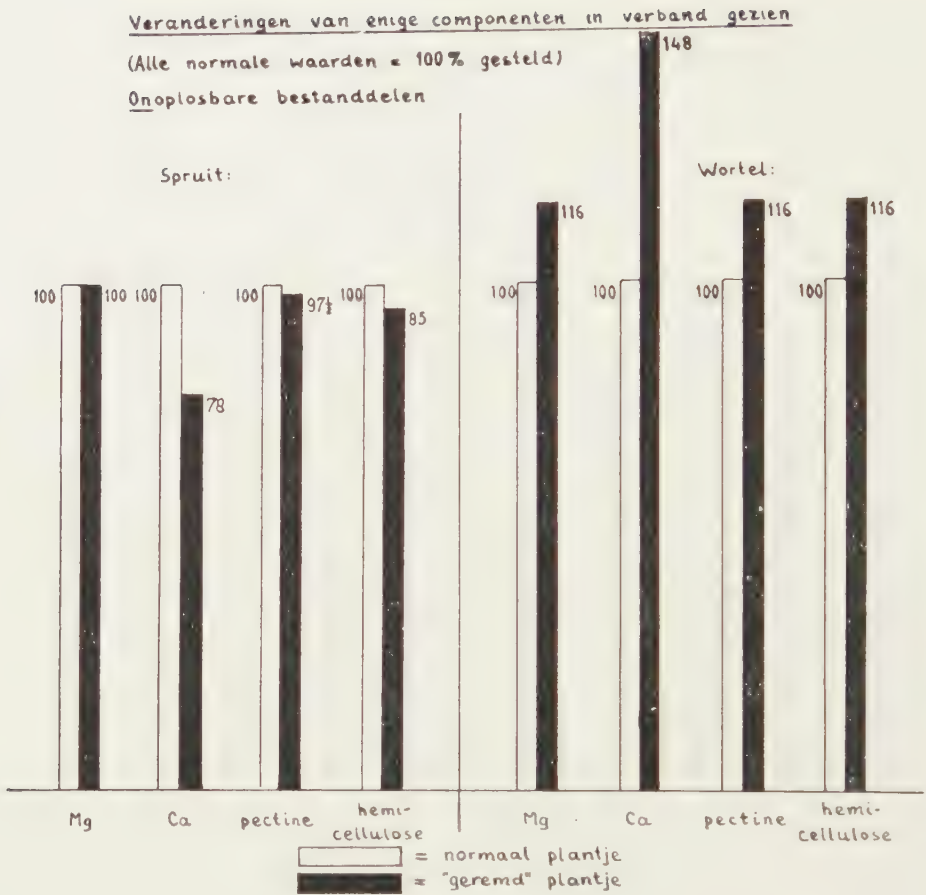


Fig. 6.

in de botanische literatuur — vooral door H. BURSTRÖM [13] — gepostuleerde invloed van calciumionen op de auxine-werking.

Onze  $\text{Ca}^{++}$ - en  $\text{Mg}^{++}$ -bepalingen leidden tot verrassende resultaten. Wij dienen ons vooraf te realiseren dat onze proefplanten in de voedingszout-oplossing een dusdanig aanbod aan  $\text{Ca}^{++}$ - en  $\text{Mg}^{++}$ -ionen hebben, dat de door de wortels opgenomen hoeveelheden slechts een te verwaarlozen vermindering betekenen.

Fig. 5 doet op overtuigende wijze uitkomen dat bij de geremde wortel de relatieve percentages van water, asrest, magnesium en pectine vrijwel op hetzelfde niveau van omstreeks 65 % gezakt zijn, zulks zeer in tegenstelling tot de verhoging van het  $\text{Ca}^{++}$ -percentage van de wortel tot 125%! Overigens is het  $\text{Ca}^{++}$ -percentage van de bijbehorende spruit tot 83% teruggelopen.

Fig. 6 laat zien dat de celwand van de geremde wortel, naast een gelijkmatige verhoging van  $\text{Mg}^{++}$ , pectine en hemicellulosen tot 116%, door de bijzonder hoge  $\text{Ca}^{++}$ -waarde van 148% gekenmerkt is.

Veranderingen van enige componenten in verband gezien

(Alle normale waarden = 100% gesteld)

Oplosbare bestanddelen

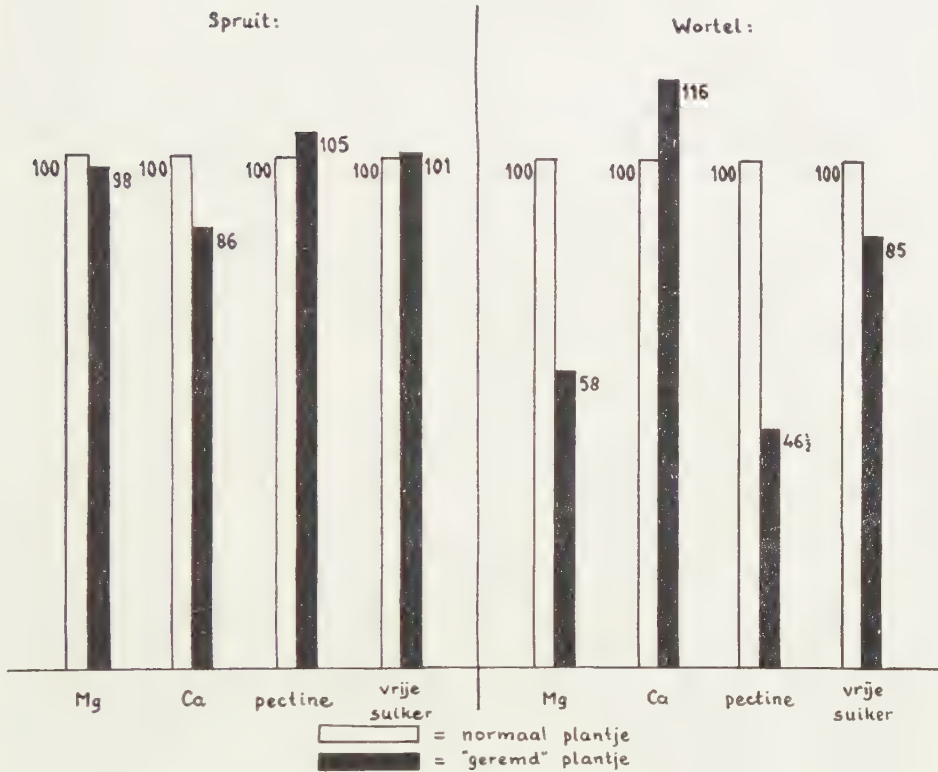


Fig. 7.

In tegenstelling hiertoe zien wij bij het oplosbare gedeelte (Fig. 7) een sterke verlaging van de  $Mg^{++}$ - en de pectine-percentages.

Hier moge nog worden vermeld dat Dr. E. F. DRION van het T.N.O. Instituut "Bewerking Waarnemingsuitkomsten" op ons verzoek de resultaten statistisch beoordeeld heeft. De door ons als belangrijk geachte verschillen zijn significant.

*Conclusies.* Bij de opzet van onze proeven was het niet de bedoeling een bepaalde theorie te toetsen. Wij wilden bij een goed gedefinieerde werking van hetero-auxine naar een invloed op biochemische processen zoeken. Voor het door ons gekozen extreem, de wortelremming, zijn inderdaad nieuwe experimentele feiten aan het licht gekomen. Het ligt voor de hand, bij de geremde wortel een verband te zien tussen de verhoogde calcium-afzetting in de celwand en de vermindering van de *permeabiliteit*, die vooral in een sterke verlaging van het watergehalte tot uiting komt. Terwijl de waarschijnlijk in de poriën van de celwand afgezette  $Ca^{++}$ -ionen — gezien de verhoging van het  $Ca^{++}$ -gehalte in het oplosbare gedeelte — bijwijze van een "turnover" nog verder kunnen

opschuiven, blijken zij een blokkade te vormen voor de overige minerale bestanddelen. Dit valt te concluderen uit de vermindering van het totale asgehalte en in het bijzonder uit de *inverse* betrekking tussen  $\text{Ca}^{++}$ - en  $\text{Mg}^{++}$ -ionen.

Het meest frappeert wel de nauwe correlatie tussen *magnesium* en de *pectinen*. De veranderingen van de relatieve percentages liepen bij beide bestanddelen steeds parallel, in de regel omlaag; alleen in de onoplosbare fractie (Fig. 9) zijn beide percentages evenveel verhoogd.

Helaas is over de *biosynthese van pectinen* en de daarbij werkzame enzymen nog nauwelijks iets bekend. Daarentegen weet men dat *magnesium* bij tal van enzymen een essentiële functie als *co-factor* uitoefent. Hiertoe behoren enzymen die rechtstreeks bij de koolhydraat stofwisseling betrokken zijn, zoals b.v. hexokinase en phospho-gluco-mutase en verder ook phosphatasen en andere enzymen die bij de ademhalingsketen een rol spelen. Er tekent zich dus een verband af tussen groeistofwerking en enzymatische processen. Natuurlijk is het beeld nog vaag, maar men ziet nu toch een concrete mogelijkheid hoe permeabiliteitsverschijnselen, membraan-evenwichten en algemeen het transport als tussenschakels in de lange keten der groei-regulatie kunnen fungeren.

De hier aangeduide ontwikkeling van het probleem laat uiteraard vele vragen open, doch deze zullen ten dele experimenteel te benaderen zijn. Natuurlijk zal het heel moeilijk worden om bij *positieve* groei-verschijnselen soortgelijke analyses uit te voeren als hier bij het extreme geval van de wortelremming gebeurd is. De veronderstelling, dat b.v. *optimale* auxine-concentraties een verlaging van het  $\text{Ca}^{++}$ -gehalte en daarmee een verhoging van de permeabiliteit veroorzaken, is vooralsnog slechts een werkhypothese.

Indien men concluderen wil dat onze experimentele resultaten bij pathologische planten verkregen zijn en dus weinig bijdragen tot het begrijpen der fysiologische verschijnselen, dan zou deze zienswijze zeker niet juist zijn. Ten eerste is de toegepaste concentratie aan hetero-auxine voor de *spruit* fysiologisch. Bovendien zijn wij nagegaan in hoeverre onze geremde plantjes *levensvatbaar* zijn. Te dien einde werd bij de dagelijkse verversing van de cultuur-vloeistof na afloop van de drie "remdagen" het hetero-auxine weggelaten. Het bleek dat dan reeds op de volgende dag nieuwe wortels groeien en op de 10e dag heeft men al moeite om te zien of de oorspronkelijk geremde planten nog verschillen van de contrôles. De door ons onderzochte wortelremming is dus zeker geen studie aan een letaal veranderd plantenmateriaal.

### Summary

A study was made of the effect of heteroauxin (3-indole-acetic acid) on biochemical processes in oat seedlings. Etiolated seedlings of *Avena sativa* (Svalöfs "Victory Oats") were grown during three days at 25° C on a solution of several mineral salts in distilled water. When heteroauxin ( $5 \cdot 10^{-8}$  g per ml) was added to the solution, the roots of the plants



became short and thick, whereas in the sprouts no visible changes occurred. Bacterial inactivation of growth substance was prevented by adding the sodium salt of penicillin G ( $5.10^{-5}$  g per ml) to the culture solution, the solution being changed daily. Chemical differences were looked for between normal seedlings and such with "inhibited" roots. A quantitative determination was therefore made of free sugar, the hemicellulose components (galactose, glucose, arabinose and xylose), cellulose, pectin, nitrogen, ash, calcium and magnesium; free amino acids and proteins were only examined qualitatively.

As expected, the sprouts did not show any significant difference. The "inhibited" roots had a fresh weight of only 47 % and a dry weight of 67 % of that of the normal roots, so the water content is also relatively reduced. Moreover, the most important result seems to be the analogy between the decrease in water, ash, magnesium and pectin content of the "inhibited" root, whereas the calcium content is increased. The decrease in pectin appears principally to be due to the soluble part of it and in this case too, is coupled with a strong reduction of soluble magnesium. The rise in calcium is caused by a strongly increased deposition in the cell wall.

The experimental results lead to the assumption that hetero-auxin effects primarily a deposition of calcium in the cell membranes and that in this way the permeability of the root is lowered. The resulting decrease in magnesium content may lower the activity of several enzymes which need  $Mg^{++}$  as a co-factor. Perhaps the relation with pectin biosynthesis could be found in this direction. Of course the results are not appropriate to draw conclusions with regard to the growth *promotion* by the auxins. Nevertheless it may be seen how permeability, membrane equilibria and generally the transport could act as links in the long chain of growth-regulating processes.

#### LITERATUUR

1. WENT, F. W., Recueil Trav. bot. néerl. **25**, 1 (1928).
2. KÖGL, F., A. J. HAAGEN SMIT en H. ERXLEBEN, zie o.a. Proc. Kon. Akad. Wet. **35**, 1 (1931); Z. physiol. Chem. **214**, 241 (1933); **215**, 215 (1934); **228**, 89 (1934); **228**, 104 (1934).
3. Zie o.a. E. POHL, Naturwiss. **41**, 392, 414 (1954).
4. GOLDACRE, R. J., Intern. Rev. Cytol. **1**, 135 (1952).
5. MÜHLETHALER, K., Ber. schweiz. bot. Ges. **60**, 614 (1950).
6. HACKETT, D. P. en K. V. THIMANN, Amer. J. Bot. **40**, 183 (1953) en vroegere mededelingen.
7. BONNER, J., Am. J. Bot. **36**, 429 (1949).
8. BOYSEN-JENSEN, P., Kgl. Danske Vidensk. Selsk., biol. Med. **13**, 1 (1936).
9. GEIGER-HUBER, M. en E. BURLET, Jb. wiss. Bot. **84**, 231 (1937).
10. SOMOGYI, M., J. Biol. Chem. **160**, 61 (1945).
11. LEFÈVRE, K. U. en B. TOLLENS, Ber. **40**, 4513 (1907); zie ook G. G. MAHER: Anal. Chem. **21**, 1142 (1949).
12. SCHWARZENBACH, G., E. KAMPITSCH en R. STEINER, Helv. chim. Acta **28**, 828 (1945).
13. BURSTRÖM, H., Physiol. Plantarum **5**, 391 (1952).

# STRUCTURE OF HETEROCYCLIC MOLECULES CONTAINING NITROGEN

## III. ON THE CONFIGURATION OF NITROGEN IN CONJUGATED SYSTEMS

BY

H. F. HAMEKA AND A. M. LIQUORI <sup>1)</sup>

(Communicated by Prof. J. J. HERMANS at the meeting of March 24, 1956)

### 1. Introduction

The high accuracy which has been achieved in the measurement of bond angles and bond distances of aromatic molecules by careful X-ray investigations has enabled the results of theoretical calculations of various kinds to be checked. The fairly high degree of accuracy which appears to have been obtained in the structure determination of melamine [1], *s*-triazine [2], phenazine [3], and *s*-tetrazine [4] might be considered a reliable basis for drawing some conclusions concerning the relations between electronic configuration and molecular structure.

Recently, attempts in this direction have been made by comparing the observed bond distances with those calculated by means of the molecular orbital method [3, 5]. The results support the conception of complete conjugation in these molecules.

An inspection of the published values of the bond angles found for all these molecules (see fig. 1) shows a slight but systematic variation, the bond angle of nitrogen being always smaller and the bond angle of carbon always larger than 120°. This effect, although rather small, attracted our attention, and its appearance in all the results lead us to believe that some significance should be attached thereto.

An attempt has been made to explain this deviation of the bond angles from the normal value of 120° on the basis of an admittedly crude, but often successful model of the chemical bond. In this model it is assumed that a molecule like *s*-triazine contains 6 electrons, which form  $\pi$ -bonds extending over all of the carbon and nitrogen atoms. The others are localized electron pair bonds, the wave functions of which are constructed in the usual way from atomic orbitals of nitrogen and carbon or of hydrogen and carbon. In addition each nitrogen atom has two electrons located as a lone pair in an atomic orbital. The inner shell electrons are disregarded.

<sup>1)</sup> Present address: Istituto di Chimica Farmaceutica, Centro di Strutturistica Chimica del C.N.R., University of Rome, Italy.

According to this model the total energy of the valence electrons consists of three parts: 1) the energy necessary to bring the atoms to their valence states, which depends on the promotion energy i.e. the energy required to promote an electron from a  $2s$  to a  $2p$  state; 2) the energy of the bonds; and 3) the repulsion energy between electrons in different bonds and lone pairs.

It should be realized that the variations in bond angles are small from an energy point of view. Some factors which have been neglected in this model could be presumably of at least the same order of magnitude. A more refined treatment of the problem may reveal that these calculations cover the most important part of the electronic interactions responsible for change in bond angle.

## 2. General considerations

The usual way of describing the state of an atom in a planar heterocyclic molecule is to assume that its  $p_z$  electrons give rise to  $\pi$  bonds while the other electrons occupy hybrid  $s$ ,  $p_x$ ,  $p_y$  states which form the  $\sigma$  bonds (the  $z$  axis considered perpendicular to the molecular plane).

To construct the hybrid ( $s$ ,  $p_x$ ,  $p_y$ ) orbitals it will be assumed that

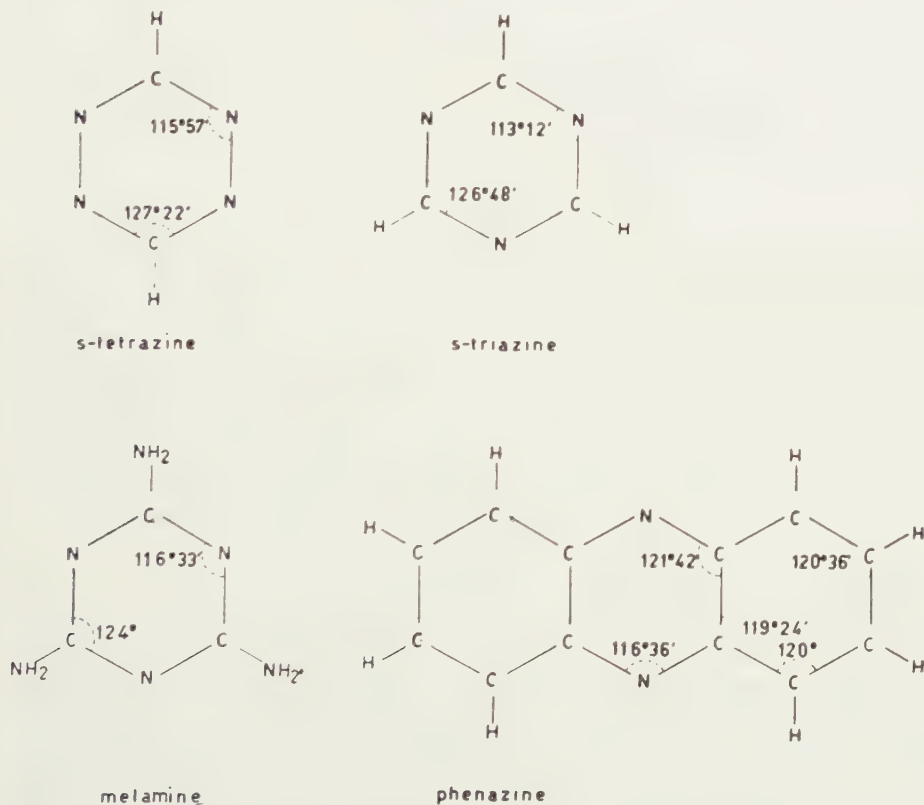


Fig. 1. Bond lengths and bond distances in *s*-tetrazine, *s*-triazine, melamine and phenazine.

the lines connecting the adjacent atomic nuclei are also the axes of quantization of the hybrid orbitals taking part in bond formation, i.e. it is assumed that bent bonds do not occur. Therefore, the bond angles are equal to the angles between hybrid orbitals.

An attempt may then be made to calculate these bond angles by determining the energy of a molecule as a function of these bond angles and by minimizing this expression. To get some idea of the position of this minimum, a molecule will be considered first where each nitrogen atom has been depleted of one lone pair electron.

1) The first term which then occurs in the energy expression is constructed from the repulsions of all the electrons. It is not profitable to account for all interactions, so that some simplifications will have to be made. The repulsions between electrons on different atoms have not been considered because these terms are not markedly affected by variations of the bond angles, although their magnitude is not small compared to the other terms. Furthermore it will be assumed that the charge distribution of a doubly occupied bonding orbital will be replaced by that of two singly occupied atomic orbitals from which the bonding orbital has been constructed. The part of the repulsion energy dependent on bond angles will not be greatly affected by this assumption, since it will be increased by the greater concentrations of charge near the nucleus and decreased by the neglect of the overlap charge. With these two simplifications the repulsion energy can be calculated without any difficulty.

2) The promotion energy need not be taken into account because in the case of three electrons in three orthonormal hybrid orbitals in a plane, the  $s$ ,  $p_x$  and  $p_y$  states are always equally occupied so that the promotion energy does not depend on the bond angle.

3) It is generally known that the energy of a covalent bond is closely connected with the overlap integral of the two hybrid orbitals of both atoms from which the bonding orbital has been constructed. This overlap integral depends on the degree of hybridization which is determined by the bond angle, consequently the bond energy depends on the valence angle. MULLIKEN [6] has investigated the relationship between bond energy and overlap integral more closely. This author offered a formula which fitted most of the experimental data. This semi-empirical formula will be used to calculate the energy of the C-N and C-H bonds as a function of the bond angles.

The energy of a heterocyclic compound composed of carbon and nitrogen atoms, each depleted of one lone pair electron, as a function of the bond angle consists of two terms. It is generally known that in the case of three  $\sigma$  bonds in one plane, the strongest bonds are formed when the valence angles are  $120^\circ$ , if it is assumed that the C-N and C-H bond are equivalent. From symmetry considerations it may be concluded that the repulsion energy of the electrons also is a minimum if the valence angles are  $120^\circ$ . Therefore the energy of the heterocyclic compound



mentioned above must be a minimum if all the bond angles are  $120^\circ$ .

The energy of a heterocyclic molecule may now be obtained by adding the energy which results from placing one lone pair electron on each nitrogen atom the energy mentioned above. Since the partial distributions over the  $s$  and  $p$  states of these electrons are affected by the degree of hybridization of the orbital, the promotion energy now depends on the bond angles. It may be seen that this quantity, as well as the interaction of these lone pair electrons with the other valence electrons on the same atom, will be lowered with decreasing C-N-C angle. Consequently the addition of these lone pair electrons will cause the C-N-C angles to close as the other effects tend to maintain these angles. Therefore C-N-C angles slightly smaller than  $120^\circ$  must be expected if the method mentioned above is applied. This agrees with the experimental data. It is necessary, nevertheless, to investigate the numerical results for these deviations more closely to see whether they are of the correct order of magnitude. For this purpose the molecule of  $s$ -triazine has been chosen because of its symmetry properties, which facilitate the calculations. It must be expected that for other molecules the deviations from  $120^\circ$  of the C-N-C angles will have the same order of magnitude.

### 3. Calculation of the energy

In order to calculate the valence angles in  $s$ -triazine we must first construct the appropriate hybridized atomic wave functions. If in the nitrogen atom the orbital of the lone pair is taken in the direction of the  $X$  axis, the corresponding wave functions may be represented by:

$$(1) \quad t_1 = a_1 s + b_1 p_x$$

and the two valence functions may be written as:

$$(2) \quad \begin{cases} t_2 = a_2 s - b_2 p_x + c_2 p_y \\ t_3 = a_2 s - b_2 p_x - c_2 p_y \end{cases}$$

since the orbitals point in two directions which are symmetric with respect to the  $X$  axis (see fig. 2).

After applying the conditions of normalization and orthogonality (1) and (2) become:

$$(3) \quad \begin{cases} t_1 = as + (1-a^2)^{\frac{1}{2}} p_x \\ t_2 = (1-a^2)^{\frac{1}{2}} 2^{-\frac{1}{2}} s - a 2^{-\frac{1}{2}} p_x + 2^{-\frac{1}{2}} p_y \\ t_3 = (1-a^2)^{\frac{1}{2}} 2^{-\frac{1}{2}} s - a 2^{-\frac{1}{2}} p_x - 2^{-\frac{1}{2}} p_y. \end{cases}$$

From our assumption that the molecule does not have bent bonds it may be concluded that changes in the C-N-C angles will also affect the N-C-N angles in the triazine molecule. If for a carbon atom the  $X$  axis is taken in the C-H direction the orbitals of the carbon atom are, by analogy with (3):

$$(4) \quad \begin{cases} u_1 = bs + (1-b^2)^{\frac{1}{2}} p_x \\ u_2 = (1-b^2)^{-\frac{1}{2}} s - b^{-\frac{1}{2}} p_x + 2^{-\frac{1}{2}} p_y \\ u_3 = (1-b^2)^{-\frac{1}{2}} s - b^{-\frac{1}{2}} p_x - 2^{-\frac{1}{2}} p_y \end{cases}$$

The valence angles may now be derived from:

$$(5) \quad \begin{cases} \varphi = \pi - 2 \operatorname{tg}^{-1} a \\ \psi = \pi - 2 \operatorname{tg}^{-1} b \\ \varphi + \psi = 4.73 \end{cases}$$

where  $\varphi$  is the C-N-C and  $\psi$  the N-C-N angle.

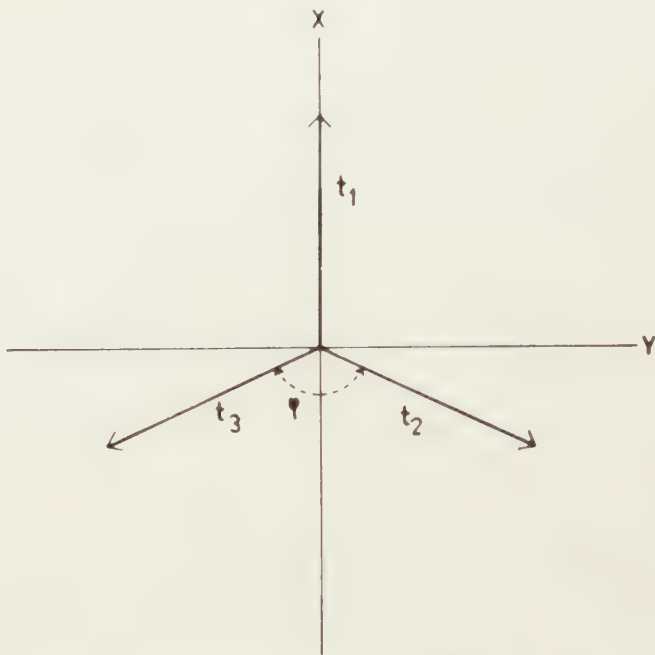


Fig. 2. Directions of  $sp^2$  hybrid orbitals of nitrogen.

As has already been mentioned, we first wish to consider a triazine molecule from which one lone pair electron has been removed from each nitrogen atom. The electronic repulsion energies of the nitrogen atoms may then be written as:

$$(6) \quad E_N = 6 \int t_1^2(1) (e^2/r_{12}) t_2^2(2) d\tau_1 d\tau_2 + 3 \int t_2^2(1) (e^2/r_{12}) t_3^2(2) d\tau_1 d\tau_2$$

and the repulsion energy of the carbon atoms may be represented by:

$$(7) \quad E_C = 6 \int u_1^2(1) (e^2/r_{12}) u_2^2(2) d\tau_1 d\tau_2 + 3 \int u_2^2(1) (e^2/r_{12}) u_3^2(2) d\tau_1 d\tau_2.$$

If the integrals occurring in (6) are denoted by  $T_{12}$  and  $T_{23}$  and those in (7) by  $U_{12}$  and  $U_{23}$ , then:

$$(8) \quad \begin{cases} 4T_{12} = (-2I_1 - 2I_2 + 4I_4 + 8I_6)a^4 - (-2I_1 - 2I_2 + 2I_3 + 2I_4 + 8I_6)a^2 + \text{const.} \\ 4T_{23} = (I_1 + I_2 - 2I_4 - 4I_6)a^4 - (2I_2 - 2I_3 + 4I_5 - 8I_6)a^2 + \text{const.} \\ 4U_{12} = (-2J_1 - 2J_2 + 4J_4 + 8J_6)b^4 - (-2J_1 - 2J_2 + 2J_3 + 2J_4 + 8J_6)b^2 + \text{const.} \\ 4U_{23} = (J_1 + J_2 - 2J_4 - 4J_6)b^4 - (2J_2 - 2J_3 + 4J_5 - 8J_6)b^2 + \text{const.} \end{cases}$$

where:

$$(9) \quad \begin{cases} I_1 = \int p_{\text{xN}}^2(1) (e^2/r_{12}) p_{\text{xN}}^2(2) d\tau_1 d\tau_2 \\ I_2 = \int s_{\text{N}}^2(1) (e^2/r_{12}) s_{\text{N}}^2(2) d\tau_1 d\tau_2 \\ I_3 = \int p_{\text{xN}}^2(1) (e^2/r_{12}) p_{\text{yN}}^2(2) d\tau_1 d\tau_2 \\ I_4 = \int s_{\text{N}}^2(1) (e^2/r_{12}) p_{\text{xN}}^2(2) d\tau_1 d\tau_2 \\ I_5 = \int p_{\text{xN}}(1) p_{\text{yN}}(1) (e^2/r_{12}) p_{\text{xN}}(2) p_{\text{yN}}(2) d\tau_1 d\tau_2 \\ I_6 = \int s_{\text{N}}(1) p_{\text{xN}}(1) (e^2/r_{12}) s_{\text{N}}(2) p_{\text{xN}}(2) d\tau_1 d\tau_2 \end{cases}$$

and  $J_k$  are the analogous quantities for the carbon atoms. It is then found that:

$$(10) \quad \begin{cases} 4E_{\text{N}} = 3(-3I_1 + 3I_4 + 12I_6)a^4 - 3(-2I_1 + 2I_4 + 8I_6)a^2 + \text{const.} \\ 4E_{\text{C}} = 3(-3J_1 + 3J_4 + 12J_6)b^4 - 3(-2J_1 + 2J_4 + 8J_6)b^2 + \text{const.} \end{cases}$$

For an estimation of the energy of a C-N bond as a function of  $a$  and  $b$ , it is necessary to calculate the overlap integral  $S$ :

$$S = \int t_2 u_2 d\tau$$

of the two corresponding valence functions. It may be deduced from (3) and (9) that:

$$(12) \quad \begin{cases} 2S(a, b) = (1 - a^2)^{\frac{1}{2}} (1 - b^2)^{\frac{1}{2}} \int s_{\text{N}} s_{\text{C}} d\tau + (1 + a^2)^{\frac{1}{2}} (1 - b^2)^{\frac{1}{2}} \int p_{\text{N}} s_{\text{C}} d\tau + \\ + (1 - a^2)^{\frac{1}{2}} (1 + b^2)^{\frac{1}{2}} \int s_{\text{N}} p_{\text{C}} d\tau + (1 + a^2)^{\frac{1}{2}} (1 + b^2)^{\frac{1}{2}} \int p_{\text{N}} p_{\text{C}} d\tau. \end{cases}$$

According to MULLIKEN [6] the bond energy may now be approximated by

$$(13) \quad E_{\text{CN}} = \frac{6AS(a, b)(I_{\text{N}}I_{\text{C}})^{\frac{1}{2}}}{1 + S(a, b)}$$

where  $A$  is roughly equal to one for  $\sigma$  bonds and  $I_{\text{N}}$  and  $I_{\text{C}}$  are the ionization energies of carbon and nitrogen.

In the same way the energy of the C-H bonds is given by:

$$(14) \quad E_{\text{CH}} = \frac{3A'S(b)(I_{\text{C}}I_{\text{H}})^{\frac{1}{2}}}{1 + S(b)}$$

where

$$(15) \quad S(b) = b \int s_{\text{C}} s_{\text{H}} d\tau + (1 - b^2)^{\frac{1}{2}} \int p_{\text{C}} s_{\text{H}} d\tau.$$

The energy of a triazine molecule without three lone pair electrons may thus be represented by

$$(16) \quad E = E_{\text{N}} + E_{\text{C}} - E_{\text{CN}} - E_{\text{CH}}.$$

The addition of the three lone pair electrons, which were supposed to be removed until now will affect the energy because of their electrostatic interaction with the other outer electrons of the nitrogens and because of their promotion energy. The first of these energies may be written as:

$$(17) \quad E'_1 = 3(T_{11} + 2T_{12})$$

where:

$$(18) \quad T_{11} = \int t_1^2(1) (e^2/r_{12}) t_1^2(2) d\tau_1 d\tau_2.$$

From (3) and (9) one finds that:

$$(19) \quad 4T_{11} = (4I_1 + 4I_2 - 8I_4 - 16I_6)a^4 - (8I_1 - 8I_4 - 16I_6)a^2 + \text{const.}$$

With the aid of (8) one finds:

$$(20) \quad E'_1 = -3(I_1 - I_2 + I_3 - I_4)a^2 + \text{const.}$$

If the energy difference of an electron in a  $2p$  and in a  $2s$  state is denoted by  $A_N$ , then it may be derived from (3) that the promotion energy  $E'_2$  is:

$$(21) \quad E'_2 = -3A_N a^2 + \text{const.}$$

so that the addition of these lone pair electrons will affect the energy by an amount  $E'$ , which is the sum of  $E'_1$  and  $E'_2$ .

#### 4. Numerical calculations

For a numerical calculation of the formulae indicated above, it is necessary to determine first the effective nuclear charge which occurs in the exponentials of the Slater wave functions of the carbon and nitrogen atoms. In agreement with SLATER [7] and ZENER [8] we assume that  $q_N = 3.90$  and  $q_C = 3.18$ . The energies  $E_C$  and  $E_N$ , expressed in electron volts, are then:

$$(22) \quad \begin{cases} E_N = 34.877 a^4 - 23.251 a^2 + \text{const.} \\ E_C = 28.438 b^4 - 18.959 b^2 + \text{const.} \end{cases}$$

The C-N distance in triazine is 1.319 Å [2]. For this distance the overlap integral  $S(a, b)$  is [9]:

$$(23) \quad \begin{cases} S(a, b) = 1/2 \{ (1-a^2)^{\frac{1}{2}} (1-b^2)^{\frac{1}{2}} 0.387 + (1-a^2)^{\frac{1}{2}} (1-b^2)^{\frac{1}{2}} 0.350 + \\ + (1-a^2)^{\frac{1}{2}} (1+b^2)^{\frac{1}{2}} 0.445 + (1+a^2)^{\frac{1}{2}} (1+b^2)^{\frac{1}{2}} 0.322 \} \end{cases}$$

Since  $I_N = 14.480$  eV and  $I_C = 11.217$  eV,  $E_{CN}$  may now be calculated from:

$$(24) \quad E_{CN} = \frac{76.467 S(a, b)}{1 + S(a, b)}.$$

The energy of the C-H bonds may be derived from

$$(25) \quad E_{CH} = \frac{48.173 S(b)}{1 + S(b)}$$

because  $I_H = 13.502$  eV,  $I_C = 11.217$  and the constant  $A'$  from (13) has



to be taken equal to 1.3 to get the correct value of the C-H bond energy at the equilibrium position. The overlap integral  $S(b)$  is given by [9]

$$(26) \quad S(b) = 0.294 b + 0.188 (1 - b^2)^{\frac{1}{2}}.$$

The values of  $E$  as a function of the C-N-C angle may now be determined without any difficulty (cf. Table I).

The promotion energy of a carbon atom which will be denoted by  $\Delta_{\text{C}}$  here, has been determined from spectroscopic data to be 4.17 eV [10, 11]. We will assume that the corresponding quantity for nitrogen may be obtained by multiplying by  $q_{\text{N}}/q_{\text{C}}$ , so that  $\Delta_{\text{N}} = 5.12$  eV. Then:

$$(27) \quad E'_2 = -15.36 a^2 + \text{const.}$$

With the aid of the integrals calculated in the appendix one finds that:

$$(28) \quad E'_2 = -5.58 a^2 + \text{const.}$$

It may thus be concluded that the effect of the promotion energy is much stronger than the electrostatic interactions.

The values of  $E'$ , which are given by:

$$(29) \quad E' = -20.94 a^2 + \text{const.}$$

may also be found in Table I.

TABLE I <sup>1)</sup>

	$E(\varphi)$	$E'(\varphi)$	$E_{\text{t}}(\varphi)$
120°	— 50.77	— 6.94	— 57.71
115°	— 50.07	— 8.50	— 58.57
112°	— 49.28	— 9.53	— 58.81
110°	— 48.58	— 10.27	— 58.85
108°	— 47.77	— 11.05	— 58.82
106°	— 46.68	— 11.89	— 58.57
100°	— 42.19	— 14.74	— 56.93

On considering the total energy  $E_{\text{t}}$  as a function of the C-N-C angle it may be seen, again from Table I, that this energy is a minimum for  $\varphi = 110^\circ$ .

$E(\varphi)$  and  $-E'(\varphi)$  have been plotted in fig. 3, where it may be seen that  $E(\varphi)$  is a minimum near  $120^\circ$  and the addition of  $E'(\varphi)$  tends to displace this minimum towards smaller values of the angle.  $E'(\varphi)$  has been shifted in fig. 3, so that its value will coincide with  $E(\varphi)$  for  $\varphi = 120^\circ$ .

## 5. Discussion

The result of the calculation is that in the equilibrium position of a *s*-triazine molecule without strain the C-N-C angle is  $110^\circ$ , whereas

<sup>1)</sup> These calculations have partly been carried out by Mr. P. SELIER, chem. cand.

the experimental value is  $113^\circ$ . Whether this difference is due to the approximations in the calculations of the electronic interactions, the bond energies and the promotion energy has not been investigated since this would involve a rather tedious procedure.

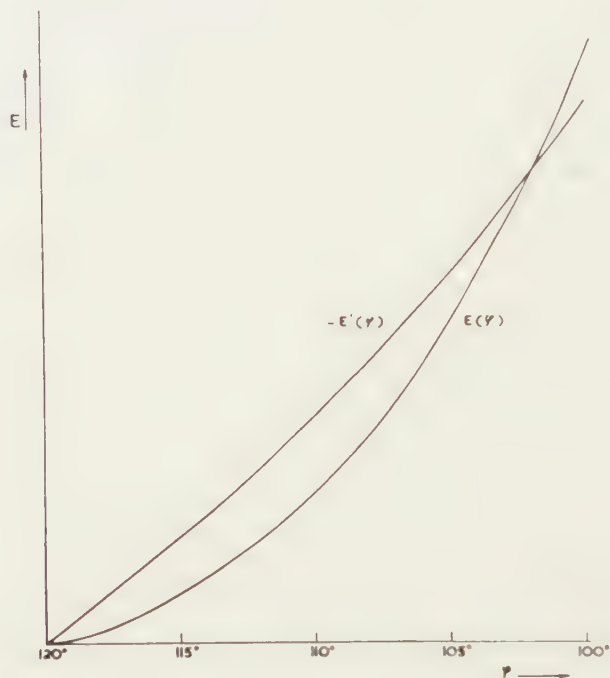


Fig. 3. The energies  $E$  and  $E'$  as functions of the C-N-C angle  $\varphi$ .

On the other hand it might as well be taken as an indication that ring formation in this molecule may be achieved only at the expense of some strain in all the C-N bonds. In this case not only the angle between the valence orbitals of both the carbon and the nitrogen will be forced to open, but also a bent bond will be formed. In any case the expected variations in the bond angles will be in the same sense as those observed experimentally, i.e. the bond angle of the carbon larger and the bond angle of the nitrogen smaller than  $120^\circ$ .

It has been found that if  $E_C$  is not taken into consideration, a valence angle of  $106^\circ$  is found for the isolated nitrogen atom, which does not differ much from the value obtained by considering also the carbon atoms. From geometrical considerations it may be concluded that the deviations from  $120^\circ$  would become smaller if the number of nitrogen atoms is either decreased or increased, but as in the first case the amount of strain in the molecule will also decrease, in the second case it is to be expected that the bonds are more bent, so that the stability of six membered heterocyclic should decrease with increasing number of nitrogen atoms.

On the other hand, this straining of the nitrogen atom should be considerably reduced in five membered conjugated rings, so that strain of the ring should be relieved with increasing number of nitrogen atoms.

Tentatively, the great stability of pyridine and of tetrazole among six- and five-membered heterocycles may be explained on this basis.

## 6. Appendix

The integrals  $I_k$  were calculated according to the well known procedure of introducing polar coordinates  $(r, \theta, \varphi)$  and expanding  $r_{12}^{-1}$  into a series of Legendre functions, viz.:

$$(30) \quad \frac{1}{r_{12}} = \sum_{n=0}^{\infty} \sum_{m=-n}^n \frac{r_1^n}{r_2^{n+1}} \frac{(n-|m|)!}{(n+|m|)!} P_n^{(m)}(\cos \theta_1) P_n^{(m)}(\cos \theta_2) e^{im(\varphi_2 - \varphi_1)}$$

if  $r_1 \leq r_2$ .

Substituting this into (9) yields, after integrating over  $\varphi_1$  and  $\varphi_2$  and taking into account the orthogonality relations of the Legendre functions:

$$(31) \quad \left\{ \begin{array}{l} I_6 = (qe^2/384 a_0) \int r_1^5 r_2^2 e^{-r_1 - r_2} \cos^2 \theta_1 \cos^2 \theta_2 \sin \theta_1 \\ \sin \theta_2 dr_1 dr_2 d\theta_1 d\theta_2. \end{array} \right.$$

Here,  $s$  and  $p_x$  are taken to be Slater functions:

$$(32) \quad \left\{ \begin{array}{l} s = (96 \pi)^{-\frac{1}{2}} r' e^{-ir'} \\ p_x = (32 \pi)^{-\frac{1}{2}} r' \cos \theta e^{-ir'} \end{array} \right. \quad r' = qr/a_0$$

where  $q$  is a screening constant and  $a_0$  is the radius of the hydrogen atom. This yields  $I_6 = 185 A/9$  if  $A = qe^2/512 a_0$ .

In the same way one finds:

$$(33) \quad \left\{ \begin{array}{ll} I_1 = 100.2 A & I_4 = 93.0 A \\ I_2 = 93.0 A & I_5 = 2.7 A \\ I_3 = 94.8 A & I_6 = 20.1 A. \end{array} \right.$$

The authors wish to express their gratitude to Prof. Dr. L. J. OOSTERHOFF for helpful suggestions and many discussions, to Prof. Dr. J. J. HERMANS for his stimulating interest and to Dr. R. M. LONGWORTH for correcting the English and for discussions.

## Summary

It has been experimentally observed that six membered heterocyclic compounds containing nitrogen have a planar structure and that the valence angles deviate from  $120^\circ$ . In order to find an explanation for this last effect, the energy has been minimized with respect to the C-N-C bond angles assuming that  $sp^2$  hybridization of the lone pair electrons of the nitrogen atoms takes place. A value of  $110^\circ$  has been found for the C-N-C angle of *s*-triazine, which should be compared with the experimental

value of  $113^{\circ}12'$ . The possibility that "bent bonds" are present in this molecule is advanced.

*Department of Theoretical Organic Chemistry.  
Laboratory of Physical and Inorganic Chemistry  
University of Leiden, The Netherlands.*

## LITTERATURE

1. HUGHES, E. W., J.A.C.S. **63**, 1737 (1941).
2. WHEATLEY, P. J., Acta Cryst. **8**, 224 (1955).
3. HERBSTSTEIN, F. H. and G. M. SCHMIDT, Acta Cryst. **8**, 406 (1955).
4. BERTINOTTI, F., G. GIACOMELLO and A. M. LIQUORI, Acta Cryst., In the Press.
5. LIQUORI, A. M. and A. VACIAGO, Ric. Scient. **26**, 181 (1956).
6. MULLIKEN, R. S., J.A.C.S. **72**, 4493 (1950).
7. SLATER, J. C., Phys. Rev. **36**, 57 (1930).
8. ZENER, N., Phys. Rev. **36**, 51 (1930).
9. MULLIKEN, R. S., C. A. RIEKE, D. ORLOFF and H. ORLOFF, J. Chem. Phys. **17**, 1248 (1949).
10. SHENTONE, A. G., Phys. Rev. **72**, 411 (1947).
11. LONG, L. H., Experientia **7**, 195 (1951).



NIVEO-ÄOLISCHE SANDE IM SAARGEBIET

VON

C. H. EDELMAN UND K. J. ZANDSTRA

(Communicated by Prof. H. A. BROUWER at the meeting of January 28, 1956)

Der Mittlere Buntsandstein (sm) setzt sich im Saargebiet vorwiegend aus ziemlich losen Sandsteinen zusammen, die mit einem Spaten leicht gebrochen werden können. Es ist denn auch kaum erstaunlich, dass diese Gesteine auch unter natürlichen Umständen leicht in Sand zerfallen. Dies ist im besonderen der Fall gewesen während des Jungpleistozäns, als das Saargebiet, ebenso wie andere ausgedehnte Teile Westeuropas, durch ein periglaziales Klima gekennzeichnet wurde.

Schon KESSLER [1], einer der ersten, der das fossile Periglazial erkannte, machte uns auf die Erscheinung aufmerksam, dass der Frost damals eine hervorragende Rolle spielte bei der Verbröckelung und Versetzung der obersten Schicht des Buntsandsteins.

HOPKINS [2] unterscheidet zwei Arten „frost riving“, nämlich: „large-scale riving“, wobei grössere und kleinere Steine entstehen, und „small-scale riving“, wobei das Gestein in Sand oder noch feinere Teilchen zerfällt.

Prozesse wie „frost-heaving“, Kryoturbation und dergleichen haben mit dem „frost-riving“ zusammengewirkt. Auf hügeligem Gelände wurde das durch Zerfallen gebildete Material durch Solifluktion nach den Tälern befördert. Während dieser Beförderung wurden die Kongelifrakten durch Korrosion noch stärker zerkleinert.

An zahlreichen Orten kann im Saargebiet festgestellt werden, dass die Solifluktion im Buntsandsteingebiet eine hervorragende Rolle gespielt hat. Trotz des sandigen Charakters der Gesteine war doch genügend feines Material vorhanden, insbesondere Eisenhydroxyd, um Solifluktion verursachen zu können. Dieser Solifluktion und des Schneeschmelzwassers zufolge wurde das Gelände beträchtlich denudiert.

Das periglaziale Klima hat eine dürftige Tundravegetation hervorgerufen, mit einem geringen Bedeckungsgrad, und in den Sandgebieten sicherlich mit offenen Stellen. Zwar war der Boden schlecht drainiert durch das Vorhandensein der „perenne Tjäle“, dennoch gab es Zeiten, wo Solifluktion wenig oder gar nicht vorkam, und der Wind überhand nehmen könnte.

Mitten im Buntsandsteingebiet hat letzterer der Verfasser, eine detaillierte Bodenkarte hergestellt, aus der ersichtlich wird, dass man die Landschaft nicht begreifen kann, wenn man die periglazialen äolischen Ablagerungen nicht kennt.

Die Verbreitung dieses niveo-äolischen Sandes ist nicht willkürlich. Dieser Sand wird zumal den Rändern der kleinen, tief eingeschnittenen Trockentäler entlang vorgefunden. Pseudo-kare sind bisweilen gänzlich mit Sand bedeckt, ebenso wie einige der flacheren Mulden. Auch auf den Plateaus wird äolischer Sand angetroffen und weiterhin in einigen unregelmässig verbreiteten Depressionen. Die Mächtigkeit der Sandschicht beträgt 1 bis 2 m, bisweilen mehr. Unter dem „Brownpodzolic“-bodenprofil erblickt man sehr lockeren hellrosafarbigem horizontal geschichteten Sand. Der Unterschied zwischen diesem niveo-äolischen Sand und dem Buntsandsteinmaterial (sm) ist folgendermassen:

- 1) *Farbe*:  
hellrosafarbig;  
sm. im allgemeinen stärker rot gefärbt, zahlreiche Abtönungen von weiss bis dunkelrot.
- 2) *Schichtung*:  
dutzende dünne Schichten, parallel zu der Oberfläche;  
sm. Neigung 5° S.
- 3) *Lockerung*:  
sehr lockerer Sand, mit Ausnahme einiger braunroter Einspülhorizonte;  
sm. mehr kompakt.
- 4) *„Desert pavement“*:  
auf der Grenze des Niveo-äolischen und sm. liegt mitunter eine Schicht versetzten gebrochenen Brauneisensteins, ein Stein stark. Unter dieser Steinsohle findet man zuweilen kryoturbat gestörtes sm. mit Eiskeilen.
- 5) *Unterliegender stark verwitterter Löss*:  
stellenweise liegt das Niveo-äolische auf einem, aus einer älteren Eiszeit stammenden, Löss (Lit. 3).
- 6) *Uebergang vom Niveo-äolischen und Solifluktsdecke*:  
entlang der Abhänge wechselt der niveo-äolische Sand wiederholt mit Solifluktsablagerungen ab.

Ausser dem eigentlichen Buntsandsteingebiet wird niveo-äolischer Sand in zahlreichen Aufschlüssen an den Flüssen Saar und Blies entlang, angetroffen. Dieser erreicht Mächtigkeiten bis 12 m und findet u.a. als Maurersand Anwendung. Der Sand ist weniger kompakt, lockerer, weniger lehmig und gleichartiger als das sm.

Es ist klar, dass die besagten Flüsse, deren Lauf grösstenteils im Buntsandstein und Perm liegen, während des Periglazials beträchtliche Mengen Sand befördert haben. Dies ergibt sich deutlich aus Sandstellen auf Talebenen oder an Abhängen im Muschelkalkgebiet, wo sonst nur Kalk, Ton und ein wenig Lehm das Anstehende bildet. Bei Sarreguemines ist

der ganze Hang des Bliestals von unten bis zu den höchsten Gipfeln mit 1 bis 1,5 m oder mehr niveo-äolischem Sand bedeckt, unmittelbar auf dem schweren Ton von Muschelkalk und Keuper. Der Sand ist sogar über die Wasserscheide herübergeweht in der Richtung der Saar. Morphologen haben dort eine sehr hohe Terrasse entdeckt, die in Wirklichkeit nichts anders ist als Würmglazialer niveo-äolischer Sand.

Die schönsten Gruben im niveo-äolischen Sand findet man bei Dillingen und Beaumarais in der Umgebung von Saarlouis vor. Der Sand ist milli-

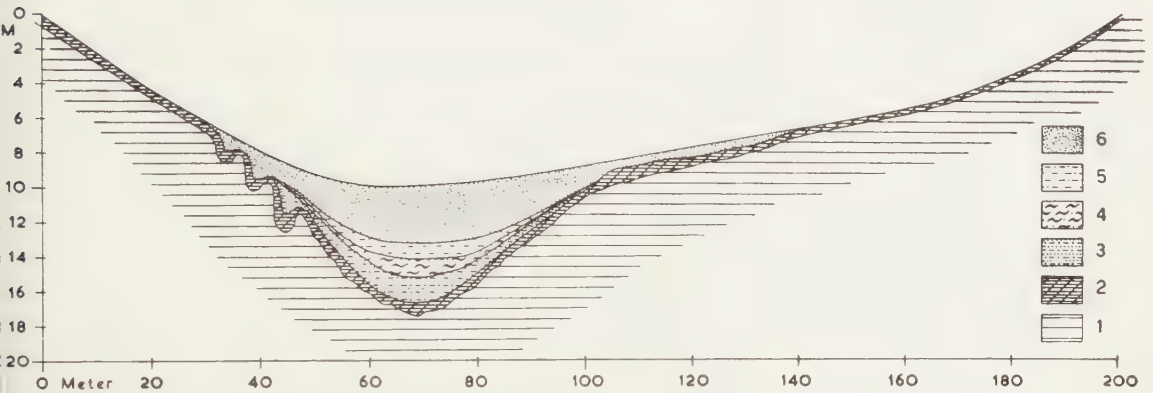


Fig. 1. Querschnitt durch ein Trockental in der Nähe von Saarlouis an der Saar.

- 6 = jung niveo-äolischer Sand (post Alleröd)
- 5 = rot-brauner niveo-äolischer Lehm (Ton-Sand); prae Alleröd
- 4 = grauer niveo-äolischer Lehm (Ton-Sand); prae Alleröd
- 3 = niveo-äolischer Sand (prae Alleröd)
- 2 = Fliesserde
- 1 = Buntsandstein.

meterfein geschichtet und zeigt eine Abwechslung von größerem und feinerem Sand auf. In dieser Ablagerung kommen eine oder mehrere Schichten rotbraunen lehmigen Sandes vor, die zirka 1 m stark sind. Diese auffälligen Lehmschichten verlaufen sehr regelmässig und neigen sich, ebenso wie die Sandschichten, dem Flusse zu. Korngrössenanalysen zeigen auf, dass der Gehalt an Teilchen  $< 2\mu$  gross ist, und dass die typische Lössfraktion vernachlässigt werden kann. Im Nachstehenden wollen wir auf das Entstehen dieser Lehmschichten zurückkommen.

Der niveo-äolische Sand längs der Abhänge des Flusstals bei Dillingen versetzt uns in die Lage, das periglaziale Milieu besser zu charakterisieren als durchweg der Fall ist. Vorausgeschickt sei, dass die Anhäufung dieses Sandes nicht als Solifluktionerscheinung aufzufassen ist. Die Schichtung ist besonders fein und regelmässig. Ausserdem wird der Sand auch an Abhängen entlang angetroffen, die sich aus fettem Ton und Kalkstein zusammensetzen. Der Hang des Tales ist zurzeit weniger schroff als ursprünglich der Fall war. Das Niveo-äolische hat die Formen vertuscht. Der Neigungswinkel der feinen Schichten kann wechseln, aber setzt sich in der Regel auf 3 bis 4° an.

Wenn auch die Basis des niveo-äolischen Sandes nicht immer abgeschlossen ist, kann dennoch an einigen Stellen festgestellt werden, dass sie sich auf die Niederterrasse aufstützt, ein einziges Mal mit einem Uebergang von kleinen Dünen. Daraus geht hervor, dass die fluviatile

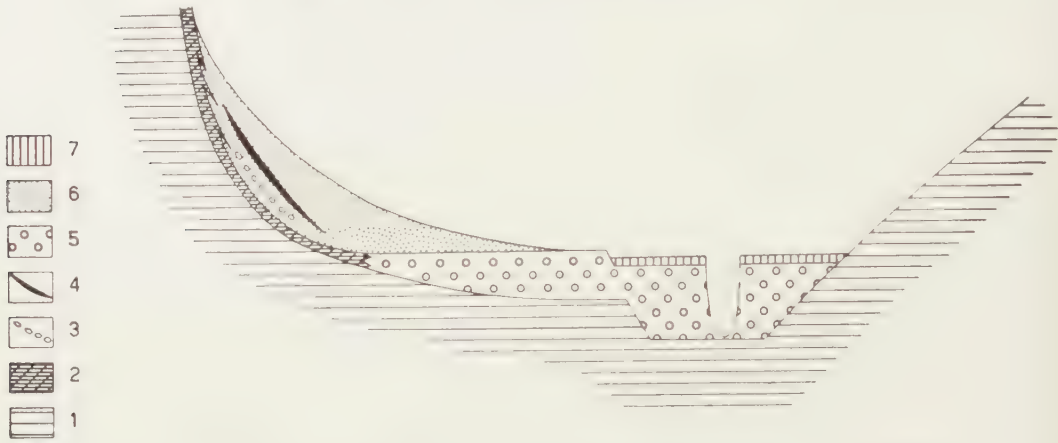


Fig. 2. Schematischer Querschnitt durch die niveo-äolische Decke des Saar- und Bliestaales zwischen Homburg und Mettlach.

- 7 = Alluvium der Saar
- 6 = niveo-äolischer Sand
- 5 = Niederterrasse Schotter
- 4 = Rotbrauner Lehm
- 3 = Steinsohle
- 2 = Fließerde
- 1 = Buntsandstein.

Sedimentation und alles, was damit zusammenhängt, schon vorüber war, als der niveo-äolische Sand an Ort und Stelle angehäuft wurde. Dies ist nur denkbar in der jüngsten Dryaszeit, nach dem ersten Einschnitt der Flüsse in der Niederterrasse während der Allerödzeit.

Die Tatsachen, welche die Ablagerungsweise am besten beleuchten, sind:

- 1) die feine regelmässige Schichtung;
- 2) keine Kreuz-schichtung;
- 3) die vollkommen konkordanten Lehmschichten;
- 4) Kryoturbation;
- 5) das Auftreten einiger Kieslinsen, in denen Windkanter angetroffen werden.

Diese Tatsachen lassen sich mit Hilfe des „snow drift“ wie folgt erklären:

- 1) Die Hänge und die Täler waren mit Schnee bedeckt, in dem ein wenig Sand vorkam. Der Schnee taute wahrscheinlich nicht, denn in diesem Fall würde die Regelmässigkeit der Sandschichten gestört sein. Der Schnee muss sublimiert sein, was auf grosse Kälte in der Zeit, wo der niveo-äolische Sand abgelagert wurde, hindeutet.



- 2) Kreuz-schichtung würde dem Prozess der Anhäufung von Schnee mit Sand nicht entsprechen. Die kleinen Dünen, die bisweilen am Fusse des niveo-äolischen Sandes angetroffen werden, deuten im Vergleich zu dem übrigen Teil der Ablagerung auf eine Klimaänderung.
- 3) Die Lehmschichten (Ton-Sand) werden verständlich durch Annahme von Verwehungen von Ton mit Sand aus der Flussebene, zusammen mit Schnee. Das Einzugsgebiet der Flüsse ist tonreich: Karbon, Perm und Muschelkalk.
- 4) Im niveo-äolischen Sand findet man stellenweise schöne einmalige Frostkeile (Lit. 4) vor. Eine andere Form von Kryoturbation sind kleine „Taschen“ mit hellrosafarbigem Sand gefüllt, die oft halb abgeschnürt sind und die übrigens die Regelmässigkeit der Schichtung kaum stören. Auch kommen kleine Sandwellen vor und ein einziges Mal kleine Aufpressungen.
- 5) Die Windkanter sind zu gross, um von unten nach oben befördert zu sein. Bei Dillingen stammen sie offenbar von der höher gelegenen Terrasse, bzw. vom solifuierten Terrassenmaterial. Die Windkanterlinsen selbst können nicht durch Solifluktion auf ihrem Platz angelangt sein. Wahrscheinlich sind sie durch die Schwerkraft heruntergerollt und über den gefrorenen Boden geglitten. Sie liegen niemals ordnungslos durch die Sandmasse verbreitet. Offenbar sind sie festgefroren und längere Zeit dem Winde ausgesetzt gewesen.

Nach oben bildet der niveo-äolische Sand einen Uebergang mit der Fliesserde des Abhanges. Dieser Uebergang kann eine Verzahnung aufweisen, wobei Solifluktionsmaterial einerseits, und niveo-äolischer Sand mit Steinlinsen anderseits, einander abwechseln. Je nachdem man sich nach unten weiter von der Solifluktionsdecke entfernt, werden die Steinlinsen stets dünner, um schliesslich ganz zu verschwinden.

Im Vorstehenden haben wir schon darauf hingewiesen, dass die Niederterrasse bisweilen von dem Niveo-äolischen überlagert wird und dass der Sand folglich aus der jüngsten Dryaszeit stammen muss. In diesem Fall entspricht er dem jungen Decksand der niederländischen Quartärgeologen.

In einigen anderen Fällen setzt sich das Liegende des niveo-äolischen Sandes aber aus Perm, Buntsandstein und Muschelkalk zusammen. In diesem Zusammenhang ist es von Bedeutung, dass die Lehm-(Ton-Sand)schichten niemals vorgefunden worden sind an Orten, wo das Material nachweisbar aus der jüngsten Dryaszeit stammt. Dasselbe gilt für die kryoturbaten Erscheinungen. Wir glauben denn auch annehmen zu dürfen, dass es möglich ist, die niveo-äolische Ablagerung in zwei Gruppen einzuteilen:

## 2. Spätglazial (nach Alleröd)

### 1. Pleniglazial und Spätglazial (vor Alleröd)

Die Lehmschichten würden dann dem Pleniglazial angehören, ebenso wie die kryoturbaten Erscheinungen.

Zum Schlusse sei noch darauf hingewiesen, dass der niveo-äolische Sand längs Abhängen bedeckt sein kann mit einer Solifluktsdecke, die im jüngsten Pleistozän gebildet worden ist. Diese Solifluktsdecke aus der jüngsten Dryaszeit darf nicht verwechselt werden mit dem im Obigen wiederholt genannten Solifluktsmaterial, das am Fusse des niveo-äolischen Sandes angetroffen wird.

*Wageningen.*

*Geol. Institut der Landwirtschaftlichen Hochschule.*

#### LITERATUR

1. KESSLER, P., Ueber diluviale Frostspalten bei Saarbrücken. Ztschr. Dtsch. Geol. Ges., **79** (1927).
2. HOPKINS, D. M., Thaw lakes and thaw sinks in the Imuruk lake area, Alaska. The Journal of Geology, **57**, 2 (1949).
3. ZANDSTRA, K. J., Un dépôt pollinifère mindelien en Sarre. Revue de Géomorphologie Dynamique, 5e Année, no. 5 (1954).
4. DÜCKER, A., Ueber die Entstehung von Frostspalten. Karl Gripp Festschrift. Schriften des Nat. Vereins für Schleswig-Holstein, **25** (Kiel, 1951).
5. EDELMAN, C. H., Over de bodemgesteldheid van Midden-Nederland (Utrecht, 1947).
- , Inleiding tot de Bodemkunde van Nederland (Amsterdam, 1950).
6. HAMMEN, TH. v. D., Late-glacial flora and periglacial phenomena in the Netherlands. Dissertation (1951).

OBSERVATIONS ABOUT SOME DIFFERENTIAL EQUATIONS  
CONCERNING RECESSION OF MOUNTAIN SLOPES. I

BY

H. LOOMAN

(Communicated by Prof. F. A. VENING MEINESZ at the meeting of January 28, 1956)

The object of this paper is to make some observations about the differential equations as found in the publications mentioned in the list of literature (cf. p. 284) under the numbers [1] . . . . . [5]; we shall indicate these equations by I, II, III and IV in the order found in [5], getting:

- I. Parallel rectilinear recession of a plateau wall . . . . . Cf. [1]
- II. Parallel rectilinear recession of a crest . . . . . Cf. [2]
- III. Central rectilinear recession of a plateau wall. . . . . Cf. [3]
- IV. Central rectilinear recession of a crest . . . . . Cf. [4]

We shall keep the notations used in the publications mentioned and shall derive the differential equations anew according to a method also applicable when  $\alpha$ ,  $\beta$  and  $c$  are variable.

I and III. *In the cases I and III a point P moves between two horizontal lines (their distance being h), on which the points A and B move in such a way that the infinitesimal area described by PB is (1-c) times as large as the infinitesimal area described by PA; PA and PB form with the horizontal plane the angles  $\alpha$  and  $\beta$  respectively, which are in general variable.*

According to fig. 1 PB describes the infinitesimal area

$d\{\frac{1}{2}(h-y)^2 \cot \beta\} + (h-y)dx = -(h-y) \cot \beta dy + \frac{1}{2}(h-y)^2 d \cot \beta + (h-y)dx$   
and PA:

$d(\frac{1}{2}y^2 \cot \alpha) - ydx = y \cot \alpha dy + \frac{1}{2}y^2 d \cot \alpha - ydx$

giving (also, when  $\alpha$ ,  $\beta$  and  $c$  are variable):

$-(h-y) \cot \beta dy + \frac{1}{2}(h-y)^2 d \cot \beta + (h-y)dx =$   
 $= (1-c) \{y \cot \alpha dy + \frac{1}{2}y^2 d \cot \alpha - ydx\}$

Special cases

I.  $c$ =constant,  $\alpha$  and  $\beta$  are constant,  $\cot \alpha = a$ ,  $\cot \beta = b$ .

We find:

$-(h-y)b dy + (h-y)dx = (1-c) \{a y dy - y dx\}$

or:

$\frac{dx}{dy} = \frac{b(h-y) + (1-c)ay}{h-y + (1-c)y} = \frac{bh + \{a(1-c) - b\}y}{h - cy}$  Cf. [1]

III.  $c = \text{constant}$ ,  $\cot \alpha = \text{constant} = a$ ,  $\cot \beta = (x/y)$

$$-(h-y) \frac{x}{y} dy + \frac{1}{2} (h-y)^2 \frac{y dx - x dy}{y^2} + (h-y) dx = (1-c) (ay dy - y dx)$$

or:

$$\frac{dx}{dy} = \frac{(h^2 - y^2)x + 2a(1-c)y^3}{y\{h^2 + (1-2c)y^2\}} \quad \text{Cf. [3].}$$

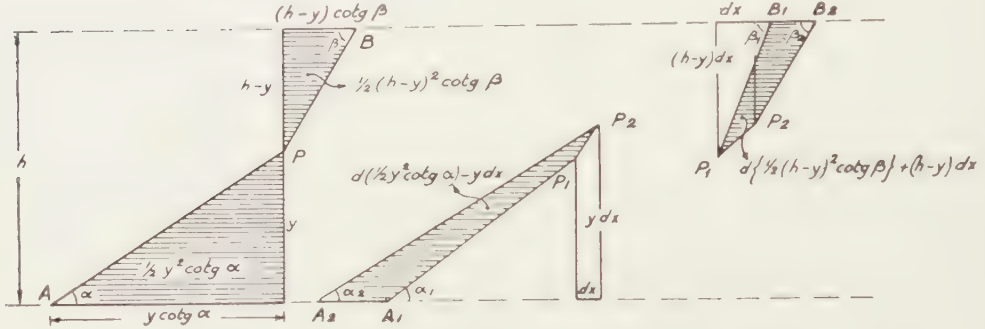


Fig. 1. Rectilinear recession of a plateau (I and II)

II and IV. In the cases II and IV a point  $P$  moves in an angle formed by a horizontal and a vertical line, a fixed point  $O$  on the horizontal line being at a distance  $k$  from the vertical one, a point  $B$  on the vertical line and a point  $A$  on the horizontal one moving in such a way that the infinitesimal area described by  $PB$  is  $(1-c)$  times as large as the infinitesimal area described by  $PA$ ;  $PA$  and  $PB$  forming with the horizontal plane the (generally variable) angles  $\alpha$  and  $\beta$  respectively.

According to fig. 2  $PB$  describes the infinitesimal area:

$$-d\left\{\frac{1}{2}(k-x)^2 \tan \beta\right\} - (k-x)dy$$

and  $PA$ :

$$d\left\{\frac{1}{2}y^2 \cot \alpha\right\} - ydx$$

giving (with in general mutually independent  $\alpha$ ,  $\beta$  and  $c$ ):

$$-d\left\{\frac{1}{2}(k-x)^2 \tan \beta\right\} - (k-x)dy = (1-c) \{d\left\{\frac{1}{2}y^2 \cot \alpha\right\} - ydx\}$$

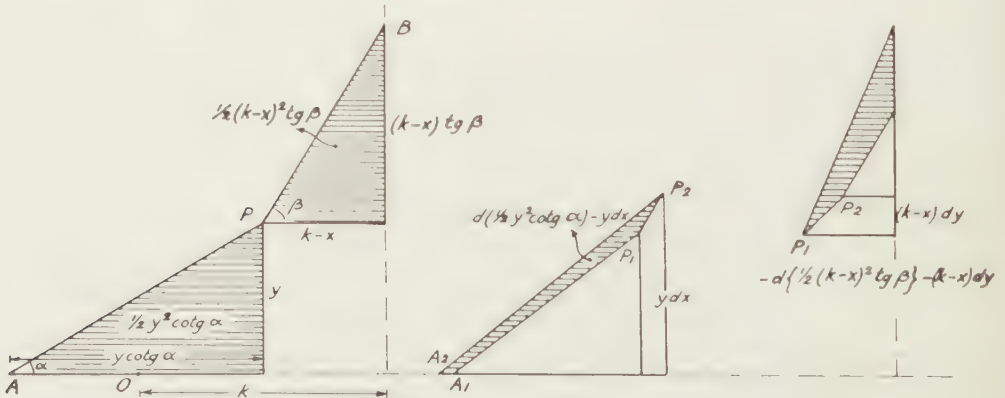


Fig. 2. Rectilinear recession of a crest (II and IV)



*Special cases*

II.  $c = \text{constant}$ ,  $\alpha$  and  $\beta$  are constant,  $\cot \alpha = a$ ,  $\cot \beta = b$ .

We find:

$$(k-x)bdx - (k-x)dy = (1-c) \{yady - ydx\}$$

or:

$$\frac{dx}{dy} = \frac{b(k-x) + ab(1-c)y}{k-x + b(1-c)y} \quad \text{Cf. [2].}$$

Point  $O$  is not used here.

IV.  $c = \text{constant}$ ,  $\cot \alpha = \text{constant} = a$ ,  $\tan \beta = (y/x)$ , if the origin of the co-ordinates system is in  $O$  and the produced part of  $PB$  passes through  $O$ .

We find:

$$-\frac{1}{2}(k-x)^2 \frac{xdy - ydx}{x^2} + (k-x) \frac{y}{x} dx - (k-x) dy = (1-c) y (ady - dx)$$

or:

$$\frac{1}{2}(k-x)^2 \frac{ydx - xdy}{x^2} + (k-x) x \frac{ydx - xdy}{x^2} = (1-c) y (ady - dx)$$

or:

$$\frac{1}{2}(k^2 - x^2) \frac{ydx - xdy}{x^2} = (1-c) y (ady - dx)$$

or:

$$\frac{dx}{dy} = \frac{x(k^2 - x^2) + 2ax^2y(1-c)}{y\{2x^2(1-c) + k^2 - x^2\}} \quad \text{Cf. [4].}$$

*Observations:*

1. The constants  $h$  and  $k$  act as *similarity factors* which may be put  $= 1$ ; this means that  $x/h$ ,  $y/h$  in I and III,  $x/k$  and  $y/k$  respectively in II and IV are introduced as new variables.

2. In *affine transformations* (*parallel projection*) the nature of the problem does not change, as the ratio of areas remains the same. Parallel remains parallel, central remains central, the constants  $a$  and  $b$  of I and II changing independently into any other constants just as the constant  $a$  in III and IV, while the perpendicular position in III and IV may be replaced by any oblique position. *Here the constant  $c$  does not change*, consequently it is (mathematically speaking) the most important constant.

3. From the data it appears that in I the integral-curves pass into each other by translation in a horizontal direction; in III by a similarity transformation with respect to the point of intersection of the given lines. In III and IV it will become evident that the (relevant) integral-curves pass through the point  $O$ , the slope of the tangent being considered an integration constant. The latter has been called  $1/b$  in [3] and [4],  $b$  being a constant in the differential equation in I and II.

4. By applying an affine transformation the perpendicular position in II and IV can be replaced by any oblique position,  $c$  remaining unchanged. It can be demonstrated now that by a limiting process case I

is to be deduced from II and III so that: *the integral curves of I can be deduced from those of II and the integral curves of III from those of IV by a limiting process, c remaining unchanged.*

5. The equations III and IV do not change under the substitution  $x' = -x$  and  $y' = -y$ . When integrating we shall find that the relevant integral curves pass through  $(0, 0)$  and that  $x/y$  can be developed in a power series of  $y^2$ , so that we get:

$$x = by + \lambda y^3 + \mu y^5 + \dots$$

Thus the integral curves have an inflexion point in 0 and there is a cubic parabola  $x = by + \lambda y^3$ , which has a contact of the 4th order with the integral curve there. Thus the lowest part is to be considered straight (to the 2nd order) which is not the case in I and II. Cf. fig. 3.

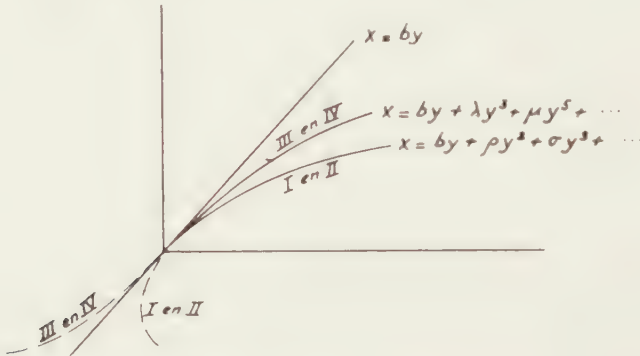


Fig. 3. Approximating parabolic lines

#### Parallel rectilinear recession

With respect to the *tangent constructions* to the integral curves in the cases I ( $a, b, c$ ) and II ( $a, b, c$ ), the behaviour of the *isoclines* (loci of points with given  $dy/dx$ ) and the behaviour of the integral curves themselves we observe the following:

*Case I* ( $a, b, c$ ). From the equation:

$$\frac{dx}{dy} = \frac{b(h-y) + (1-c)ay}{h-y + (1-c)y} = \frac{bh + \{a(1-c) - b\}y}{h - cy}$$

it follows that the isoclines are horizontal straight lines.

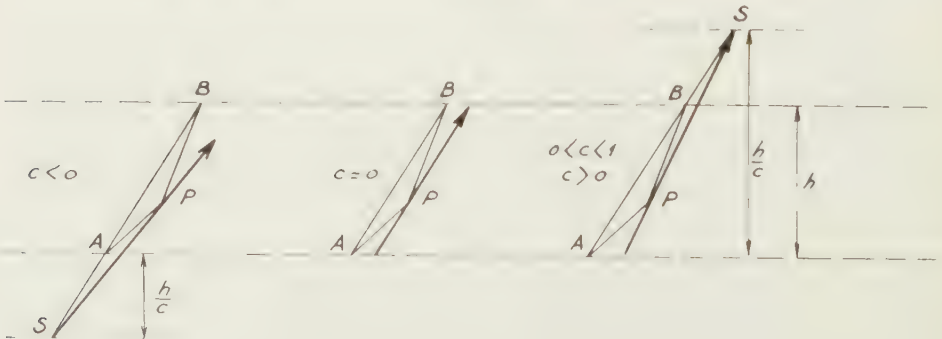


Fig. 4. First tangent construction for case I

*First Tangent Construction:* Draw through the point  $P(x, y)$  the lines  $PA$  and  $PB$  of the original definition and determine (for  $c \neq 0$ ) the point of intersection  $S$  of the produced line  $AB$  with the line  $y = h/c$ ; then  $SP$  is the tangent in  $P$ . For  $c = 0$  the tangent in  $P$  is parallel to  $AB$ . Cf. fig. 4.

*Demonstration:*

If  $X, Y$  are the coordinates of any point of the line through

$$A(x-ay, 0) \text{ and } B\{x+b(h-y), h\},$$

then

$$X = x - ay + \frac{ay + b(h-y)}{h} Y,$$

so that  $S$  has the co-ordinates

$$X_s = x - ay + \frac{ay + b(h-y)}{h} \frac{h}{c} = x + a\left(\frac{1}{c} - 1\right)y + \frac{b}{c}(h-y) \text{ and } Y_s = \frac{h}{c}.$$

Consequently:

$$\frac{X_s - x}{Y_s - y} = \frac{a\left(\frac{1}{c} - 1\right) + \frac{b}{c}(h-y)}{\frac{h}{c} - y} = \frac{a(1-c)y + b(h-y)}{h - cy} = \frac{dx}{dy}.$$

If  $c = 0$ , then  $\frac{dx}{dy} = \frac{ay + b(h-y)}{h}$ , consequently the tangent  $\parallel AB$ .

*Second Tangent Construction:* Draw (for  $c \neq 0$ ) through the point  $G(0, h/c)$  the lines  $GC$  and  $GD$  at angles  $\beta$  and  $\alpha$  with the horizontal plane,  $C\left(-\frac{bh}{c}, 0\right)$  being on the  $X$  axis and  $D\left(-\frac{ah(1-c)}{c}, h\right)$  on the line  $y = h$ . Connect  $P(x, y)$  on the line  $CD$  with  $G$ , then  $PG$  is the tangent in  $P$ . Cf. fig. 5.

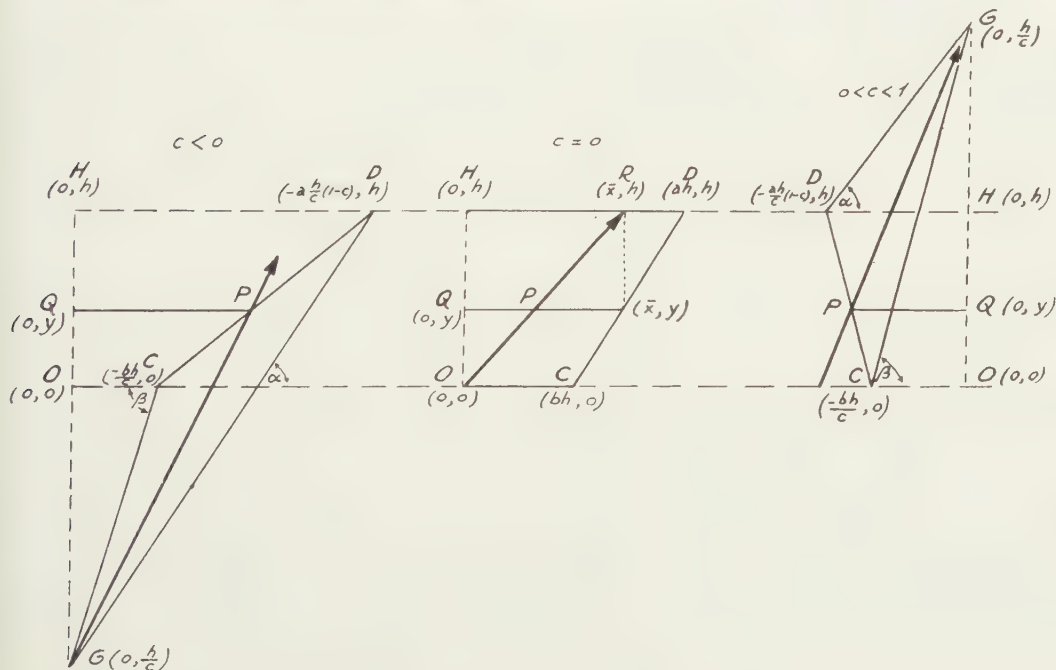


Fig. 5. Second tangent construction for case I

*Demonstration:*

The points  $C$  and  $D$  form with  $O(0, 0)$  and  $H(0, h)$  the angular points of a trapezium in which the distance from  $P(x, y)$  to  $Q(0, y)$  can be calculated from

$$PQ = \frac{ah(1-c)}{c} \frac{y}{h} + \frac{bh}{c} \frac{h-y}{h},$$

so that

$$PQ:GQ = \frac{\frac{ah(1-c)}{c} \frac{y}{h} + \frac{bh}{c} \frac{h-y}{h}}{\frac{h}{c} - y} = \frac{a(1-c)y + b(h-y)}{h-cy} = \frac{dx}{dy}.$$

If  $c=0$  we can use  $C(bh, 0)$  and  $D(ah, h)$  so that  $CD$  has the equation

$$x = bh + (a-b)y = ay + b(h-y)$$

the line from  $O(0, 0)$  to  $R(x, h)$  consequently yielding the value

$$\frac{HR}{OH} = \frac{ay + b(h-y)}{h} = \frac{dx}{dy}.$$

Cf. fig. 5 middle.

By constructing the tangent directions for a number of values of  $y$  between 0 and  $h$ , a quick diagram of the integral-curves is obtained. These can also be constructed point by point by virtue of the following property:

*If we take the point  $(0, 0)$  as the origin of the integral-curve, and if we indicate the curve determined by  $a, b, c$ , by  $I(a, b, c)$  we get:*

*$I(a, b, 0)$  is a parabola:*

*$I(a, b, c)$  with  $c \neq 0$  is: an affine representation of the ordinary logarithmic line (consequently also of  $y=e^{-x}$  and  $y=-e^{-x}$ ).*

*Demonstration:*

By integrating we find, if  $c \neq 0$

$$x - by = (a-b) \frac{1-c}{c} \frac{h}{c} \left\{ \frac{-y}{h} \lg \left( 1 - \frac{cy}{h} \right) \right\}$$

or:

$$x = (a-b) \frac{1-c}{c} \frac{h}{c} \lg \left( 1 - \frac{cy}{h} \right) + \frac{b-a(1-c)}{c} y.$$

Putting  $1 - \frac{cy}{h} = e^{-t}$ , then  $y = \frac{h}{c} (1 - e^{-t})$  and

$$x = (a-b) \frac{1-c}{c} \frac{h}{c} t + \frac{b-a(1-c)}{c} \frac{h}{c} (1 - e^{-t})$$

$$y = 0 \cdot t + \frac{h}{c} (1 - e^{-t}).$$

After introducing the vectors

$$\vec{r} = \begin{vmatrix} x \\ y \end{vmatrix}, \quad \vec{v}_1 = \begin{vmatrix} (a-b) \frac{1-c}{c} \frac{h}{c} \\ 0 \end{vmatrix} \quad \text{and} \quad \vec{v}_2 = \begin{vmatrix} \frac{b-a(1-c)}{c} \frac{h}{c} \\ \frac{h}{c} \end{vmatrix},$$



we get:

$$\vec{r} = \vec{v}_1 t + \vec{v}_2 (1 - e^{-t}) = \vec{v}_1 t + \vec{v}_2 - \vec{v}_2 e^{-t}.$$

If  $c=0$ , the parabola  $x = by + \frac{a-b}{h} \frac{1}{2} y^2$  passes into

$$x = bht + (a-b)h \frac{1}{2} t^2$$

$$y = ht + 0 \cdot \frac{1}{2} t^2$$

after the substitution  $y = ht$ .

After the introduction of the vectors

$$\vec{r} = \begin{vmatrix} x \\ y \end{vmatrix}, \quad \vec{v}_1 = \begin{vmatrix} (a-b)h \\ 0 \end{vmatrix} \quad \text{and} \quad \vec{v}_2 = \begin{vmatrix} bh \\ h \end{vmatrix}$$

we get:

$$\vec{r} = \vec{v}_1 \frac{1}{2} t^2 + \vec{v}_2 t.$$

*Observations:*

From  $\vec{r} = \vec{v}_1 t + \vec{v}_2 - \vec{v}_2 e^{-t}$  and  $t \rightarrow +\infty$  it appears that the asymptote  $y = (h/c)$  is represented by  $\vec{r} = \vec{v}_1 t + \vec{v}_2$ . When  $t \rightarrow -\infty$  the asymptotic direction proves to be that of  $-\vec{v}_2$ .

From

$$\vec{r} = (\vec{v}_1 + \vec{v}_2) t + \vec{v}_2 \{1 - t - (1 - t + \frac{1}{2} t^2 - \dots)\} = (\vec{v}_1 + \vec{v}_2) t + \vec{v}_2 (-\frac{1}{2} t^2 + \dots)$$

and  $t \rightarrow 0$  it appears that the curve touches  $\vec{v}_1 + \vec{v}_2$  in 0. For the relevant values of  $a$ ,  $b$  and  $c$  the vector  $\vec{v}_1$  lies on the positive  $X$ -axis, while the end of  $\vec{v}_2$  is on the asymptote, consequently if  $c > 0$  above and if  $c < 0$ , under the  $X$ -axis; so when  $c > 0$  we must take  $t \geq 0$  and when  $c < 0$  we must take  $t \leq 0$  in order to get  $y \geq 0$ .

*Construction integral curves.* Draw  $OA$  and  $OB$  (cf. figs. 6 and 7) at the

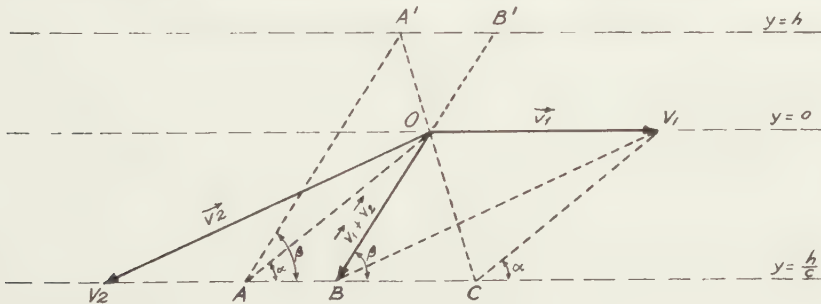


Fig. 6. Construction basevectors for case II,  $c < 0$

angles  $\alpha$  and  $\beta$  with the  $X$ -axis and make  $B'A'$  on  $y=h$  equal to  $BA$  on  $y \parallel (h/c)$ ; draw  $OA'$ , which intersects  $y=h/c$  in  $C$  and draw  $CV_1 \parallel V_1B$ .

Then  $OV_1$  represents the vector  $\vec{v}_1$ ,  $OB$  the vector  $\vec{v}_1 + \vec{v}_2$  and  $OV_2 \parallel V_1B$

the vector  $\vec{v}_2$ . Let  $t$  pass through an arithmetical progression and add  $\vec{v}_1 t + \vec{v}_2$  and  $\vec{v}_2 e^{-t}$  (the latter passing through a geometric progression).

When  $c=0$ ,  $OA$  acts as  $\vec{v}_1$  and  $OB$  as  $\vec{v}_2$ . Cf. fig. 7.

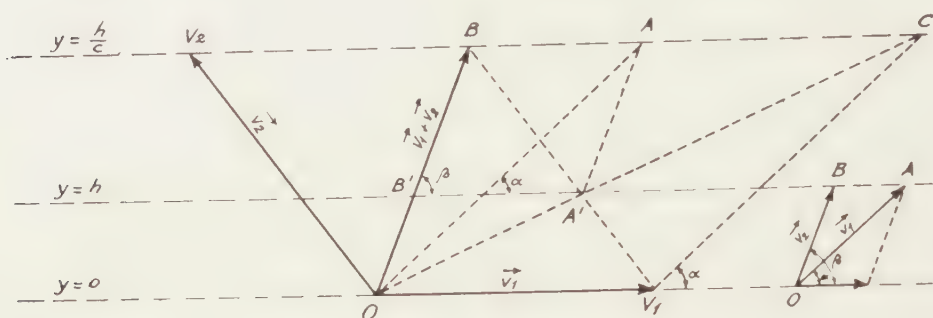


Fig. 7. Construction basevectors for case II,  $c > 0$  and  $c = 0$

*Demonstration:*

Obviously

$$AB = A'B' = (a-b) \frac{h}{c},$$

so

$$BC = \left(\frac{h}{c} : h\right) A'B' = \frac{1}{c} (a-b) \frac{h}{c},$$

so

$$AC = OV_1 = BC - AB = \left(\frac{1}{c} - 1\right) (a-b) \frac{h}{c},$$

so  $OV_1$  represents the vector

$$\vec{v}_1 = \begin{vmatrix} (a-b) \frac{1-c}{c} \frac{h}{c} \\ 0 \end{vmatrix}.$$

Besides:

$$\vec{v}_1 + \vec{v}_2 = \begin{vmatrix} (a-b) \frac{1-c}{c} \frac{h}{c} \\ 0 \end{vmatrix} + \begin{vmatrix} b \frac{a(1-c)}{c} \frac{h}{c} \\ \frac{h}{c} \end{vmatrix} = \begin{vmatrix} b \frac{h}{c} \\ \frac{h}{c} \end{vmatrix}$$

consequently  $OB$  (tangent in  $O$ ) represents the vector  $\vec{v}_1 + \vec{v}_2$ . From this follows the construction of  $OV_2$  and  $\vec{v}_2$ .

*Observation:*

The direction of  $\vec{v}_1$  is that of the asymptote  $y = (h/c)(t \rightarrow \infty)$ ; the direction of  $-\vec{v}_2$  is the second asymptotic direction ( $t \rightarrow -\infty$ ),  $\vec{v}_2$  besides representing the constant part cut out on the asymptote by the tangent in any point  $P$  of the curve and the line through  $P$  parallel to the line of  $\vec{v}_2$ .

The last mentioned property is characteristic of the (affine transformations of the) exponential curve and may also be used for the tangent construction.

Case II ( $a, b, c$ ). From the equation

$$\frac{dx}{dy} = \frac{b(k-x) + ab(1-c)y}{k-x + b(1-c)y} = \frac{b \frac{k-x}{y} + ab(1-c)}{\frac{k-x}{y} + b(1-c)}$$

(homogeneous equation) it follows that the isoclines are the straight lines through the point of intersection  $(k, 0)$  of the horizontal and vertical lines along which move  $A$  and  $B$ .

*First tangent construction.* Draw through  $P(x, y)$  the lines  $PA$  and  $PB$  of the definition and determine on (the produced part of)  $AB$  the point  $S$ , situated in such a way that (the direction taken into consideration)  $SA:SB=1:(-c)$ , so that  $S$  is on the side of  $A$  when  $c < 0$ , and on the side of  $B$  when  $0 < c < 1$ . Then  $SP$  is the tangent in  $P$ . When  $c=0$  the tangent is  $\parallel AB$ .

*Demonstration:*

If the infinitesimal strips described by  $PA$  and  $PB$  are taken to be parallelograms with a common base i.e. the line element situated on the tangent in  $P$ , then the distances of  $B$  and  $A$  to that tangent have the ratio  $(1-c):1$ . If we call the point of intersection of the produced part of  $AB$  with the just mentioned tangent  $S_1$  we get  $S_1A:S_1B=1:(1-c)$  or  $S_1A:AB=1:(-c)$  consequently  $S_1$  and  $S$  coincide.

*Observations:*

1. If  $c$  increases from  $-\infty$  to 1, then the slope of the tangent increases from  $\tan \alpha$  to  $\tan \beta$ .
2. The demonstration given above holds also in case I, then yielding for the ordinate of  $S$  the value  $h/c$ .
3. On constructing for a number of lines through  $(k, 0)$ , hence for a number of values of  $(k-x)/y$ , the tangential positions, we obtain a quick diagram of the integral-curves.

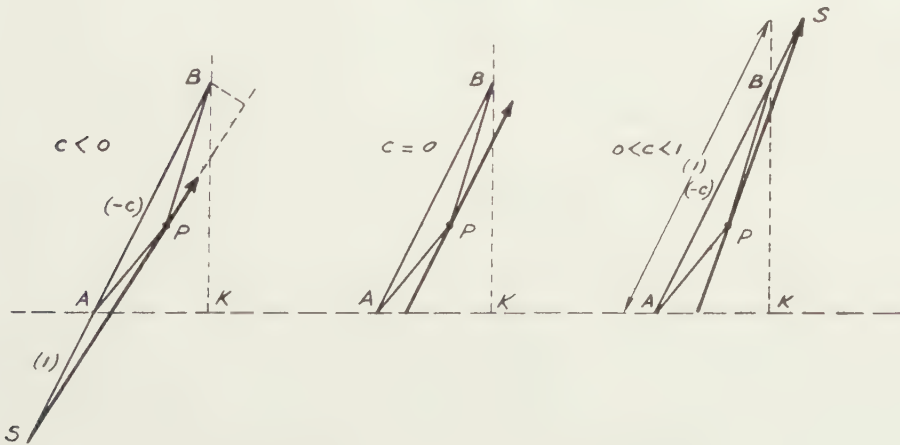


Fig. 8. First tangent construction for case II

4. The tangent constructions for I and II may be executed at the same time as follows: Draw through  $B(k, h)$  the line  $BC$  at the angle  $\beta$  with the  $X$ -axis and through any point  $P$  of  $BC$  the line  $PA$  at the angle  $\alpha$  with the  $X$ -axis and determine the point of intersection of  $AB$  (produced) with the line  $y = (h/c)$ . Then  $PS$  is the tangent position: in I for all the points of the horizontal line through  $P$  and in II for all the points of  $PK$ , if  $K$  is the point  $(k, 0)$ .

Second Tangent Construction: Draw any circle through  $K(k, 0)$  e.g. one that touches the  $X$ -axis  $OK$ , and draw  $KA$  and  $KB$  at the slope angles  $\alpha$  and  $\beta$  and  $KL$  and  $KM$  at the angles  $\gamma$  and  $\delta$ , in such a way that  $\tan \gamma = \{1/(1-c)\} \tan \alpha$  and  $\tan \delta = \{1/(1-c)\} \tan \beta$  (either suffices), then the tangential positions  $KB$ ,  $KA$ ,  $KO$  and  $KH$  correspond with the isoclines  $KO$ ,  $KH$ ,  $KM$  and  $KL$ . The points of intersection of  $KA$  with  $HB$ ,  $KO$  with  $BM$ ,  $KH$  with  $LB$ ,  $KL$  with  $HM$  are on one line  $p$ . With an isocline  $K_1$  corresponds the

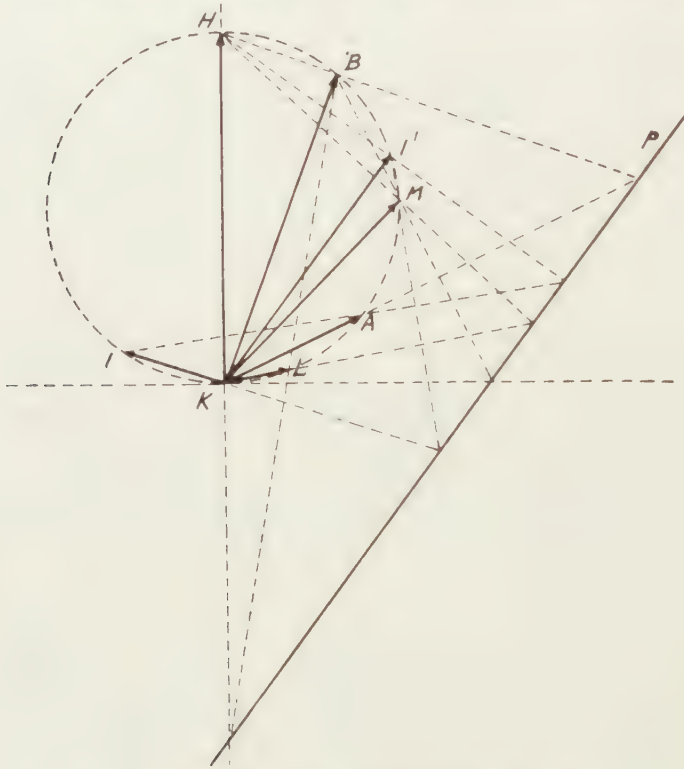


Fig. 9. Second tangent construction for case II

tangential position  $K1'$  (and inversely) by virtue of the property that  $1B$  and  $1'K$ ,  $1K$  and  $1'M$ ,  $1H$  and  $1'L$ ,  $1A$  and  $1'H$  cut each other on  $p$ . If  $K1$  and  $K2$  are any isocline respectively and  $K1'$  and  $K2'$  the corresponding tangential positions, then  $12'$  and  $21'$  always cut each other on  $p$ .

The symbols (except 0) and the figures all indicate points on the auxiliary circle. Cf. fig. 9.



*Demonstration :*

This follows from propositions of projective geometry, by virtue of the fact that there is a *projective correspondence* between the pencil of the isoclines and that of the tangential positions. We also demonstrate:

*We have the cases  $II_e$ ,  $II_h$  or  $II_p$  (see below) according as  $p$  has no, two different or two coinciding points in common with the auxiliary circle. The (possible) points of intersection of  $p$  with the auxiliary circle give, when joined to  $K$ , the tangent in  $K$  to the integral-curve and its asymptotic direction.*

Consequently the integral-curve in fig. 9 is a spiral.

The differential equation of  $II$  is

$$\frac{dx}{dy} = \frac{b(k-x) + ab(1-c)y}{k-x + b(1-c)y}$$

or

$$\frac{d(k-x)}{dy} = - \frac{k-x + a(1-c)y}{\frac{k-x}{b} + (1-c)y}$$

and can be replaced by

$$\begin{aligned} \frac{d(k-x)}{dt} &= -(k-x) - a(1-c)y \\ \frac{dy}{dt} &= \frac{k-x}{b} - (1-c)y \end{aligned}$$

after the introduction of a parameter  $t$ .

Cf. [2]. pp. 120 and 121, where  $t$  has the opposite sign.

In the relevant integral-curves is the value of  $t$ , employed here,  $> 0$ .

When integrating we distinguish three cases:

$$II_e: \quad (1-c) \frac{a}{b} - \left(1 - \frac{c}{2}\right)^2 > 0 \quad \text{or} \quad c^2 - 4(1-c) \frac{a-b}{b} < 0$$

$$II_h: \quad (1-c) \frac{a}{b} - \left(1 - \frac{c}{2}\right)^2 < 0 \quad \text{or} \quad c^2 - 4(1-c) \frac{a-b}{b} > 0$$

$$II_p: \quad (1-c) \frac{a}{b} - \left(1 - \frac{c}{2}\right)^2 = 0 \quad \text{or} \quad c^2 - 4(1-c) \frac{a-b}{b} = 0.$$

Here too  $0 < b < a$ ,  $1 - c > 0$ .

The curves  $II_e$  are affine transformations of logarithmic spirals (Bernoulli's spirals), circles included among them. The curves  $II_h$  are affine transformations of the lines  $y = x^n$  (polytropic lines).

The curves  $II_p$  are affine representations of  $y = x \lg|x|$ , hence also projective representations of the well-known logarithmic line.

*Demonstration :*

In  $II_e$  the solution is:

$$\begin{aligned} k-x &= \varrho_1 e^{-\frac{1}{2}ct} \cos \omega t + \varrho_2 e^{-\frac{1}{2}ct} \sin \omega t \\ y &= \sigma_1 e^{-\frac{1}{2}ct} \cos \omega t + \sigma_2 e^{-\frac{1}{2}ct} \sin \omega t, \end{aligned}$$

in which

$$\omega = \frac{1}{2} \sqrt{\left\{ 4(1-c) \frac{a-b}{b} - c^2 \right\}}.$$

By putting  $t=0$  we get  $k=\varrho_1$  and  $0=\sigma_1$  and from the differential-equations:

$$\frac{dx}{dt} = k \text{ and } \frac{dy}{dt} = \frac{k}{b} \text{ or } -k = -\frac{1}{2}kc + \varrho_2\omega \text{ and } \frac{k}{b} = \sigma_2\omega,$$

so that

$$\varrho_2 = \frac{-k(1-\frac{1}{2}c)}{\omega} \text{ and } \sigma_1 = \frac{k}{b\omega}.$$

After introducing the vectors

$$\vec{r} = \begin{vmatrix} k-x \\ y \end{vmatrix}, \vec{v}_1 = \begin{vmatrix} k \\ 0 \end{vmatrix} \text{ and } \vec{v}_2 = \begin{vmatrix} \frac{-k(1-\frac{1}{2}c)}{\omega} \\ \frac{k}{b\omega} \end{vmatrix}$$

we get:

$$\vec{r} = \vec{v}_1 e^{-\frac{1}{2}ct} \cos \omega t + \vec{v}_2 e^{-\frac{1}{2}ct} \sin \omega t.$$

In  $II_h$ , when

$$d = \sqrt{c^2 - 4(1-c) \frac{a-b}{b}},$$

the solution is:

$$\begin{aligned} k-x &= \varrho_1 e^{-\frac{1}{2}ct} \cosh\left(\frac{1}{2}d\right)t + \varrho_2 e^{-\frac{1}{2}ct} \sinh\left(\frac{1}{2}d\right)t \\ y &= \sigma_1 e^{-\frac{1}{2}ct} \cosh\left(\frac{1}{2}d\right)t + \sigma_2 e^{-\frac{1}{2}ct} \sinh\left(\frac{1}{2}d\right)t \end{aligned}$$

with

$$\varrho_1 = k, \sigma_1 = 0, -k = -\frac{1}{2}kc + \frac{1}{2}\varrho_2 d, \frac{k}{b} = \frac{1}{2}\sigma_2 d,$$

or

$$\varrho_2 = \frac{-k(2-c)}{d}, \sigma_2 = \frac{2k}{bd}.$$

After introducing the vectors:

$$\vec{r} = \begin{vmatrix} k-x \\ y \end{vmatrix}, \vec{v}_1 = \begin{vmatrix} k \\ 0 \end{vmatrix} \text{ and } \vec{v}_2 = \begin{vmatrix} \frac{-k(2-c)}{d} \\ \frac{2k}{bd} \end{vmatrix}$$

we get:

$$\vec{r} = \vec{v}_1 e^{-\frac{1}{2}ct} \cosh\left(\frac{1}{2}d\right)t + \vec{v}_2 e^{-\frac{1}{2}ct} \sinh\left(\frac{1}{2}d\right)t.$$

Hence also:

$$\vec{r} = \frac{\vec{v}_1 + \vec{v}_2}{2} e^{p_1 t} + \frac{\vec{v}_1 - \vec{v}_2}{2} e^{p_2 t}$$

in which  $p_1 = \frac{1}{2}(-c+d)$  and  $p_2 = \frac{1}{2}(-c-d)$ .

In  $II_p$  the solution is:

$$k-x = \varrho_1 e^{-\frac{1}{2}ct} + \varrho_2 t e^{-\frac{1}{2}ct} \quad y = \sigma_1 e^{-\frac{1}{2}ct} + \sigma_2 t e^{-\frac{1}{2}ct}$$

if

$$\varrho_1 = k, \sigma_1 = 0, \varrho_2 = -k \left(1 - \frac{c}{2}\right) = -k \sqrt{\left(1-c\right) \frac{a}{b}}, \sigma_2 = \frac{k}{b}.$$

After introducing the vectors:

$$\vec{r} = \begin{vmatrix} k-x \\ y \end{vmatrix}, \vec{v}_1 = \begin{vmatrix} k \\ 0 \end{vmatrix}, \vec{v}_2 = \begin{vmatrix} -k\left(1-\frac{c}{2}\right) \\ \frac{k}{b} \end{vmatrix}$$

this becomes:

$$\vec{r} = \vec{v}_1 e^{-\frac{1}{2}ct} + \vec{v}_2 t e^{-\frac{1}{2}ct} = \vec{v}_1 e^{-\frac{1}{2}ct} + \frac{2}{c} \vec{v}_2 \left(\frac{1}{2}ct\right) e^{-\frac{1}{2}ct}.$$

*Observations:*

1. The curve  $II$  ( $a, b, 0$ ) has

$$\omega = \sqrt{\frac{a-b}{b}}, \vec{v}_1 = \begin{vmatrix} k \\ 0 \end{vmatrix} \text{ and } \vec{v}_2 = \begin{vmatrix} \frac{-kb}{\sqrt{b(a-b)}} \\ \frac{k}{\sqrt{b(a-b)}} \end{vmatrix},$$

hence  $\vec{r} = \vec{v}_1 \cos \omega t + \vec{v}_2 \sin \omega t = \vec{v}_1 \cos \varphi + \vec{v}_2 \sin \varphi$ ,

and is consequently an *ellipse* with the equation:

$$b(a-b)y^2 + \{(k-x) + by\}^2 = k^2$$

cutting the  $Y$ -axis in  $\left(0, \frac{k}{\sqrt{ab}}\right)$ , the  $X$ -axis and the line  $PB$  having conjugate directions, just as the  $Y$ -axis and the line  $PA$ . This ellipse approximates a *circle*, if  $b \rightarrow 0$ ,  $a \rightarrow \infty$  and  $ab \rightarrow 1$ .

2. In case  $II_h$  the degree  $n$  of the curve satisfies the equation

$$n + \frac{1}{n} - 2 = \frac{c^2 b}{(1-c) \frac{a-b}{b}} - 4 = \frac{c^2 b - 4(1-c) \frac{a-b}{b}}{(1-c) \frac{a-b}{b}} > 0$$

for the relevant values of  $a$ ,  $b$  and  $c$ .

Consequently  $n > 0$ .

OBSERVATIONS ABOUT SOME DIFFERENTIAL EQUATIONS  
CONCERNING RECESSION OF MOUNTAIN SLOPES. II

BY

H. LOOMAN

(Communicated by Prof. F. A. VENING MEINESZ at the meeting of January 28, 1956)

*Central rectilinear recession**Case III* ( $a, b, c$ ). From the linear differential equation

$$\frac{dx}{dy} = \frac{h^2 - y^2}{\{h^2 + (1 - 2c)y^2\}y} x + \frac{2a(1 - c)y^2}{h^2 + (1 - 2c)y^2}$$

it follows that the isoclines  $(dx/dy) = p$  are cubic curves with the equation:

$$p\{h^2 + (1 - 2c)y^2\}y = (h^2 - y^2)x + 2a(1 - c)y^3$$

More especially we find if  $p = 0$  (zero isocline, locus of the points where the integral-curves have vertical tangents) the curve

$$x = \frac{-2a(1 - c)y^3}{h^2 - y^2}.$$

*Construction isoclines:* Construct the 0-isocline  $x = \frac{-2a(1 - c)y^3}{h^2 - y^2}$  and divide the horizontal parts bounded by the 0-isocline and the line  $x = ay$  at the ratio  $p : (a - p)$ ; the locus of these dividing points is the  $p$ -isocline.

*Demonstration:*

We have

$$\begin{aligned} p &= \frac{h^2 - y^2}{\{h^2 + (1 - 2c)y^2\}y} (x - ay) + \frac{a(h^2 - y^2)}{h^2 + (1 - 2c)y^2} + \frac{2a(1 - c)y^2}{h^2 + (1 - 2c)y^2} = \\ &= \frac{h^2 - y^2}{\{h^2 + (1 - 2c)y^2\}y} (x - ay) + a \frac{h^2 + (1 - 2c)y^2}{h^2 + (1 - 2c)y^2} = \\ &= \frac{h^2 - y^2}{\{h^2 + (1 - 2c)y^2\}y} (x - ay) + a, \end{aligned}$$

hence

$$a - p = \frac{h^2 - y^2}{\{h^2 + (1 - 2c)y^2\}y} (ay - x).$$

Also

$$\begin{aligned} p &= \frac{h^2 - y^2}{\{h^2 + (1 - 2c)y^2\}y} x + \frac{2a(1 - c)y^2}{\{h^2 + (1 - 2c)y^2\}y} = \\ &= \frac{h^2 - y^2}{\{h^2 + (1 - 2c)y^2\}y} \left\{ x - \left( \frac{-2a(1 - c)y^3}{h^2 - y^2} \right) \right\} = \\ &= \frac{h^2 - y^2}{\{h^2 + (1 - 2c)y^2\}y} (x - x_1), \text{ if } x_1 = \frac{-2a(1 - c)y^3}{h^2 - y^2} = \text{abscis 0-isocline.} \end{aligned}$$



Consequently  $p : (a-p) = (x-x_1) : (ay-x)$ , which was to be demonstrated. For  $c=0$  cf. fig. 14 [4] p. 1079.

*Observation :*

From  $(a-p) : a = (ay-x) : (ay-x_1)$  it follows that the isoclines form a system of curves which have an common affinity axis in the line  $ay=x$ . Consequently we can start from any other isocline and derive the others through affinity.

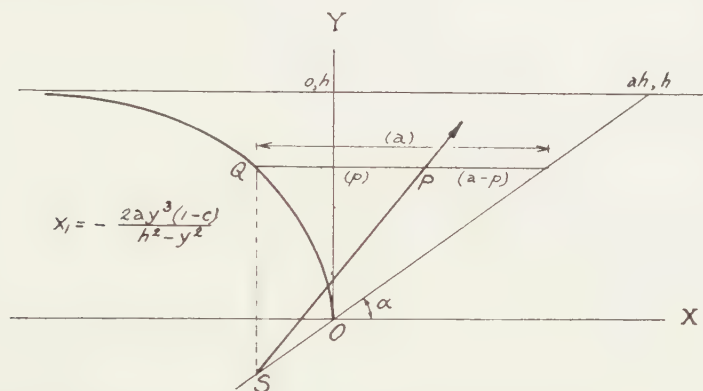


Fig. 10. Tangent construction and construction isoclines for case III

*Tangent construction for the integral-curves.* Draw through  $P(x, y)$  the horizontal line; the latter cuts the 0-isocline in point  $Q(x_1, y)$ , with  $x_1 = \frac{-2a(1-c)y^3}{h^2-y^2}$ . Draw through  $Q$  the vertical line; it cuts the line  $x=ay$  in the point  $S(x_1, y_1)$ . Then  $PS$  is the tangent in  $P$ . Cf. fig. 10.

*Demonstration :*

We have

$$\begin{aligned} \frac{dx}{dy} &= \frac{h^2-y^2}{\{h^2+(1-2c)y^2\}y} x + \frac{2a(1-c)y^2}{h^2+(1-2c)y^2} = \\ &= \frac{h^2-y^2}{\{h^2+(1-2c)y^2\}y} \cdot \left\{ x - \left( \frac{-2a(1-c)y^3}{h^2-y^2} \right) \right\} = \\ &= \left\{ x - \left( \frac{-2a(1-c)y^3}{h^2-y^2} \right) \right\} : \frac{\{h^2+(1-2c)y^2\}y}{h^2-y^2} = \\ &= \left\{ x - \left( \frac{-2a(1-c)y^3}{h^2-y^2} \right) \right\} : \left\{ y - \left( \frac{-2(1-c)y^3}{h^2-y^2} \right) \right\} = \\ &= (x-x_1) : (y-y_1) \end{aligned}$$

with

$$x_1 = \frac{-2a(1-c)y^3}{h^2-y^2}, \quad y_1 = \frac{-2(1-c)y^3}{h^2-y^2},$$

consequently  $x_1=ay_1$ .

*Observation :*

Point  $S(x_1, y_1)$  depends on  $y$ , not on  $x$ . The tangents, drawn in the points  $(x, y)$  of a line of constant  $y$ , pass through a centre  $S(x_1, y_1)$ , situated on  $x_1=ay_1$ , independent of  $x$ .

The solution of the equation III is (cf. [3] p. 964 for  $c \neq \frac{1}{2}$ ).

$$x = ay - (a-b)y \left\{ \frac{h^2}{h^2 + (1-2c)y^2} \right\}^{\frac{1-c}{1-2c}}, \text{ if } c \neq \frac{1}{2}$$

$$x = ay - (a-b)y e^{\frac{-y^2}{2h^2}}, \text{ if } c = \frac{1}{2}.$$

Here we distinguish three cases:

$$III_e : c < \frac{1}{2}$$

$$III_h : \frac{1}{2} < c < 1$$

$$III_v : c = \frac{1}{2}.$$

In case  $III_e$  we can write:

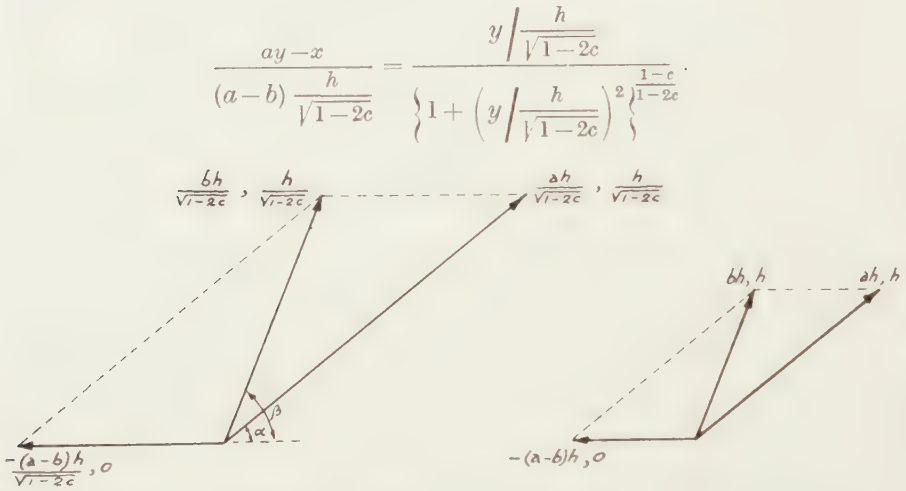


Fig. 11. Construction basevectors for case III,  $c < \frac{1}{2}$  and  $c = \frac{1}{2}$

Putting  $\frac{ay-x}{(a-b)\frac{h}{\sqrt{1-2c}}} = u$  and  $y/\frac{h}{\sqrt{1-2c}} = t = \tan \varphi$ , we have:

$$u = \frac{t}{(1+t^2)^{\frac{1-c}{1-2c}}} = \frac{\tan \varphi}{(\sec \varphi)^{\frac{2(1-c)}{1-2c}}} = \tan \varphi (\cos \varphi)^{\frac{2(1-c)}{1-2c}} = \sin \varphi (\cos \varphi)^{\frac{1}{1-2c}}.$$

Besides  $ay-x = u(a-b)\frac{h}{\sqrt{1-2c}}$  or

$$x = \frac{ah}{\sqrt{1-2c}} - \frac{y}{h/\sqrt{1-2c}} = u \frac{(a-b)h}{\sqrt{1-2c}}.$$

When introducing the vectors

$$\vec{r} = \begin{pmatrix} x \\ y \end{pmatrix}, \vec{v}_1 = \begin{pmatrix} -\frac{(a-b)h}{\sqrt{1-2c}} \\ 0 \end{pmatrix} \text{ and } \vec{v}_2 = \begin{pmatrix} \frac{ah}{\sqrt{1-2c}} \\ h/\sqrt{1-2c} \end{pmatrix}$$

we get:

$$\vec{r} = \vec{v}_1 \sin \varphi (\cos \varphi)^{\frac{1}{1-2c}} + \vec{v}_2 \tan \varphi$$

or

$$\vec{r} = \vec{v}_1 \frac{t}{(1+t^2)^{1-2c}} + \vec{v}_2 t.$$

In case  $III_h$  we can write:

$$ay - x = (a - b) y \left\{ 1 - (2c - 1) \left( \frac{y}{h} \right)^2 \right\}^{\frac{1-c}{2c-1}}$$

$$\frac{ay - x}{(a - b)h/\sqrt{2c-1}} = \frac{h}{h/\sqrt{2c-1}} \left\{ 1 - \left( \frac{y}{h/\sqrt{2c-1}} \right)^2 \right\}^{\frac{1-c}{2c-1}}.$$

Put  $\frac{y}{h/\sqrt{2c-1}} = \sin \varphi$ , then  $\frac{ay - x}{(a - b)h/\sqrt{2c-1}} = \sin \varphi (\cos \varphi)^{2\frac{1-c}{2c-1}}.$

Or after introduction of the vectors  $\vec{r} = \begin{vmatrix} x \\ y \end{vmatrix}$ ,  $\vec{v}_1 = \begin{vmatrix} -(a-b)h \\ \sqrt{2c-1} \\ 0 \end{vmatrix}$  and

$$\vec{v}_2 = \begin{vmatrix} ah \\ \sqrt{2c-1} \\ h \\ \sqrt{2c-1} \end{vmatrix} :$$

$$\vec{r} = \vec{v}_1 \sin \varphi (\cos \varphi)^{\frac{1-c}{2c-1}} + \vec{v}_2 \sin \varphi.$$

In case  $III_p$  we have:

$$\frac{ay - x}{(a - b)h} = \frac{y}{h} e^{-1\left(\frac{y}{h}\right)^2}$$

or after introducing the vectors:

$$\vec{r} = \begin{vmatrix} x \\ y \end{vmatrix}, \vec{v}_1 = \begin{vmatrix} -(a-b)h \\ 0 \end{vmatrix}, \vec{v}_2 = \begin{vmatrix} ah \\ h \end{vmatrix}$$

and substituting  $y/h = t$ :

$$\vec{r} = \vec{v}_1 t e^{-t^2} + \vec{v}_2 t.$$

*Observation:*

The curve  $III(a, b, 0)$  is the cubic curve

$$x = ay - \frac{(a-b)h^2y}{y^2+h^2} = by + \frac{(a-b)y^3}{y^2+h^2} \quad \text{or} \quad \frac{x-by}{ay-x} = \frac{y^2}{h^2}$$

and is the locus of points that divide the horizontal parts between  $x=by$  and  $x=ay$  at the ratio  $y^2:h^2$ ; consequently it can be easily constructed. It cuts the line  $y=h$  halfway between  $(bh, h)$  and  $(ah, h)$  just as  $I(a, b, 0)$ . Cf. [4], p. 1079, fig. 14.

*Case IV*  $(a, b, c)$ . The isoclines in IV can be derived from those of III by means of the following construction:

We use the line connecting  $O(0, 0)$  and  $(k, h)$  as transformation axis by making correspond two points  $(x, y)$  and  $(x_1, y_1)$ , which are on one line with  $O$ , while the vertical line through  $(x, y)$  and the horizontal line through  $(x_1, y_1)$  cut each other on the transformation-axis. If  $(x_1, y_1)$  describes an isocline of

III, then  $(x, y)$  describes the isocline of IV corresponding to the same tangential slope.

According to a figure this transformation is expressed by the formulae:

$$x = \frac{k}{h} y_1, \quad y = y_1^2 \frac{k}{hx_1} \quad \text{Cf. fig. 12.}$$

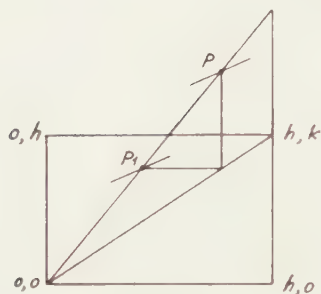


Fig. 12. Derivation isoclines IV from isoclines III, also tangent construction

*Demonstration:*

Putting in the differential equation for IV  $dy/dx=p$  we get:

$$2x^2y(1-c)(ap-1) + (k^2-x^2)(xp-y) = 0$$

or

$$2x^2y(1-c)(ap-1) + (k^2-x^2)\left(x\left(p-\frac{1}{a}\right) + \left(\frac{x}{a}-y\right)\right) = 0$$

or

$$\begin{aligned} (k^2-x^2)\left(y-\frac{x}{a}\right) &= 2x^2y(1-c)(ap-1) + (k^2-x^2)\frac{ap-1}{a} = \\ &= \frac{ap-1}{a} x \{2axy(1-c) + k^2-x^2\} \end{aligned}$$

$$(k^2-x^2)(ay-x) = (ap-1)[(x-ay)(k^2-x^2) + ay\{(1-2c)x^2+k^2\}]$$

$$ap(k^2-x^2)(ay-x) = (ap-1)ay\{(1-2c)x^2+k^2\}$$

$$\frac{ay-x}{y} = \frac{ap-1}{p} \frac{k^2+(1-2c)x^2}{k^2-x^2}.$$

After substituting

$$x = \frac{k}{h} y_1, \quad y = y_1^2 \frac{k}{hx_1},$$

we get:

$$\frac{ay_1^2 \frac{k}{hx_1} - \frac{k}{h} y_1}{y_1^2 \frac{k}{hx_1}} = \frac{ap-1}{p} \frac{k^2 + (1-2c) \frac{k^2}{h^2} y_1^2}{k^2 - \frac{k^2}{a^2} y_1^2}$$

or:

$$\frac{ay_1-x_1}{y_1} = \frac{ap-1}{p} \frac{h^2 + (1-2c) y_1^2}{h^2 - y_1^2}.$$

This, however, is the isocline of III with

$$p_1 = \frac{dx_1}{dy_1} = \frac{1}{p} \quad \text{or} \quad \frac{dy_1}{dx_1} = p.$$

From this follows immediately the:



*Tangent construction for the integral-curves.* To the point  $P(x, y)$  corresponds  $P_1(x_1, y_1)$  by virtue of  $x_1 = x^2(h/ky)$ ,  $y_1 = (h/k)x$  (see above). Draw in the way treated in III the tangent  $P_1S$  to the integralcurve of III, which passes through  $P_1$ . The line through  $P$  and  $||P_1S$  is the required tangent.

With the help of this we can easily obtain a diagram of the field of line elements and consequently of the integral-curves. See also for  $c=0$  [4] p. 1080 (algebraic curve) and p. 1372.

The integration of IV has not been executed in the publications mentioned, but can be got by the substitution  $a^2y^2/k^2 = v$ ,  $x/ay = t$ . For we have:

$$\begin{aligned}(1-c) \frac{2x^2y}{y^2} (dx - ady) + (k^2 - x^2) \frac{ydx - xdy}{y^2} &= 0 \text{ or} \\ (1-c) 2ya^2t^2(aydt + atdy - ady) + (k^2 - a^2y^2t^2)adt &= 0 \\ (1-c) at^2k^2(2vdt + tdv - dv) + k^2(1 - vt^2)adt &= 0 \\ (1-c) t^2 \left( 2v + t \frac{dv}{dt} - \frac{dv}{dt} \right) + 1 - vt^2 &= 0 \\ (1-c) t^2(t-1) \frac{dv}{dt} + (1-2c) vt^2 + 1 &= 0 \\ \frac{dv}{dt} = \frac{1-2c}{1-c} \frac{v}{1-t} + \frac{1}{(1-c)t^2(1-t)}.\end{aligned}$$

This is linear differential equation for  $v$ .

Integration of this with initial condition  $y=0$ ,  $t=b/a$  yields the solution:

$$v = (1-t)^{-\frac{1-2c}{1-c}} \cdot \frac{1}{1-c} \int_{b/a}^t \frac{(1-\lambda)^{\frac{-c}{1-c}}}{\lambda^2} d\lambda$$

or

$$\frac{(ay)^2}{k^2} \cdot \left( 1 - \frac{x}{ay} \right)^{\frac{1-2c}{1-c}} = \frac{1}{1-c} \int_{b/a}^{\frac{x}{ay}} \frac{(1-\lambda)^{\frac{-c}{1-c}}}{\lambda^2} d\lambda$$

or

$$(ay)^{\frac{1}{1-c}} (ay-x)^{\frac{1-2c}{1-c}} = \frac{k^2}{1-c} \int_{b/a}^{\frac{x}{ay}} \frac{(1-\lambda)^{\frac{-c}{1-c}}}{\lambda^2} d\lambda.$$

*Observation:*

The curve IV  $(a, b, 0)$  is the curve with the equation

$$bxy(ay-x) = k^2(x-by).$$

It cuts the line  $x=k$  in point  $\left(0, \frac{k}{\frac{1}{ab}}\right)$  (just as II  $(a, b, 0)$ ). Rendering the equation in the form  $(x-by):(ay-x) = xy:k(k/b)$  we see the connexion with III  $(a, b, 0)$ . Cf. [4], p. 1080, fig. 15. The equation can also be written

$$\frac{b}{a} \frac{x}{k} \frac{y}{k/a} \left( \frac{y}{k/a} - \frac{x}{k} \right) = \frac{x}{k} - \frac{b}{a} \frac{y}{k/a}.$$

Consequently, after the introduction of the base vectors  $\begin{vmatrix} k \\ 0 \end{vmatrix}$  and  $\begin{vmatrix} 0 \\ k/a \end{vmatrix}$  it

can be reduced to  $(b/a)xy(y-x)=x-(b/a)y$ . The constant  $b/a$  cannot be eliminated. In the general case we can use as base vectors

$$\begin{vmatrix} k/\sqrt{1-c} \\ 0 \end{vmatrix} \quad \text{and} \quad \begin{vmatrix} 0 \\ k/a/\sqrt{1-c} \end{vmatrix} \quad (\text{cf. case III});$$

then the equation only has the constants  $b/c$  and  $c$ .

### *Limiting cases. Knick formation*

In the foregoing we have always supposed  $0 < b < a < +\infty$ ,  $-\infty < c < 1$ . It is important to investigate limiting cases, in which one or more of the conditions:  $b \rightarrow 0$ ,  $a \rightarrow +\infty$ ,  $c \rightarrow -\infty$ ,  $c \rightarrow 1$  or  $a \rightarrow b$  respectively, have been fulfilled. It is also of importance to find if a form such as  $xy = \delta$  (with small positive  $\delta$ ) can occur in the neighbourhood of  $(0, 0)$ , which can practically be called a *knick*. This will require checking of the curvature of the integral curves; in [4], part II an other measure has been chosen for the flat part which, however, involves drawbacks.

1. In case I  $b \rightarrow 0$  yields nothing special, while  $a \rightarrow +\infty$  means an affine transformation with  $x = by$  as affinity axis and the curve approximates  $y = 0$ ; the curvature in  $(0, 0)$  increases to  $+\infty$ . The condition  $a \rightarrow b$  also yields an affine transformation with respect to  $x = by$  as affinity axis;  $d^2x/dy^2$  uniformly converging to 0, just as the curve.

For we have

$$\frac{d^2x}{dy^2} = (a-b)(1-c) \frac{h}{(cy-h)^2}$$

so that

$$\frac{d^2x}{dy^2} \Big|_{y=0} = \frac{(a-b)(1-c)}{h}$$

and

$$\frac{d^2x}{dy^2} \Big|_{y=h} = \frac{a-b}{(1-c)h},$$

hence curvature  $\Big|_{y=0} = \frac{(a-b)(1-c)}{h(1+b^2)^{3/2}}$ , curvature  $\Big|_{y=h} = \frac{a-b}{(1-c)h(1+a^2)^{3/2}}$ .

The osculating parabola in  $(0, 0)$  is  $x = by + \frac{1}{2} \frac{(a-b)(1-c)}{h} y^2$  which passes into I  $(a, b, 0)$  when  $c=0$ . The curvature  $\Big|_{y=h}$  varies when  $y=h$  from 0 to 0 via a maximum; this phenomenon has been pointed out in [4]. The form for  $c \rightarrow -\infty$  is found by letting the similarity factor tend to  $+\infty$  in such a way that  $h/c \rightarrow -l$ . We get

$$x - by = (a-b)l \left\{ \frac{y}{l} - lg \left( 1 + \frac{y}{l} \right) \right\}$$

with osculating parabola

$$x = by + \frac{1}{2} \frac{(a-b)(1-c)}{l} y^2.$$

So there is no sign of knick-formation.

1. In case I the change of  $b$  (see [1], fig. 4) yields an affine trans

formation (dilatation) with respect to  $x=ay$  as affinity axis, as is clear from the equation:

$$ay-x = \frac{a-b}{c} \left( \frac{y}{h/c} - (1-c) \lg \frac{1}{1-y/\frac{h}{c}} \right)$$

in which  $ay-x$  changes proportionally to  $a-b$ . The supposition  $b \rightarrow 0$  produces nothing special.

The change of  $a$  produces an affine transformation with respect to  $x=by$  as affinity axis, as is clear from:

$$x-by = (a-b) \frac{1-c}{c} \frac{h}{c} \left( \frac{-y}{h/c} + \lg \frac{1}{1-\frac{cy}{h}} \right)$$

in which  $x-by$  changes proportionally to  $a-b$  and consequently  $\rightarrow \infty$ , if  $a \rightarrow +\infty$ , with given  $y > 0$ . With given  $x$ :

$$-\frac{cy}{h} + \lg \frac{1}{1-\frac{cy}{h}} = \frac{1}{2} \left( \frac{cy}{h} \right)^2 + \frac{1}{3} \left( \frac{cy}{h} \right)^3 + \frac{1}{4} \left( \frac{cy}{h} \right)^4 + \dots$$

must consequently tend to 0, hence also  $y$ , while the curvature in  $(0, 0)$  namely  $\frac{(a-b)(1-c)}{h(1+b^2)^{3/2}}$  tends to  $\infty$ . The osculating parabola in  $(0, 0)$  is

$$x = by + \frac{1}{2} \frac{(a-b)(1-c)}{h} y^2$$

which passes for  $c=0$  into I  $(a, b, 0)$ .

If  $a \rightarrow b$ , the curve approximates the affinity axis  $x=by$ , while  $d^2x/dy^2$  and also the curvature uniformly tend to 0.

For we have

$$\frac{d^2x}{dy^2} = (a-b)(1-c) \frac{h}{(cy-h)^2} \text{ and } (1+b^2)^{3/2} \leq \left\{ 1 + \left( \frac{dx}{dy} \right)^2 \right\}^{3/2} \leq (1-a^2)^{3/2}.$$

For  $y=0$  and  $y=h$  we find respectively:

$$\begin{aligned} \frac{d^2x}{dy^2} \Big|_{y=0} &= \frac{(a-b)(1-c)}{h}, \text{ curvature } \Big|_{y=0} = \frac{(a-b)(1-c)}{h(1+b^2)^{3/2}} \\ \frac{d^2x}{dy^2} \Big|_{y=h} &= \frac{(a-b)}{(1-c)h}, \text{ curvature } \Big|_{y=h} = \frac{a-b}{(1-c)h(1+a^2)^{3/2}}. \end{aligned}$$

The curvature  $\Big|_{y=h}$  varies if  $a$  varies from 0 to  $\infty$ , from 0 to 0 via a maximum; for case IV this phenomenon has been pointed out in [4] pp. 1369–1371.

If  $c$  varies from 0 to  $-\infty$ , then it follows from the first tangent construction (for  $y > 0$ ) that the tangent in  $P$  turns from the position.  $AB$  to the position of  $PA$ , so that the line  $x=ay$  is the limit. The form for  $c \rightarrow -\infty$ , in the neighbourhood of  $(0, 0)$  is found by letting the similarity factor  $h$  tend to  $+\infty$  in such a way that  $h/c \rightarrow -l$ . We get

$$x-by = (a-b) l \left\{ \frac{y}{l} - \lg \left( 1 + \frac{y}{l} \right) \right\}$$

with osculating parabola

$$x = by + \frac{1}{2} \frac{(a-b)(1-c)}{l} y^2$$

See [1] fig. 5.

So there is no sign of knick-formation.

2. In case II it appears from

$$\{(k-x) + b(1-c)y\} \frac{dx}{dy} = b(k-x) + ab(1-c)y$$

that for  $b \rightarrow 0$  we find besides  $x=k$  also  $dx/dy=0$ , so the  $y$ -axis.

If at the same time we let  $c$  tend to  $-\infty$ , so that  $\lim -bc = \lim b(1-c) = m$  we get in the limit

$$\{(k-x) + my\} \frac{dx}{dy} = amy.$$

Putting  $x = \mu y^2 + \nu y^3 + \dots$  we find

$$(k + my - \mu y^2 - \nu y^3 - \dots) (2\mu y + 3\nu y^2 + \dots) = amy,$$

which gives  $2k\mu = am$ ,  $\mu = \frac{am}{2k}$

$$3k\nu + 2m\mu = 0, \quad \nu = \frac{-2\mu m}{3k} = -\frac{am^2}{3k^2}$$

so:

$$x = \frac{am}{2k} y^2 - \frac{am^2}{3k^2} y^3 - \dots$$

so in the first approximation a parabola;  $x = (am/k) \frac{1}{2} y^2$ , so no *knic* formation.

The first tangent construction now becomes as follows. *Erect a line through O at an angle  $\alpha$  and drop a line through  $K(k, 0)$  to the left at an angle whose  $\cot = m$ . Draw through a point P of the first line a vertical line cutting the second in a point C and call the point of intersection of the horizontal line through C with the Y-axis S, then PS is the tangential position for all the points of KP. The integralcurve cuts the X-axis perpendicularly.*

The demonstration follows from  $\frac{dx}{dy} = \frac{ay}{\frac{k-x}{m} + y}$ .

If at the same time we let  $b$  tend to 0 and  $a$  to  $\infty$ , in such a way that  $\lim ab = g$ , we get:

$$(k-x) \frac{dx}{dy} = g(1-c)y \quad \text{or} \quad g(1-c)y^2 + (k-x)^2 = k^2.$$

This is an ellipse with half axes  $k$  and  $\frac{k}{\sqrt{g(1-c)}}$  and passes into a circle if  $g(1-c) = 1$ .

The behaviour if  $a \rightarrow b$  is found from:

$$\frac{dy}{dx} = \frac{1}{b} - \frac{1}{b} \frac{k-x+(1-c)by}{k-x+(1-c)ay} = \frac{1}{b} \frac{(1-c)(a-b)y}{k-x+(1-c)ay}$$



or approximated:

$$\frac{1}{b} - \frac{dy}{dx} = \frac{(1-c)(a-b)y}{bk}$$

$$dx - b dy = \frac{(1-c)(a-b)}{bk} y dx = \frac{(1-c)(a-b)}{k} y dy$$

$$x - by = \frac{1}{2} (1-c) \frac{a-b}{k} y^2.$$

The limit is the line  $x = by$ . In order to find the behaviour if  $c \rightarrow -\infty$  we start from the differential equation

$$\frac{dy}{dx} = \frac{\frac{1}{b}(k-x) + (1-c)y}{k-x + (1-c)ay}$$

and let  $k$  tend to  $\infty$  in such a way that  $k/(1-c) \rightarrow l$ . As  $k$  is a similarity factor, the form is preserved.

We get

$$\frac{dy}{dx} = \frac{\frac{1}{b} \left( \frac{k}{1-c} - \frac{x}{1-c} \right) + y}{\frac{k}{1-c} - \frac{x}{1-c} + ay}.$$

So the limit is:

$$\frac{dy}{dx} = \frac{(l/b)+y}{l+ay} \text{ or } \frac{dx}{dy} = \frac{l+ay}{(l/b)+y} = a + \frac{l(1-(a/b))}{(l/b)+y}$$

$$x = ay + l \left( 1 - \frac{a}{b} \right) \lg \frac{y+(l/b)}{l/b}$$

$$x = ay - l \frac{a-b}{b} \lg \left( 1 + \frac{by}{l} \right)$$

$$\frac{ay-x}{l} = \frac{a-b}{b} \lg \left( 1 + \frac{by}{l} \right) = (a-b) \frac{y}{l} - \frac{a-b}{b} \frac{1}{2} \frac{b^2 y^2}{l^2} + \dots$$

$$x - by = \frac{1}{2} \frac{a-b}{bl} y^2 \quad (\text{osculating parabola}).$$

*So no sign of knick-formation.*

In full:

$$x - by = (a-b) y - l \frac{a-b}{b} \lg \left( 1 + \frac{by}{l} \right)$$

$$= \frac{a-b}{b} l \left\{ \frac{by}{l} - \lg \left( 1 + \frac{by}{l} \right) \right\}$$

so the same form as in I.

3. The influence of the variation of  $b$  on the form of III ( $a, b, c$ ) (see [3], p. 1157, fig. 8) may be found by writing the equation of the integral-curve as follows:

$$ay - x = (a-b) y \left\{ \frac{b^2}{b^2 + (1-2c)y^2} \right\}^{\frac{1-c}{1-2c}} \quad \text{when } c \neq \frac{1}{2}$$

$$ay - x = (a-b) y e^{\frac{-y^2}{2b^2}}, \quad \text{when } c = \frac{1}{2}.$$

$ay-x$  varying proportionally to  $a-b$ , this means an affinity with respect to  $x=ay$  as affinity axis. The case  $b \rightarrow 0$  produces nothing special.

The variation of  $a$ , hence also of  $a-b$  yields an affine transformation with respect to  $x=by$  as affinity axis, as is clear from:

$$x-by = (a-b) y \left[ 1 - \left\{ \frac{l^2}{h^2 + (1-2c)y^2} \right\}^{\frac{1-c}{1-2c}} \right], \text{ if } c \neq \frac{1}{2}$$

$$x-by = (a-b) y \left\{ 1 - e^{-\frac{y^2}{2h^2}} \right\}, \text{ if } c = \frac{1}{2}$$

so that for  $a \rightarrow \infty$  the curve approximates  $y=0$ .

Cf. [3], p. 1158, fig. 9.

All the curves have an inflexion point in  $(0, 0)$  so the curvature 0, while for large  $x$  the curvature is again near to 0. There is a point with maximum curvature which tends to  $(0, 0)$  if  $a$  increases. Then the curvature assumes any large value so that the shape of a *knick* is approached.

Consequently we have this shape:



Fig. 13. Knick formation in III

For III  $(a, b, 0)$  we have the progression

$$x = by + (a-b) \left\{ \frac{y^3}{h^2} - \frac{y^5}{h^4} + \dots \right\}.$$

So there is in  $(0, 0)$  the cubic parabola  $x = by + (a-b/h^2)y^3$ , which has a contact of the 4th order with III  $(a, b, 0)$ .

For this the curvature is

$$\frac{b \frac{y}{h^2}}{\left\{ 1 + \left( b + \frac{3(a-b)}{h^2} y^2 \right)^{3/2} \right\}}$$

from which the point with maximum curvature can be found.

In order to find the form of III  $(a, b, c)$  if  $c \rightarrow -\infty$ , we let the similarity factor tend to  $\infty$ , so that  $\lim \frac{h}{\sqrt{1-2c}} = l$ .

We then get from:

$$ay-x = (a-b) y \left\{ 1 + \frac{(1-2c)y^2}{h^2} \right\}^{-\frac{1-c}{1-2c}}$$

the limit equation.

$$ay-x = (a-b) y \left( 1 + \frac{y^2}{l^2} \right)^{-1/2} = l(a-b) \cdot \frac{y/l}{\sqrt{1+(y^2/l^2)}}$$

with asymptote  $ay-x = (a-b)l$ . See [3], p. 1155, fig. 6.

4. In case IV  $x=0$  is an integral-curve, corresponding to  $b=0$ , for any values of  $a$  and  $c$ , as is clear from the differential equation. If,

however, we let  $b$  tend to 0 and  $c$  to  $-\infty$ , so that  $bc \rightarrow -l$ , we get as limit, besides  $x=0$ , also a line parallel to  $ay-x=0$ . Hence there are curves that have the shape of  $xy-\delta$  in the neighbourhood of the origin and which, consequently, have practically a *knick*.

In general for the point of intersection  $(k, y)$  of an integral-curve with  $x=k$  we have:

$$(ay_1)^{\frac{1}{1-c}} (ay_1 - k)^{\frac{1-2c}{1-c}} = \frac{k^2}{1-c} \int_{b/a}^{\frac{k}{ay_1}} \frac{(1-t)^{\frac{-c}{1-c}}}{t^2} dt.$$

If  $c \rightarrow -\infty$ ,  $1/(1-c) = \delta$  tends to 0 and  $-c/(1-c) = 1-\delta$ , so the right term becomes:

$$\begin{aligned} & \frac{k^2}{1-c} \int_{b/a}^{\frac{k}{ay_1}} \frac{(1-t)^{1-\delta}}{t^2} dt - k^2 \delta \int_{b/a}^{\frac{k}{ay_1}} \frac{1 - (1-\delta)t - \frac{(1-\delta)\delta}{2}t^2 + \dots}{t^2} dt = \\ & = k^2 \delta \left[ -\frac{1}{t} + (1-\delta) \lg \frac{1}{t} - \frac{(1-\delta)\delta}{2} t + \dots \right]_{b/a}^{\frac{k}{ay_1}} = \\ & = \delta k^2 \left[ -\frac{ay_1}{k} + (1-\delta) \lg \frac{ay_1}{k} - \dots + \frac{a}{b} - (1-\delta) \lg \frac{a}{l} + \dots \right] \\ & \rightarrow k^2 \lim \frac{\delta a}{b} = k^2 \lim \frac{a}{(1-c)b} = k^2 \lim \frac{a}{-bc} = k^2 \frac{a}{l}, \end{aligned}$$

if  $b \rightarrow 0$  and  $c \rightarrow -\infty$  and  $\lim -bc = l$ .

So we get in the limit:

$$(ay_1 - k)^2 = k^2 \frac{a}{l} \text{ or } ay_1 = k + k \sqrt{\frac{a}{l}} \text{ or } y_1 = \frac{k}{a} + \frac{k}{\sqrt{al}}.$$

The curve approximates

$$ay - x = k + k \sqrt{\frac{a}{l}}.$$

So we have the shape of fig. 14. Just as in III the integral-curves have

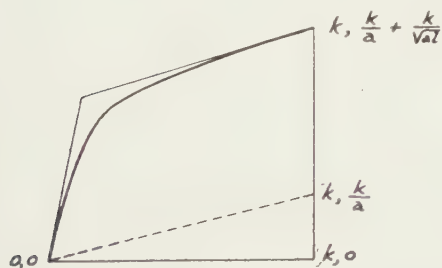


Fig. 14. Knick formation in IV

an inflexion point in  $(0, 0)$  and there is a cubic parabola with a contact of the 4th order.

Now we let  $c$  tend to  $-\infty$  and at the same time the similarity factor  $k$  to  $+\infty$  in such a way that  $\frac{k}{1-c}$  has the limit  $m$ . We find as above:

$$\begin{aligned}
m^2 \int_{b/a}^{\frac{x}{ay}} \frac{(1-t)^{1-\delta}}{t^2} dt &= m^2 \int_{b/a}^{\frac{x}{ay}} \frac{1-t}{t^2} dt = m^2 \left[ -\frac{1}{t} + lg \frac{1}{t} \right]_{b/a}^{\frac{x}{ay}} = \\
&= m^2 \left( -\frac{ay}{x} + lg \frac{ay}{x} + \frac{a}{b} - lg \frac{a}{b} \right) = m^2 \left( \frac{a(x-by)}{bx} + lg \frac{by}{x} \right),
\end{aligned}$$

hence the limit equation:

$$(ay-x)^2 = m^2 \left[ \frac{a}{b} \left( 1 - \frac{by}{x} \right) + lg \left( 1 - \left( 1 - \frac{by}{x} \right) \right) \right].$$

## LITERATURE

(The articles mentioned below have appeared in the *Proceedings of the Koninklijke Nederlandse Akademie van Wetenschappen*).

1. BAKKER, J. P. and J. W. N. LE HEUX, Projective-geometric treatment of O. Lehmann's theory of the transformation of steep mountainslopes. *Proc.* **49**, 533-547 (1946).
2. DIJK, W. VAN and J. W. N. LE HEUX, Theory of parallel rectilinear slope-recession, part I and II. *Proc.* **55**, 155-122 and 123-129 (1952). On page 121 the solution for  $d = 0$  is given incorrectly: (20) sub 2 should be

$$\begin{aligned}
x' &= \lambda_1 e^{\frac{1}{2}ct} + \lambda_2 t e^{\frac{1}{2}ct} \\
y &= \mu_1 e^{\frac{1}{2}ct} + \mu_2 t e^{\frac{1}{2}ct}
\end{aligned}$$

while (22) should be

$$\begin{aligned}
\lambda_1 &= k, \quad \lambda_2 = -\frac{c}{2} k \\
\mu_1 &= 0, \quad \mu_2 = -\frac{k}{h}.
\end{aligned}$$

3. BAKKER, J. P. and J. W. N. LE HEUX, Theory on central rectilinear recession of slopes, part I and II. *Proc.* **50**, 959-966 and 1154-1162 (1947).

On page 962 the symbol  $b$  is used for the variable  $\cotg \beta = x/y$  whereas further down  $b$  represents a constant (integration constant, namely the value of  $\cotg \beta$  for  $x = y = 0$ ).

On page 965 footnote 6) the condition  $b \rightarrow a$  is wrongly mentioned. This should be  $a - b \rightarrow +\infty$ . If  $a - b$  remains limited, the limit is  $x = ay + 0$ . In general we get:

$$x = ay - \lim \frac{(a-b)h}{\sqrt{1-2c}}.$$

On page 1154 we read the incorrect statement that if  $c = \frac{1}{2}$  the formula (14a) assumes the form  $x = by$ . This should be:

$$x = ay - (a-b)ye^{-\frac{1}{2}\frac{y^2}{h^2}}.$$

4. ——— and ———, Theory on central rectilinear recession of slopes, part III and IV. *Proc.* **53**, 1073-1084 and 1364-1374 (1950).
5. ——— and ———, A remarkable new geomorphological law, part I and II. *Proc.* **55**, 339-340 and 554-571.

On page 407 we find incorrectly, as in 3,  $b \rightarrow a$ .



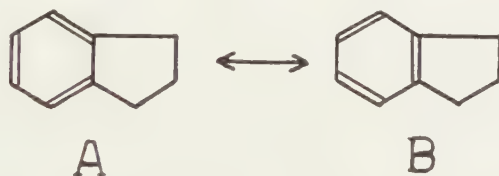
# OZONOLYSIS OF INDAN, 4,7-DIMETHYLINDAN AND 5,6-DIMETHYLINDAN IN CONNECTION WITH THE SO-CALLED MILLS-NIXON EFFECT \*) \*\*)

BY

J. P. WIBAUT AND F. P. K. DE JONG

(Communicated at the meeting of March 24, 1956)

A preferential stabilization of one Kekulé form has been discussed by MILLS and NIXON <sup>1)</sup> in the case of indan, on the strength of geometrical considerations. These authors concluded that the form A, in which the carbon atoms common to the two rings are joined by a single bond, should be more free from strain, or more stable than the alternate form B with double linkage of the rings.



According to the original postulate of MILLS and NIXON the ringsystem of indan exists in the rigid structure A. To test this theory MILLS and NIXON and other authors investigated the diazo-coupling of hydroxy-indans. The observations as a whole indicate that there is no rigid fixation of bonds in the indan system, although there may exist a slight preference for one structure.

According to several authors the Kekulé structure according to MILLS and NIXON (structure A) is privileged.

In 1946 LONGUETT-HIGGINS and COULSON published a theoretical study on the Mills-Nixon effect.<sup>2)</sup> Their conclusion—based on the molecular orbital method—was that contrary to the generally adopted theory, the common carbon-carbon bond of the two nuclei must be shortened resulting in a stronger double bond character of that bond; the other aromatic bonds have also changed. In indan the differences in bond order and length

\*) F. P. K. DE JONG: "Het Mills-Nixon Effect", Thesis Amsterdam 1951. (printed by Firma P. Harte, Bergen op Zoom, Netherlands).

\*\*) Complete experimental data will be published in the *Recueil des Travaux Chimiques des Pays-Bas*.

<sup>1)</sup> W. H. MILLS and J. G. NIXON, *J. Chem. Soc.* **1930**, 2510.

<sup>2)</sup> H. C. LONGUETT-HIGGINS and C. A. COULSON, *Trans. Farad. Soc.* **42**, 756 (1946).

from those in benzene are very small and in the opposite direction to those commonly postulated.

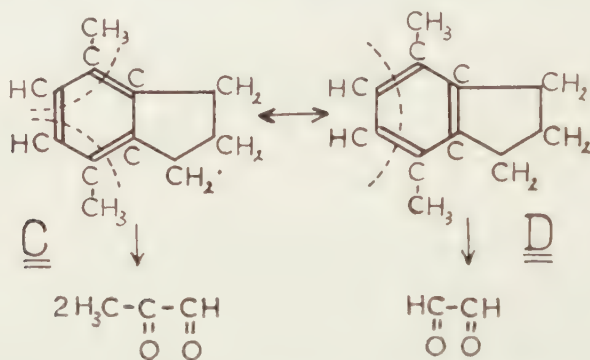
We studied the ozonolysis of indan, of 4,7-dimethylindan and of 5,6-dimethylindan. The ozonizations of the indans were carried out in chloroform solution at a temperature from -25 to -30 centigrades.

In the ozonolysis of indan there is formed glyoxal which has been isolated in the form of glyoxime; yield of glyoxime 15% and 17% calculated on the intake of indan.

In the ozonization of indan there occurs a side reaction, i.e. the oxidation of a part of the hydrocarbon to indanon-1. In one experiment we isolated the *p*-nitro-phenylhydrazone of indanon-1, melting point 233°; melting point of an authentic preparation 238°, mixed melting point 234°. Yield: 0.5 millimol from 12 millimol indan.

Similar side-reactions occur in the ozonolysis of the dimethylindans.

The ozonolysis of 4,7-dimethylindan yields methylglyoxal and glyoxal. Therefore the dimethylindan reacts with ozone according to both Kekulé structures C and D.



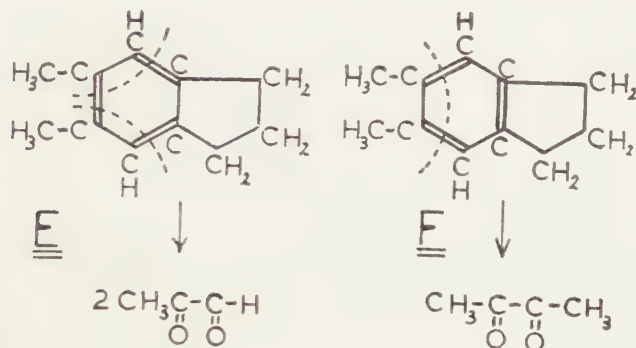
Methylglyoxal and glyoxal have been isolated in the form of the oximes. These oximes have been identified by melting points and mixed melting points. In four experiments the following results were obtained.

The total yield of oximes amounted to 9.7%, 10.4%, 9% and 9.6% of the theoretical yield, calculated on the intake of dimethylindan. The mixtures of oximes were analysed; from the percentage of methylglyoxime and the percentage of glyoxime we have calculated the molecular ratio glyoxim: methylglyoxim = 1.66, 1.77, 1.44, 1.43, mean value 1.57.

The molecular ratio glyoxim: methylglyoxim = 1.57 indicates that 4,7-dimethylindan reacts for about 76% according to form D and for 24% according to form C. This result is the opposite from what would be expected from the theory of MILLS and NIXON.

Similar results were obtained in the ozonolysis of 5,6-dimethylindan. The scission products methylglyoxal and dimethylglyoxal have been isolated in the form of the di-oximes; methylglyoxime and dimethylglyoxime have been identified by means of melting points and mixed

melting points. In three experiments the total yield of oximes amounted to 4.7 %, 5.1 %, and 3.7 % of the theoretical yield, calculated on the intake of dimethylindan. For the molecular ratio dimethylglyoxime: methylglyoxime we found 3.4, 3.1 and 4.1, mean value 3.5. This means that 5.6-dimethylindan reacts for about 87 % according to form F and for about 13 % according to form E.



### Conclusion

The experimental results represent only a first approximation from the quantitative side because of the low yields of diones, which have been obtained. However, these results warrant the following conclusion:

In the reaction with ozone 4.7-dimethylindan and 5.6-dimethylindan react according to both Kekulé structures. From the molecular ratio of the oxidation products, namely glyoxal and methylglyoxal, respectively methylglyoxal and dimethylglyoxal it follows that one Kekulé structure is privileged; this is the form in which the carbon atoms common to the two rings are joined by a double bond. This result is the opposite from what would be expected from the theory of MILLS and NIXON, but seems in agreement with the theoretical study of LONGUETT-HIGGINS and COULSON.

*Amsterdam, March 1956.*

*Laboratory for Organic Chemistry  
of the University of Amsterdam*

### BIBLIOGRAPHY

Some results of this investigation have been mentioned by WIBAUT in several lectures:

- WIBAUT, J. P., The application of ozonolysis to the study of the fine structure of aromatic compounds. *Comptes Rendus de la quinzième conférence de l'Union Internationale de Chimie pure et appliquée*, Amsterdam 1949, p. 79.
- , L'ozonation et l'ozonolyse des composés aromatiques et hétérocycliques dans la détermination de la réactivité du système cyclique. *Ind. chim. Belge* 20, 1 (1955).
- , L'ozonation et l'ozonolyse des composés aromatiques et hétérocycliques dans la détermination de la structure fine des molécules. *J. Chim. Phys.* France, p. 111 (1956).

AN X-RAY INVESTIGATION OF THE WHITE TO GREY  
TRANSFORMATION OF TIN

BY

KEHSIN KUO AND W. G. BURGERS

(Communicated at the meeting of March 24, 1956)

1. *Introduction*

Tin exists in two allotropic forms: white tin ( $\beta$ -Sn) with a tetragonal lattice above 13° C and grey tin ( $\alpha$ -Sn) with a diamond structure below this temperature. The transformation from white to grey tin is accompanied by an unusual large increase in volume (about 20 %), with the result that the grey tin falls into pieces. The so-called tin disease is a direct consequence of this volume expansion.

Earlier experiments (GROEN & BURGERS, 1954; GROEN, 1954) carried out in this laboratory showed that compact pieces of grey tin can be obtained, provided that the white tin contains a small amount of mercury. Starting from a single crystal of white tin, GROEN and BURGERS (1954) obtained in one case a single crystal of the grey form. Recently HALL (1955) confirmed the importance of the presence of a small amount of mercury for the compactness of grey tin, which, however, is always polycrystalline in Hall's experiments.

The present investigation was undertaken in order to study by means of Laue X-ray method the crystallographic aspects of the formation of grey tin from single crystals of white tin.

These aspects are:

1. The physical state of grey tin = single crystal or polycrystalline.
2. The orientation-relationship between white and grey tin.
3. The deformation of white tin caused by the formation of grey tin. — Earlier HALL (1955) has observed slip lines and kink bands in the white tin near the transformation front.

2. *Preparation and transformation of single crystals of white tin*

A master alloy of tin (MERCK, pro analysi, >99.93 %) containing 2.22 atomic per cent mercury was first prepared by melting in vacuum, from which the tin-mercury alloy with 0.052 atomic per cent mercury was later prepared in a fireclay crucible. This alloy was homogenized at 150° C for two days and thereafter was rolled down to 1 mm. From this thin sheet specimens of about 10 × 30 mm with a pointed end of 20 mm long were cut. Single crystals of white tin were grown, starting from



the pointed end of the specimen, in a horizontal moving furnace according to the method of ANDRADE and ROSCOE (1937); the temperature was 270–300° C and the moving speed 80 mm per hour.

According to GROEN and BURGERS (1954), the essential conditions for the formation of compact grey tin are:

1. The use of thin sheets.
2. A slow rate of transition.
3. The growth of only one nucleus.

These conditions should also apply to the formation of single crystals of grey tin.

At –20° C, the rate of nucleation of grey tin is extremely slow, whereas that of growth is measurable, about 10 mm per day; therefore this temperature would be favourable for the growth of single crystals of grey tin. However, the incubation period is extremely long (more than two months) and therefore grey tin powder has been put into the refrigerator, so that the white tin crystals are “infected” (not “inoculated”, as direct contact between white and grey tin did not appear to be a necessary condition for this infection). In this way the incubation period was shortened to 3 to 10 days. Commonly only one grey colony forms at a corner of the specimen and grows from one end of the white crystal to the other (figures 1a and 1b). Cracks are always present in the grey tin, so formed, the largest compact piece ever obtained was  $7 \times 10$  mm. If the transformation starts somewhere along the long sides, the white crystal becomes bent and a large crack occurs invariably in the middle part of the grey nodule (figure 1c). Of the twenty white tin crystals fifteen started to transform at the corners and the rest at the sides.

The orientation of both white and grey tin near and at the transformation front was determined by the glancing Laue method. Sometimes it was necessary to extend the X-ray examination over a length of 5 mm on both sides of the boundary in order to study the rotation of the lattice (see paragraph 4). The molybdenum tube was operated at 50 kV and 15 mA, the collimator had a diameter of 0.5 mm and a length of 40 mm and the film-specimen distance was 40 mm.

Since grey tin has the diamond structure, its orientation could easily be determined by comparing the stereographic projection of the Laue reflections with a set of standard projections for cubic crystals using SCHIEBOLD and SACH's method (1926). Generally, it was enough to use one side of the Laue photograph to determine the orientation of the grey tin crystal.

In the case of white tin, which has a body-centred tetragonal lattice, specially prepared standard projections were required <sup>1</sup>). The important

---

<sup>1</sup>) The (001)- and (111)-projections of white tin ( $a = 5.84$  Å, and  $c = 3.17$  Å) were prepared by Mr. J. H. PALM in this laboratory.

reflections are from the (100)-, (110)-, (101)- and (211)-planes and their angular relationship is shown in table I. By measuring the angles between the intense Laue spots and comparing them with those listed in table I, the orientation of the white tin could thus be determined.

TABLE I<sup>1)</sup>  
Angular relationship between important planes of white tin

	(100)	(101)	(110)	(211)
(100)	90°	—	—	—
(101)	61° ; 90°	40° ; 57°	—	—
(110)	45°	70°	90°	—
(211)	46° ; 70°	27° ; 44° 67° ; 77°	43° ; 76°	28° ; 40° 66° ; 79° 86° ; 88°

Of the twenty transformed single crystals of white tin, twelve were single crystals of grey tin, five polycrystalline, and three consisted of large grey crystals, the orientation of which could sometimes still be determined. This confirms the finding of GROEN and BURGERS (1954) that a single crystal of grey tin can be obtained from a single crystal of white tin in spite of the large volume expansion. This seems to be unusual and the possible explanation is that the transformation strain is borne mainly by the ductile white tin (cf. paragraph 4).

HALL (1955) used a lower temperature ( $-78^{\circ}\text{C}$ ) for the nucleation of grey tin and found that several grey nodules formed simultaneously and the resulting grey pieces were always polycrystalline. The difference in transformation temperature, hence the rate of nucleation, may account for the different transformation behaviours observed by HALL and the present authors. However, this point has not been further investigated.

It is perhaps also of interest to note that in one case a single crystal of grey tin has also been obtained when starting from polycrystalline white tin.

### 3. *The orientation-relationship between white and grey tin*

As mentioned above, the transition of white into grey tin is accom-

<sup>1)</sup> See for a more extensive table J. F. NICHOLAS, *J. Metals* 3, 1142 (1951).

Fig. 1. Formation of a grey nodule in white tin crystals (magnif.  $2\times$ ). a. Crystal 2D. At one end; b. Crystal 3F. At one corner; c. Crystal 4J. At one side.

Fig. 2. Laue-photographs (crystal 3G). a. Undeformed white tin crystal; b. The same deformed white crystal as shown in figure 2a (asterism) and undeformed grey tin crystal (sharp spots) close to the transformation front.

Fig. 3. Laue-photographs (crystal 4E). a. Another example of a deformed white crystal (asterism) and an undeformed grey tin crystal (sharp spots) close to the transformation front; b. The same crystal of grey tin as shown in figure 3a, but deformed, 1 mm from the transformation front.

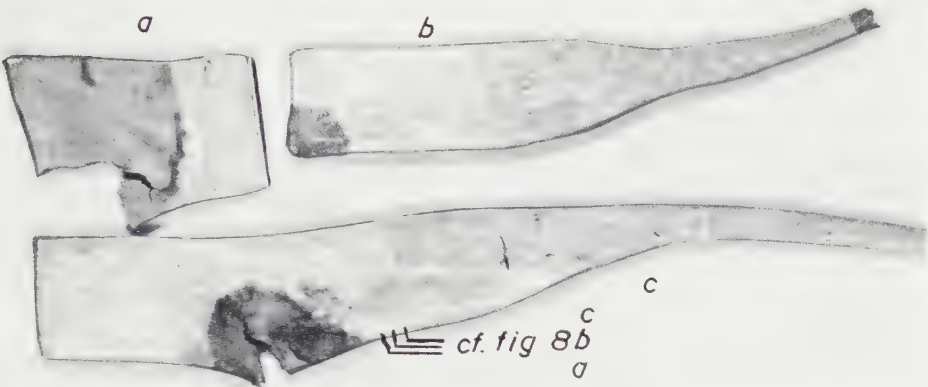


Fig. 1

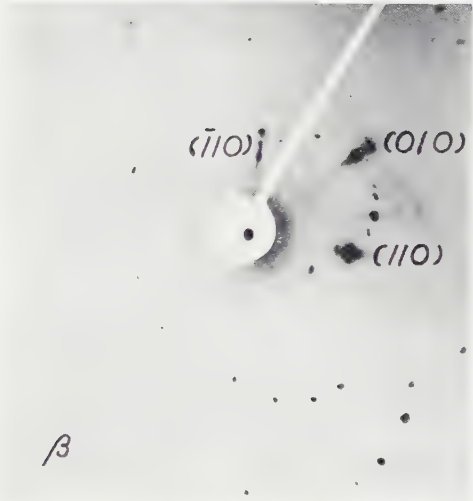


Fig. 2a



Fig. 2b



Fig. 3a



Fig. 3b



Fig. 4



Fig. 7

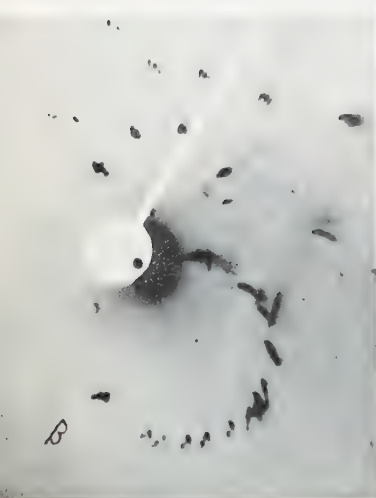


Fig. 8a



Fig. 8b



Fig. 8c



Fig. 10a



Fig. 10b



panied by a volume increase no less than 20 % and therefore a considerable amount of transformation strain is to be expected. However, it seems that this strain is borne by the white tin, which deforms to an extent according to its distance from the transformation front. Figure 2a shows the Laue-photograph of an undeformed white tin crystal (crystal 3G) at a distance about 2 mm away from the boundary, whereas figure 2b shows the elongated Laue-streaks (or asterism) of the deformed white tin together with the sharp Laue-spots of the undeformed grey tin at the transformation front. Another example is shown in figure 3a.

This phenomenon is not unexpected, however. White tin is very ductile and grey tin is extremely brittle and rigid. During transformation, the white tin crystal deforms (it is no longer a truly single crystal, as is shown by the fine structure of the Laue-streaks and by the Debeye-Scherrer arcs in figure 3a), leaving the lattice of the newly formed grey tin undistorted. The deformation of white tin, especially the lattice rotation and fragmentation, will be discussed in paragraph 4.

As the transformation front moves away, the grey tin loses contact with the white tin. Then, in the absence of ductile material capable of taking up the stress produced at the transformation front, the grey tin itself becomes deformed. Figure 3b shows the Laue-photograph of the same grey tin crystal as shown in figure 3a, however, at a distance about 1 mm away from the transformation front. Comparing with figure 3a, the main zone of the deformed grey tin can still be recognized. This phenomenon is very common and therefore good single crystals of grey tin can, though not always, only exist at the transformation front in direct contact with white tin. Figure 4 is a Laue-photograph of a not so severely deformed grey crystal.

Another way to accommodate the transformation stress is to expand sidewise (figure 1a), resulting in a gradual change in lattice orientation of the grey tin crystal.

In several other cases, two distinctly different grey crystals were found within a distance of 2 mm, and the change in orientation is too abrupt to be considered as due to the above-mentioned continuous change of lattice-orientation. It seems very likely that in this case the formation of a new grey crystal from the single crystal of white tin has taken place.

Fig. 4. Laue-photograph of a grey single crystal formed in crystal 2D.

Fig. 7. Laue-photograph (crystal 4K) showing the complex nature of the transformation-deformation in the original white tin crystal.

Fig. 8. Laue-photographs of a white tin crystal (crystal 4J). a. 1 mm from the transformation front. Fragmentation; b. 2 mm from the transformation front. Fragmentation and lattice rotation; c. 3 mm from the transformation front. Undeformed crystal.

Fig. 10. Laue-photographs showing the [001]-zone of two deformed white tin crystals, at some distance from the transformation front; rotation around the slip-direction [001]. a. Crystal 4G; b. Crystal 4I.

From the above discussion it becomes clear that the orientation-relationship between white and grey tin should be studied in the immediate neighbourhood of the transformation front, despite the fact that in this region the orientation of the white tin crystal, owing to asterism, cannot always be accurately determined. As appears from figure 5, the orientations thus determined for twelve pairs of white-grey crystals showed a random scattering without any indication of preferred grouping.

Figure 6 shows the results of another related experiment. In this case for a definite white tin crystal (4G) the orientation of both the white crystal and the grey crystals formed from it were determined at the transformation front in three successive transformation stages. It appears from figure 6 that in this case the orientations of the grey tin crystals formed at the transformation front from the same white tin crystal are also different and spread considerably <sup>1)</sup>.

From these results it would be impossible to conclude the existence of a definite orientation-relationship accompanying the allotropic transformation of tin. It seems more probable that they have to be seen in favour of the absence of such a relationship. Also the combined occurrence of

- (a) fragmentation of the white tin crystal at the transformation front (see below) and
- (b) the formation of only one crystal of grey tin from the fragments with slightly different orientations

seems to us to point in this direction. If such a definite orientation-relationship between the forms of tin was actually present, then it would be expected that, instead of a nearly perfect single grey crystal, many small grey crystals with a certain preferred orientation would form from the same white crystal. Experimental results show the contrary to be true.

The lack of orientation-relationship between white and grey tin does not seem to be unnatural, if we take into consideration the large difference both in specific volume and in mechanical properties. This latter circumstance in particular has perhaps not always been given due consideration. Coherency and overgrowth may have survived lattice strain caused by the differences in lattice and in specific volume, if both lattices could share this strain. This is certainly not the case with the white-grey transformation of tin.

However, it should be pointed out that the present investigation only proves the absence of what we may call a "macro-orientation relationship" between the two modifications of tin. The Laue-method used here is incapable of dealing with the existence of two-dimensional coherency of a few atomic layers.

<sup>1)</sup> It may be argued that in the first experiment, in order to stimulate the transformation, the white tin crystals were "infected" with grey tin (cf. paragraph 2) and that, consequently, the formation of grey tin may not have been spontaneous. This, however, cannot be held against the second experiment.

HALL (1955) and PRASAD and WOOSTER (1956) both have suggested, from purely structural considerations, the following orientation-relationship:

White Tin		Grey Tin
(100)	//	(110)
(001)	//	(001)

Then, the white tin lattice, on transformation into grey, would suffer a compression of about 21 % along the  $a$ -axis and an expansion of about 105 % along the  $c$ -axis. HALL calculated the lattice strain and concluded that this coherency will break down when the grey tin becomes one unit-cell thick. The present investigation demonstrates that this orientation-relationship does not seem to exist macroscopically.

#### 4. Deformation of white tin at the transformation front

The deformation suffered by the white tin crystals at the transformation front is manifested by the asterisms in the Laue-photographs (see figures 2b and 3a). Similar observations have been made earlier by

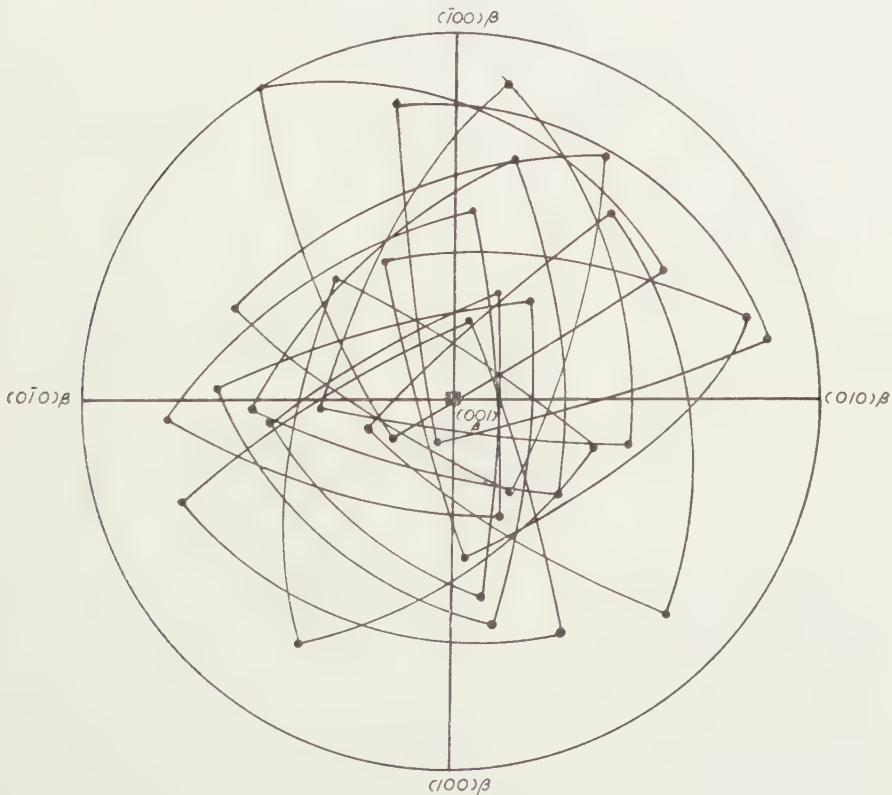


Fig. 5.  $\{100\}$ -poles of twelve grey tin single crystals formed from twelve white tin single crystals. The orientations of the latter are rotated in the stereographic projection so as to coincide with the  $(001)$ -projection of the white tin.

(GROEN<sup>1</sup>). Generally, the deformation is heavy, especially, as it is easy to perceive, when the transformation does not start at the end of the specimen. Only in two out of the twenty crystals of white tin examined, the deformation was slight. The nature of this deformation is very complicated: an example is given in figure 7. As the distance from the transformation front increases, the degree of deformation decreases and asterism commonly cannot be observed at a distance about 3 to 5 mm from the transformation front.

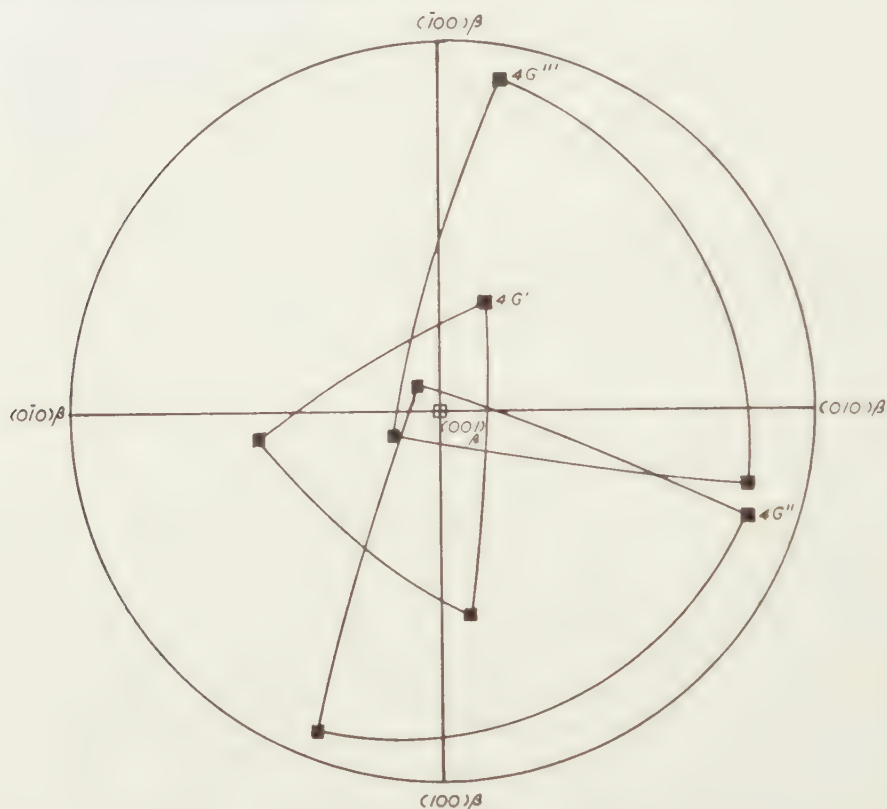


Fig. 6. Orientation of three grey tin crystals formed from the *same* white tin crystal (4G) in three successive stages of the transformation process.

Fragmentation is one of the results of this deformation, as is shown in figure 8a which relates to the crystal shown in figure 1c. The triple Laue-spots indicate that the white tin crystal under consideration breaks down into three slightly differently orientated crystals (the disorientation between two crystals is about  $1-1.5^\circ$ ) and the presence of Debye-Scherrer arcs<sup>2</sup>) implies that numerous crystallites have been formed. Figure 8b is taken at a place where apparently both fragmentation and lattice bending have taken place. Figure 8c shows the undeformed lattice. This series of

<sup>1</sup>) To be published by Mr. GROEN in a forthcoming doctor thesis.

<sup>2</sup>) Not clearly visible in the reproduction.



Laue-photographs demonstrates clearly the kind of inhomogeneous lattice rotation found in plastic deformation of crystals. From figure 9, which is the stereographic projection of the original (figure 8c) and final (figure 8a) positions of crystal 4J (the plane of projection is taken parallel to the crystal plate), it can be seen that its lattice has rotated about  $22^\circ$  around  $[110]$ .

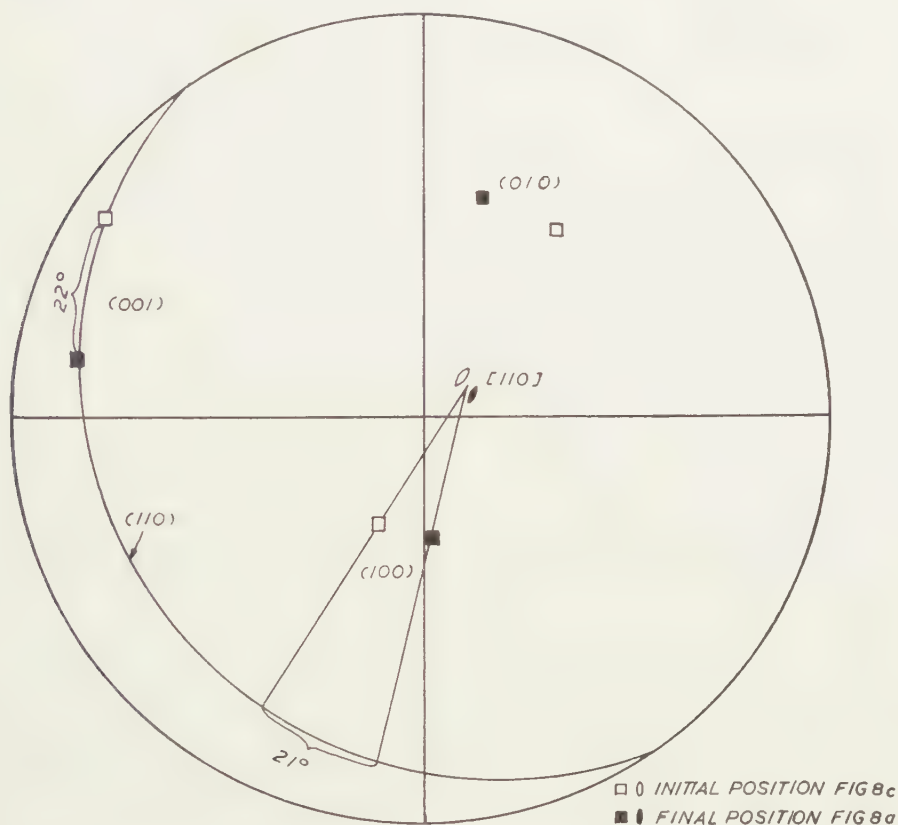


Fig. 9. Stereographic projection of figures 8a and 8c, showing the lattice rotation of a white tin crystal at some distance from the transformation front; axis of rotation:  $[110]$ .

Lattice rotation can also be determined, though less accurately, from the Laue-streaks. The lattice rotation found from figure 8b alone is about  $12^\circ$ . A stereographic plot of the main Laue-streaks visible in figure 2b (belonging to the  $[001]$ -zone, the indices are shown in figure 2a) shows that the lattice has rotated about  $5^\circ$  around  $[100]$ .

According to MARK and POLANYI (1923) and OBINATA and SCHMID (1933), the main slip systems of white tin are  $\{110\}$ ,  $\langle 001 \rangle$  and  $\{100\}$ ,  $\langle 001 \rangle$ ; which of these two systems is really active depends upon the orientation of the crystal with respect to the stress direction. The Taylor-axes of rotation (i.e., the axis in the slip plane normal to the slip direction)

for these two systems are  $\langle 110 \rangle$  and  $\langle 100 \rangle$  respectively, and these are, as described above, actually the rotation axes found experimentally <sup>1)</sup>.

It is of interest to note that also lattice rotation around the slip direction [001] has been observed. The Laue-spots belonging to the [001]-zone in figures 10a <sup>2)</sup> and 10b are smeared out or broken into fragments along the zone-ellipse, though the deformation is very complex and a second rotation also exists. This kind of rotation has been reported earlier by COLLINS and MATHEWSON (1940) for aluminium.

Fragmentation in deformed crystals has been found before by various investigators in extended or bent sodium (ANDRADE and TSIEN, 1937), aluminium (HEIDENREICH and SHOCKLEY, 1948; YEN and HIBBARD, 1949; HONEYCOMBE, 1951; LALOEUF and CRUSSARD, 1951; CHEN and MATHEWSON, 1951; CALNAN, 1952), molybdenum (AUST, MADDIN and CHEN, 1953), tungsten (RIECK, 1956) and zinc (CONARD, AVERBACH and COHEN, 1953) and the rotation axis, where kink bands existed, was always the Taylor-axis. The present investigation agrees with this general principle and adds white tin to the group of metals which deforms, without separate annealing and polygonization, into slightly differently orientated fragments.

However, as it is known (VAN ARKEL and PLOOS VAN AMSTEL, 1928; also GAY and KELLER, 1953) that deformed tin may recrystallize spontaneously at room-temperature within a short interval (for example a few seconds), the possibility of polygonization in the course of the deformation-process may not be overlooked for metals with a low melting-point.

From the above description it is clear that the nature of the transformation deformation in this metal is extremely complicated. For this reason, it would be unwise to speculate too much about the different kinds of lattice rotation. A clean-cut solution of this problem could only be arrived at by studying unidirectionally stressed single crystals with predetermined orientations.

### *Summary*

Single crystals of white  $\beta$ -tin have been transformed at  $-20^\circ\text{C}$  into

<sup>1)</sup> The slip-plane normals for  $\{110\}$  and  $\{100\}$  are also  $\langle 110 \rangle$  and  $\langle 100 \rangle$ , and since we do not know the stress direction, it is impossible to ascertain whether the rotation axes are the Taylor-axes or the slip-plane normals. Since kink bands have also been observed in white tin by HALL (1955) near the transformation front, Taylor-rotation is considered to be more probable. However, in view of the recently discovered "rotational slip" [WILMAN *et al.* (1950) (1951); WHAPHAM (1956)], the possibility of rotations around slip-plane normals cannot be definitely excluded.

<sup>2)</sup> GAY and KELLER (1953) observed in their study of the rolling of coarse-grained white tin (grain-size  $\sim \frac{1}{2}$ –1 mm) that after only a few per cent rolling the Laue-reflections were completely replaced by Debye-Scherrer arcs. The spots within the arcs were very often joint by a continuous background. The same phenomenon is visible in figure 10a.

the grey  $\alpha$ -modification. In many cases single crystals of the latter were obtained. The orientations of the two allotropic forms co-existing in the immediate neighbourhood of the transformation front have been determined by the glancing Laue-method. No regular orientation-relationship between the two lattices could be found, though the possibility of two-dimensional coherency of a few atomic layers could not be excluded. The lack of an orientation-relationship was considered to be due to

- a) the large volume expansion (about 20 %) accompanying the  $\beta \rightarrow \alpha$  transformation and
- b) the large difference in mechanical properties between white (extremely ductile) and grey (very brittle) tin.

Fragmentation and lattice rotation have often been observed in the white tin crystals in the neighbourhood of the transformation front. This deformation could in some cases be explained by a rotation around the Taylor-axis (line in slip-plane perpendicular to slip-direction) or around the slip-direction.

*(Laboratory of Physical Chemistry,  
Technical University, Delft, Netherlands)*

#### REFERENCES

- ANDRADE, E. N. DA C. and R. ROSCOE, *Proc. Phys. Soc.* **49**, 152 (1937).  
 ——— and L. C. TSIEN, *Proc. Roy. Soc. A* **163**, 1 (1937).  
 ARKEL, A. E. VAN and J. J. A. PLOOS VAN AMSTEL, *Z. Physik* **51**, 534 (1928).  
 AUST, K. T., R. MADDIN and N. K. CHEN, *J. Metals* **5**, 1477 (1953).  
 CALNAN, E. A., *Acta Cryst.* **5**, 557 (1952).  
 CHEN, N. K. and C. H. MATHEWSON, *J. Metals* **3**, 653 (1951).  
 COLLINS, J. A. and C. H. MATHEWSON, *Trans. AIME* **137**, 150 (1940).  
 CONARD, G. P., B. L. AVERBACH and M. COHEN, *J. Metals* **5**, 1036 (1953).  
 EVANS, D. M., D. N. LAYTON and H. WILMAN, *Proc. Roy. Soc. A* **205**, 17 (1951).  
 GAY, P. and A. KELLER, *Acta Cryst.* **6**, 172 (1953).  
 GROEN, L. J., *Nature* **174**, 836 (1954).  
 ——— and W. G. BURGERS, *Proc. Kon. Ned. Akad. Wet., Amsterdam B* **57**, 79 (1954).  
 HALL, E. O., Symposium on the mechanism of phase transformations in metals, p. 87. Institute of Metals, London (1955).  
 HEIDENREICH, R. D. and W. SHOCKLEY, "Strength of Solids" (Bristol Conference), p. 57. The Physical Society (1948).  
 HONEYCOMBE, R. W. K., *J. Inst. Met.* **80**, 45 (1951).  
 LALOEF, A. and C. CRUSSARD, *Rev. Métall.* **48**, 462 (1951).  
 MARK, H. and M. POLANYI, *Z. Physik* **18**, 75 (1923).  
 OBINATA, J. and E. SCHMID, *Z. Physik* **82**, 224 (1933).  
 PRASAD, S. C. and W. A. WOOSTER, *Acta Cryst.* **9**, 35 (1956).  
 RIECK, G. D., *Acta Met.* **4**, 47 (1956).  
 SCHIEBOLD, E. and G. SACHS, *Z. Krist.* **63**, 34 (1926).  
 WHAPHAM, A. D., *J. Inst. Met.* **84**, 109 (1956).  
 WILMAN, H., *Nature* **165**, 321 (1950).  
 YEN, M. K. and W. R. HIBBARD JR., *Trans. AIME* **185**, 710 (1949).

# LIGHT-SCATTERING BY SOLUTIONS OF SOME SODIUM ALKYL-1-SULFATES

BY

W. PRINS AND J. J. HERMANS

(Communicated at the meeting of March 24, 1956)

A number of alkyl-1-sulfates have been examined both in water and in aqueous solutions of sodium chloride. It was found that none of the detergents, if pure, showed any perceptible dissymmetry in the light-scattering. The 90° scattering is compared with data in the literature and is interpreted in terms of the theoretical considerations developed in a previous article. The conclusion is reached that the micellar weight increases with increasing salt content and that the effective charge is of the order of 0.1 times the number of monomers per micelle. This effective charge shows no systematic change with changes in salt content. Furthermore, it is found that the activity correction resulting from the electrical double layer around the micelles is quite important.

The light-scattering results for polyvinylacetate in the presence of sodium decyl-1-sulfate support the belief that the solubilized polymer molecules are considerably expanded.

The light-scattering instrument was calibrated by means of Ludox solutions. The Rayleigh numbers of benzene, toluene, carbon disulfide and water obtained in this way are given in table I. That of water was obtained by an extrapolation to zero dissymetry as described in section 4.

In addition to light-scattering, some measurements of surface tension, density and viscosity are reported. An impure detergent which showed a very high limiting viscosity number gave a large dissymmetry and showed a pronounced peak in turbidity in the neighbourhood of the critical micelle concentration. The pure detergents, however, gave much lower viscosities, in accordance with results reported by PHILIPPOFF.

The method of light-scattering was applied to detergent solutions by DEBYE [1], who investigated solutions of kationic soaps. Subsequent experiments on kationic soaps were carried out by TRAP [2]. It was the aim of the work described below to extend these experiments to a number of anionic detergents. During and after the completion of our program, several other articles have appeared dealing with the same subject [3, 4, 5, 6]. The results of these measurements will be compared with ours and among each other in sections 6 and 7.

## 1. *Preparation of the detergents*

Some of the experiments were carried out with a few grams of sodium octyl-1-sulfate ( $C_8Na$ ) and sodium tetradecyl-1-sulfate ( $C_{14}Na$ ), put at our disposal by DU PONT DE NEMOURS (Wilmington, Delaware). Another sample of  $C_{14}Na$  was obtained from the Shell laboratory at Amsterdam.



Most of the experiments, however, were performed on preparations made by W. DORST in the department of organic chemistry of the university at Leiden. The procedure followed in the preparation of the  $C_9C_{10}$  and  $C_{12}$  soaps has been described in a previous article [7]. The  $C_{14}$  and  $C_{16}$  products were prepared from the corresponding alcohols in a similar manner, except that after the addition of a small amount of the alcohol to the mixture of acetic acid and chlorosulfonic acid at  $4^\circ\text{C}$ , the temperature was raised to  $10\text{--}20^\circ\text{C}$ , where the reaction started, forming HCl fumes and foam. The rest of the alcohol was then added gradually; foaming was suppressed by the addition of a few ml ether. The temperature was then raised to about  $35^\circ\text{C}$  and the solution was stirred for another half hour. The handling of the reaction mixture from here on was the same as described previously [7]. For all the samples, about 80 % of the theoretically possible amount of alkyl sulfate was obtained. A determination of the sodium content of the  $C_9\text{Na}$  soap showed that the amount of inorganic salt was 1 % at most, which was considered insignificant for our experiments.

## 2. *Miscellaneous properties of the detergents*

a) X-ray data obtained for our samples have been published elsewhere [8].

b) The *surface tension*  $\gamma$  of detergent solutions usually decreases rapidly with increasing concentration and approaches a constant value. Sometimes the curve exhibits a minimum at the critical micelle concentration (CMC), a phenomenon which has been attributed by DREGER *et al.* [9] and by BRADY [10] to the presence of traces of the long-chain alcohol used for the preparation of the soap. In the case of alkyl sulfates DREGER found that on prolonged ethereal extraction the minimum disappears.

We determined the surface tension of solutions of  $C_9\text{Na}$  and  $C_{10}\text{Na}$  in doubly distilled water of specific conductivity  $2.10 \cdot 10^{-6}$  mho/cm, having a surface tension  $\gamma = 73.9$  dynes/cm. For  $C_9\text{Na}$  solutions a minimum of 34 dynes/cm was found at a concentration 0.014 g/ml; at higher concentrations  $\gamma$  was constant and equal to 39 dynes/cm. The minimum for  $C_{10}\text{Na}$  solutions was 37 dynes/cm at a concentration of 0.011 g/ml, while  $\gamma$  assumed the constant value of 39.5 dynes/cm at higher concentrations. All the experiments were carried out with a sensitive torsion balance equipped with a wire frame.

These results seem to indicate the presence of small traces of  $C_9\text{OH}$  and  $C_{10}\text{OH}$  respectively. Light-scattering, however, did not confirm this, although PHILLIPS and MYSELS [4] have shown that the presence of 0.03 % of the alcohol already gives rise to an enormous peak in the turbidity, just below the CMC (see also section 7).

c) The *densities* of dilute  $C_9\text{Na}$  and  $C_{10}\text{Na}$  solutions were measured in a pycnometer. A plot of the volume of 1 mole of solution versus mole

fraction was linear within experimental error. As a result of the fact that the densities were very close to that of pure water, no change in the partial molar volume  $v$  of the detergent could be detected at the CMC. The  $v$ -value for  $C_9Na$  was 198 which gives a density of  $M/198=1.24$ ,  $M$  being the molecular weight 246.3. Similarly, for  $C_{10}Na$ ,  $v$  was 212, and thus the density 1.25.

d) *Viscosity* measurements were made at  $37.5 \pm 0.05^\circ \text{C}$  in a capillary viscometer. No great accuracy is claimed, but some of the results are interesting in connection with the light-scattering data.

Solutions of one of the  $C_{14}Na$  samples put at our disposal, in concentrations ranging from 0 to 0.0025 g/ml were examined in the presence of various amounts of NaCl (0.05 to 0.3 N). Qualitatively the following conclusions could be made.

(I) none of the viscosities differed more than 4 % from that of pure water. The high viscosities reported by PILPEL [11] were not found, not even at the highest salt content examined.

(II) the limiting viscosity number

$$[\eta] = \lim_{c \rightarrow c_0} \frac{t - t_0}{t_0(c - c_0)}$$

had the rather high value of  $48 \pm 10$  ml/g. Here  $t$  is the efflux time for the solution,  $t_0$  that for the same solution at the CMC,  $c$  the detergent concentration and  $c_0$  the CMC. Below the CMC, the limiting viscosity number  $[\eta] = \lim_{c \rightarrow 0} [(t - t_0)/t_0c]$  had about the same value. Similarly, when NaCl is present and  $c_0$  is almost zero, while  $t_0$  represents the efflux time for the NaCl solution in the absence of detergent, the limiting viscosity number has the same order of magnitude.

PHILIPPOFF [12] reports limiting viscosities of only 4 to 7 ml/g for a large number of detergents, both below and above the CMC. The high viscosities found by us for this particular  $C_{14}Na$  sample indicate the existence of very asymmetric particles. If these particles are prolate ellipsoids of rotation with a short axis of 20 Å, the  $[\eta]$ -value of 48 leads to a length of 800 Å. For oblate ellipsoids of rotation the diameter would be 2000 Å. Approximately the same large dimensions are found from the dissymmetry of the light scattered by this sample in water. Moreover, on diluting to a concentration less than the CMC, a large peak appeared in the turbidity. It is therefore almost certain that the viscosity results must be attributed to the presence of impurities, which give rise to large asymmetric micelles above the CMC, and to asymmetric microcrystalline particles below the CMC where the impurities are no longer solubilized. This is confirmed by the viscosities of solutions of our own  $C_9Na$  sample which showed neither the dissymmetry nor the peak in light-scattering. The viscosities both below and above the CMC were found to be of the same order of magnitude as reported by PHILIPPOFF.

### 3. Light-scattering apparatus and calibration

The measurements were carried out with the light-scattering apparatus (fig. 1) described by TRAP and HERMANS [2] after some minor changes were made.

A magnetic coil voltage stabilizer was introduced for the 220 volts input of the mercury arc transformer, in order to get a stable light source. For the separation of the 4358 Å mercury line, three Ilford colour filters (nrs. 805, 806 and 809) were chosen. For the 5461 Å line a combination of a green Ilford filter (nr. 807) and an interference filter (Bairdwell, 70 % transmission of 5461 line) proved to be satisfactory.

The photomultiplier current was measured directly with a sensitive galvanometer (Kipp, Delft, type A5, internal resistance 340  $\Omega$ ), with a parallel external damping resistance of 7.10<sup>4</sup>  $\Omega$ . The current could be read on a scale to within 2.10<sup>-11</sup> amp. A second resistance box, in series with the galvanometer was used when investigating solutions of higher turbidity.

It was found that large rectangular cells (made by van Oortmerssen, The Hague) gave no false reflection when fitted in the manner shown in fig. 1, top view. One of these cells was equipped with a Pyrex side vessel filled with analytical grade benzene, distilled and dried over sodium. This

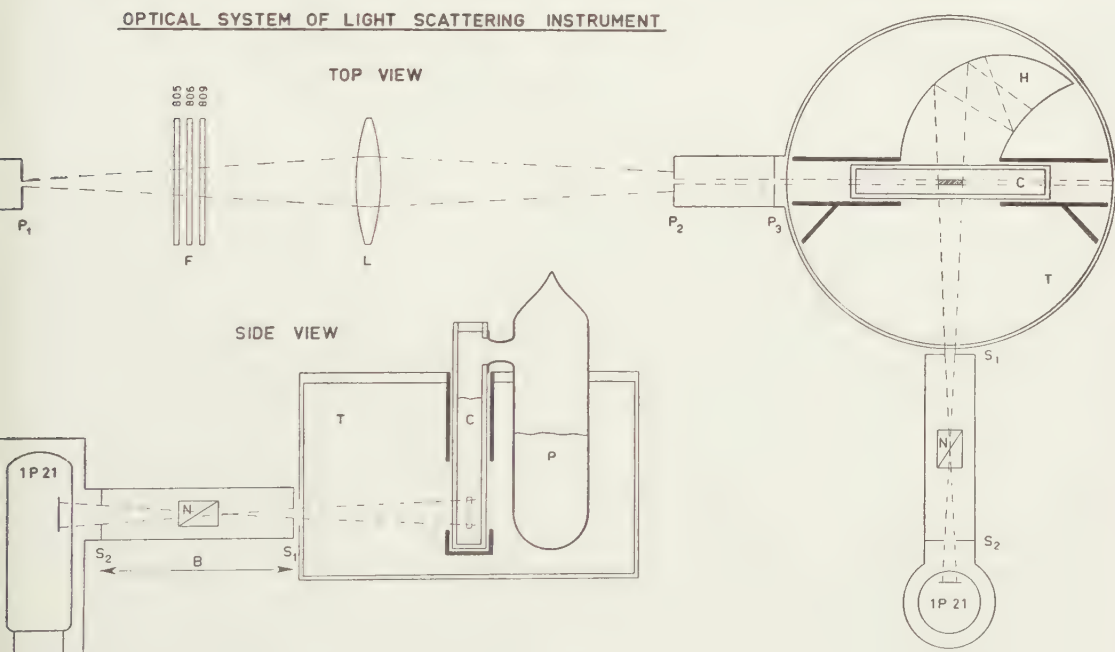


Fig. 1. Light-scattering instrument.  $P_1$  = adjustable slit 12  $\times$  2 mm in front of mercury arc; F = colour filters (Ilford) for  $\lambda = 4358$ ; L = lens; T = temperature bath made of glass and filled with water;  $P_2$  and  $P_3$  are entrance slits; C = rectangular scattering cell 14  $\times$  80  $\times$  90 mm outside dimensions, optical glass 2 mm thick; H = black-walled Rayleigh horn;  $S_1$  and  $S_2$  are receiver slits, 4  $\times$  4 and 4  $\times$  8 mm respectively; N = Nicol prism.

cell was sealed in vacuo (fig. 1, side view). After repeated distillation, effected by placing the cell in acetone and dry ice, the benzene in the cell showed no dissymmetry: it was used as a standard after calibration with Ludox (see below).

Proper correction was made for refraction at the cell wall when the refractive index of the liquid examined differed from that of the water in the temperature bath.

Since we used pure benzene as a standard, it was necessary to know its absolute scattering power, usually expressed as the Rayleigh number  $R_{90}$ . There exists, however, a disagreeable uncertainty in the value of this number [13, 14, 15, 16]. Our own calibration of the benzene was based on a comparison with an aqueous silica suspension "Ludox" (DU PONT) in a manner similar to that described by TRAP and HERMANS [16].

TABLE I

Refractive index  $\nu$ , depolarization factor  $\varrho$  and Rayleigh number  $R_{90}$  for four liquids at 25° C, using unpolarized incident light of wavelength  $\lambda$ .  $R'_{90}$  was obtained from our own calibration (see text),  $R_{90}$  from the benzene values of CARR and ZIMM [14].

Liquid	$\lambda(\text{m}\mu)$	$\nu$	$\varrho$	$10^6 R'_{90}$ ( $\text{cm}^{-1}$ )	$10^6 R_{90}$ ( $\text{cm}^{-1}$ )
benzene . . . . .	436	1.5193	0.43	$48.7 \pm 1$	48.5
b.p. 79.7–79.8/756 mm . .	546	1.5019	0.42	$17.9 \pm 1$	16.3
toluene . . . . .	436	1.5151	0.51	58.5	57.7
b.p. 110.4–110.5/761 mm .	546	1.4940	0.49	20.2	18.4
carbon disulfide . . . . .	436	1.6699	0.67	280	274
b.p. 45.7–45.9/749 mm . .	546	1.6322	0.68	81.7	67.6
water . . . . .	436	1.3397	0.15	2.93	2.92
ultrafiltered . . . . .	546	1.3340			

Table I gives some  $R_{90}$  values found in this way. Benzene was measured against Ludox, the other liquids against benzene. The organic liquids were analytical grade samples, fractionated by us through a Todd column, collecting the fraction boiling to within 0.1° C of the boiling point given in the literature. Slow filtration through ultraline Pyrex sintered glass filters under nitrogen pressure directly into dust free cells gave liquids with negligible dissymmetry. The treatment of the water is described in the next section.

#### 4. Preparation of dust-free water and aqueous solutions

The optical clarification of water was a matter of considerable difficulty, the more so because the experiments had to be done under unfavorable conditions. Several methods were tried, and we finally adopted filtration through a commercial membrane of the Membrangesellschaft, Göttingen, Germany, using a chromiumplated support and housing.



Doubly distilled water, prefiltered through a collodion membrane [2, 17, 18] and repeatedly filtered through a commercial membrane gave a dissymmetry of 1.5, the best we could attain. By measuring the scattered intensities at 45, 135 and 90 degrees of various water samples with different "dust contents", the graph of fig. 2 was obtained where the intensities are

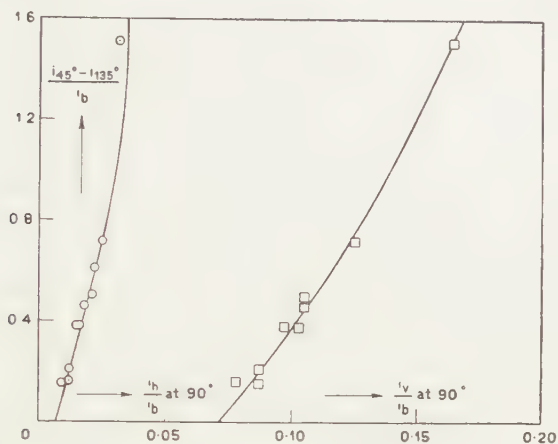


Fig. 2. Influence of dust on the 90° scattering of water; ○ horizontal component  $i_h$ ; □ vertical component  $i_v$ . All  $i$ 's relative to benzene ( $i_b$ ).

relative to that for benzene at 90°. Extrapolation to  $i_{45} - i_{135} = 0$  gives for the Rayleigh number of water the value mentioned in table I. After completing this work it was found that the careful measurements of KRAUT and DANDLIKER [19] gave the result 2.89, in excellent agreement with our value.

Filtration of NaCl-solutions through the membrane filter gave high and erratic turbidities, caused by very small dust particles extracted from the membrane. Centrifuging, or filtration through ultrafine glass filters, however, gave reasonably good results.

Detergent solutions were treated in the same way as salt solutions. These solutions exhibited at higher concentrations and on addition of salt a dissymmetry below 1.05, which was assumed to be due to dust in the solvent. For all detergent concentrations we could therefore make use of the "dust correction" graph of fig. 2 for the determination of the 90° scattering of the solute particles. Solutions of the  $C_{14}Na$  and  $C_{16}Na$  products had to be kept at 50° C. When filtered through a glass filter, kept at this temperature by a heating mantle, these solutions often gave erratic turbidities caused by very small dust particles. These were, at least in part, extracted from the sintered glass plate, since repeated filtration often gave an increase in turbidity. To avoid this difficulty, centrifuging was carried out instead. This was done at a temperature where part of the detergent crystallized and thus was centrifuged out, thereby removing also the dust particles. A final correction for dust was

made as in fig. 2, since for these detergent solutions no intrinsic dissymmetry was found at high concentrations and on addition of salt.;

### 5. Refractive index increments

The  $\partial n/\partial c$  values were measured in a Zeiss Löwe interferometer. Since white light is used, this excludes the determination of the dispersion which, however, is small.

For  $C_{10}Na$ ,  $\partial n/\partial c$  in pure water differed only 4 % from that in concentrated NaCl (1.2 N). This makes it permissible, in the dilute salt solutions investigated, to consider  $\partial n/\partial c$  of the detergent as independent of salt content. For  $C_{11}Na$  and  $C_{16}Na$  the temperature bath in the interferometer was heated at  $50.0 \pm 0.1^\circ C$  by circulating water through a copper box placed at the bottom. Although the stirrer in the temperature bath was handoperated, the interference pattern in the eye-piece of the interferometer was sufficiently steady to allow of readings equally accurate as at room temperature: one part in the sixth decimal place of the refractive index. Only in the case of  $C_9Na$  and  $C_{10}Na$  could we detect the critical micelle concentration (CMC) in a plot of refractive index  $n$  versus concentration  $c$ . This gave 13.5 g/l for  $C_9Na$  and 8.5 g/l for  $C_{10}Na$ .

### 6. Light-scattering

When necessary, soap concentrations were determined by evaporating the solvent from 5 or 10 ml of solution at  $110^\circ C$  and weighing, subtracting the amount of added salt, if any. Dilutions were frequently made in the light scattering cell with dust-free water or NaCl solutions. All meas-

TABLE II

Results of light scattering by solutions of sodium alkyl-1 sulfates; wavelength 436 m $\mu$ .

deter- gent	NaCl m-mole per l	CMC $-c_0$ g/l	$\partial n/\partial c$ ml/g	$10^3 K$ cm <sup>2</sup> /g <sup>2</sup>	$f_e$	$M_m^*$	$10^3 \cdot 2B$ cm <sup>3</sup> /g <sup>2</sup>
$C_8Na$	0	30					
$C_9Na$	0	14.5	0.101	1.66	0.84	7.730	4.6
	75	12	0.101	1.66			
$C_{10}Na$	0	8.4	0.108	1.89 <sub>5</sub>	0.84	9.300	10.5
	75	4.2	0.108	1.89 <sub>5</sub>	1.00	20.300	2.2
	1200	0.4	0.104	1.76	0.95	19.250	0
$C_{12}Na$	75	0.1	0.119	2.31	0.96	23.000	1.9
$C_{14}Na$	0	0.6	0.116	2.17	1.0	~2.900	
	12.5	0.5 <sub>5</sub>	0.116	2.17	1.0	34.000	7.0
	25	0.5	0.116	2.17	1.0	37.000	3.1 <sub>5</sub>
	50	0.3 <sub>5</sub>	0.116	2.17	1.0	40.500	1.9
	100	0.1	0.116	2.17	1.0	43.500	1.0 <sub>5</sub>
$C_{16}Na$	0	0.2	0.117	2.23	1.0	~4.850	
	12.5	0.1	0.117	2.23	1.0	47.000	3.6 <sub>5</sub>
	25	0.08	0.117	2.23	1.0	53.000	1.6
	50	0.05	0.117	2.23	1.0	63.000	0.7 <sub>5</sub>

urements were made at  $25.00 \pm 0.05^\circ \text{C}$ , except for  $\text{C}_{14}\text{Na}$  and  $\text{C}_{16}\text{Na}$  where the temperature was  $50.0 \pm 0.1^\circ \text{C}$ . No dissymmetry was found in any of the soap solutions examined, except for the impure samples of  $\text{C}_9\text{Na}$  and  $\text{C}_{14}\text{Na}$  (see below). The experimental results are summarized in table II. In addition, figs 3, 4, 5 and 6 give examples of light-scattering curves. The constant  $K$  in table II and fig. 5 is defined by

$$K = 2\pi^2 n^2 (\partial n / \partial c)^2 / \lambda^4 N_A,$$

$n$  being the refractive index,  $\lambda$  the wave-length in vacuo and  $N_A$  Avogadro's number. The quantity  $B$  (second virial coefficient) is determined by the relation

$$K(c-c_0)/R_{90} = 1/M_m^* + 2B(c-c_0),$$

where  $c_0$  is the critical micelle concentration and  $M_m^*$  the apparent micellar weight (see discussion).

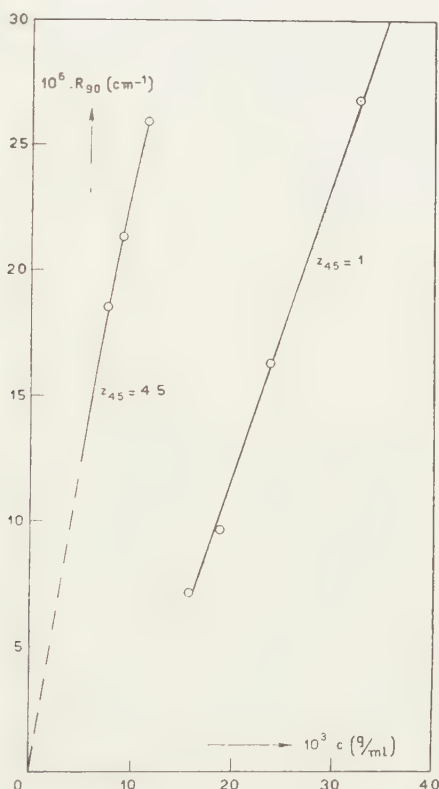


Fig. 3. Effect of traces of nonyl alcohol on the scattering of  $\text{C}_9\text{Na}$  in 0.075 N NaCl at  $25^\circ \text{C}$ ;  $z_{45}$  is the dissymmetry  $i_{135}/i_{45}$ .

## 7. Special remarks

**$\text{C}_8\text{Na}$ .** Very little material was available. The value of  $c_0$  in table II is only approximate.

**$\text{C}_9\text{Na}$ .** The large depolarization in pure water may be due to our method of correction for dust which for systems of low turbidity is less reliable, especially with regard to depolarization [20]. A less pure sample of the same detergent showed the behaviour seen in fig. 3. The peak is

probably caused by a trace of nonyl alcohol, which is insoluble below the CMC. The appearance of the peak was accompanied by a sudden decrease of the depolarization  $\rho$  from 0.11 to 0.02, and a strong dissymmetry  $z_{45} = 4.5$ . This suggests that the insoluble nonyl alcohol which is liquid at room temperature is present in the form of droplets with a diameter of about 1500 Å. When left overnight,  $z_{45}$  increased to about 6, showing that the micro emulsion is not stable.

**C<sub>10</sub>Na.** Our results are consistent with those of HUTCHINSON and MELROSE [3] who found  $M_m^* = 13,000$  at a salt content of 1 mole/l. For C<sub>10</sub>Na in water TARTAR and LELONG [6] have quite recently published the value 8.1 g/l for  $c_0$  and 0.113 for  $\partial v/\partial c$ , both of which agree well with table II. Their value for  $M_m^*$ , however, is 13,000 instead of our 9,300.

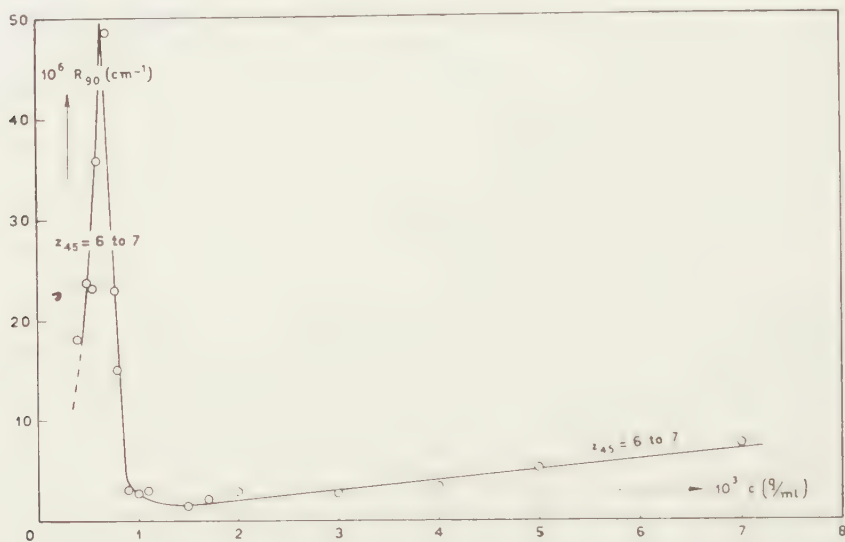


Fig. 4. The scattering of an impure C<sub>14</sub>Na sample in water at 50° C.

**C<sub>12</sub>Na.** The value of  $M_m^*$  tallies well with that mentioned by HUTCHINSON and MELROSE [3], but is 30 % lower than that reported by PHILLIPS and MYSELS [4]. This discrepancy may be attributed partly to a difference of 4 % between their  $\partial v/\partial c$  and ours. It may be noted in this connection that our  $\partial v/\partial c$ -value is in excellent agreement with that found in the more recent experiments of KUSHNER and HUBBARD [5]. Furthermore, there is a systematic difference between the  $M_m^*$  values found by PHILLIPS and MYSELS and those reported by KUSHNER and HUBBARD:

NaCl (mole/l)	0	0.02	0.03	0.04	0.08	0.2
$M_m^*$ (Ph. and M.)	23,000	27,000	28,800	—	—	34,000
$M_m^*$ K. and H.)	11,400	19,000	21,700	23,100	24,400	26,800

Our value of  $M_m^*$  at 0.075 mole NaCl per liter is more in line with the data of KUSHNER and HUBBARD. On the other hand, according to TARTAR and



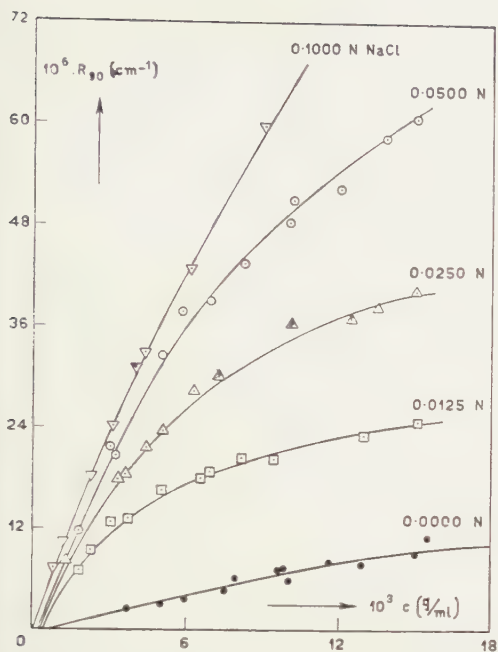


Fig. 5. Rayleigh number for our own  $C_{14}Na$  sample in water and dilute NaCl solutions at  $50^\circ C$ .

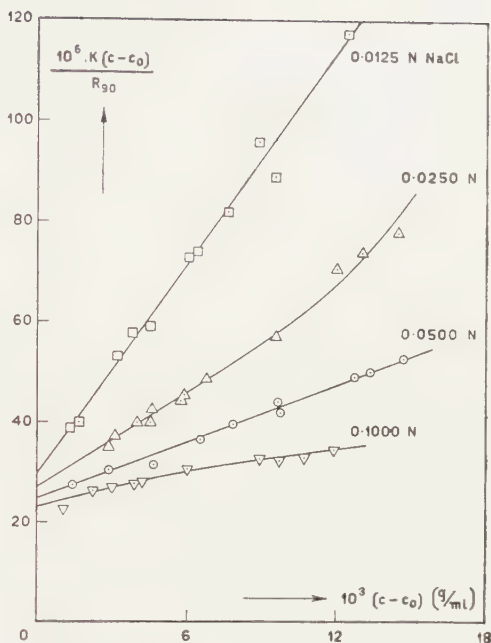


Fig. 6. Reduced turbidity  $K(c - c_0)/R_{90}$  versus  $c - c_0$  for  $C_{14}Na$  solutions.

LELONG [6] the value of  $M_m^*$  in pure water is 20,500, which is closer to the Phillips-Myers than to the Kushner-Hubbard result.

**$C_{14}Na$ .** Our own preparation gave the results shown in figs 5 and 6. Another sample gave the curve of fig. 4. This is in line with the high solution viscosity found for this sample and described in section 2. The values of  $c_0$  and  $\partial r/\partial c$  given in table II agree very well with those mentioned by TARTAR and LELONG [6]. Their  $M_m^*$  value in 0.01 molar NaCl is 43,500 whereas we find 34,000 in 0.0125 molar salt. TARTAR and LELONG find it very difficult to get reliable scattering data for  $C_{14}Na$  in pure water and attribute this to insufficient screening of the micellar charge by the small amount of monomer,  $c_0$  being very low. It is also possible, however, that the very low excess turbidity found by us in pure water as a solvent is in error as a result of our dust correction (compare section 4).

#### 8. Solubilization of polyvinyl acetate by $C_{10}Na$

It was shown by SATA and SAITO [21] that a colloidal suspension of polyvinylacetate (PVA) in water clarifies after some days when  $C_{12}Na$  is added. Their viscosity measurements indicate a stretching of the PVA molecules. This solubilization takes place also at soap concentrations below the CMC, and it seems likely that the polymer is solubilized by a protective layer of detergent molecules. The stretching may then be explained by the electric charges of the soap ions attached to the polymer.

We have observed a similar interaction between PVA and  $C_{10}Na$ . The solution which was optically clear to the eye showed a light-scattering 17 times as high as that of a  $C_{10}Na$  solution of the same concentration in the absence of PVA. The dissymmetry  $\tau_{45}$  was about 2. Since the molecular weight of the polymer was about 150,000, this dissymmetry is much higher than that observed when PVA of this molecular weight is dissolved in a good solvent like butanone. This confirms the expansion of the PVA molecules.

### 9. Discussion

Several authors [2, 3, 5, 6, 22-27] have stressed the effect of electric charge on the determination of particle weight by means of light-scattering. In a previous paper [28] we have investigated the consequences of a frequently discussed model: (a) it is assumed that the micelle size distribution is narrow, (b) the concentration of the monomer is assumed to remain constant when the detergent concentration is increased beyond the CMC, (c) if a micelle contains  $m$  monomer ions, a fraction  $1 - p/m$  of the counter ions is supposed to be bound to the micelle. The ratio  $\alpha = p/m$  may be called effective degree of dissociation. An activity coefficient for the micelles is derived from the volume exclusion principle, using the hard sphere approximation, the radius of the sphere being determined by the extension of the electrical double layer.

It was found that under these circumstances a plot of  $K(c - c_0)/R_{90}$  versus  $c$  yields an apparent molecular weight

$$M_m^* = M_m/g,$$

where the correction factor  $g$  is determined by the concentrations of soap monomer and of added salt, by the values of  $p$  and  $m$ , and by the ratio between the refractive index increment for the salt and that for the detergent. The slope of the curve is determined by the same quantities and contains in addition a term proportional to the excluded volume, which can be calculated from the ionic strength of the solution. For details the reader is referred to the paper quoted [28].

The experimental data thus give two informations: the slope and the intercept, from which the two quantities  $m$  and  $p$  can be derived. The equations from which these quantities must be obtained are complicated, but it was found that in all cases examined approximations could be made which considerably simplified the procedure. Among other things, it is legitimate to replace the value of the second virial coefficient given in Eq. 30 of the previous article [28] by the simplified expression:

$$2B = \frac{p^2}{2(n_1 + n_3)M_m M_m^*} + \frac{8v_m N_A}{(M_m^*)^2}.$$

The effect of this approximation on the calculated value of  $m$  proved to be negligible, while that of  $p$  is affected by at most a few percent. The

TABLE III

Sodium alkyl-1-sulfates in water and aqueous NaCl. Actual number  $m$  of monomers and residual charge  $p$  per micelle, calculated from the apparent value  $m^*$  and the experimental value of  $B$ , using the equations of the preceding article [28].

$n_1$  = monomer concentration (= CMC) in mole/ml;  $n_3$  = salt content in mole/ml;  $f$  = ratio between refractive index increment of salt and that of detergent;  $\kappa$  = Debye-Hückel reciprocal characteristic length which serves to calculate the excluded volume  $v_m$ ;  $a$  = radius of micelle, assumed spherical with a density 1.2;

$$D_h = 2a + 2/\kappa.$$

deter- gent	$10^6 m_1$	$10^6 m_3$	$10^{-6} \kappa$ cm <sup>-1</sup>	$f$	$m^*$ exp.	$10^3$ ( $2B$ ) exp.	$10^8 a$ cm	$10^8 D_h$ cm	$\frac{10^3 \cdot 8 v_m N_A}{(M_m^*)^2}$	$m$	$p$
C <sub>9</sub> Na	58.9	0	7.96	0.38	31	4.6	13.6	52.4	6.2	~31	—
C <sub>10</sub> Na	32.3	0	5.90	0.33	36	10.5	14.6	62.9	7.1	40	4.6
C <sub>10</sub> Na	16.1	75	9.90	0.33	78	2.2	18.9	58.0	1.2	87	9.1
C <sub>12</sub> Na	0.35	75	9.01	0.28	80	1.9	19.7	61.6	1.1	88	8.4
C <sub>14</sub> Na	1.90	0	1.45	0.26	~9	—	9.8	157.5	—	—	—
C <sub>14</sub> Na	1.74	12.5	3.98	0.26	107	7.0	22.4	95.0	1.9	120	13.9
C <sub>14</sub> Na	1.58	25	5.44	0.26	117	3.2	23.0	82.9	1.0	130	13.1
C <sub>14</sub> Na	1.11	50	7.55	0.26	128	1.9	23.8	74.0	0.6	144	15.5
C <sub>14</sub> Na	0.32	100	10.57	0.26	137	1.1	24.3	67.5	0.4	153	16.3
C <sub>16</sub> Na	0.58	0	0.80	0.24	~14	—	11.7	272	—	—	—
C <sub>16</sub> Na	0.29	12.5	3.36	0.24	137	3.7	25.0	109	1.5	148	11.6
C <sub>16</sub> Na	0.23	25	5.49	0.24	154	1.6	26.0	88.4	0.6	165	11.6
C <sub>16</sub> Na	0.14	50	7.48	0.24	183	0.8	27.5	81.8	0.4	196	13.1

TABLE IV

Quaternary alkyl ammonium bromides in water and aqueous KBr [2]. The symbols have the same meaning as in table III.

deter- gent	$10^6 m_1$	$10^6 m_3$	$10^{-6} \kappa$ cm <sup>-1</sup>	$f$	$m^*$ exp.	$10^3$ ( $2B$ ) exp.	$10^8 a$ cm	$10^8 D_h$ cm	$\frac{10^3 \cdot 8 v_m N_A}{(M_m^*)^2}$	$m$	$p$
C <sub>10</sub> Br	63	0	8.26	0.26	44	6.6	16.0	56.2	2.9	52	9.1
C <sub>10</sub> Br	59	12.5	8.80	0.26	46	6.8	16.2	55.1	2.5	56	11.1
C <sub>10</sub> Br	50	25	9.02	0.26	48	5.8	16.5	55.2	2.3	58	10.6
C <sub>10</sub> Br	45	50	10.15	0.26	52	4.8	16.8	53.3	1.8	64	12.2
C <sub>12</sub> Br	14.7	0	3.99	0.24	62	15.2	18.5	87.1	4.6	73	11.6
C <sub>12</sub> Br	10.8	12.5	5.02	0.24	68	7.4	19.1	78.0	2.7	78	10.5
C <sub>12</sub> Br	9.1	25	6.07	0.24	77	4.2	19.9	72.8	1.7	87	10.3
C <sub>14</sub> Br	3.6	0	1.98	0.23	92	37.2	21.7	144.7	7.2	107	15.5
C <sub>14</sub> Br	2.1	12.5	3.98	0.23	117	5.8	23.5	97.3	1.4	131	14.5
C <sub>14</sub> Br	1.6	25	5.37	0.23	122	1.6	23.8	84.8	0.8	131	8.7

result of the calculation is given in table III. A similar calculation was carried out for the results of measurements on some quaternary alkyl ammonium bromides [2] and is summarized in table IV. The ratio  $f$  between the refractive index increment for the salt and that for the detergent was derived from the value for NaCl quoted by EDSALL *et al.* [29] and from that for the soaps given in table II. For the quaternary ammonium salts we used the values found by TRAP [2], while that for the added

KBr was derived from the work of BAXTER *et al.* [30] and adapted to the correct wave-length by using similar data published by BÖTTCHER and SCHOLTE [31]. From these calculations we may draw the following conclusions.

a) The difference between the true micellar weight and the apparent one is comparatively small. The effective degree of dissociation is of the order of 10 %.

b) HUTCHINSON's assertion [24] that the change in apparent micellar weight on addition of salt is completely due to the charge of the micelles is not confirmed. Rather must we conclude that the real micellar weight is changed as well.

c) There is no clear-cut tendency of  $p$  to change with salt content, but it must be remarked that the experimental error in  $B$ , and thus in  $p$ , may be large, and also that the calculation of the excluded volume effect is crude. The effect of these two factors on the calculated values of  $m$  is very much smaller.

d) The excluded volume term in  $B$  is often of the same order as the  $p^2$ -term, and thus has a notable effect on the calculated  $m$ -value, and a very pronounced effect on the calculated  $p$ -value.

e) The values of  $M_m^*$  for  $C_{14}Na$  and  $C_{16}Na$  in pure water are astonishingly low. It must be remembered that these results may be in error because of incomplete "dust-correction". Moreover, it is possible that  $p$  is particularly large in this case; and so is  $D_h$ , which means that the excluded volume term becomes very large and rather unreliable. This becomes particularly apparent from the fact that in some cases subtraction of the volume term from the experimental  $B$ -value left us with a negative result, indicating that the volume term overestimated the effect of the electric double layer on the activity coefficient of the micelles. This was the case, for instance, for  $C_9Na$  in the first row of table III, which explains why no  $p$ -value is given.

*Laboratorium voor Anorganische en Fysische Chemie  
Rijks Universiteit, Leiden*

#### REFERENCES

1. DEBYE, P., Ann. N. Y. Acad. Sci. **51**, 575 (1949); J. Phys. Coll. Chem. **53**, 1 (1949); P. DEBYE and E. W. ANACKER, J. Phys. Coll. Chem. **55**, 644 (1951).
2. TRAP, H. J. L., thesis Groningen 1953; H. J. L. TRAP and J. J. HERMANS, Proc. Kon. Ned. Akad. van Wetensch. **B 58**, 97 (1955).
3. HUTCHINSON, E. and J. C. MELROSE, Z. physikal. Chem., N. F. **2**, 363 (1954).
4. PHILLIPS, J. N. and K. J. MYSELS, J. Phys. Chem. **59**, 325 (1955).
5. KUSHNER, L. M. and W. D. HUBBARD, J. Colloid Sci. **10**, 428 (1955).
6. TARTAR, H. V. and A. L. M. LELONG, J. Phys. Chem. **59**, 1185 (1956).
7. DORST, W., W. PRINS and J. J. HERMANS, Proc. Kon. Ned. Akad. van Wetensch., Amsterdam, **B 59**, 190 (1956).
8. PRINS, W. and J. A. PRINS, Nature **177**, 535 (1956).



9. DREGER, E. E., G. I. Keim, G. D. MILES, L. SHEDLOWSKI and J. ROSS, Ind. Eng. Chem. **36**, 610 (1944).
10. BRADY, A. P., J. Phys. Chem. **53**, 59 (1949).
11. PILPEL, N., J. Colloid Sci. **9**, 285 (1954).
12. PHILIPPOFF, W., Discuss. Faraday Soc. **11**, 96 (1951).
13. ROUSSET, A. and R. LOCHET, J. Polymer Sci. **10**, 319 (1953).
14. ZIMM, B. H., J. Polymer Sci. **10**, 351 (1953).
15. HALWER, M., G. C. Nutting and B. A. BRICE, J. Chem. Phys. **21**, 1425 (1953).
16. TRAP, H. J. L. and J. J. HERMANS, Rec. trav. chim. **73**, 167 (1954).
17. ELFORD, W. J., Trans. Faraday Soc. **33**, 1094 (1937).
18. GORING, D. A. J. and P. JOHNSON, J. Chem. Soc. **33** (1952).
19. KRAUT, J. and W. B. DANDLIKER, J. Polymer Sci. **18**, 563 (1955).
20. HORN, P. and H. BENOIT, J. Chim. Physique **48**, 530 (1951).
21. SATA, N. and S. SAITO, Kolloid Z. **128**, 154 (1952).
22. HERMANS, J. J., Rec. trav. chim. **68**, 859 (1949); Proc. Intern. Colloq. Macromol., Amsterdam, 238, (1949).
23. DOSCHER, T. M. and K. J. MYSELS, J. Chem. Physics **19**, 254 (1951).
24. HUTCHINSON, E., J. Colloid Sci. **9**, 191 (1954).
25. MYSELS, K. J., J. Phys. Chem. **58**, 303 (1954).
26. PRINS, W. and J. J. HERMANS, J. Phys. Chem. **59**, 576 (1955).
27. MYSELS, K. J., J. Colloid Sci. **10**, 507 (1955).
28. PRINS, W. and J. J. HERMANS, Proc. Kon. Ned. Akad. Wet., Amsterdam, **B 59**, 162 (1956).
29. EDSALL, J. T., H. EDELHOCH, R. LONTIE and P. R. MORRISON, J. Amer. Chem. Soc. **72**, 4641 (1950).
30. BAXTER, G. P., A. C. BOYLSTON, E. MÜLLER, N. H. BLACK and P. B. GOODE, J. Amer. Chem. Soc. **33**, 914 (1911).
31. BÖTTCHER, C. J. F. and TH. G. SCHOLTE, Rec. trav. chim. **70**, 221 (1951).

# PHASE DETERMINATION IN THE HEAVY ATOM METHOD IN THE CASE OF NON-CENTROSYMMETRIC CRYSTALS

BY

A. F. PEERDEMAN AND J. M. BIJVOET

(Communicated at the meeting of March 24, 1956)

Even when a compound contains a heavy atom the phase determination in X-ray analysis still presents difficulties when a centre of symmetry is absent. A solution of the problem was reached in the isomorphous replacement method. After the heavy atom is located by the Patterson method the difference  $\Delta F$  in the structure factors (Fourier coefficients)  $F_B$  and  $F_A$  of the two isomorphous structures  $A$  and  $B$  can be calculated in magnitude and phase. With the aid of the absolute values of the observed structure factors their phases can then be determined by simple calculation. Still the phase angle  $\alpha$  may be positive or negative. This difficulty originally has been surmounted by including both signs in a Fourier map which, however, causes the superposition of the structure by its inverted structure [1]. As has been suggested [2] the ambiguity in the sign of the phase angle can be removed by anomalous diffraction. In this way the direct synthesis of a non-centrosymmetrical structure by means of isomorphous replacement has been performed in the case of the hydrochloride and hydrobromide of tyrosine [3].

Since it appeared that anomalous scattering can generally be effected by ordinary X-rays it became worth while to investigate its use in phase determination beyond the above case. A Patterson method has been devised by PEPINSKY *et al.* [4]. Another application in the single heavy atom technique may be pointed out.

The figure shows the resultant structure factor  $F$  from a heavy atom contribution  $A$  and a normal contribution  $N$  from the rest of the cell, together with the anomalous component.

It is seen that the difference in the resultant  $R$  for reflection and counter-reflection is determined by the angle  $\pi/2 - \alpha$  between  $N'$  and  $F$ . So the phase angle  $\alpha$  can be judged from the difference  $\Delta I = I_{hkl} - I_{\bar{h}\bar{k}\bar{l}}$ .

In algebraic formulation:

$$\sin\left(\frac{\pi}{2} - \alpha\right) = \frac{N'}{|F|}$$

$$\Delta I = (N' + A)^2 - (N' - A)^2 = 4 N' A.$$

From the observed value of  $\Delta I$  and the known value of  $A$ , the component  $N'$  is found in sign and magnitude, hence  $\alpha$  can be calculated except for

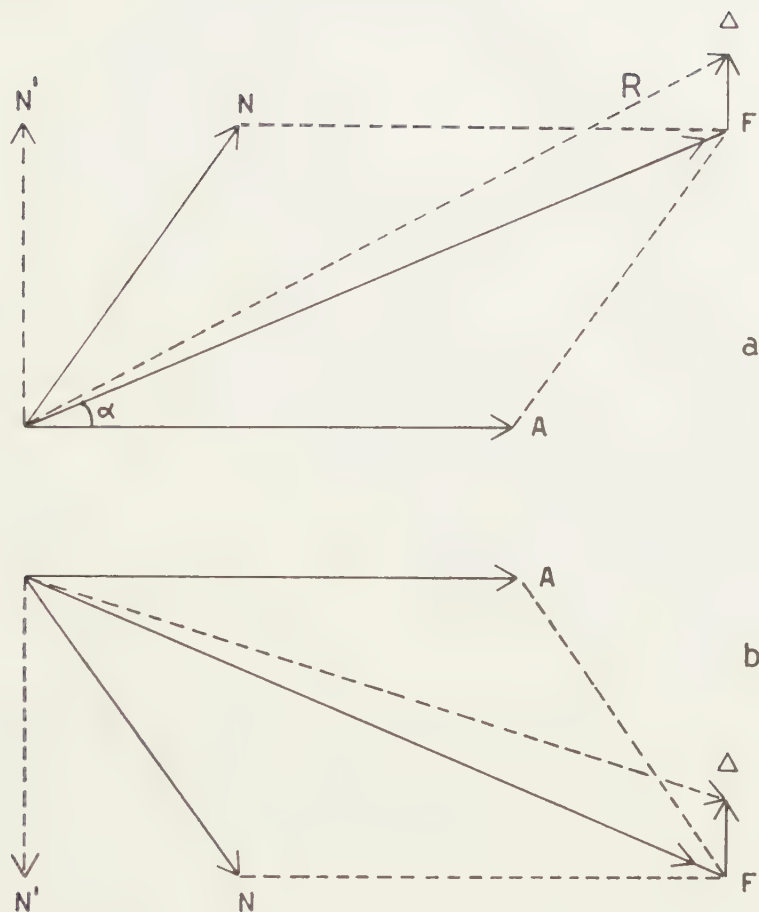


Fig. 1. Influence of anomalous scattering in the heavy atom method for reflection (a) and counter reflection (b).

the choice between  $\alpha$  and  $\pi - \alpha$ . However, the contribution of the heavy atom generally predominates and therefore  $\alpha$  will have the smaller value. The opposite case may arise only with very small intensities which are of no influence in a first Fourier synthesis.

An example of the above method will be given in due time.

*Laboratorium voor Kristalchemie der  
Rijks-Universiteit te Utrecht*

#### REFERENCES

1. BOKHOVEN, C., J. C. SCHOONE and J. M. BIJVOET, *Acta Cryst.* **4**, 275 (1951).
2. BIJVOET, J. M., *Nature* **173**, 888 (1954).
3. PETERSON, S. W., *Nature* **176**, 395 (1955).
4. OKAYA, Y., Y. SAITO and R. PEPINSKY, *Phys. Rev.* **98**, 1857 (1955).

## GEOLOGY

### GRADED BEDDING IN LIMESTONES

BY

PH. H. KUENEN AND E. TEN HAAF

(Communicated at the meeting of April 28, 1956)

#### *Abstract*

Attention is drawn to the fact that graded bedding is not restricted to graywackes and similar resedimented arenaceous rocks. Detrital limestones may show the same features indicative of deposition by turbidity currents. Because in limestones these features tend to be less obvious, few instances have been recorded so far. Three newly discovered examples are briefly described, and it appears probable that several regularly bedded geosynclinal limestone series, with or without intercalated shales, may turn out to have been deposited in bathyal depths by turbidity currents.

Many graded graywackes, attributed to the action of turbidity currents, contain some calcite, in the form of shells or of a slightly calcareous groundmass. Recent graded deep-sea sands with shallow-water benthonic foraminifera or pelecypods have also been described (ERICSON, EWING and HEEZEN, 1952).

In these cases the calcite is merely an admixture to terrigenous materials, but true limestones with graded bedding are also known.

MIGLIORINI, in collaboration with the senior author (KUENEN and MIGLIORINI, 1950) described graded detrital limestones, the so-called Brecciolas of the Apennines, and considered them as a product of resedimentation.

A few years later CAROZZI (1952) gave a description of the Upper Malm of the Nappe de Morcles, northwest of Chamonix. He attributed its coarse detrital limestone beds to resedimentation by turbidity currents. The same investigator, in a joint paper with the senior author (KUENEN and CAROZZI, 1953), showed that turbidity currents played an important part in the transport and deposition of certain detrital limestone beds in the Nappe de la Brèche of the Pic Marcellly chain, near Geneva. Among the rocks of this overthrust sheet, composed mainly of coarse limestone breccias and calcareous pelagic shales, there are many calcarenites with graded bedding.

The senior author found a few graded detrital limestones on the beach of the Girvan area, Scotland, which he attributed to resedimentation of calcareous detritus by turbidity currents (KUENEN, 1953). NEWELL *et al.*



(1953) connected several limestone beds bordering the foot of the Permian Reefs of the Guadalupe Mountains, U.S.A., with the action of turbidity currents.

CLARKE (1917) published a photograph of a wonderful succession of Silurian limestone beds at Mt. Joli-Percé, Gaspé Peninsula, Canada, which exhibit flute casts (flow marks) and tracks in addition to ripple marks and regular bedding. Pending local investigation, it appears highly probable that here is another example of graded calcarenites.

Mention can also be made of graded calcarenites observed by the senior author among the regularly bedded Malm limestones exposed along the river Var in the Alpes Maritimes. But until features indicating current action, such as current ripple lamination or flute casts, have been noted, the assumption of resedimentation by turbidity currents is not justified.

This short review shows that graded bedding in detrital limestones has been observed repeatedly and attributed to the action of turbidity currents. Yet most of these rock series are somewhat exceptional in character one way or another and it would be possible to maintain that resedimentation of calcareous detritus in deep water has been a very unusual occurrence in the geological past. It is therefore of some importance to draw attention to the finding by the present authors of three limestone series of normal character in which graded bedding is well developed, although only preliminary observations could be made.

Two occur in the northern part of the Abruzzi mountains northeast of Rome, one in the northern Apennines east of La Spezia.

#### *Middle Liassic limestone*<sup>1)</sup>

Near the Canapine pass between Norcia and Capodacqua a thick series of regularly stratified limestones is exposed. Owing to a strong development of chert and to tectonic crushing most sedimentary features are obscured, except west of the watershed along the road. There, well developed flute casts were observed on the soles of two beds, both distinctly graded. One was 50 cm thick. Of the other, at least two meters, the upper limit could not be ascertained because from a grain size of 2 or 3 mm at the base, it graded upwards into a jointed calcilutite with conchoidal fracture, indistinguishable from the supposedly pelagic beds intercalated between the graded calcarenites.

This thick bed, together with the underlying bed only 25 cm thick, could be traced over 300 meters and showed no change of thickness or character.

The upper surfaces of some other beds showed drag marks (=groove casts) and current ripple marks. On weathered joints of some fine grained beds parallel or current-ripple lamination was clearly discernible. In one bed convolute lamination was strongly developed, and elongate chert

<sup>1)</sup> The writers wish to thank Professor SCARSELLA for indicating the age of the rocks described here.

nodules, formed along the lamination planes, were bent and upended. Such abnormal position of cherts had already been recognised as typical of this formation <sup>1)</sup>, so that, apparently, convolute lamination is by no means rare.

On the eastern side of the pass there are thin seams of shale between some of the limestone beds. Here, slump structures containing balled-up masses of limestone were found.

#### *Miocene limestone*

A second series of graded limestones was discovered in the Miocene exposed on highway no. 80 north of the Gran Sasso massif. Again these rocks had the appearance of an ordinary well-bedded limestone without any considerable interstratification of shale or marl. West of Montorio al Vomano, the inverted limb of a recumbent fold crops out along the road. Here several soles showed the same kind of tracks and burrows as are typical of many Flysch-type graywackes. Many of the limestone beds had a uniform crystalline texture, but several, up to a meter in thickness, exhibited distinct grading from coarse calcarenite to calcilutite. Current ripple lamination was not very distinct, but characteristic flute casts occurred on half a dozen soles.

#### *Eocene limestone*

The Calcare Alberese is a marly limestone known only as displaced masses occurring in the Argille Scagliose of the northern Apennines. The age is probably Eocene.

The second author examined a few outcrops and discovered plenty of evidence for resedimentation: grading in beds a few dozen centimeters thick, flow marks and tracks on the soles, current ripple lamination and convolute lamination. Further details will be given in a later publication.

#### *Conclusions*

These observations, in spite of their preliminary and incidental nature, allow of a few conclusions.

In the first place, the discovery of graded bedding in three normal, pure limestones series, in addition to its occurrence in the less usual formations cited earlier, shows that a search for resedimented calcareous deposits should comprise all regularly bedded, geosynclinal series, whether they show shales and marls between the limestone beds or not. It is not improbable that several such resedimented rocks will be discovered. Separate limestone beds occurring here and there between graded graywackes may prove to be of the same nature.

In the second place, both limestone formations of the northern Abruzzi described in this paper showed current directions from the southwest, that is, transversal to the geosynclinal trough. The Miocene limestone is

<sup>1)</sup> SCARSELLA, personal communication.

directly overlain by a sandy Flysch formation, a "marnoso arenacea", with a longitudinal direction of supply from the north and northwest. The abrupt change in detrital material is thus explicable by a shifting of the source area of the sediment.

In the third place, we now know that most of the complex of features characteristic of graded graywackes can also occur in resedimented limestones: grading, lamination in the upper part of beds, flute and groove casts, current ripple marks, convolute and ripple lamination, tracks and burrows, regular stratification of alternating detrital and pelagic beds, and occasional slump structures. Thereby these features are proved to be typical of the process of resedimentation itself, and independent of the chemical nature of the sediment.

But in a calcareous formation these phenomena tend to be much less conspicuous. Recrystallization often obliterates the internal sedimentary structures, and superficial solution effaces sole markings. Because resedimented and pelagic limestone beds present a similar resistance to weathering, the markings on bedding planes are but rarely exposed. On the other hand both positive and negative forms can be preserved, while in graywacke outcrops the pelagic shales or marls weather away rapidly, destroying the moulds while exposing the casts on the soles.

#### REFERENCES

- CAROZZI, A., Tectonique, courants de turbidité et sédimentation. *Rev. Génér. des Sciences*, **59**, 229-245 (1952).
- CLARKE, J. M., Strand and undertow markings of Upper Devonian time as indications of prevailing climate. *N.Y. State Mus., Bull.*, **196**, 199-238 (1917).
- ERICSON, D. B., M. EWING and B. C. HEEZEN, Turbidity currents and sediments in North Atlantic. *Am. Ass. Petr. Geol., Bull.*, **36**, 489-511 (1952).
- KUENEN, PH. H., Graded bedding, with observations on Lower Paleozoic rocks of Britain. *Verh. Kon. Ned. Akad. Wet. Amsterdam, Afd. Natuurk.*, **22**, 3, 47 (1953).
- , (in press) Sole markings of graded graywacke beds.
- and A. CAROZZI, Turbidity currents and sliding in geosynclinal basins of the Alps. *Journ. of Geol.*, **61**, 363-373 (1953).
- and C. I. MIGLIORINI, Turbidity currents as a cause of graded bedding. *Journ. of Geol.*, **58**, 91-127 (1950).
- NEWELL, N. D. *et al.*, The Permian reef complex of the Guadalupe Mountain Region, Texas and New Mexico (San Francisco, 1953).

# GEBISSRESTE VON MENSCHENAFFEN AUS DEM UNTER- PLIOZÄN RHEINHESSENS. I

VON

G. H. R. VON KOENIGSWALD

(Communicated at the meeting of March 24, 1956)

Unter den tertiären Menschenaffen nimmt *Paidopithecus rhenanus* POHLIG aus dem Unterpliozän (Pont) von Eppelsheim in Rheinhessen eine besondere Stellung ein: diese Art ist auf Grund eines Femurs aufgestellt worden, während beinahe alle anderen Affenarten auf Gebissresten beruhen und von ihnen kein vergleichbares Skelettmaterial bekannt ist. Erst kürzlich haben LE GROS CLARK & LEAKEY (1951) einen Affenfemur beschrieben, auf den wir noch eingehen müssen, aber dieser stammt aus sehr viel älteren Schichten und ausserdem noch aus Ostafrika.

So ist es begreiflich, dass der Affe aus Rheinhessen nicht ohne weiteres mit anderen Funden zu vergleichen ist. Gehört das Femur zu *Dryopithecus* oder zu einer anderen Gattung? Dürfen die gleichaltrigen Zähne aus den schwäbischen Böhmerzen mit der eppelsheimer Form vereinigt werden (SCHLOSSER) oder muss man sie davon getrennt halten (ABEL)? Diese Fragen werden sich nur beantworten lassen, wenn genügend aus Gebissresten aus Rheinhessen vorliegen.

Solche scheinen bereits mehrfach gefunden zu sein, sind aber entweder verloren gegangen oder nicht als solche erkannt worden. Während eines kurzen Besuches an das Mainzer Museum im Februar 1937 zeigte mir der inzwischen leider verstorbene Direktor Prof. O. SCHMIDTGEN drei Primatenzähne, die vom Wissberg in Rheinhessen stammten. Es waren dies ein auffällig einfach gebauter unterer Molar, ein langer, sehr stark komprimierter oberer Eckzahn (ähnlich dem eines Pavians) und ein unterer Milchzahn, an den ich jedoch keine Erinnerung mehr besitze. Später scheinen noch weitere Zähne gefunden worden zu sein. In einer Zusammenfassung erwähnt WAGNER den unteren Molaren merkwürdigerweise nicht. „Eine mündliche Mitteilung von SCHMIDTGEN bezeichnet die am Wissberg gefundenen Affenzähne als schimpansoid. Nach ihm liegen vor: 2 Prämolare des Oberkiefers, zwei Eckzähne und einige fragliche Reste“ (1946, p. 8). Die kostbaren Funde waren Herrn Dr. W. ABEL zur Bearbeitung anvertraut, sind aber, wie Herr Conservator K. STADELMANN vom Mainzer Museum mir freundlicherweise mitteilte, nach dem Kriege verloren gegangen.

Einen oberen Eckzahn von Eppelsheim den KAUP schon abbildete, hat HAUPT (1935) als *Semnopithecus eppelsheimensis* bezeichnet. Wie



HÜRZELER (1954, p. 51) sehr richtig bemerkt, kann der Zahn nicht von einem Cynomorphen stammen; er ist jedoch zu klein um zu der gleichen Form zu gehören, die durch das eppelsheimer Femur belegt ist.

Nach dem Kriege sammelte Herr Prof. W. FREUDENBERG am Wissberg einen unteren Molaren und einen oberen Incisiven, die er als Menschenaffen-zähne bestimmte und die sich heute im Besitz von Herrn Dr. E. O. SCHOCH in München befinden. Der untere Molar stammt ohne Zweifel aus dem gleichen Gebiss wie der Molar, den ich 1937 in SCHMIDTGEN's Sammlung gesehen hatte. Über die Zuweisung des Schneidezahnes bin ich mir nicht ganz im klaren; die Basis scheint mir für einen Menschenaffen-zahn etwas breit, möglicherweise stammt er von einem Carnivoren. Da mir das Original nicht vorliegt, möchte ich hier von einer Besprechung dieses Zahnes absehen.

Erst im letzten Jahre, 1955, erwarb Herr Dr. SCHOCH einen weiteren jedoch viel kleineren unteren Molaren, der von der gleichen Fundstelle stammt. Alle soeben erwähnten Reste vom Wissberg bei Gau-Weinheim stammen aus der Grube von Herrn NAUTH auf der Höhe des Berges. Es ist dies, neben der reichen Sandgrube von Herrn Weingutsbesitzer H. SCHWAHN in Westhofen bei Worms, wohl die wichtigste Fundstelle pliozäner Säugetiere in Rheinhessen, nachdem der klassische Fundplatz Eppelsheim schon lange erschöpft und ausser Betrieb ist.

Herrn Dr. E. O. SCHOCH möchte ich an dieser Stelle herzlich dafür danken, dass er mir die wichtigen Reste zur Bearbeitung anvertraut hat. Es handelt sich also um zwei untere Molaren, von sehr verschiedener Grösse die wir getrennt beschreiben müssen.

#### I. *Paidopithecus rhenanus* POHLIG 1895.

Typus: Oberschenkelknochen, gefunden 1820 in Eppelsheim, Rheinhessen, bewahrt im Museum in Darmstadt.

Alter: Unterpliozän (Pont).

Fundstellen: Eppelsheim und Wissberg bei Gau-Weinheim in Rheinhessen; schwäbische Bohnerze von Salmendingen, Melchingen, Trochtelfingen und Ebingen; Seu d'Urgell bei Lerida, Spanien.

#### A. Femur

1861 *Hylobates fontani* OWEN, in KAUP, Beiträge etc. p. 1, Taf. I, Fig. 3.

1895 *Paidopithecus rhenanus* POHLIG, Bull. Soc. Belge de Geologie etc., 9, p. 149.

1895 *Pliohylobates eppelsheimensis* DUBOIS, idem, p. 155.

#### B. Gebiss; grosse Form

1867 *Dryopithecus*, QUENSTEDT, Handbuch etc., p. 32.

1898 *Dryopithecus fontani* v. BRANCO, Jahreshefte p. 16.

1898 *Dryopithecus* sp. v. BRANCO, idem, p. 61.

1901 *Dryopithecus rhenanus* SCHLOSSER, Die menschenähnlichen Zähne etc., p. 267.

- 1905 *Dryopithecus suevicus* KOKEN, Führer durch die Sammlungen des geol. Institutes Tübingen, p. 81.  
 1914 *Dryopithecus fontani* WOODWARD, On the lower jaw etc. p. 316.  
 1919 *Dryopithecus germanicus* ABEL, Das Entwicklungszentrum etc., pp. 27–29.

Der grössere der vorliegenden Zähne ist ein zweiter Molar des rechten Unterkiefers. Der Zahn scheint leicht abgerollt zu sein; die Wurzeln sind abgebrochen, aber die vollständige Zahnkrone ist erhalten. Diese ist bereits recht stark abgeschliffen, denn an allen drei Höckern der Aussen-seite liegt das Dentin bloss. Der Zahn, der eine gelbliche Farbe besitzt und der ausgezeichnet fossilisiert ist, ist 10.9 mm lang und 9.3 mm breit, woraus sich ein Index von 85,3 ergibt.

Wie üblich bei Anthropoiden besteht die Krone aus fünf leicht alter-nierenden Haupthöckern. Von diesen sind die drei labialen sehr viel stärker betont als die lingualen. Im Trigonid ist das Protoconid grösser als das Metaconid, beide sind durch eine einfache, unterbrochene Leiste mit einander verbunden. Davor liegt eine langgestreckte Grube, die Fovea anterior. Im Talonid fällt zunächst das lateral scharf abgegrenzte, bis über die Zahnmitte hineinragende Hypoconid auf. An der Aussenseite des Zahnes ist die Begrenzung vorne durch einen deutlichen Einschnitt, hinten durch einen Einschnitt mit einer vorgelagerten kleinen Grube markiert. Das Hypoconulid ist labial verschoben und mit dem kleinen Entoconid durch eine leicht unterbrochene Leiste verbunden. Diese setzt am Hinterende der Entoconidspitze an und zieht zum Vorderende des Hypoconulids, sodass sie etwa parallel zur Trigonidleiste läuft. Hinter Entoconid und Hypoconulid befindet sich eine einfache, abgegrenzte hintere Grube, die Fovea posterior. Zwischen Entoconid und Metaconid liegt ein kleiner Randhöcker wie er bei Anthropoiden vielfach vorkommt und in dem wir wohl den Rest eines ursprünglich vorhanden gewesenen Metastylids erblicken dürfen.

Vom Basalband ist nichts mehr zu sehen. Das Zahnrelief ist von grösster Einfachheit, was wohl mit der starken Abkautung zusammen hängt. Nur am hinteren Abhang des Metaconids lässt sich der Rest einer grösseren Schmelzfalte erkennen.

Zu einem Vergleich müssen zunächst die von BRANCO (1898) und SCHLOSSER (1902) ausführlich beschriebenen „menschenähnlichen Zähne“ aus den schwäbischen Bohnerzen herangezogen werden, welche SCHLOSSER zwar zur eppelsheimer Art gestellt hat, jedoch der Gattung *Dryopithecus* zurechnet.

Die Zähne aus den Bohnerzen sind untereinander recht variabel; leider zeigt kein einziger den gleichen Grad der Abkautung wie das vorliegende Stück. Die Grösse ist dieselbe, auch die Verteilung der Höcker. Das Entoconid ist verschieden ausgebildet, so bei dem Molaren von Melchingen (SCHLOSSER 1902, Taf. I, fig. 7) deutlich stärker als bei dem von Trochtel-fingen (idem, Fig. 6), der in dieser Hinsicht, in seiner Grösse (Länge: 10.6 mm; Breite 9.2 mm) sowie in der Ausbildung seiner Querleisten und

in der Abgrenzung des Hypoconids und der verschiedenen Gruben besonders gut mit dem Zahn vom Wissberg übereinstimmt. Nur ist er noch nicht abgekaut, und daher ist das Leistensystem deutlicher, aber dieses verschwindet schon bei leichter Abkaunung und ist auch an der Unterseite des Schmelzes nicht mehr zu sehen (BRANCO 1898, Taf. I, Fig. 6). Alle am hinteren Abhang des Metaconids am Wissberger Zahn noch erkennbaren Schmelzrunzeln finden sich auch, nur deutlicher, am Zahne von Trochelfingen, der wohl ebenfalls ein zweiter Molar ist. (BRANCO 1898, Taf. II, Fig. 6; SCHLOSSER 1902, Taf. I, Fig. 6; SCHLOSSER bezeichnete diesen Zahn p. 127 als zweiten, in der Tafelerklärung als  $M_2$  ( $M_3?$ )). Die deutliche Ausbildung von Querleisten hängt mit der Formation einer solchen zwischen Metaconus und Hypoconus in den oberen Molaren zusammen (SCHLOSSER 1902, Taf. I, Fig. 2), und muss daher der gleiche Molarentyp auch für die eppelsheimer Form angenommen werden. Es kann kein Zweifel bestehen, dass SCHLOSSER recht behalten hat, und die Zähne aus dem Bohnerz tatsächlich zu gleichen Art gehören wie das Femur von Eppelsheim.



Fig. 1. Zweiter unterer Molar von *Paidopithecus rhenanus* POHLIG. A. Aus dem Unterpliozän von Wissberg bei Gau-Weinheim, Rheinhessen (Sammlung SCHOCH-München). B. Aus dem Unterpliozän von Sue d'Urgell, Lerida, Spanien. (Spiegelbildlich nach einem von Herrn Dr. M. CRUSAFONT PAIRÓ—Sabadell zur Verfügung gestellten Abguss).  $1\frac{1}{2}$  natürliche Grösse.

Kommen wir nun zu einem Vergleich mit den ausserdeutschen Funden, so fällt direkt eine fast völlige Übereinstimmung mit dem entsprechenden Zahn des Kiefers von Seu d'Urgell bei Lerida in Spanien auf, den SMITH WOODWARD (1914) als zu *Dryopithecus fontani* gehörig beschrieben hat. Die Zahnreihe besitzt tatsächlich beinahe die gleiche Masse wie die des *Dryopithecus fontani* von St. Gaudens, aber doch ergeben sich wichtige morphologische Unterschiede, die nicht als einfache Variabilität aufgefasst werden dürfen, da zwischen diesen Funden ebenfalls ein grosser Altersunterschied besteht. Der typische *Dryopithecus fontani* kommt aus dem Obermiozän (Torton-Sarmat) von St. Gaudens — Reste von 3 Unterkiefern und 2 isolierte untere Molaren — und La Grive St. Alban — isolierter oberer Molar —. Hiervon ist scharf zu trennen der Unterkiefer von Seu d'Urgell. Nach seiner Begleitfauna, die wie am Wissberg, *Hipparion gracile*, *Mastodon longirostris*, *Tapirus priscus*, *Chalicotherium goldfussi*, *Dicerorhinus schleiermacheri*, *Cervus dicranocerus* u.s.w. enthält (VILLALTA & CRUSAFONT 1947) sind diese Schichten von unterpliozänem Alter (Pont) und völlig gleichaltrig mit unserm rheinhessischen Dinotheriumsand und den Bohnerzen von Salmendingen. Nun gibt es wohl einige wenige Arten,



die vom Miozän ins Pliozän reichen, aber das ist keine Selbstverständlichkeit. v. ZITTEL hat eine Zuweisung des eppelsheimer Femurs *Dryopithecus* ausdrücklich von der Hand gewiesen, da dies „jedoch bei dem beträchtlich verschiedenen Alter der Ablagerungen von Eppelsheim und St. Gaudens höchst unwahrscheinlich ist“. (1893, p. 710).

Weiter kommt hinzu, dass, wenigstens morphologisch, ein Spezialist wie GREGORY den spanischen Kiefer von dem französischen trennt. „*Dryopithecus fontani*, the genotype, approaches the gorilla in the nipple-like form of the molar cusps, in the retention of an external cingulum in the molars, as well as in the important characters noted by REMANE. The jaw from Lerida, Spain, referred by SMITH WOODWARD to this species, approaches the chimpanzee in certain characters“ (1926, p. 83).

Wir haben also stratigraphische und morphologische Gründe, den Anthropoiden von Lerida von *Dryopithecus fontani* abzuscheiden. Unser Zahn vom Wissberg stimmt in den Massen mit dem entsprechenden der Leridamandibel beinahe bis auf Bruchteile eines Millimeters überein. ( $M_2$  von Lerida: Länge 11.0, Breite 9.5 mm). In der Verteilung der Höcker, dem deutlich abgegrenzten breiten Hypoconid und der Art der schwachen durch die Abkauung bereits verschwundenen Runzelung sind sich die Zähne völlig gleich. Der einzige, unwesentliche Unterschied besteht in der Anwesenheit eines Cingulums am vorderen Aussenrande des Leridazahnes, doch ist dieses Merkmal nicht einmal bei *Dryopithecus fontani* konstant.

Die geologische Gleichaltrigkeit, die Unterschiede mit dem typischen *Dryopithecus fontani* und die ausgezeichnete Übereinstimmung der zweiten Molaren sprechen dafür, dass der Unterkiefer von Lerida zur gleichen Art gehört, die auch vom Wissberg vorliegt.

Die nächste Frage hat nun zu lauten: *Dryopithecus* oder *Paidopithecus*? Wir haben soeben bereits gehört, dass das Gebiss von *Dryopithecus fontani* als mehr „gorilloid“, das von *Dryopithecus rhenanus* als mehr „schimpansoid“ bezeichnet worden ist. Bei der ersteren Form sind die Höcker mehr randständig, und scheint die Schmelzfältelung auch schwächer gewesen zu sein. Auch dürfte bei dem Leridakiefer die Symphyse steiler, der Kieferbogen breiter und der aufsteigende Ast trotz kleinerer Zähne massiver gewesen sein als bei *fontani*. REMANE äussert sich vorsichtig: „Zusammenfassend kann man von *Dryopithecus rhenanus* sagen, dass die bisher vorhandenen Reste die Einordnung in die Gattung *Dryopithecus* zwar nicht mit absoluter Sicherheit gestatten, dies aber bei dem augenblicklichen Stande unseres Wissens die einzige angemessene ist“ (1921). Wenn wir jedoch gleichzeitig noch die stratigraphischen Unterschiede und die andersartige Morphologie der Kiefer hinzunehmen, so glaube ich hieraus doch ableiten zu dürfen, dass beide Formen nicht nur artlich, sondern auch generisch verschieden sind, und möchte daher vorschlagen, den Gattungsnamen *Paidopithecus* bei zu behalten.



## C. Gebiss; kleine Form

- 1901 *Anthropodus brancoi* SCHLOSSER, Die menschenähnlichen Zähne etc., Zool. Anz. 24, p. 264.  
 1902 *Neopithecus brancoi* ABEL, Zwei neue Menschenaffen etc., p. 1173.  
 1921 *Dryopithecus rhenanus* REMANE, Zur Beurteilung etc. p. 337.  
 1931 *Dryopithecus brancoi* ABEL, Die Stellung des Menschen etc., p. 122.  
 1954 ? *Pliopithecus brancoi* HÜRZELER, Contribution etc., Anal. Pal. 11, p. 52.

Unter den „menschenähnlichen“ Zähnen von Salmendingen befindet sich einer, den BRANCO ursprünglich wegen seiner Kleinheit für einen Milchzahn gehalten hat, bis SCHLOSSER in ihm einen letzten unteren Molaren erkannte, den er als *Anthropodus brancoi* von den übrigen Primatenzähnen trennte. Später veränderte ABEL (1902) den Namen in *Neopithecus*.

Über die Selbständigkeit weder der Art noch der Gattung besteht Einigkeit. GREGORY und vor allem REMANE (1921, p. 337) wollen den fraglichen Zahn einem schwachen Individuum des „*Dryopithecus germanicus*“ zuschreiben. ABEL (1931) stellt ihn später wohl ebenfalls zu *Dryopithecus*, behält aber den Artennamen *brancoi* bei. Neuerdings scheint HÜRZELER (1954) geneigt zu sein, die Gattung als mögliche Terminalform der *Pliopithecus*-Gruppe zu betrachten.

Es ist nun interessant zu sehen, dass sich unter dem Material vom Wissberg ein Molar befindet, der in seinen Massen wohl zu der „kleinen Form“ aus dem Bohnerz passen würde, sich jedoch morphologisch soweit von dieser entfernt, dass sie nicht zur gleichen Art gehören kann. Was die erstere betrifft scheint mir die Zugehörigkeit zu *Paidopithecus* sehr wohl möglich — was auf einen ausgesprochenen sexuellen Dimorphismus weisen würde — aber nicht erwiesen.

Immer wieder ist bei den Zähnen aus dem schwäbischen Bohnerz ihre Menschenähnlichkeit betont worden. Wie BRANCO mitteilt, hielt JÄGER die Zähne für menschlich. Ein Molar von Salmendingen „wurde seiner Zeit an R. OWEN nach London geschickt und dort ebenfalls als „unzweifelhafter Menschenzahn“ bestimmt, wie uns QUENSTEDT berichtet. Ein gleiches Urteil fällte Professor ARNOLD in Tübingen, der damalige Anatom, über drei weitere derartige Zähne, welche von QUENSTEDT inzwischen erworben worden waren. Der Vergleich zeigte, dass dieselben ebenfalls den drittletzten bei „Mongolen, Finnen und Mohren“ glichen“. (BRANCO, 1898, p. 18). QUENSTEDT (1867) und nach ihm SCHLOSSER (1887) scheinen die ersten gewesen zu sein, die dann die Zähne als äffisch und zu *Dryopithecus* gehörig bezeichneten. BRANCO berichtet weiterhin: „Die Schwierigkeit des Vergleiches unserer fraglichen Zähne mit den französischen des *Dryopithecus* ist so gross, dass Herr GAUDRY, welchem ich anfänglich nur die vergrösserten Zeichnungen unserer Zähne mit der Bitte um freundliche Vergleichung derselben zusandte, eine sichere Bestimmung derselben, selbst auch nur eine generische, ablehnen musste“ (1898, p. 21). Die Menschenähnlichkeit unserer Zähne wird sogar noch

grösser, wenn man die ähnlich komplizierten Molaren des vorzeitlichen Menschen, vor allem des *Sinanthropus pekinensis*, mit ihnen vergleicht (WEIDENREICH, 1937).

REMANE (1921) findet in den Molaren aus den Böhnerzen eine gewisse Annäherung an den Schimpansen, und GREGORY (teste ABEL 1931, p. 122) scheint sogar geneigt zu sein, um zu erklären „According to this view the European *Dryopithecus fontani* may even be directly intermediate between the Asiatic types on one hand and the modern African Gorilla on the other; while the allied *D. rhenanus* may stand nearer to the direct ancestors of the Chimpanzee“. SCHLOSSER hingegen bezeichnet den Orangutan, *Simia* als „den vermutlichen Nachkommen der Gattung *Dryopithecus*“ (1902, p. 116).

Es scheint mir sehr die Frage, ob wir auf Grund des Gebisses so weit gehen dürfen. Mir vorliegende Schimpansenzähne (siehe auch WEIDENREICH 1937, Fig. 158) weisen ein sehr viel feineres und komplizierteres Relief auf als die fossilen Zähne, und solange nicht einmal die pleistozäne Entwicklungsgeschichte der beiden afrikanischen Grossaffen bekannt ist, lässt sich über den Verlauf der Spezialisierung nichts aussagen.

Vom Gebiss des *Paidopithec* können wir noch einige interessante Einzelheiten vermelden. v. SCHEURLEN teilt mit: „Eine Röntgenaufnahme der zwei einzigen *Dryopithecus*-Zähne, bei denen die Wurzeln erhalten sind, durch Fräulein Dr. HAUG ergab, dass diese im Gegensatz zu rezenten Anthropomorphenzähnen dieselbe schmale Pulpahöhle aufweisen wie der Mensch“. (v. SCHEURLEN 1938, p. 28). Diese Bemerkung ist nur beschränkt richtig und trifft nur auf den heutigen Menschen zu, denn der fossile Mensch wie der Neanderthaler und der Peking Mensch (WEIDENREICH, 1937, Fig. 307) besitzen gerade eine weite Pulpahöhle.

Herr Prof. C. ARAMBOURG, Paris, war so freundlich, mir von dem von GAUDRY beschriebenen *Dryopithecus*-Kiefer, von St. Gaudens ein Originalphoto zur Verfügung zu stellen. Hierbei zeigt es sich, dass der erste untere Prämolare trotz Überbetonung des Protoconids einen deutlichen Innenhöcker besitzt. Die ganze linguale Seite wird von einem Basalband umfahren, das vorne noch eine leichte Schmelzknospe aufweist, vielleicht der letzte Rest eines Paraconids. Wenn eine obermiozäne Form mit so starken Eckzähnen noch so ursprüngliche Verhältnisse erkennen lässt, so dürfte der entsprechende Zahn des schwächeren *Paidopithec* vermutlich noch ausgesprochen zweihöckrig gewesen sein, wie wir dies auch bei dem entsprechenden Zahne von *Ramapithecus* cf. *brevirostris* aus den gleichaltrigen indischen Siwaliks beobachten können (GREGORY, HELLMAN & LEWIS 1938, Taf. 8, Fig. C).

Bei der Beschreibung der Lerida-Mandibel weist SMITH WOODWARD auf den unspezialisierten Zustand der Symphyse. „Hence, sofar as the mandibular symphysis is concerned, the Miocene“ — dies in Anlehnung an die französische Nomenklatur; in unserm Sinne Unterpliozän — „*Dryopithecus* resembles the large modern Anthropoids no more closely

than it agrees with the earliest known true Man. By slight changes in two different directions it may have passed into the one as readily as into the other" (1914, p. 320).

Ein Vergleich mit den Gebissen bisher bekannten, meist ebenfalls auf dürftige Reste basierten fossilen Anthropoiden ist nicht leicht. Gleichaltrig in Europa ist nur der kleinere *Hispanopithecus laietanus* DE VILLALTA & CRUSAFONT aus dem Pont von Viladecaballs in Nordspanien, (DE VILLALTA & CRUSAFONT 1944), der in seinen Molaren durch die Verteilung der glatten Höcker stark an *Symphalangus* erinnert, was noch durch einen einspitzigen ersten unteren Prämolaren unterstrichen wird. Von den miozänen Formen sind wir auf *Dryopithecus fontani* bereits eingegangen. *Dryopithecus darwini* (= *Griphopithecus suessi* ABEL) aus dem Mittelmiozän des Wiener Beckens, von Lewis zu *Sivapithecus* gestellt (1937, p. 144), besitzt ein anderes Kronenrelief und hat weder in den unteren noch in den oberen Molaren (GLÄSSNER 1932) die für unsere Form charakteristischen Querleisten; *Pliopithecus* (HÜRZELER 1954) ist viel zu klein, und die Molaren des spanische *Sivapithecus occidentalis* DE VILLALTA & CRUSAFONT (1944) haben ein zu gefältes Kronenrelief.

Von den asiatischen Formen ist der Anthropeide aus dem Pont von Anatolien zu gross (OZANSOY 1955); das Gebiss, das Herr OZANSOY mir in Paris freundlicherweise zeigte, ist zu ausgekauht um irgend einen Vergleich zu ermöglichen. Auch unter den verschiedenen Arten der indischen Sivaliks kann ich nicht viel Vergleichbares finden: eine Ausnahme macht vielleicht PILGRIM's *Dryopithecus punjabicus* (1915, Taf. 3), der die gleiche Querleiste zwischen Hypoconus und Metaconus in den oberen Molaren zeigt, wie sie für den schönen Molaren aus Salmendingen (SCHLOSSER 1902, Taf. I, Fig. 2) so charakteristisch ist. LEWIS stellt diese indische Art zu *Bramapithecus* (1937, p. 141), worin ich ihm nicht folgen kann. Von den zahlreichen aus dem Untermiozän von Kenya von LE GROS CLARK & LEAKEY beschriebenen Arten kommt *Proconsul* für einen Vergleich nicht in Frage, da dieser einen Pseudohypoconus besitzt und wohl mit keiner jüngeren Art verwandt ist. *Sivapithecus africanus* ist zu gross und ohne Querleiste in den oberen Molaren, die zwar bei *Limnopithecus macinnesi* vorkommt (LE GROS CLARK & LEAKEY 1951, Taf. 7, Fig. 8), der aber durch überspezialisierte untere Prämolaren nicht als möglicher Vorläufer in Frage kommt. Die kleinen schlechterhaltenen Anthropoiden aus dem Untermiozän Ägypten, von den alttertiären brauchen wir hier nicht zu sprechen, ergeben ebenfalls keine Vergleichspunkte.

Schliesslich müssen wir noch auf das Femur von Eppelsheim eingehen, welches ja das eigentliche Typusexemplar unserer Art darstellt, wobei wir uns vor allem auf die zusammenfassende Arbeit von GIESELER (1926) stützen wollen. Seinen Massen nach kann es nur von einem grösseren Anthropoiden stammen. Es handelt sich um einen schlanken Oberschenkelknochen von 284 mm Länge (nach DUBOIS 286 mm); wie Röntgenaufnahmen vermuten lassen, ist er wohl nicht ganz richtig zusammen-



gesetzt und war vielleicht ein wenig kürzer. Eine Neubearbeitung des Fundes durch Herrn Prof. R. BAY und Herrn Dr. J. HÜRZELER (Basel) scheint im Gange zu sein, sodass wir hier nicht näher darauf einzugehen brauchen. Die Epiphysenfugen sind geschlossen; der Knochen stammt also von einem vollkommen erwachsenen Individuum.

SCHLEIERMACHER scheint den Oberschenkelknochen ursprünglich einem 12 jährigen Menschenkinde zu geschrieben zu haben; OWEN, LARTET, DUBOIS, WALKHOFF und GIESELER (1926) finden ihn gibbonartig, und auch ABEL (1931, p. 124) reiht *Paidopithec* ausdrücklich unter die Hylobatiden ein. SCHLOSSER stellt ihn zu *Dryopithecus*, das gleiche tut auch POHLIG der ihn jedoch für menschenähnlicher hält als irgend ein Anthropoidenfemur. Er vermutet sogar „ein häufiges Üben des aufrechten Ganges“; eine Röntgenuntersuchung des Originalstückes sowohl durch WALKHOFF als durch GIESELER (1926, Taf. X, Figs. 10–11) lässt keinerlei „Trajektorium der aufrechten Haltung“ erkennen; POHLIG's Schlussfolgerungen werden von DUBOIS, WALKHOFF und GIESELER widersprochen.

Ist nun *Paidopithec* ein Hylobatide oder ein Simiide? Der heutige Gibbon, charakterisiert durch überlange Gliedmassen, hat auch eine sehr charakteristische Lebensweise: er bewegt sich, hangelnd und laufend durch die Baumkronen, von Baum zu Baum springend. Ein solches Geschöpf darf nicht gross sein, da sonst die Zweige unter ihm abbrechen, und dass der lebende Siamang Indonesiens in der Tat das Maximum an Grösse darstellt, lässt sich sehr deutlich an Hand von Verletzungen zeigen. SCHULTZ (1939, p. 576) fand in einer Serie von 118 wilden Gibbons nicht weniger als 42, d.h. 36 %, mit geheilten Knochenbrüchen. Das ist deutlich genug. Die Länge des Siamangfemurs gibt GIESELER mit 195–234 mm (Mittelwert nach SCHULTZ 206 mm) an; ein Femur von 286 mm kann also niemals von einem Hylobatiden s.str. stammen.

Man muss überhaupt sehr aufpassen, um jeden kleinen Affen gleich als Hylobatiden zu bezeichnen. Neurere Funde von *Pliopithecus*, der meist zu dieser Gruppe gestellt wird (vide ABEL 1931, p. 109) haben gezeigt, dass dieser weder nach seinen Körperproportionen (ZAPFE, 1952) noch nach seinem Gebiss (HÜRZELER 1954) dieser Gruppe eingereiht werden darf.

Wir müssen also annehmen, dass das eppelsheimer Femur trotz seiner gibbonähnlichen Form einen generalisierten Typus darstellt. Dies scheint SCHLOSSER bereits gesehen zu haben, und auch GREGORY & HELLMAN schliessen sich dieser Ansicht an (1926, p. 14). LE GROS CLARK & LEAKEY (1951, Fig. 23) bilden einen Femur aus dem Untermiozän der Insel Maboko im Kavirondogolf des Victoria Sees in Ostafrika ab, der nicht nur die gleiche Länge (ca. 285 mm) sondern auch den gleichen schlanken Schaft wie das eppelsheimer Femur besitzt, und sich von diesem nur unwesentlich unterscheidet, wie Fig. 2 zeigt. Leider lässt sich nicht mit Sicherheit feststellen, ob dieser Knochen von *Proconsul* oder dem in den gleichen Schichten vorkommenden *Sivapithecus* stammt.



Die relative Länge der Gliedmassen bei den fossilen Menschenaffen war offensichtlich eine ganz andere als bei den heutigen Formen. Zu diesem Resultat kommen sowohl LE GROS CLARK & LEAKEY auf Grund des untermiozänen Materiales aus Ostafrika (1951, p. 113) wie ZAPFE

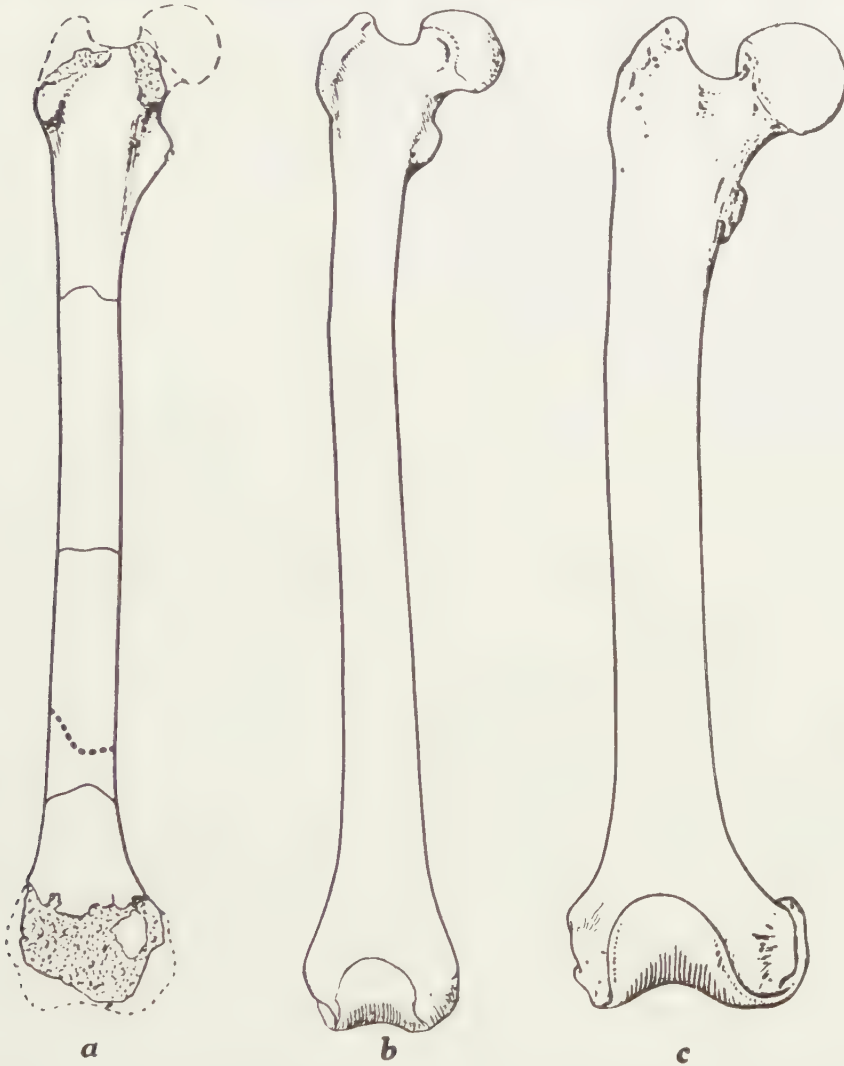


Fig. 2. Femur des *Paidopithecus rhenanus* POHLIG (b) im Vergleich mit den Femur von ? *Proconsul* (a) aus dem Untermiozän Ostafrikas und dem des lebenden Schimpansen (c). Alle drei Figuren im gleichen Maszstab verkleinert.

(Nach LE GROS CLARK & LEAKEY, 1951).

(1952) bei der Beschreibung des Skelettes des obermiozänen *Pliopithecus*. Auch der Humerus von St. Gaudens mit nur ca. 230 mm ohne Epiphysen (ergänzt ca. 260 mm) ist im Vergleich mit den Unterkiefern des *Dryopithecus fontani* auffällig klein. „Entweder gehört jener Oberarm des

*Dryopithecus*, den LARTET abbildet, einem sehr viel jüngeren Individuum an, als der von ihm gezeichnete Unterkiefer. Dafür spricht vielleicht das Fehlen der Epiphysen. Oder wir haben in diesem miozänen Menschenaffen eine Gattung vor uns, welche kurzarmiger, also menschenähnlicher war, als alle lebenden Anthropomorphen" (BRANCO 1898, p. 14). Auch hier fand sich ein in den Proportionen durchaus vergleichbares Stück auf Mboko (LE GROS CLARK & LEAKEY 1951, p. 98, Fig. 24), dessen Zuweisung, zu einer bestimmten Art leider ebenfalls unmöglich ist.

Immerhin zeigt es sich, dass sich sowohl zu dem *Dryopithecus* Humerus von St. Gaudens wie zu unserm Eppelsheimer *Paidopithecus* Femur vergleichbare Stücke bereits im Untermiozän finden. Nun dürfte dieser *Dryopithecus* etwa ebenso gross wie *Paidopithecus* gewesen sein, eher etwas grösser nach den kräftigeren Unterkiefern zu urteilen im Vergleich mit der Mandibel von Lerida. Hätte nun *Paidopithecus* einen ebenso kurzen Humerus besessen wie *Dryopithecus fontani*, so hätte diese Form einen Oberarmknochen gehabt, der kürzer gewesen wäre als sein Oberschenkel. Das letztere ist heute nur beim Menschen der Fall. Die Länge des Humerus geteilt durch die des Femur ergibt für den modernen Menschen Indices zwischen 70.4 und 74.8, für den Pekingmenschen 79.3, für die grossen Menschenaffen 101.4–138.2 (nach WEIDENREICH 1941, p. 51). Eppelsheimer Femur und Humerus von St. Gaudens würden kombiniert einen Index von nur ca. 90.9 ergeben. Was übrigens die Länge unseres Femur betrifft, so ist diese gleich an den Mittelwert für den weiblichen Schimpansen (286 mm), nur das er eben sehr viel schlanker ist. Der zugehörige Humerus des letzteren ist jedoch 290 mm lang. Dem Unterkiefer nach zu urteilen hat *Paidopithecus* etwa Schimpansengrösse gehabt, er scheint nur sehr viel schlanker gewesen zu sein und, wenn unsere Spekulationen richtig sind, auch andere Proportionen gehabt zu haben. Übrigens hat ZAPFE SCHLOSSER's Ansicht, dass „jene auffallende Länge des Oberarmes der Anthropomorphen lediglich eine neue, und zwar sicher nicht weiter als in das Pliozän zurückdatierende Spezialisierung" sei, gerade bei der Beschreibung des scheinbar gibbonähnlichen *Pliopithecus* bestätigen können.

Zusammenfassend kommen wir zu dem Resultat, dass *Paidopithecus rhenanus* ein Simier (und also kein Hylobatide) von etwas Schimpansengrösse gewesen sein muss, vermutlich mit ausgesprochenem Sexualdimorphismus. Die Symphyse des Unterkiefers war noch unspezialisiert, der erste untere Prämolare vermutlich zweihöckrig, die Schmelzrunzelung der Molaren von einem Typ, wie er sowohl bei fossilen Simiiden und Hominiden als auch noch beim modernen Menschen vorkommt. Die Körperproportionen waren wahrscheinlich noch nicht so extrem wie bei den lebenden Anthropoiden. Das dürftige vorliegende Material lässt keine definitiven Schlussfolgerungen über eine mögliche Verwandtschaft, weder mit den Simiiden als etwa mit den Hominiden, zu.

So bleibt die Herkunft von *Paidopithecus* vorläufig in Dunkel gehüllt.

Mit *Dryopithecus* dürfte er auf eine gemeinsame Wurzel zurückgehen. Direkt mit unserer Form verwandt ist möglicherweise *Dryopithecus punjabicus* Pilgrim aus der Nagri Zone — Mittelplozän — der indischen Siwaliks von Hari Talyangar, Simila Hills, der dann wohl auch zu *Paidopithecus* gestellt werden müsste. Übrigens braucht die Querleiste zwischen Hypononus und Metaconus in den oberen Molaren nicht ohne weiteres als eine Überspezialisierung angesehen werden, denn Reste hiervon finden wir bei Orang, Schimpansen und primitiven Hominiden.

(To be continued)

# GEBISSRESTE VON MENSCHENAFFEN AUS DEM UNTER- PLIOZÄN RHEINHESSENS. II

VON

G. H. R. VON KOENIGSWALD

(Communicated at the meeting of March 24, 1956)

## II. *Rhenopithecus eppelsheimensis* (HAUPT)

Typus : ein oberer Eckzahn von Eppelsheim, bewahrt im Museum in Darmstadt.

Alter : Unterpliozän (Pont).

Fundstellen: Eppelsheim und Wissberg, Rheinhessen.

1861 ? *Semnopithecus* KAUF, Beiträge etc., Taf. I, Fig. 4.

1888 *Dryopithecus fontani* SCHLOSSER, Die Affen, Lemuren etc., p. 15.

1935 *Semnopithecus eppelsheimensis* HAUPT, Andere Wirbeltiere etc.

1954 ? *Pliopithecus eppelsheimensis* HÜRZELER, Contribution etc., p. 51, Fig. 35.

Gleichzeitig mit dem eppelsheimer Femur hat KAUF einen oberen Eckzahn beschrieben, in dem er einen *Semnopithecus* vermutet. SCHLOSSER (1888) stellt ihn zu *Dryopithecus fontani* und meint dass er wegen seiner mässigen Grösse „möglicherweise von einem Weibchen“ stamme. Später ist HAUPT wieder auf diesen Fund zurückgekommen, den er jetzt ohne Bedenken zu *Semnopithecus* stellt, während HÜRZELER ihm wegen seiner Kleinheit und seines einfachen ovalen Durchschnittes auf *Pliopithecus* beziehen möchte mit dem er in der Grösse etwa übereinkommt. Dieser Eckzahn ist tatsächlich für eine Art, von der auch das Femur stammen könnte, zu klein, und bildet somit den ersten Hinweis darauf, dass in Eppelsheim zwei Anthropoiden von verschiedener Grösse vorkommen. Im übrigen handelt es sich wohl eher um den grossen männlichen Eckzahn einer kleinen Art; die gebogene Wurzel weist auf ausgesprochene Prognathie hin.

Unter dem neuen Material vom Wissberg befindet sich ein Zahn der schon in seinen Massen gut zu diesem kleinen Eckzahn passt und den ich darum zur gleichen Art stellen möchte. Es handelt sich um die Schmelzkappe eines rechten Molaren, der leider stark beschädigt ist, da der grösste Teil des Protoconids beim Finden verloren gegangen ist. Die Zahnkrone ist dünn, Usuren sind nicht zu sehen, so dass es sich ohne Zweifel um einen Zahnkeim handelt.

Der erste Eindruck (auch von Herrn Dr. SCHUCH) war, dass es sich um einen Milchmolaren handle. Indessen weicht er in seiner Form so



weitgehend von dem einzigen bekannten Milchzahn von *Dryopithecus* von Salmendingen ab (SCHLOSSER 1902, Taf. I, Fig. 14) und besitzt auch keinerlei durchlaufende Trigonidleiste, wie ihn die Milchzähne der Anthropoiden ganz allgemein besitzen, und die sogar noch bei *Meganthropus* und *Sinanthropus* (WEIDENREICH 1937, Fig. 343), ja in seltenen Fällen noch beim rezenten Menschen vorkommt, dass ich mich gezwungen gesehen habe, den Zahn als einen Dauermolaren zu klassifizieren. Seine Länge dürfte 8.4, seine Breite 7.3 mm betragen haben, woraus sich ein Index von 85.7 berechnet. Seiner Form nach dürfte es sich um einen ersten Molaren handeln.



Fig. 3. Erster unterer Molar von *Rhenopithecus eppelsheimensis* (HAUPT) aus dem Unterpliozän vom Wissberg bei Gau-Weinheim, Rheinhessen (Sammlung SCHOCH-München). a. von oben, b. lingual, c. distal.  $1\frac{1}{2}$  natürliche Grösse.

Unser Zahn besitzt ein leicht zusammengekniffenes Metaconid an welches sich als distale Verlängerung ein kurzer Wulst anschliesst, der hier zwar keine Höckerform besitzt, den ich aber doch als Equivalent des Mesostylids betrachten möchte. Das Protoconid ist leider abgebrochen, sodass über seine Form nichts ausgesagt werden kann.

An ein breites Trigonid schliesst sich ein erstaunlich verkürztes Talonid an. Das Hypoconid ist schmal, scharf abgegrenzt und ein wenig über die Zahnmitte reichend. Entoconid und Hypoconulid sind gleich gross. Diese drei Höcker sind scharf und spitz, und an der Aussenseite steil abfallend.

Die Trigonidleiste ist durch einen Einschnitte unterbrochen. Eine kurze Schmelzfalte läuft vom Metaconid in die vordere Grube, eine breitere ist nach hinten gerichtet – sie entspricht REMANE's hinterer Metaconidnebenleiste – und begrenzt lateral die das Talonid durchschneidende Furche, die gradlinig die ganze Krone in zwei ungleiche Hälften teilt, das Hypoconid hinten abschneidet und auch Entoconid und Hypoconulid von einander scheidet. Hinten wird der Zahn durch eine wohlgeformte Grube, die Fovea posterior, begrenzt, an deren Rande ein ganz schwaches Tuberculum sextum zu erkennen ist.

Von dem grösseren Zahn von Wissberg unterscheidet sich der kleinere durch seine Dimensionen, ein verkürztes Talonid, einen anderen Verlauf der zentralen Furche, mehr zentrale Lage des Hypoconulids einen ausgesprochenen Grössenunterschied zwischen Metaconid und Entoconid, und offensichtlich spitzere, im Talonid, schärfer von einander separierte Höcker. Durch die gleichen Merkmale, vor allem die deutlich abgegrenzten Höcker unterscheidet er sich auch vom dritten kleinen Molar aus den Böhnerzen von Melchingen, der bei einer Länge von 10.3 eine Breite von nur 7.8 mm besitzt, also einen ersten Molaren von etwa der gleichen Grösse wie der vorliegende besessen haben könnte. Bei dem Zahn von

Melchingen begrenzen die dicht nebeneinander stehenden Höcker ein langgestrecktes Becken und sind nicht messerscharf von einander getrennt, sodass dieser Zahn einen ganz andern Charakter erhält und beide nicht zur gleichen Art gehören.

Unser Molar ist nur wenig grösser als der entsprechende von *Pliopithecus*; von diesem ist er leicht durch die stärker separierten und spitzeren Höcker zu unterscheiden, denn bei dieser Art besteht die Tendenz, dass die Höcker sowohl der lingualen wie der buccalen Seite zu mehr oder weniger geschlossenen Wand zusammenschmelzen zu scheinen (HURZELER 1954, Fig. 39). Er besitzt etwa die gleiche Länge wie ein erster Molar des sumatranischen Siamang, — maximale Länge nach DE TERRA 1905, p. 267, 8.0 mm), dessen Höcker jedoch runder sind, keine Schmelzrunzeln aufweisen, und bei dem das Hypoconulid noch etwa in der Zahnmitte liegt. Bei dieser Art beträgt die Länge des Femur 191–219 mm, mit einem Mittelwert von 206 mm, sodass das Femur — selbst wenn man an eine Überspezialisierung nach Art der heutigen Gibbons denken würde wozu nicht der mindeste Grund besteht — doch noch beträchtlich kürzer sein müsste als das klassische Femur von Eppelsheim.

Unser Zahn ist kürzer als der von allen europäischen und asiatischen Menschenaffen, wie ein Blick auf die von GREGORY, HELLMAN & LEWIS gegebene Tabelle zeigt (1938, p. 7), selbst kürzer als der von „*Dryopithecus*“ *rhenanus* stammende letzte Milchzahn (SCHLOSSER 1902, Taf. 1, Fig. 14; Länge 8.8 mm). Am nächsten kommt ihm noch ein erster Molar von *Ramapithecus* cf. *brevirostris* aus den Siwaliks mit einer Länge von 9.1 mm und einer Breite von 8.1 mm. Aber dieser Zahn, leider stark abgekaut, besitzt einen gänzlich anderen Kronenumriss (Trigonid schmäler als Talonid) und ein viel breiteres Hypoconid (1938, Taf. 2, Fig. 3). Morphologisch gleicht er noch am meisten einem isolierten, von LEWIS zu *Dryopithecus cautleyi* gestellten Molaren (LEWIS 1934, Taf. II, Fig. 2; die Bestimmung scheint mir anfechtbar) aber dieser besitzt eine stärkere Schmelzrunzelung die auch auf das Talonid übergreift und ein Hypoconulid, welches noch kleiner ist als das Entoconid; dieser Zahn besitzt auch ein im Verhältnis zum Metaconid kleines Entoconid, ähnlich wie der vorliegende Zahn. Auch *Bramapithecus thorpei* (LEWIS, 1934, Taf. I, Fig. 4), besitzt ein kleines Entoconid, ist aber viel breiter und zeigt anders geformte Höcker.

Auch zu den afrikanischen Anthropoiden (LE GROS CLARK & LEAKEY 1951) lassen sich keine Beziehungen nachweisen. Die Molaren höcker des kleinen *Limnopithecus* sind flacher und kantiger, und zeigen ebenso wie die von *Proconsul nyanzae* (der kleinsten der *Proconsul*-Arten) keine Schmelzrunzelung.

Da ich den kleinen Molaren vom Wissberg bei keiner der bekannten Anthropoiden Gattungen unterzubringen vermag, schlage ich hierfür einen neuen Namen vor, und zwar

*Rhenopithecus n.g.*

Als Artname kommt wohl *eppelsheimensis* in Frage, und als Typus darf der schon von KAUP abgebildete Eckzahn gelten. Welcher Art die Beziehungen der neuen Gattung zu den bisher beschriebenen ist, lässt sich bei dem dürftigen Material leider nicht feststellen.

## LITERATUR

- ABEL, O., Zwei neue Menschenaffen aus dem Leithakalkbildungen des Wiener Beckens. Sitz. K. Akad. Wiss. Wien. Math.-Nat. Kl. **111**, 1171–1202 (1902).
- , Zwei neue Menschenaffen aus den Leithakalkbildungen des Wiener Beckens. Centralbl. f. Min., 167–182 (1903).
- , Das Entwicklungszentrum der Hominiden. Mitt. Anthropol. Ges. Wien, 27–29 (1919).
- , Die Stellung des Menschen in Rahmen der Wirbeltiere, 1–398 (Jena, Fisher 1934).
- BRANCO, W., Die menschenähnlichen Zähne aus dem Böhnerz der schwäbischen Alb. Jahrb. Ver. Vaterl. Natk. Württemberg, **54**, 1–144 (1898).
- DUBOIS, E., *Pithecanthropus erectus*. P. V. Bull. Soc. Belge de Geologie etc. **9**, 151–160 (1895).
- GAUDRY, A., Le *Dryopithecus*. Mem. Soc. Geol. France, Pal. nr. **1**, 1–11 (1890).
- GIESELER, W., Zur Beurteilung des Eppelsheimer Femur. Verh. Ges. Phys. Anthropol., 34–45 (1926).
- GLAESSNER, M., Neue Zähne von Menschenaffen aus dem Miozän des Wiener Beckens, An. Nat. Hist. Mus. Wien **46**, 15–27 (1932).
- GREGORY, W. K. & M. HELLMANN, The dentition of *Dryopithecus* and the origin of Man. Anthropol. P. Am. Mus. Nat. Hist. **28**, 1–125 (1926).
- GREGORY, W. K., M. HELLMAN & G. E. LEWIS, Fossil Anthropoids of the Jale-Cambridge India Expedition of 1935. Publ. Carnegie Inst. Washington, nr. 495, pp. 1–27.
- HARLÉ, E., Une machoire de *Dryopithecus*. Bull. Soc. Geol. France **26**, 377–383 (1898).
- , Nouvelle pièce de *Dryopithecus*. idem **27**, 304–310 (1899).
- HAUPT, O., Andere Wirbeltiere des Neozoikums. In: SALOMON-CALVI, Ober-rheinischer Fossilkatalog Liefg. **4**, nr. (1935).
- HÜRZELER, J., Contribution à l'Ontologie et à la phylogenese du genre *Pliopithecus* GERVAIS., Ann. Pa. **11**, 5–63 (1954).
- KAUP, I. J., Beiträge zur näheren Kenntnis der urweltlichen Säugetiere **5**, 1–32 (1861).
- LARTET, E., Note sur un grand singe fossile qui se rattache au groupe des singes supérieurs. C. R. Ac. Sci. Paris, **43**, 219–223 (1856).
- LE GROS CLARK, W. L. & L. S. B. LEAKEY, The Miocene Hominoidea of East Africa. British Museum, Fossil Mammals of Africa, **1**, 1–117 (1951).
- LEWIS, E. G., Preliminary notice on new Man-like apes from India. Am. J. Sc. **27**, 161–179 (1934).
- , Taxonomic syllabus of Siwalik fossil Anthropoids. Am. J. Sc. **34**, 139–147 (1937).
- OZANSOY, F., Sur les gisements continentaux et les mammifères du Néogène et du Villafranchien d'Ankara (Turquie). C. R. Paris. Séance 21 février 1955.
- PHILGRIM, G. F., New Siwalik Primates and their bearing on the question of the evolution of Man and the Anthropoids. Rec. Geol. Surv. India, **45**, 1–74 (1915).

- POHLIG, H., *Paidopithecus rhenanus* n.g. n.sp., le singe anthropomorphe du Pliocène rhénan. P. V. Bull. Soc. Belge de Géologie etc., **9**, 149-151 (1895).
- QUENSTEDT, W., Handbuch der Petrefaktenkunde (2. Aufl., 1867).
- REMANE, A., Zur Beurteilung der fossilen Anthropoiden. Centralbl. f. Min. etc. **11**, 335-339 (1921).
- , Beiträge zur Morphologie des Anthropoidengebisses. Arch. Natgesch. **87**, Abt. A, 1-179 (1922).
- SCHEURLLEN, E. VON, Die Bedeutung des Steinheimer Schädels für die Entwicklungsgeschichte. Jahrb. Ver. Vaterl. Natk. Württemberg, **94**, 15-40 (1938).
- SCHLOSSER, M., Die Affen, Lemuren, Chiropteren etc. des europäischen Tertiärs. Beitr. Pal. Österreich-Ungarns **6**, 1-224 (1888).
- , Die menschenähnlichen Zähne aus dem Bohnerz der schwäbischen Alb. Zool. Anz. **24**, 261-271 (1901).
- , Beiträge zur Kenntnis der Säugetierreste aus den süddeutschen Bohnerzen. Geol. Pal. Abh. N. F. **5**, H. 3, 117-258 (1902).
- SCHULTZ, A. H., Notes on diseases and healed fractures of wild Apes. Bull. Hist. Med. **7**, 571-582 (1939).
- SMITH WOODWARD, A., On the lower jaw of an anthropoid ape (*Dryopithecus*) from the Upper Miocene of Lerida (Spain). Quart. J. Geol. Soc. **70**, 316-320 (1914).
- TERRA, M. DE, Beiträge zu einer Odontographie der Menschenrassen Diss. Zürich, 1-302 (1905).
- VILLALTA, J. F. DE & M. CRUSAFONT, Hallazoo del "*Dryopithecus fontani*" Lartet en en vindobomiense de la cuenca Vallés-Penedés. Bol. Inst. Geol. y Min. España, **55**, 131-143 (1941.)
- & ———, Dos nuevos antropomorfos del Miocene español y su situation dentro de la moderna sistematica de los simidos. Not. y Com. Inst. Geol. Madrid, **13**, 91-135 (1944).
- & ———, Les gisements de mammifères du Néogène espagnol. IV. C. R. somm. Soc. Géol. France, 28-30 (1947).
- WAGNER, W., Die unterpliozäne Wirbeltierfauna vom Wissberg bei Gau-Weinheim in Rheinhessen. W. Ver. T. H. Darmstadt, **1**, 2-11 (1946).
- WEIDENREICH, F., The dentition of *Sinanthropus pekinensis*. Pal. Sinica **101**, 1-180 (1937).
- , The extremity bones of *Sinanthropus pekinensis*. idem, **116**, 1-82 (1941).
- ZAPFE, H., Die *Pliopithecus* Funde aus der Spaltenfüllung von Neudorf an der March., Verh., Geol. Bundesanst., Sonderh. C, 1-5 (1952).
- ZITTEL, K. A. VON, Palaeozoologie, **4** (1893).



## ASTRONOMY

### REPORT OF THE NETHERLANDS EXPEDITION TO CEYLON FOR THE OBSERVATION OF THE TOTAL SOLAR ECLIPSE ON JUNE 20<sup>TH</sup> 1955

BY

J. HOUTGAST

(Communicated by Prof. M. MINNAERT at the meeting of March 24, 1956)

The area of the totality of the solar eclipse on June 20th 1955 extended over Ceylon, Farther India and the Philippine Islands. Ceylon was to be preferred for the observations, as it could be reached more easily from the Netherlands. The totality would take place at about 8.15 a.m. with a duration of about five minutes.

At the meeting of the Eclipse Commission of the "Koninklijke Nederlandse Akademie van Wetenschappen" on September 14th, 1954, Professor MINNAERT presiding, it was considered desirable to send out an expedition. An eclipse duration of five minutes gives a good opportunity to observe the spectrum of the chromosphere up to a height of 20.000 km, where the chromosphere passes into the corona. Professor W. BLEEKER, meteorological member of the Eclipse Commission, reported on the meteorological conditions. His report was based on statistical data showing that in the month of June the rainfall in Ceylon east of the higher regions is very slight. The coastal area was considered less favourable, on account of fog occurring in the morning hours. Moreover, in view of the possibilities of housing and accomodation along the central line of the totality, the region around Minneriya appeared to be the most suitable for setting up an observation camp.

#### *The programme of observation*

As after the expedition of 1954 only a relatively short time was available for preparation, there was only the possibility to continue the observations of the chromosphere as they had been started on the occasion of the two previous expeditions. The purpose was again, to take as great a number of spectra of the chromosphere as possible, in order to deduce from them how the chromospheric emission in each of the spectral lines depends on the height in the chromosphere. By making use of former experience, it proved possible to modify our apparatus within the required time and to make it ready for supplementary observations. The observations in 1952 (Khartum) and in 1954 (Gotland) had been made by means of an

objective prism<sup>1)</sup>). The spectra, taken at Khartum with exposure times of 0.5 and 1.0 seconds, yield absolute intensities and gradients of about 130 emission lines of medium strength. The Gotland spectra, taken with an exposure time of 0.1 second, comprise, besides the Fraunhofer spectrum before and after the contacts, about ten of the strongest chromospheric lines from K to H<sub>γ</sub> in all phases of the totality. Obviously spectra that can yield a more exact knowledge of the behaviour of the weak lines are still lacking. In addition to the continuum, only the weaker lines and perhaps also the wings of the stronger ones can inform us about the structure of the lower chromosphere, since only for these lines the optical depth of the chromosphere is small enough. As can be deduced from the self-reversals in many chromospheric emission lines, the temperature goes through a rather sharp minimum at a relatively small height above the base of the chromosphere. This temperature-course can only be studied from pictures with a short time of exposure.

A second aim, during this eclipse, would be to measure the strongest chromospheric emission lines up to as great a height as possible; in view of this the long duration of the eclipse would be favourable.

In order to obtain these observations during the eclipse in Ceylon the spectrograph was provided with a specially constructed slit. This was shaped like a semi-circle with a diameter of 32.0 mm, thus of the same size as the solar image, and outside it had two straight parts (fig. 1).

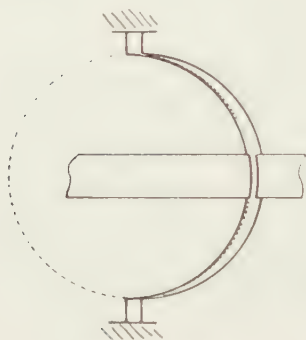


Fig. 1. The semicircular-shaped slit with a radius of curvature of 16 mm. During the eclipse the focussing of the widths of the slit was: 1 mm of the broad parts, 0.02 mm of the narrow part. The moon's limb would have to coincide with the dotted line.

Of the central part, 6 mm high, the slit width could be independently regulated. The purpose was, to take the spectrum, during the eclipse, with a narrow central slit 0.02 mm wide and with broader outer parts of about 1 mm. At about the middle of the totality, the slit would be turned over 180° in a few seconds and shifted sideways from the position for the second contact to that for the third. When the comparison spectra of the sun on the days before the eclipse were taken, a platinum step weakener had been put on the narrow part of the slit, while the broader parts were covered.

<sup>1)</sup> J. HOUTGAST: Atti dell' XI „Convegno Volta”, Rome 1952; A. C. S. VAN HEEL, J. HOUTGAST and M. G. J. MINNAERT: These Proceedings, series B, 57, No. 5, 1954.

The spectrograph, the former Cooke spectrograph of the Netherlands Eclipse Commission, was used in autocollimation and was provided with 2 flint prisms of  $45^\circ$  measuring  $15 \times 18 \text{ cm}^2$ ; as a collimator-camera lens a simple lens with a focal distance of 3 m was used, with an effective diameter of  $13 \text{ cm}^1$ ). This lens replaced the former Cooke triplet, which does not yield sufficiently sharp images at full aperture. As the focal distance of the original Cooke lens was 260 cm, the spectrograph-tube had to be made 40 cm longer. The wavelength region selected extended from 3900 to  $4050 \text{ \AA}$  and covered a length of 12 cm of the spectrum. The spectra would be taken on Kodak film 103 0 with the same automatic camera that had been used in Gotland in 1954; now, however, by means of a specially built motor, it was possible to vary the times of exposure, during the course of the eclipse, from  $0^{\text{s}}.1$  to  $3^{\text{s}}$ . Around the middle of totality, the times of exposure were even longer, and then the electric switches were worked by hand. The moments of opening and shutting the focal plane shutter were recorded on a tape by a chronograph. All new parts of the mechanical equipment were made by the technicians Mr. N. VAN STRATEN and Mr. J. VAN DEN BROEK of the Utrecht Astronomical Observatory.

The sun's image on the slit was formed by a photographic objective of Steinheil with a focal distance of 350 cm at  $4000 \text{ \AA}$  and 25 cm diameter, on which the light was thrown about horizontally by the coelostat mirror of 30 cm diameter. About 30 cm before the sun's image the beam was reflected vertically downward by means of a small flat mirror. The image with a diameter of 32 mm fell on the horizontal plane of the slit. The light penetrating through the slit was reflected horizontally, by a  $45^\circ$  prism, placed just outside the axis of the spectrograph-tube; it reached the spectrograph lens and behind it the prisms and the flat mirror, placed in autocollimation. The returning beam pictured the spectrum on the film. In order to prevent vignetting in the spectrograph for all parts of the slit, the objective had to be diaphragmed up to a diameter of 7 cm. It was intended to use the full aperture around the middle of the totality, so as to obtain a brighter picture of the corona on the slit-plate for a correct reorientation of the slit.

It was hoped that by means of this apparatus the spectra of the extreme limb of the sun and of the chromosphere could be taken in quick succession. From the spectra of the low chromosphere, obtained with the narrow part of the slit, the profiles of the strong lines could be deduced. The spectra taken with the broad parts of the slit would yield the integrated intensities of the emission lines. As only a small part of the corona would enter the slit, the emission lines of the chromosphere would show up to a great height against a very weak corona-continuum.

<sup>1)</sup> This Zeiss lens, diameter 15 cm,  $f = 296 \text{ cm}$  at  $\lambda = 3980 \text{ \AA}$ , was bought in 1925 by the Netherlands Eclipse Commission for the observations of the limb-darkening of the sun on the Gornegrat.

It was planned to take the spectra until about 2 minutes after the 2nd contact, while 20 seconds before we would start to take pictures of the spectrum of the extreme limb of the sun, followed by an analogous series at the 3rd contact. Another advantage of the slit thus constructed would be that the position of the emission lines, taken with the narrow slit, with respect to those taken with the broader parts, would allow to determine from what part of the chromosphere the recorded line profiles originate.

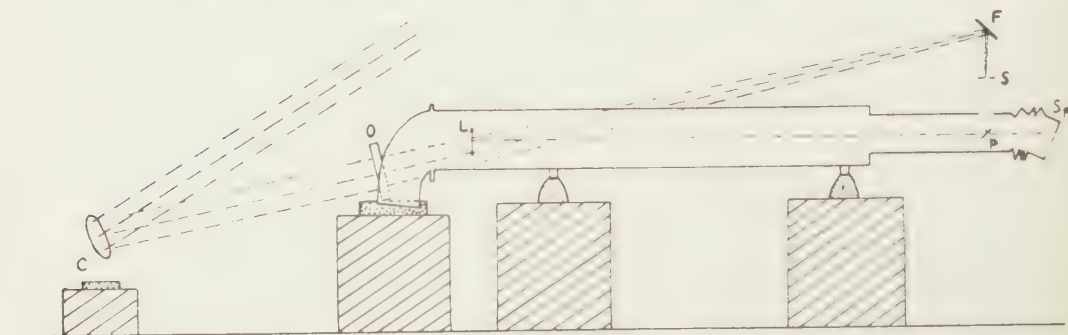


Fig. 2. The position of the optical instruments. *C* coelostat with 25 cm-mirror; *O* photographic objective,  $f = 350$  cm; *F* flat mirror; *S* slit (see fig. 1); *p* totally reflecting prism, a little outside the axis of the spectrograph-tube; *L* simple lens as a collimator- and cameralens,  $f = 296$  cm; the two prisms and the flat mirror in the curved part of the spectrograph have not been drawn; *Sp* spectrum and mechanism of the jumping film. The vertical plane through the beam reflected by the coelostat mirror forms an angle of  $17^\circ$  with the vertical plane through the axis of the spectrograph.

### *The preparations*

The Netherlands Eclipse Commission made an application, on September 30th, 1954, to the Netherlands Organization for Pure Scientific Research (Z.W.O.) for obtaining the necessary subsidy, and presented details as to the forthcoming expedition. This subsidy was granted in December. The construction of the new instrumental implements had already been started, for which the prime cost was met by the annual grant from the Academy, assigned in view of provisions in the periods between the expeditions. The three mirrors required by the expedition were aluminized in the Technical College at Delft by Professor A. C. S. VAN HEEL.

After a medical examination, Mr. N. VAN STRATEN, chief instrument maker at the Astronomical Observatory in Utrecht, was appointed as second member of the expedition in January 1955.

Various authorities provided valuable information, which facilitated the choice of a place of observation. Professor REDMAN sent a general report on conditions in Ceylon and practical matters, prepared by J. E. JACKSON. Information as to weather-conditions and accomodation was supplied by Professor DASSANAYAKE of the Metereological Department



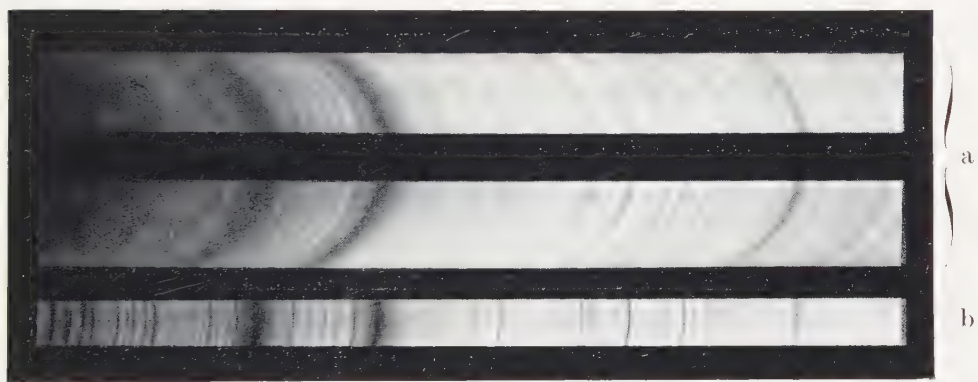


Fig. 3. The spectral area selected, taken at full sunlight. *a*) with the broad parts of the slit (strongly weakened with filter); *b*) with the narrow part of the slit.



in Colombo. Valuable assistance was also rendered by Mr. DESMIT and the staff of the Netherlands Legation in Colombo. Especially during the expedition the assistance of Mr. KORTHALS ALTES and other members of the Legation, who gave advice as to local conditions, was of great value.

The steam navigation companies "Nederland" in Amsterdam and the "Rotterdamse Lloyd" in Rotterdam saw to the sending of the instruments to and from Colombo. The Eclipse Commission are very grateful to these companies for the transportation of the instruments, free of charge.

The members of the expedition arrived at Ceylon by K.L.M. on May 11th and there found the chests with the instruments well stored. These had to be sent on to the area of observation, for which no definite choice had as yet been made. As a consequence of the advice and with the cooperation of Mr. SCHOLTEN of the Royal Shell at the Hague, the Shell in Colombo was contacted. There Mr. BERGNE appeared to be able to supply us with a lorry and some employees, to transport the instruments to the regions desired and take them again to Colombo after the eclipse.

The next important step was to choose the place of observation. There was some uncertainty as regards conditions in Habanera, where a few months before rooms had already been reserved in the Resthouse through the intermediacy of the Meteorological Department and of the Netherlands Legation in Colombo. Fortunately, Professor MAILVAGANAM, of the Physical Department of the University of Ceylon, could then be contacted, who himself was a member of the combined British-Potsdam-Ceylon eclipse expedition. His preparations on the Hingurakgoda aerodrome and its surroundings, where this expedition had taken up its abode, made it possible for him to introduce us there. On June 15th the two members of the expedition left Colombo and after visiting some grounds that might be suitable for the observation of the eclipse, they arrived at the Hingurakgoda aerodrome. Here Professor A. VON KLÜBER, the leader of the British-Potsdam expedition, after consultation with Professor MAILVAGANAM, could put a circuit bungalow of the agricultural station at the disposal of the Netherlands expedition<sup>1)</sup>. The circuit bungalow lay three miles west of the aerodrome and was very suitable for the purpose, especially because it appeared possible to set up our instruments in the immediate neighbourhood. It was a genuine pleasure to work on these grounds of the agricultural station, where all possible assistance was rendered by the manager, Mr. NANAYAKARA. Especially Mr. WEERASINGHE, our faultless guide and interpreter in these (Sinhalese) surroundings, gave help of inestimable value. During the stay in Hingurakgoda nearly all the members of the other expeditions visited our camp, while we also visited theirs, which again and again led to fruitful exchanges of views.

---

<sup>1)</sup> The Eclipse Commission here again expresses its gratitude to the Director of Agriculture at Peradenia for putting these housing-facilities and opportunities for working at its disposal.

Apart from this, seldom a day passed without a group of Sinhalese society paying a visit to our camp.

When the instruments arrived on May 17th, their places had been established and the two tents had been set up; one as a place of storage, the other to protect the spectrograph and its accessories. The coelostat, placed outside the latter tent, was covered with canvas at night. The orientation of the coelostat and the spectrograph took place by means of a theodolite, lent to the Eclipse Commission by Professor A. KRUIDHOF of Wageningen. The instruments were mounted on tables of L-shaped aluminum, constructed beforehand, and covered by multiplex plates, of which the legs were driven into the ground.

All the activities made good progress and on May 31st the first pictures for the focussing could be taken. In order to get films that could be easily handled, each series consisted of about 6 to 7 pictures on a strip of a little less than 1 m, which was developed in plastic tins. It appeared that extra-hardening was superfluous, even at temperatures of 30° Centigrade, after developing with a borax developer and fixing in Kodak acid fixing salt as a means of hardening.

Extensive series of comparison spectra and standardizing spectra of the solar disc's centre were taken, with and without a step-weakening on the slit and with various widths of the slit. These spectra were taken on previous days, preferably at the time of the eclipse, i.e. about 8.15 a.m. The correct times of the second and the third contact would, in our place of observation situated at  $80^{\circ} 57' 07''$  Eastern longitude,  $8^{\circ} 03' 08''$  Northern latitude correspond with  $8^h 12^m 11^s.6$  and  $8^h 16^m 52^s.3$  Ceylon time ( $5^h 30^m$  ahead of Greenwich time). Time-signals of the B.B.C. were received via the Ceylon wireless by means of a wireless apparatus, fitted out with batteries, which had been kindly lent to us by the Netherlands Posts, Telegraphs and Telephones.

During the last ten days the rather intricate programme of observation was rehearsed, experiments being made with various widths of the slit and various times of exposure. During this practice the adjustments during the middle of the totality were carried out within 40 seconds, so that exposures could be made until 120 seconds after the second and from 120 seconds before the third contact. Three days before the eclipse we decided not to rely on the automatic control of the jumping film, but to bring about the contact by hand. After some experience it appeared from what was recorded on the chronograph-tape that even the time of exposure of  $0^s.1$  could be reproduced easily. Deviations, however, would be recorded and be taken into account afterwards. When two days before the eclipse our batteries were exhausted, they could be loaded anew through the kind help of Dr. DAS of the Kodaikanal Observatory, in the latter's camp of observation, after all other efforts to do so had failed.

During the weeks of preparation the sky was overcast at the time of



the eclipse on more than half of the days and the situation grew worse as the day of the eclipse approached. In the last week only two days were favourable for our observations. On June 18th a complete series of comparison pictures could be recorded with a clear sky between 8.15 and 8.30 on a part of the same film which had to be used for the eclipse.

As the sky became overcast, the exposures on the second film could only be taken at 11.30. Part of these pictures were developed, for checking purposes. The next day another series of exposures for standardizing, on each film, could only be taken at 10.30. We could be completely confident as to the quality of these pictures and the way our apparatus worked.

### *The day of the eclipse*

At 5<sup>h</sup>.30 two policemen took up their stand before our camp, a precautionary measure against the possibility of a troublesome display of interest, for which we are very much indebted to the police-authorities of Hinrakgoda.

At 7 o'clock we were still rather hopeful as to the condition of the sky and between 7 and 8 we could now and then observe the sun, which was partly covered by the moon, so that the instruments could be focussed. By 8 o'clock, however, the cloud-layer became so dense that all hope had to be abandoned. The second contact could not be observed, but nevertheless 20 seconds before the calculated time of the second contact our chronograph and the film transportation were put into operation, with a considerably longer time of exposure than was on the programme for a clear sky. At about the moment of middle totality a dim inner corona could be observed through the clouds. The situation was hopeless, however; the dark-grey cloud-layer extended across the greater part of the sky, while along part of the horizon orange-coloured smudges were visible.

After the moment of the third contact the shadow, which was visible as a dark area on the cloud-layer, was seen to disappear in north-easterly direction. We went on with the pictures until six minutes after the third contact. To change the films during the middle of the totality had been considered superfluous, as the number of pictures, because of the longer times of exposure, was relatively small. It was not to be expected, however, that any valuable record of this eclipse had been photographed on our film. Soon afterwards we heard that none of the scientific eclipse-expeditions had had any success with optical observations.

### *After the eclipse*

On June 24th the Dutch observers, after packing their instruments, left Hingurakgoda. The next day they were present in Colombo at the reunion of the eclipse observers, organised by the "Ceylon Association

for the Advancement of Science" at the University of Ceylon, where experiences were communicated to a large audience.

On June 28th Mr. VAN STRATEN left Ceylon and Dr. HOUTGAST did so on June 29th. After arrival in Holland the first eclipse film was developed and appeared to contain no more than the calibration spectra and some solar spectra after the third contact.

#### *Acknowledgements*

The Eclipse Commission are very much indebted to the Netherlands Organization for Pure Scientific Research (Z.W.O.), which made the money for this expedition available.

They also express their gratitude to all authorities and persons, some of whom have already been mentioned in this report, who in any way helped this expedition. They especially want to call to mind the help given by Professor A. W. MAILVAGANAM and his assistants in material matters and in matters of organization.

Finally, the author expresses his thanks to Professor and Mrs. H. von KLÜBER for the many encouraging talks and for the pleasant and valuable contact, which have been of genuine importance for the expedition.

*Sterrewacht "Sonnenborgh" der  
Rijksuniversiteit te Utrecht.*

# ELECTROCHEMICAL BEHAVIOUR OF ION-EXCHANGING SUBSTANCES

## XII. ROOT POTENTIALS IN ACID POTASSIUM CHLORIDE SOLUTIONS

BY

D. MACGILLAVRY AND H. J. C. TENDELOO

(Communicated by Prof. C. H. MACGILLAVRY at the meeting of April 28, 1956)

### Summary

Potentials of Lucerne clover were measured in KCl-HCl solutions. Both salt and acid concentration were varied. An apparent isoionic point was found experimentally at a pH close to 3.0. A significant difference between root potentials was found for seedlings grown in nutrient solution and those grown in distilled water. Estimates obtained for the buffer capacity of the non-permeating root material were of the order  $0.3$  to  $1.0 \times 10^{-2}$  M.

### Introduction

The investigation of root potentials of Lucerne clover, *Medicago Sativa*, in electrolyte solutions has been extended <sup>1</sup>).

Measurements have been taken in KCl-HCl solutions. It was explained in previous publications <sup>2</sup>) that the observed trends of potentials in KCl solutions might be expected for Donnan membrane potentials of systems of the following type.

DIAGRAM I



<sup>1</sup>) Earlier potential measurements with Lucerne clover are described in communications VIII and IX of this series.

H. J. C. TENDELOO and D. MACGILLAVRY, Proc. Kon. Ned. Akad. v. Wetenschappen 57, 509 (1954) VIII;

D. MACGILLAVRY and H. J. C. TENDELOO, Proc. Kon. Ned. Akad. v. Wetenschappen 57, 513 (1954) IX.

<sup>2</sup>) H. J. C. TENDELOO, G. J. VERVELDE and A. J. ZWART VOORSPUY, Rec. trav. chim. 63, 97 (1944) I; 65, 539 (1946) II; Versl. Ned. Akad. v. Wetenschappen 53, 169 (1944) III.

W. H. VAN DER MOLEN and H. J. C. TENDELOO, Proc. Konink. Ned. Akad. v. Wetenschappen 50, 763 (1947) IV.

G. J. VERVELDE, Proc. Konink. Ned. Akad. v. Wetenschappen 51, 308 (1948) V.

G. J. VERVELDE and H. J. C. TENDELOO, Rec. trav. chim. 72, 62 (1953) VI.

D. MACGILLAVRY and H. J. C. TENDELOO, Rec. trav. chim. 73, 15 (1954) VII.

The anions  $A^-$  and cations  $B^+$ , the non-permeating ions, are supposed to derive from weakly ionizing substances.

In publication VI by VERVELDE and TENDELOO the theory was developed of changes of potential with composition of solution  $S_B$ . Besides the influence of KCl concentration at constant pH also the influence of varying pH at constant KCl concentration was discussed. It was explained that at the isoionic point of the non-permeating material the membrane potential will be zero and will not depend on the  $K^+$  ion concentration.

In publication IX on ion-exchanging substances, several series of measurements of Lucerne clover in KCl solutions were described and discussed. The pH just outside the root wall was not measured. It may be presumed that it was near 5 on account of the ordinary content of  $CO_2$  and of an additional small content of plant acids formed in the roots.

#### *Measurements in KCl-HCl Solutions*

As suggested by VERVELDE and TENDELOO it was decided to measure root potentials of Lucerne clover at constant KCl concentration while varying the pH by adding HCl. One series was measured while keeping the KCl concentration constant at  $10^{-4}$  M; the other series of measurements was done at the constant KCl concentration of  $10^{-2}$  M.

At these two concentrations potentials were measured at pH = 5, 4, and 3. If the actual behaviour of potentials would have a fair resemblance to the pattern of potentials for our model, the two plots of potential vs. pH at constant KCl concentration should intersect at an apparent isoionic point for the root material.

The electric chain and experimental procedure were as described in communication IX<sup>3)</sup>.

The measured potentials are listed in Table I.

#### *Variance Analysis of Data*

It is seen that the behaviour of the root potentials with varying pH in  $10^{-4}$  M KCl is strikingly different from that in  $10^{-2}$  M KCl. Thus, for each concentration an independent variance analysis was made (Table II).

The residual variance estimate 38.20 for potentials in  $10^{-4}$  M KCl is smaller than the estimate found for the sets of measurements in KCl solutions when no HCl was added (see publ. IX). Thus, to get more precise measurements it appears advantageous to stabilize the pH by adding at least a small concentration of HCl.

The estimate of residual variance of 2.95 for potentials in  $10^{-2}$  M KCl

<sup>3)</sup> For convenience of reading the Cambridge pH-electrometer the experimental cell and a standard cell were placed in series; the two cells were bucking each other. In this way a reversal of sign of the chain potential was avoided.



TABLE I  
Potentials <sup>1)</sup> of Lucerne clover in KCl-HCl Solutions

$\log c_{K^+}$	- 4			- 2		
$\log c_{H^+}$	- 5	- 4	- 3	- 5	- 4	- 3
+ <sup>2)</sup>	- 96	- 50	+ 2	- 10	- 9	- 1
+	- 85	- 48	+ 4	- 8	- 8	- 1
+	- 82	- 34	+ 8	- 4	+ 2	+ 10
+	- 75	- 39	+ 9	- 9	- 7	0
+	- 84	- 42	+ 8	+ 1	- 2	+ 5
+	- 83	- 50	+ 10	- 16	- 14	- 8
- <sup>3)</sup>	- 96	- 60	- 16	- 17	- 16	- 6
-	- 90	- 58	- 25	- 19	- 17	- 11
-	- 73	- 48	- 7	- 18	- 16	- 11
-	- 93	- 58	- 15	- 16	- 13	- 6

<sup>1)</sup> The potentials are given in mV relative to a reading of 900 mV on the Cambridge pH-electrometer. This reference point was selected for convenience as it is very close to what may be called the apparent isoionic points of the + roots and - roots as explained below.

<sup>2)</sup> Seedlings marked + were grown in nutrient solution (see VERVELDE, Diss. p. 86).

<sup>3)</sup> Seedlings marked - were grown in distilled water.

happens to be smaller than variance estimates previously found for individual measurements. This low estimate has little meaning and must be due to chance. Even if we use, however, the estimate 38.20 as a reference level also for Table IIB, it is seen that both an effect due to HCl concentration and a root effect are always indicated.

TABLE II  
A. Variance analysis of potentials in  $10^{-4}$  M KCl

Source of variation	Sum of squares	Dimension	Variance estimate
HCl concentration . .	35,011.67	2	17,505.84
Root level . . . . .	1,992.14	9	221.34
Residual . . . . .	687.66	18	38.20
Total . . . . .	37,691.47	29	

B. Variance analysis of potentials in  $10^{-2}$  M KCl

Source of variation	Sum of squares	Dimension	Variance estimate
HCl concentration . .	428.87	2	214.44
Root level . . . . .	1,148.84	9	127.65
Residual . . . . .	53.12	18	2.95
Total . . . . .	1,630.83	29	

In the usual manner the root effects were analyzed for a possible effect due to nutrient solution (Table III).

TABLE III  
Differences between Roots  
A. Potentials in  $10^{-4}$  M KCl

Source of variation	Sum of squares	Dimension	Variance estimate
Effect due to nutrient solution . . . . .	1,180.94	1	1,180.94
Differences within groups. . . . .	811.20	8	101.40
	1,992.14	9	

B. Potentials in  $10^{-2}$  M KCl

Source of variation	Sum of squares	Dimension	Variance estimate
Effect due to nutrient solution . . . . .	642.22	1	642.22
Differences within groups. . . . .	506.62	8	63.33
	1,148.84	9	

Comparison of variance estimates of Table III clearly shows that growing roots in nutrient solution or distilled water makes a difference and is a factor determining the observed differences between roots. This holds true for measurements in  $10^{-4}$  M KCl and also in  $10^{-2}$  M KCl.

It is noteworthy that, while the effect of HCl concentration strongly decreases with increasing KCl concentration, and also the variance of root level tends to decrease, the effect due to nutrient solution still is pronounced at the higher KCl concentration.

#### Regression Equations

On account of the given analysis four sets of potential averages have to be calculated. These are listed in Table IV.

TABLE IV  
Potential averages

$\log c_{K^+}$	- 4			- 2		
$\log c_{H^+}$	- 5	- 4	- 3	- 5	- 4	- 3
+ roots	- 84.2	- 43.8	+ 6.8	- 7.7	- 6.3	+ 0.8
- roots	- 88.0	- 56.0	- 15.8	- 17.5	- 15.5	- 8.5

In accordance, four regression equations have to be derived for the dependence of potential on pH. By means of orthogonal polynomials variance estimates may be found for linear and quadratic components (Table V).

TABLE V  
Analysis Concentration Effect  
A. Roots grown in nutrient solution

$\log c_{K^+}$	Component	Sum of squares	$F$
- 4	linear	24,843.00	650.34
	quadratic	106.78	2.79
- 2	linear	216.75	7.56
	quadratic	34.03	1.19

B. Roots grown in distilled water

$\log c_{K^+}$	Component	Sum of squares	$F$
- 4	linear	10,440.12	273.30
	quadratic	45.38	1.19
- 2	linear	162.00	5.65
	quadratic	16.67	0.58

Since the dimension of each component is one, the sum of squares at the same time is a variance estimate. In order to judge the possible significance of components it must be remembered that the estimate of residual variance for potentials in  $10^{-4}$  M KCl,  $s^2=38.20$ , would be a rather high estimate for potentials in  $10^{-2}$  M KCl. In case a variance analysis had been made for the data of Table I all taken together, instead of subdividing the data as was done, the estimate for residual variance would have come to 28.66. Even this estimate apparently would not be an underestimate.

For proper comparison the variance estimates for  $10^{-4}$  M KCl were divided by 38.20, and those for  $10^{-2}$  M KCl were divided by 28.66. The resulting  $F$  values so obtained are given in the last column of Table V. At the 5 % confidence level, all linear components are significant ( $F > 4.41$ ), while no quadratic component can be considered significant ( $F < 4.41$ ).

For the regression equations for potential  $y$  on  $pH=x$  we find:

for roots grown in nutrient solution

- (1)  $\log c_{K^+} = -4 \quad y = -45.50 x + 141.61;$
- (2)  $\log c_{K^+} = -2 \quad y = -4.25 x + 12.61;$

for roots grown in distilled water

- (3)  $\log c_{K^+} = -4 \quad y = -36.13 x + 91.25;$
- (4)  $\log c_{K^+} = -2 \quad y = -4.5 x + 4.17;$

The four equations and the experimental points are plotted in graph I.

### *Effective Isoionic Points*

To obtain an estimate of the pH where the root potentials for + roots,

resp. -roots, become independent of the  $K^+$  ion concentration, i.e. the apparent isoionic point, the coordinates of the point of intersection were determined for both pairs of regression equations. We find

for the +roots  $(x_+; y_+) = (+3.1; -0.7)$ , and

for the -roots  $(x_-; y_-) = (+2.8; -8.2)$ .

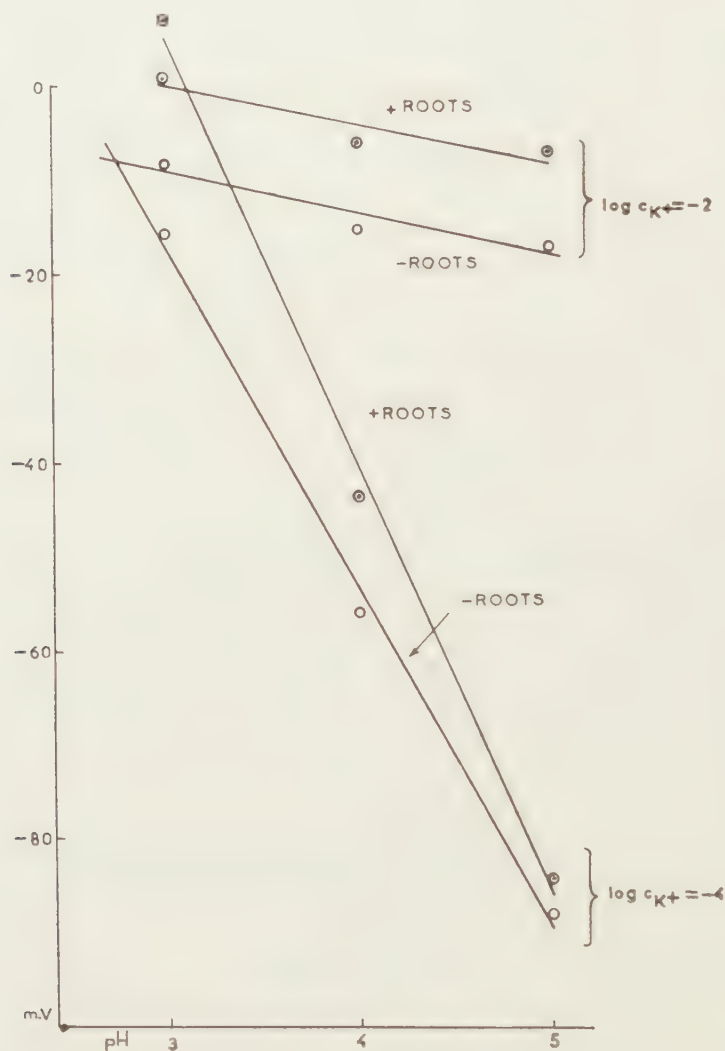


Fig. 1

Although the potential vs. pH plots all appear to be distinct, the pH-values of the two isoionic points need not be significantly different. To settle this, the confidence intervals of the two abscissae have to be determined.

For  $x_+$  the confidence limits are 3.0 and  $3.2_5$ , and

For  $x_-$  the confidence limits are  $2.4_5$  and 3.0.



The two intervals do not overlap but they are adjacent to each other. It might be argued that the null hypothesis for this case should be rejected. It appears prudent to await further results before drawing a definite conclusion in this respect.

It must be added that further accumulation of data might well show that an apparent isoionic point as found by us is not an entirely fixed point. It could be, for instance, that the plot  $\log c_{K^+} = -3$  would not go through this experimental point, but intersect the first two plots in neighbouring points. This could be formulated in this way that the pH of an apparent isoionic point would shift with the concentration of the  $K^+$  ions. Such a dependence would be analogous to the drifting with increasing electrolyte concentration as was observed by KRUYT and TENDELOO <sup>4)</sup> for the electrophoretic effect of colloidal systems.

In case the pattern of root potentials is actually similar to that of potentials for a one membrane system of the type shown in Diagram I, the term isoionic point would have a definite meaning. For a seedling, the potential difference measured, the root potential, need not be zero at the point of intersection of graph I, since it would include also other membrane potentials and diffusion potentials. Still, such a point would be a natural zero point of the potential scale. It would seem fair to assume that the other contributions to the total potential difference of the seedling remain constant or at least that any variations would be negligible.

#### *Effective Buffer Capacity of Root Material*

On the assumption that the membrane system represented in Diagram I is a reliable model, the Vervelde-Tendeloo equation would be applicable. We would have

$$(5) \quad K_1 \log c_H + K_2 - K_1 \log v = (c_K + c_H) \left( \frac{1}{v} - v \right).$$

For numerical calculations, it is convenient to make the following substitutions.

$$v = e^z, \quad K_1 = -L, \quad \text{and} \quad K_2 = -L\alpha.$$

Hence,

$$(6) \quad E - E_0 = \frac{RT}{F} \ln v = \frac{RT}{F} z = 25 z.$$

Equation (5) takes the form

$$(7a) \quad LpH - L\alpha + 0.43 Lz = -(c_K + c_H) (e^z - e^{-z}).$$

Hence,

$$(7b) \quad L = \frac{-2(c_K + c_H) \sinh z}{pH - \alpha + 0.43 z} = \frac{A(z)}{B(z)}.$$

---

<sup>4)</sup> H. J. C. TENDELOO, "Lading en Hydratie" (H. J. Paris, Amsterdam, 1926). H. R. KRUYT and H. J. C. TENDELOO, Verslag Kon. Akad. v. Wetenschappen, Amsterdam 34, 408-16 (1925); J. Phys. Chem. 29, 1303-11 (1925).

It should be noted that at the isoionic point  $E - E_0 = 0$  for the effective membrane; thus  $z = 0$  in (7a) and  $v = 1$  in (5). It is easily seen that in relation (5) all terms containing  $v$  cancel out or vanish at this point, and in (7a) all terms with  $z$ . Equation (7a) then reduces to

$$(8) \quad LpH - L\alpha = 0.$$

This shows that  $\alpha$  is the pH of the apparent isoionic point.  $L$  is the buffer capacity<sup>5)</sup> of the non-permeating material.

In the present investigation of potentials in KCl-HCl solutions  $\alpha$  is determined experimentally as explained. Although it is uncertain whether the apparent isoionic points of the +roots and -roots are really different, we shall use for the numerical calculations  $\alpha = 3.1_4$  for the +roots and  $\alpha = 2.7_8$  for the -roots. The reference potential for the +roots is  $-0.7$  mV and for the -roots the reference level is  $-8.2$  mV. On this new basis experimental points and regression equations are plotted again in Fig. II. The  $z$  values then are calculated from the measured potentials by (6). Hence,  $L$  is the only unknown. For each experimental point ( $c_K$ ,  $c_H$ ,  $E$ ) a value for  $L$  can be calculated. Results of the numerical calculations are tabulated in Table VI.

TABLE VI  
Estimates for the effective Buffer Capacity  $L$   
A. Roots grown in nutrient solution

$\log c_{K^+}$	$\log c_{H^+}$	$E - E_0$ in mV	$A(z)$	$B(z) \times 10^3$	$L \times 10^3$
-4	-5	-83.5	+0.39	+3.10	8.0
-4	-4	-43.1	+0.11	+1.08	9.8
-4	-3	+7.5	-0.01	-0.67	(67.0)
-2	-5	-7.0	+1.74	+5.69	3.3
-2	-4	-5.6	+0.76	+4.57	6.0
-2	-3	+1.5	-0.12	-1.14	(9.5)

B. Roots grown in distilled water

$\log c_{K^+}$	$\log c_{H^+}$	$E - E_0$ in mV	$A(z)$	$B(z) \times 10^3$	$L \times 10^3$
-4	-5	-79.8	+0.83	+2.67	3.2
-4	-4	-47.8	+0.39	+1.32	3.4
-4	-3	-7.6	+0.09	+0.68	(7.5)
-2	-5	-9.3	+2.06	+7.63	3.7
-2	-4	-7.3	+1.09	+6.02	5.5
-2	-3	-0.3	+0.21	+0.26	(1.2)

<sup>5)</sup> An increase of base  $dB$  added to the internal solution equals the increase of free anions  $dA$  of the assumed uniform mixture of weak acids. This concentration is given by  $A = LpH - L\alpha + 0.43Lz$ , where pH refers to the bathing solution, or  $LpH^* - L\alpha$ , where  $pH^*$  refers to the internal solution of our Donnan system. Buffer capacity is defined as  $dB/dpH$ ; cf. D. A. MACINNES, "The Principles of Electrochemistry", p. 276, (Reinhold Publishing Corporation, New York, 1939); D. D. VAN SLIJKE, J. Biol. Chem. 52, 525 (1922).

It is seen that for  $L$  an order of magnitude of  $5 \times 10^{-3}$  M is indicated. Values range from  $0.3$  to  $1.0 \times 10^{-2}$  M. Estimates between parentheses are very uncertain; these points are too close to the isoionic point where both  $A(z)$  and  $B(z)$  vanish.

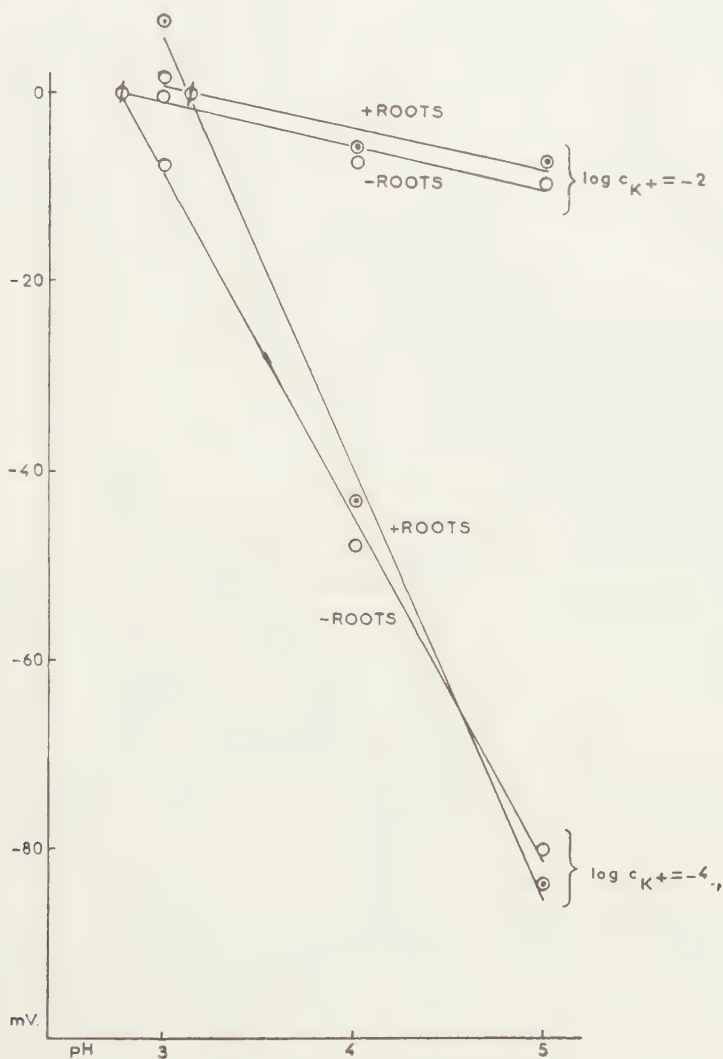


Fig. 2

The  $L$  values so calculated seem to show a certain pattern. Whether this has any meaning is hard to say at present, as a confidence interval for  $L$  would be wide. An increased  $L$  value at  $\text{pH} = 3$  might indicate a higher concentration of non-diffusing plant acids, or of acids diffusing at a much reduced rate, with titration constants near  $10^{-3}$ .

It must be added that it was assumed that  $L$  would be constant. The  $L$  values for  $\text{pH} 4$  and  $5$  do fall fairly close together. Whether this indicates

a really constant buffer capacity  $L$  in this pH range, is hard to decide at present on account of the wide confidence interval for  $L$ .

For the time being, we might formulate a conclusion as follows. The central points of the plots for pH=4 would give the better estimates for  $L$ , especially in the present case where  $L$  values calculated for pH=3 are not reliable for the reason mentioned above. Thus, we might average the  $L$  values for pH=4, ignoring any possible difference between + and -roots. The four values are 9.8, 6.0, 3.4 and  $5.5 \times 10^{-3}$  M; these give the average value  $6.2 \times 10^{-3}$  M. The range of the four values happens to be narrow, probably much narrower than the confidence interval. Thus, all we may conclude to at present from our measurements with Lucerne clover is an order of magnitude for  $L$ .

### *Discussion*

These findings appear to be in qualitative agreement with results obtained by HOPE and STEVENS<sup>6)</sup> by an independent method. They measured the amount of KCl freely diffusing in or out broad bean roots when the KCl concentration of the outside solution is increased or decreased. They could account for their results by assuming that KCl could penetrate an appreciable part of the total root volume.

Since non-permeating material is contained in these cells, Donnan equilibria, it seems, should be approached when momentary diffusion has subsided. After this, ions of KCl are taken up according to metabolic needs at steady but much smaller individual rates. These steady fluxes would occur primarily at the root apex.

Hope derived estimates for the concentration of non-permeating ions by making use of the Donnan theory. It was assumed that the concentration of non-permeating ions was constant. In this way it was found that for broad bean roots this concentration is  $6 \times 10^{-3}$  M at the root tip, first 5 mm from the root apex, and runs to  $4 \times 10^{-2}$  M for the third cm from the root apex.

In our experiments the concentration of non-permeating ions is not fixed, but will have to vary with pH as explained above and in previous communications. The concentration of ionizable groups, however, should be constant and would be the upper limit attainable for the concentration of ionized groups. Still, regardless of the difference of plant species and of the manner of obtaining estimates, their estimates and ours would likely be of the same order of magnitude, as was found.

### *Conclusions*

Root potentials of Lucerne clover in KCl-HCl solutions of constant KCl concentration were found to vary linearly with pH in the range 3-5.

---

<sup>6)</sup> A. B. HOPE and P. G. STEVENS, Australian J. Sci. Research B 5, 335 (1952); A. B. HOPE, *ibid.* B 6, 396 (1953).



This was verified for two KCl concentrations,  $10^{-2}$  M and  $10^{-4}$  M resp.

The two plots intersect at about  $\text{pH}=3$ . This point may be interpreted as an effective isoionic point of the non-permeating root material.

This was found for seedlings grown in nutrient solution and also for seedlings grown in distilled water, +roots and -roots resp. The potentials of these two classes of roots appear to be different. The isoionic point of the +roots had a  $\text{pH}=3.1$ , that of the -roots a  $\text{pH}=2.8$ . It is not certain whether also the two isoionic points should be considered distinctly different.

The root potentials of Lucerne clover as measured by us conform to a behaviour of potentials to be expected for a Donnan system of the type as represented in Diagram I. Estimates for the buffer capacity of the root material fall in the range 0.3 to  $1.0 \times 10^{-2}$  M.

#### *Acknowledgements*

We wish to express our appreciation to Prof. Dr. N. H. KUIPER, Ir. L. C. A. CORSTEN and Ir. S. H. JUSTESEN of the Department of Mathematics for assistance and advice concerning the variance analysis.

# ON THE FLEXURAL RIGIDITY OF A BEAM, WEAKENED BY TRANSVERSE SAW CUTS. I

BY

W. T. KOITER

(Communicated by Prof. C. B. BIEZENO at the meeting of April 28, 1956)

## 1. Introduction

The rotors of two-pole turbogenerators have a reduced flexural rigidity with respect to one of the principal axes, due to the longitudinal slots for the electric windings. This may introduce a secondary critical speed at half the normal critical speed. It has been suggested [ref. 1] to overcome this difficulty by restoring equality of the flexural rigidities by means of transverse saw cuts in the pole faces (see fig. 1). This solution does not

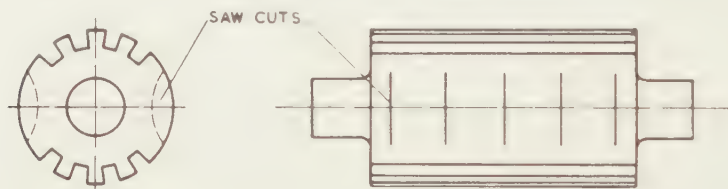


Fig. 1. Two-pole turbogenerator with saw cuts in pole faces.

interfere with the magnetic circuit, and the stress concentration at the root of the cuts presents no major problem because the bending stresses are very low. An experimental investigation on the effect of these saw cuts on the flexural rigidity is now being made in the Laboratory of Applied Mechanics under the direction of Prof. KOCH.

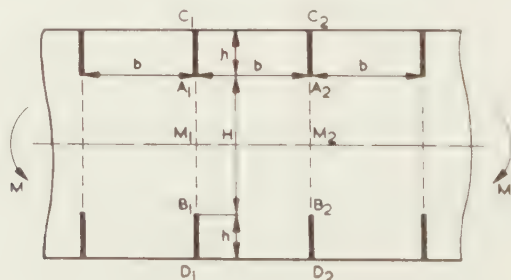


Fig. 2. Bending of a strip with saw cuts.

A theoretical approach to the problem may be obtained by considering the corresponding two-dimensional bending problem in generalized plane stress of an infinite strip, weakened by an infinite number of equal and equally-spaced saw cuts perpendicular to the boundaries (fig. 2). The

stress distribution and the stiffness of the weakened strip will depend on the two parameters  $b/H$ , the ratio of pitch  $b$  to remaining height  $H$ , and  $b/h$ , the ratio of pitch  $b$  to depth  $h$  of the saw cuts. We introduce the concept of an "equivalent height"  $h_e$  of the notch depth  $h$ , defined by the height  $H + 2h_e$  of an unnotched strip with the same flexural rigidity as the notched strip of height  $H + 2h$ . The two-dimensional problem is solved when the ratio of equivalent height  $h_e$  to notch depth  $h$  has been determined as a function of the two parameters  $b/H$  and  $b/h$ . Obviously we have  $0 < h_e/h < 1$ . The basic result of our analysis is formula (9), where the nondimensional coefficients  $\alpha_{11}$ ,  $\alpha_{12}$  and  $\alpha_{22}$  only depend on the parameter  $\beta = b/h$  if the parameter  $b/H$  is sufficiently small, say  $b/H < \infty$ . These coefficients are given in figs. 9 to 11 (para. 5).

An approximate solution to our rotor problem is now obtained by calculating the flexural rigidity of an *equivalent or reduced cross-section* of the rotor, using the appropriate two-dimensional value  $h_e$  for each vertical strip of the cross-section (fig. 3). This solution is approximate in

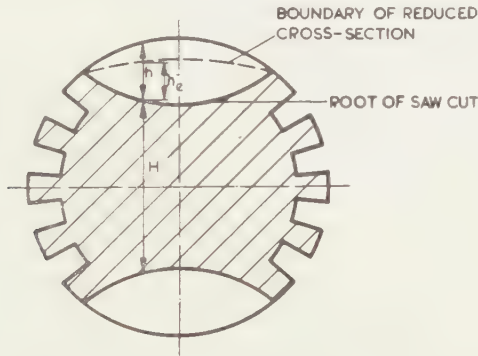


Fig. 3. Reduced cross-section of rotor.

character because we have assumed a state of generalized plane stress in each vertical "slice" cut out of the beam in fig. 3. We may observe that the actual flexural rigidity of the rotor cross-section is larger than our approximation because we have neglected the connection between the vertical "slices".

## 2. The two-dimensional problem

We observe that in the two-dimensional problem (fig. 2) the lines  $A_1B_1$ ,  $A_2B_2$  etc. will remain straight and that no shear stresses will be transmitted across these lines. Denoting the average curvature of the strip by  $\alpha_0$ , the angle between the lines  $A_1B_1$  and  $A_2B_2$  will be  $\alpha_0 b$ ; the line  $M_1M_2$  is the neutral axis.

We now consider the rectangle  $C_1C_2D_2D_1$  in fig. 2, loaded by (as yet unknown) normal stresses  $p_y$  along  $A_1B_1$  and  $A_2B_2$ , antisymmetrical with respect to the neutral axis  $M_1M_2$  (fig. 4). The boundaries  $A_1C_1C_2A_2$  and

$B_1D_1D_2B_2$  are unloaded. The loads  $p_y$  are to be determined from the condition that the edges  $A_1B_1$  and  $A_2B_2$  remain straight and make an angle  $\kappa_0 b$ .

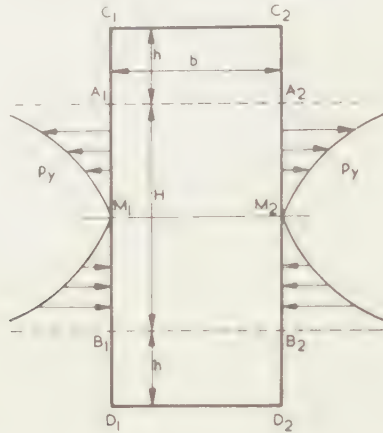


Fig. 4. The rectangle  $C_1C_2D_2D_1$  of fig. 2.

If the strip were cut along  $A_1A_2$  and  $B_1B_2$ , the solution would be very simple: the loads  $p_y$  would be proportional to the distance from the neutral axis, and the energy of flexure of the rectangle per unit thickness, i.e. the flexural energy in the strip of fig. 2 per unit thickness over a length  $b$  would be

$$(1) \quad A_0 = \frac{1}{24} EH^3 b \kappa_0^2.$$

The fact that the parts  $A_1A_2C_2C_1$  and  $B_1B_2D_2D_1$  are connected to  $A_1A_2B_2B_1$  causes a variation of the distribution of loads  $p_y$  from a linear distribution and an increase in strain energy. Our problem is to find this increase in strain energy.

An important simplification of our two-dimensional problem is achieved if the ratio  $b/H$  is sufficiently small. A self-equilibrating system of stresses acting along  $A_1A_2$  then has a negligible effect on the stresses in the neighbourhood of  $B_1B_2$  and vice versa (SAINT-VÉNANT'S principle). Indeed it is well-known from similar problems that the interaction of the stresses along  $A_1A_2$  and  $B_1B_2$  is already negligible for  $b/H < \infty 1$ . Henceforward we shall assume that our dimensions satisfy this inequality.

We may now obtain the increase in strain energy, due to the connection of the part  $A_1A_2C_2C_1$  to  $A_1A_2B_2B_1$ , by considering the problem of a *half-plane*, weakened by an infinite number of equal and equally-spaced saw cuts, and loaded in tension parallel to the boundary (fig. 5). The stress approaches to  $E(\epsilon_0 - \kappa_0 x)$  at infinity, where  $\epsilon_0 = \frac{1}{2} \kappa_0 H$ .

Likewise the problem for the rectangle of fig. 4 may now be replaced by the problem for the semi-infinite strip  $C_1C_2F_2F_1$  (fig. 6). The loads  $p_y$  are to be determined from the requirement that the displacements  $v$  in



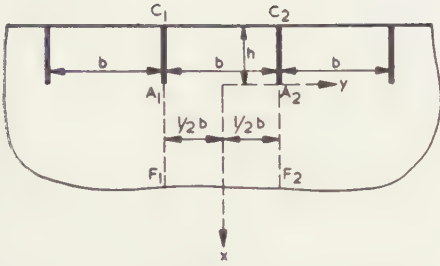


Fig. 5. Half-plane with saw cuts.

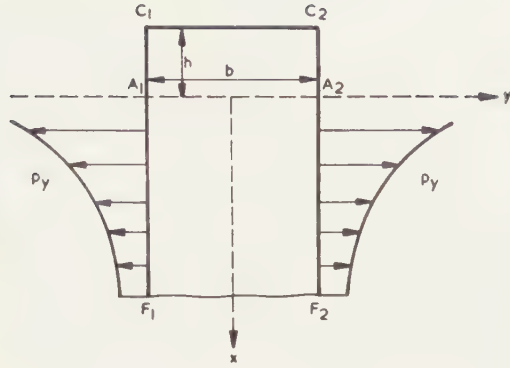


Fig. 6. Problem for semi-infinite strip.

the direction of the  $y$ -axis satisfy along the boundaries  $y = \pm \frac{1}{2}b$ ,  $x > 0$

$$(2) \quad (v)_{y=\frac{1}{2}b} - (v)_{y=-\frac{1}{2}b} = (\varepsilon_0 - \kappa_0 x) b,$$

where again  $\varepsilon_0 = \frac{1}{2}\kappa_0 H$ .

The loads  $p_y$  are obviously linear functions of  $\varepsilon_0$  and  $\kappa_0$ . If the strip were cut along  $A_1 A_2$  these loads would be given by

$$(3) \quad p_{y0} = E(\varepsilon_0 - \kappa_0 x),$$

where  $E$  is YOUNG'S modulus. The increase in strain energy per unit thickness of the strip, due to the connection of the part  $A_1 A_2 C_2 C_1$  to the semi-infinite strip  $A_1 A_2 F_2 F_1$  is given by

$$(4) \quad \begin{cases} \Delta A = \frac{1}{2} b \int_0^\infty (p_y - p_{y0}) (\varepsilon_0 - \kappa_0 x) dx = \\ = \frac{1}{2} b \int_0^\infty [p_y - E(\varepsilon_0 - \kappa_0 x)] (\varepsilon_0 - \kappa_0 x) dx. \end{cases}$$

When  $p_y$  has been obtained as a function of  $x$ ,  $\varepsilon_0$  and  $\kappa_0$ , the integral in (4) may be evaluated and the result written in the form

$$(5) \quad \Delta A = \frac{1}{2} E b h (\alpha_{11} \varepsilon_0^2 + \alpha_{12} \varepsilon_0 \kappa_0 h + \frac{1}{3} \alpha_{22} \kappa_0^2 h^2),$$

with nondimensional coefficients  $\alpha_{11}$ ,  $\alpha_{12}$  and  $\alpha_{22}$ . Remembering that  $\varepsilon_0 = \frac{1}{2}\kappa_0 H$  we have

$$(6) \quad \Delta A = \frac{1}{2} E b H^3 \left( \frac{1}{4} \alpha_{11} \frac{h}{H} + \frac{1}{2} \alpha_{12} \frac{h^2}{H^2} + \frac{1}{3} \alpha_{22} \frac{h^3}{H^3} \right) \kappa_0^2.$$

Bearing in mind that the increase in strain energy (6) occurs at both ends of the rectangle  $A_1 A_2 B_2 B_1$  in fig. 4, we obtain for the energy per unit thickness over a length  $b$  in the strip of fig. 2

$$(7) \quad A = A_0 + 2\Delta A,$$

where  $A_0$  is given by (1) and  $\Delta A$  by (6). Equating this expression to the

corresponding energy in an unnotched strip of height  $H + 2h_e$

$$(8) \quad A = \frac{1}{24} Eb (H + 2h_e)^3 \kappa_0^2,$$

we obtain the equivalent height  $h_e$  of the notch depth in the form

$$(9) \quad h_e = \frac{1}{2} H \left[ \left( 1 + 6\alpha_{11} \frac{h}{H} + 12\alpha_{12} \frac{h^2}{H^2} + 8\alpha_{22} \frac{h^3}{H^3} \right)^{1/3} - 1 \right].$$

A complete solution of the two-dimensional problem (on the assumption  $b/H < \infty$ ) is achieved as soon as the coefficients  $\alpha_{11}$ ,  $\alpha_{12}$  and  $\alpha_{22}$  have been determined as functions of the single parameter  $b/h = \beta$ , the ratio of pitch to depth of the saw cuts. Although such a complete solution is not yet available, the extreme cases of *small* pitch to depth ratio ( $\beta \ll 1$ ) and of *large* pitch to depth ratio ( $\beta \gg 1$ ) are solved comparatively easily. Moreover, on the basis of the rigorous results for these extreme cases a satisfactory approximation may be established for intermediate values of  $\beta$ . The case of small pitch to depth ratio is discussed in para. 3 and the case of large values of this ratio in para. 4. The interpolation for intermediate values of  $\beta$  is given in para. 5.

Finally it should be noted that the result (5) may also serve to calculate the "equivalent height"  $h'_e$  of the parts  $A_1A_2C_2C_1$  and  $B_1B_2D_2D_1$  (fig. 2) of the strip in *tension*. The strain energy per unit thickness of the rectangle in fig. 4 is given by

$$(10) \quad A = \frac{1}{2} EbH \epsilon_0^2 + Ebbh \alpha_{11} \epsilon_0^2,$$

whereas the corresponding energy of an unnotched strip of height  $H + 2h'_e$  amounts to

$$(11) \quad A = \frac{1}{2} Eb (H + 2h'_e)^2 \epsilon_0^2.$$

Equating these expressions we obtain the result

$$(12) \quad h'_e = \alpha_{11} h_e.$$

### 3. The case of small pitch to depth ratio ( $\beta \ll 1$ )

In the case of small pitch to depth ratio the free boundary  $C_1C_2$  (fig. 5) has a negligible effect on the stress distribution, and we may consider the simplified problem of an *infinite* strip ( $-\infty < x < \infty$ ), loaded by unknown normal stresses  $p_y$  along the boundaries  $y = \pm \frac{1}{2}b$ ,  $x > 0$  and unloaded along the boundaries  $y = \pm \frac{1}{2}b$ ,  $x < 0$ ; this analysis for small  $\beta$  remains valid for values of  $\beta$  up to about 1. The transverse displacements along the boundaries  $y = \pm \frac{1}{2}b$  have to satisfy condition (2) for  $x > 0$ . The stress distribution is of course symmetric with respect to the  $x$ -axis.

Introducing the AIRY stress function  $f(x, y)$ , we have

$$(13) \quad \sigma_x = \frac{\partial^2 f}{\partial y^2}, \quad \sigma_y = \frac{\partial^2 f}{\partial x^2}, \quad \tau_{xy} = -\frac{\partial^2 f}{\partial x \partial y},$$

where  $f(x, y)$  satisfies the biharmonic equation

$$(14) \quad \left( \frac{\partial^2}{\partial x^2} + \frac{\partial^2}{\partial y^2} \right)^2 f = 0.$$

The boundary conditions for  $f(x, y)$  are

$$(15) \quad y = \pm \frac{1}{2} b: \frac{\partial^2 f}{\partial x^2} = p_\nu, \quad \frac{\partial^2 f}{\partial x \partial y} = 0.$$

We have from Hooke's law in generalized plane stress

$$(16) \quad \frac{\partial v}{\partial y} = \frac{1}{E} \left( \frac{\partial^2 f}{\partial x^2} - \nu \frac{\partial^2 f}{\partial y^2} \right),$$

where  $\nu$  is Poisson's ratio. Remembering the boundary conditions (15) we may now put condition (2) in the form

$$(17) \quad (v)_{y=+b} - (v)_{y=-b} = \frac{1}{E} \int_{-ib}^{ib} \frac{\partial^2 f}{\partial x^2} dy = (\varepsilon_0 - \kappa_0 x) b,$$

where the second equality only holds for  $x > 0$ .

We assume that  $e^{-\gamma x} f(x, y)$  and  $e^{-\gamma x} p_\nu(x)$  are absolutely integrable from  $x = -\infty$  to  $x = \infty$  and from  $x = 0$  to  $x = \infty$  for all  $\gamma$  in a range  $0 < \gamma < \gamma_1$ . The FOURIER-transforms [ref. 2]

$$(18) \quad \frac{1}{\sqrt{2\pi}} \int_{-\infty}^{\infty} f(x, y) e^{i\lambda x} dx = F(\lambda, y), \text{ regular for } 0 < \text{Im}(\lambda) < \gamma_1,$$

$$(19) \quad \frac{1}{\sqrt{2\pi}} \int_0^{\infty} p_\nu(x) e^{i\lambda x} dx = P_+(\lambda), \text{ regular for } \text{Im}(\lambda) > 0,$$

$$(20) \quad \frac{1}{\sqrt{2\pi}} \int_{-\infty}^0 [(v)_{y=+b} - (v)_{y=-b}] e^{i\lambda x} dx = V_-(\lambda), \text{ regular for } \text{Im}(\lambda) < \gamma_1,$$

$$(21) \quad \frac{1}{\sqrt{2\pi}} \int_0^{\infty} (\varepsilon_0 - \kappa_0 x) b e^{i\lambda x} dx = \frac{i}{\sqrt{2\pi}} \frac{\varepsilon_0 b}{\lambda} + \frac{1}{\sqrt{2\pi}} \frac{\kappa_0 b}{\lambda^2}, \text{ regular for } \text{Im}(\lambda) > 0,$$

exist and are regular in the strip and half-planes indicated with each transform.

We now apply a FOURIER transformation to (14), (15) and (17) and reduce various terms by integration by parts. From (14) we obtain the ordinary differential equation for  $F(\lambda, y)$

$$(22) \quad \frac{d^4 F(\lambda, y)}{dy^4} - 2\lambda^2 \frac{d^2 F(\lambda, y)}{dy^2} + \lambda^4 F(\lambda, y) = 0$$

with the general solution

$$(23) \quad F(\lambda, y) = A(\lambda) \cosh \lambda y + B(\lambda) \lambda y \sinh \lambda y + C(\lambda) \sinh \lambda y + D(\lambda) \lambda y \cosh \lambda y.$$

The functions  $A$ ,  $B$ ,  $C$ ,  $D$  are determined from the transformed boundary conditions (15)

$$(24) \quad y = \pm \frac{1}{2} b: -\lambda^2 F(\lambda, y) = P_+(\lambda), \frac{dF(\lambda, y)}{dy} = 0.$$

Substitution in the transformed equation (17) then yields an equation for the unknown transforms  $P_+(\lambda)$  and  $V_-(\lambda)$

$$(25) \quad \frac{4}{E} P_+(\lambda) \frac{\cosh \lambda b - 1}{\lambda b (\sinh \lambda b + \lambda b)} = \frac{1}{\sqrt{2\pi}} \left( \frac{i\varepsilon_0}{\lambda} + \frac{\kappa_0}{\lambda^2} \right) + \frac{1}{b} V_-(\lambda),$$

holding in the strip  $0 < \text{Im}(\lambda) < \gamma_1$ .

Equation (25) is an equation between FOURIER-transforms of the WIENER-HOPF type [ref. 2, art. 11.17], and it may be solved by the standard technique. We put

$$(26) \quad \frac{\cosh \lambda b - 1}{\lambda b (\sinh \lambda b + \lambda b)} = \frac{1}{\sqrt{\lambda^2 b^2 + 16}} \chi(\lambda b),$$

where

$$(27) \quad \chi(\lambda b) = \frac{\sqrt{\lambda^2 b^2 + 16} (\cosh \lambda b - 1)}{\lambda b (\sinh \lambda b + \lambda b)}$$

is regular and not zero in a strip  $-\gamma_1 < \text{Im}(\lambda) < \gamma_1$ . Because  $\log \chi(\lambda b)$  tends to zero as  $|\lambda|^{-2}$  for  $|\lambda| \rightarrow \infty$  in this strip, we have by CAUCHY's theorem

$$(28) \quad \log \chi(\lambda b) = \log \chi_+(\lambda b) - \log \chi_-(\lambda b),$$

where

$$(29) \quad \log \chi_+(\lambda b) = \frac{1}{2\pi i} \int_{i\gamma' b - \infty}^{i\gamma' b + \infty} \frac{\log \chi(z)}{z - \lambda b} dz, \quad \text{Im}(\lambda) > \gamma', \quad -\gamma_1 < \gamma' < \gamma_1;$$

$$(30) \quad \log \chi_-(\lambda b) = \frac{1}{2\pi i} \int_{i\gamma'' b - \infty}^{i\gamma'' b + \infty} \frac{\log \chi(z)}{z - \lambda b} dz, \quad \text{Im}(\lambda) < \gamma'', \quad -\gamma_1 < \gamma'' < \gamma_1.$$

We note that the integrals (29) and (30) remain convergent for  $\lambda b \rightarrow 0$  if we choose  $\gamma' = \gamma'' = 0$ , because  $\log \chi(z)$  has a double zero at  $z = 0$ . We have therefore  $\chi_+(0) = \chi_-(0) = 1$ .

We now write eq. (25) in the form

$$(31) \quad \begin{cases} \frac{4}{E} P_+(\lambda) \frac{1}{\sqrt{\lambda b + 4i} \sqrt{\lambda b - 4i}} \frac{\chi_+(\lambda b)}{\chi_-(\lambda b)} \\ = \frac{1}{\sqrt{2\pi}} \left( \frac{i\varepsilon_0}{\lambda} + \frac{\kappa_0}{\lambda^2} \right) + \frac{1}{b} V_-(\lambda), \end{cases}$$

where the principal value of the square roots is to be taken. We remember that  $\chi_+(\lambda b)$  and  $\chi_-(\lambda b)$  are regular and free from zero's in the upper half-plane  $\text{Im}(\lambda) > \gamma' > -\gamma_1$  and lower half-plane  $\text{Im}(\lambda) < \gamma'' < \gamma_1$  respectively. Both  $\chi_+(\lambda b)$  and  $\chi_-(\lambda b)$  tend to unity for  $|\lambda| \rightarrow \infty$  in their half-planes



of regularity. The solution for  $P_+(\lambda)$  and  $V_-(\lambda)$  must satisfy the following requirements

- a)  $P_+(\lambda)$  is regular for  $\text{Im}(\lambda) > 0$ ;
- b)  $V_-(\lambda)$  is regular for  $\text{Im}(\lambda) < \gamma_1$ ;
- c)  $P_+(\lambda)$  and  $V_-(\lambda)$  tend to zero for  $|\lambda| \rightarrow \infty$  in their half-planes of regularity.

It is easily seen that the solution of (31) is unique because the homogeneous equation, obtained from (31) by putting  $\varepsilon_0 = \kappa_0 = 0$ , does not admit a solution for  $P_+(\lambda)$  and  $V_-(\lambda)$  which both tend to zero for  $|\lambda| \rightarrow \infty$  in their half-planes of regularity. It is easily verified that the required solution is given by

$$(32) \quad \begin{cases} P_+(\lambda) = E\varepsilon_0 b \frac{i\sqrt{-4i}}{4\sqrt{2\pi}} \frac{\sqrt{\lambda b + 4i}}{\lambda b \chi_+(\lambda b)} + \\ + E\kappa_0 b^2 \frac{\sqrt{-4i}}{4\sqrt{2\pi}} \frac{\sqrt{\lambda b + 4i}}{\lambda^2 b^2 \chi_+(\lambda b)} \left\{ 1 + \left[ \frac{i}{8} + \chi'_-(0) \right] \lambda b \right\}, \end{cases}$$

$$(33) \quad \begin{cases} V_-(\lambda) = -\varepsilon_0 b^2 \frac{i}{\sqrt{2\pi}} \frac{1}{\lambda b} \left[ 1 - \sqrt{-4i} \frac{1}{\sqrt{\lambda b - 4i}} \frac{1}{\chi_-(\lambda b)} \right] + \\ - \kappa_0 b^3 \frac{1}{\sqrt{2\pi}} \frac{1}{\lambda^2 b^2} \left[ 1 - \sqrt{-4i} \frac{1}{\sqrt{\lambda b - 4i}} \frac{1}{\chi_-(\lambda b)} \left\{ 1 + \left[ \frac{i}{8} + \chi'_-(0) \right] \lambda b \right\} \right], \end{cases}$$

where  $\chi'_-(0)$  denotes the derivative of  $\chi_-(\lambda b)$  with respect to  $\lambda b$  at the point  $\lambda b = 0$ . It is now easily verified that our assumptions on the introduction of the FOURIER-transforms (18) to (20) are justified.

The load distribution  $p_v(x)$  may now be obtained from (32) by the inverse transformation

$$(34) \quad p_v(x) = \frac{1}{\sqrt{2\pi}} \int_{i\gamma - \infty}^{i\gamma + \infty} P_+(\lambda) e^{-i\lambda x} d\lambda, \quad 0 < \gamma < \gamma_1.$$

Evaluation of (34) is not readily possible. However, we do not need the load distribution  $p_v(x)$  itself but rather expression (4) which may be computed directly from (32). Putting

$$(35) \quad \Delta A(\lambda) = \frac{1}{2} b \int_0^\infty [p_v - E(\varepsilon_0 - \kappa_0 x)] (\varepsilon_0 - \kappa_0 x) e^{i\lambda x} dx,$$

we have

$$(36) \quad \begin{cases} \Delta A(\lambda) = \frac{1}{2} b \varepsilon_0 \int_0^\infty p_v e^{i\lambda x} dx - \frac{1}{2} b \kappa_0 \int_0^\infty p_v x e^{i\lambda x} dx + \\ - \frac{1}{2} b E \varepsilon_0^2 \int_0^\infty e^{i\lambda x} dx + b E \varepsilon_0 \kappa_0 \int_0^\infty x e^{i\lambda x} dx - \frac{1}{2} b E \kappa_0^2 \int_0^\infty x^2 e^{i\lambda x} dx = \\ = \frac{1}{2} b \varepsilon_0 \sqrt{2\pi} P_+(\lambda) + \frac{1}{2} i b \kappa_0 \sqrt{2\pi} \frac{d}{d\lambda} P_+(\lambda) + \\ - \frac{1}{2} i b E \varepsilon_0^2 \frac{1}{\lambda} - b E \varepsilon_0 \kappa_0 \frac{1}{\lambda^2} + i b E \kappa_0^2 \frac{1}{\lambda^3}, \end{cases}$$

and the required expression (4) is obtained by substituting (32) into (36) and taking the limit of this result for  $\lambda \rightarrow 0$ .

We now write with  $\lambda b = w$

$$(37) \quad \sqrt{2\pi} P_+(\lambda) = E \varepsilon_0 b \varphi_+(w) + E \kappa_0 b^2 \psi_+(w),$$

where

$$(38) \quad \varphi_+(w) = \frac{i}{4} \sqrt{-4i} \frac{\sqrt{w+4i}}{w \chi_+(w)},$$

$$(39) \quad \psi_+(w) = \frac{1}{4} \sqrt{-4i} \frac{\sqrt{w+4i}}{w^2 \chi_+(w)} \left\{ 1 + \left[ \frac{i}{8} + \chi'_-(0) \right] w \right\}.$$

Expression (4) may now be reduced to

$$(40) \quad \left\{ \begin{aligned} \Delta A &= \lim_{w \rightarrow 0} \left\{ \frac{1}{2} E b^2 \varepsilon_0^2 \left[ \varphi_+(w) - \frac{i}{w} \right] + \right. \\ &\quad + \frac{1}{2} E b^3 \varepsilon_0 \kappa_0 \left[ \psi_+(w) + i \varphi'_+(w) - \frac{2}{w^2} \right] + \\ &\quad \left. + \frac{1}{6} E b^4 \kappa_0^2 \left[ 3i \psi'_+(w) + \frac{6i}{w^3} \right] \right\}, \end{aligned} \right.$$

where primes again denote differentiations. Comparing this result to (5) we obtain the nondimensional coefficients  $\alpha_{11}$ ,  $\alpha_{12}$ ,  $\alpha_{22}$

$$(41) \quad \alpha_{11} = \frac{b}{h} \lim_{w \rightarrow 0} \left[ \varphi_+(w) - \frac{i}{w} \right],$$

$$(42) \quad \alpha_{12} = \frac{b^2}{h^2} \lim_{w \rightarrow 0} \left[ \psi_+(w) + i \varphi'_+(w) - \frac{2}{w^2} \right],$$

$$(43) \quad \alpha_{22} = \frac{b^3}{h^3} \lim_{w \rightarrow 0} \left[ 3i \psi'_+(w) + \frac{6i}{w^3} \right].$$

The evaluation of (41) to (43) requires some straightforward algebra, in which the definition of our square roots should be remembered. Expression (43) is evaluated more easily if it is rewritten in the form

$$(44) \quad \alpha_{22} = 3i \frac{b^3}{h^3} \lim_{w \rightarrow 0} \frac{d}{dw} \left[ \psi_+(w) - \frac{1}{w^2} \right].$$

We obtain the results with  $\beta = b/h^2$

$$(45) \quad \alpha_{11} = \beta \left[ \frac{1}{8} - i \chi'_+(0) \right],$$

$$(46) \quad \alpha_{12} = \beta^2 \left[ \frac{1}{64} - \frac{i}{8} \{ \chi'_+(0) + \chi'_-(0) \} - \{ \chi'_+(0) \}^2 \right],$$

$$(47) \quad \left\{ \begin{aligned} \alpha_{22} &= 3\beta^3 \left[ -\frac{1}{512} - \frac{3i}{128} \chi'_+(0) + \frac{i}{128} \chi'_-(0) - \frac{1}{8} \chi'_+(0) \chi'_-(0) + \right. \\ &\quad \left. + \frac{1}{2} i \chi'_+(0) \chi''_+(0) - \frac{1}{6} i \chi'''_+(0) \right]. \end{aligned} \right.$$

---

<sup>1)</sup> Depending on the way in which the limits are obtained for  $w \rightarrow 0$ , the results may have various forms which are all equivalent on account of eq. (49), i.e.  $\chi'_+(0) = \chi'_-(0)$ .

In order to evaluate this result numerically we have to compute the required derivatives of  $\chi_+(w)$  and  $\chi_-(w)$  at  $w=0$ . The first derivatives are given by

$$(48) \quad \left. \begin{array}{l} \frac{\chi'_+(w)}{\chi_+(w)} \\ \frac{\chi'_-(w)}{\chi_-(w)} \end{array} \right\} = \frac{1}{2\pi i} \int_{i\gamma-\infty}^{i\gamma+\infty} \frac{\log \chi(z)}{(z-w)^2} dz, \quad \begin{cases} \gamma < \text{Im}(w) \\ \gamma > \text{Im}(w) \end{cases}$$

For  $w=0$  the integral remains convergent for  $\gamma=0$ , and we obtain

$$(49) \quad \chi'_+(0) = \chi'_-(0) = \frac{1}{\pi i} \int_0^{\infty} \frac{1}{z^2} \log \chi(z) dz = -0,03646 i,$$

where the numerical result has been obtained by numerical integration.

By differentiation of (48) we obtain

$$(50) \quad \frac{d}{dw} \frac{\chi'_+(w)}{\chi_+(w)} = \frac{1}{2\pi i} \int_{i\gamma-\infty}^{i\gamma+\infty} \frac{2 \log \chi(z)}{(z-w)^3} dz, \quad \gamma < \text{Im}(w).$$

We deform the path of integration for  $w=0$  into the real axis, indented by a small half-circle below the origin. The contributions of the positive and negative parts of the real axis cancel each other, due to the symmetry of  $\chi(z)$ , and we obtain

$$(51) \quad \chi''_+(0) - \{\chi'_+(0)\}^2 = \frac{\pi i}{2\pi i} \frac{1}{2} \left[ \frac{d^2}{dz^2} 2 \log \chi(z) \right]_{z=0} = \frac{1}{32} = 0,03125.$$

By repeated differentiation of (50) and partial integration we obtain

$$(52) \quad \left\{ \begin{array}{l} \frac{d^2}{dw^2} \frac{\chi'_+(w)}{\chi_+(w)} = \frac{1}{2\pi i} \int_{i\gamma-\infty}^{i\gamma+\infty} \frac{6 \log \chi(z)}{(z-w)^4} dz = \\ = \frac{1}{2\pi i} \int_{i\gamma-\infty}^{i\gamma+\infty} \frac{1}{(z-w)^3} \frac{d^2}{dz^2} \{\log \chi(z)\} dz, \quad \gamma < \text{Im } w. \end{array} \right.$$

From (27) we have

$$(53) \quad \left[ \frac{d^2}{dz^2} \log \chi(z) \right]_{z=0} = \frac{1}{16}.$$

We rewrite the righthand member of (52)

$$(54) \quad \frac{1}{2\pi i} \int_{i\gamma-\infty}^{i\gamma+\infty} \frac{1}{16(z-w)^2} dz + \frac{1}{2\pi i} \int_{i\gamma-\infty}^{i\gamma+\infty} \frac{1}{(z-w)^2} \left[ \frac{d^2}{dz^2} \{\log \chi(z)\} - \frac{1}{16} \right] dz,$$

and observe that the first integral is zero. The second integral may be

taken along the real axis for  $w=0$ . Hence we obtain from (52)

$$(55) \quad \begin{cases} \chi_+'''(0) - 3\chi_+'(0)\chi_+''(0) + 2\{\chi_+'(0)\}^3 = \\ = \frac{1}{\pi i} \int_0^\infty \frac{1}{z^2} \left[ \frac{d^2}{dz^2} \{\log \chi(z)\} - \frac{1}{16} \right] dz = 0.0283 i, \end{cases}$$

where the numerical value is again the result of a numerical integration.

By substitution of the values (49), (51) and (55) into (45) to (47) we obtain the final result for the case of small pitch to depth ratio  $\beta$

$$(56) \quad \begin{cases} \alpha_{11} = 0.08854 \beta, \\ \alpha_{12} = 0.00783 \beta^2, \\ \alpha_{22} = 0.00702 \beta^3. \end{cases}$$

*(To be continued)*



ON THE FLEXURAL RIGIDITY OF A BEAM,  
WEAKENED BY TRANSVERSE SAW CUTS. II

BY

W. T. KOITER

(Communicated by Prof. C. B. BIEZENO at the meeting of April 28, 1956)

4. *The case of large pitch to depth ratio ( $\beta \gg 1$ )*

In the extreme case of a very large ratio of pitch to depth, the effects of the saw cuts do not interfere mutually. The increase in strain energy, due to the material of depth  $h$  between two saw cuts may now be written in the form

$$(57) \quad \Delta A = \frac{1}{2} E b h (\varepsilon_0^2 + \varepsilon_0 \kappa_0 h + \frac{1}{3} \kappa_0^2 h^2) - \Delta A^*,$$

The first term is the strain energy in the rectangle  $A_1 A_2 C_2 C_1$  of figs. 5 and 6 in the absence of saw cuts for a bending strain distribution  $\varepsilon_y = \varepsilon_0 - \kappa_0 x$ . The second term  $-\Delta A^*$  represents the decrease in strain energy, occurring when one saw cut is applied. If we write

$$(58) \quad \Delta A^* = \frac{1}{2} E h^2 (\alpha_{11}^* \varepsilon_0^2 + \alpha_{12}^* \varepsilon_0 \kappa_0 h + \frac{1}{3} \alpha_{22}^* \kappa_0^2 h^2),$$

where the numerical coefficients  $\alpha_{11}^*$ ,  $\alpha_{12}^*$  and  $\alpha_{22}^*$  are as yet unknown, the required coefficients in (5) are

$$(59) \quad \left\{ \begin{array}{l} \alpha_{11} = 1 - \frac{\alpha_{11}^*}{\beta}, \\ \alpha_{12} = 1 - \frac{\alpha_{12}^*}{\beta}, \\ \alpha_{22} = 1 - \frac{\alpha_{22}^*}{\beta}, \end{array} \right.$$

where again  $\beta = b/h$ .

Our problem has now been reduced to the problem of a half-plane with a single saw cut perpendicular to the boundary (fig. 7), the faces of the saw cut being loaded by compressive stresses  $E(\varepsilon_0 - \kappa_0 x)$ . Obviously, the line  $AF$  will remain straight and no shear stresses will be transmitted across this line.

We now consider the quarter-plane  $GCF$  (fig. 8), unloaded along the boundary  $CG$  and loaded by normal stresses  $-E(\varepsilon_0 - \kappa_0 x)$  along  $CA$  and by as yet unknown normal stresses  $p_y$  along  $AF$ . The latter loads are to be determined from the condition that  $AF$  remains straight.

We introduce the AIRY stress function  $f(r, \theta)$  in polar coordinates and put  $r = \rho h$ ; we have

$$(60) \quad h^2 \sigma_r = \frac{1}{\rho^2} \frac{\partial^2 f}{\partial \theta^2} + \frac{1}{\rho} \frac{\partial f}{\partial \rho}, \quad h^2 \sigma_\theta = \frac{\partial^2 f}{\partial \rho^2}, \quad h^2 \tau_{r\theta} = \frac{1}{\rho^2} \frac{\partial f}{\partial \theta} - \frac{1}{\rho} \frac{\partial^2 f}{\partial \rho \partial \theta},$$

where  $f(r, \theta)$  satisfies the biharmonic equation

$$(61) \quad \left( \frac{\partial^2}{\partial \rho^2} + \frac{1}{\rho} \frac{\partial}{\partial \rho} + \frac{1}{\rho^2} \frac{\partial^2}{\partial \theta^2} \right)^2 f = 0.$$

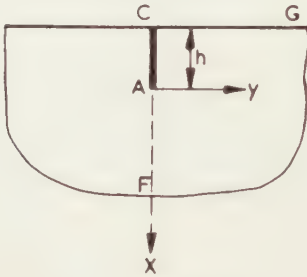


Fig. 7. Half-plane with a single saw cut.

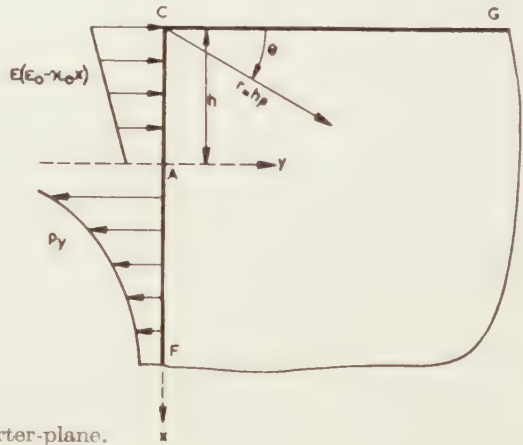


Fig. 8. Problem of quarter-plane.

The boundary conditions for  $f(r, \theta)$  are

$$(62) \quad \theta = 0: \frac{\partial^2 f}{\partial \rho^2} = 0, \quad \frac{1}{\rho^2} \frac{\partial f}{\partial \theta} - \frac{1}{\rho} \frac{\partial^2 f}{\partial \rho \partial \theta} = 0;$$

$$(63) \quad \theta = \frac{\pi}{2}: \frac{1}{\rho^2} \frac{\partial f}{\partial \theta} - \frac{1}{\rho} \frac{\partial^2 f}{\partial \rho \partial \theta} = 0;$$

$$(64) \quad \theta = \frac{\pi}{2}: \frac{1}{h^2} \frac{\partial^2 f}{\partial \rho^2} = \begin{cases} -E(\epsilon_0 + \kappa_0 h - \kappa_0 h \rho) & \text{for } \rho < 1, \\ p_y(\rho) & \text{for } \rho > 1. \end{cases}$$

From Hooke's law in generalized plane stress we have

$$(65) \quad h \epsilon_\theta = \frac{1}{\rho} \frac{\partial v}{\partial \theta} + \frac{u}{\rho} = \frac{1}{Eh} \left[ \frac{\partial^2 f}{\partial \rho^2} - \nu \left( \frac{1}{\rho^2} \frac{\partial^2 f}{\partial \theta^2} + \frac{1}{\rho} \frac{\partial f}{\partial \rho} \right) \right],$$

$$(66) \quad h \epsilon_r = \frac{\partial u}{\partial \rho} = \frac{1}{Eh} \left[ \frac{1}{\rho^2} \frac{\partial^2 f}{\partial \theta^2} + \frac{1}{\rho} \frac{\partial f}{\partial \rho} - \nu \frac{\partial^2 f}{\partial \rho^2} \right],$$

$$(67) \quad h \gamma_{r\theta} = \frac{1}{\rho} \frac{\partial u}{\partial \theta} + \frac{\partial v}{\partial \rho} - \frac{v}{\rho} = \frac{2(1+\nu)}{Eh} \left[ \frac{1}{\rho^2} \frac{\partial f}{\partial \theta} - \frac{1}{\rho} \frac{\partial^2 f}{\partial \rho \partial \theta} \right],$$

where  $u$  and  $v$  denote the radial and tangential displacements.

We assume that  $\rho^{\mu-2} f(r, \theta)$  and  $\rho^\mu p_y(\rho)$  are absolutely integrable from  $\rho=0$  to  $\rho=\infty$  and from  $\rho=1$  to  $\rho=\infty$  respectively, for all  $\mu$  in a range

$0 < \mu < \mu_1$ . The MELLIN-transforms [ref. 3, art. 49]<sup>2)</sup>

$$(68) \quad \int_0^{\infty} \varrho^{s-2} f(r, \theta) d\varrho = F(s, \theta), \text{ regular for } 0 < \operatorname{Re}(s) < \mu_1,$$

$$(69) \quad \int_1^{\infty} \varrho^s p_v(\varrho) d\varrho = P_-(s), \text{ regular for } \operatorname{Re}(s) < \mu_1,$$

$$(70) \quad \int_0^{\infty} \varrho^{s-1} u(r, \theta) d\varrho = U(s, \theta), \text{ regular for } 0 < \operatorname{Re}(s) < \mu_1,$$

$$(71) \quad \int_0^{\infty} \varrho^{s-1} v(r, \theta) d\varrho = V(s, \theta), \text{ regular for } 0 < \operatorname{Re}(s) < \mu_1,$$

exist and are regular in the strip and half-plane indicated with each transform. Because  $AF$  in fig. 8 remains straight, we may put

$$v\left(r, \frac{\pi}{2}\right) = 0 \text{ for } \varrho > 1.$$

Hence

$$(72) \quad \int_0^1 \varrho^{s-1} v\left(r, \frac{\pi}{2}\right) d\varrho = V_+(s) = V\left(s, \frac{\pi}{2}\right)$$

is regular in the half-plane  $\operatorname{Re}(s) > 0$ .

We now apply a MELLIN transformation to (61) by multiplying both members by  $\varrho^{s+2}$  and integrating from  $\varrho=0$  to  $\varrho=\infty$ . Integrating by parts those terms which contain derivatives with respect to  $\varrho$ , we obtain the ordinary differential equation for the MELLIN-transform  $F(s, \theta)$

$$(73) \quad \left[ \frac{d^2}{d\theta^2} + (s-1)^2 \right] \left[ \frac{d^2}{d\theta^2} + (s+1)^2 \right] F(s, \theta) = 0,$$

with the general solution

$$(74) \quad \begin{cases} F(s, \theta) = A(s) \sin(s-1)\theta + B(s) \cos(s-1)\theta + \\ + C(s) \sin(s+1)\theta + D(s) \cos(s+1)\theta. \end{cases}$$

The functions  $A, B, C, D$  are determined by the transformed boundary conditions (62) to (64), obtained by multiplying by  $\varrho^s$  and integrating from  $\varrho=0$  to  $\varrho=\infty$ ,

$$(75) \quad \theta = 0 : F(s, \theta) = 0, \frac{d}{d\theta} F(s, \theta) = 0;$$

$$(76) \quad \theta = \frac{\pi}{2} : \frac{d}{d\theta} F(s, \theta) = 0;$$

$$(77) \quad \theta = \frac{\pi}{2} : \frac{1}{h^2} s(s-1) F(s, \theta) = -\frac{E(\varepsilon_0 + \kappa_0 h)}{s+1} + \frac{E\kappa_0 h}{s+2} + P_-(s).$$

<sup>2)</sup> In order to obtain somewhat simpler expressions we have replaced SNEDDON's  $(s+1)$  by  $s$ .

The resulting solution (74) which satisfies the boundary condition (75) to (77) is

$$(78) \quad \left\{ \begin{aligned} F &= h^2 \left[ -\frac{E(\varepsilon_0 + \kappa_0 h)}{s+1} + \frac{E\kappa_0 h}{s+2} + P_-(s) \right] \frac{s+1}{\cos \pi s + 2s^2 - 1} \\ &\cdot \left[ -\frac{\cos \frac{\pi}{2} s}{s-1} \sin(s-1)\theta + \frac{\cos \frac{\pi}{2} s}{s+1} \sin(s+1)\theta + \right. \\ &\left. + \frac{\sin \frac{\pi}{2} s}{s} \cos(s-1)\theta - \frac{\sin \frac{\pi}{2} s}{s} \cos(s+1)\theta \right]. \end{aligned} \right.$$

Next we transform equations (65) to (67) by multiplying by  $\varrho^s$  and integrating from  $\varrho=0$  to  $\varrho=\infty$ , obtaining

$$(79) \quad \frac{d}{d\theta} V(s, \theta) + U(s, \theta) = \frac{1}{Eh} \left[ \{s^2 - (1-\nu)s - \nu\} F(s, \theta) - \nu \frac{d^2}{d\theta^2} F(s, \theta) \right],$$

$$(80) \quad -sU(s, \theta) = \frac{1}{Eh} \left[ \{-\nu s^2 - (1-\nu)s + 1\} F(s, \theta) - \frac{d^2}{d\theta^2} F(s, \theta) \right],$$

$$(81) \quad \frac{d}{d\theta} U(s, \theta) - (s+1)V(s, \theta) = \frac{2(1+\nu)}{Eh} s \frac{d}{d\theta} F(s, \theta).$$

Solving for  $V(s, \theta)$ , we have

$$(82) \quad \left\{ \begin{aligned} V(s, \theta) &= \\ &= -\frac{1}{Eh} \frac{1}{s(s+1)} \left[ \{2 - \nu s^2 - (1-\nu)s + 1\} \frac{d}{d\theta} F(s, \theta) + \frac{d^3}{d\theta^3} F(s, \theta) \right]. \end{aligned} \right.$$

Substituting (78) into (82) we may calculate  $V(s, \pi/2)$  by putting  $\theta = \pi/2$ . Remembering (72) we get after some elementary algebra the WIENER-HOPF equation

$$(83) \quad V_+(s) = 2h \frac{\sin \pi s}{s(\cos \pi s + 2s^2 - 1)} \left[ -\frac{\varepsilon_0 + \kappa_0 h}{s+1} + \frac{\kappa_0 h}{s+2} + \frac{1}{E} P_-(s) \right],$$

holding in the strip  $0 < \operatorname{Re}(s) < \mu_1$ .

In order to solve this equation, we write with a constant  $B > 1$

$$(84) \quad -\frac{\sin \pi s}{s(\cos \pi s + 2s^2 - 1)} = \frac{\sqrt{B^2 - s^2}}{s^2} H(s),$$

where

$$(85) \quad H(s) = \frac{-s \sin \pi s}{\sqrt{B^2 - s^2} [\cos \pi s + 2s^2 - 1]}$$

is regular in a strip  $-\mu_1 < \operatorname{Re}(s) < \mu_1$ , where  $\mu_1 > 1$ . In this strip  $H(s)$  tends to unity for  $|s| \rightarrow \infty$ .

We now write

$$(86) \quad H(s) = \frac{H_+(s)}{H_-(s)},$$

where  $H_+(s)$  and  $H_-(s)$  are defined by

$$(87) \quad \left\{ \begin{aligned} \log H_+(s) \\ \log H_-(s) \end{aligned} \right\} = -\frac{1}{2\pi i} \int_{\mu-i\infty}^{\mu+i\infty} \frac{\log H(z)}{z-s} dz, \quad \left\{ \begin{aligned} \mu < \operatorname{Re}(s), \\ \mu > \operatorname{Re}(s), \end{aligned} \right.$$



and  $-\mu_1 < \mu < \mu_1$ . Obviously  $H_+(s)$  and  $H_-(s)$  are regular and free from zero's in the half-planes  $\operatorname{Re}(s) > \mu$  and  $\operatorname{Re}(s) < \mu$  respectively. Both  $H_+(s)$  and  $H_-(s)$  tend to unity for  $|s| \rightarrow \infty$  in their half-planes of regularity.

Our WIENER-HOPF equation (83) may now be rewritten in the form

$$(88) \quad V_+(s) = -2h \frac{\sqrt{B+s} \sqrt{B-s} H_+(s)}{s^2 H_-(s)} \left[ -\frac{\varepsilon_0 + \kappa_0 h}{s+1} + \frac{\kappa_0 h}{s+2} + \frac{1}{E} P_-(s) \right],$$

where the arguments of the square roots do not exceed  $\pi/2$  in absolute value. The solution for  $P_-(s)$  and  $V_+(s)$  must satisfy the following requirements

- a)  $V_+(s)$  is regular for  $\operatorname{Re}(s) > 0$ ;
- b)  $P_-(s)$  is regular for  $\operatorname{Re}(s) < \mu_1$ ;
- c)  $V_+(s)$  and  $P_-(s)$  tend to zero for  $|s| \rightarrow \infty$  in their half-planes of regularity.

A difficulty now arises out of the fact that the solution of (88) which satisfies the above requirements is *not unique*. In fact, the homogeneous equation, obtained from (88) by putting  $\varepsilon_0 = \kappa_0 = 0$ , possesses the solution

$$(89) \quad V_+(s) = Qh \frac{\sqrt{B+s} H_+(s)}{s^2},$$

$$(90) \quad P_-(s) = -\frac{1}{2}QE \frac{H_-(s)}{\sqrt{B-s}},$$

which satisfies our requirements for arbitrary values of the constant  $Q$ . The general solution of (88) is now obtained by adding a suitable particular solution to (89) and (90). It is easily verified that

$$(91) \quad \begin{cases} V_+(s) = -2h \frac{\varepsilon_0 + \kappa_0 h}{s+1} \frac{\sqrt{B+1}}{H_-(-1)} \frac{1}{s} \sqrt{B+s} H_+(s) + \frac{\kappa_0 h^2}{s+2} \cdot \\ \quad \cdot \frac{\sqrt{B+2}}{H_-(-2)} \frac{1}{s} \sqrt{B+s} H_+(s) \end{cases}$$

$$(92) \quad \begin{cases} P_-(s) = E \frac{\varepsilon_0 + \kappa_0 h}{s+1} \left[ 1 + \frac{\sqrt{B+1}}{H_-(-1)} \frac{sH_-(s)}{\sqrt{B-s}} \right] + \\ \quad - E \frac{\kappa_0 h}{s+2} \left[ 1 + \frac{\sqrt{B+2}}{2H_-(-2)} \frac{sH_-(s)}{\sqrt{B-s}} \right] \end{cases}$$

is such a particular solution.

The ambiguity is removed by observing that

$$(93) \quad \begin{cases} P(s) = -\frac{E(\varepsilon_0 + \kappa_0 h)}{s+1} + \frac{E\kappa_0 h}{s+1} + P_-(s) = \\ \quad = \int_0^1 -E(\varepsilon_0 + \kappa_0 h - \kappa_0 \varrho) \varrho^s d\varrho + \int_1^\infty p_\nu(\varrho) \cdot \varrho^s d\varrho \end{cases}$$

is the MELLIN-transform of the normal loads along the *entire* boundary  $\theta = \pi/2$  (the line  $CF$  in fig. 8). In order that the resulting normal force be zero, a plausible requirement from a physical point of view, we must

have  $P(0) = 0$ . The particular solution (91), (92) satisfies this condition, whereas the general solution (89), (90) of the homogeneous equation does not. Hence we must have  $Q = 0$ , and the required solution of (88) is given by (91) and (92).

We arrive at the same result  $Q = 0$  in a completely rigorous way by investigating the physical significance of the general solution (89), (90) of the homogeneous equation. The corresponding transformed stress function  $F(s, \theta)$  may be calculated by substituting (90) and  $\varepsilon_0 = \kappa_0 = 0$  into (78). The stress distribution may now be obtained by the inverse MELLIN-transforms [ref. 3, art. 49]<sup>3)</sup>

$$(94) \quad h^2 \sigma_r = \frac{1}{2\pi i} \int_{\mu-i\infty}^{\mu+i\infty} \left[ \frac{d^2}{d\theta^2} F(s, \theta) - (s-1) F(s, \theta) \right] \cdot \varrho^{-s-1} ds,$$

$$(95) \quad h^2 \sigma_\theta = \frac{1}{2\pi i} \int_{\mu-i\infty}^{\mu+i\infty} s(s-1) F(s, \theta) \cdot \varrho^{-s-1} ds,$$

$$(96) \quad h^2 \tau_{r\theta} = \frac{1}{2\pi i} \int_{\mu-i\infty}^{\mu+i\infty} s \frac{d}{d\theta} F(s, \theta) \cdot \varrho^{-s-1} ds,$$

where  $0 < \mu < \mu_1$ . After some elementary algebra it appears that the integrands of both (95) and (96) are regular for  $\text{Re}(s) > -\mu_1$ . Remembering that  $\mu_1 > 1$  we may now shift the line of integration to the line  $\text{Re}(s) = \mu'$ , where  $\mu_1 > \mu' > -1$ . Hence we obtain for  $\varrho \rightarrow 0$ :  $\sigma_\theta \rightarrow 0$  and  $\tau_{r\theta} \rightarrow 0$ . On the other hand, the integrand of (94) has a simple pole at  $s = 0$  with residue

$$(97) \quad h^2 QE \frac{H_-(0)}{(\pi^2 - 4) \sqrt{B}} [2\pi \cos \theta - 4 \sin \theta] \frac{1}{\varrho}.$$

Hence, the radial stress for  $\varrho \rightarrow 0$  is approximated by

$$(98) \quad \sigma_r \rightarrow QE \frac{H_-(0)}{(\pi^2 - 4) \sqrt{B}} (2\pi \cos \theta - 4 \sin \theta) \frac{1}{\varrho}.$$

This singularity corresponds to a concentrated force at the corner  $C$  in fig. 8 in the direction  $GC$  of magnitude

$$(99) \quad \frac{1}{2} QEh \frac{H_-(0)}{\sqrt{B}}$$

per unit thickness. Obviously no concentrated force occurs at the corner  $C$  in fig. 8 in our problem, and we have to put  $Q = 0$ .

We are now able to calculate the reduction in strain energy  $\Delta A^*$  when a saw cut is applied in our half-plane, this reduction being given by twice the strain energy in the quarter-plane, loaded by normal stresses

<sup>3)</sup> Cf. footnote 2.

$-E(\varepsilon_0 + \kappa_0 h - \kappa_0 r)$  along  $CA$ , i.e.

$$(100) \quad \left\{ \begin{aligned} \Delta A^* &= - \int_0^h E(\varepsilon_0 + \kappa_0 h - \kappa_0 r) v\left(r, \frac{\pi}{2}\right) dr = \\ &= -E(\varepsilon_0 + \kappa_0 h) h \int_0^1 v\left(r, \frac{\pi}{2}\right) d\rho + E\kappa_0 h^2 \int_0^1 v\left(r, \frac{\pi}{2}\right) \cdot \rho d\rho = \\ &= -E(\varepsilon_0 + \kappa_0 h) h V_+(1) + E\kappa_0 h^2 V_+(2), \end{aligned} \right.$$

where  $V_+(s)$  is given by (91). and we obtain the following values for the coefficients  $\alpha_{11}^*$ ,  $\alpha_{12}^*$  and  $\alpha_{22}^*$  in (58)

$$(101) \quad \alpha_{11}^* = 2(B+1) \frac{H_+(1)}{H_-(-1)},$$

$$(102) \quad \alpha_{12}^* = 4(B+1) \frac{H_+(1)}{H_-(-1)} - \frac{2}{3} \sqrt{(B+1)(B+2)} \left[ \frac{H_+(1)}{H_-(-2)} + \frac{H_+(2)}{H_-(-1)} \right],$$

$$(103) \quad \left\{ \begin{aligned} \alpha_{22}^* &= 6(B+1) \frac{H_+(1)}{H_-(-1)} + \frac{3}{4}(B+2) \frac{H_+(2)}{H_-(-2)} + \\ &\quad - 2 \sqrt{(B+1)(B+2)} \left[ \frac{H_+(1)}{H_-(-2)} + \frac{H_+(2)}{H_-(-1)} \right]. \end{aligned} \right.$$

In order to evaluate these results numerically, we have to calculate the required values of  $H_+(s)$  and  $H_-(s)$ . It is convenient to choose

$$(104) \quad B = \frac{2\pi}{\pi^2 - 4} = 1,0705.$$

Bearing in mind the symmetry property of  $H(s)$ , viz.  $H(-s) = H(s)$ , we have

$$(105) \quad \left\{ \begin{aligned} \log \frac{H_+(1)}{H_-(-1)} &= -\frac{1}{2\pi i} \int_{-i\infty}^{i\infty} \left( \frac{1}{z-1} - \frac{1}{z+1} \right) \log H(z) dz = \\ &= \frac{2}{\pi} \int_0^\infty \frac{1}{y^2+1} \log \frac{y \sinh \pi y}{\sqrt{B^2+y^2} [\cosh \pi y - 2y^2 - 1]} dy = -0,0468 \end{aligned} \right.$$

$$(106) \quad \left\{ \begin{aligned} \log \frac{H_+(1)}{H_-(-2)} &= -\frac{1}{2\pi i} \int_{-i\infty}^{i\infty} \left( \frac{1}{z-1} - \frac{1}{z+2} \right) \log H(z) dz = \\ &= \frac{3}{\pi} \int_0^\infty \frac{y^2+2}{(y^2+2)^2+y^2} \log \frac{y \sinh \pi y}{\sqrt{B^2+y^2} [\cosh \pi y - 2y^2 - 1]} dy = -0,0469, \end{aligned} \right.$$

$$(107) \quad \left\{ \begin{aligned} \log \frac{H_+(2)}{H_-(-1)} &= -\frac{1}{2\pi i} \int_{-i\infty}^{i\infty} \left( \frac{1}{z-2} - \frac{1}{z+1} \right) \log H(z) dz = \\ &= \frac{3}{\pi} \int_0^\infty \frac{y^2+2}{(y^2+2)^2+y^2} \log \frac{y \sinh \pi y}{\sqrt{B^2+y^2} [\cosh \pi y - 2y^2 - 1]} dy = -0,0469, \end{aligned} \right.$$

$$(108) \quad \left\{ \begin{aligned} \log \frac{H_+(2)}{H_-(-2)} &= -\frac{1}{2\pi i} \int_{-\infty}^{\infty} \left( \frac{1}{z-2} - \frac{1}{z+2} \right) \log H(z) dz = \\ &= \frac{4}{\pi} \int_0^{\infty} \frac{1}{y^2+4} \log \frac{y \sinh \pi y}{\sqrt{B^2+y^2} [\cosh \pi y - 2y^2 - 1]} dy = -0.0470. \end{aligned} \right.$$

where the numerical values have been obtained by numerical integration. It is easily verified that (107) is the mean of (105) and (108). The fact that (105) and (108) are nearly equal leads to the suspicion that they should be exactly equal; this suspicion, however, has not been proved.

The resulting values for the nondimensional coefficients  $\alpha_{11}^*$ ,  $\alpha_{12}^*$  and  $\alpha_{22}^*$  are

$$(109) \quad \begin{cases} \alpha_{11}^* = 3.952, \\ \alpha_{12}^* = 4.696, \\ \alpha_{22}^* = 4.429. \end{cases}$$

##### 5. Interpolation for intermediate values of the ratio of pitch to depth ( $0 < \beta < \infty$ )

The results of our analysis for *small* pitch to depth ratio are pictured in the left-hand part of figs. 9 to 11. In accordance with (56) these curves are a straight line for  $\alpha_{11}$ , a parabola for  $\alpha_{12}$  and a cubic parabola for  $\alpha_{22}$ . The hyperbolas (59) for *large* pitch to depth ratio with the numerical coefficients (109) are given in the right-hand part of figs. 9 to 11.

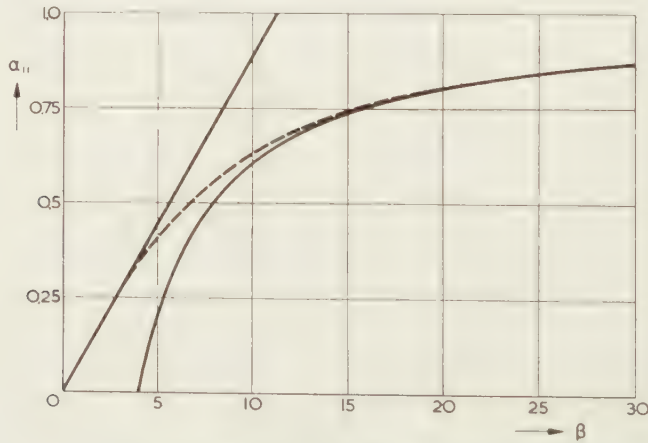


Fig. 9. Graph of  $\alpha_{11}$  as function of  $\beta$ .

The actual curves for  $\alpha_{11}$ ,  $\alpha_{12}$  and  $\alpha_{22}$  as functions of  $\beta$  must approach to the curves for small pitch to depth ratio when  $\beta \rightarrow 0$  and to the curves for large pitch to depth ratio for  $\beta \rightarrow \infty$ . Moreover, we know that the actual values of  $\alpha_{11}$  and  $\alpha_{22}$  will always be smaller than the values given by (56), because the latter values have been derived for infinite depth  $h$ .



(cf. para. 3). On the other hand, the asymptotic formulas (59) underestimate the actual equivalent height because the interaction of two saw cuts leads to a smaller decrease of strain energy in the half-plane than the sum of these decreases for two independent saw cuts.

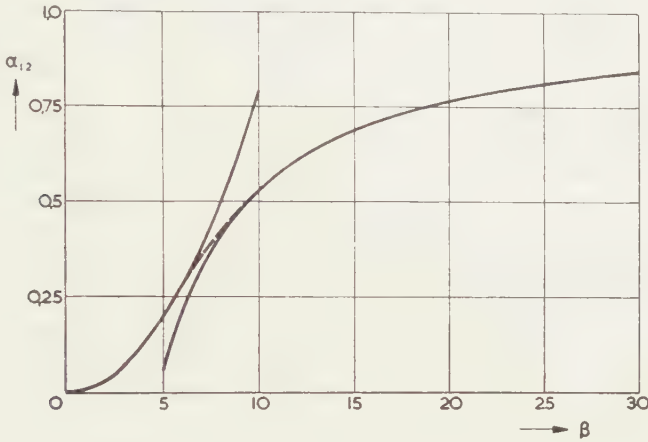


Fig. 10. Graph of  $\alpha_{12}$  as function of  $\beta$ .

A satisfactory interpolation for intermediate values of  $\beta$  may now be obtained by drawing the dotted curve through the point half-way between the two limiting curves at the value of  $\beta$  where their vertical distance is a minimum. The error of this approximation is always smaller than

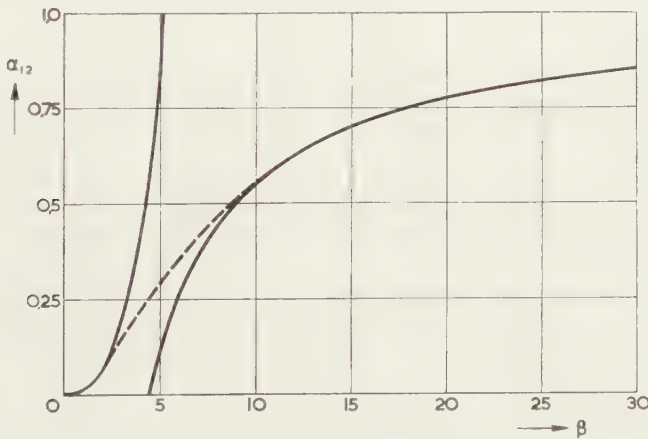


Fig. 11. Graph of  $\alpha_{22}$  as function of  $\beta$ .

half the minimum vertical distance between the two limiting curves (i.e.  $\pm 0.09$  in fig. 9,  $\pm 0.03$  in fig. 10 and  $\pm 0.28$  in fig. 11). The actual error is probably even much smaller; it may be estimated at about  $\pm 0.02$  in fig. 9,  $\pm 0.01$  in fig. 10 and  $\pm 0.08$  in fig. 11. The resulting error in equivalent height will not exceed  $\pm 0.02h$  because the effect of

the larger error in  $\alpha_{22}$  will be greatly diminished by the factor  $8h^3/H^3$  in eq. (9).

The dotted curves in figs. 9, 10 and 11 should therefore give a satisfactory approximation for the nondimensional coefficients  $\alpha_{11}$ ,  $\alpha_{12}$  and  $\alpha_{22}$  over the entire range  $0 < \beta < \infty$ , and the corresponding equivalent height may be calculated by means of (9). It should be remembered, however, that this result is valid only if our basic assumption  $b/H < \sim 1$  is applicable.

*Delft, April 16, 1956.*

---

#### REFERENCES

1. DISPAUX, J., Grote turbo-generatoren met waterstofkoeling, *Electrotechniek* 33, 291 (1955).
2. TITCHMARSH, E. C., *Theory of Fourier integrals* (Oxford University Press, Oxford, 1937).
3. SNEDDON, I. N., *Fourier transforms* (Mc Graw-Hill, New York, 1951).

## METEOROLOGY

### THE NOVAYA-ZEMLYA PHENOMENON

BY

S. W. VISSER

(Communicated by Prof. H. P. BERLAGE at the meeting of May 26, 1956)

*Id fieri potest per leges repercussorias.*  
JOHANNES KEPLER, 1604.

1. The sailors from Holland hibernating on the isle of Novaya Zemlya, 1596–1597, saw the sun on the 24th of January 1597, 14 days before the calculated day. The abnormal refraction should have amounted to more than  $4^\circ$ . Analogous phenomena have been observed January 27th and 31st and February 8th (the sun rising in SSE, setting in SSW). In Holland the report of the observations met with sharp criticism. S. P. L'HONORÉ NABER too, who edited in 1917 the story of GERRIT DE VEER for the Linschoten-Society (ref. No 8) ventilated his grievances in an extremely stern fashion. He calculated the deviation of the sun's rays above normal ( $36'$ ) to be respectively  $4^\circ 17'$ ,  $4^\circ 3'$ ,  $2^\circ 58'$  and  $1^\circ 9'$  and declared these results to be impossible. Just like the critics of the 16th century, he interpreted the story as a too far pushed joke, based upon a change of the Gregorian Calendar into the Julian one. So only three days would remain!

As a devoted defender of DE VEER since 1918 J. W. VAN NOUHUYS entered the arena. He has made an extensive study of the literature concerning the phenomenon. I wish to extend my thanks to him for permission to consult his archives. He has found a similar observation made by SHACKLETON during the expedition to Antarctica, 1914–1917 [7]. I shall discuss this matter at the end of this paper. VAN NOUHUYS has remarked that the Encyclopaedia Britannica [2] even reduced all time records, starting with the departure from Texel, to the Old Style, though beyond doubt during the whole voyage the New Style has been practised.

His researches revealed an idea of KEPLER, who, in 1604, fully discussed the observations of 1597 [3]:

Alter modus consistit in repercussione facta . . . . a superiore superficie aeris nos ambientis. . . . Id fieri potest per leges repercussorias. . . . Nec metus est, ut superficies ista radios transmittat, propterea, quod post superficiem convexam illam occurrat rarius medium.

The phenomenon may be caused, KEPLER said, by total reflection by an upper air-layer in accord with the laws of reflection. VAN NOUHUYS

had advanced this same explanation long before he came to know KEPLER's idea [5].

Modern views lead to the conception of repeated total reflection at the upper boundary of a ground inversion. The rays entering below this boundary at its beginning where the sun rises normally, cannot leave the trap and, repeatedly reflected, must follow the surface of the earth to the end of the inversion. The phenomenon is the same as that of the totally reflected radio-rays in the ionosphere and the sound-waves in the ozonosphere. The sun is no simple point. The case is most favourable when for the rays of the lowest edge of the sun the critical angle of total reflection is reached or exceeded. After a few reflections the whole space between the surface of the earth and the ground inversion is filled up with light and the phenomenon becomes visible everywhere below the inversion.

2. *Method.* We have tested KEPLER's conception in its modern fashion as follows.

2.1. To begin with we consider a fictive atmosphere with constant pressure and temperature below the inversion. Then the propagation is rectilinear. We shall finally apply the necessary corrections.

2.2. A sharp temperature boundary being present at a height  $H$  above the surface of the earth the critical angle of the incident rays for total reflection can be calculated. As the radius of the earth I have assumed 6.370.000 meters.

Table 1 contains some results.

TABLE 1

Height and critical angle	
400 m	89° 20,2'
300 m	89° 26,5'
200 m	89° 33,0'
150 m	89° 36,5'
100 m	89° 41,5'
50 m	89° 46,0'

2.3 The absolute refractive indices  $n_a$  for an atmospheric pressure of 1013 mb and for temperatures ranging from  $-50^\circ$  to  $+40^\circ$  C have been calculated with the aid of H. A. LORENTZ's equation [4] in its simplified form

$$(n_a - 1)/d = \text{constant}$$

in which  $d$  is the density of the air.

We may divide  $d$  by  $d_0$  (density at  $0^\circ$  C and 1013 mb) and therefore replace  $d$  by the relative density  $\delta$ . Then

$$n_a - 1 = c\delta$$



or, applying the gas-laws

$$(1) \quad n_a - 1 = c \frac{p}{1013} \cdot \frac{273}{T}$$

in which  $p$  is the pressure and  $T$  the absolute temperature.

For  $p = 1013$  mb and  $T = 273^\circ$  the absolute refractive index of the air is 1,000 293

hence  $c = 0,000\ 293$ .

Table 2 contains some of the results.

TABLE 2  
Absolute refractive index

$t$	$n_a$	$t$	$n_a$
$-50^\circ \text{ C}$	1,000 359	$0^\circ \text{ C}$	1,000 293
$-40^\circ \text{ C}$	1,000 343	$+10^\circ \text{ C}$	1,000 283
$-30^\circ \text{ C}$	1,000 329	$+20^\circ \text{ C}$	1,000 273
$-20^\circ \text{ C}$	1,000 316	$+30^\circ \text{ C}$	1,000 264
$-10^\circ \text{ C}$	1,000 304	$+40^\circ \text{ C}$	1,000 256

2.4. The refractive index, when the ray passes from a layer with a temperature  $T_0$  to a layer with temperature  $T_1$ , is to be found by the equation

$$n = \frac{1 + 0,000\ 293 \frac{p}{1013} \cdot \frac{273}{T_0}}{1 + 0,000\ 293 \frac{p}{1013} \cdot \frac{273}{T_1}}$$

Rejecting quadratic and higher power terms we have

$$(2) \quad n = 1 + 0,000\ 079 \frac{p}{T_0 T_1} \cdot \Delta T$$

in which  $\Delta T$  = temperature difference.

Expressing the pressure in mm of mercury

$$(2a) \quad n = 1 + 0,000\ 105 \frac{p}{T_0 T_1} \cdot \Delta T.$$

For constant pressure (1013 mb or 760 mm)

$$n = 1 + 0,079\ 99 \frac{\Delta T}{T_0 T_1}.$$

We have calculated the refractive indices for temperature differences  $\Delta T$  of  $5^\circ$ ,  $10^\circ$ ,  $15^\circ$  and so on for temperatures at the ground ranging from  $-50^\circ \text{ C}$  to  $+40^\circ$  and the critical angles for each  $\Delta T$ . Fig. 1 represents the results graphically. The abscissae indicate the ground temperatures, the ordinates those at the boundary from  $+40^\circ$  to  $-50^\circ$ . The difference between abscissa and ordinate indicates the temperature jump at the

boundary. The inclining lines connect points with equal critical angle for steps of  $5'$  between  $89^\circ 15'$  and  $90^\circ$ .

The figure shows the critical angle to be more than  $89^\circ$  even for extreme temperature differences amounting to  $90^\circ$ . Therefore it is clear that explanation of the phenomenon by refraction only, caused by temperature differences, is quite impossible (LITTROW; see PERNTER-EXNER, ref. 6, p. 68).

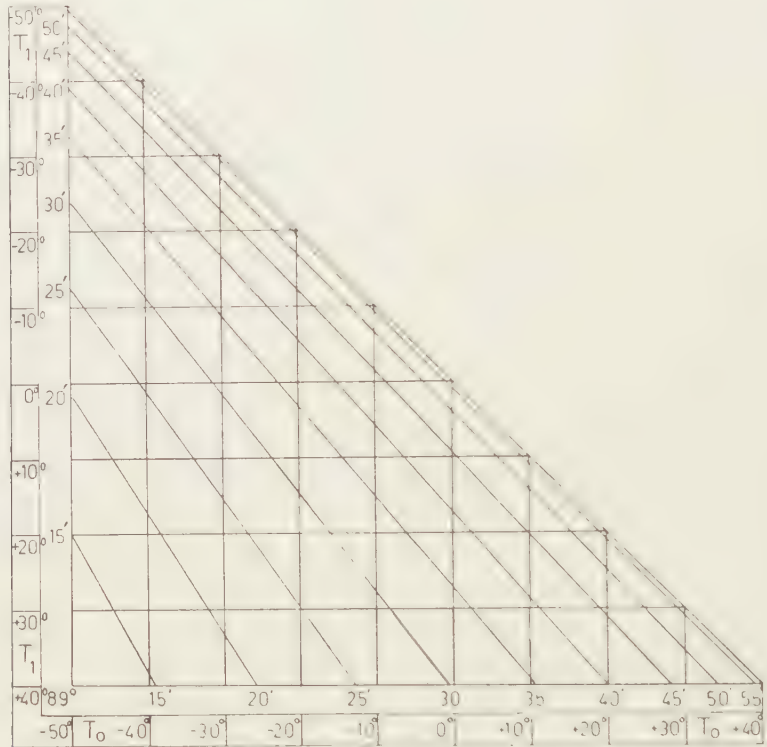


Fig. 1

2.5. We have now found relations between the height  $H$  and the critical angle (Table 1) and between the critical angle and the temperature difference (fig. 1). From these data we have derived graphically the desired relation between the height and the temperature difference for all surface temperatures from  $-50^\circ$  to  $+40^\circ$ . The results cannot yet serve us, because they hold good only for our fictive atmosphere. We only give the data for  $0^\circ\text{C}$  as an example.

TABLE 3  
Height and temperature differences for fictive atmosphere

height in m . . . .	50	100	150	200	250	300	350	400
temp. difference in $^\circ\text{C}$	7,3	15,0	23,5	33,0	43,0	53,9	66,3	81,0

2.6. We now proceed to the application of the necessary corrections.

a. *Pressure.* How to change the temperature when the pressure is normally decreasing, in order that the refractive index or, which is the same, the density remains unchanged? The last question which also arises in other meteorological investigations, leads to an atmosphere with a temperature-lapse rate of  $-3,42^{\circ}\text{C}$  per 100 m, the so called "homogeneous atmosphere".

b. *Temperature.* We assume dry-adiabatic conditions with the temperature-lapse rate of  $-1^{\circ}\text{C}$  per 100 m.

c. *Humidity.* When considering wet adiabatic conditions we have to take a smaller lapse-rate, but the difference may be neglected at the very low temperatures in the arctic regions.

The result is that we have to apply a lapse-rate of  $3,42 - 1,00 = 2,42^{\circ}$  per 100 m, which must be subtracted from the above-mentioned graphically deduced temperatures (2.5). So the critical temperature differences dependent on the height and the surface temperature have been found. See Table 4 and fig. 2.

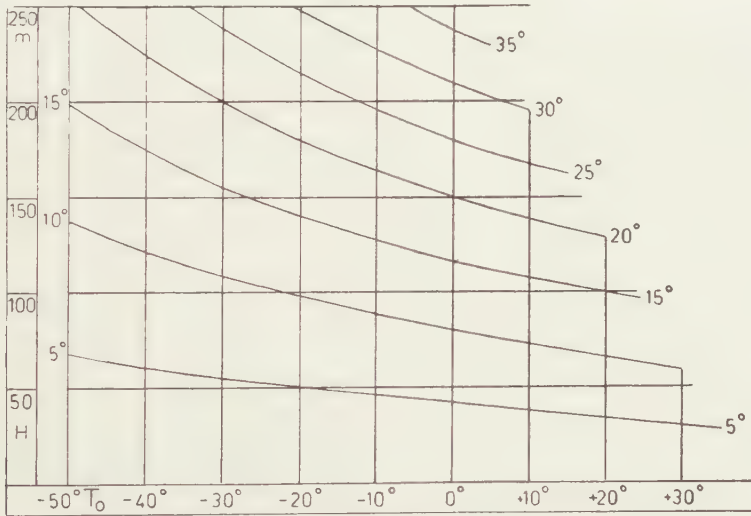


Fig. 2

We see that the temperature differences are considerably smaller at very low temperatures than at high ones:  $8,1^{\circ}$  at  $-40^{\circ}\text{C}$ ,  $15,2^{\circ}$  at  $+20^{\circ}$ .

TABLE 4  
Critical temperature differences

H	surface temperatures									
	- 50	- 40	- 30	- 20	- 10	0	+ 10	+ 20	+ 30	+ 40
250	19,7	23,1	26,5	30,0	33,5	36,9				
200	15,1	17,6	20,2	22,8	25,6	28,2	31,2			
150	10,9	12,6	14,4	16,2	18,0	19,9	21,8	23,8		
100	7,2	8,1	9,1	10,2	11,4	12,6	13,9	15,2	16,5	
50	3,8	4,2	4,6	5,0	5,5	6,1	6,8	7,6	8,5	9,5

The conditions for the development of the Novaya-Zemlya phenomenon are most favourable at low temperatures; it must be especially a phenomenon of the arctic regions.

3. *The investigations of Wegener.* ALFRED WEGENER [9] has studied the same atmospheric conditions occurring during deformations of the disk of the sun at low heights above the horizon.

3.1. He followed the instructions of practical geodesy. The curved light-ray may be considered to be the arc of a circle, under normal atmospheric conditions with radius  $\varrho = 6,5 R$ ,  $R$  being the radius of the earth, or

$$k = R/\varrho = 0,13.$$

According to experience the curvature is larger for the abnormal optical phenomena and therefore WEGENER applied  $k=0,5$  and  $k=0,2$ . He stated that  $p/T_0T_1$  (equation 2a) for  $p = 750$  and  $T_0 = 273$  nearly equals 0.01

$$\text{hence} \quad \Delta T = 10^6 (n - 1).$$

This approximation, however, is not allowed, least of all for other temperatures and pressures. He has given the following example (table 5).

TABLE 5  
Wegener's approximation

$10^6 (n - 1)$	$t_1 - t_2$	error
2,1	2	+ 0,1
5,2	5	+ 0,2
10,3	10	+ 0,3
15,2	15	+ 0,2
19,9	20	- 0,1
24,4	25	- 0,6
28,8	30	- 1,2

We have added the figures below the horizontal line and WEGENER's errors, amounting to more than  $1^\circ$ .

WEGENER calculated the left hand part of the next table for  $T_0 = 273$  and  $p = 750$  mm and assumed the results to be "offenbar näherungsweise" equal to the temperature difference at the inversion. I have added the values for  $k = 0,13$  and the right part of the table containing the conditions needed for 760 mm at  $0^\circ \text{C}$ .

TABLE 6  
Critical values after Wegener

Minimalwerte für $10^6(n - 1)$			for 760 mm		Table 4	residuals
$k = 0,5$	$k = 0,2$	$k = 0,13$	correction	corrected		
15,7	25,1	27,3	+ 0,5	27,8	28,2	- 0,4
11,8	18,8	20,5	+ 0,1	20,4	19,9	+ 0,5
7,3	12,6	13,7	+ 0,4	13,3	12,6	+ 0,7
3,9	6,3	6,8	- 0,4	6,4	6,1	+ 0,3



The values of table 4 have been added at the right hand side of table 6. The residuals are small, in the mean  $+0,3^{\circ}$ , and must be attributed to small differences in the method made use of by me and by WEGENER.

3.2. There is an important difference with the real conditions in the free atmosphere, since, a ground inversion being present, the temperature does not change in the way accepted thus far. As a rule the temperature rises from the surface of the earth up to the level where the temperature-decrease starts. Assuming the earth to be flat this feature does not make a difference; for parallel layers with different refractive indices the refraction depends upon the differences between the lowest and the highest layers. PERNTER (ref. 6, p. 63) has calculated for this case a minimum lapse-rate of  $11^{\circ}/100$  m at  $0^{\circ}$  C. With the spherical earth the curvature of the rays must be greater and this is accounted for by the enlarged lapse-rate amounting to  $12,6^{\circ}$  as derived above. But then, also in this case of the spherical surface of the earth with concentric air layers the refraction depends on the temperature difference between the lowest and the highest layers only.

#### 4. *Meteorological considerations*

The last word rests with the meteorologist.

4.1. Is an extension of the ground-inversion up to a distance of  $4^{\circ}$ , more than 400 km, as is necessary for the observation of January 24, 1597, acceptable? We have to do with a frozen and snow-covered sea-surface from Novaya Zemlya to the Siberian coast along a distance of 300 km and farther to the south with a snow-covered plain. Here lies the source-region of the arctic air masses and the atmospheric circumstances are specially favourable for the development of an extended ground-inversion. Furthermore the polar night was still uninterrupted and the temperature-increase upward may develop in an undisturbed fashion.

4.2. Are the temperature jumps needed at 100 m or corresponding lapse-rates admissible ( $12,6^{\circ}$  at  $0^{\circ}$  C,  $8,1^{\circ}$  at  $-40^{\circ}$ )? They are vigorous but beyond doubt possible. This compels us to deal with our last question.

4.3. May we find such temperature-conditions amongst modern meteorological observations? I had two series of observations at my disposal, one from Siberia and one from Greenland.

a. *Siberia*. From the incomplete daily weather reports of three aerological stations on the north coast of Siberia opposite Novaya Zemlya during the winter months 1949–1952 nine observations of ground-inversions could be gathered; Marian Mar ( $67\frac{1}{2}^{\circ}$  N,  $53^{\circ}$  E, numbers 6 and 7 of fig. 3), Dikson ( $73\frac{1}{2}^{\circ}$  N,  $80^{\circ}$  E, the numbers 3 and 8), and Cap Chelidskin ( $78^{\circ}$  N,  $105^{\circ}$  E, the numbers 1, 2, 4, 5 and 9). The position of "Behouden Huys" was  $76^{\circ}$  N and  $69^{\circ}$  E.

These observations have been plotted in the upper part of fig. 3. The abscissae represent the temperature-differences with the surface temperature (average  $-32,7^{\circ}$  C), the ordinates the pressure-differences with the surface

pressure (average 1030 mb). The drawn lines refer to the months of December and January, the dash-lines to February in which month the sun is daily rising above the horizon. The curve through the origin represents the critical line for total reflection, constructed for the average

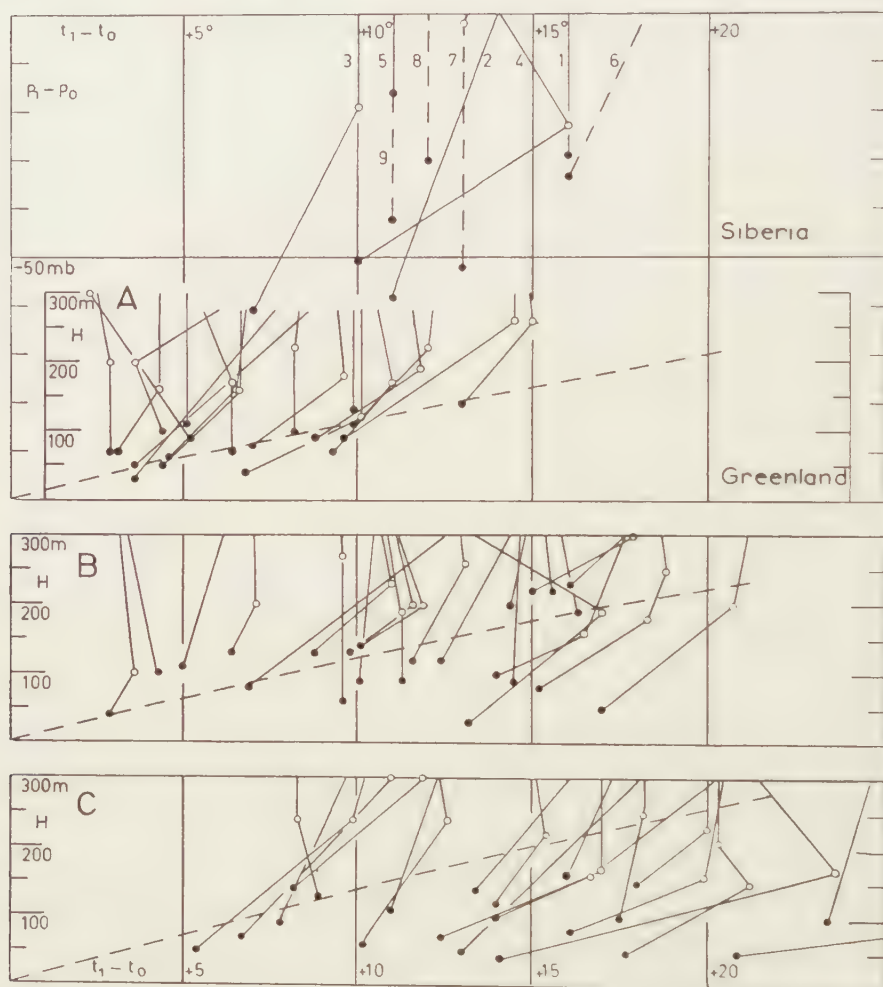


Fig. 3

temperature. The upper air-observations start only at pressure lapses between  $-40$  and  $-50$  mb (heights between 280 and 300 m). Therefore a considerable uncertainty is present in the lower 300 m, but we need not violate some of the diagrams (2, 7, 1) when extending them to the origin by curves approaching the critical line.

b. *Greenland.* The observations on Greenland are those of the French expedition led by P. E. VICTOR in the years 1949-1951 [1]. The station was situated in Central Greenland ( $70^{\circ} 55' N$ ,  $40^{\circ} 38,4' W$ , 2993 m above sealevel). For each sounding by radiosonde the characteristic

points of the registration and their heights above the station have been published (starting at 30 m). We have studied 73 of them out of a total of 190, 40 giving good results. They always refer to observations in arctic air in the months October to March. The surface temperatures run from  $-28,0^{\circ}\text{C}$  to  $-58,2^{\circ}$ . We have divided them in three groups: A, from  $-28,0^{\circ}$  to  $-37,5^{\circ}$  (mean-temperature of 9 cases  $-34,5^{\circ}$ ), B, from  $-38,2^{\circ}$  to  $-47,0^{\circ}$  (mean-temperature  $-42,6^{\circ}$ , 12 cases), C, from  $-48,0^{\circ}$  to  $-58,2^{\circ}$  (mean-temperature  $-52,1^{\circ}$ , 19 cases). From these three groups a number of observations (totally 62) have been plotted in fig. 3 up to 300 m.

Group A concerns temperatures equalling approximately those of Siberia. The observations have been plotted in the upper part of the figure with the Siberian ones and at the same height-scale. Groups B and C have been represented in the central and the lower part of the figure. All diagrams start at their lowest characteristic points, indicated by black spots. The first part beginning in the origin has been omitted. Groups B and C contain also the critical lines constructed for the average temperature of the group. Where the inclination of the diagram is less than that of the critical line total reflection occurs. Obviously this is the case only in the lowest air-layer before the first nod in the diagram. Higher on total reflection is no longer possible though the inversion proper has not yet been reached. In the groups B and C the number of favourable cases is notably large. All Greenland groups show strong inversions especially at the lowest surface temperatures. In a good number of cases the first nod lies considerably high: we found 11 of them between 30 and 60 m, 18 between 70 and 100 m, 8 between 110 and 140 m, 3 between 150 and 190 m.

In the upper part the Siberian and Greenland observations suit remarkably well. We should not, however, attach too much value to this feature because the circumstances differ considerably, Siberia having a sea-level climate, and Greenland a highland climate at 3000 m with strong outward radiation stimulating very low ground temperatures. On the other hand the cold air above the sea stagnates whereas in the highland it will flow down hampering the formation of a ground inversion. Yet, as summed up above well developed inversions upward to 190 m occur in Greenland.

5. *Conclusions.* As the result of the investigation we arrive at the conclusion that the Novaya-Zemlya phenomenon may be explained fairly satisfactorily. Neither the theory of optics, nor meteorological evidence are opposed to our conclusion.

The Novaya-Zemlya phenomenon is caused by repeated total reflection at the upper boundary of a ground inversion. In accord with the laws of optics the vertical temperature-distribution must be a definite increase upward depending on the surface temperature and the height of the inversion above the surface. The conditions are most favourable in the arctics and the

phenomenon must be confined to the polar regions. Yet here too it must be rare. An important deviation of the position of the sun from normal requires a ground inversion along a large distance, amounting to 90 km for each three-days deviation in sun-rise; it must be situated above a plain area (sea-surface) in the direction of the sun. The temperature must rise upward considerably, 7 to 9° at 100 m, for temperatures at the ground of -50 to -30°. For this a calm atmosphere and a clear sky are needed. Finally it is visible only during two short time intervals at the beginning and at the end of the polar night.

The meteorological researches showed the necessary temperature-conditions to be present in a good number of cases on the highland of Greenland. Here, however, the topographical features are unfit for a good development of the phenomenon. Also the position of the Siberian stations is unfavourable because the surface in southern direction is not as plain as required. Though the material at hand is not sufficient to allow a definite conclusion concerning the development of good inversions at sea-level we may on good grounds accept their possibility.

#### *6. Shackleton's observations*

p. 49. The sun which had made "positively his last appearance" seven days earlier, surprised us by lifting more than half its disk above the horizon on May 8. A glow on the northern horizon resolved itself into the sun at 11 a.m. that day. A quarter of an hour later the unseasonable visitor disappeared again, only to rise again at 11.40 a.m., set at 1 p.m., rise at 1.10 p.m. and set lingeringly at 1.20 p.m. These curious phenomena are due to refraction, amounted to 2° 37' at 1.20 p.m. The temperature was 15° below zero Fahrenheit, and we calculated that the refraction was 2° above normal. In other words, the sun was visible 120 miles farther south than the refraction tables gave it any right to be. The navigating officer naturally was aggrieved. He had informed all hands on May 1 that they would not see the sun again for seventy days and now had to endure the jeers of friends who affected to believe that his observations were inaccurate for a few degrees.

p. 56. Just before noon today (July 26) the top of the sun appeared by refraction for one minute, seventy-nine days after our last sunset. A few minutes earlier a small patch of the sun had been thrown up on one of the black streaks above the horizon.

The positions of the "Endurance" were on May 2nd 75° 23' S, 42° 14' W, on August 1st 72° 26' S, 48° 10' W. The table contains the positions of the ship on May 8th and July 26th, estimated on the map of the voyage, the geographical latitude where the sun just reaches the horizon, corrected for normal atmospheric refraction and the difference with the ship's position.



Position		Geographical latitude of sun in horizon	Difference with position
May 2nd	75° 23'	75,6°	+ 0,2°
May 8th	75,5°	73,6°	+ 1,9° Shackleton 2°
July 26th	72,5°	71,0°	+ 1,5°
August 1st	72° 26'	72,2°	+ 0,2°

Also on July 26th an important deviation occurs, the sun becoming visible 5 days before the normal day.

The question whether we have to do with the Novaya-Zemlya phenomenon leads to the question of the reliability of the ship's position. As appears from the report of JAMES sufficient care has been bestowed on the measurements to avoid errors caused by abnormal refraction. We may attribute the differences for a small part only to errors in the ship's position and we conclude that indeed SHACKLETON and his crew must have seen the Novaya-Zemlya phenomenon.

The observations of the Dutch of 1597 find their best confirmation in the Weddell-sea observations of 1915.

#### REFERENCES

1. BEDEL, B., Les observations météorologiques de la station française du Groenland. Conditions atmosphériques en altitude du 17 sept. 1949 au 10 août 1951. Expéd. pol. franç. missions P.-E. Victor. Expéd. arct. Rés. scient. No N V, Paris, 1954.
2. *Encyclopaedia Britannica*, Arctic regions, 2, 107 (1936).
3. KEPLER, J., *Ad Vitellionem paralipomena, quibus astronomiae pars optica traditur*. Francfort 1604. De observatione Hollandorum in alto septentrione. (W. von Dyck u. M. Caspar, *Gesamm. Werke*, Band 2, 128-132, München 1939).
4. LORENTZ, H. A., *Verh. Kon. Ned. Akad. v. Wet. Amsterdam*, 18, (1878); *Wied. Ann.* 9, 641 (1880).
5. NOUHUYS, J. W. VAN, *Het Nova-zembla-verschijnsel*, Voordracht Bat. Gen. Proefond. Wijsbeg. (Rotterdam, 2 februari 1930).
6. PERNTER, J. M. und F. M. EXNER, *Meteorologische Optik* (2. Auflage, 1922).
7. SHACKLETON, E., *South—the story of Shackleton's last expedition 1914-1917* (London, 1920).
8. VEER, G. DE, *Reizen van Willem Barentz, Jacob van Heemskerck, Jan Cornelisz Rijp en anderen naar het noorden (1594-1597)*. Edited by S. P. L'Honoré Naber, *Linschoten-vereeniging*, XV (1917). *English translation*, Hackluyt Society (1853).
9. WEGENER, A., *Elementare Theorie der atmosphärischen Spiegelungen*, *Ann. der Phys.* 4. Folge, 57, 203-230 (1918).

HETEROSTEGINES DU MIOCENE DE L'ANGOLA

PAR

A. J. WISSINK<sup>1)</sup>

(Communicated by Prof. I. M. VAN DER VLIERK at the meeting of April 28, 1956)

Par l'intermédiaire de M. le Professeur UBAGHS de l'Université de Liège, qui fournissait les matériaux, j'avais l'occasion d'étudier une collection de Foraminifères miocènes, originaires de l'Atoquéro près de Porto Amboim, Angola.

Il s'avérait qu'à l'aide des Foraminifères il était possible de distinguer entre une partie inférieure avec une Heterostegine primitive dont les cloisons secondaires ne se sont pas développées entièrement et une partie supérieure avec une Heterostegine beaucoup plus développée, dont les cloisons secondaires ne sont courtes que par exception.

Les Heterostegines dont les cloisons secondaires restent courtes ont déjà été décrites par plusieurs auteurs comme des Operculines, mais je suis d'avis, que, pour éviter des confusions, il vaut mieux se servir de la classification proposée par PAPP et KÜPPER (1954) et, par conséquence, les décrire comme des Heterostegines.

DESCRIPTION

Pour l'explication des expressions c.n.,  $W_3W_4/W_1W_2$  et d.o. je me permets de renvoyer le lecteur à la thèse de BANNINK (1948).

*Heterostegina costata levitesta* PAPP et KÜPPER

Le test est très plat, égal, avec une spire à accroissement rapide. Les cloisons secondaires se développent dès le deuxième tour. En général elles restent courtes, mais par endroits on en voit quelques unes, qui se sont développées entièrement. Il n'était pas possible de distinguer entre une forme A et une forme B.

Loge initiale: 90-140 microns.

Diamètre du 2<sup>e</sup> tour: 1140-1500 microns.

Diamètre du 3<sup>e</sup> tour: 3450-5200 microns.

Les cloisons sont au nombre de 12-15 sur le 2<sup>e</sup> tour.

Les cloisons sont au nombre de 21-28 sur le 3<sup>e</sup> tour.

c.n.: 0.53-0.8  $W_3W_4/W_1W_2$ : 7-8 d.o. 0.25.

Vu le développement des cloisons et la surface égale, cette espèce est identique à *Heterostegina costata levitesta* PAPP et KÜPPER. Elle se distingue de *Operculina beneyidea* DACT par l'absence d'ornementation.

<sup>1)</sup> La Direction de la Compagnie Financière Belge des Pétroles a libéralement consenti à la publication de cette note; je l'en remercie sincèrement.

*Heterostegina complanata spiralis* PAPP et KÜPPER,  
 faisant transition vers  
*Heterostegina complanata sculpturata* PAPP et KÜPPER

Le test est très plat, avec une spire à accroissement très rapide. La spire montre un épaississement net. Les cloisons secondaires se développent dès la première cloison primaire et ne sont courtes que par exception. La surface peut être égale ou ornementée avec des granules le long des cloisons.

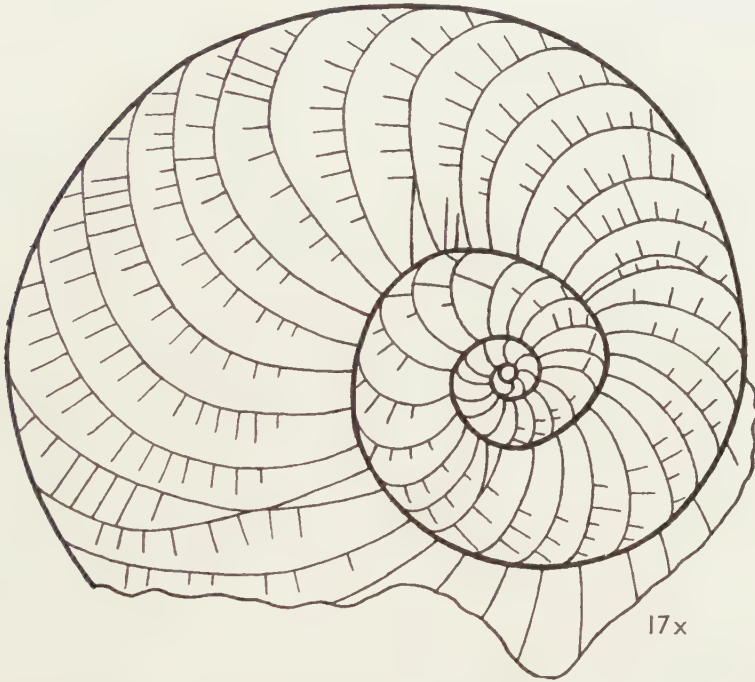


Fig. 1. *Heterostegina costata levitesta* PAPP ET KÜPPER Porto Amboim, Angola

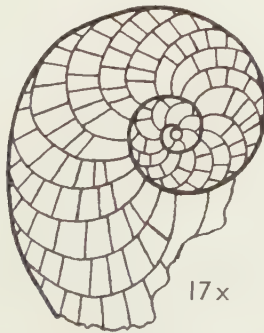


Fig. 2. *Heterostegina compl. spiralis* PAPP ET KÜPPER faisant transition vers  
*Heterostegina complanata sculpturata* PAPP ET KÜPPER. Porto Amboim, Angola

Loge initiale: 120–240 microns.

Diamètre du 2<sup>e</sup> tour: 1350–5160 microns.

Les cloisons sont au nombre de 15–22 sur le 2<sup>e</sup> tour.

c.n.: 0.9–1.2.  $W_3W_4/W_1W_2$ : 12–15. d.o.: peu important.

Vu le développement des cloisons, de la surface et de la spire, cette espèce fait transition de *Heterostegina complanata spiralis* PAPP et KÜPPER vers *Heterostegina complanata sculpturata* PAPP et KÜPPER.

#### BIBLIOGRAPHIE

- BANNINK, D. D., Een Monografie van het genus *Operculina* d'Orbigny 1826. Thèse Leiden (1948).
- DACI, A., Description d'*Operculina benevidea* nov. sp. Comunicacoes dos Servicos Geológicos de Portugal, 35 (1954).
- PAPP, A. et K. KÜPPER, Über die Entwicklung der Heterosteginen im Torton des Wiener Beckens. Anzeiger der math.-naturw. Klasse der Österreichischen Akademie der Wissenschaften, Nr. 10 (1952).
- et ———, The genus *Heterostegina* in the Upper Tertiary of Europe. Contributions from the Cushman Foundation for Foraminiferal Research, 5, Part 3 (July, 1954).



# ON THE THEORY OF EMISSION LINES IN EXPANDING NEBULAE

BY

H. ZANSTRA

*(Circular No. 10 of the Astronomical Institute of the University of Amsterdam)*

*(Communicated at the meeting of May 26, 1956)*

## *Summary*

The ratio of the radiation produced to the radiation emitted by a volume element of an expanding nebula or gaseous envelope in any spectral line was derived in 1947 by SOBOLEV for a rectangular thermal Doppler profile with redistribution. It is now found to be approximately the same for a Maxwell Doppler profile with redistribution, provided the expansion is rapid enough. Applications made in 1947 by SOBOLEV to the relative intensities and shapes of emission lines in bright line stars can therefore be maintained from this point of view.

For radiation pressure of Lyman alpha radiation in an expanding nebula the situation appears to be much more involved and one cannot state that the rectangular profile used by SOBOLEV in his Chapter III would lead to the same results as the Maxwell profile, even for rapid expansions.

## 1. *Introduction*

In 1947 SOBOLEV <sup>1)</sup> published a treatise on moving envelopes of stars which constitutes an important and probably decisive step in the development of the subject of expanding envelopes of stars and of expanding nebulae. Among other things he introduced the extremely fruitful idea of considering the radiation which ultimately escapes from the nebula in a certain spectral line as a leakage which results inside the nebula in a corresponding excess of emission over absorption in this line, provided the expansion is sufficiently rapid. Stated otherwise, for any line there is an energy production inside the nebula which is equal to this excess and of which the equivalent ultimately escapes, which is the way in which we shall look upon it in the next sections.

Further he pointed out that the Doppler effect due to the thermal motion of individual atoms should lead to the re-emitted frequency being

---

<sup>1)</sup> V. V. SOBOLEV, Moving envelopes of stars, Publ. of the Leningrad State Univ. of the order of Lenin (Leningrad, 1947) (in Russian).

different from the absorbed frequency. This he took approximately into account by the assumption that any frequency absorbed would, upon re-emission in the same line, be redistributed in frequency with a probability proportional to the absorption coefficient  $\alpha_\nu$  for the line in question. This may be called non-coherent scattering with complete redistribution, or briefly scattering with redistribution. More generally one may say that any re-emission, not necessarily by scattering, takes place with complete redistribution, as he also assumes. However, he approximates the line profile of absorption coefficient by a rectangular profile of half-width corresponding to the mean thermal velocity, and the emission in a volume element is thus simply spread out uniformly across the profile.

The first discussion of LYMAN  $\alpha$  radiation in an expanding nebula was attempted by the writer in 1934<sup>1)</sup>. Though the main idea that the  $L_\alpha$  density and radiation pressure are cut down by the expansion was qualitatively correct, the treatment was criticized by us in 1938, because "one should consider interaction of individual atoms having velocities of different directions" and it was pointed out that "this will cut down the density and radiation pressure of  $L_\alpha$  still further, probably by a large factor".<sup>2)</sup> It was not until 1949 that the writer, in B.A.N. No. 401,<sup>3)</sup> took this effect into account by introducing scattering with redistribution, as explained above. It was done for an actual thermal profile  $e^{-(\Delta\nu/\Delta\nu_D)^2}$  for Maxwell distribution, but only for a nebula *at rest*. One of the most recent publications of this case is by KOELBLOED<sup>4)</sup> in 1956. He gave an accurate solution for various total optical depths of  $L_\alpha$ . For a review of other work in this connection by various writers the reader may be referred to KOELBLOED's paper and our 1949 paper. However, particular mention should be made of UNNO's work.<sup>5)</sup>

For a nebula *at rest* the situation may be summed up as follows. The case of  $L_\alpha$  density and  $L_\alpha$  radiation pressure for ordinary scattering (i.e. without change in frequency) was treated by AMBARZUMIAN in 1932<sup>6)</sup> and 1933.<sup>7)</sup> He used a rectangular thermal profile, but the result is practically the same for a Maxwell profile with ordinary scattering. The introduction of scattering with redistribution for a Maxwell profile by the writer in 1949 resulted in an enormous cutting down of  $L_\alpha$  density and radiation pressure, the latter by a factor of about 300, as compared with AMBARZUMIAN. The nebula considered has a total optical depth for  $L_c$  radiation (the continuous spectrum beyond the Lyman series)  $\tau$  of about unity.

<sup>1)</sup> H. ZANSTRA, M.N. 95, 84 (1934).

<sup>2)</sup> H. ZANSTRA, The Observatory 61, 295 (1938), p. 297, foot note.

<sup>3)</sup> H. ZANSTRA, B.A.N. 11, 1 (1949), No. 401.

<sup>4)</sup> D. KOELBLOED, B.A.N. 12, 339 (1956), No. 465.

<sup>5)</sup> W. UNNO, Publ. A.S. Japan 3, 160, 178 (1952); 4, 100 (1952); 7, 81 (1955).

<sup>6)</sup> V. A. AMBARZUMIAN, M.N. 93, 50 (1932).

<sup>7)</sup> V. A. AMBARZUMIAN, Bull. de l'Obs. centr. à Poulkovo 13, 3 (1953), No. 114.

Now pass to Sobolev's case of an *expanding* nebula with rectangular  $L_a$  thermal profile, and redistribution. SOBOLEV finds that under those assumptions both the  $L_a$  radiation density and radiation pressure are cut down enormously for an expanding nebula as compared with a nebula at rest. The unsatisfactory point of his treatment however is that he should have used a Maxwell profile, and so his treatment for the nebula at rest is erroneous (see Section 4). But how is it for an expanding nebula? In the present paper the case of an expanding nebula with Maxwell profile and redistribution is treated. The outcome will be that for the  $L_a$  source function and radiation density there is very little difference between the results of rectangular and Maxwell profile, provided the expansion is rapid enough (Sections 2 and 3). This applies, not only to  $L_a$ , but to any kind of transition, as considered at the beginning of this section.

As regards  $L_a$  radiation pressure the situation is much less clear. Some remarks on this question will be made in Section 4.

2. *Expanding nebula: Linear flow,  $v$  proportional to  $s$ ,  $j$  constant, re-emission with redistribution for a Maxwell profile. Resulting  $G/(2j)$  compared with Sobolev's rectangular profile*

In the present section we are treating individual velocities of atoms in an expanding nebula by a method similar to that used in our 1934 paper. However we introduce scattering (or re-emission) with redistribution for a thermal Maxwell profile of the absorption coefficient in the same way as was done for a stationary nebula in our 1949 paper, B.A.N. No. 401. We consider the case of a homogeneous nebula, as SOBOLEV does in his Chapter I, and an expansion proportional to depth. This means that all physical quantities are independent of depth, but the results hold also if they are varying slowly, of which fact SOBOLEV makes use in his applications.

To fix the ideas, we think of scattering of Lyman  $\alpha$  radiation by hydrogen atoms, but the result holds as well for any other spectral line, and for re-emission other than by scattering.

Assuming for the atoms a Maxwell distribution corresponding to a kinetic temperature  $T_1$ , the atomic absorption coefficient at a distance  $\Delta\nu$  from the central frequency  $\nu_0$  is given by the thermal Doppler formula:

$$(1) \quad \alpha_\nu = \alpha e^{-x^2},$$

where

$$(1a) \quad x = \frac{w}{w_D}, \quad (1b) \quad w_D = \sqrt{\frac{2kT_1}{m_A}}$$

$$(1c) \quad \Delta\nu = \nu_0 \frac{w}{c}, \quad \Delta\nu_D = \nu_0 \frac{w_D}{c},$$

$\alpha$  being the absorption coefficient at the line centre,  $w$  the atomic thermal velocity in one direction, and  $m_A$  the mass of the atom. We may call  $w_D$  the thermal Doppler velocity.

Let  $s_g$  be the geometrical depth, reckoned from the inside of the nebula and  $N$  the local number of atoms per  $\text{cm}^3$ . Though the nebula is expanding, we yet define the "optical depth for the line centre" by

$$(2) \quad s = \int N \alpha ds_g = \alpha \int N ds_g.$$

Then, using (1)

$$(2a) \quad ds(\Delta\nu) = e^{-x^2} ds.$$

Now consider a nebula consisting of plane parallel layers, expanding with a velocity  $v$  perpendicular to these layers, and simplify the problem in such a way that only an inward and an outward flow of radiation is considered in the direction of  $v$ , so that  $s_g$  and  $s$  also refer to this direction (see Fig. 1), while the physical situation only depends on  $s_g$  or  $s$ . Let further this velocity of matter in bulk  $v$  be proportional to  $s$

$$(3) \quad v = \frac{dv}{ds} \cdot s$$

with  $dv/ds$  independent of  $s$ . For the sake of convenience we choose  $v$  zero at the inner boundary.

The absolute velocity of individual atoms  $V$  (linear component) is then

$$(4) \quad V = v + w,$$

or, expressing all velocities in the unit  $w_D$

$$(4a) \quad V/w_D = v/w_D + w/w_D = v/w_D + x,$$

using (1a).

In Fig. 1 this quantity  $V/w_D$  is plotted against  $s$ . The central straight line  $OP$ ,  $x=0$ , represents equation (3) and therefore has the slope

$$(5) \quad a = \frac{v/w_D}{s} = \frac{1}{w_D} \frac{dv}{ds} = \frac{1}{c} \frac{v_0}{\Delta\nu_D} \frac{dv}{ds}, \quad x = ay$$

in virtue of (1c). It is flanked by the two full-drawn lines for  $x = +1$  and  $-1$  and the two broken lines  $x = +2$  and  $-2$ , and so one could continue.

Choose an element of matter at central optical depth  $s$ , then the atoms with thermal velocity zero are represented by  $P$  in the diagram. For an observer  $A$  at the inside of the nebula at absolute rest it has the individual velocity  $V = v = s dv/ds$  and emits the frequency

$$(6) \quad \nu = \nu_0 - \frac{V}{c} \nu_0.$$

All atoms observed by him to emit this frequency  $\nu$  have the same individual velocity  $V$  given by (6) and are therefore situated on the line  $AB$ . Using (2a) and (5), the optical depth in  $\nu$  for the portion  $AQ = s - y$  (central) becomes

$$(7) \quad s_\nu = \int_A^Q ds(\Delta\nu) = - \int_A^Q e^{-x^2} dy = \frac{1}{a} \int_x^{x_A} e^{-x^2} dx$$





for the radiation over all frequencies referred to the optical depth of the line centre.

The emerging flux or intensity per frequency unit  $I'_\nu$  for observer  $A$  or  $I_\nu$  for observer  $B$  is given by

$$(10) \quad I_\nu = I'_\nu = \int_{s_\nu=0}^{s_{\nu m}} j_\nu e^{-s_\nu} ds_\nu,$$

where  $I'_\nu$  is towards the left and  $I_\nu$  towards the right in Fig. 1.

Substituting (9) and the upper limit (7a) and (10), we obtain

$$(11) \quad I_\nu = I'_\nu = \frac{1}{\Delta\nu_D \sqrt{\pi}} j [1 - e^{-s_{\nu m}}] = \frac{1}{\Delta\nu_D \sqrt{\pi}} j \left[1 - e^{-\frac{\nu\pi}{a}}\right].$$

Let the energy produced per  $\text{cm}^3$  be  $G\alpha N$ , that is  $Gds$  per  $\text{cm}^2$  within  $ds$ . For  $ds=1$ , the point  $P$  in Fig. 1 moves to a neighbouring point  $P'$  along the central line, and since the slope of the curve in Fig. 1 is  $a$ , the line  $AB$  moves upward by  $dV/w_D = a$ , corresponding to the Doppler shift for observer  $A$ :  $d\nu = \Delta\nu_D dV/w_D = a\Delta\nu_D$ . Following Sobolev's reasoning (see Section 1) that the energy generated  $Gds$  must flow away in the outward plus the inward emerging flux ( $I_\nu + I'_\nu$ ) $d\nu$ , we have ( $ds=1$ ):

$$(12) \quad (I_\nu + I'_\nu)d\nu = 2I_\nu d\nu = 2I_\nu a\Delta\nu_D = G.$$

Sobolev's principle really holds for the nebula as a whole, but for the homogeneous nebula it can be applied to an element as was done following him.

Substituting (11) in (12), we obtain the *desired ratio of energy produced into energy emitted by a volume element*

$$(13) \quad \frac{G}{2j} = \frac{a}{\sqrt{\pi}} \left[1 - e^{-\frac{\nu\pi}{a}}\right] = \frac{1}{s_{\nu m}} [1 - e^{-s_{\nu m}}]$$

for Maxwell profile.

For a transparent line,  $s_{\nu m} \ll 1$ , we get  $G/(2j) = 1 - \frac{1}{2}s_{\nu m} \simeq 1$ , as is also clear physically.

The most important case is that of an *opaque line*,  $s_{\nu m} \gg 1$ , where (13) and (5) yield

$$(14) \quad \frac{G}{2j} = \frac{a}{\sqrt{\pi}} = \frac{1}{w_D \sqrt{\pi}} \frac{dv}{ds} = \frac{1}{w_D \sqrt{\pi}} \cdot \frac{dv}{\alpha N ds_g}, \quad s_{\nu m} \gg 1.$$

Then  $a \ll 1$ .

Sobolev's case of a rectangular profile with absorption coefficient  $\alpha N$  for the total width  $2w_D$  and zero outside is quite readily worked out directly, as was done by him in his Chapter I. Then  $j = j_\nu 2\Delta\nu_D$  within the line, and one obtains

$$(15) \quad \frac{G}{2j} = \frac{a}{2} [1 - e^{-(2/a)}] \simeq \frac{a}{2} = \frac{1}{2w_D} \cdot \frac{dv}{\alpha N ds_g} = \beta_{ik},$$

where the approximation holds if the nebula is opaque. This is the same as Sobolev's expression for  $\beta_{ik}$  (transition between levels  $i$  and  $k$ ) in his Chapter I holding for linear treatment, if we use  $w_D$  for Sobolev's mean thermal velocity  $u$ . For a transparent line  $G/(2j) = 1 - 1/a \simeq 1$ .

The only difference between the formulae (14) and (15) is the replacement of  $\sqrt{\pi}$  or 1.77 by 2. Replacement of the rectangular by the Maxwell profile would therefore hardly influence the results of Sobolev's Chapter I, in particular the relative populations of levels and the relative intensities of hydrogen lines for bright line stars. As remarked, the application of the formulae is there justified for the main body of the gaseous envelope, since  $G$ ,  $j$  and  $dv/ds$  vary but slowly, by which is meant that the variation is small for an increase of the order  $s_{vm}$  or order  $2/a$ , the portion of the line  $AB$  cut off between the two extreme drawn lines in Fig. 1.

Also Sobolev's discussion of line shapes of bright line stars in his Chapter II is not influenced appreciably if the rectangular profile he uses is replaced by a Maxwell profile.

The equations (1) to (14) hold for any type of line, that is for downward and upward transitions between any two levels of the atom, and for any dilution of the incident stellar radiation. Their operation may be illustrated for the simple case of  $L_a$  scattering in an expanding hydrogen nebula exposed to very dilute stellar  $L_c$  radiation. If the known incident  $L_c$  flux per  $\text{cm}^2$  is  $S_c$ , and  $u$  is the ratio of the  $L_c$  absorption coefficient to the central  $L_a$  absorption coefficient, one has approximately

$$(16) \quad G = \frac{\nu_\alpha}{\nu_c} S_c u e^{-us}$$

for the production of  $L_a$  subsequent on recombination. (Equation (11) of B.A.N. No. 401.) Since the line is sufficiently opaque,  $j$  is then given by (14) and the emerging intensity per frequency unit by (11). Inside the nebula at any  $s$  one has large optical depth in  $\nu$  outward and inward for the portion of the profile which matters for excitation, and then, by a similar reasoning as for (11), one obtains  $I_\nu = I'_\nu = \frac{1}{\Delta\nu_D\sqrt{\pi}} j = j_\nu$  and a radiation density per frequency unit  $u_\nu = (I_\nu + I'_\nu)/c = 2j_\nu/c$ , which in its turn determines the population of level 2 as compared with the ground level 1. All those quantities are indirectly proportional to  $a$  or to the velocity gradient  $dv/ds$  (for the case of dilute  $L_c$  radiation considered) and are therefore cut down more and more when the expansion gets more rapid.

### 3. *Expanding nebula: Radiation all directions*

For the sake of completeness, we now give the treatment taking the direction of the radiation properly into account for the spectral line considered.

The radiation emitted per  $\text{cm}^3$  per second is then  $4\pi\lambda NJ$ , evenly in all

directions, where we use a capital  $J$ . We can then consider Fig. 1 to apply to the inward and outward radiation in a certain fixed direction in the element of solid angle  $d\Omega$  and replace  $j$  in (8) by  $Jd\Omega$ ,  $j_v$  in (9) by  $J_v d\Omega$  and  $I_v$  or  $I'_v$  in (10) by  $I_v d\Omega$  only. Then  $J_v$  is the source function per unit frequency, which is independent of direction and  $I_v$  the emerging intensity per unit frequency per unit solid angle, which in general depends on direction.

The energy produced per  $\text{cm}^3$  is defined by  $\alpha NG$ , as before. Then condition (12) passes into

$$(12') \quad \int I_v a \Delta v_D d\Omega = G,$$

the integration for  $\Omega$  taking place over the whole sphere.

Now however  $s_{vm}$ , i.e.  $\sqrt{\pi}/a$  depends on direction. Then (13) passes into

$$(13') \quad \frac{G}{4\pi J} = \frac{1}{\sqrt{\pi}} \int a \left[ 1 - e^{-\frac{\sqrt{\pi}}{a}} \right] \frac{d\Omega}{4\pi},$$

or, for an opaque line,  $s_{vm} \gg 1$ , or  $a/\sqrt{\pi} \ll 1$ , for all directions

$$(14') \quad \frac{G}{4\pi J} = \frac{1}{\sqrt{\pi}} \int a \frac{d\Omega}{4\pi} = \frac{1}{w_D \sqrt{\pi} \cdot \alpha N} \int \frac{dv}{ds_g} \frac{d\Omega}{4\pi}, \quad s_{vm} \gg 1.$$

For *isotropic expansion*  $dv/ds_g$  is independent of direction, and the ratio of energy produced to energy emitted by a volume element is the same as (14). Other cases were considered by SOBOLEV. His case of radial outflow with constant velocity is interesting, since there is no expansion in the radial direction and the maximum expansion occurs perpendicular to the radius, in which direction also the intensity of escaping radiation is maximum.

#### 4. *Remarks on $L_\alpha$ density and radiation pressure in static and expanding nebulae*

Consider the case of a hydrogen nebula as discussed at the end of Section 2, and let the optical depth  $\tau$ , or  $us$ , for  $L_c$  radiation be appreciable, say unity for the whole nebula.

In his Chapter III SOBOLEV has worked out this case rigorously, using a rectangular profile with redistribution, both for an expanding nebula and for a nebula at rest, or with zero velocity gradient.

Now first take the nebula at rest with constant kinetic temperature, that is constant thermal width. Then a rectangular profile gives the same result for  $L_\alpha$  scattering with redistribution as for ordinary  $L_\alpha$  scattering, and then, as remarked in Section 1, the source function or the radiation density is entirely erroneous, being much larger than under the correct assumption of a Maxwell distribution. For this case Sobolev's solution is



therefore not correct.<sup>1)</sup> The main outcome of our paper is now that, when the nebula expands, the discrepancy between the source function for rectangular and Maxwell profile becomes less glaring until, for rapid expansion there is practically no difference. The position at present is therefore that we have the correct  $J$  for the two extreme cases of a nebula at rest (Koelbloed's solution) and rapidly expanding, and in the future one might attempt to link up these two extremes by a reasonable approximation for intermediate cases.

SOBOLEV has also worked out the  $L_a$  radiation pressure. Here again, the rectangular profile he uses gives wrong results for a nebula at rest, while the correct radiation pressure for a Maxwell profile is now known from the work of 1949 and later reviewed in Section 1. We had considerable hope that for rapid expansion his radiation pressure would become about the same as for Maxwell profile. In fact, we derived expressions for it for the case of linear flow, but they involve a double integral over rather complicated functions, and it did not appear possible to reduce them to simple formulae which could be compared with the results for a rectangular profile. Nor is it easy to get a numerical solution by quadrature, and it is doubtful whether it is worth while to pursue this further.

We wish to express our special thanks to Dr. SERGEI I. GAPOSHKIN for providing us with the English translation of Sobolev's 1947 treatise carried out by him in collaboration with Dr. CECILIA H. P. GAPOSHKIN and Miss JANE A. CONNELL.

---

<sup>1)</sup> When writing our 1949 paper B.A.N. No. 401 we did not know that SOBOLEV had used a rectangular profile and thought from information available, that his treatment for a nebula at rest might be correct. This is not the case, and we wish to withdraw the corresponding statement made there.

BIOLOGICAL PROCESSES IN THE ESTUARINE ENVIRONMENT

VIII. IRON BACTERIA AS GRADIENT ORGANISMS

BY

L. G. M. BAAS BECKING, E. J. FERGUSON WOOD AND I. R. KAPLAN <sup>1)</sup>

(Communicated at the meeting of June 30, 1956)

SUMMARY

(1) Iron bacteria develop only where there is a sudden increase in the electrode potential of the milieu; they are "gradient-organisms".

(2) This fact was first recognized by PRINGSHEIM (1949) and by VAN BENEDEN (1951) and we could confirm this work, extending it by using a freshwater as well as a marine milieu. Aeration of water that has percolated through a layer of mud showed, at the point of aeration, a development of iron bacteria, often in a surprisingly short time.

(3) If sulphate reduction occurs in the mud and the effluent contains  $H_2S$  or (and)  $SH^-$ , *Thiothrix*, *Thiovulum*, and *Beggiatoa* may appear. These organisms also require a steep change of the electrode potential, but at a lower level than the iron bacteria.

(4) There is evidence to assume that hydrogen is generated during the oxidation of the percolates.

(5) The pH-Eh limits of iron bacteria, based upon 23 sets of measurements, are outlined.

INTRODUCTION

A long overdue revival of the interest in iron bacteria has taken place in the last decade. The taxonomic situation, which was chaotic, has been cleared up by PRINGSHEIM (1949) who has reduced the number of genera to two, to wit *Sphaerotilus* (Kützing 1833), synonymous with both *Leptothrix*, *Cladothrix* and, perhaps, with *Crenothrix*; and *Gallionella* (Ehrenberg 1836), synonymous with *Toxothrix* and *Spirophyllum*. The coccoid forms, such as *Siderocapsa*, seem insufficiently studied to be included in the iron bacteria. While many forms of *Sphaerotilus* may be cultured on organic media, *Gallionella* has thus far defied attempts at pure culture (TEICHMANN 1935, cited by PRINGSHEIM, has apparently come close to this, however). The work of TEMPLE and COLMER (1951), who obtained, at low pH, a pure culture of *Thiobacillus ferrooxidans*, has shown the relation of *Thiobacteria* and iron bacteria, which seems also

<sup>1)</sup> C.S.I.R.O. Division of Fisheries and Oceanography, Cronulla, N.S.W.

to hold for *Crenothrix*, as the growth of this organism may be stimulated by reduced S-compounds.

#### OCCURRENCE IN SEAWATER

Although the authors have repeatedly observed both *Sphaerotilus* and *Gallionella* in brackish water, in seawater, and in brines, confirming the observations of PERFILIEV (1927), BUTKEVITCH (1928), and CHOLODNY (1931), this fact is not generally recognized. PRINGSHEIM (1952) states (p. 214): "No iron organisms are known to occur in seawater, which precipitates humus substances and other complex-forming agents and in which ferrous bicarbonate does not seem to be found owing to the alkaline reaction and the presence of too large concentrations of magnesium and calcium salts".

BAAS BECKING and MACKAY (1956) called attention to pectin derivatives as chelating agents and while we have observed a positive pectin reaction in the sheaths of *Sphaerotilus* it may well be that the ferrous salts (whether bicarbonate, carbonate, or hydroxide) are directly absorbed by the sheaths and that therefore the organisms will be independent of ferrous ion and, consequently, of pH. Moreover, at the pH of seawater, the bicarbonate ion is at maximum concentration. So there is no reason to suppose that ferrous bicarbonate will not be present. The noxious effect of calcium salts, also claimed by VAN BENEDEN (1951) does not seem to exist in seawater (antagonism?). Moreover, VAN BENEDEN himself observed development of iron bacteria at pH 7.7. It should be remembered also that marine muds are often quite acid (down to pH 5.1, Port Hacking, South-west Arm, March 1956). From this paper it will appear that iron bacteria can actually develop in seawater.

#### OXIDATION GRADIENTS

PRINGSHEIM (1949) was the first to recognize the importance of this gradient. He states (p. 215) "organisms dependent on the oxidation of ferrous compounds can live only in the very zone, narrow though it may be, where ferrous iron and oxygen meet. From this it appears that their capacity for multiplication depends not on the total amount or concentration of iron compounds found by analytical methods but on the reduction-oxidation potential and the intensity with which such chemical transformations take place". VAN BENEDEN (1951), although apparently ignorant of these considerations, obtained copious cultures of *Sphaerotilus* from soils percolated by the mineral water of Spa and subsequently oxidized in the air.

The idea of the gradient is already implicit in Winogradsky's classical paper of 1888, but never properly realized as such (WINOGRADSKY (1949).

Our field observations confirm Pringsheim's ideas. The following cases will illustrate this:

- (a) At Palm Cave, near Warrah, in the Hawkesbury sandstone, a

formation of iron stalactites and stalagmites occurs (Fig. 1). At the surface of these structures as well as in the drip water *Gallionella* is found in the winter months. The oxidized iron, occurring in the topsoil burdening the

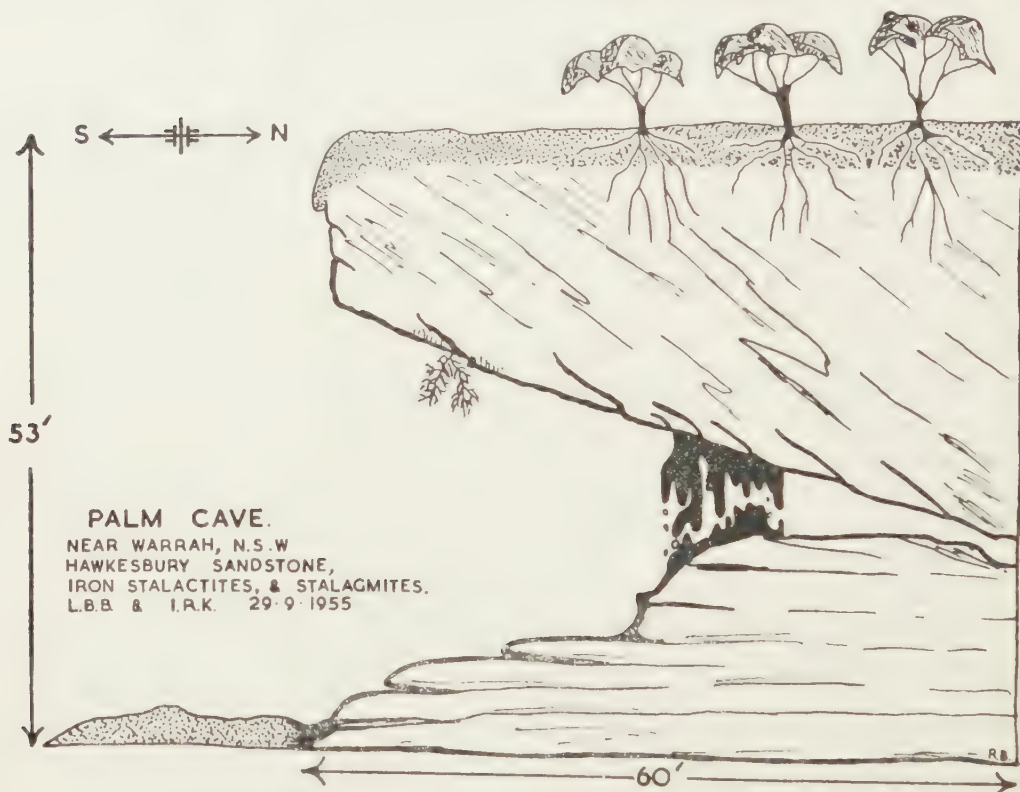


Fig. 1

sandstone, is reduced at the rhizosphere of the plants growing in this soil. The roots often penetrate deeply into the underlying sandstone. As ferrous salts (bicarbonate) the iron finally reaches the roof of the cave, where it is oxidized to goethite. As STERRY HUNT (1881) already remarked, the alteration of siderite into limonite is attended by a contraction of 27.5 per cent., whence these bodies are often porous or spongy (we measured an apparent density of 1.48 in a 40 cm long stalactite, weighing almost a pound). The outer layer consists of fairly pure siderite, probably originating from ferrous bicarbonate.

(b) Less conspicuous, but equally illuminating, is the occurrence of *Sphaerotilus* in the Hawkesbury Sandstone region, wherever water issues from between the sandstone layers (Patonga, Dover Heights, Burraneer Bay, Salmon Point, National Park).

(c) *Crenothrix* was observed coating machinery at a manufacturing plant at Matraville, New South Wales. It appeared when cooling water, obtained from deep bores and containing much reduced iron, was aerated in the cooling spray.



(d) At The Hole, Lake Macquarie, water from a *Salicornia* swamp seeps over a reduced mud containing *Desulphovibrio* and *Thiobacillus denitrificans*, and *Gallionella* forms a thick felt at the interface. The Eh profile is: surface of mud +95 mV, 5 cm depth -10 mV, 10 cm depth -55 mV, while in the felt the Eh was +240 mV, the pH varying from 7.1-7.8.

In all cases mentioned bacteria developed only on the spot where the oxidation took place. Even in shallow (so-called aerobic) cultures, containing ferrous salts, most of the culture fluid remains unutilized *as the oxidation proceeds only at the interphase*.

#### EXPERIMENTAL

In order to obtain a more or less controllable gradient both freshwater and marine muds were percolated with freshwater and seawater, fortified with .2 per cent.  $\text{NH}_4\text{Cl}$  and .2 per cent.  $\text{KH}_2\text{PO}_4$  (Fig. 2).  $2\frac{1}{2}$  litre bottles

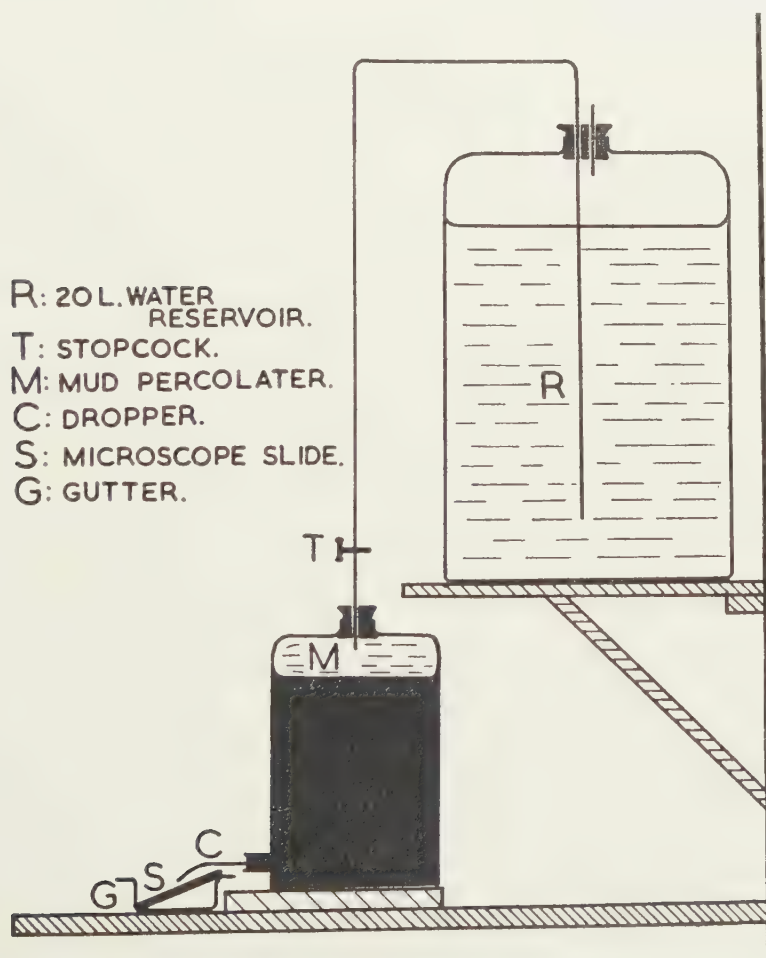


Fig. 2

TABLE 1  
Percolation of muds

F = Freshwater

S = Seawater

A and C contain steelwool

1. Affluent

2. Top of mud

3. Bottom of mud

4. Effluent

Incub. one month	pH	E <sub>b</sub> (mv)	Aeration of effluent pH E <sub>b</sub> (mV)	Iron in p.p.m.	Acid soluble Fe = 0 — OH	Acid insol. Fe = 0 — OH	dry matter accum.	N base 10 %	H <sub>2</sub> S	cultures
FA	1	7.90	+422	144						
	2	7.02	+137							
	3	7.51	-658*							
	4	7.25	+222	190	22 %	1.5 %	.183 g			4 wks
FB	1	7.71	+382	272						
	2	6.85	+177							
	3	6.62	+172							
	4	6.60	+364	211	29 %	1.8 %	.120 g		+	4 wks
FC	1	6.51	+267	251						
	2	7.30	-535*							
	3	7.30	-458*							
	4	7.11	+345	206					+	4 wks
FD	1	6.42	+273	176						
	2	6.30	+073							
	3	6.50	+212							
	4	6.72	+360	195					+	4 wks
SA	1	7.42	+272	14				2.28		
	2	7.48	-024							
	3	8.09	-266							
	4	8.05	0	8.02 +321	14				+	4 wks
SB	1	7.42	+176	12				2.42		
	2	7.35	-002							
	3	7.22	-048							
	4	6.95	+089	7.00 +331	12				+	6 wks
SC	1	7.68	+484							
	2	7.48	-162							
	3	8.10	-443*							
	4	7.95	-402*	12					+	4 wks
SD	1	7.28	+426						+	4 wks
	2	7.58	+081						+	4 wks
	3	7.28	+031							
	4	7.13	+413	14					-	9 wks

\* These very low Eh values are due to hydrogen generated from steel wool.

TABLE 2  
Percolation of muds continued

S.Z.	Seawater, mud + <i>Zostera</i>	1. Affluent
S.E.	Seawater, mud + <i>Enteromorpha</i>	2. Top of mud
		3. Bottom of mud
		4. Effluent

	pH	E <sub>h</sub> mV	X Base × 10.3	Cultures	H <sub>2</sub> S		
S.Z.A	1	7.90	+221	2.54	pos. in 10 days	Averages	<i>Zostera</i>
	2	8.30	+132				
	3	8.52	-052			pH	E <sub>h</sub>
	4	7.30	-024		++		mV
						1	8.00 +217
S.Z.B	1	8.10	+213	pos. in 10 days		2	8.43 +021
	2	8.55	-091			3	8.29 -146
	3	8.05	-239			4	7.56 -067
	4	7.82	-109		++		<i>Enteromorpha</i>
S.E.A	1	7.90	+219	2.36	pos. in 15 days		
	2	7.70	-239			1	8.00 +225
	3	6.90	-124			2	7.98 -239
	4	7.30	-129		+	3	7.32 -157
						4	8.01 -134
S.E.B	1	8.09	+231	pos. in 17 days			
	2	8.25	-239				
	3	7.75	-191				
	4	8.73	-139		+		

with an opening at the bottom were filled for two-thirds with mud and perfused from 20 litre demijohns at a rate of about 10 litres in 24 hours. Three series of four bottles each were prepared. The effluent issued through a dropper at the bottom of the jars and was caught on inclined microscope slides which could be renewed at will. Tables 1 and 2 show the composition of mud and water, and also the pH and E<sub>h</sub> at four different levels: affluent, top of the mud, bottom of the mud, and effluent. In the steelwool percolates, particularly in the freshwater, a large amount of oxide (chiefly goethite) had to be removed from the slide by acid prior to examination. This often spoiled the preparations. The best results were obtained with thin coatings, which were washed in freshwater to remove the salt, dried, and mounted in balsam without staining (Fig. 4). From Table 1 it appears that, in the freshwater percolates, the addition of steelwool to the mud caused abnormally low potentials. This is due to the fact that, without sulphate reduction (no H<sub>2</sub>S was observed in the effluent), the hydrogen generated by the steelwool remains unutilized. In the percolate from SA (seawater, mud from Lake Mallacoota, Victoria, steelwool) some *Sphaerotilus* appeared after a few weeks, but only at the extreme surface. On the surface of the slide, filamentous, sulphur-containing *Thiothrix* was

observed. The addition of steelwool to the marine muds caused a large accumulation of non-biogenic iron rust on the slide, more than 8 mm in 4 weeks. Only after six weeks of continuous percolation the seawater series (Mallacoota mud, no steelwool) showed the development of *Sphaerotilus* (culture S B, Fig. 4a). After replacing the slide the new slide showed copious growth of the *Spirophyllum*-form of *Gallionella* in five days (Fig. 4b). The characteristics of the effluent were pH 7.15,  $E_h$  +290 mV.

Table 2 shows the characteristics of seawater percolated through marine mud with the addition of *Zostera* and *Enteromorpha*. The latter from seems to produce more acid. After two weeks the oxidized effluent had deposited a heavy layer of sulphur on the slides. There appeared a copious development of *Thiothrix*. Under the sulphur layer, close to the surface of the slide, black ferrous sulphide was formed, protected against oxidation by the oxygen absorbing cover of Thiobacteria. A permanent mount made of this sulphide has kept its black colour for over two months.

The data presented in Tables 1 and 2 tend to show that both the Beggiatoaceae and the iron bacteria are to be considered as "gradient organisms".

#### LIMITS OF THE MILIEU

Figure 3 shows the characteristics controlling the presence or the

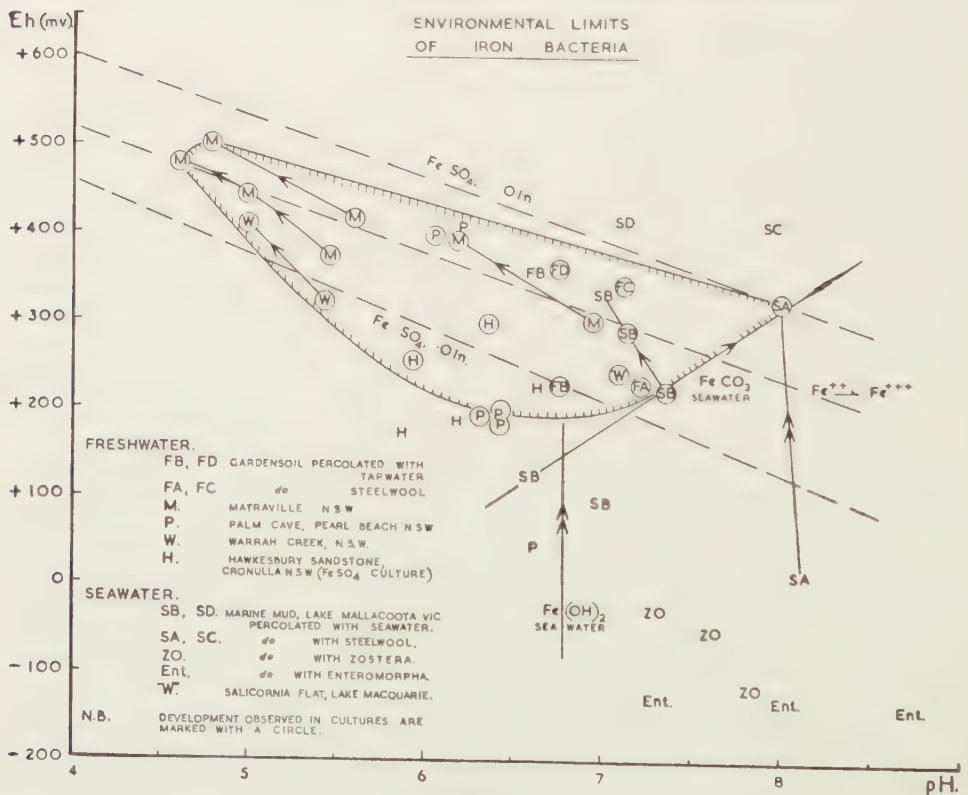


Fig. 3



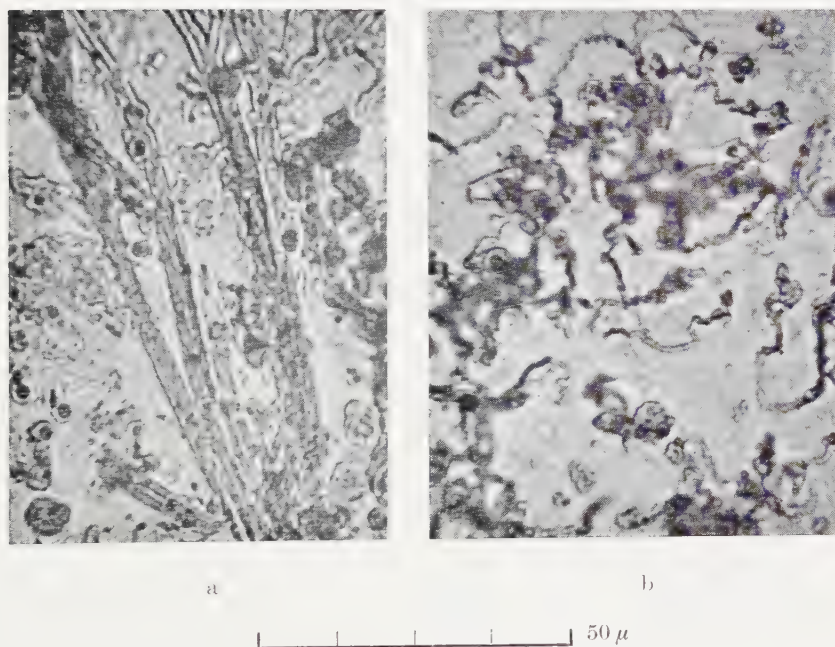


Fig. 4. a. *Sphaerotilus* sp. (some *Spirophyllum*) seawater, mud from Lake Mallacoota, Vic.  
b. *Spirophyllum*-form of *Gallionella ferruginea* Ehr. seawater, mud from Lake Mallacoota, Vic.



absence of iron bacteria. Apart from the percolation experiments, measurements from freshwater occurrences (Palm Cove, Matraville, Hawkesbury Sandstone, Lake Macquarie) are included. The data on *Thiothrix* are too few to enable us to draw conclusions; it is probable, however, that their

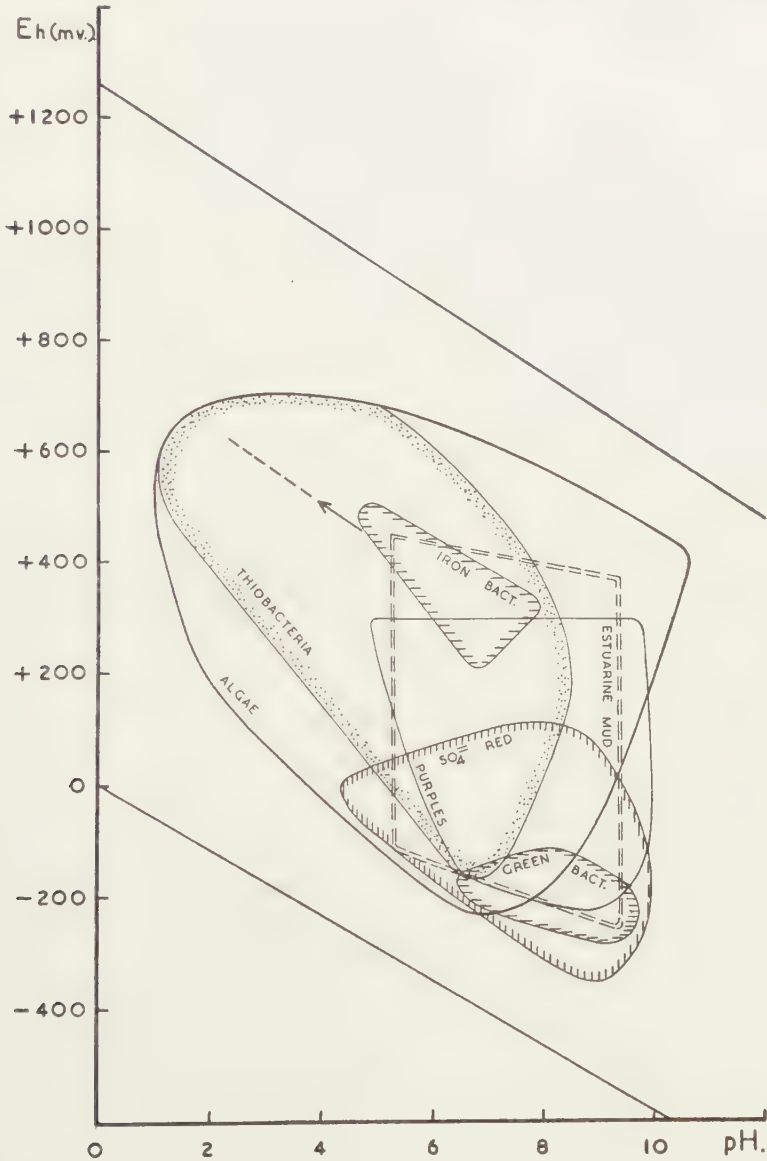


Fig. 5

milieu lies entirely outside the region in which iron bacteria occur. It seems that the latter do not tolerate  $H_2S$ . In Figure 3 we also depict: (1) the characteristics of the oxidation of  $.01n FeSO_4$  at various pH (limits); (2) the theoretical curve for the oxidation of  $1.0n Fe^{++}$ ; and (3) characteristics for the oxidation of a mixture of  $.01n Fe(OH)_2$  and

.01M  $\text{FeCO}_3$  (suspensions)<sup>1</sup>). While the abovementioned curves may not completely outline the environment of the iron bacteria, they seem suggestive.

#### RELATION TO OTHER GROUPS

Figure 5 shows the pH- $E_h$  region of the iron bacteria relative to the regions occupied by other forms in the marine environment (see BAAS BECKING and WOOD (1955)). The milieu-limits of the iron bacteria are well within those of both algae and *Thiobacteria*, while the region overlaps the upper part of the region in which purple bacteria occur. In this upper part no more  $\text{H}_2\text{S}$  is present in the environment, the purple bacteria oxidizing their sulphur to sulphate. The region of the iron bacteria, on the other hand, is widely separated from that of the sulphate reducers. It seems probable that the milieu limits of the Beggiatoaceae should be outside the boundaries of the iron bacteria, but overlapping the region of the sulphate reducers. The arrow near the limits of the iron bacteria suggests a possible extension of the region to include the milieu of *Thiobacillus ferrooxidans* Temple and Colmer.

#### ROLE OF THE HYDROGEN

The close relation of *Thiobacteria* and iron bacteria, exemplified by both *Thiobacillus ferrooxidans* and *Crenothrix polyspora* (= *Sphaerotilus*?) may be accounted for by the primary requirement of these bacteria; the hydrogen. The origin of this hydrogen may, in certain cases, be unimportant, whether from organic matter, sulphur, ferrous iron, or from sulphite. The older, inorganic-chemical literature contains many references

TABLE 3  
Compounds yielding hydrogen on oxidation  
(literature from GMELIN-PIETSCH 1953, SIDGWICK 1951)

Substance	Conditions	Authors	Year
FeO	in water vapour	MOISSAN	1877
Fe(OH) <sub>2</sub>	in presence of H-acceptor	DUNSTAN & DYMOND	1887
	heated in water	BERL & VAN TAACK	1928
	in the cold	FRICKE & RIHL	1943
FeCO <sub>3</sub>	heated in steam	KNOP	1873
	heated in water	TRAUBE, LANGE & JUSTH	1925
FeS	boiling water	REGNAULT	1836
	water at 56° C	DE CLERMONT & FROMMEL	1878
	steam	GAUTIER	1906
	steam, very pure H <sub>2</sub>	FISCHER & TROPSCH	1922/23
FeS <sub>2</sub>	steam, 500° C	GRÜNERT	1929
H <sub>2</sub> S	steam, 400° C	GAUTIER	1906
SO <sub>3</sub> <sup>-</sup>	with organic matter	GMELIN (no author cited)	

<sup>1</sup>)  $\text{Fe}(\text{HCO}_3)_2$  probably present.



to the generation of hydrogen by oxidation of iron and sulphur compounds, some of which are gathered in Table 3.

Experiments on the development of iron bacteria in hydrogen are under way and will be reported on in another place.

#### ACKNOWLEDGMENTS

We gratefully acknowledge the help of Mr. L. CROSBY and Mr. C. PURDAY in the preparation of the microphotographs.

#### LITERATURE

- BAAS BECKING, L. G. M. and E. J. F. WOOD, *Proc. Kon. Ned. Akad. v. Wet.* **B 58**, 160 (1955).  
 ——— and MARGARET MACKAY, *Proc. Kon. Ned. Akad. v. Wet.* **B 59**, 109 (1956).  
 BENEDEN, G. VAN, *Hydrologia* **3**, 1 (1951).  
 BUTKEWITCH, W. S., *Ber. Wiss. Meeresinst. U.S.S.R.* **3**, 10 (1928).  
 CHOLODNY, N., *Beih. Bot. Zentrbl. I*, **48**, 399 (1931).  
 GMELIN-PIETSCH, *Handbuch der Anorganischen Chemie* (8th ed., Weinheim Verlag "Chemie", 1935).  
 HUNT, F. STERRY, *Canad. Naturalist* **9**, 431 (1881).  
 PERFILIEV, B. V., *Journ. Micr. Soc. Leningrad* **1**, 179 (1927).  
 PRINGSHEIM, E. G., *Biol. Rev.* **12**, 200 (1949).  
 ———, *Endeavour* **11**, 207 (1952).  
 SIDGWICK, N. V., *The chemical elements and their compounds* (Oxon. Clarendon, 1951).  
 TEMPLE, K. L. and A. R. COLMER, *Journ. of Bact.* **62**, 605 (1951).  
 WINOGRADSKY, S., *Microbiologie du Sol* (Paris, Masson and Co., 1949).

BIOLOGICAL PROCESSES IN THE ESTUARINE ENVIRONMENT

IX. OBSERVATIONS ON TOTAL BASE

BY

L. G. M. BAAS BECKING <sup>1)</sup>

(Communicated at the meeting of September 29, 1956)

*Summary*

Titration of total base carried out in the last few years allow of the following conclusions.

1. The empirical  $K_1$  of the carbonic acid-bicarbonate system (abt.  $4 \times 10^{-7}$  at  $20^\circ\text{C}$ ) approaches closely to the value for pure water given by HARNED and DAVIS (1943) while it is significantly different from the values derived from ionic activity in seawater by BUCH *et al.* (1932);  $10^{-6}$  for 20 ‰ Cl at  $20^\circ\text{C}$ .

2. Other buffering systems were observed in estuarine waters, the most important of which is the  $\text{SH}^- \rightleftharpoons \text{H}_2\text{S}$  system which may cause a hundredfold increase in the total base. Moreover, the presence of ammonia, amines, phosphate and organic acids might influence the total base in the estuarine environment.

3. From the study of eleven estuaries and lagoons on Australia's east and south coast the dilution effect could be represented by

$$B \times 10^{-3} n = 1.12 + .0445 S \text{ ‰}$$

Freshwater of a very high base content was found in the southern part of New South Wales.

4. Apart from the relation mentioned above, the base may be considerably lowered at a high, constant salinity. This effect was further studied in over 227 estuarine samples, plotting base against pH. No simple relation was found.

5. Shaking seawater with air, with several types of mud, with purified sand or with calcium carbonate caused no significant changes in the base.

6. Apart from dilution, the changes in total base in the estuarine environment are most probably caused by biological processes.

A preliminary survey shows the multiplicity of these changes, the causes of which are mainly obscure.

I. *The carbonic acid system*

The total base of seawater varies only within narrow limits;

$$2.45 - 2.55 \times 10^{-3} n.$$

<sup>1)</sup> C.S.I.R.O. Division of Fisheries & Oceanography, Cronulla, N.S.W.

Higher values were observed by the author 2 miles outside Port Price, South Australia ( $2.70 \times 10^{-3} n$ ) and at Lakes Entrance, Victoria ( $2.65 \times 10^{-3} n$ ). Although a systematic survey of this value for our waters is lacking (especially the influence of plankton swarms might yield valuable data) it is safe to assume that this characteristic will show but little change.

It is in the estuarine environment that great changes occur, not only because of the admixture with freshwater but also because of the influence of living beings (much more pronounced than in the open sea) and of the bottom upon the invading seawater.

From older field observations by the author (mostly unpublished) it will be seen that the estuarine system *per se* does not cover the entire range of variability. Figure 1 gives an aspect of "comparative hydrology"

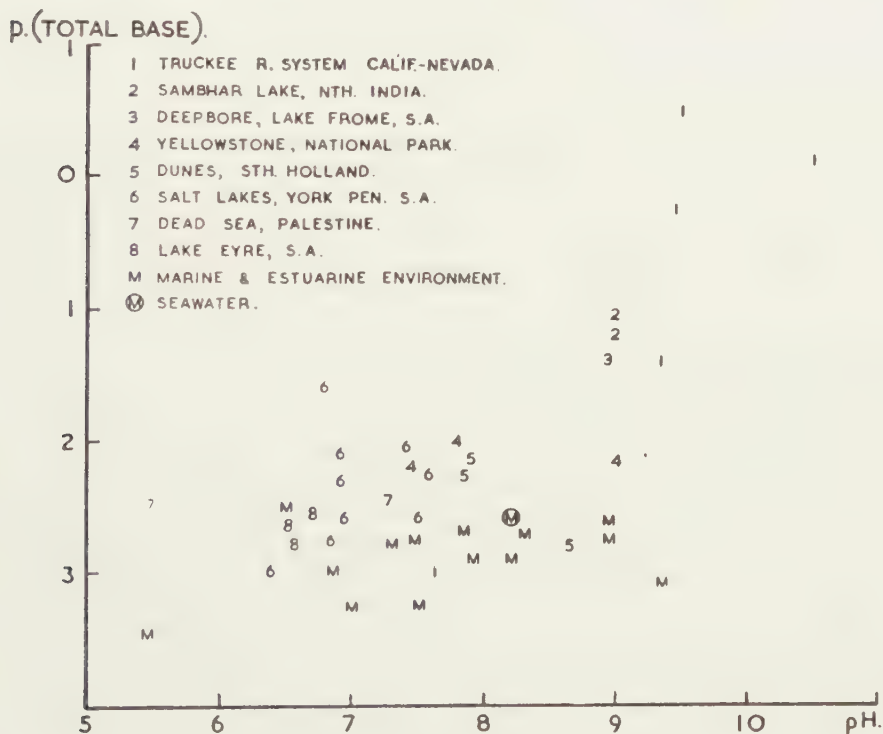


Fig. 1

in which (taking pB total base as a function of pH) the marine (inclusive of the estuarine) environment is compared with other groups of terrestrial waters. With the exclusion of soft fresh waters the base content of both ocean and estuaries is low.

In the carbon-dioxide system the total base, according to Rakestraw (1949) equals

$$B = (\text{HCO}_3^-) + 2(\text{CO}_3^{--}) + (\text{H}_2\text{BO}_3^-)$$

neglecting the borate, the influence of which is negligible at  $\text{pH} < 8.5$ , and taking

$$(\text{H}_2\text{CO}_3) + (\text{HCO}_3^-) + 2 (\text{CO}_3^{2-}) = 1$$

it follows \* that the fraction  $(\text{HCO}_3^-)$  amounts to

$$(1) \quad (\text{HCO}_3^-) = \frac{K_1 (\text{H}^+)}{(\text{H}^+)^2 + K_1 (\text{H}^+) + 2 K_1 K_2}$$

which fraction may be calculated if  $K_1$  and  $K_2$  are known.

At  $20^\circ \text{C}$  in freshwater the older values for these constants are slightly smaller than the values given by HARNED and DAVIS (1943). They are, however, much smaller than those derived by BUCH (1932) *et al.*

Accounting for the activities of the ions in solution, he derived for

$$\begin{aligned} \text{p}K_1 &= 6.47 - .188 \quad \text{‰Cl}^0/_{00} \text{ at } 20^\circ \text{C} \\ \text{p}K_2 &= 10.35 - .498 \quad \text{‰Cl}^0/_{00}. \end{aligned}$$

The following table gives a comparison of these various constants at  $20^\circ \text{C}$ .

TABLE 1

	$\text{Cl}^0/_{00}$	$K_1 \times 10^{-7}$	$K_2 \times 10^{-11}$
FLEMMING 1949	0	3.5	4.4
HARNED & DAVIS 1943	0	4.16	4.84
BUCH <i>et al.</i> 1932	20	10.	100.

Application of (1) will yield the percentage of  $\text{HCO}_3^-$  at various values of pH.

Figure 2 and Table 2 give, besides the theoretical figures, the results of 14 electrometric titrations.

Titration both under  $\text{CO}_2$  pressure (30 ml Erlenmeyer) and in open vessels yielded the same results. The end point should be at pH 4.5, but in certain cases this was difficult to attain as a small plateau appeared at pH 4.8–4.9, probably due to the presence of salts of fatty acids – in this case the end value had to be obtained from extrapolation. From this table and from Figure 2 it appears that while the empirical curves show an inflection at about pH 6.40, according to BUCH this point should be situated at pH 6.00. Another four seawater titrations yielded, for the apparent pK, 6.42, 6.40, 6.50 and 6.51.

As will be seen later, waters rich in  $\text{H}_2\text{S}$  show, on titration, a buffer plateau at pH 6.9–7.0, the  $\text{p}K \text{ H}_2\text{S} \rightleftharpoons \text{SH}^-$  for distilled water at  $20^\circ \text{C}$  being 6.96. Here again the experimental data are in agreement with the dissociation constants for fresh water. As this report is concerned only with actual observations it would be out of place to discuss the causes of this discrepancy. It seems that the theoretical superstructure which

\*)  $K_1(\text{H}_2\text{CO}_3) = (\text{H}^+) (\text{HCO}_3^-)$   
 $K_2(\text{HCO}_3^-) = (\text{H}^+) (\text{CO}_3^{2-})$



TABLE 2  
Per cent  $\text{HCO}_3^-$  as determined by titration

		8.0	7.5	7.0	6.5	6.0	5.5	5.0	pH	$\bar{X}$ base $\times 10^{-3}$	$\bar{X}$ base % of seawater	Cl‰	Locality
BUCH	1932	83	97	89	71	50	29	9				20	
FLEMING	1949	98	90	78	50	26	11	3				0	
LATIMER	1952	98	91	81	54	80	15	4				0	
	sample												
Seawater	1	100	86	67	39	21	9	4	8.00	2.47		19.6	Port Hacking
19.4-19.6	5	94	84	75	54	21	11	4	8.21	2.59		19.4	Jetty Laboratory
% Cl	7	100	87	76	53	10	5	1	8.00	2.58		19.4	Jetty, shaken with air, 4h
	14	98	77	66	58	32	11	4	8.08	2.50		19.3	Port Hacking, filtered
Average		98	84	71	51	21	9	3	8.07	2.53	100		
	3	100	91	79	59	27	13	7	7.81	2.41	95	19.4	Shaken with reduced silt, S.W.Arm, 4h
Seawater	8	94	85	72	32	14	7	2	8.10	2.76	110	19.4	Shaken with washed sand, 4h
shaken	9	100	89	76	53	27	13	5	7.80	2.36	93	19.4	Shaken with reduced silt, 18h S.W.Arm
with	11	100	85	69	51	23	12	6	7.98	2.46	97	19.4	2 weeks contact with Enteromorpha
mud													percolate from Mallacoota mud
	12	95	87	73	53	20	9	4	8.24	2.52	100	19.4	2 weeks contact with Zostera percolate
													from Mallacoota mud
	13	95	82	70	47	24	12	5	8.23	2.48	98	19.4	2 weeks contact, Mallacoota mud plus steelwool
Average		97	87	73	49	23	11	5	8.02	2.50	99		
Seawater	2	100	92	81	58	29	15	8	7.72	2.59	103	19.4	
shaken with	10	100	93	80	58	27	15	8	7.75	2.55	101	19.4	Shaken 18h with shelly mud from Pitt-
shelly mud													water, Tasmania
or with $\text{CaCO}_3$	4	100	93	78	51	24	12	4	7.63	2.44	97	19.4	Shaken with shell grit, Lab. fish pond, 4h
	6	100	88	70	44	24	12	4	7.95	2.25	90	19.4	Shaken with calcium carbonate, 4h
Average		100	92	77	53	26	14	6	7.76	2.46	97		

reached, about twenty years ago, its maximum complexity, should be reconsidered and perhaps simplified (RAKESTRAW 1949). Even the dissociation constants given by HARNED and DAVIS assume that all aqueous  $\text{CO}_2$

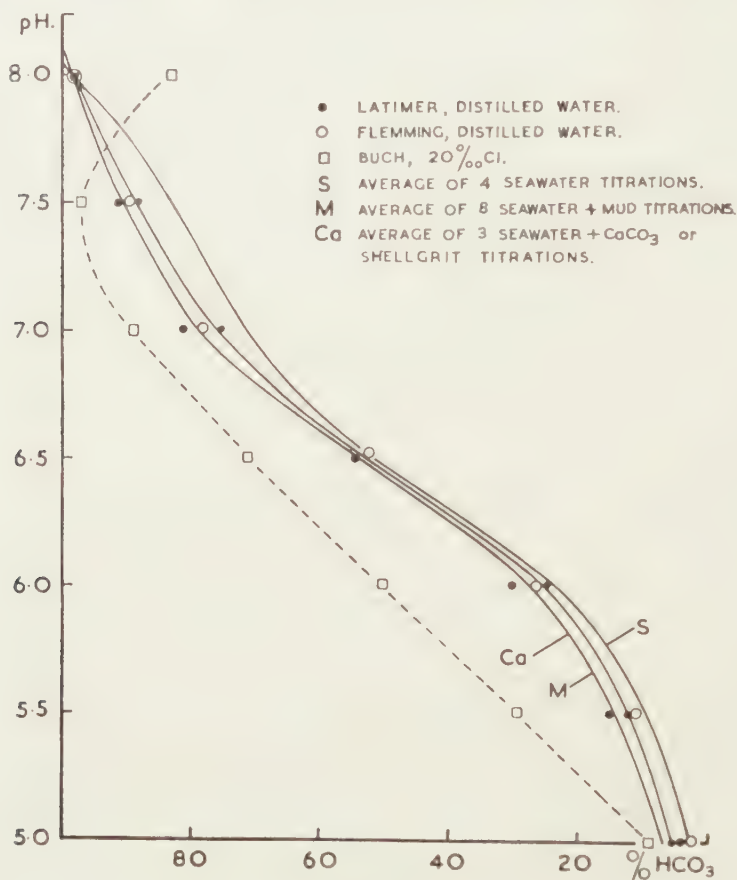


Fig. 2

is present as  $\text{H}_2\text{CO}_3$ . If  $K_1$  is corrected for unhydrated  $\text{CO}_2$ , it increases 2000 fold! (OLSEN and YOUNG 1940). So it seems safer to use the experimental data without too much effort at further interpretation.

From Table 2 it also appears that the theoretical titration curve for distilled water is approached more closely after the seawater has been shaken with calcium carbonate or with shell grit.

## II. Other buffering systems

a. If *Enteromorpha* decomposes in seawater (10 gr fresh weed in 100 ml seawater) the base is reduced by 80 % in two weeks, while the pH drops to about 6. After this time, both pH and buffering value of the water increase. In one case  $9.4 \times 10^{-2} n$  "base" was found, pH 8.35, after six weeks. As titration with iodine yielded the equivalent of about  $1n \text{H}_2\text{S}$  this

confirms the idea that the base should be chiefly  $\text{SH}^- + \text{H}_2\text{S}$ . The titration curve shows plateaus at pH 6.40 (bicarbonate system) and between pH 7.0 and pH 6.9. For the reaction  $\text{K}_1 (\text{H}_2\text{S}) = (\text{H}^+) (\text{SH}^-)$  LATIMER (1952) gives  $\text{K}_1 = 1.1 \times 10^{-7}$ ,  $\text{pK}_1 = 6.96$  (Fig. 3).

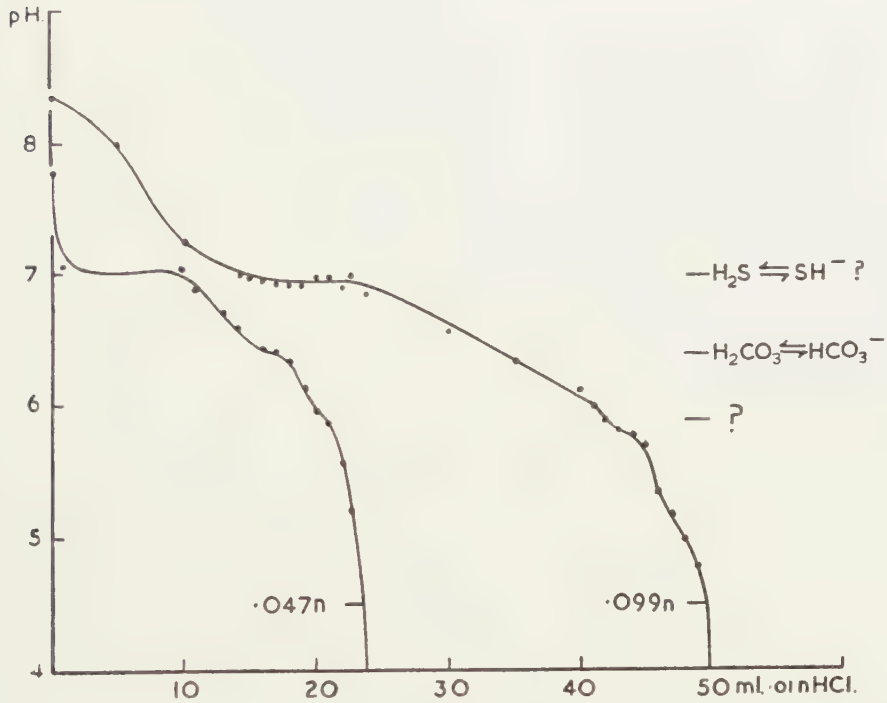


Fig. 3

TABLE 3  
High base accompanied by  $\text{H}_2\text{S}$

pH	Base $\times 10^{-3}n$	log base + 3	
8.2	2.50	.400	Seawater
8.35	99	1.998	<i>Enteromorpha</i> rotting, green bacteria present
7.79	47	1.672	<i>Enteromorpha</i> rotting
6.85	44	1.642	<i>Enteromorpha</i> rotting
7.20	9.06	.957	Hole dug in mangrove swamp, near Kone, New Caledonia *
7.10	9.04	.954	<i>Cymodocea</i> flat, Bay of Gouaro, New Caledonia *
7.30	7.20	.856	<i>Zostera</i> mud, Hartley Point, Lake Macquarie
7.40	5.12	.708	Hole dug in mangrove swamp, Santa Maria Isle, New Caledonia *
6.50	4.45	.648	Lake Mallacoota, shore, ironstone
5.85	3.60	.556	<i>Ecklonia</i> , rotting
6.52	3.18	.504	<i>Brachydontes</i> mud, Lake Macquarie

\* Collected by Mr. I. R. KAPLAN, May 1956.

Abnormally high base is usually accompanied by  $H_2S$  (Table 3).

In Figure 4 these data are shown together with some values for rotting *Ecklonia* and *Enteromorpha*, to mark the end of the preliminary process of putrefaction, with the reduction of total base. The calculated regression

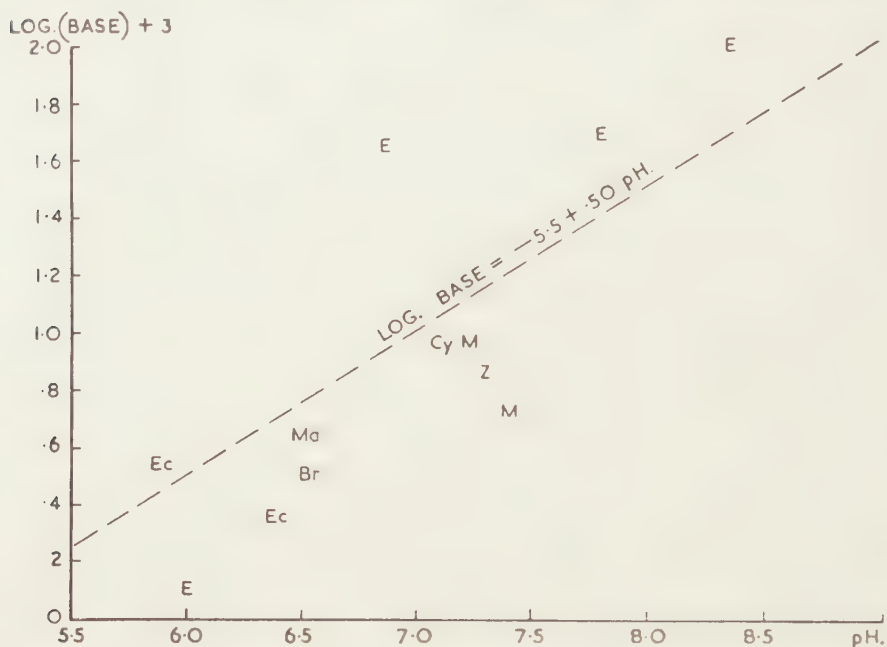


Fig. 4

is;  $\log \text{base} = -2.5 + .50 \text{ pH}$ . In this milieu the electrode potentials are low, values  $E_h = -200 \text{ mV}$  are frequent. Apart from this instance, there is no correlation between total base content and electrode potential.

#### b. Organic acids

When, prior to filtering, much algal matter had been present in the water, decided buffer plateaus were observed in the range  $\text{pH } 4.7 - 4.9$ , corresponding to  $K_a = 1 - 2 \times 10^{-5}$ . As *Enteromorpha* produces a propionic acid-sulphonium salt (BYWOOD and CHALLENGER, 1955) and as both *Desulphovibrio* and *Thiobacillus* may produce similar salts it is interesting to observe that, for

$$\begin{aligned} \text{propionic acid, } K_a &= 1.40 \times 10^{-5} \\ \text{butyric acid } ,, &= 1.40 \times 10^{-5} \\ \text{isobutyric acid } ,, &= 1.50 \times 10^{-5} \end{aligned}$$

(again on the assumption that chlorinity does not interfere).

#### c. Phosphate

In the bicarbonate range ( $\text{pH } > 8$ ) we might expect a titration plateau, in  $H_2S$  containing acid muds, where phosphate is released in sufficient



quantities.  $\text{H}_2\text{PO}_4^- \rightleftharpoons \text{H}^+ + \text{HPO}_4^-$  shows a  $\text{pK}_2=7.1$ . Although such an inflection point has not been observed thus far, it seems well to keep this in mind.

d. In many cases a small but unmistakable plateau was observed at pH 5.8 corresponding to  $K=1.6 \times 10^{-6}$ . The origin of this plateau is unknown.

e. At the alkaline side the production of both ammonia and amines could be demonstrated in *Enteromorpha*. Furthermore, hydroxyl ions might be excreted as such, in analogy with the activity of freshwater algae, like *Chara*.

From the above it appears that titration curves will only yield significant results when  $\text{H}_2\text{S}$ ,  $\text{SH}^-$  and organic acids are absent. Especially the sulphide system may interfere considerably.

### III. The influence of dilution

If seawater with a total base of  $2.5 \times 10^{-3} n$  be diluted with distilled water, the following relation will hold,  $B \times 10^{-3} n = .075 S \text{ ‰} - .005$ . The correction lies without our limits of accuracy.

In the estuaries the seawater is diluted with a mixture of rainwater and river (creek) water. Some of the river waters show a low total base, as Table 4 shows.

TABLE 4  
Total base of Victorian waters

	total base $\times 10^{-3}$	pH
Genoa River	.65	7.1
Timbilican Creek	.75	7.5
Nicholson River	.85	7.5
Lake Wellington	.75	7.2
Latrobe River	.85	7.3
Average	.77	7.32
Waters from the Hawkesbury sandstone, N.S.W., are even lower in base.		

However, Boggy Creek or Bald Hill Creek, one of the feeding creeks of Lake Merimbula, shows a very high base, the nature of which could not be further ascertained.

TABLE 5  
Characteristics of Bald Hill Creek

	pH	ppm	total base $\times 10^{-3}$
1952 at Lake	7.60	375	5.30
1952 300 yds from outflow	7.80	540	4.75
1955 300 yds from outflow	7.50	465	2.40
1955 1 mile upstream	8.06	405	4.80

This creek has little influence on the base content of Lake Merimbula, however.

The dilution curve, obtained from 45 determinations of 8 estuarine stations, is given in Figure 5. The regression line is  $B 10^{-3} = 1.12 + .0445 S^{0/100}$ . This regression line does not fit the data obtained for seawater. It describes conditions only in the estuarine environment.

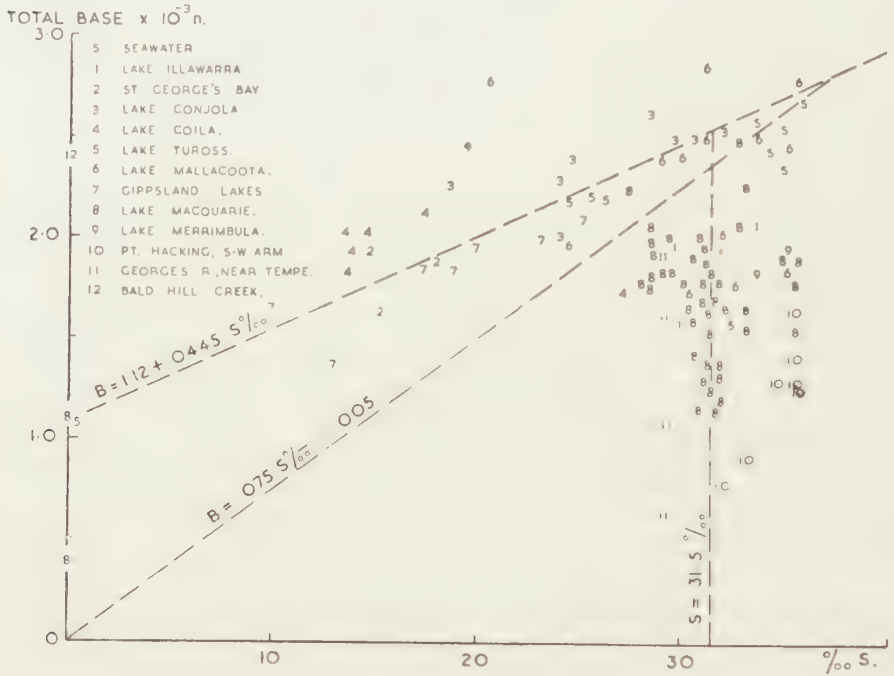


Fig. 5

From Figure 5 it may also be seen that there is a large group of values in which the total base is lowered in relation to seawater at a fairly constant salt content (28–36 S ‰), regression  $S = 31.5^{0/100}$ .

Table 6 shows how the points on Figure 5 may be divided into two sets.

TABLE 6

Locality	$B = 1.12 \times 10^{-3} + 0.0445 S^{0/100}$	$S = 31.5^{0/100}$
1. Lake Illawarra, N.S.W.	0	3
2. George's Basin, N.S.W.	3	0
3. Lake Conjola, N.S.W.	7	0
4. Lake Coila, N.S.W.	5	0
5. Lake Tuross, N.S.W.	4	1
6. Lake Mallacoota, N.S.W.	9	3
7. Gippsland Lakes, N.S.W.	7	0
8. Lake Macquarie, N.S.W.	8	39
9. Lake Merimbula, N.S.W.	1	1
10. Port Hacking, S.W.Arm, N.S.W.	0	7
11. George's River, N.S.W.	0	4
	44	58

#### IV. *Abiological influences on the base*

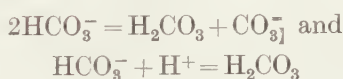
The high spread of the points around the dilution line and the group with a low base at constant salinity are probably all mainly due to biological activity.

The examination of Table 2 shows that seawater, shaken with air, with various types of mud, with sand, with shell grit and with calcium carbonate did not materially change its characteristics, the total base decreasing or increasing not more than 10 %. It may very well be that there is an abiological influence (ionic exchange perhaps) but the preliminary experiments have failed to find a significant effect of the mud. In view of the great biological influences, experiments (which have to extend over several days) should be carried out with sterile seawater under sterile conditions. Inasmuch as sterilization will materially influence both structure and composition of the mud, this seems, at present, beyond us.

#### V. *Biological influences*

In 1924 the author, together with Dr. IRVING, published results on the influence of various algae on the total base. From the few observations it already appeared that the changes in base could not be solely accounted for (as is often claimed) by changes in the bicarbonate-carbonate system.

Photosynthesis, apart from using the free  $\text{CO}_2$  or  $\text{H}_2\text{CO}_3$ , will change bicarbonate into carbonate according to



Here pH will increase with very little change in base, ( $\text{HCO}_3^-$ ) being about  $2.5 \times 10^{-3}$  while ( $\text{H}^+$ ) is only  $10^{-8}$ . As repeatedly observed by several authors, in seawater photosynthesis will reach an endpoint at pH 9.3–9.4. If BUCH's data are correct, at this pH the  $\text{HCO}_3^-$  content will be very low. In freshwater the endpoint of photosynthesis lies much higher, values of nearly pH 11 are on record.

From the above it is clear that the production of  $\text{OH}^-$  ions will also change the pH without appreciably changing the base. Similarly, both respiration or the production of acid will lower the base, although, due to the large buffering effect, the changes are not as rapid as those caused by  $\text{CO}_2$  uptake.

Figure 6 shows the relation of pH and total base in ten New South Wales and Victorian estuaries, (227 points). If seawater were diluted with rainwater or distilled water (pH about 5.8) the dotted line through S would be followed. The regression, however, follows a line through *a* if extreme values are omitted. There are many of these extreme values and a distinct correlation between pH and total base does not exist. The average is situated at pH 8.08, total base  $1.82 \times 10^{-3}$  while the pH is close to that of seawater, the base is only 73 % that of seawater, showing that the base may be lowered in many cases without a change in pH.

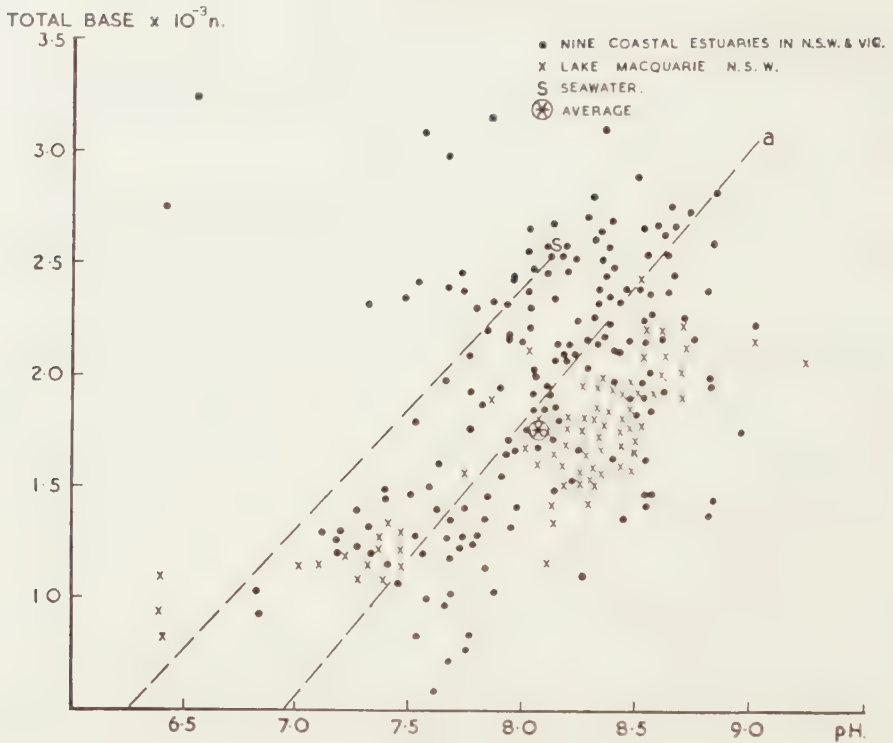


Fig. 6

TABLE 7

Values marked with \* from IRVING and BAAS BECKING (1924)

		Base at start		Base	
		$\times 10^{-3}$	pH		
Spirorbis	48h	1.90	7.58	1.10	
			7.54	1.54	
			7.52	1.60	
			7.45	1.55	
			7.32	1.50	
			7.65	1.00	
			6.80	1.10	
			6.80	.90	
Corallina *	24h	2.55	8.55	1.36	light
	24h	2.55	8.55	1.80	dark
Ulva *	24h	2.55	8.65	3.44	light
	24½h	2.55	8.35	3.09	dark
Gigartina *	24h	2.55	8.40	2.41	light
	24h	2.55	8.25	2.52	dark
Leathesia *	24h	2.55	8.80	2.53	light
	24h	2.55	8.60	2.54	dark
Pyrazus herculeus	4 days	1.95	8.37	2.82	
Anedra trapezia	4 days	1.95	8.38	2.61	
Enteromorpha	12h	2.45	9.00	4.41	light
	24h	2.45	9.40	3.20	light
	12h	2.45	8.05	2.70	dark
	24h	2.45	8.15	2.70	dark

Table 7 and Figure 7 show the changes caused by organisms observed in the laboratory. The influence of decaying algal vegetation and of sulphate reduction are not shown. From Figure 4 it appears that sulphate reduction causes an increase in pH, which might be expected on theoretical grounds (BAAS BECKING & KAPLAN 1956).

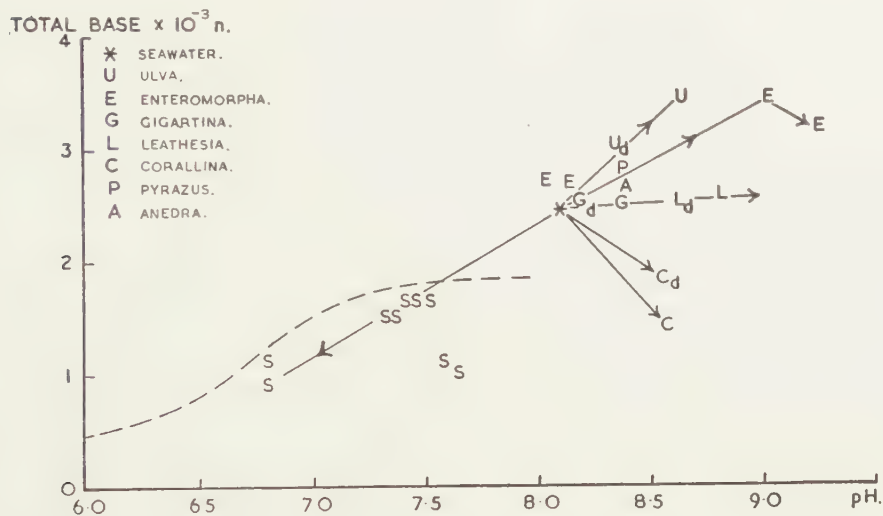


Fig. 7

Lime depositing and lime-secreting organisms, like shells, coralline algae and tube-worms, all seem to behave differently in relation to base and pH (Fig. 7). *Spirorbis* may abstract more than a gram of  $\text{CaCO}_3$  from seawater per square metre of colony per day.

The coralline algae seem to abstract  $\text{HCO}_3^-$  from the water as well as carbonate. The tube-worm *Spirorbis* reduces the base in many instances almost on the titration curve for its original base, (hatched line in Fig. 7). Shells, *Pyrazus herculeus* and *Anedra trapezia*, seem to abstract little bicarbonate and actually slightly increase the base. This may be due to the secretion of alkali, e.g. ammonia. While the photosynthetic effect was marked in *Enteromorpha* together with the probable production of alkali in the light, the difference between light and dark treatment of other algae is only slight. *Ulva*, like *Enteromorpha*, seems to produce alkali, while *Leathesia* and *Gigartina* cause, both in the light and the dark, an increase in pH at constant base. It seems possible that they take in bicarbonate in the dark.

It seems clear that the effect of organisms on the total base is both varied and profound, but much laboratory work will be needed to clarify these effects. While the carbon dioxide system is the most important it certainly is not the only one to be considered in the study of the buffering systems in seawater.



In the study of the CO<sub>2</sub> system the amount of biological work done does not seem commensurate with the large physico-chemical superstructure which may even have impeded rather than furthered research.

#### LITERATURE

- BAAS BECKING, L. G. M. and MARGARET MACKAY, *Proc. Kon. Ned. Akad. v. Wetensch. B* **59**, 109 (1956).  
 ——— and I. R. KAPLAN, *Proc. Kon. Ned. Akad. v. Wetensch. B* **59**, 85 (1956).  
 BUCH, K., H. W. HARVEY, H. WATTENBERG and S. GRIPENBERG, *Cons. Perm. Inst. p. l'Explor. de la Mer. Rapp. et Proc-Verb.* **5**, 79 (1932).  
 BYWOOD, R. and F. CHALLENGER, *Biochem. Journ.* **55**, 4 (1953).  
 FLEMING, R. H., in Sverdrup, Johnson and Fleming, *The Oceans* (New York, Prentice-Hall, 1949).  
 HARNED, H. S. and R. DAVIS Jr., *J. Am. Chem. Soc.* **65**, 2030 (1943).  
 IRVING, L. and L. G. M. BAAS BECKING, *Proc. Soc. Exp. Biol. & Med.* **22**, 1 (1924).  
 LATIMER, W. U., *Oxidation Potentials* (New York, Prentice-Hall, 1952).  
 OLSON, A. R. and P. V. YOULE, *J. Am. Chem. Soc.* **62**, 1027 (1940).  
 RAKESTRAW, N. W., *Sears. Found. Journ. Mar. Res.* **8**, 14 (1949).

## THE OZONOLYSIS OF PHENANTHRENE

(Preliminary Communication)

BY

J. P. WIBAUT AND TH. J. DE BOER

(Communicated at the meeting of September 29, 1956)

As part of the work in our laboratory on the ozonolysis of aromatic and heterocyclic compounds [1] we have investigated the ozonolysis of phenanthrene.

Half a century ago, HARRIES and WEISS [2] described for the first time the ozonolysis of phenanthrene in chloroform. They isolated a crystalline, explosive reaction product which was formulated as a diozonide on the basis of elementary analysis. No fission products from the alleged diozonide could be identified. This result is surprising for the following reason.

Considering the marked olefinic character of the phenanthrene molecule, formation of a diozonide is very surprising. In phenanthrene the 9-10 C-C-bond has by far the highest bond multiplicity [3] and the lowest localisation energy (16.2 kcal) [4]. The vulnerability of the 9-10 bond is furthermore illustrated by reaction with osmium tetroxide [5] and diazoacetic acid [6]. Therefore ozone should attack the 9-10 C-C-bond first of all. The resulting diphenyl derivative (formula Ia) would, like benzene, be relatively stable towards further attack of ozone and therefore phenanthrene and ozone would be expected to react in a molar ratio 1 : 1. This assumption is fully confirmed by our experiments.

Ozone reacts so quickly with phenanthrene, that the "olefinic content" can be determined quantitatively by the titrimetric method of BOER and KOOYMAN [7]. A constant stream of ozone (and oxygen) is passed through a solution of the unsaturated compound. The gases escaping from the reaction vessel are continuously titrated iodometrically and the amounts of escaping ozone plotted against time. From this plot the amount of reacted ozone can be calculated. In two typical experiments with 2.80 mmol of phenanthrene in 14 ml of chloroform at  $-30.5^{\circ}\text{C}$  the calculated amount of reacted ozone was 2.86 resp. 2.78 mmol. This shows that phenanthrene reacts quickly with one mole of ozone.

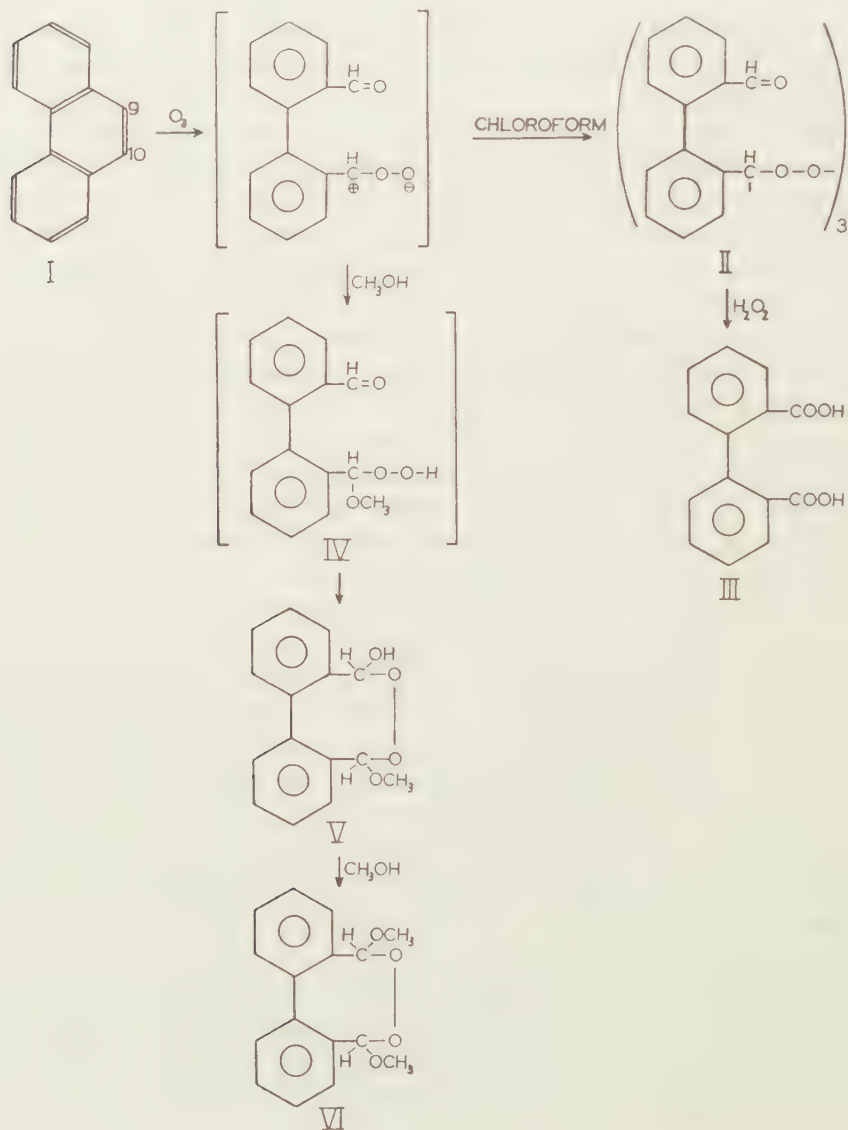
Our next aim was to identify the reaction product(s). For this purpose phenanthrene was ozonised in *thoroughly dry* chloroform at  $-65$  to  $-70^{\circ}\text{C}$ . After completion of the reaction, ether was added. A precipitate was formed which melted, after careful washing with ether, at  $128-129^{\circ}\text{C}$ .

The following data apply to this compound:

	C	H	O	Active O	Mol. weight
Anal. found	73.23	4.71	21.12	6.75	675
Calc. for $C_{14}H_{10}O_3$	73.33	4.46	22.21	7.07	226

Active oxygen was determined by dissolving the product in a little benzene, followed by addition of a small piece of solid  $CO_2$ , acetic acid and NaJ [8]. Active oxygen was not due to a hydroperoxide function because the lead-tetraacetate test was negative.

The molecular weight was determined cryoscopically in benzene. The value of 675 is about three times the calculated value for a monoözonide. We therefore conclude that the reaction product is a trimeric ozonide. The reaction scheme is given on the basis of the Criegee mechanism [9].



The structure of the trimeric ozonide (II) is supported by the infrared spectrum, which contains a relatively strong carbonyl band at about  $1690\text{ cm}^{-1}$ . Furthermore oxidation with boiling hydrogen peroxide solution yields (at least 20 %) diphenic acid (III), identified by admixture with an authentic sample.

It may be noted that the trimer (II) can also be obtained from the chloroform solution by precipitation with methanol. Products in this way obtained have a lower melting point (round  $120^\circ$ ) and a higher mol. weight (e.g. 775, 795). This shows that the lower melting point is probably caused by contamination with higher polymers.

Our results are somewhat different from those of SCHMITT, MORICONI and O'CONNOR [10] who recently reported the isolation of a phenanthrene monoözonide (m.p.  $65\text{--}90^\circ$ ) from a chloroform solution by precipitation with methanol. Their conclusion is based on a.o. infrared data and the mol. weight (Rast). However, the cited "characteristic ozonide bands" of BRINER [11] as found in "phenanthrene monoözonide" were recently shown to be actually carbonyl bands by CRIEGEE [12]. In the meantime BRINER [13] has admitted the correctness of Criegée's findings. Besides the Rast mol. weight determination is unreliable. We have found that our trimeric ozonide with mol. weight 675, decomposes easily in camphor at its melting point, thus giving much too low mol. weight values (e.g. 290, 324). It seems therefore to us that the product of SCHMITT, MORICONI and O'CONNOR may have been an impure trimeric phenanthrene ozonide, rather than the suggested monoözonide.

For further information we studied the ozonolysis reaction in methanol as a solvent. Though this part of our work is not yet completed we are prompted to give our results at this stage, because of a recent publication of BAILEY [14] which also deals with the ozonolysis of phenanthrene in methanol. Some of our conclusions agree with Bailey's, others are essentially different. Our results are summarised below.

Phenanthrene was ozonised in methanol at  $-15^\circ\text{C}$ . The initial suspension becomes a clear solution when reaction is complete. Upon addition of water a precipitate is formed which melts, after thorough washing with ether, at  $96.5\text{--}97.5^\circ\text{C}$ . We have assigned to this product structure V on the basis of analysis, mol. weight, chemical properties and the infrared spectrum.

	C	H	Active O	OCH <sub>3</sub>	Mol. weight
Anal. found	69.27	5.64	6.01	13.64	246
Calc. for C <sub>15</sub> H <sub>14</sub> O <sub>4</sub>	69.75	5.46	6.20	12.02	258

The mol. weight was determined according to Rast in camphor. Contrary to compound II, there was no sign of decomposition. The mol. weight could not be determined in benzene, owing to insolubility. The product liberates immediately iodine from NaI in acetic acid and gives a negative lead tetraacetate test in acetic acid as well as in benzene, indicating the absence of a hydroperoxy group.

The infrared spectrum in nujol gives no absorption in the region  $1700\text{ cm}^{-1}$  (no carbonyl). All these properties are in accordance with the proposed structure V.

The course of the reaction is illustrated in the reaction scheme (p. 422). As in chloroform, the primary reaction product is Ia, which is attacked immediately by methanol to yield the methoxy hydroperoxide IV. Similar products have been obtained by CRIGEE [9] when ozonizing olefinic compounds in methanol. It is well known that an aldehyde and a hydroperoxide may form a semiacetal [15]. In our case this happens by intramolecular reaction ( $\text{IV} \rightarrow \text{V}$ ). No catalyst is required since the hydroperoxide itself seems to be sufficiently acidic to promote reaction. Intermolecular reaction between the aldehyde and hydroperoxide groups of IV can be discarded because this would lead to a product with a much higher molecular weight than actually found.

BAILEY has isolated by a similar technique a product with m.p.  $84\text{--}88^\circ$  to which he assigns structure IV because of a positive hydroperoxide test and an infrared spectrum with a carbonylband. We think it possible that this product is impure V, the impurity containing perhaps a hydroperoxide group and the carbonylband in the infrared spectrum being due to decomposition of V while being dispersed in KBr.

We found that spectra in nujol are absolutely "carbonyl-free", whereas in KBr a strong CO band appears. The intensity of this band is roughly doubled (other bands remaining equal) if the sample is vibrated with powdered KBr over twice as long a period (2 resp. 4 minutes). It is obvious that these spectra in KBr discs must be interpreted with care.

If after ozonisation at  $0^\circ\text{C}$  no water is added but the clear methanolic solution is left for a few hours, a new compound m.p.  $174\text{--}175^\circ$  with structure VI separates.

	C	H	Active O	$\text{OCH}_3$	mol. weight (in benzene)
Anal. found	70.00	5.96	5.88	22.87	254
Calc. for $\text{C}_{16}\text{H}_{16}\text{O}_4$	70.58	5.92	5.82	22.80	272

The product gives a negative lead tetraacetate test and the infrared spectrum contains no carbonylbands. Apparently the intermediate semiacetal V is slowly converted into the acetal VI. BAILEY has also obtained this product with m.p.  $180\text{--}181^\circ\text{C}$  after recrystallisation from methyl-ethylketone, whereas we used methanol. It may be noted that we have formulated only one of the possible stereoisomers of VI.

We are studying the effect of benzaldehyde when this is added immediately after ozonisation, in order to find out whether this can prevent intramolecular acetalisation ( $\text{IV} \rightarrow \text{V}$ ) and effect acetalisation with benzaldehyde instead. These and other experimental details will be published elsewhere.

We thank Mr. H. v. D. DONK for experimental assistance in the earlier stages of this work.

*Amsterdam, 27th September 1956.*



## BIBLIOGRAPHY

1. WIBAUT, J. P. *et al.*, Rec. trav. chim. **60**, 842 (1941); **65**, 141, 413 (1946); **66**, 705 (1947); **67**, 945 (1948); **69**, 1355 (1950); **70**, 509, 1005 (1951); **71**, 761, 1124 (1952); **73**, 431 (1954); **74**, 241 (1955); Proc. Koninkl. Ned. Akad. Wetenschap. B **56**, 333 (1953); Verslagen Koninkl. Ned. Akad. Wetenschap. **59**, 93 (1950); *ibid.* **64**, 40 (1955).
2. HARRIES, C. and V. WEISS, Ann. **343**, 373 (1905).
3. INGOLD, C. K., Structure and mechanism in Organic Chemistry, p. 169 (Bell and Sons, London, 1953).
4. BROWN, R. D., J. Chem. Soc., **1950**, 3249.
5. COOK, J. W. and R. SCHOENTAL, J. Chem. Soc. **1948**, 170; Nature **161**, 237 (1948).
6. DRAKE, N. L. and T. R. SWEENEY, J. Org. Chem. **11**, 67 (1946).
7. BOER, H. and E. C. KOOYMAN, Anal. Chim. Acta **5**, 550 (1951).
8. CRIEGEE, R., G. BLUST and G. LOHAUS, Ann. **583**, 2 (1953).
9. CRIEGEE, R. *et al.*, Ann. **564**, 9 (1949); Chem. Ber. **86**, 1 (1953); Ann. **583**, 2 (1953); Chem. Ber. **37**, 766, 993, 1708 (1954); Chem. Ber. **88**, 795, 1878, 1889 (1955).
10. SCHMITT, W. J., E. J. MORICONI and W. F. O'CONNOR, J. Am. Chem. Soc. **77**, 5640 (1955).
11. BRINER, E. *et al.*, Helv. chim. Acta **35**, 340, 353, 2145 (1952) *ibid.* **36**, 1166 (1953); *ibid.* **37**, 1558, 1561 (1954); Compt. rend. **234**, 1932 (1952); *ibid.* **237**, 504 (1953).
12. CRIEGEE, R., A. KERCKOW and H. ZINKE, Chem. Ber. **88**, 1878 (1955).
13. BRINER, E. and E. DALLWIGK, Helv. chim. Acta **39**, 1446 (1956).
14. BAILEY, P. S., J. Am. Chem. Soc. **78**, 3811 (1956).
15. CRIEGEE, R., Fortschr. der Chem. Forsch. **1**, 542 (1950).

INVESTIGATION OF THE ALKALOIDS OF PUNICA GRANATUM L.  
(3rd communication)<sup>1)</sup>

BY

J. P. WIBAUT AND U. HOLLSTEIN

(Communicated at the meeting of June 30, 1956)

The alkaloid pelletierine  $C_8H_{15}ON$  has been mentioned in the chemical, pharmaceutical and medical literature for about eighty years. Pelletierine is said to occur in the bark of *Punica Granatum* L. together with pseudopelletierine,  $C_9H_{17}ON$ , isopelletierine,  $C_8H_{15}ON$ , and methylisopelletierine  $C_9H_{17}ON$ . It is thought that pelletierine has anthelmintic properties and that the anthelmintic activity of the mixture of alkaloids from *Punica granatum* is mainly (or at least to a considerable extent) due to the presence of pelletierine in these mixtures.

On the strength of various reactions HESS [1], in 1917/18, ascribed the structure of 3-(2'-piperidyl)propanal to pelletierine. Although the degradation evidence as given by him seems to support this conclusion, there may be an unsuspected weak link in his chain of argument.

Several attempts during the period 1940–1953 to synthesize the 3-(2'-piperidyl)propionaldehyde were unsuccessful [2, 3, 4]. Though the diethylacetal of this aldehyde has been synthesized, it has not been possible to obtain the aldehyde itself. Although this aldehyde is no doubt formed primarily through hydrolysis of the acetal, only resinous substances are obtained. Other synthetic approaches also failed. Therefore, in recent years the existence of pelletierine has been questioned.

GALINOVSKY and VOGL [5] prepared the N-benzoyl derivative from synthetic isopelletierine, 1(2'-piperidyl)propanone. On the other hand, from a commercial sample of "pelletierine hydrobromide", in which according to their investigation the hydrobromides of some alkaloids from *Punica granatum* were present, they prepared N-benzoylisopelletierine; it appeared from the melting point and mixed melting point that this preparation was identical with the synthetic product.

On the strength of these as well as other observations GALINOVSKY and HÖLLINGER [6] hold the view that the so-called pelletierine does not exist, but that the alkaloid described as such is in reality isopelletierine.

We have made similar observations: a sample of so-called "d,l-pelletierine hydrobromide", which had been isolated from the bark of *Punica*

<sup>1)</sup> U. HOLLSTEIN, "Onderzoek naar het voorkomen van Pelletierine in *Punica Granatum* L.", Thesis, Amsterdam, 1956.

Granatum by Wellcome Research Laboratories (England), was found to be identical with the hydrobromide of synthetically prepared d,1-isopelletierine [4].

Obviously, these observations do not warrant a definite answer to the question as to whether a substance having the structural formula of 3(2'-piperidyl)propanal occurs in *Punica Granatum*. Therefore we started a new investigation, using modern analytical methods [7].

In the second communication [8] on this subject we described the separation of the alkaloids of *Punica Granatum* L. by means of chromatography on paper <sup>2)</sup>. We examined three samples of bark of different origin. All the three samples contain in addition to pseudopelletierine, isopelletierine and methylisopelletierine other basic components, which give a colour reaction with DRAGENDORFF's reagent.

We have improved the chromatographic separation. The results obtained with three samples of bark of different origin are given in this communication.

Table I <sup>3)</sup> first of all gives the  $R_f$  values of some still unknown bases, which for the time being are indicated by  $A_0$ ,  $A_1$ ,  $A_2$ ,  $A_3$  and  $A_4$ , and the  $R_f$  values of pseudopelletierine, methylisopelletierine and isopelletierine.

TABLE I

	A-total	$A_0$	$A_1$	$A_2$	$A_3$	$A_4$	pseudop.	methylisop.	isop.
$R_f$		0.03	0.07	0.11	0.17	0.21	0.35	0.48	0.55
	%	%	%	%	%	%	%	%	%
extract 1	11						86	3	
extract 2	9	2	—	5	—	2	83	3	5
extract 3									
neutral	11	< 1	< 1	2	< 1	9	78	4	7
extract 3									
alkaline	15	< 1	< 1	2	3	10	79	—	6
extract 3									
combined	9	< 1	1	3	< 1	5	82	4	5

The numbers 1, 2 and 3, respectively, relate to: 1. bark of unknown origin, obtained from England; 2. bark of Italian origin and 3. bark of Spanish origin. The percentages of pseudo-, methyliso- and isopelletierine have been calculated from calibration curves representing the relation

<sup>2)</sup> In this communication we assumed that methylisopelletierine in basic milieu is converted into condensation products. However, after having repeated these experiments under the same conditions as used by GALINOVSKY *et al.* [11]. We found only racemisation in agreement with the results of these Austrian authors.

<sup>3)</sup> In the 2nd communication reference is made to a substance C, which was found in chromatography on a buffered kieselguhr column during elution with ether. It has now been found that this substance, as regards  $R_f$  value and specific violet colour of the spot, is identical with  $A_4$  ( $R_f = 0.21$ ).

between the size of the spots and the quantity of synthetic alkaloid deposited. The percentages of the unknown bases A have been calculated from a fictitious calibration curve, which we obtained by averaging the three wellknown calibration curves. Relative errors of about 50 % should be taken into account for percentages under 10 %. In paper chromatography of bark 1 the technique had not yet been developed to such an extent as to permit separation of substances A into their components, so that we can only give A-total.

The alkaline and neutral extraction, respectively, of bark 3 depends on whether the bark has been subjected to an alkaline pretreatment (with  $\text{Ca}(\text{OH})_2$ ). The combined extraction has been described in our previous communication [8].

By adapting the circular preparative paper chromatography according to GIRI [9] to our separation problem we succeeded in isolating the bases  $A_1$ ,  $A_2$  and  $A_4$  as picrolonates from the combined extract of bark 3. The  $A_0$  and  $A_3$  concentrations were so low that isolation was not possible. On the assumption that the unknown bases contain only one nitrogen atom per molecule, we find from the analyses of the picrolonates the following simplest formulas for the bases:  $A_1 : \text{C}_9\text{H}_{17}\text{O}_2\text{N}$ ;  $A_2 : \text{C}_{10}\text{H}_{19}\text{O}_2\text{N}$ ;  $A_4 : \text{C}_7\text{H}_9\text{ON}$ . These formulas show that, in comparison with  $A_1$ ,  $A_2$  contains an additional  $\text{CH}_2$  group, so that the bases  $A_1$  and  $A_2$  might be considered as homologues; the low hydrogen content of  $A_4$  points towards an aromatic character. The principal conclusion, however, is that apart from isopelletierine, the bark does not contain an isomeric compound of the composition  $\text{C}_8\text{H}_{15}\text{ON}$ . The slight quantities of  $A_0$  and  $A_3$ , which cannot be isolated, can be left out of consideration.

Besides, in quite a different way we could demonstrate that the various bark extracts examined do not contain a substance of the structure 3(2'-piperidyl)propanal. In spite of the instability of this aldehyde, former investigations by GALINOVSKY and co-workers [3] showed that this substance is formed as an intermediary during the last step of the synthesis before resinification occurs. This conclusion could be confirmed by experiments in which the 3(2'-piperidyl)propanal-2,4-dinitrophenylhydrazone hydrochloride was formed from the acetal after acid hydrolysis. The presence in the hydrolysis product of an aldehyde group could be demonstrated with SCHIFF's reagent and by means of a - though less specific - reaction with ammoniacal silver solution.

The 3(2'-piperidyl)propanal was prepared in dilute solution in three ways, which have previously been tested for a synthesis, viz. by acid hydrolysis of the acetal [2], by dehydrogenation of 4(2'-piperidyl)butanediol-1,2 [4] and by reduction of 3-ketooctahydropyrrocoline [3].

From the close agreement of  $R_f$ -values of these three reaction products in each of 11 different paper chromatographic systems we concluded that these products are identical.

These spots, which we therefore ascribe to 3(2'-piperidyl)propanal, do

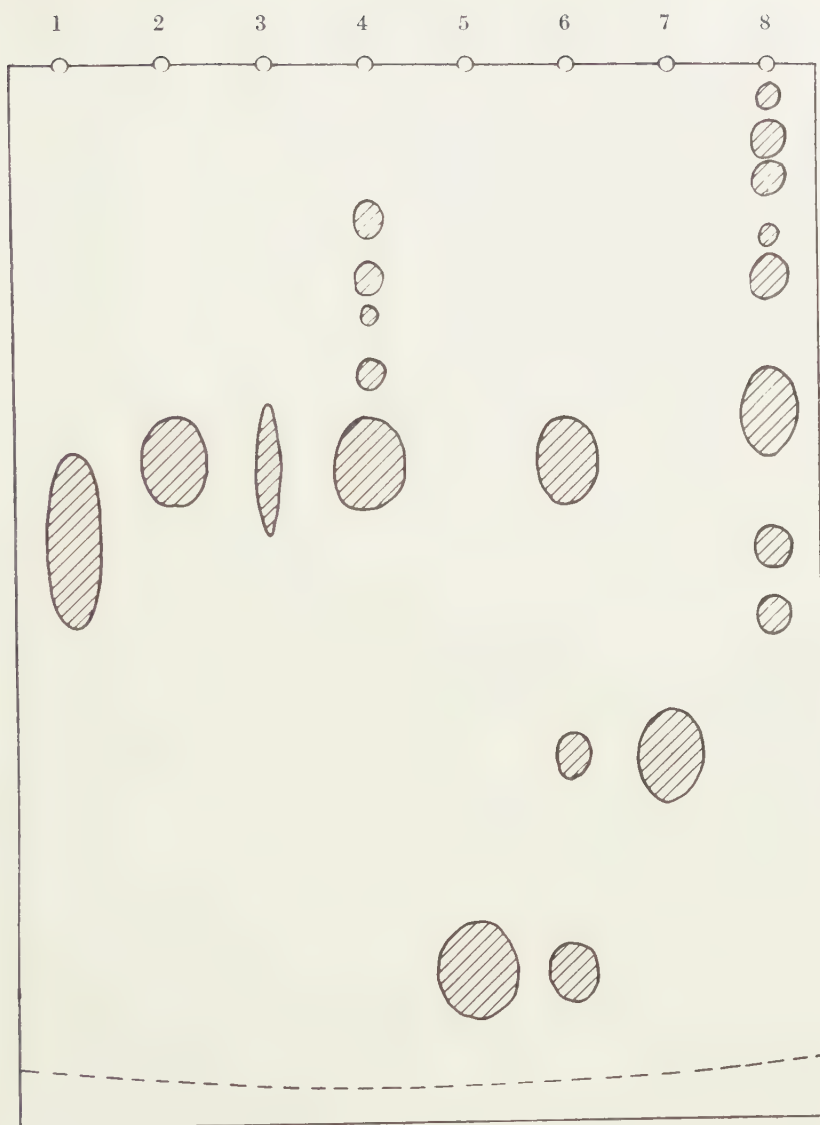


Fig. 1. Paperchromatogram

Whatmanpaper No. 1. Solvent n-butanol/9.5 % HCl 15 : 4.

----- = solvent front

1. 3(2'-piperidyl) propanal diethylacetal.
2. Hydrolysis product of 1.
3. 4(2'-piperidyl) butanediol-1.2.
4. Dehydrogenation product of 3.
5. 3-ketooctahydropyrrocoline..
6. Reduction product of 5.
7. Octahydropyrrocoline.
8. Extract "3. combined" of Punica Granatum L.



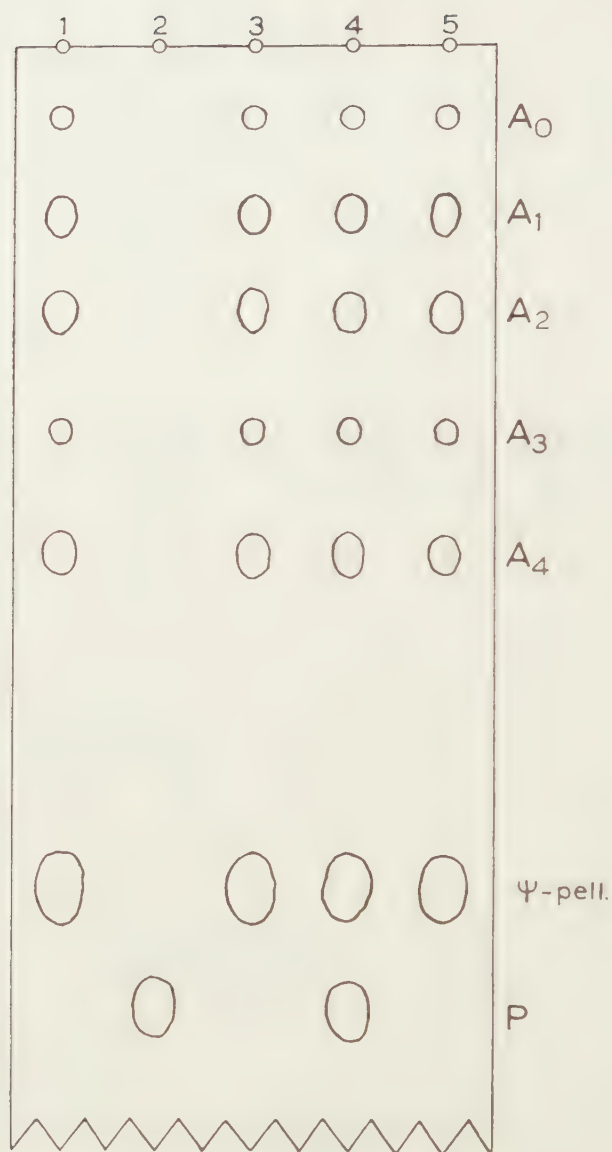


Fig. 2. Paperchromatogram

Whatmanpaper No. 1. Solvent n-butanol/9.5 % HCl 15 : 4.  
The front has flown off the paper.

1. Extract "3. combined" of *Punica Granatum* L.
2. Hydrolysed 3(2'-piperidyl) propanal diethylacetal (P).
3. Sample 1.
4. Mixture of sample 1. and sample 2. (1 : 1).
5. Sample 1.

not occur in the bark extracts of the samples under investigation.

By way of illustration we give two pictures of chromatograms. In fig. 1 the spots of the three above-mentioned starting materials are compared with 3(2'-piperidyl)propanal formed from them and with a chromatogram of "bark extract 3 combined". Fig. 2 represents an elution chromatogram (where the solvent front has flown off the paper), in which this bark extract is compared with hydrolysed acetal (P).

*We now consider it very improbable that the aldehyde 3(2'-piperidyl)propanal occurs in nature.*

The fact that the resinification of 3(2'-piperidyl)propanal is actually based on autocondensation, as presumed by former investigators, has now been proved in our opinion by the I.R.spectra of the hydrolysis product of 3(2'-piperidyl)propanal acetal in carbon tetrachloride and of the hydrobromide of this hydrolysis product in a potassium bromide disc. Using carbon tetrachloride as solvent we observed bands at  $1682\text{ cm}^{-1}$  and at  $1643\text{ cm}^{-1}$ ; for the potassium bromide disc the bands were found at  $1677\text{ cm}^{-1}$  and at  $1632\text{ cm}^{-1}$ . We ascribe these bands to an  $\alpha$ - $\beta$ -unsaturated aldehyde and to a carbon-carbon double bond. The resinification is therefore based on a polyaldol condensation, followed by dehydration.

GALINOVSKY's supposition that the pelletierine described in the literature is identical with isopelletierine would now seem to us to be correct. The melting points of the hydrochloride, the hydrobromide and the picrate of isopelletierine closely approximate the values stated in the literature for the hydrochloride, the hydrobromide and the picrate of pelletierine.

The same applies to the melting point of the N-benzoyl compound of isopelletierine compared with the literature value for the N-benzoyl compound of pelletierine.

We have prepared the oxime of d,l-isopelletierine and its picrate. The melting points of these compounds do not differ much from the values stated by HESS for the melting points of the pelletierine oxime and its picrate, respectively.

In connection with indications in the literature that pelletierine shows anthelmintic activity it is interesting to find out to what extent 3(2'-piperidyl)propanal possesses this property in comparison with  $\psi$ -pelletierine, isopelletierine and methylisopelletierine.

This investigation has been made by Dr. J. VAN NOORDWIJK at the Pharmaco-therapeutical laboratory of the University of Amsterdam. We are indebted to Prof. Dr. B. MENDEL, director of this laboratory, who placed the necessary equipment at our disposal and to Dr. J. VAN NOORDWIJK, who permitted us to mention the results obtained by him in this communication.

For this investigation dilute solutions of the hydrochlorides of  $\psi$ -pelletierine, d,l-isopelletierine and d,l-methylisopelletierine were used; these substances have been synthesized at our laboratory.

The pharmacological activity of these substances has been investigated on the liver fluke according to the method of CHANCE and MANSOUR [10]. *Isopelletierine hydrochloride is still active at a concentration of 1/16,000 to 1/32,000, whilst the hydrochloride of 3(2'-piperidyl)propanal is not active at a concentration of 1/1000.*

Methylisopelletierine and  $\psi$ -pelletierine (as hydrochlorides) are still active in a solution of 1/4000 to 1/8000.

Of the *Punica Granatum* alkaloids the isopelletierine shows the greatest activity (with respect to the liver fluke), methylisopelletierine and  $\psi$ -pelletierine being less active.

It follows therefore that the anthelmintic activity of extracts from *Punica Granatum* is chiefly due to isopelletierine. This is in agreement with our concept that the pelletierine mentioned in the literature is identical with isopelletierine.

### Experimental

#### Isolation of $A_1$ , $A_2$ and $A_4$ picrolonates.

For all chromatograms n-butanol/9.5 % HCl 15:4 was used as solvent.

$A_1$  was isolated with  $3 \times 10$  sheets of Whatman paper No. 3, on which 1350 mg of alkaloid hydrochlorides had been deposited. 8.5 mg of paper chromatographically pure  $A_1$  picrolonate was isolated.

	C	H	N	m.pt (KOFER)
$A_1$ picrolonate	52.7	5.9	15.9	162°–166°
calc. for $C_{19}H_{25}O_7N_5$	52.41	5.79	16.09	

Assuming that the base contains only one nitrogen atom, a calculation from the analysis figures gives  $C_9H_{17}O_2N$ .

Of  $A_2$  three portions were isolated, viz. 3.1 mg (I) from 6 sheets with 240 mg total mixture, 13.1 mg (II) from 6 + 7 sheets with 944 mg total mixture and 23 mg (III) from 3 + 10 sheets with 1350 mg total mixture.

$A_2$ picrolonate	C	H	N	m.pt (KOFER)
I	52.6	5.8		190°–193°
II	53.1	6.0	15.2	181°–185°
III	53.0	6.4	15.15	188°–192°
calc. for $C_{20}H_{27}O_7N_5$	53.44	6.06	15.58	

The picrolonates were paper chromatographically pure. The simplest formula for  $A_2$  is  $C_{10}H_{19}O_2N$ .

Of  $A_4$  22.5 mg was isolated from 12 + 6 + 7 sheets with 1184 mg total mixture.

	C	H	N	m.pt (KOFER)
$A_4$ picrolonate	52.6	4.55	18.2	155°–158°
calc. for $C_{17}H_{17}O_6N_5$	52.71	4.42	18.08	

The base was calculated as being  $C_7H_9ON$ .

*Hydrochloride of 3(2'-piperidyl)propanal-2,4-dinitrophenylhydrazone.* To 45 ml of a 2,4-dinitrophenylhydrazine solution in about 18 % of hydrochloric acid, 0.3 g of 3(2'-piperidyl)propanal acetal was added at 50° C. After 10 minutes an orange-red crystalline product precipitated, which after recrystallisation from ethanol melted with decomposition at 191°–193° (Kofler).

	C	H	N	Cl
found	47.0	5.6	19.4	10.1
calc. for $C_{14}H_{20}O_4N_5Cl$	46.99	5.63	19.57	9.91

*Isopelletierine oxime.*

This substance could be prepared from isopelletierine hydrochloride according to the directions given by HESS and EICHEL [1] for the preparation of pelletierine oxime. After recrystallisation from diethyl ether the melting point (Kofler) was 100°–104°. HESS reports for the melting point of the oxime of "pelletierine" 96°–97° (from petr. ether) and 80° (from diethyl ether).

	C	H	N
found	62.1	10.3	17.9
calc. for $C_8H_{16}ON_2$	61.50	10.32	17.93

*Isopelletierine oxime picrate.*

This substance was prepared according to the directions given by HESS and co-workers for pelletierine oxime picrate. After recrystallisation from ethanol the picrate melted at 175°–176° (Kofler). HESS reports for the melting point of pelletierine oxime picrate 179°–180°.

	C	H	N
found	43.8	4.9	18.0
calc. for $C_{14}H_{19}O_8N_5$	43.64	4.97	18.18

*Preparation of a dilute 3(2'-piperidyl)propanal hydrochloride solution*

A solution of the hydrochloride of d,l-3(2'-piperidyl)propanal was obtained as follows. Dilute hydrochloric acid was added to 3(2'-piperidyl)propanal diethylacetal until the pH of the liquid was about 4. The solution was warmed for a short time. The colourless solution thus obtained which, in addition to the hydrochloride of piperidyl propanal, contained some ethanol, was used as soon as possible for the biological experiment. (The quantity of ethanol present was smaller than the value which shows pharmacological activity).

BIBLIOGRAPHY

1. HESS, K. and A. EICHEL, Ber. **50**, 1192 (1917).
2. BEETS, M. G. J. and J. P. WIBAUT, Rec. Trav. Chim. **60**, 905 (1941).  
SPIELMAN, M. A., S. SWADESH and C. W. MORTENSON, J. Org. Chem. **6**, 780 (1941).

3. GALINOVSKY, F., O. VOGL and R. WEISER, *Monatsch.* **83**, 114 (1952).
4. WIBAUT, J. P. and M. J. HIRSCHER, *Rec. Trav. Chim.* **75**, 225 (1956).
5. GALINOVSKY, F. and O. VOGL, *Monatsh.* **83**, 1055 (1952).
6. ——— and R. HÖLLINGER, *Monatsh.* **85**, 1012 (1954).
7. WIBAUT, J. P., H. C. BEYERMAN and P. H. ENTHOVEN, *Rec. Trav. Chim.* **73**, 102 (1954).
8. ———, ———, U. HOLLSTEIN, YVONNE M. F. MULLER and E. GREVELL, *Proc. Koninkl. Nederl. Akad. Wetensch., Amsterdam*, **B 58**, 56 (1955).
9. GIRI, K. V., *J. Ind. Inst. Science* **37**, 1 (1955).
10. CHANCE, M. R. A. and T. E. MANSOUR, *Brit. J. Pharmacol.* **4**, 7 (1949)  
NOORDWIJK, J. v. and U. HOLLSTEIN, *Acta Physiol. Pharmacol. Neerl.* in  
the press.
11. GALINOVSKY, F., G. BIANCHETTI and O. VOGL, *Monatsch.* **84**, 1221 (1953).



# THE DEHYDRATION OF ALUMINA HYDRATES. III FORMATION OF THE PORE SYSTEM DURING THE DEHYDRATION OF GIBBSITE

BY

J. H. DE BOER, J. J. STEGGERDA AND P. ZWIETERING

(Communicated at the meeting of June 30, 1956)

In previous publications [1] we discussed the phase transformations occurring during the dehydration of gibbsite. The present article deals with the formation of the pore system during this process.

## A. The development of the internal surface

In addition to our experiments on the adsorption of lauric acid on partially dehydrated gibbsite [1], we have examined the development of the internal surface area by means of nitrogen adsorption. Measurements were made on normal gibbsite, prepared by the Bayer process. Dehydration was effected by heating the gibbsite for about 8 hours at temperatures between 165 and 700° C, under atmospheric pressure and humidity conditions. The surface areas were calculated by the method of BRUNAUER, EMMET and TELLER from the data of the adsorption of nitrogen at 77.3° K.

The results of this investigation are given in figures 1 and 2.

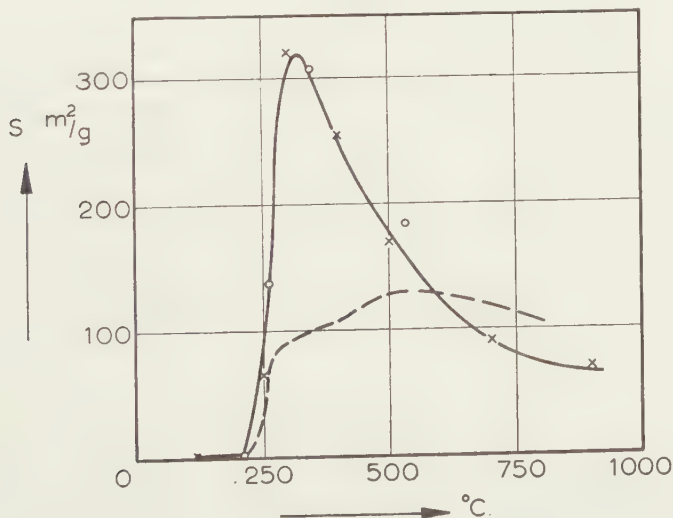


Fig. 1. The surface area of gibbsite as a function of the dehydration temperature.  
 ————— from N<sub>2</sub>-adsorption data  
 - - - - - from lauric acid-adsorption data

In Fig. 1 the surface area per gram of  $\text{Al}_2\text{O}_3$  is plotted as a function of the dehydration temperature; Fig. 2 shows this area as a function of the water content (calculated on dry  $\text{Al}_2\text{O}_3$ ).

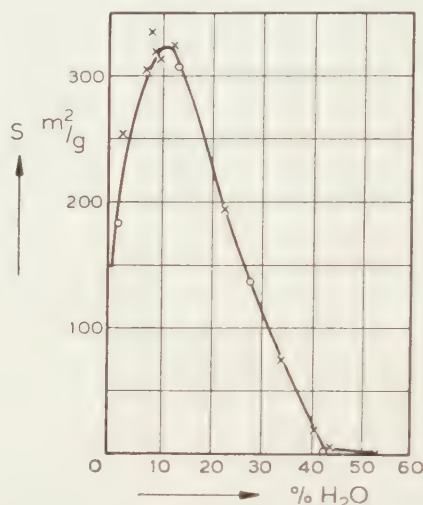


Fig. 2. The surface area of gibbsite from  $\text{N}_2$ -data as a function of the water content (calculated on anhydrous  $\text{Al}_2\text{O}_3$ ).

Our results are in good agreement with those obtained by other investigators, in particular with BLANCHIN's [3]. The maximum surface area, 300 sq. m/g, was found at 300° C at a water content of about 10 %. As clearly illustrated by Fig. 2 the surface area remains remarkably small during the first stage of dehydration. Practically no available surface area is found at water contents between 53 % and 44 %, the region where boehmite is formed. Only below 44 %, water does the surface area begin to develop more strongly, indicating that the  $\gamma$ - $\text{Al}_2\text{O}_3$ , formed in this region, has an extended surface area. This is in complete agreement with the theory advanced by us on the intragranular hydrothermal formation of boehmite [1, 2]. Also the surface area accessible to laurie acid showed the characteristic described above [1, art. I]. However, the shape of the curve, shown again in Fig. 1, is quite different in this case. This is to be attributed to the fact that the fraction of the total surface area which is accessible to laurie acid varies owing to a change in the pore width occurring during dehydration.

#### B. The pore size distribution during dehydration

Adsorption and desorption isotherms of nitrogen at 77.3° K were measured of four samples, chosen from different regions of the dehydration range of gibbsite. The pore size distributions of the samples were calculated from the desorption branches by the method of BARRETT, JOYNER and HALENDA [4]. In some cases the form of the adsorption branches enabled us to draw conclusions with respect to the shape of the pores.

We shall now discuss the results obtained by examination of the four samples.

### Sample PSH200

After having been heated at 200° C for 8 hours this sample had a water content of 47.8 %, showing that part of the gibbsite had been converted into boehmite. The isotherm of the sample is given in Fig. 3.

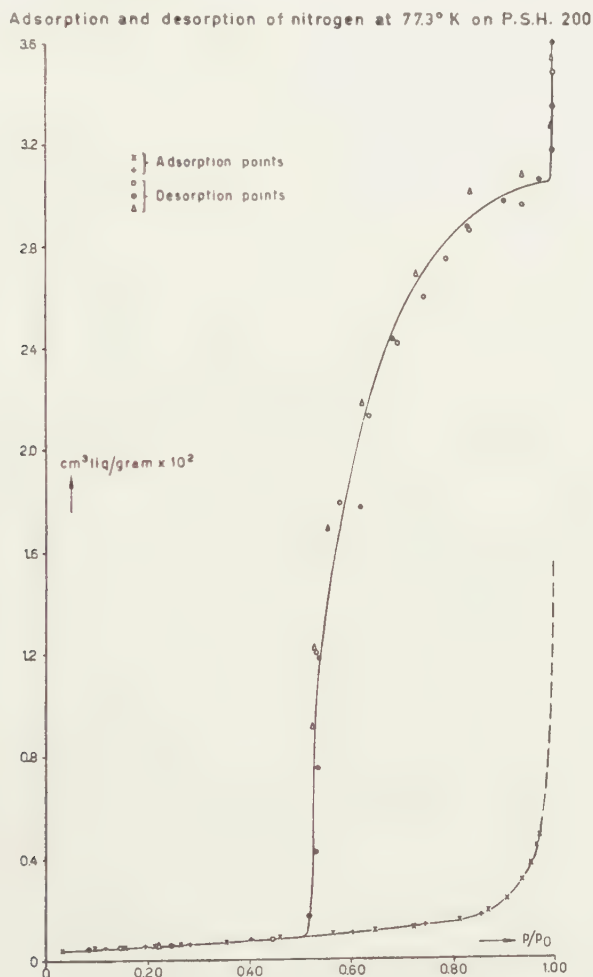


Fig. 3. The N<sub>2</sub>-adsorption-desorption-isotherm at 77.3° K on PSH 200.

The available internal surface area of this sample, calculated by the B.E.T. method, is 1.3 sq. m/g. If the surface area is calculated by the method of BARRETT, JOYNER and HALENDA, a value of about 40 sq. m/g is found. This discrepancy, and the shape of the hysteresis, point to a pore system—which consists of pores 500 Å wide—being closed by very short, 30 Å wide “bottlenecks”. We intend to revert to this question in a following article.

## Sample PSH 259

The sample was heated at 259° C for eight hours, after which it had a water content of 28.1 %. This shows it to consist of boehmite,  $\chi$ - $\text{Al}_2\text{O}_3$  and unconverted gibbsite. The surface area calculated by the B.E.T. method was 137 sq. m/g. The shape of the hysteresis in the isotherm (Fig. 4) enables us to conclude that the greater part of the pore volume consists of fissure-like pores [5]. The pore size distribution was calculated

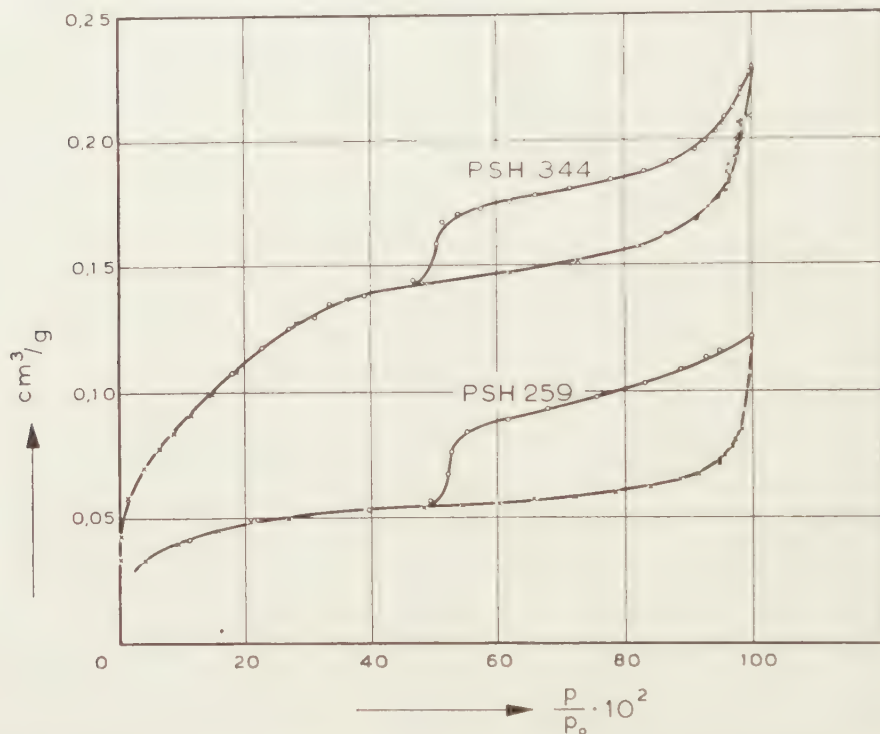


Fig. 4. The  $\text{N}_2$ -adsorption-desorption-isotherms at 77.3° K on PSH 259 and PSH 344.

by means of the method of BARRETT, JOYNER and HALENDA [4], modified to apply to fissure-like pores [2]. Results are given in Figs. 5 and 6, which show the cumulative pore volume and the cumulative surface area respectively as functions of the pore diameter.

Three types of pores are found to occur in this sample:

1) Very wide pores, which are formed during the formation of the boehmite, and which, during this first stage of dehydration, were not freely accessible to gases. In the later stages of dehydration they are freely accessible.

2) Fissure-like pores, having a width of about 28 Å. In the discussion of the optical investigation further information will be given on the nature of these pores.

3) Very narrow pores of unknown shape, having a width of about 7 Å.

#### Sample PSH 344

Gibbsite was heated at 344°C for eight hours, under atmospheric pressure and humidity conditions. After this, the sample had a water content of 13.8 %. The gibbsite had been completely converted; the sample consisted of a mixture of boehmite and  $\chi$ - $\text{Al}_2\text{O}_3$ . The isotherm

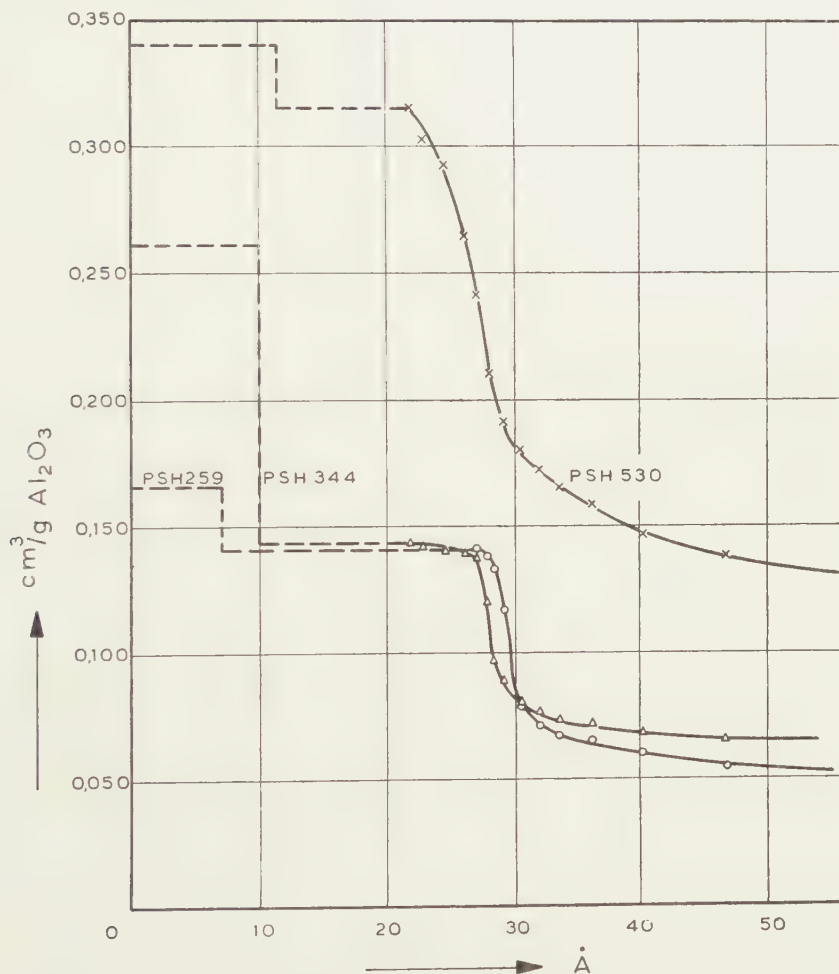


Fig. 5. The cumulative pore volume as a function of the pore width.

and the pore size distribution, calculated from it, are also given in Figs. 4, 5 and 6, which show that when dehydration advances between 28 % and 13 % water, only very narrow pores—scarcely 10 Å wide—are formed. The fissure-like 29 Å-wide pores remain unchanged.

#### Sample PSH 530

Gibbsite was heated at 530°C for eight hours. After this the water



content of the sample was 2.0 %. The nitrogen isotherm is given in Fig. 7, the pore size distributions, calculated from it, are shown in Figs. 5 and 6.

As a result of sintering, the surface area of this sample, 190 sq. m/g, has already become considerably smaller than the maximum available surface area of 300 sq. m/g (see Fig. 1). Also the pore size distribution proved to have changed considerably as a result of the sintering process. The difference between the abovementioned three types of pores is diminished;

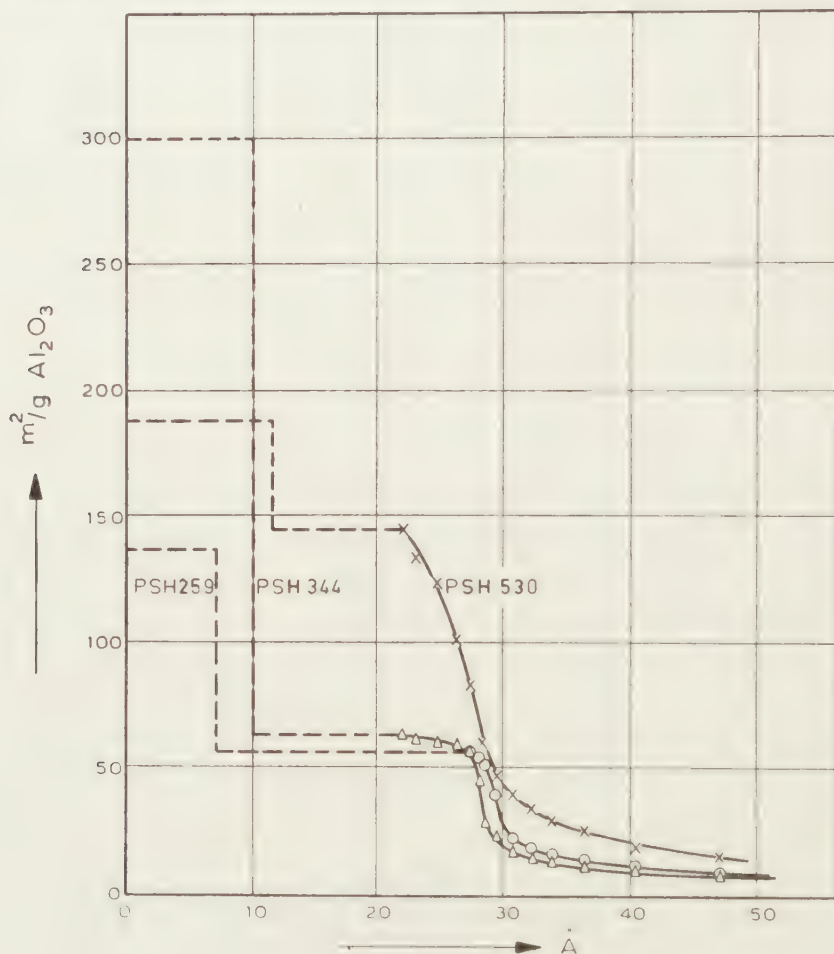


Fig. 6. The cumulative surface area as a function of the pore width.

the pore width is increased. From the shape of the hysteresis it is seen, moreover, that the pore shape also had undergone a change: it seems as if no fissure-like pores are left.

The results obtained from the investigation of the four samples enable us to derive the following picture of pore genesis during the dehydration of gibbsite:

- 1) During the intragranular hydrothermal formation of boehmite wide

pores ( $> 500 \text{ \AA}$ ) are formed, which, at first, are not accessible for gases.

During the formation of the  $\chi\text{-Al}_2\text{O}_3$  two more types of pores are formed in the order as given:

2) Fissure-like pores having a mean width of  $30 \text{ \AA}$ .

3) Very narrow pores (about  $10 \text{ \AA}$ ), which make the greatest contribution to the total internal surface area.

4) At temperatures above  $300^\circ \text{C}$  the surface area decreases as a result of sintering. In this process the pore structure is changed considerably; as the temperature rises, the pores grow wider.

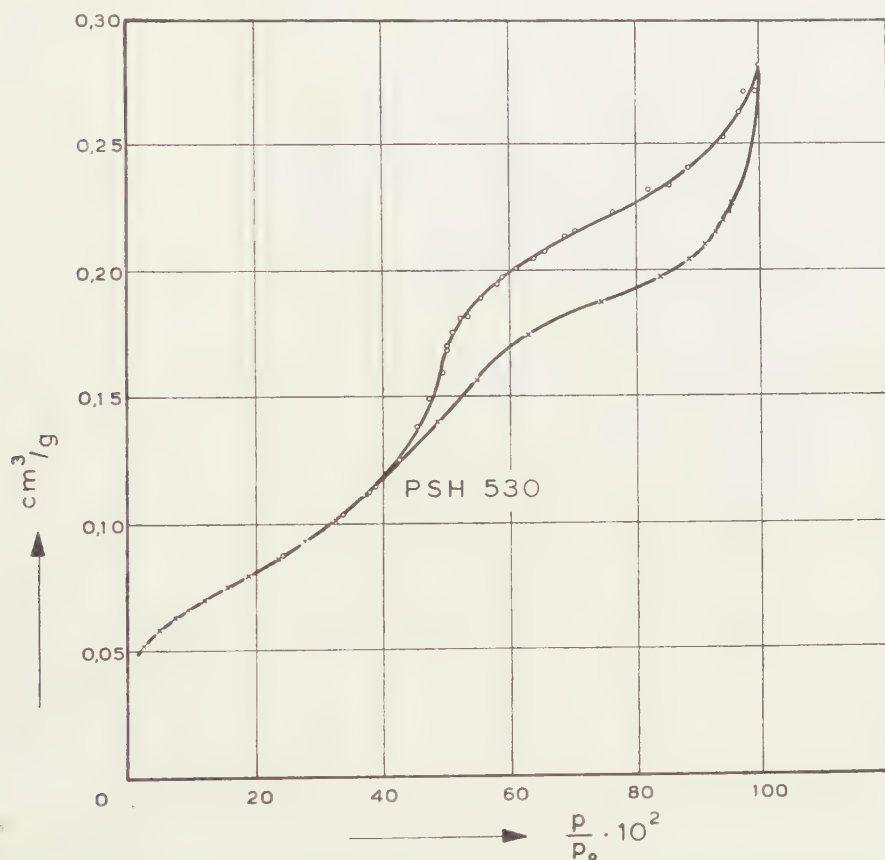


Fig. 7. The  $\text{N}_2$ -adsorption-desorption-isotherm at  $77.3^\circ \text{K}$  on PSH 530.

### C. Microscopic investigation

We have found that the microscopic investigation of gibbsite and its dehydration products constitutes an entirely new source of information on the pore structure, completely independent of all adsorption problems. A synthetic and a natural gibbsite were examined under the microscope. The synthetic gibbsite was prepared by passing carbon dioxide through a hot, concentrated sodium aluminate solution. In this process gibbsite is precipitated in the form of small rod-like crystals, which are developed

in the [001] direction. The crystals of natural gibbsite were isolated from a sample of coarse-crystalline bauxite from Surinam<sup>1)</sup>. They consisted of rather large (some tenths of mm), thin hexagonal cleavage plates (the cleavage plane of gibbsite is (001)). These crystals also lent themselves to conoscopic examination; because of their small size ( $10\ \mu$ ) the synthetic crystals could not be examined conoscopically. Both products gave only a small yield of boehmite when heated. This boehmite proved to have no effect on the phenomena which will be mentioned below and which we attribute exclusively to the presence of  $\chi\text{-Al}_2\text{O}_3$ . The observations made on the two types of gibbsite are in complete agreement with each other.

The optical behaviour of the products formed during the dehydration of the gibbsite to  $\chi\text{-Al}_2\text{O}_3$  is as follows:

a) In the first stage of the dehydration process the positively birefringent gibbsite (practically uniaxial; its axis is nearly perpendicular to the cleavage plane) is converted into a negatively birefringent product the optical axis of which is about perpendicular to the cleavage plane (001) of the original gibbsite.

b) When the decomposition of the gibbsite advances, the dehydration product again becomes positively birefringent; the optical axis, however, has turned through  $90^\circ$ , and now lies in the cleavage plane of the original gibbsite. This situation remains unaltered, even after the product is heated at  $1200^\circ\text{C}$  and converted into  $\alpha\text{-Al}_2\text{O}_3$ .

$\chi\text{-Al}_2\text{O}_3$  belongs to the cubical system; consequently the birefringence observed by us is not to be attributed to the  $\chi\text{-Al}_2\text{O}_3$  itself. An explanation of the phenomena may be found in WIENER's theory on the optical behaviour of heterogeneous finely-dispersed systems [6, 7]. If a heterogeneous system is composed of two phases differing in refractive index and one of the phases is present in the form of particles oriented according to a specific axis, while both the size of the particles and the distance between them are smaller than the wave length of the light employed for the investigation, the system is optically anisotropic. It behaves like an optically uniaxial crystal. It is not essential for the occurrence of this phenomenon that one of the phases is anisotropic itself. This phenomenon is mostly referred to by the term "form-birefringence". It will be clear that the birefringence observed in dehydrated gibbsite may be interpreted as such a form-birefringence, as we are here concerned with two phases, viz.  $\chi\text{-Al}_2\text{O}_3$  and pores, the sizes of which are of the order of  $10\text{--}100\ \text{\AA}$  and which are filled with air. We must conclude that the  $\chi\text{-Al}_2\text{O}_3$  and the pores possess a very distinct orientation.

In his theory WIENER gives the following two possibilities as regards orientation:

<sup>1)</sup> We wish to thank Dr. H. EBBINGE of Billiton Mij., The Hague and Professor Dr. E. NIGGLI, formerly at Leyden University, who kindly supplied us with the samples.



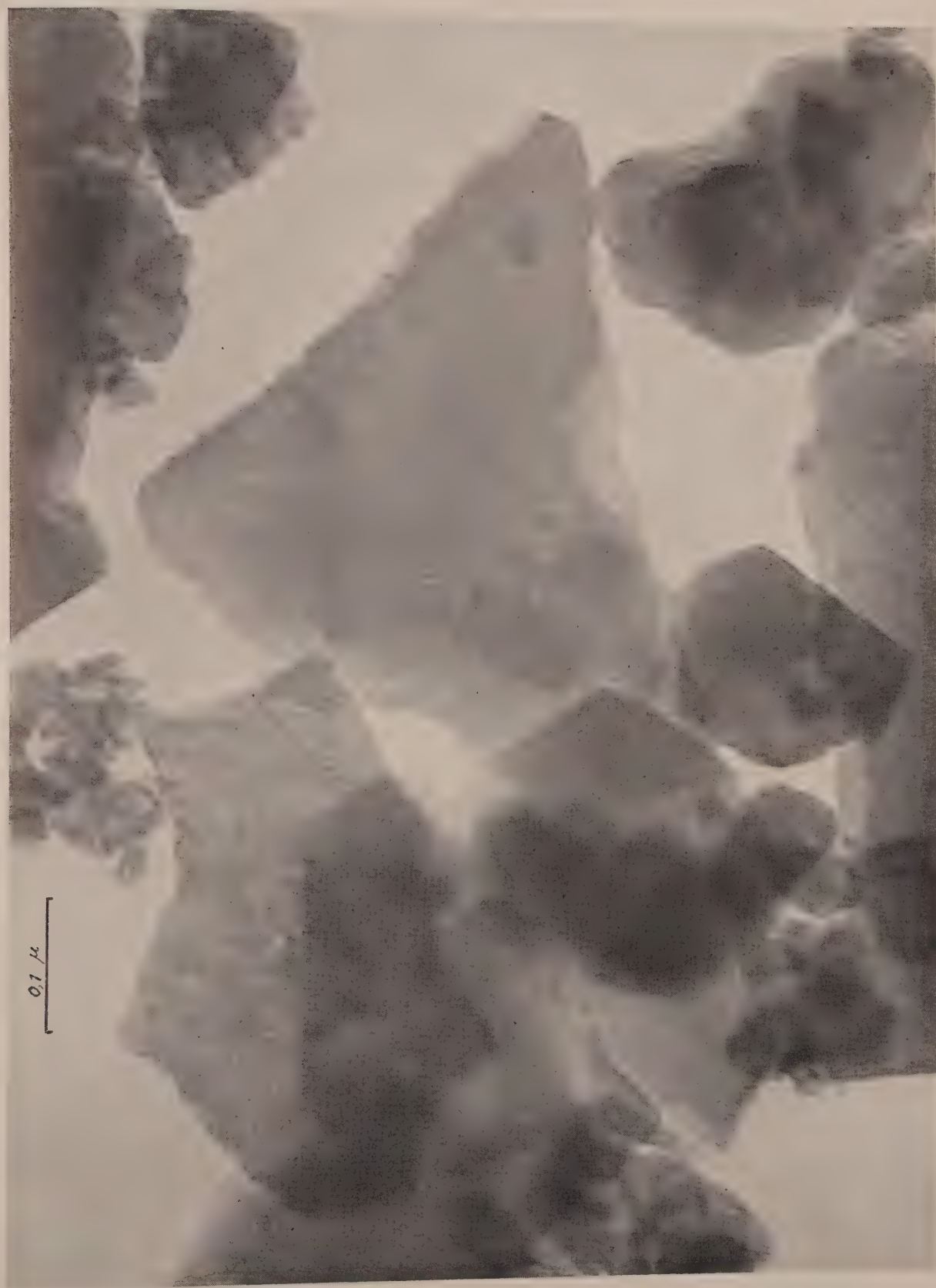


Fig. 8. Electron-microscope photo of gibbsite, dehydrated at 300° C.



Fig. 9. Electron microscope photo of gibbsite, dehydrated at 300° C. Remark that there is no parallel structure visible on the pseudohexagonal cleavage planes.



Fig. 10. Laue pattern of  $\chi\text{-Al}_2\text{O}_3$ , formed by dehydration of one crystal gibbsite. Incident  $X$ -ray beam perpendicular to the cleavage plane of the original gibbsite.



a) One of the phases consists of cylindrical particles oriented parallel to each other. In this case the optical axis coincides with the direction of the cylinder axes, and the system is positively birefringent.

b) One of the phases consists of plate-like particles, lying parallel to each other. Here, the optical axis is perpendicular to the plates and the system is negatively birefringent.

With reference to what has been said above we may draw the following conclusions:

a) During the first stage of the dehydration of gibbsite to  $\chi$ - $\text{Al}_2\text{O}_3$  fissure-like pores are formed, which are separated by plate-like particles lying parallel to each other. The pores are oriented in the, very distinct, cleavage direction of the original gibbsite crystal (001). The splitting off of water results in a breaking up of the gibbsite lattice along its cleavage plane. The plate-like particles, thus formed, have an average thickness of 200 Å. In the foregoing we have seen that also the  $\text{N}_2$  adsorption isotherm points to a formation of fissure-like pores in the initial stage of dehydration.

b) When dehydration advances the plate-like particles are divided into rod-like particles, all of which lie parallel to each other in the cleavage plane, hence perpendicular to the [001] direction of the original gibbsite. Consequently, a second type of pores must have been formed. This view is fully confirmed by the adsorption isotherms of nitrogen described above.

c) During sintering, even up to 1200° C, the rod-like structure of the  $\text{Al}_2\text{O}_3$  is left undisturbed, in spite of the fact that the  $\chi$ - $\text{Al}_2\text{O}_3$  is converted, via a number of intermediate stages, into  $\alpha$ - $\text{Al}_2\text{O}_3$  and despite the fact that a sintering process results in a widening of the pores and a serious decrease of the internal surface area.

#### D. *Investigation by means of the electron microscope*

In Figs. 8 and 9 electron microscope photos of gibbsite dehydrated at 300° C, are given <sup>1)</sup>. These photos confirm fully the picture of parallel pores, which we developed from birefringence investigations.

#### E. *X-Ray-investigation*

Laue patterns (Fig. 10) of a dehydrated natural gibbsite crystal reveal that all the parallel oriented  $\chi$ - $\text{Al}_2\text{O}_3$  particles have an octahedron plane parallel to the cleavage plane (001) of the original gibbsite crystal. The assembly of  $\chi$ - $\text{Al}_2\text{O}_3$  particles resulting from one gibbsite crystal, therefore, shows a distinct orientation texture.

#### *Summary*

The formation of the pore system during the dehydration of gibbsite to anhydrous  $\text{Al}_2\text{O}_3$  was studied by means of nitrogen adsorption and by microscopic, electron-microscopic and X-ray examinations. Experimental

<sup>1)</sup> We thank Dr. R. WESTRIK and Mr. A. M. KIEL of the Central Laboratory S.M. for making the electron microscope photos.

results obtained by these methods led to the following picture of the pore system:

During the intragranular hydrothermal formation of boehmite wide cavities, which are at first inaccessible for gases, are formed in the granules.

During the subsequent formation of  $\chi$ - $\text{Al}_2\text{O}_3$ , the real "active" component, two types of pores are formed in succession:

1) Plate-like pores having a width of about 30 Å. These pores are all parallel to each other and lie in the direction of the cleavage plane of the original gibbsite crystal. They are separated by plate-like particles of a thickness of about 200 Å.

2) Subsequently, a second type of pores is formed. These pores have a width of about 10 Å and divide the  $\chi$ - $\text{Al}_2\text{O}_3$  into parallel rod-like crystals.

At about 300° C a maximum internal surface area of 300 sq. m/g is reached. Above this temperature sintering occurs, as a result of which the pore width increases; the differences between the three types of pores described above are gradually lost. The pseudomorphy of the assembly with respect to the original gibbsite crystal and the orientation of the rod-like crystals in the assembly, however, are preserved up to a very high temperature (1200° C).

*Delft, Laboratory for Chemical Technology of the  
Technological University  
Geleen, Central Laboratory of the Netherlands State Mines*

#### REFERENCES

1. BOER, J. H. DE, J. M. H. FORTUIN and J. J. STEGGERDA, The dehydration of alumina hydrates I, Proc. Kon. Ned. Ak. van Wetensch. B 57, 170 (1954); II, ibid B 57, 434 (1954).
2. STEGGERDA, J. J., Thesis, Delft (1955).
3. BLANCHIN, L., Thèse, Lyons (1952).
4. BARRETT, E. P., L. G. JOYNER, P. P. HALENDA, J. Am. Chem. Soc. 73, 373 (1951).
5. BOER, J. H. DE, Verslag van de gewone vergadering van de afd. Natuurkunde van de Kon. Ned. Ak. van Wetensch. 63, No. 7 (1952).
6. WIENER, O., Abhandgn. d. Sächs. Ges. d. Wiss. Math.-Phys. Kl. 32 (1912).
7. AMBRONN, H. and A. FREY, Das Polarisationsmikroskop, seine Anwendung in der Kolloidforschung und in der Färberei. (Leipzig, 1926).

THE REACTIONS OF ORGANIC HALOGEN COMPOUNDS WITH  
SOLUTIONS OF METALS IN NON-AQUEOUS SOLVENTS

(Preliminary Communication)

BY

A. BEVERLOO, M. C. DIELEMAN, K. S. DE VRIES,  
P. E. VERKADE AND B. M. WEBSTER

(Communicated at the meeting of June 30, 1956)

The reactions of various types of organic compounds with solutions of metals, such as sodium and lithium, in non-aqueous solvents, such as liquid ammonia and methylamine, have in recent years again been investigated in various laboratories from different view-points<sup>1</sup>). For this reason it seems expedient to us to report briefly on some of the results obtained during our own investigations in this field. In doing so, we will mainly confine ourselves to the reactions of alkyl halides with sodium in liquid ammonia.

As a rule the experiments have hitherto been performed by adding the alkyl halide dropwise to a solution of sodium in liquid ammonia, which is stirred vigorously and cooled to about  $-60^\circ$ , until the blue colour of the solution disappears; the colour change is almost invariably very sharp, *i.e.* the reactions proceed very rapidly. The ammonia is then slowly evaporated and collected in water, and the residue as well as the volatile products not soluble in water are investigated.

The products formed in these experiments — in proportions dependent on the nature of the alkyl halide  $RX$ ; we are at present confining ourselves to this cause of the variation of the results — are alkane  $RH$ , alkene  $R(ene)$ , amine, and "bialkyl"  $RR$ . The three first-mentioned products have been found previously, among others by CHABLAY<sup>2</sup>); the formation of bialkyl has not been observed before.

Some of the facts observed by us are mentioned below in a more or less general form.

1) Methyl iodide gives methane in a yield of about 50 %; probably practically the only other product formed is monomethylamine.

2) With all the other alkyl chlorides, bromides, and iodides examined the corresponding alkane is the main product.

<sup>1</sup>) See *e.g.* G. W. WATT, Chem. Revs. **46**, 317 (1950); A. J. BIRCH, Quart. Revs. (London) **4**, 69 (1950); R. A. BENKESER *et al.*, J. Am. Chem. Soc. **77**, 6042 (1955).

<sup>2</sup>) E. CHABLAY, Ann. chim. (Paris) (9) **1**, 469 (1914).

3) The quantity of bialkyl varies widely. Starting from primary as well as secondary and tertiary chlorides, this product is formed at most in minor quantities. Starting from primary bromides and iodides, the quantity of bialkyl is as a rule considerable; in the case of *n*-heptyl bromide and *n*-heptyl iodide, for example, about 30 % by weight of the hydrocarbons formed is tetradecane. Secondary and tertiary bromides and iodides exhibit less tendency to form bialkyl than the corresponding primary compounds.

4) One or more isomeric alkenes are formed from all alkyl bromides and alkyl iodides which contain a hydrogen atom in  $\alpha$ -position. The *n*-alkyl bromides give 2–4 % of alkene; *n*-propyl iodide yields about 15 % of propene. More alkene is formed from secondary and tertiary than from primary bromides and iodides. The composition of the alkene mixture formed from *sec.*butyl bromide — it consists of butene-1 and *cis*- and *trans*-butene-2 — is very similar to that obtained in the reaction of this compound with potassium amide in liquid ammonia, and also — as regards the proportion butene-1 : butene-2 — to that obtained in the case of typical E2 eliminations in an alcoholic medium <sup>3)</sup>.

Here, too, the chlorides occupy a special position. The mixture of hydrocarbons obtained from primary and secondary chlorides contains at most a few tenths per cent of alkene, and even with tertiary chlorides, *e.g.* with *tert.*butyl chloride, no more than a few per cent of alkene is formed.

5) Especially the reaction of primary, secondary, and tertiary alkyl chlorides with sodium in liquid ammonia is interesting from the preparative point of view; in fact, by means of this reaction a practically quantitative yield of the corresponding alkane can be obtained. We have found — we are not going into this fact here — that when applying this reaction to higher alkyl chlorides a medium of ammonia and ether is to be recommended.

6) Amines without doubt occur as reaction products, but no direct identifications or quantitative determinations of such compounds have hitherto been performed. It is, however, certain that in many cases the quantity of these products is not large; thus, the results of experiments with *n*-heptyl bromide leave scope for at most a few per cent of heptylamine.

The available data do not yet allow to give an answer to the question whether we are concerned here with ionic reactions in which carbanions play a prominent part, or with radical reactions, or possibly with both. The formation of the reaction products mentioned can be explained with the aid of both reaction mechanisms, for example in the following way:

---

<sup>3)</sup> Compare *e.g.* C. K. INGOLD, *Structure and Mechanism in Organic Chemistry* (Cornell University Press, Ithaca, N.Y., 1953).

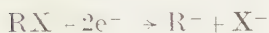


A. *Ionic mechanism.*

Primary reaction:



or



Secondary reactions:



Mechanism:

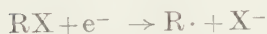
hydrogen ion abstraction

 $S_N2$  $E2$ B. *Radical mechanism.*

Primary reaction:



or



Secondary reactions:



Mechanism:

hydrogen atom abstraction

colligation <sup>3)</sup>

disproportionation

In support of the ionic mechanism it may for example be brought forward that it provides a simple explanation of the fact that the quantity of bialkyl formed from a chloride is generally so much smaller than that formed from a bromide or iodide with the same hydrocarbon residue. This can easily be understood if the bialkyl is indeed formed according to the  $S_N2$  mechanism formulated above; in fact, chlorides always undergo substitution reactions much more slowly than bromides and iodides <sup>3)</sup>. If, on the contrary, the bialkyl would be formed from two free radicals  $R\cdot$ , it would rather have to be expected that all halides with the same hydrocarbon residue would yield this product in the same quantity.

A radical mechanism is suggested by the fact that even neopentyl iodide yields a not inconsiderable amount of bialkyl (bincopentyl). Indeed, on the one hand it is known that  $S_N2$  reactions of neopentyl halides proceed particularly slowly <sup>3)</sup>; on the other hand it may be accepted that the formation of bialkyl by colligation of two free (neopentyl) radicals is practically unimpeded.

In view of this uncertainty concerning the reaction mechanism we will for the moment refrain from a further discussion of the many problems



involved. It may only be remarked that it is not unreasonable to suppose that different halides react according to different mechanisms.

As regards the reactions of other organic halogen compounds we will only mention that 1,3-dibromopropane gives cyclopropane in a yield of about 35 %, whereas 1,4-dibromobutane does not give any cyclic products. Allyl chloride and allyl bromide give considerable quantities of biallyl.

These investigations are being extended in various directions, *viz.* by varying the nature of the compounds examined, the solvent, the metal used, and the experimental conditions. It is self-evident that attention will be devoted to theoretical aspects as well as to preparative applications.

Our thanks are due to the Management of the Koninklijke/Shell Laboratorium, Amsterdam (N.V. De Bataafsche Petroleum Maatschappij) for financial support and to Dr. A. F. BICKEL and Dr. E. C. KOOYMAN for helpful suggestions.

*Laboratory of Organic Chemistry,  
Technical University, Delft, Netherlands*

THE ELECTRON MICROSCOPY OF MINUTE CRYSTALLINE  
DETAIL

BY

LOUIS W. LABAW AND RALPH W. G. WYCKOFF

(Communicated at the meeting of September 29, 1956)

Preparations consisting of a combined metal-shadowed and evaporated carbon film reveal under the electron microscope the molecular order on the surfaces of many macromolecular crystals [1]. The resolution attained with such preparations has been so much higher than needed to record the molecules of the crystals for which the method was developed that additional experiments have been undertaken to ascertain what is the smallest detail that can thus profitably be examined. This should indicate the minimum molecular size of crystals worth investigating by replication; and it should also show if significant submolecular detail exists in photographs of crystals composed of the larger macromolecules. Now that resolving powers of less than  $15\text{\AA}$  can regularly be obtained with the available electron microscopes, the factors that must limit the size of useful detail in these photographs are of two sorts. One is the faithfulness with which the microscopic images of the preparations reproduce the crystalline surfaces. This depends, not so much on the original faithfulness of the replications as on changes occurring in the preparations during the electron bombardment involved in their examination at high magnifications. The other limiting factor is the essentially chemical one of getting crystalline surfaces free enough from contaminating salt and amorphous molecular deposits to reveal the ordered molecular arrays that are the crystals themselves. Experience has already shown that this becomes more serious the smaller the molecules and the greater the concentration of salt required for their crystallization.

To evaluate these limitations several crystalline proteins of progressively smaller molecular size have been examined and photographs have been made at high resolution of macromolecular crystals with faces unusually free of contamination. Figures 1 and 2 are examples of such pictures of crystals having very large molecules. Figure 1 shows an area of a (120) face of a crystal of the southern bean mosaic virus protein, Figure 2 a portion of a (111) face of a tobacco necrosis virus protein crystal. These molecular particles, with diameters of ca.  $250\text{\AA}$ , have surfaces studded with particulate detail that is sometimes repeated on neighboring molecules. This detail could be related to the characteristic shape of the desiccated molecules or it could be due to small quantities of salt attached preferentially to areas of the molecular surfaces. Many more observations

will be needed to decide between these alternatives and to show how much useful information can thus be gained about the internal structure of such large molecular particles and their orientations within the crystals they form. Many photographs of which these are typical nevertheless demonstrate that the preparations from which they were made are sufficiently faithful to yield information bearing upon these questions.

Figure 3 shows the surface of a needle-shaped crystal of the jack bean protein concanavallin B. Its molecules, with a weight of about 42,000, are the smallest thus far replicated. The net visible here is rectangular with a short dimension of ca. 62A and a long dimension of ca. 87A. The images of the particles themselves are not in contact and have an average diameter of 30–40A. Probably crystalline order involving molecules much smaller than this cannot be well-recorded through the use of metal-carbon replicas.

Recent experiments by MENTER [2] have shown that far smaller molecular separations can be seen by the direct observation of sufficiently thin crystals. His photographs of platinum phthalocyanine show successions of stripes ca. 11A apart, which is the separation to be expected from its crystal structure as established by X-ray diffraction [3]. That this can legitimately be considered as a direct visualization of these rows gains support from the theoretical work of NIEHRS [4] who has shown that the diffraction phenomena accompanying the passage of electrons through crystals should enhance contrast and give unusually good resolution when the crystals are properly oriented and of an optimal thickness.

Experiments we have made confirm those of MENTER. Very few crystals in our preparations have, as might be expected, shown molecular detail but when, as in the photograph of copper phthalocyanine reproduced in Figure 4, the correct crystallographic orientation is achieved, the molecular rows become evident, separated from one another by 12A and enhanced in contrast by constructive interference between the electrons scattered in them. Evidently electron microscopy is now in a position to render visible order in crystals having molecules of a few hundreds as well as of many thousands molecular weight.

*National Institute of Arthritis and Metabolic Diseases  
National Institutes of Health  
Public Health Service  
U.S. Department of Health, Education, and Welfare  
Bethesda 14, Maryland*

#### REFERENCES

1. LABAW, L. W. and R. W. G. WYCKOFF, *Proc. Koninkl. Nederl. Akad. v. Wet.* Amsterdam **B 59**, 171 (1956).
2. MENTER, J. W., Paper read at Symposium of International Union of Crystallography (Madrid, April 1956).
3. ROBERTSON, J. M., *J. Chem. Soc. (London)*, **1935**, 615.
4. NIEHRS, H., *Z. Physik*, **138**, 570 (1954); likewise a paper read at Symposium of International Union of Crystallography (Madrid, April 1956).





Fig. 1. A small portion of a crystal of the southern bean mosaic virus protein. The face at the right, with the molecular particles separate from one another, is (120). The face at the left, having its molecules in rows, is (110). On the (120) face the interparticle distance, in a vertical direction on this photograph, is  $\sqrt{3}d$ , where  $d$  is the distance between particles in contact, as they are in the rows on (110). Along the horizontal rows of (120) the particle separation is  $\sqrt{2}d$ . Magnification 170,000  $\times$ .



Fig. 2. A portion of a (111) face of a crystal of one of the tobacco necrosis virus proteins. The opaque (white) regions are places where the underlying crystal has not been completely digested away. Magnification 210,000  $\times$ .



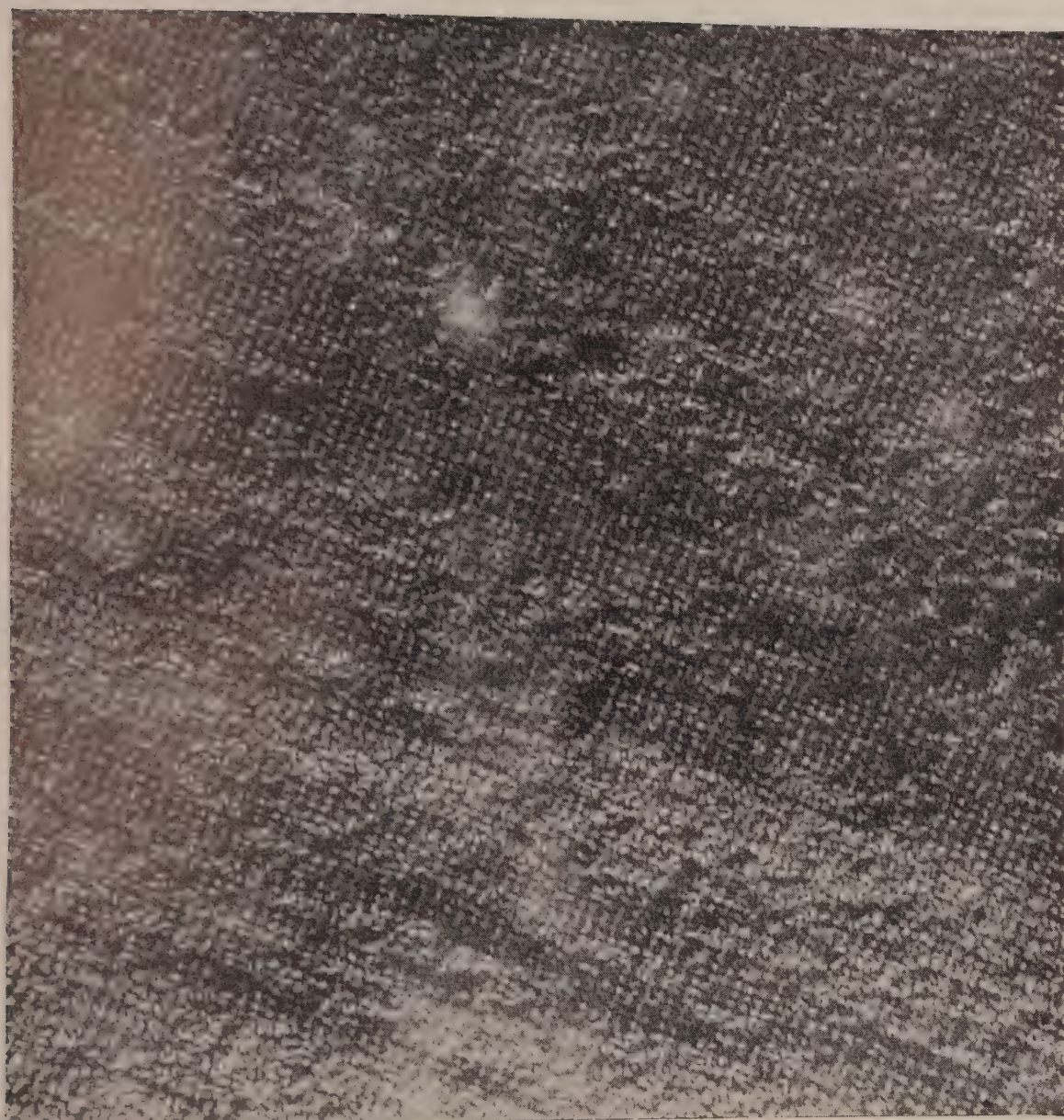


Fig. 3. Molecular distribution on a predominant face of needle-shaped crystals of the protein concanavallin B. Magnification 160,000  $\times$ .

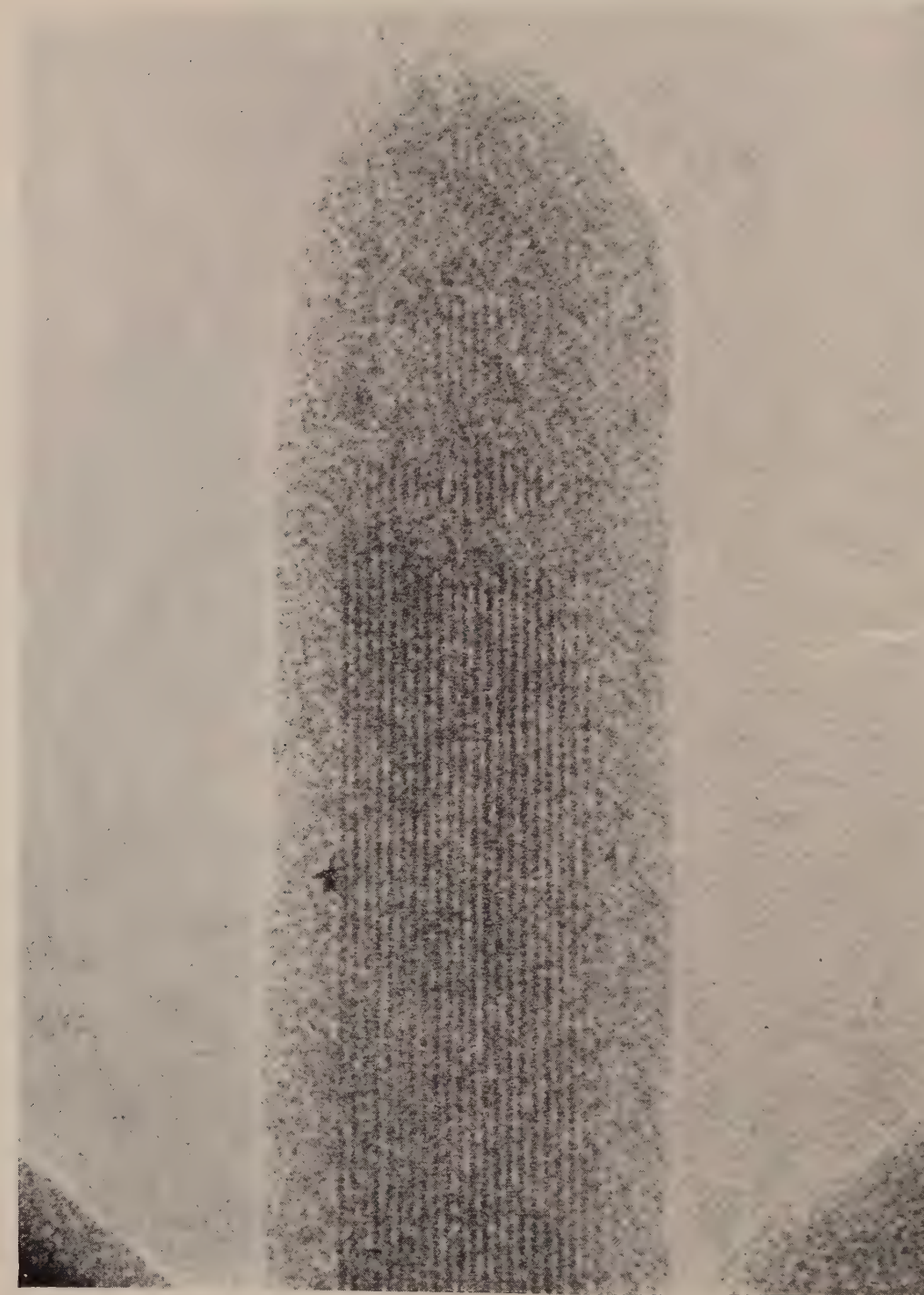


Fig. 4. A crystal of copper phthalocyanine showing rows of lines ca 12Å apart. Photographed at an original magnification of 45,000 times. Enlarged ca 20-fold optically to final magnification of 1,000,000  $\times$ .



ACCELERATED SPHERICAL LIGHT WAVE CLOCKS IN  
CHRONOGEOMETRY

BY

A. D. FOKKER

(Communicated at the meeting of June 30, 1956)

Every motion has its own proper time. This fact was put into evidence by MINKOWSKI soon after EINSTEIN had published his theory of relativity. Two motions starting from the same point-instant, on meeting again, will show different lapses of time between the events of their parting and their meeting. This fundamental absolute statement of chronogeometry must be taken as describing the actual behaviour of two identical clocks, following the specified motions. Therefore an analysis is wanted of the chronogeometry of ideal accelerated clocks.

No model of a clock, in fact no clock can be conceived without a spatial extension. I shall take a model of an ideal clock, based upon and representing the essentials of MICHELSON and MORLEY's famous experiment. The model thus idealizes *empirical fact*. It will consist of a closed perfectly rigid, perfectly reflecting spherical mirror, at the centre of which a spherical light pulse has been started. The test for the perfection and rigidity of the sphere is that the light pulse after reflections will ever and ever again concentrate in the centre, and that this focussing will not be disturbed by rotating the body of the spherical mirror. I want to show that the focussing quality will not be disturbed by accelerations either.

One may thus take the successive reflections of the light pulse as the clock ticks which, if counted, measure the time lapse. Moreover, these reflections mark events simultaneously over the surface of the spherical mirror. The situation in case of a uniform motion may be illustrated in a  $cT$ - $X$ -diagram, where the motions of the extremities of a diameter parallel to the  $X$ -axes are represented by straight time tracks and the pulsating light wave by optical lines under 45 degrees (fig. 1).

A uniformly accelerated motion along  $X$  is represented on the  $cT$ - $X$ -diagram by a hyperbola:

$$(1) \quad ct = rSh\psi, \quad x = rCh\psi,$$

The proper acceleration, referred to a Lorentz frame following the motion, is uniform,  $c^2/r$ . Let (1) be the motion of the hindmost extremity of the diameter parallel to the acceleration. Let the motion of the foremost

extremity of that diameter be given by  $ct = R \text{Sh} \psi$ ,  $x = R \text{Ch} \psi$ , with a uniform proper acceleration  $c^2/R$ . Any particle defined on the sphere by polar angles  $\theta$  and  $\varphi$  will move according to

$$(2) \quad \begin{cases} ct = \left\{ \frac{1}{2}(R+r) + \frac{1}{2}(R-r) \cos \theta \right\} \text{Sh} \psi \\ x = \left\{ \frac{1}{2}(R+r) + \frac{1}{2}(R-r) \cos \theta \right\} \text{Ch} \psi \\ y = \frac{1}{2}(R-r) \sin \theta \cos \varphi \\ z = \frac{1}{2}(R-r) \sin \theta \sin \varphi \end{cases}$$

with acceleration  $2c^2/\{R + r + (R-r) \cos \theta\}$ . A specified value of  $\psi$  defines a (flat) space of simultaneity, which contains the spherical surface defined by  $\theta$  and  $\varphi$  at constant  $(r, R)$ .

Notwithstanding the differences of acceleration, even thanks to these

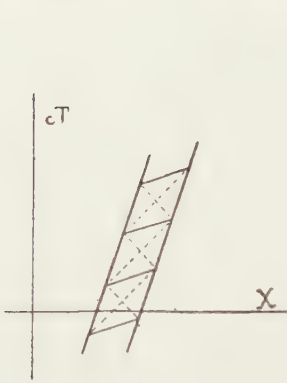


Fig. 1. Time tracks showing uniform motion of the diameter of a sphere and the light cones of a spherical wave repeatedly reflected.

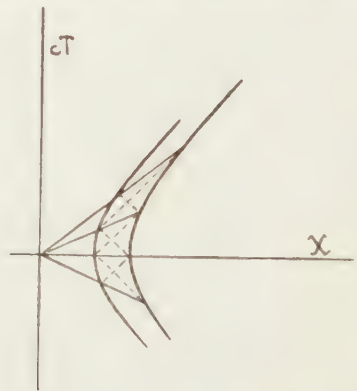


Fig. 2. Time tracks showing accelerated motion of the diameter of a rigid sphere and the light cones of a spherical wave repeatedly reflected.

differences, the invariant space interval between any pair of instants on the sphere at the same value of  $\psi$  will remain constant and perpendicular to the time tracks of constant  $R, r, \theta, \varphi$ . Thus (2) defines the motion of the sphere as an acceleration of a rigid body<sup>1)</sup>.

We shall concentrate our attention to the diameter connecting  $\theta = 0$  and  $\theta = \pi$ , which points in the direction of the acceleration.

Now let a reflection of the spherical light wave occur at  $\psi = 0$ ,  $ct = 0$ , at  $x = r$  and at  $x = R$ . We shall presently see that at the next reflection the wave again reaches the extremities  $x = r$  and  $x = R$  at identical values of  $\psi$ . On the one hand one has  $r \text{Sh} \psi' = R - r \text{Ch} \psi'$ , and hence  $\exp \psi' = R/r$ ; on the other hand one gets  $R \text{Sh} \psi'' = R \text{Ch} \psi'' - r$ , and  $\exp(-\psi'') = r/R$ . Thus  $\psi' = \psi'' = \psi_1 = \ln(R/r)$ . This shows that the next reflection occurs on the mirror in the simultaneity space  $\psi = \psi_1$ . Likewise another reflection will occur on the surface in the space  $\psi = 2\psi_1$ , and so on.

<sup>1)</sup> FOKKER, A. D., Space-time geometry of a moving rigid body, *Rev. mod. Phys.* 21 (1949) 406.

A similar line of argument shows that the wave front repeatedly collapses to a focus on a time track defined by  $(x, ct) = \sqrt{rR}(\text{Ch}\psi, \text{Sh}\psi)$ , at  $\psi = (n + \frac{1}{2})\psi_1$ ,  $n = 0, 1, 2 \dots$ . According to this assertion, the first focus of this pulse will occur at

$$\begin{aligned} ct &= \sqrt{rR} \text{Sh}(\tfrac{1}{2}\psi_1) = \sqrt{rR} \tfrac{1}{2}\sqrt{R/r} - \sqrt{r/R} = \tfrac{1}{2}(R-r) \\ x &= \sqrt{rR} \text{Ch}(\tfrac{1}{2}\psi_1) = \tfrac{1}{2}(R+r), \quad y = 0, \quad z = 0, \end{aligned}$$

It is easily verified that this focussing event in fact is the tip of a light cone on the sphere, given by

$$\begin{aligned} ct &= 0, \quad x = \tfrac{1}{2}(R+r) + \tfrac{1}{2}(R-r) \cos \theta, \\ y &= \tfrac{1}{2}(R-r) \sin \theta \cos \varphi, \quad z = \tfrac{1}{2}(R-r) \sin \theta \sin \varphi. \end{aligned}$$

Again, it must be shown that this focussing event is the tip of a light cone, having as a base the sphere at the instant  $\psi = \psi_1$ , where  $\text{Sh}\psi_1 = (R^2 - r^2)/2rR$  and  $\text{Ch}\psi_1 = (R^2 + r^2)/2rR$ .

This sphere is given by

$$\begin{aligned} ct_1 &= \{ \tfrac{1}{2}(R+r) + \tfrac{1}{2}(R-r) \cos \theta \} (R^2 - r^2)/2rR \\ x_1 &= \{ \tfrac{1}{2}(R+r) + \tfrac{1}{2}(R-r) \cos \theta \} (R^2 + r^2)/2rR \\ y_1 &= \tfrac{1}{2}(R-r) \sin \theta \cos \varphi, \quad z_1 = \tfrac{1}{2}(R-r) \sin \theta \sin \varphi. \end{aligned}$$

The interval from the typical point of the sphere to the preceding focus is given by

$$\begin{aligned} \Delta ct &= ct_1 - \tfrac{1}{2}(R-r) = \{ (r^3 - r^2R)(\cos \theta - 1) + (R^3 - R^2r)(\cos \theta + 1) \} / 4rR \\ \Delta x &= x_1 - \tfrac{1}{2}(R+r) = \{ -(r^3 - r^2R)(\cos \theta - 1) + (R^3 - R^2r)(\cos \theta + 1) \} / 4rR \\ \Delta y &= \tfrac{1}{2}(R-r) \sin \theta \cos \varphi, \quad \Delta z = \tfrac{1}{2}(R-r) \sin \theta \sin \varphi. \end{aligned}$$

Squaring and subtracting, one finds

$$\begin{aligned} (\Delta ct)^2 - (\Delta x)^2 &= 4r^2(r-R)R^2(R-r)(\cos^2 \theta - 1)/16r^2R^2 \\ &= \tfrac{1}{4}(R-r)^2 \sin^2 \theta \end{aligned}$$

and therefore

$$(\Delta ct)^2 - (\Delta x)^2 - (\Delta y)^2 - (\Delta z)^2 = 0$$

which shows that we *do* have a light cone between the focus at  $\psi = \frac{1}{2}\psi_1$  and the sphere at  $\psi = \psi_1$ .

One has to be careful and to be aware, that there is no light ray between the ends of a diameter from  $(\pi - \theta, -\varphi)$  at  $\psi = 0$  to  $(\theta, \varphi)$  at  $\psi = \psi_1$ . The light rays do not travel along diameters of the accelerated spherical mirror.

It is clear that the focussing is not disturbed by accelerations of the type defined by (2) which describe a motion of the mirror as a rigid sphere, provided the proper accelerations are uniform during the intervals between successive reflections.

Infinitesimal spherical light-wave clocks therefore will not be disturbed by any non-uniform acceleration. More specifically the diameter  $(R-r)$

of the clock must be negligible in comparison with  $R$  which defines the acceleration  $\gamma = c^2/R$ .

The motions of different surface elements of the sphere are not the same. Therefore, between two positions defined by two values of  $\psi$ , differing by  $\Delta\psi$ , the surface elements experience unequal time lapses. For a particular particle the time lapse is defined to be

$$c\tau = \left\{ \frac{1}{2}(R+r) + \frac{1}{2}(R-r) \cos \theta \right\} \Delta\psi.$$

The mean of the time lapses taken for all elements of the sphere turns out to be  $\overline{c\tau} = \frac{1}{2}(R+r)\Delta\psi$ , *i.e.* the time lapse for the centre of the sphere.

A count of the number of reflections measures  $\Delta\psi$  in units

$$\psi_1 = \ln(R/r) = 2 \left\{ \frac{R-r}{R+r} - \frac{1}{3} \left( \frac{R-r}{R+r} \right)^3 - \frac{1}{5} \left( \frac{R-r}{R+r} \right)^5 + \dots \right\}$$

and the corresponding unit of time lapse is

$$\tau_1 = \frac{2}{c} (R-r) \left\{ 1 + \frac{1}{3} \left( \frac{R-r}{R+r} \right)^2 + \frac{1}{5} \left( \frac{R-r}{R+r} \right)^4 + \dots \right\}.$$

Here  $(R-r)/(R+r) = c^{-1}(R-r)\gamma/c$  is half the velocity gain of the sphere's centre between two reflections as compared to the velocity of light. Whenever this ratio is infinitesimal, the absolute counting rate for the accelerated clock is the same as for the clock in uniform motion.

The spherical light wave and rigid mirror not only gives a measure for time-like intervals, for lapses of time, but also provides for measuring spatial distances. The diameters of the mirror supply a collection of measuring rods pointing in all directions.

It has already been remarked that the reflections of the light pulse define simultaneity on the surface for an eventual observer moving with the clock.

The dynamical problem of how to produce the specified accelerated motion lies outside the scope of the present investigation.

**Conclusion.** It has been shown that a model of a spherical light wave rigid clock, based on the empirical evidence of the Michelson and Morley experiment, behaves in agreement with chronogeometry in giving a measure both for lapses of time and for spatial distances.

To reverse the argument is to recall that the above mentioned absolute statement of chronogeometry (special relativity) is supported by the empirical evidence of the rudimentary spherical light wave rigid clock device used in Michelson and Morley's experiment.



THE GEOLOGICAL AGE OF WADJAK MAN FROM JAVA

BY

G. H. R. VON KOENIGSWALD

(Communicated at the meeting of September 29, 1956)

In 1889 Mr. VAN RIETSCHOTEN discovered in a kind of rock fissure in the marble quarries at Wadjak near Tulung Agung on the South coast of Eastern Java a human skull which was given to the Royal Natural History Society in Batavia and in turn sent to E. DUBOIS, at that time working in Sumatra. Already in a first report (1890 p. 19) DUBOIS remarks that the skull belongs to a type very different from the Malayan race, and in a second (1890, p. 12), after he visited the site in September 1890 and collected a second skull, that here we had an indication that Java formerly was inhabited by a population related to the "present day Australian aboriginals (or Papuans)".

We had to wait till 1920, before DUBOIS gave a more detailed description. The title of his publication "The Proto-Australian Fossil Man of Wadjak, Java" leaves no doubt about his interpretation. He unnecessarily attached the name of "*Homo wadjakensis*" to these skulls, which belong merely to a type of *Homo sapiens*. (PINKLEY, 1936).

The only other person, as far as I am aware, to study the original material was PINKLEY (1936), who was the first to reproduce photographs; DUBOIS had only given drawings in his own paper. PINKLEY, in also drawing attention, to the unusual robustness of the skulls, points out the fact, that the braincapacity is rather high – according to DUBOIS Wadjak I 1550 ccm, Wadjak II 1650 ccm – and that in spite of the massive jaw the teeth are smaller than in many Australians. Besides that the second lower molar of Wadjak Man has only 4 cusps, while usually in the Australians we find 5. He calls the skull "Australimorphic" and even suggests "that Wadjak Man was perhaps not a proto-Australian". (1936, p. 198).

We will not go into further anthropological details; of importance to us for the reconstruction of the history of Java is the geological age of Wadjak Man. DUBOIS suggests that he "must probably date from Pleistocene time" (1920, p. 1016), his main reason being besides the archaic type of skull, the relatively heavy fossilisation. That the latter is not a valid reason for a considerable antiquity is well known. In the collection of the Smithsonian Institute of Washington are some indian skulls, perfectly fossilized, yet found together with pottery and neolithic arrow heads.



DUBOIS mentioned some mammalian remains from Wadjak, but according to him "as far as can be ascertained not different from species now living in Java". It is worth mentioning that in the DUBOIS' collection from Wadjak Mr. D. A. HOOIJER has discovered an upper molar of *Tapirus indicus* (1947, pl. 1, fig. 16). This species is extinct in Java, but still living in Sumatra. It has not yet been observed in other prehistoric sites in Java, where, together with neolithic implements, we find several species, now disappeared from that Island, as *Elephas indicus*, *Cervus eldi*, *Felis rubiginosa* etc. So the presence of tapir, which in Java is well known from Pleistocene beds and rock fissures, is interesting, but by itself not necessarily a sign of great antiquity.

There are many indications that, before in the (late) Neolithic the present-day Malays have arrived, Java was inhabited by a probably mixed population of australo-melanesoid affinities (literature vide v. KOENIGSWALD, 1952). That is the reason, why the present author already earlier has placed Wadjak Man in the post-Pleistocene (v. KOENIGSWALD, 1935, p. 190); while others (MOVIUS, 1944, p. 109) still regard him as a Pleistocene form, although with a questionmark.

We are now able to produce several arguments, which all are in favour of a young, even very young geological age. In Puger, Eastern Java Mr. B. VAN HEEKEREN excavated three skeletons, which have been studied by SNELL (1938). The exact age is difficult to determine, but objects of bronze have been found during the excavations; that would indicate an age of maximal 2000 years. One of the skulls (Puger II) has clear australo-melanesoid affinities. Besides this SNELL found a typical "wadjakoid" palate still present in the modern Javanese. All this must be taken as a sign that the time the older australo-melanesoid population (which now has completely disappeared from Java) and the modern Javanese had contact with each other, cannot be older than a few 1000 years.

This is, in the author's opinion, confirmed by the discovery of Keilor Man, found in 1940 at Keilor near Melbourne. WEIDENREICH (1945) has shown, that the Keilor skull is just a Wadjak type from Australia. We will not discuss here the various opinions, formerly expressed about the age of this skull - mostly: Last Interglacial -, but only give the radio-carbon dating, as published by RUBIN & SUESS (1955, p. 488):

W-125	3010 $\pm$ 160 years
W-169	8500 $\pm$ 250 years

#### KEILOR TERRACE, VICTORIA

"Two charcoal samples from aboriginal hearths found and submitted by E. D. GILL, National Museum of Victoria. These samples were expected to date the Keilor terrace and therefore the Keilor skull, previously believed by some workers to be the oldest remains

of *Homo sapiens* ever found. However, the collector, E. D. GILL, expected the terrace to have formed during a relatively recent pluvial period, possibly contemporaneous with the Mankato, and the skull to be of about the same age. No charcoal has been found at the exact site where the Keilor skull was discovered, but there seems to be no reason to assume that the skull is substantially older than the hearths from which the samples were collected.

W-125: relatively large pieces of charcoal collected from a number of hearths with bones and artifacts buried in the Keilor Terrace at Braybrook south of Keilor. The age suggests that the material was at least in part intrusive; W-169: charcoal from aboriginal hearth in Keilor Terrace collected from middle of terrace (vertically) at the east end of a molding-sand quarry on the south bank of the river at Braybrook, Victoria, about 200 yds. west (upstream) from where Milleara Road crosses the river. According to the collector this material and the terrace are no doubt of the same age".

As we have seen above—here again we might point to the advanced pattern of the second lower molars—we have no reason to believe in a great antiquity of Wadjak Man in Java. We have now a confirmation of that in the absolute age determination of the Wadjak type from Australian. Wadjak Man in Java must not necessarily be much older than in Australia; even the opposite might be possible. The by DUBOIS suggested Pleistocene age of the Wadjak finds is not confirmed by our observations: they belong to the post-Pleistocene or—in terms of culture—to the Mesolithic or even a younger period of Java.

#### LITERATURE

- DUBOIS, E., Kwartaalverslagen van het Mijnwezen, Batavia. 2e Kwartaal. (1890).  
 ———, idem. 3e Kwartaal (1890).  
 ———, The Proto-Australian fossil Man from Wadjak, Java. Proc. Kon. Akad. Wetensch. Amsterdam, 23, 1013–1051 (1920).  
 HOOIJER, D. A., On fossil and prehistoric remains of *Tapirus* from Java, Sumatra and China. Zool. Mededel., 27, 253–299 (1947).  
 KOENIGSWALD, G. H. R. VON, Die fossilen Säugetierfaunen Javas. Proc. Kon. Akad. v. Wetensch. Amsterdam, 38, 188–198 (1935).  
 ———, Evidence of a prehistoric australomelanesoid population in Malaya and Indonesia. Southw. J. of Anthropol., 8, 92–96 (1952).  
 MOVIUS, H. L., Early Man and Pleistocene Stratigraphy in Southern and Eastern Asia. Pap. Peabody Mus., Harvard Univ., 19, nr. 3, 1–125 (1944).  
 PINKLEY, G., The significance of Wadjak Man, a fossil *Homo sapiens* from Java. Peking Nat. Hist. Bull., 10, 183–200 (1936).  
 RUBIN, M. and H. E. SUESS, U.S. Geological Survey Radiocarbon Dates II. Science, 121, 481–488 (1955).  
 SNELL, C. A. R. D., Menschelijke skeletresten uit de duinformatie van Java's Zuidkust nabij Poeger (Z. Banjoewangi) Diss. Batavia, pp. 1–129 (1938).  
 WEIDENREICH, F., The Keilor skull: a Wadjak type from Southeast Australia. Am. J. Phys. Anthropol., 3, 21–32 (1945).

PARALLEL EVOLUTIONARY TRENDS IN LARGER  
FORAMINIFERA

BY

C. W. DROOGER

(Communicated by Prof. G. H. R. VON KOENIGSWALD at the meeting of Sept. 29, 1956)

*Abstract.* Adaptation as a result of selection of random mutations is a possible explanation of the numerous parallel trends towards greater radial symmetry in the evolution of many unrelated groups of larger Foraminifera. The successive stages of the sequences offer a better basis for refined time-stratigraphic correlation than the commonly used associations of fossils, which do not belong to groups with changes in constant direction during evolution. Many detailed data on the foraminiferal series are still required for the elimination of different rates of development in each group in geographically remote areas.

In several groups of the fossil Foraminifera the existence of evolutionary trends is nowadays a well-established fact. In each of them there are commonly one or more of the morphological features that show gradual changes into a constant direction. Such series are known in many, among themselves unrelated groups above the species level, both among smaller and larger forms. The successive stages fit into logical schemes that seem to be dependent on geologic time only. Consequently, the importance of these so-called bioseries for time-stratigraphic correlation is getting more and more recognized. It is generally acknowledged that predictions concerning as yet unknown stages in such a series are allowed.

Up to now there have been very few speculations in the literature about the background of these series. At least for some of them, some hypothesis may be advanced, namely for the orbitoidal groups. Such a hypothesis is considered recommendable as a working basis that may direct and stimulate future research. It, moreover, allows a better evaluation of the exactness of correlations by means of these groups.

Larger Foraminifera may be distinguished from their smaller counterparts by greater dimensions, more numerous chambers and a more complex growth pattern. The boundary between both groups is vague, and it may be interpreted in somewhat different ways. At some places it cuts through homogeneous units of family rank. As a consequence, the larger Foraminifera comprise many unrelated groups. Their growth pattern enables a further subdivision into two fairly distinct parts, the components of which are again unrelated.

Individuals of the first, operculinid type grow by repeated addition



of a single chamber at a time, mostly according to a constant spiral system. Each chamber has a single, basal (proximal) larger opening. Besides in most smaller Foraminifera, this operculinid type is fundamentally present in several well-known groups of the larger ones, such as the genera *Operculina* and *Nummulites*. The proximal opening may be multiplied and the chambers correspondingly subdivided into numerous chamberlets, such as for instance in the representatives of the Alveolinidae, but the simple spiral system remains unaltered.

The second, orbitoidal type differs from the operculinid one by the possession of an additional, distal larger opening. After the forming of a variable number of operculinid chambers, the later chambers have at least these two larger openings (stolons), which results in the addition of a steadily increasing number of chambers at a time. Such genera as *Orbitoides* and *Lepidocyclus* clearly demonstrate this mode of growth, in which chambers are simultaneously added in all horizontal directions to the median layer, as well as in vertical directions to the lateral systems.

The value of operculinid larger Foraminifera for correlation purposes cannot be denied, but this value is nearly entirely based on empirical data. No uniform directions are apparent in the changes of the morphology of each of the groups, such as *Nummulites* (SCHAUB), *Operculina* (BANNINK) or the Alveolinidae (REICHEL).

On the other hand the orbitoidal groups are known to have evolved into fairly constant directions, which are moreover, more or less similar in unrelated groups. These parallel trends have been recognized by several authors, and consequently uniform terms have been introduced for ontogenetic stages and evolutionary phenomena (TAN SIN HOK).

Three successive ontogenetic stages have been defined for all orbitoidal individuals: embryonic, nepionic and neanic<sup>1</sup>).

The embryonic stage consists of the initial chambers, commonly two, protoconch and deutoconch, but occasionally some more, which together are morphologically clearly distinct from the later chambers.

The nepionic stage comprises either all chambers directly encircling the embryonic ones, or all chambers, in which continuous spiral systems that begin at the embryonic chambers, are recognizable.

The neanic stage contains all later chambers; they are commonly of uniform shape.

All chambers of these three stages are situated in a single growth plane; they form the so-called median layer. Many orbitoidal genera have systems of lateral chambers in addition, which systems grow continuously with the enlarging of the median layer.

During the evolution of the various groups, all three stages of the median

---

<sup>1</sup>) For these and the following terms a choice has been made from the literature. This does not imply that these terms are considered more appropriate than others.

layer gradually changed. The evolutionary trends will be dealt with separately for each of the stages. Because of the more numerous available data, the middle stage will be treated first.

The nepionic stage. The schematic drawings in fig. 1 show various arrangements of the nepionic chambers in horizontal sections. The drawings have been placed in the logical order *a* to *k*. The operculinid spiral (either trochoid or planispiral) of *a* shows orbitoidal later chambers in *b*, and it

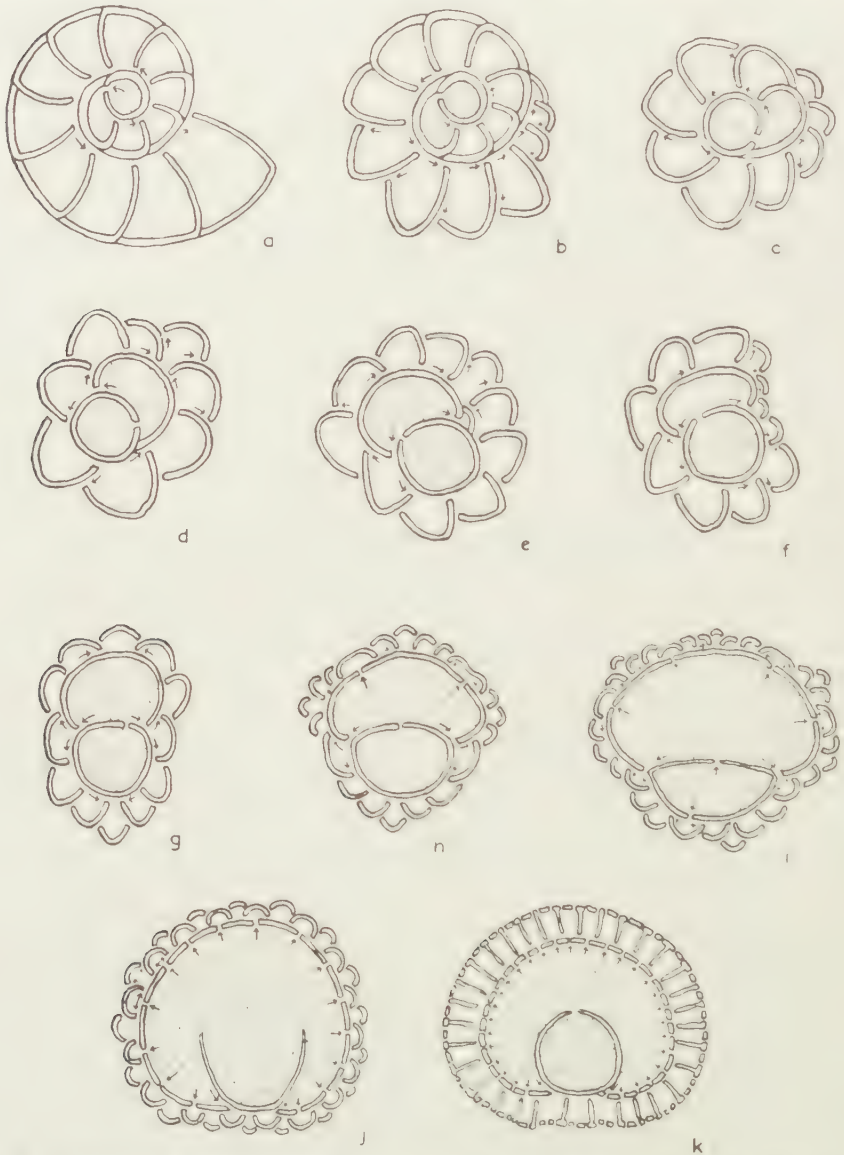


Fig. 1. Schematic drawings of various arrangements of the nepionic chambers in horizontal sections. Arrows indicate directions of growth. The embryonic chambers have been dotted.



has further been shortened in *c* and *d*. In the latter type the third chamber already possesses two stolons; as a result there are two nepionic spirals in opposite directions. In *e* there are two stolons in the deuteroconch and consequently two chambers (auxiliary chambers) that have direct connection with the embryonic stage. From *e* to *g* we see increasing length of the spirals that originate from the second auxiliary chamber. In *h* to *j* the number of stolons in the walls of the embryonic chambers has been further increased and correspondingly the number of auxiliary chambers and of nepionic spirals becomes greater. No more than two steps are needed in *j* for the complete envelopment of the embryonic stage. Finally we see in *k* a type, in which all nepionic chambers are alike, probably having been formed together.

These types, though often with minor deviations, have been found in all groups of orbitoidal Foraminifera. In none of the groups are they all known; in several groups most of them have been found, in others but a few. No doubt many data are still lacking.

The logical order from *a* to *k* is generally considered to correspond to successive levels in the evolution of the various groups. This implies the disappearance of the operculinid system, the increase in the number of nepionic spirals, and the encircling of the embryonic stage in a decreasing number of steps. This complex of changes TAN SIN HOK gave the name of nepionic acceleration. In general outline nepionic acceleration is apparently true of all groups, but more detailed data are still few. Some examples will be given below, but first the various aspects of the embryonic stage will be reviewed.

For the embryonic chambers a similar logical series has been established (fig. 2). In the series *l* to *r*, the type *l*, frequently found among operculinid forms, changes towards complete envelopment of the protoconch by the deuteroconch. The shorter series *m-s-t* shows the disappear-

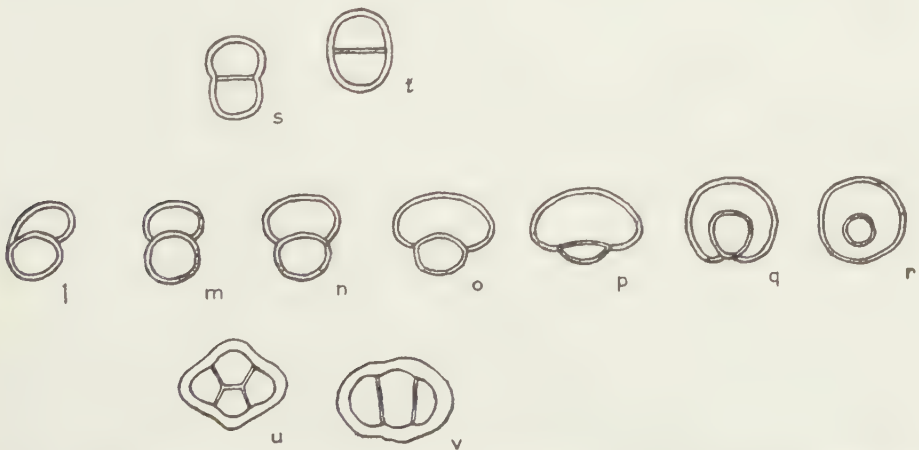


Fig. 2. Schematic drawings of the embryonic chambers after horizontal sections of various existing types. Stolons have not been drawn.

ance of the difference between both embryonic chambers. In *u* two additional chambers, which correspond to auxiliary chambers, have been incorporated in the embryonic stage, which is separated from the later chambers by a thick wall. In *v* the four chambers of *u* have lost still more of their individual character.

Again there are many indications that the logical orders of these types correspond at many places with a succession in time. For these tendencies towards a more globular shape of the embryonic stage the term embryonic acceleration may be introduced, analogous to the nepionic acceleration. Both types of acceleration were found to go often together.

The following examples give a review of our present knowledge of a number of groups. It is not tried to give a complete account. Nearly all evidence concerns the more frequent megalospheric generations, since data on the corresponding microspheric individuals are very scarce.

Three families of orbitoidal Foraminifera occurred about contemporaneously during the Late Cretaceous.

The Pseudorbitoididae are a remarkable group of the central American Upper Cretaceous (BRONNIMANN, 1954/6). Their median layer is characterized by the presence of vertical plates in different arrangements. Their descent from the operculinid genus *Sulcoperculina* is fairly certain. Several nepionic types of the series *a-f* have been described, but a reliable time sequence could as yet not be established. Some indications of nepionic acceleration may be concluded from the literature.

The Orbitoididae are characterized by a thick-walled embryo of the types *u* and *v*. In the most common genus, *Orbitoides*, it has been found that *v* is younger than *u*. The nepionic types in this genus are also of fairly high development; they belong to the group *h-j*. The arrangements with 10 to 14 auxiliary chambers appear later than those with 4 and 6 of such chambers. The known species of the Orbitoididae nearly all show considerable specialization. KUPPER (1954b) recently demonstrated from features of the microspheric generation that this rootless group probably descended from a biserial, *Gumbelina*-like ancestor.

Also the third family of the Cretaceous, the Lepidorbitoididae, are rootless. They show fairly thick-walled embryonic types *l-o* and several nepionic types of the series *b-j* with up to eight auxiliary chambers. The stratigraphic sequence of these types is not yet thoroughly known, but according to PAPP and KUPPER in Austria the general outline is in good accordance with both nepionic and embryonic accelerations.

Another family of unknown origin are the Paleocene-Eocene Discocyclinidae. They show embryonic types *m* to *r*, but no embryonic acceleration is apparent (VAN DER WEIJDEN, SCHWEIGHAUSER). Throughout the stratigraphic range of the group, the nepionic chambers are nearly always arranged according to a more or less stable type *k*. Connections with more primitive types are unknown.

Better data are available on the nepionic development of the family Helicolepidinidae of the American Eocene. In most representatives the primary spiral is a persistent character. Since the descent from an Early Eocene *Amphistegina*-species (BARKER and GRIMSDALE), the main spiral gradually lost its operculinid character. In the genus *Helicolepidina*, VAN RAADSHOOVEN found in stratigraphic order the gradual transition from type *d* to type *g*.

The Helicolepidinidae have their *Amphistegina*-ancestor in common with at least part of the Lepidocyclinidae (BARKER and GRIMSDALE), in which family the primary spiral has no particular length. As to the nepionic development in the Lepidocyclinidae, there is a general change from type *b* in the species of *Eulinderina* of the American Middle Eocene to about type *i* in the Middle Miocene *Lepidocyclina* species of Indonesia (RENTZ and KUPPER). One nice example deserves special mention (MOHLER). In three successive assemblages of *Lepidocyclina* from the Miocene of Borneo, the number of auxiliary chambers was shown to increase from 2-5 in the lowermost sample to 8-13 in the uppermost one. No doubt future research of the Lepidocyclinidae will yield numerous valuable data, both biological and stratigraphic. It is considered likely that several lineages are involved; possibly the family, or even the main genus, *Lepidocyclina*, is heterogeneous. There are, for instance, no distinct links between the majority of *Lepidocyclina* species and those of the subgenus *Eulepidina*, which are highly specialized with embryonic type *q* and nepionic arrangements that resemble type *j*. *Eulepidina* appeared as early as the Oligocene, while the contemporaneous other subgenera of *Lepidocyclina* look less advanced in both embryonic and nepionic respects. The latter possess embryonic types *m* to *p* and *m* to *t*. Although probably not rigorously so, embryonic acceleration may be present, but the total record still looks somewhat irregular and again we lack detailed data.

The Miogypsinidae are a fairly well-known family, beginning with the early descendents from the genus *Rotalia* in the Oligocene, till the last representatives in the Middle Miocene (TAN SIN HOK, DROOGER). Embryonic acceleration is distinct, but slight in this group; it does not surpass type *o*. Nepionic acceleration, from *b* to about *h*, was repeatedly found to be true in general outline, while at some places it could be confirmed also for minor steps. In the Miogypsinidae there are some indications that nepionic retardation might have occurred, but if true, it would have been of but slight importance, during the early development of the group.

Another good example of nepionic acceleration is known from the genus *Cycloclypeus* in Indonesia (TAN SIN HOK, 1932). In this genus of the Nummulitidae, the ontogenetic stages have an appearance that is somewhat different from those in the orbitoidal Foraminifera (fig. 3). The nepionic chambers are elongate-operculinid, most of them being subdivided into chamberlets, while the neanic chambers are annular with the same subdivision. TAN found that the number of nepionic



chambers continuously decreased (acceleration) from about 25 in Oligocene assemblages to about 3 in those from Pliocene and recent deposits. The changes are probably gradual (DROOGER, 1955).

Two more or less distinct trends of the neanic stage in orbitoidal Foraminifera will be advanced.

The first one concerns the connections between the neanic chambers. These chambers, which are of fairly uniform type, are connected with the adjoining ones through stolons. Several stolon arrangements have been observed. Especially among the *Lepidocyclinidae* (VAN DE GEYN and VAN DER VLERK, TAN SIN HOK) and the *Miogypsinidae* (TAN SIN HOK, BRONNIMANN, 1940) it was found that the number of stolons per chamber increased, both in the course of ontogeny of single individuals, and at comparable ontogenetic stages of individuals during the evolution of the groups. As a result, there is an increase of connections between the neanic chambers.

The second trend is found in but a single family, the *Miogypsinidae*, in which it is very distinct. In all other orbitoidal groups the embryonic-nepionic stage always has a central position in the median layer. In the main lineage of the *Miogypsinidae*, the subgenus *Miogypsinina*, the early stages remain in a peripheral position, but there have been more or less successful side branches, in which they shifted towards a more central position in the median layer. As far as we know, these centripetal trends occurred some six times, independently of one another, at various levels of development of the group, and in widely separated geographic areas (fig. 6).

The enumerated changes in all three ontogenetic stages of orbitoidal Foraminifera point to the acquiring of greater radial symmetry throughout the organisms. Radial symmetry increases in the trends towards a more globular shape and a more rapid encircling of the embryonic stage (embryonic and nepionic accelerations), as well as in those towards more numerous connections between the neanic chambers and a central position of the early stages. The parallelism of these trends in many unrelated groups favours the assumption of adaptation as a result of selection of random mutations.

Radial symmetry in invertebrates is generally thought to be connected with a mode of life, in which the organism is passive with respect to its environment. Geologic history furnishes several examples, in which the change from an active to a passive relation to environment is accompanied by the acquiring of greater radial symmetry.

The treated groups of Foraminifera were certainly not passive by attachment to other organisms or objects, but their active capacities may be considered ineffective because of the turbulence and other movements of the shallow water in which they evidently all thrived. The influence



of repeated passive displacement is thought to follow, among other things, from the frequent regeneration, as well as from the strengthening of the test, which were observed in some of the groups (DROOGER, 1955). In such an environment free connections of the protoplasm in all directions may be considered more efficient. Hence, the selective value of a more adequate radial symmetry.

Similar ideas of radial symmetry have been advanced before, among others by TAN SIN HOK and SMOUT. Both authors, however, connect the parallel trends with the increase in absolute size of the organisms, while TAN moreover, continuously thought to refute the adaptive nature of the trends. The increase in size is postulated as a general (unexplained) phyletic tendency in most groups of Foraminifera. Once this being accepted, SMOUT emphasizes that there is a limited size of the organism, above which the protoplasm will be unable to preform the next, greater operculinid chamber of constant shape. Consequently, beyond this limit the organism should possess preadapted additional stolons in order to increase its size, which increase is then achieved by breaking up of the protoplasm for an orbitoidal or other more complex growth pattern.

In our opinion, however, the increase in absolute size may be another adaptive response to the shallow water environment, since greater size and weight may be favourable factors against the dangers of burial and transportation. Furthermore, tests consisting of more numerous smaller units are thought to have a more solid structure, another advantage in turbulent water.

Summarizing, it may be postulated that, once the size restriction of simple operculinid chambers has been overcome, the more or less interdependent factors of increase in absolute size, increase of mechanical strength and greater radial symmetry, all have more or less selective value in the shallow water environment. The next question along this line would be why these organisms are restricted to this unstable environment. Possibly there has been some dependence on commensal algae, as were found by CUSHMAN, among others in recent *Cycloclypeus*, but this and other questions have as yet to remain unanswered because of our scanty knowledge of living Foraminifera.

The trends towards increased radial symmetry may be expected in other, as yet hardly explored orbitoidal groups, such as *Halkyardia* (BURSCH), the Calcarinidae (KUPPER, 1954a), and possibly the Planorbulinidae and Orbitolininae.

Other ways of acquiring greater radial symmetry occur in the many unrelated groups, in which the individuals develop a series of broad and shallow, uniserial or annular chambers, together with a conical shape of the test (fig. 4). Some examples are *Dictyoconus* and *Orbitolina* with more or less arenaceous walls, *Taberina* and *Rhapydionina* among the Peneroplidae, *Fabiania* and the *Chapmanina* group (FRIZZELL) among the per-

forated genera. Yet another way of increasing radial symmetry occurs in some offshoots of operculinid families, in which the spiral is repeatedly doubled with the result that several spirals follow one another along the

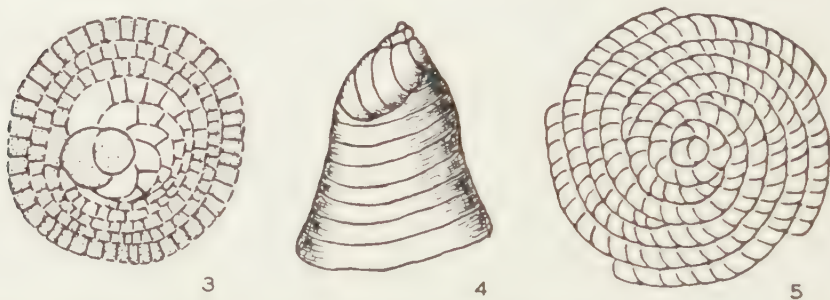


Fig. 3. Schematic drawing of a *Cycloclypeus* individual in horizontal section. The embryonic and neanic chambers have been dotted.

Fig. 4. Radial symmetry of a conical series of uniserial chambers (redrawn after FRIZZELL).

Fig. 5. Radial symmetry by repeated bifurcation of an operculinid spiral (horizontal section, redrawn after SMOUT).

circumference of the test (fig. 5). This peculiar type has been encountered in *Multispirina* of the Alveolinidae (REICHEL) and in *Dictyoconoides* and *Dictyokathina* of the Rotaliidae (SMOUT). Also several species of *Nummulites* may have these intercalary whorls.

In the orbitoidal groups rapid development of the nepionic stage enables the distinction of several, narrowly delimited stages in the sequences. The adaptive character of the trends more or less guarantees the irreversibility of the evolution. It is self-evident that the successive stages are very welcome for long-range time-stratigraphic correlation and age determinations. For these purposes they are considered to yield a more refined and sounder basis than the common practice of using associations of frequently encountered species, each of which stands alone in the fossil record, without ancestors and descendants in a phylogenetic series of uniform trend. Such faunal associations are highly dependent on all kinds of environmental conditions and the index value of the components is often a matter of discussion. Hence, the wealth of literature on correlation and age determination of many stratigraphic units. After the Mesozoic with its phylogenetic lines and numerous index fossils among the Cephalopoda, time correlation of Tertiary marine sediments has been mainly based on associations of other mollusks without distinct evolution patterns. Extensive use of the trends in several groups of larger Foraminifera is one of the ways to develop better correlation methods, especially for the Tertiary.

An important drawback of this method is that we are as yet unacquainted with the speed of the changes in the groups. Since we are

dealing with benthonic organisms, a series did not necessarily develop with exactly the same rate in widely separated parts of the globe. For a check of the respective rates we will need many data of independent groups.

Embryonic, nepionic and neanic changes are no doubt more or less correlated within a group, but this correlation is not necessarily constant, as may be seen from the following example. In the Miocene of northern Italy *Miolepidocyclus* developed in a relatively short time as a side branch of the *Miogypsina* s.str.series. Although based on but few data,

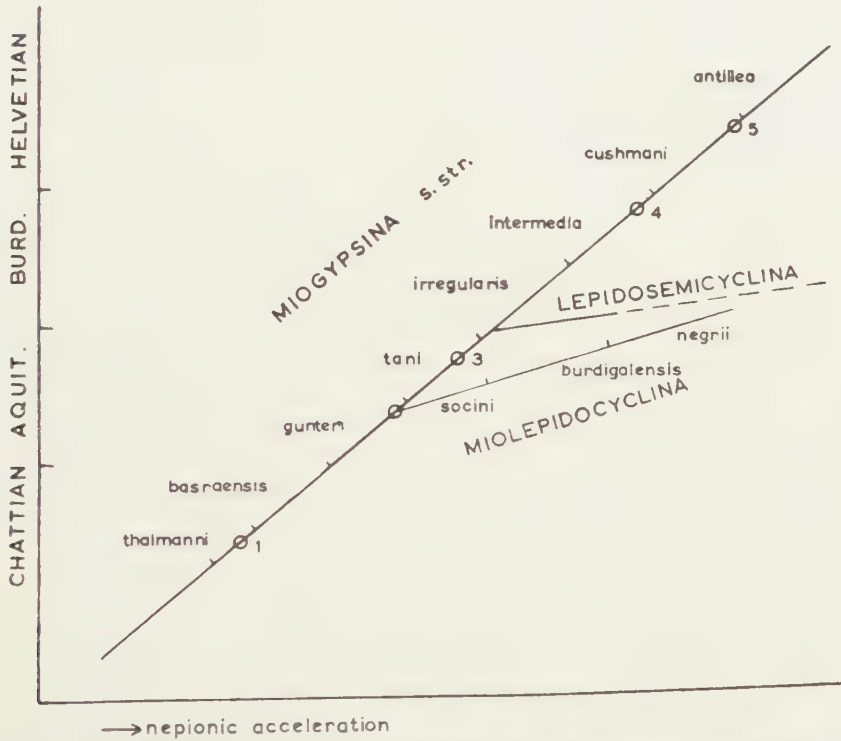


Fig. 6. Different rates of nepionic acceleration in the *Miogypsinidae*. The relation between nepionic acceleration and geologic time is given as a straight reference-line for the series of *Miogypsina* s.str.species. The approximate location of departure of centripetal lineages from the main *Miogypsina* series has been entered: 1, *M. panamensis*-*M. ecuadorensis* (America); 2, *M. socini*-*M. burdigalensis*-*M. negrii* (Mediterranean); 3, *M. bronnimanni* (America); 4, *M. mexicana* (America); 5, *M. mediterranea* (Mediterranean). The centripetal trend of *Miogypsina* (*Miogypsinoides*) *dehaarti cupulaeformis* (Western Pacific) cannot be shown in this figure.

the speed of centripetal movement and that of nepionic acceleration show variable correlation in a number of samples in stratigraphic succession (DROOGER, 1954). The *Miolepidocyclus* lineage furthermore shows a more rapid nepionic acceleration than the contemporaneous *Miogypsina* s.str. in adjoining regions. For it appears that the last representative of *Mio-*



*lepidocyclina* in this area. *M. negrii*, was distinctly more highly developed in this respect than *M. irregularis* of the *Miogypsina* s. str. lineage, which species invaded the area after the extinction of the *Miolepidocyclina* group (fig. 6). Possibly, the side branch of the Indonesian subgenus *Lepidosemicyclina* possesses a similar, more rapid nepionic acceleration.

Although different rates in a group are thus very likely, the stratigraphic value of the already established series is probably greater than that of the previously used faunal associations. For instance, the recent trans-atlantic correlation of Oligo-Miocene stratigraphic units, based on the parallel trends in the Miogypsinidae (DROOGER, 1956) is considered more reliable than the one that was founded earlier, mainly on various arbitrary associations. Furthermore, the new correlation was found to be supported by the zones of planctonic Foraminifera.

Evidently the evolutionary trends of several groups of larger Foraminifera offer a good future basis for stratigraphic correlation as soon as the various groups will have been carefully analysed and compared with one another for the tracing of differences in the adaptive rates. Distinct stages in the development of the microplankton may give additional reference points. Unfortunately, the evolution of the planctonic Foraminifera up to now has looked rather haphazard (the rise of *Orbulina* may again be an example of the acquiring of greater radial symmetry (BLOW)), but the faculty of rapid geographic dispersal may yield a number of reliable datum surfaces over great parts of the world.

Consequently, it may be concluded that micropaleontologists will obtain many valuable results, if they continue along these promising lines of research.

#### REFERENCES

- BARKER, R. W. and T. F. GRIMSDALE, A contribution to the phylogeny of the orbitoidal Foraminifera, with description of new forms from the Eocene of Mexico. *Journ. Pal.*, **10**, 231-247 (1936).
- BANNINK, D. D., Een monografie van het genus *Operculina*. Acad. thesis Leiden (1948).
- BLOW, W. H., Origin and evolution of the foraminiferal genus *Orbulina* d'Orbigny. *Micropaleontology*, **2**, 57-70 (1956).
- BRONNIMANN, P., Über die tertiären Orbitoididen und Miogypsiniden von Nordwest-Marokko. *Schweiz. Pal. Abh.*, **63** (1940).
- , Upper Cretaceous orbitoidal Foraminifera from Cuba, I-V. *Contrib. Cushman Found. Foram. Res.*, **5**, 55-62, 91-105; **6**, 57-76, 97-104; **7**, 60-66 (1954-1956).
- BURSCHE, J. G., Mikropalaontologische Untersuchungen des Tertiärs von Gross Kei (Molukken). *Schweiz. Pal. Abh.*, **65** (1947).
- CUSHMAN, J. A., Shallow-water Foraminifera of the Tortugas region. *Publ. Carnegie Inst., Wash.*, **17** (1922).
- DROOGER, C. W., Study of American Miogypsinidae. Acad. thesis Utrecht (1952).
- , Miogypsina in northern Italy. *Proc. Kon. Ned. Ak. Wetensch.*, ser. B, **57**, 227-249 (1954).



- , Remarks on *Cyclocypeus*. id., 58, 415–433 (1955).
- , Transatlantic correlation of the Oligo-Miocene by means of foraminifera. *Micropaleontology*, 2, 183–192 (1956).
- FRIZZELL, DON. L., Rotallid Foraminifera of the Chapmanininae: their natural distinction and parallelism to the *Dictyoconus* lineage. *Journ. Pal.*, 23, 481–495 (1949).
- GEYN, W. A. E. VAN DE and I. M. VAN DER VLERK, A monograph on the Orbitoididae, occurring in the Tertiary of America. *Leidsche Geol. Meded.*, 7, no. 2 (1935).
- KÜPPER, K., Note on *Schlumbergerella* Hanzawa and related genera. *Contrib. Cushman Found. Foram. Res.*, 5, 26–30 (1954a).
- , Notes on Upper Cretaceous larger Foraminifera, I, II. id., 5, 63–67, 179–184 (1954b).
- MOHLER, W. A., *Lepidocyclus crucifera* n.sp. aus dem Burdigal von Ost-Borneo. *Ecl. geol. Helv.*, 39, 302–309 (1946).
- PAPP, A. and K. KÜPPER, Die Foraminiferen von Guttaring und Klein St. Paul (Kärnten), II–IV. *Sitzungsber. Österr. Ak. Wiss., Math.-nat. Kl., Abt. I*, 162, 65–82, 345–357; 164, 317–334 (1953, 1955).
- RAADSHOOVEN, B. VAN, On some Paleocene and Eocene larger Foraminifera of Western Venezuela. *Proc. Third World Petr. Congr., The Hague, sect. 1*, 476–487 (1951).
- REICHEL, M., Étude sur les Alvéolines. *Schweiz. Pal. Abh.*, 57, 59 (1936, 1937).
- , *Multispirina iranensis* n. gen. n. sp., Foraminifère nouveau du Crétacé supérieur de l'Iran. id., 65 (1947).
- RENZ, O. and H. KÜPPER, Über morphogenetischen Untersuchungen an Grossforaminiferen. *Ecl. geol. Helv.*, 39, 317–342 (1946).
- SCHAUB, H., Stratigraphie und Paläontologie des Schlierenflysches. *Schweiz. Pal. Abh.*, 68 (1951).
- SCHWEIGHAUSER, J., Mikropaläontologische und stratigraphische Untersuchungen im Paleocaen und Eocaen des Vicentin (Norditalien). id., 70 (1953).
- SMOUT, A. H., Lower Tertiary Foraminifera of the Qatar Peninsula. *Publ. British Museum Nat. History* (1954).
- TAN SIN HOK, On the genus *Cyclocypeus* Carpenter. *Wetensch. Meded. Dienst Mijnb. Ned. Indië*, 19 (1932).
- , Die peri-embryonalen Äquatorialkammern bei einigen Orbitoididen. *De Mijning.*, 2, 113–116 (1935).
- , Beitrag zur Kenntnis der Lepidocyclusiniden. *Proc. Kon. Ak. Wetensch.*, 39, 990–999 (1936a).
- , Zur Kenntnis der Lepidocyclusiniden. *Natuurk. Tijdschr. Ned. Indië*, 96, 235–280 (1936b).
- , Zur Kenntnis der Miogypsiniden. *De Mijning.*, 3, 45–61, 84–98, 109–123 (1936c).
- , Weitere Untersuchungen über die Miogypsiniden. id., 4, 35–45, 87–111 (1937).
- , On *Polylepidina*, *Orbitocyclus* and *Lepidorbitoides*. id., 6, 53–84 (1939).
- WEYDEN, W. J. M. VAN DER, Het genus *Discoeyclus* in Europa. *Acad. thesis Leiden* (1940).

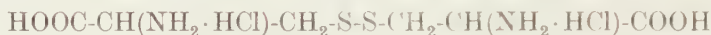
ON THE CRYSTAL STRUCTURE OF L-CYSTINE  
HYDROCHLORIDE

BY

A. F. CORSMIT, A. SCHUYFF AND D. FEIL

(Communicated by Prof. J. M. BIJVOET at the meeting of June 30, 1956)

A recent publication by STEINRAUF and JENSEN (1956) on the unit-cell parameters and space group of L-cystine hydrochloride



brings us to publish preliminary data of our structure determination of this compound.

The unit-cell parameters determined from rotation and Weissenberg photographs (CuK radiation) are in agreement with the values given by STEINRAUF and JENSEN, but our values are probably less accurate.

With two molecules of  $\text{C}_6\text{H}_{12}\text{N}_2\text{O}_7\text{S}_2\cdot 2\text{HCl}$  per cell the calculated density

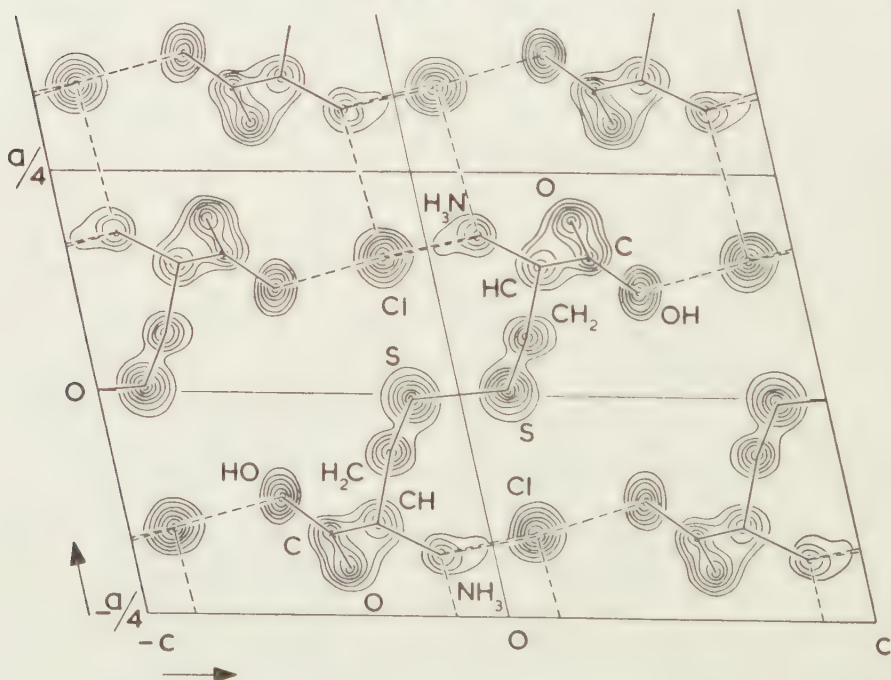


Fig. 1. The electron density of L-cystine hydrochloride projected on the  $ac$ -plane. Contours are at arbitrary intervals, the intervals around the sulphur and chlorine atoms being three times as large as that around the other atoms. Hydrogen bonds are indicated by broken lines.

is  $1.53 \text{ g.cm}^{-3}$ , while by flotation a density of  $1.525 \text{ g.cm}^{-3}$  was found.

The space group was determined to be C2. All atoms are in general (fourfold) positions, so the cystine molecule must possess a twofold axis. The sulphur and chlorine positions were determined from Patterson projections along the b and c axes. The projection of the electron density on the ac-plane was determined by subsequent Fourier syntheses, until none of the reflexions changed sign any more. The disagreement factor R for the (h0l) reflexions was 22 % at this stage.

The structure of the cystine molecule is clearly evident from the last Fourier projection (see figure 1). The electron density projection of the cystine molecule on the ac-plane is almost identical with that of the cystine group in N, N'-diglycyl-L-cystine dihydrate (YAKEL and HUGHES, 1954).

Inspection of the Patterson projection along the c axis of L-cystine hydrochloride showed that the y parameters in this compound also are very similar to the corresponding parameters in N, N'-diglycyl-L-cystine dihydrate.

Our structure determination had been interrupted by other work; as the determination has now been started by others, we do not intend to continue it.

*Laboratorium voor Kristalchemie  
der Rijks-Universiteit Utrecht*

#### REFERENCES

- STEINRAUF, K. L. and L. H. JENSEN, *Acta Cryst.* **9**, 539 (1956).  
YAKEL Jr., H. L. and E. W. HUGHES, *Acta Cryst.* **7**, 291 (1954).

# CHEMISTRY

## THE SYNTHESIS OF CIS, CIS-9, 11- AND CIS, CIS-10, 12-OCTADECADIENOIC ACIDS

BY

S. SPARREBOOM

(Communicated by Prof. J. H. DE BOER at the meeting of June 30, 1956)

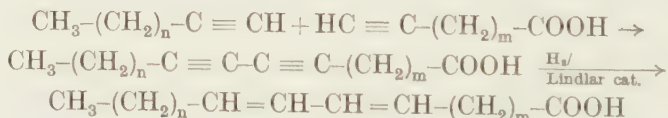
In this communication the synthesis of cis, cis-9, 11- and cis, cis-10, 12-octadecadienoic acids is described. The purification of these compounds was followed by means of infra-red spectra measurements.

### INTRODUCTION

In the course of an investigation into the mechanism of the alkali-isomerisation of polyenoic fatty acids, two conjugated cis, cis isomers of linoleic acid have been synthesized, viz. cis, cis-9, 11- and cis, cis-10, 12-octadecadienoic acids.

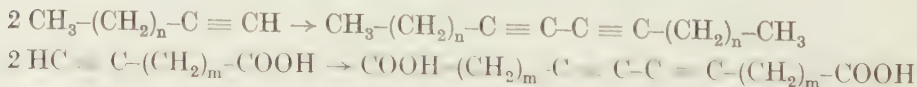
There are several literature data relating to the isolinoleic acids with conjugated trans, trans [1-10] and conjugated cis, trans [8-10] systems of double bonds, but hitherto no data are available on the conjugated cis, cis acids.

The syntheses were carried out in accordance with the following reaction scheme:



in which  $n=4$  and  $m=8$  or  $n=5$  and  $m=7$  respectively.

A variation of the oxidative coupling method of GLASER [11] was applied to prepare 10, 12-octadecadiynoic acid from 1-heptyne with 10-undecynoic acid and 9, 11-octadecadiynoic acid from 1-octyne with 9-decynoic acid. In the asymmetrical coupling the yield was relatively low, since symmetrical coupling reactions occurred simultaneously between the molecules of the starting materials:



The yields of symmetrical diynedioic acids obtained by the side-reactions were somewhat greater than the yields of asymmetrical diynoic acids. The diynoic acids were rather unstable as appeared from a blue coloration on standing, which was accelerated on exposure to light. This coloration is probably caused by polymerisation or cyclisation of the



molecules. On heating a red colour was observed, possibly as a result of the formation of quinoid systems [12].

A Lindlar catalyst [13] was used in the partial hydrogenation of the octadecadiynoic acids, which had to be arrested when two moles hydrogen had been taken up. In each case a mixture of stereo-isomers of the relevant octadecadienoic acid was formed, as appeared from the infra-red spectra. Since, fortunately, the *cis*, *cis*-isomers readily crystallized out from solutions at low temperatures, the isolation and purification – which could be followed with the help of infra-red spectra – of the desired compounds was possible by repeated recrystallizations.

The octadecadienoic acids had the following constants:

Constants	<i>cis</i> , <i>cis</i> -9, 11 acid	<i>cis</i> , <i>cis</i> -10, 12 acid <sup>1)</sup>
M.p.	42.0–43.2° C	38.2–39.0° C
$n_D^{70}$	1.4631	1.4637
$d_4^{70}$	0.8802	0.8810
M.R. at 70° C	87.79	87.79
M.R. (Eisenlohr)	85.93	85.93
Exaltation	1.86	1.86
Acid value	200.3 (calcd. 200.1)	200.3 (calcd. 200.1)
H <sub>2</sub> -uptake	2.0 moles	1.95 moles
M.p. hydrogenated product		67.5° C
U.V. spectra at $\lambda_{\max}$ 235 m $\mu$	$\epsilon$ = 26,000 (ethanol) $\epsilon$ = 26,700 (light petr.)	$\epsilon$ = 25,900 (ethanol) $\epsilon$ = 26,600 (light petr.)
Elementary analysis	76.90% C (calcd. 77.15) 11.80% H (calcd. 11.43)	76.47% C (calcd. 77.15) 11.50% H (calcd. 11.43)

The infra-red spectra of *cis*, *cis*-9, 11- and *cis*, *cis*-10, 12-octadecadienoic acids (Figs. 1 and 2) were measured on a Perkin–Elmer model 12 C single-beam spectrophotometer, using a rock-salt prism <sup>2)</sup>.

Both spectra show a weak absorption band at 1600/cm (6.25  $\mu$ ). This absorption may be ascribed to the C=C stretching mode, in which the conjugated double bonds vibrate out-of-phase in respect to one another. The weakness of the band is in accordance with the fact that the conjugated systems of double bonds are situated near the middle of a long chain [15].

The absence of absorptions at 948/cm, 965/cm, 982/cm and 988/cm proves that no isolated or conjugated double bonds with a *trans*-configuration are present. The weak bands present at 965/cm, 978/cm and 986/cm in the spectrum of solid *cis*, *cis*-9, 11-octadecadienoic acid (Fig. 1) are absent in the spectrum of this sample in the liquid state, so that this set of bands probably arises from the interaction between the crystal lattice and molecular vibrations.

<sup>1)</sup> ALLEN [14] recently described the synthesis of the methyl ester of this acid.

<sup>2)</sup> The preparation was carried out by melting the samples between rock-salt plates which were then pressed together and allowed to cool, so that the samples crystallized between them.

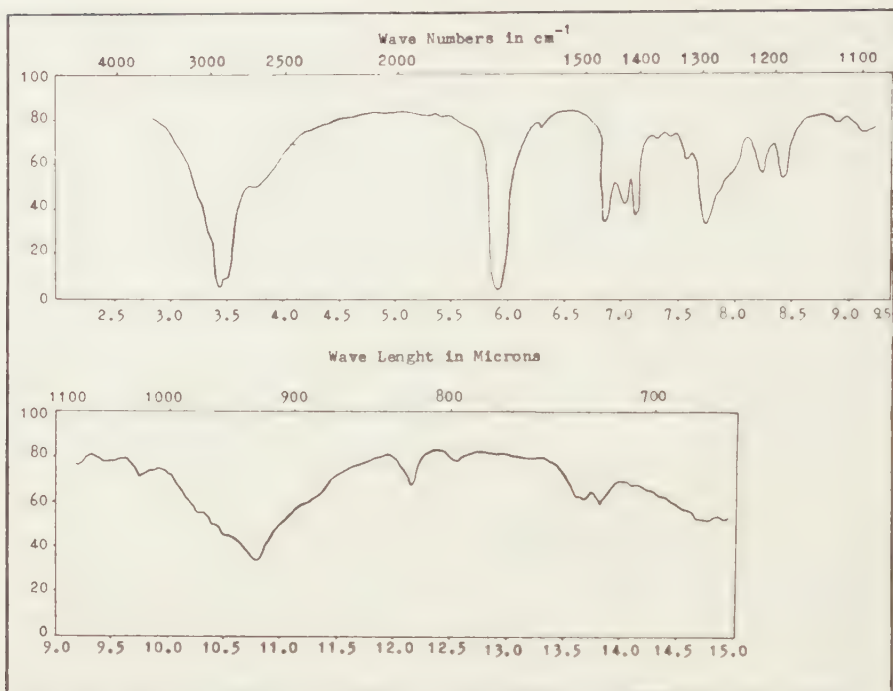


Fig. 1. Infra-red spectrum of *cis, cis*-9, 11-octadecadienoic acid.

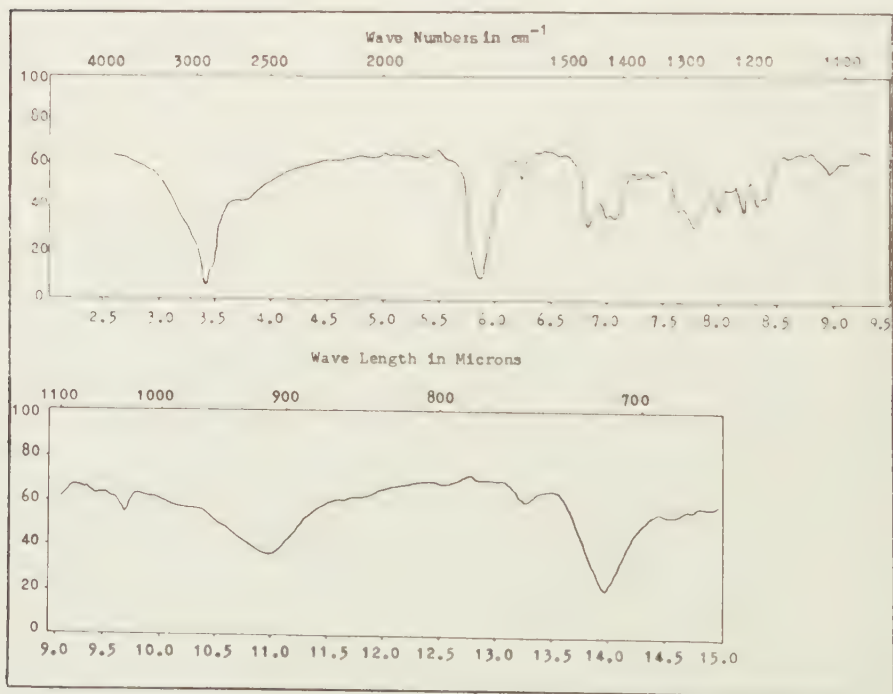


Fig. 2. Infra-red spectrum of *cis, cis*-10, 12-octadecadienoic acid.

## EXPERIMENTAL

1-*Heptyne* was obtained by the interaction of sodium acetylide and pentylbromide (prepared from pentanol [16]) in liquid ammonia solution [17, 18]. The crude product was purified by fractional distillation in a plate column, as described by SHORLAND [19]. Heptyne: B.p. 97.5–98.5°C;  $n_D^{20}$  1.4086.

10-*Undecynoic* acid was prepared from 10-undecenoic acid (slip point 19.6°C) via the dibromo-undecanoic acid. After dehydrobromating at low temperature the 11-bromo-10-undecenoic acid [20] was obtained, the potassium salt of which was thermally decomposed by SPOELSTRA's method [21]. The distilled product was recrystallized from 30 parts light petroleum at –15°C. 10-Undecynoic acid: M.p. 42.5–43.0°C;  $n_D^{65}$  1.4393.

## 10, 12-Octadecadiynoic acid

A solution of 6.5 g undecynoic acid and 1 g heptyne in 10 ml ethanol was added slowly, at 20°C, whilst stirring, to a solution of 50 g cuprous chloride and 80 g ammonium chloride in 200 ml water, to which 3.5 g heptyne had previously been added<sup>1)</sup>. The temperature was raised to 50°C and the reaction mixture stirred for 5 h. After adding hydrochloric acid (to decompose any copper-complexes), the reaction mixture was taken up in ether, washed with water and extracted with soda solution. The neutral fraction (2.8 g) contained heptyne and tetradecadiyne. The acid mixture (7.5 g) was taken up in light petroleum, in which, at low temperatures, docosadiynedioic acid does not dissolve (1.85 g). The resultant mixture (5.65 g) was dissolved in 400 ml water and excess ammonia and the magnesium salt of the octadecadiynoic acid precipitated by the addition of 60 ml 10 % ammonium chloride solution and excess 15 % magnesium sulphate solution; the undecynoic acid remained in solution.

The operation was repeated, the diynoic acid being liberated from the precipitated magnesium soap and recrystallized from 25 parts light petroleum at –20°C (yield 13.1 % calculated on undecynoic acid as starting material).

The pure 10, 12-octadecadiynoic acid had the following constants:

Melting point . . . . .	42.2–42.4°C
Refractive index $n_D^{65}$ . . . . .	1.4810
Mol. weight by titration . . . . .	276 (calcd. 276)
H <sub>2</sub> -uptake on catalytic hydrogenation (with Pt-oxide in alcoholic solution) .	3.94 moles
M.p. hydrogenated product . . . . .	67.9°C
Ultra-violet spectrum in light petroleum	$\lambda_{\text{max}}$ 226 239 252.5 m $\mu$ $\epsilon$ 450 430 250

<sup>1)</sup> By proceeding in this way an excess of heptyne is invariably ensured, reducing the chance of the formation of the symmetrical diynedioic acid, to which—as borne out by previous experiments—there is always a tendency.

As previously described, the octadecadiynoic acid turned blue on exposure to light, and red on heating to 41° C. The blue mixture can be purified by dissolving it in light petroleum in which the coloured compound is insoluble.

#### 10, 12-Docosadiynedioic acid

The crude docosadiynedioic acid (1.85 g) was recrystallized from 20 parts light petroleum at 20° C. The product obtained had a high degree of purity and had the following constants:

Acid value. . . . .	309.5 (calculated 309.9)
Melting point . . . . .	112.1–113.0° C
Ultra-violet spectrum (in alcohol) . . .	$\lambda_{\max}$ 239 253 265 m $\mu$
	$\epsilon$ 413 228 40

#### *Cis, cis*-10, 12-octadecadienoic acid

After exploratory experiments it appeared that for the partial reduction of 10, 12-octadecadiynoic acid an amount of quinoline, smaller than mentioned in the literature, did not affect the selectivity of the catalyst, and that the rate of hydrogen absorption was increased. The most favourable composition of the reaction mixture was found to be: 2 g octadecadiynoic acid, 1 g Lindlar catalyst, 0.025 g quinoline and 10 ml ethanol. Hydrogenation took place while stirring and after ca. 4 h the necessary amount of hydrogen had been taken up. From infra-red measurements it appeared that a certain amount of trans double bonds had been formed. On cooling a solution of the product in 30 parts light petroleum at –40° C the *cis, cis* compound crystallized out, whereas the greater part of the trans compounds remained in the mother liquor. With the help of the infra-red spectrum the purification could be followed. After 4 recrystallizations of the crude hydrogenation product in 100 parts light petroleum at –40° C a substance was obtained in which only about 0.5 % of *cis, trans* compounds could be detected.

By repeated recrystallization of this product from 25 parts pure acetone at –40° C, *cis, cis*-10, 12-octadecadienoic acid was obtained (overall yield of the recrystallizations, 12.5 % <sup>1)</sup>) in a very pure state, having the constants as given in the table.

*Cis, cis*-10, 12-octadecadienoic acid has a remarkably high melting point compared with that of the *trans, trans* compound (ca. 57° C). This *cis, cis* compound was very unstable <sup>2)</sup>, as appeared from the rapid changing of the refractive index.

<sup>1)</sup> The low, final yield was due to the many recrystallizations which were necessary to remove the last traces of impurities.

<sup>2)</sup> This was probably the reason for the differences between the data of the elementary analysis, as calculated and as found, it being impossible to carry out the analysis immediately after the last crystallization.



1-Octyne was prepared by coupling hexylbromide [16] with sodium acetylide in liquid ammonia [17, 18] and purifying the product by repeated fractional distillation.

Octyne: B.p. 125–127° C;  $n_D^{20}$  1.4165.

From the forerun and the residue a small amount of pure octyne ( $n_D^{20}$  1.4162) was further isolated via the silver compound.

9-Decynoic acid was obtained from 10-undecynoic acid ethyl ester (b.p. 80–85° C/0.1 mm;  $n_D^{20}$  1.4445) by the Barbier–Wieland degradation method (described by BLACK and WEEDON [22] for this compound).

Ethyl undecynoate [23] was treated with phenylmagnesiumbromide and the 1,1-diphenylundecyn-10-ol-1 obtained ( $n_D^{20}$  1.5556) was dehydrated without further purification. Upon application, however, of the simple procedure of Black and Weedon (heating at 220° C for  $\frac{1}{2}$  h), low yields were obtained, probably due to polymerization of the product. Heating in vacuo for a short time or using potassium hydrogen sulphate as a catalyst did not improve the results. On heating for 10 mins. to 220° C, with granulated clay pipe as a catalyst, a better result was obtained.

After repeated recrystallization from 8 parts light petroleum at –30° C the dehydrated product, 1,1-diphenyl-1-undecenyne-10, was obtained in a pure state (yield 47 %, m.p. 38.3–38.8° C, b.p. 175° C/0.1 mm,  $n_D^{65}$  1.5427,  $\lambda_{\max}$  251 m $\mu$ ,  $\epsilon$  15,000).

Oxidation of this product was carried out with  $\text{CrO}_3$  in acetic acid medium, giving 9-decynoic acid which could be isolated by distillation.

After repeated recrystallization from 10 parts light petroleum at –5° C, 9-decynoic acid was obtained in a pure state (yield 66 %, overall yield 31 %, m.p. 25.5–26.1° C, b.p. 88° C/0.1 mm,  $n_D^{27}$  1.4533).

The physical constants of the non-recrystallized product appeared to be in close agreement with those given by Black and Weedon. The same is applicable to the constants of 1,1-diphenyl-1-undecenyne-10. Upon further purification of these substances, however, the constants showed deviations. Since, in addition, Black and Weedon did not obtain 1,1-diphenyl-1-undecenyne-10 in a crystalline state, it is assumed that their products were not entirely pure.

### 9,11-Octadecadiynoic acid

In the preparation of 9,11-octadecadiynoic acid by coupling of 1-octyne with 9-decynoic acid, use was made of the experience gained in the previously mentioned coupling reaction of 1-heptyne with 10-undecynoic acid. The following procedure was employed:

A solution of 6.2 g 9-decynoic acid and 0.5 g octyne in 10 ml ethanol was added dropwise to the catalyst solution, while stirring, at 20° C. The latter solution contained 50 g cuprous chloride, 80 g ammonium chloride, 200 ml water, 4.0 g octyne and 6 ml 2 N ammonia. The temperature was then raised gradually to 50° C and the solution vigorously stirred for 5 h.

During the last hour air was passed repeatedly over the surface of the liquid.

The separation of the reaction products took place in the same way as described for the preparation of the 10, 12-diynoic acid. The amount of unsaponifiable matter (unconverted 1-octyne and its coupling product the symmetrical 7, 9-hexadecadiyne) was 3.25 g. The yield of 9, 11-eicosadiynedioic acid (insoluble in light petroleum at low temperature) amounted to 4.6 g (75.2 %).

The unconverted part of the 9-decynoic acid and the 9, 11-diynoic acid, when dissolved in light petroleum, could be separated via the magnesium salts, yielding 0.4 g 9-decynoic acid (6.5 %) and 1.7 g 9, 11-octadecadiynoic acid (16.7 %). The latter compound was purified by repeated recrystallization from 50 parts light petroleum at  $-20^{\circ}\text{C}$ .

On heating to the melting point no discoloration took place as in the case of the 10, 12-diynoic acid.

The purified 9, 11-diynoic acid had the following constants:

Melting point . . . . .	47.5–48.0° C
Refractive index $n_D^{25}$ . . . . .	1.4813
$\text{H}_2$ -uptake on catalytic hydrogenation (with Pt-oxide in alcoholic solution) . . . . .	4.0 moles
M.p. hydrogenated product . . . . .	67.8° C
Ultra-violet spectrum in light petroleum	$\lambda_{\text{max}}$ 226 239 253.5 $\text{m}\mu$
	$\epsilon$ 410 383 222

#### *9, 11-Eicosadiynedioic acid*

From a concentrated solution in acetone the crude product was precipitated with 15-fold excess light petroleum. It was subsequently purified by three recrystallizations from 50 parts acetone at  $-50^{\circ}\text{C}$ .

On exposure to light a blue coloration rapidly took place in the surface layer of the substance.

The purified 9, 11-eicosadiynedioic acid had the following constants:

Melting point . . . . .	117–118° C
Ultra-violet spectrum (in alcohol) . . . . .	$\lambda_{\text{max}}$ 239 253.5 $\text{m}\mu$
	$\epsilon$ 400 226

#### *Cis, cis-9, 11-octadecadienoic acid*

This compound was obtained by partial hydrogenation of 9, 11-octadecadiynoic acid with a Lindlar catalyst, by the same procedure as used in the synthesis of *cis, cis-10, 12-octadecadienoic acid*.

#### ACKNOWLEDGEMENT

I am greatly indebted to Mr. G. DIJKSTRA for the infra-red analyses and to Miss J. M. HAECCK and Mr. J. B. A. STROINK for the attentive care with which they carried out the experiments.

My thanks are further due to the Management of Unilever N.V., Rotterdam, for their kind permission to publish this paper.

*Unilever Research Laboratory*

*Vlaardingen, 2nd May, 1956.*

## REFERENCES

1. MANGOLD, C., *Monatsh.* **15**, 307 (1894).
2. BÖESEKEN, J., *Rec. trav. chim.* **46**, 623 (1927).
3. SMIT, W. C., *Rec. trav. chim.* **49**, 539 (1930).
4. MIKUSCH, J. D. VON, *J. Am. Chem. Soc.* **64**, 1580 (1942).
5. ———, *Angew. Chem.* **62**, 475 (1950).
6. ———, *J. Am. Oil Chemists' Soc.* **29**, 114 (1952).
7. ———, *Fette u. Seifen* **54**, 751 (1952).
8. JACKSON, J. E., R. F. PASCHKE, W. TOLBERG, H. M. BOYD and D. H. WHEELER, *J. Am. Oil Chemists' Soc.* **29**, 229 (1952).
9. MIKUSCH, J. D. VON, *Official Digest Fed. Paints Varnishes Prod. Club* **28**, 44 (1956).
10. NICHOLS JR., P. L., S. F. HERB and R. W. RIEMENSCHNEIDER, *J. Am. Chem. Soc.* **73**, 247 (1951.)
11. GLASER, C., *Ann.* **154**, 159 (1870).
12. SEHER, A., *Fette u. Seifen* **54**, 544 (1952); **55**, 95 (1953).
13. LINDLAR, H., *Helv. Chim. Acta* **35**, 447 (1952).
14. ALLEN, R. R., *J. Org. Chem.* **21**, 143 (1956).
15. SHEPPARD, N., and D. M. SIMPSON, *Quart. Revs.* **6**, 1 (1952).
16. KAMM, O., and C. NARVEL, *Org. Syntheses. Coll. Vol. I*, 29 (1941).
17. CAMPBELL, K. N. and B. K. CAMPBELL, *Org. Syntheses* **30**, 15 (1950).
18. VAUGHN, T. H., G. F. HENNION, R. R. VOGT, and J. A. NIEUWLAND, *J. Org. Chem.* **2**, 1 (1937).
19. SHORLAND, F. B., *J. Appl. Chem. (London)* **2**, 438 (1952).
20. KRAFT, F., *Ber.* **29**, 2232 (1896).
21. SPOELSTRA, D. B., Thesis, Utrecht, 1927.
22. BLACK, H. K. and B. C. L. WEEDON, *J. Chem. Soc.* **1953**, 1785.
23. JEFFERY, G. H. and A. I. VOGEL, *J. Chem. Soc.* **1948**, 674.

## SOLAR WEIGHTING FUNCTIONS. I

BY

H. HUBENET

(Communicated by Prof. M. MINNAERT at the meeting of October 27, 1956)

*Introduction*

Originally the chemical composition of a stellar atmosphere used to be determined by means of a "rough analysis" of the spectrum, that is, in the discussion only average values of the temperature  $T$  and electron pressure  $p_e$  of the atmosphere were used. It was considered dubious, whether the work involved in taking in account the detailed stratification, by considering the true temperature and pressure distributions, would be paid by a substantially increased accuracy. CLAAS [1] undertook such a "fine analysis" of the solar spectrum and determined the abundances relative to hydrogen of 16 elements in the solar atmosphere. In the majority of the cases he confined himself to the use of *faint* Fraunhofer lines. This has many advantages: 1) For such lines damping and turbulence have no influence on the equivalent width. 2) Faint lines are formed in the deeper layers of the photosphere ( $\tau_0 \approx 0.1$ ), whereas strong lines have higher levels of formation where uncertainties as to the prevailing temperatures and deviations from thermodynamical equilibrium introduce sources of errors. 3) Especially in this case the Unsöld-Minnaert method of the weighting functions [2] is very time saving.

Claas' method can hardly be improved, in contradistinction to its numerical basis. The basic data for his computations were: 1) The temperature distribution. 2) The assumed metal and helium content. 3) The observed equivalent widths. 4) The line strengths respectively the  $gf$ -values. Though the data mentioned under 1) and 2) can be improved, it is generally felt that the determined abundance values will not alter very much.

The equivalent width of a line is determined by the number of atoms contributing to the line formation (that is by the number of atoms in the initial state of the transition), and also by the weighting functions describing in how far these absorbing atoms are effective.

The present investigation intends to give some numerical information as to the sensitivity of abundance determinations to changes in the assumed temperature distribution and helium and metal content, but we confine ourselves to the influence of these factors on the weighting functions not considering for this moment their influence on the number of absorbing atoms. For this purpose we computed weighting functions for different cases, confining ourselves to the absorption weighting functions for the centre of the solar disc.



### Definitions and equations

CLAAS neglected the helium content, a simplification which will not be introduced here. In the basic equation for the equivalent width as used by CLAAS, the weighting function  $h_\lambda$  corresponding to a helium content zero will be replaced by a modified function  $h'_\lambda$ . It will not be difficult to verify the following equation by comparison with CLAAS [1] (page 4):

$$(1) \quad W_\lambda = 5,28 \cdot 10^6 \lambda^2 \int_0^\infty h'_\lambda(\tau_0) \cdot \frac{N_1}{N_H} d\tau_0$$

$W_\lambda$ -equivalent width expressed in mÅ,  $\lambda$ -wavelength in Å units,  $f$ -oscillator strength of the transition,  $h'_\lambda(\tau_0) = \frac{h_\lambda(\tau_0)}{1+4B}$  (weighting functions),  $B$ -abundance of helium relative to hydrogen (in numbers),  $\tau_0$ -optical depth for the continuous absorption at  $\lambda$  5000,  $N_1$ -number of atoms in the initial state of the transition,  $N_H$ -number of hydrogen atoms.

The ratio  $N_1/N_H$  can be found by application of the Boltzmann and Saha equations. In a formal way we can write:

$$(2) \quad \frac{N_1}{N_H} = g_1 A_{ei} F_i(\vartheta, p_e, u, u^+, u^{++}, \dots, \chi_1, \chi_2, \dots, E_1)$$

( $g_1$ -statistical weight of the initial state,  $A_{ei}$ -abundance of the element, that is the ratio of the total number of particles of the element (neutral and ionized states) to the total number of hydrogen particles (practically all the hydrogen is in the neutral state),  $i$ -state of ionization,  $\vartheta = T/5040$ ,  $p_e$ -electron pressure,  $u, u^+, u^{++}, \dots$ -partition functions,  $\chi_1, \chi_2, \dots$ -ionization potentials,  $E_1$ -excitation potential of the initial state).

For the explicit form of the functions  $F_i$  we refer to CLAAS [1] (page 6).

These are the basic equations that enable us to compute equivalent widths. The functions and quantities which have to be known are:

Atmospheric:  $T(\tau_0), p_e(\tau_0), h'_\lambda(\tau_0), A_{ei}$ .

Atomic :  $\lambda, g_1 f, u, u^+, u^{++}, \dots, \chi_1, \chi_2, \dots, E_1$ .

When this method is applied for abundance determinations  $W_\lambda$  is known from the observations and  $A_{ei}$  can be found.

### Computation of the atmospheric functions

We assume that on the average every metal atom is singly ionized and that only the  $H^-$ -ions and the neutral  $H$ -atoms contribute to the continuous absorption<sup>1)</sup>. Then the state of the atmosphere is defined by the temperature distribution  $T(\tau_0)$ , the inverse metal content  $A = N_H/N_{met}$  and the helium content  $B$ .

The electron pressure  $p_e$  can be found by means of an iterative process (BARBIER). For the description of this method we refer to CLAAS [1]

<sup>1)</sup> This is an approximation and in a second paper the author hopes to deal with this question.

(page 10). Since we, unlike CLAAS, assume a non-vanishing helium content Claas' equations (35a) and (39) have to be modified slightly.

We will now discuss the computations of the weighting functions in more detail. Our functions  $h'_\lambda(\tau_0)$  are defined in the following way:

$$(3) \quad h'_\lambda(\tau_0) = \frac{h_\lambda(\tau_0)}{1+4B} = \frac{g'_1(\tau_0)/\kappa_0}{1+4B} = \frac{g_1\{\tau(\tau_0)\}/\kappa_0}{1+4B}$$

( $\kappa_0$ -continuous absorption coefficient per gram stellar matter at  $\lambda$  5000,  $\tau$ -optical depth for wavelength  $\lambda$ ).

$g_1(\tau)$  is the absorption weighting function for the centre of the solar disc. We can write (cf. PECKER [3]):

$$(4) \quad g_1(\tau) = \frac{\int_0^\infty B_\lambda e^{-\tau} d\tau - B_\lambda e^{-\tau}}{\int_0^\infty B_\lambda e^{-\tau} d\tau}$$

( $B_\lambda$ -Kirchhoff Planck function for wavelength  $\lambda$  and temperature  $T\{\tau_0(\tau)\}$ ).

The optical depth for continuous absorption  $\tau$  can be found from:

$$(5) \quad \tau = \int_0^{\tau_0} \frac{\kappa}{\kappa_0} d\tau_0.$$

$\kappa$  is the continuous absorption coefficient per gram for wavelength  $\lambda$ . We have

$$(6) \quad \kappa = \frac{\kappa_H + \frac{p_e}{m_H} k_H^-}{1+4B}$$

( $\kappa_H$ -continuous absorption coefficient of neutral H per gram (tabulated by UNSÖLD [2], page 170),  $k_H^-$ -continuous absorption coefficient of  $H^-$  per H-atom and per unit of electron pressure (tabulated by CHANDRASEKHAR and BREEN [11])).

The computation of the weighting function proceeds in the order: (6), (5), (4), (3).

The computations were performed by means of the IBM card programmed calculator (CPC) of the Indiana University Research Computing Center.

### Results

The computations were carried out for 3 wavelengths:  $\lambda$  4000,  $\lambda$  5000,  $\lambda$  8000. In order to investigate the influence of the temperature distribution, weighting functions were determined for 4 models  $T(\tau_0)$  as proposed by several authors for a fixed composition  $A = 9000$ ,  $B = 0.04$  (fig. 1; tables II, III, IV, VI). By varying the composition for a fixed model the influence of the composition was investigated; we chose the average model and the following ( $A$ ,  $B$ ) combinations: (9000, 0), (9000, 0.04),

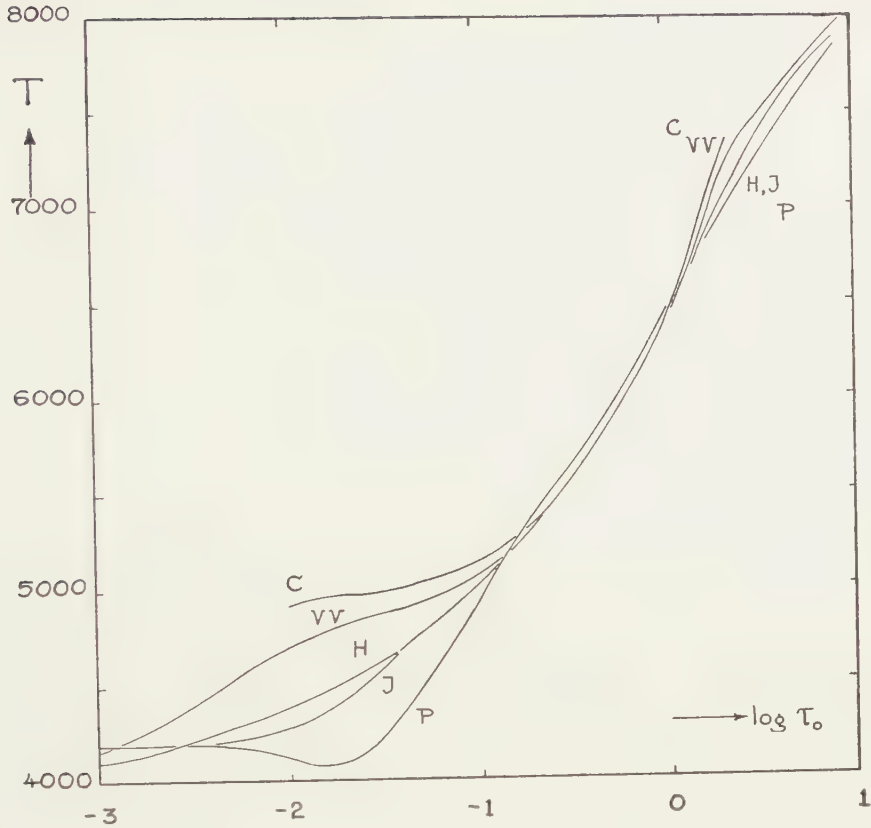


Fig. 1. The temperature distributions  $T(\tau_0)$  considered in this investigation: C — CLAAS [1], H — an average of some recently derived models, J — DE JAGER VII [6], slightly smoothed, P — PAGEL [7], VV — a combination of VITENSE II [8] and VOIGT [9].

TABLE I  
Temperature distribution CLAAS,  $A = 8000$ ,  $B = 0$ .  
Computations by CLAAS

$\tau_0$	$\vartheta$	$\log p$	$\log p_e$	$\log \kappa_0$	$\log h'_{4000}$	$\log h'_{5000}$	$\log h'_{8000}$
0,01	1,022	3,95	0,07	8,80	1,12	1,07	0,90
0,02	1,015	4,10	0,22	8,94	0,97	0,93	0,73
0,04	1,007	4,25	0,37	9,07	0,83	0,78	0,58
0,06	0,999	4,34	0,46	9,15	0,75	0,68	0,51
0,08	0,990	4,41	0,53	9,20	0,69	0,63	0,46
0,10	0,980	4,46	0,58	9,24	0,64	0,58	0,41
0,2	0,942	4,62	0,79	9,37	0,47	0,39	0,20
0,6	0,840	4,87	1,35	9,75	1,94	1,83	1,48
1,0	0,781	4,94	1,76	0,04	1,49	1,30	2,81
1,4	0,736	4,98	2,10	0,28	1,10	2,86	2,16
1,8	0,706	4,99	2,31	0,43	2,79	2,47	3,33
2,2	0,684	5,01	2,47	0,55	2,51		

TABLE II  
Temperature distribution De JAGER,  $A = 9000$ ,  $B = 0.04$

$\tau_0$	$\theta$	$\log p$	$\log p_e$	$\log \frac{N_{H^+}}{N_H}$	24000					25000					28000				
					$\tau_\lambda$	$\log x_\lambda$	$\frac{x_\lambda}{x_0}$	$\log g'_\lambda$	$\log h'_\lambda$	$\log x_0$	$\log y'_0$	$\log h'_0$	$\tau_\lambda$	$\log x_\lambda$	$\frac{x_\lambda}{x_0}$	$\log g'_\lambda$	$\log h'_\lambda$	$\log x_\lambda$	$\log h'_\lambda$
0.001	1.209	3.35	9.38	2.76	7.89 [6]	8.26	0.789	9.98	1.55	8.36	9.95	1.53	1.35 [7]	8.50	1.35	9.86	1.44	8.50	1.44
0.002	1.206	3.51	9.54	2.64	1.58 [7]	8.41	0.789	9.98	1.40	8.52	9.95	1.37	2.70 [7]	8.65	1.35	9.86	1.28	8.65	1.28
0.004	1.198	3.67	9.70	2.59	3.16 [7]	8.56	0.789	9.98	1.26	8.66	9.95	1.23	5.41 [7]	8.79	1.35	9.86	1.14	8.79	1.14
0.006	1.193	3.76	9.79	2.58	4.73 [7]	8.64	0.789	9.98	1.17	8.74	9.95	1.14	8.11 [7]	8.88	1.35	9.86	1.05	8.88	1.05
0.008	1.186	3.82	9.85	2.62	6.31 [7]	8.70	0.789	9.98	1.12	8.80	9.95	1.09	1.08 [8]	8.93	1.35	9.85	0.99	8.93	0.99
0.01	1.180	3.88	9.91	2.65	7.89 [7]	8.74	0.789	9.97	1.07	8.84	9.94	1.04	1.35 [8]	9.07	1.35	9.85	0.95	9.07	0.95
0.02	1.136	4.04	0.07	3.12	1.58 [8]	8.83	0.788	9.96	0.97	8.93	9.93	0.93	2.70 [8]	9.07	1.35	9.82	0.82	9.07	0.82
0.04	1.075	4.22	0.26	3.83	3.15 [8]	8.91	0.788	9.94	0.87	9.02	9.89	0.82	5.41 [8]	9.15	1.35	9.76	0.68	9.15	0.68
0.06	1.043	4.34	0.37	4.17	4.73 [8]	8.97	0.787	9.93	0.79	9.08	9.87	0.73	8.12 [8]	9.21	1.35	9.72	0.58	9.21	0.58
0.08	1.020	4.42	0.46	4.43	6.30 [8]	9.02	0.787	9.91	0.73	9.12	9.85	0.67	1.08 [9]	9.25	1.36	9.68	0.50	9.25	0.50
0.1	1.003	4.48	0.52	4.61	7.88 [8]	9.05	0.787	9.90	0.68	9.16	9.83	0.61	1.35 [9]	9.29	1.36	9.65	0.44	9.29	0.44
0.2	0.947	4.67	0.76	5.20	1.57 [9]	9.18	0.787	9.85	0.50	9.29	9.76	0.41	2.71 [9]	9.42	1.36	9.54	0.19	9.42	0.19
0.4	0.884	4.84	1.07	5.81	3.15 [9]	9.38	0.786	9.76	0.21	9.49	9.63	0.08	5.43 [9]	9.62	1.36	9.34	0.80	9.62	0.80
0.6	0.843	4.93	1.33	6.18	4.72 [9]	9.56	0.786	9.66	0.94	9.66	9.50	9.78	8.16 [9]	9.80	1.37	9.16	9.44	9.80	9.44
0.8	0.812	4.98	1.54	6.43	6.29 [9]	9.71	0.785	9.56	9.68	9.81	9.37	9.50	1.09	9.95	1.38	8.98	9.11	9.95	9.11
1.0	0.787	5.01	1.72	6.62	7.86 [9]	9.83	0.785	9.45	9.45	9.94	9.24	9.24	1.37	0.08	1.39	8.80	8.80	0.08	8.80
1.4	0.754	5.04	1.96	6.87	1.10	0.02	0.784	9.26	9.08	0.12	8.99	8.81	1.93	0.27	1.41	8.46	8.28	0.27	8.46
1.8	0.728	5.08	2.16	7.06	1.41	0.16	0.781	9.04	8.71	0.27	8.72	8.39	2.50	0.42	1.43	8.09	7.76	0.42	8.09
2.2	0.710	5.09	2.30	7.19	1.72	0.26	0.778	8.83	8.40	0.37	8.46	8.02	3.07	0.53	1.45	7.72	7.29	0.53	7.72
2.6	0.698	5.11	2.40	7.28	2.04	0.34	0.775	8.63	8.12	0.45	8.21	7.70	3.66	0.62	1.47	7.35	6.84	0.62	7.35
3.0	0.689	5.12	2.47	7.34	2.34	0.39	0.773	8.46	7.90	0.50	8.00	7.44	4.25	0.67	1.48	7.04	6.47	0.67	7.04
3.5	0.679	5.13	2.55	7.42	3.73	0.45	0.771	8.24	7.61	0.57	7.72	7.09	5.00	0.74	1.50	6.58	5.95	0.74	6.58
4.0	0.670	5.14	2.62	7.45	3.12	0.50	0.769	7.99	7.32	0.62	7.41	6.73	5.75	0.80	1.52	5.95	5.27	0.80	5.95
4.5	0.663	5.15	2.68	7.53	3.50	0.55	0.767	7.74	7.02	0.66	7.08	6.35	6.52	0.85	1.54			0.85	
5.0	0.658	5.16	2.72	7.56	3.88	0.58	0.766	7.52	6.76	0.70	6.76	5.99	7.29	0.89	1.55			0.89	



TABLE III

Temperature distribution VITENSE-VOIGT,  $A$  9000,  $B$  0.04

$\tau_0$	$\vartheta$	$\log p$	$\log p_e$	$\log \frac{N_{H^+}}{N_{H^-}}$	24000					25000					28000				
					$\tau_\lambda$	$\log \kappa_\lambda$	$\frac{\kappa_\lambda}{\kappa_0}$	$\log g'_\lambda$	$\log b'_\lambda$	$\log \kappa_0$	$\log g'_0$	$\log b'_0$	$\tau_\lambda$	$\log \kappa_\lambda$	$\frac{\kappa_\lambda}{\kappa_0}$	$\log g'_\lambda$	$\log b'_\lambda$		
0.001	1.210	3.34	9.36	2.75	7.88 [6]	8.25	0.789	9.98	1.57	8.35	9.96	1.54	1.35 [7]	8.48	1.35	9.87	1.46		
0.002	1.176	3.51	9.54	3.07	1.58 [7]	8.36	0.789	9.97	1.44	8.47	9.94	1.42	2.70 [7]	8.60	1.35	9.85	1.32		
0.004	1.132	3.69	9.72	3.54	3.15 [7]	8.47	0.788	9.96	1.33	8.57	9.93	1.29	5.41 [7]	8.70	1.35	9.81	1.18		
0.006	1.103	3.80	9.83	3.84	4.73 [7]	8.53	0.788	9.96	1.26	8.63	9.91	1.22	8.12 [7]	8.77	1.35	9.79	1.09		
0.008	1.085	3.87	9.90	4.03	6.30 [7]	8.58	0.788	9.95	1.21	8.68	9.90	1.16	1.08 [8]	8.81	1.35	9.77	1.03		
0.01	1.072	3.93	9.97	4.16	7.88 [7]	8.62	0.788	9.94	1.16	8.72	9.90	1.11	1.35 [8]	8.85	1.35	9.76	0.97		
0.02	1.046	4.11	0.15	4.36	1.58 [8]	8.76	0.787	9.93	1.01	8.86	9.88	0.96	2.71 [8]	8.99	1.35	9.72	0.80		
0.04	1.028	4.29	0.33	4.44	3.15 [8]	8.90	0.787	9.92	0.86	9.00	9.86	0.80	5.41 [8]	9.14	1.36	9.70	0.63		
0.06	1.015	4.39	0.43	4.53	4.72 [8]	8.98	0.787	9.91	0.77	9.08	9.85	0.70	8.13 [8]	9.21	1.36	9.67	0.53		
0.08	1.004	4.46	0.50	4.62	6.30 [8]	9.03	0.787	9.91	0.71	9.14	9.84	0.64	1.08 [9]	9.27	1.36	9.66	0.46		
0.1	0.995	4.51	0.56	4.70	7.87 [8]	9.07	0.787	9.90	0.66	9.18	9.83	0.59	1.36 [9]	9.31	1.36	9.64	0.40		
0.2	0.949	4.68	0.76	5.16	1.57 [9]	9.20	0.787	9.86	0.50	9.30	9.77	0.41	2.71 [9]	9.43	1.36	9.54	0.18		
0.4	0.887	4.85	1.06	5.78	3.15 [9]	9.38	0.786	9.78	0.23	9.49	9.65	0.11	5.43 [9]	9.62	1.36	9.37	9.82		
0.6	0.845	4.93	1.32	6.16	4.72 [9]	9.55	0.786	9.69	9.97	9.66	9.54	9.82	8.16 [9]	9.79	1.37	9.20	9.48		
0.8	0.813	4.98	1.54	6.42	6.29 [9]	9.70	0.785	9.60	9.73	9.81	9.42	9.55	1.09	9.95	1.38	9.04	9.17		
1.0	0.787	5.01	1.72	6.62	7.86 [9]	9.84	0.785	9.51	9.50	9.94	9.30	9.30	1.37	0.09	1.39	8.88	8.87		
1.4	0.746	5.05	2.02	6.93	1.10	0.06	0.783	9.30	9.08	0.16	9.05	8.82	1.93	0.31	1.42	8.53	8.31		
1.8	0.715	5.08	2.26	7.16	1.41	0.23	0.778	9.05	8.65	0.34	8.74	8.35	2.50	0.52	1.45	8.13	7.73		
2.2	0.694	5.09	2.42	7.32	1.72	0.35	0.774	8.77	8.26	0.46	8.41	7.89	3.09	0.63	1.48	7.67	7.16		
2.6	0.682	5.10	2.51	7.40	2.03	0.42	0.771	8.54	7.95	0.53	8.12	7.53	3.68	0.71	1.50	7.25	6.66		
3.0	0.675	5.11	2.57	7.46	2.34	0.46	0.770	8.35	7.71	0.58	7.87	7.23	4.29	0.76	1.51	6.85	6.21		
3.5	0.667	5.13	2.64	7.51	2.72	0.51	0.767	8.11	7.42	0.63	7.57	6.88	5.05	0.81	1.53	6.28	5.60		
4.0	0.662	5.14	2.68	7.55	3.11	0.55	0.766	7.92	7.19	0.66	7.31	6.59	5.82	0.85	1.54	5.53	4.81		
4.5	0.656	5.15	1.73	7.59	3.49	0.58	0.764	7.68	6.92	0.70	6.98	6.22	6.59	0.89	1.56				
5.0	0.653	5.15	2.76	7.61	3.87	0.60	0.764	7.52	6.74	0.72	6.74	5.96	7.37	0.92	1.56				

 $\frac{1}{2} \tau_0$

TABLE IV  
Temperature distribution PAGER,  $A = 9000$ ,  $B = 0.04$

$\tau_0$	$\theta$	$\log p$	$\log p_e$	$\log \frac{N_{H^+}}{N_H}$	$\lambda 4000$					$\lambda 5000$					$\lambda 8000$					
					$\tau_\lambda$	$\log \kappa_\lambda$	$\frac{\kappa_\lambda}{\kappa_0}$	$ \log g'_\lambda $	$\log h'_\lambda$	$\log \kappa_0$	$\log g'_0$	$\log h'_0$	$\tau_\lambda$	$\log \kappa_\lambda$	$\frac{\kappa_\lambda}{\kappa_0}$	$ \log g'_\lambda $	$\log h'_\lambda$	$\log \kappa_0$	$\log g'_0$	$\log h'_0$
0.001	1.200	3.36	9.39	2.87	7.89 [6]	8.26	0.789	9.98	1.56	8.36	9.95	1.53	1.35 [7]	8.49	1.35	9.86	1.44			
0.002	1.200	3.52	9.55	2.72	1.58 [7]	8.41	0.789	9.98	1.40	8.52	9.95	1.37	2.70 [7]	8.65	1.35	9.86	1.28			
0.004	1.200	3.67	9.70	2.57	3.16 [7]	8.57	0.789	9.98	1.25	8.67	9.95	1.22	3.40 [7]	8.80	1.35	9.86	1.13			
0.006	1.207	3.76	9.79	2.37	4.73 [7]	8.67	0.789	9.98	1.15	8.77	9.95	1.12	8.11 [7]	8.90	1.35	9.86	1.04			
0.008	1.214	3.82	9.85	2.21	6.31 [7]	8.74	0.789	9.98	1.08	8.84	9.96	1.05	1.08 [8]	8.97	1.35	9.87	0.97			
0.01	1.223	3.87	9.90	2.03	7.89 [7]	8.80	0.788	9.98	1.02	8.90	9.96	1.00	1.35 [8]	9.03	1.35	9.87	0.91			
0.02	1.231	4.01	0.04	1.78	1.58 [8]	8.95	0.788	9.98	0.87	9.05	9.96	0.84	2.70 [8]	9.18	1.35	9.88	0.76			
0.04	1.160	4.17	0.20	2.65	3.15 [8]	8.99	0.788	9.97	0.81	9.10	9.94	0.78	5.41 [8]	9.23	1.35	9.84	0.68			
0.06	1.096	4.28	0.31	3.47	4.73 [8]	9.00	0.788	9.95	0.79	9.10	9.91	0.74	8.12 [8]	9.24	1.35	9.78	0.62			
0.08	1.055	4.37	0.40	3.97	6.30 [8]	9.02	0.787	9.94	0.75	9.12	9.88	0.70	1.08 [9]	9.26	1.35	9.74	0.56			
0.1	1.032	4.44	0.47	4.25	7.88 [8]	9.05	0.787	9.92	0.71	9.15	9.86	0.65	1.33 [9]	9.29	1.35	9.71	0.50			
0.2	0.935	4.65	0.76	5.38	1.57 [9]	9.16	0.786	9.84	0.51	9.27	9.74	0.42	2.71 [9]	9.40	1.36	9.53	0.20			
0.4	0.871	4.83	1.12	5.96	3.15 [9]	9.40	0.786	9.73	0.16	9.31	9.60	0.03	3.43 [9]	9.64	1.36	9.32	9.75			
0.6	0.832	4.91	1.38	6.29	4.72 [9]	9.59	0.785	9.62	9.87	9.69	9.46	9.71	8.17 [9]	9.83	1.37	9.12	9.37			
0.8	0.800	4.96	1.60	6.54	6.29 [9]	9.75	0.784	9.49	9.58	9.85	9.30	9.39	1.09	9.99	1.38	8.91	8.99			
1.0	0.780	4.99	1.76	6.70	7.86 [9]	9.86	0.785	9.38	9.36	9.96	9.16	9.14	1.37	9.99	1.38	8.91	8.99			
1.4	0.750	5.03	1.98	6.91	1.10	0.03	0.783	9.17	8.98	0.13	8.89	8.70	1.93	9.99	1.40	8.72	8.70			
1.8	0.731	5.06	2.13	7.04	1.41	0.13	0.781	8.98	8.68	0.24	8.65	8.35	2.50	9.99	1.42	8.35	8.16			
2.2	0.716	5.08	2.25	7.16	1.72	0.23	0.779	8.77	8.38	0.33	8.39	8.00	3.08	9.99	1.43	8.02	7.72			
2.6	0.706	5.10	2.33	7.23	2.04	0.29	0.777	8.61	8.15	0.40	8.19	7.73	3.66	9.99	1.45	7.65	7.26			
3.0	0.696	5.11	2.41	7.29	2.35	0.35	0.775	8.43	7.91	0.46	7.95	7.43	4.25	9.99	1.46	7.35	6.89			
3.5	0.687	5.13	2.49	7.36	2.73	0.40	0.773	8.22	7.65	0.52	7.69	7.11	4.99	9.99	1.47	6.99	6.47			
4.0	0.679	5.14	2.55	7.41	3.12	0.45	0.771	8.02	7.39	0.56	7.42	6.80	5.73	9.99	1.49	6.55	5.97			
4.5	0.672	5.15	2.61	7.46	3.50	0.50	0.770	7.82	7.15	0.61	7.15	6.48	6.49	9.99	1.50	5.99	5.37			
5.0	0.667	5.16	2.66	7.50	3.89	0.53	0.768	7.63	6.92	0.65	6.88	6.17	7.25	9.99	1.51					

TABLE V  
Average temperature distribution,  $A = 9000, B$  zero

$\tau_\lambda$	$\vartheta$	$\log p$	$\log p_e$	$\log \frac{N_{\text{H}}^+}{N_{\text{H}}}$	24000				25000				28000				
					$\tau_\lambda$	$\log \kappa_\lambda$	$\frac{\kappa_\lambda}{\kappa_0}$	$\log g'_\lambda$	$\log h'_\lambda$	$\log \kappa_0$	$\log g'_0$	$\log h'_0$	$\tau_\lambda$	$\log \kappa_\lambda$	$\frac{\kappa_\lambda}{\kappa_0}$	$\log g'_\lambda$	$\log h'_\lambda$
0,001	1,223	3,29	9,34	2,59	7,88 [6]	8,30	0,788	9,98	1,58	8,40	9,96	1,56	1,35 [7]	8,53	1,35	9,87	1,47
0,002	1,212	3,46	9,50	2,60	1,58 [7]	8,45	0,789	9,98	1,43	8,55	9,96	1,40	2,70 [7]	8,68	1,35	9,87	1,32
0,004	1,191	3,62	9,66	2,72	3,15 [7]	8,58	0,789	9,98	1,30	8,68	9,95	1,27	5,41 [7]	8,81	1,35	9,86	1,18
0,006	1,172	3,72	9,76	2,91	4,73 [7]	8,64	0,789	9,97	1,22	8,75	9,94	1,20	8,11 [7]	8,88	1,35	9,84	1,10
0,008	1,161	3,79	9,83	2,99	6,31 [7]	8,70	0,788	9,97	1,17	8,80	9,94	1,14	1,08 [8]	8,93	1,35	9,84	1,04
0,01	1,151	3,84	9,89	3,09	7,89 [7]	8,73	0,788	9,97	1,13	8,84	9,94	1,10	1,35 [8]	8,97	1,35	9,83	0,99
0,02	1,115	4,02	0,06	3,44	1,58 [8]	8,85	0,788	9,96	1,01	8,95	9,92	0,97	2,70 [8]	9,08	1,35	9,80	0,85
0,04	1,072	4,20	0,24	3,88	3,15 [8]	8,96	0,788	9,94	0,88	9,06	9,89	0,83	5,41 [8]	9,19	1,35	9,76	0,70
0,06	1,039	4,30	0,36	4,25	4,73 [8]	9,01	0,787	9,93	0,81	9,11	9,87	0,76	8,12 [8]	9,25	1,35	9,72	0,60
0,08	1,016	4,38	0,44	4,50	6,30 [8]	9,05	0,787	9,91	0,76	9,16	9,85	0,69	1,08 [9]	9,29	1,36	9,68	0,52
0,1	1,000	4,44	0,51	4,67	7,88 [8]	9,09	0,787	9,90	0,71	9,20	9,83	0,64	1,35 [9]	9,33	1,36	9,66	0,46
0,2	0,944	4,63	0,74	5,27	1,57 [9]	9,22	0,787	9,85	0,52	9,33	9,76	0,43	2,71 [9]	9,46	1,36	9,54	0,21
0,4	0,880	4,80	1,07	5,88	3,15 [9]	9,43	0,786	9,75	0,21	9,54	9,63	0,09	5,43 [9]	9,67	1,36	9,35	9,81
0,6	0,836	4,88	1,35	6,26	4,72 [9]	9,62	0,785	9,65	9,92	9,73	9,49	9,76	8,17 [9]	9,86	1,37	9,15	9,42
0,8	0,806	4,93	1,55	6,50	6,29 [9]	9,77	0,785	9,55	9,68	9,88	9,36	9,49	1,09	0,02	1,38	8,98	9,11
1,0	0,783	4,96	1,73	6,68	7,86 [9]	9,90	0,785	9,45	9,45	0,00	9,24	9,24	1,37	0,15	1,39	8,80	8,80
1,4	0,747	4,99	1,99	6,95	1,10 [9]	0,09	0,783	9,23	9,03	0,20	8,96	8,76	1,93	0,35	1,42	8,43	8,23
1,8	0,723	5,02	2,18	7,12	1,41	0,23	0,780	9,01	8,68	0,34	8,69	8,36	2,50	0,50	1,44	8,06	7,72
2,2	0,707	5,04	2,30	7,24	1,72	0,32	0,777	8,81	8,38	0,43	8,44	8,00	3,08	0,60	1,46	7,69	7,26
2,6	0,695	5,06	2,40	7,32	2,03	0,39	0,774	8,62	8,14	0,50	8,20	7,70	3,67	0,67	1,48	7,35	6,84
3,0	0,686	5,07	2,48	7,39	2,34	0,45	0,772	8,44	7,87	0,56	7,97	7,41	4,27	0,74	1,50	6,98	6,42
3,5	0,676	5,08	2,55	7,45	2,73	0,51	0,770	8,22	7,60	0,62	7,69	7,07	5,02	0,80	1,51	6,53	5,90
4,0	0,668	5,09	2,62	7,51	3,11	0,56	0,768	7,99	7,32	0,67	7,40	6,73	5,78	0,86	1,53	5,90	5,23
4,5	0,661	5,10	2,67	7,56	3,50	0,60	0,766	7,75	7,03	0,72	7,08	6,36	6,55	0,91	1,55		
5,0	0,656	5,11	2,72	7,60	3,88	0,63	0,764	7,53	6,78	0,75	6,76	6,01	7,33	0,94	1,56		

TABLE VI  
Average temperature distribution,  $A = 9000$ ,  $B = 0.04$

$\tau_0$	$\theta$	$\lambda 44000$			$\lambda 50000$			$\lambda 80000$									
		$\log p$	$\log p_e$	$\log \frac{N_{H^+}}{N_H}$	$\tau_\lambda$	$\log \kappa_\lambda$	$\frac{\kappa_\lambda}{\kappa_0}$	$\log g'_\lambda$	$\log h'_\lambda$	$\log \kappa_0$	$\log g'_0$	$\log h'_0$	$\tau_r$	$\log \kappa_r$	$\frac{\kappa_r}{\kappa_0}$	$\log g'_r$	$\log h'_r$
0.001	1.223	3.33	9.36	2.57	7.88 [6]	8.26	0.788	9.98	1.55	8.37	9.96	1.53	1.35 [7]	8.50	1.35	9.88	1.45
0.002	1.212	3.50	9.53	2.57	1.58 [7]	8.41	0.789	9.98	1.41	8.51	9.96	1.38	2.70 [7]	8.64	1.35	9.87	1.30
0.004	1.191	3.66	9.69	2.70	3.15 [7]	8.54	0.789	9.98	1.27	8.64	9.95	1.24	5.41 [7]	8.78	1.35	9.86	1.15
0.006	1.172	3.76	9.79	2.88	4.73 [7]	8.61	0.789	9.97	1.20	8.71	9.94	1.17	8.11 [7]	8.84	1.35	9.84	1.08
0.008	1.161	3.83	9.86	2.97	6.31 [7]	8.66	0.788	9.97	1.15	8.76	9.94	1.12	1.08 [8]	8.89	1.35	9.84	1.01
0.01	1.151	3.88	9.91	3.07	7.89 [7]	8.70	0.788	9.97	1.11	8.80	9.94	1.08	1.35 [8]	8.93	1.35	9.83	0.97
0.02	1.115	4.06	0.09	3.41	1.58 [8]	8.81	0.788	9.96	0.98	8.92	9.92	0.94	2.70 [8]	9.05	1.35	9.80	0.82
0.04	1.072	4.24	0.27	3.85	3.15 [8]	8.92	0.788	9.94	0.86	9.02	9.89	0.81	5.41 [8]	9.15	1.35	9.76	0.67
0.06	1.039	4.35	0.38	4.23	4.73 [8]	8.97	0.787	9.93	0.79	9.08	9.87	0.73	8.12 [8]	9.21	1.35	9.72	0.58
0.08	1.016	4.42	0.46	4.48	6.30 [8]	9.02	0.787	9.91	0.73	9.12	9.85	0.67	1.08 [9]	9.25	1.36	9.68	0.50
0.1	1.000	4.48	0.53	4.65	7.88 [8]	9.05	0.787	9.90	0.68	9.16	9.83	0.61	1.35 [9]	9.29	1.36	9.66	0.44
0.2	0.944	4.67	0.76	5.24	1.57 [9]	9.18	0.787	9.85	0.50	9.29	9.76	0.41	2.71 [9]	9.42	1.36	9.54	0.19
0.4	0.880	4.84	1.09	5.87	3.15 [9]	9.39	0.786	9.75	0.20	9.50	9.63	0.07	5.43 [9]	9.63	1.36	9.35	9.79
0.6	0.836	4.92	1.36	6.24	4.72 [9]	9.58	0.786	9.65	0.90	9.68	9.49	9.75	8.16 [9]	9.82	1.37	9.16	9.41
0.8	0.806	4.97	1.57	6.48	6.29 [9]	9.73	0.785	9.55	9.66	9.83	9.36	9.47	1.09	9.97	1.38	8.98	9.09
1.0	0.783	5.00	1.74	6.66	7.86 [9]	9.85	0.785	9.45	9.43	9.96	9.24	9.22	1.37	0.10	1.39	8.80	8.79
1.4	0.747	5.04	2.01	6.93	1.10	0.05	0.783	9.23	9.02	0.15	8.96	8.75	1.93	0.30	1.42	8.43	8.21
1.8	0.723	5.07	2.19	7.11	1.41	0.18	0.780	9.01	8.66	0.29	8.69	8.34	2.50	0.45	1.44	8.06	7.71
2.2	0.707	5.09	2.32	7.22	1.72	0.28	0.777	8.81	8.36	0.39	8.44	7.99	3.08	0.55	1.46	7.70	7.25
2.6	0.695	5.10	2.42	7.31	2.03	0.35	0.774	8.62	8.10	0.46	8.20	7.68	3.67	0.63	1.48	7.35	6.83
3.0	0.686	5.11	2.49	7.37	2.34	0.40	0.772	8.44	7.86	0.52	7.97	7.39	4.26	0.69	1.49	6.99	6.42
3.5	0.676	5.13	2.56	7.44	2.73	0.46	0.770	8.22	7.58	0.57	7.69	7.06	5.01	0.75	1.51	6.54	5.90
4.0	0.668	5.14	2.63	7.50	3.11	0.51	0.768	7.99	7.30	0.62	7.40	6.72	5.77	0.81	1.52	5.92	5.24
4.5	0.661	5.15	2.69	7.55	3.50	0.55	0.766	7.75	7.02	0.67	7.08	6.35	6.54	0.86	1.54		
5.0	0.656	5.16	2.73	7.58	3.88	0.59	0.765	7.53	6.76	0.70	6.76	5.99	7.31	0.90	1.55		



TABLE VII  
Average temperature distribution,  $A = 9000$ ,  $B = 0.2$

$\tau_0$	$\vartheta$	$\log p$	$\log p_e$	$\log \frac{N_{\text{H}}^+}{N_{\text{H}}}$	$\lambda 4000$				$\lambda 5000$				$\lambda 8000$				
					$\tau_\lambda$	$\log \kappa_\lambda$	$\frac{\kappa_\lambda}{\kappa_0}$	$\log q'_\lambda$	$\log h'_\lambda$	$\log \kappa_0$	$\log q'_0$	$\log h'_0$	$\tau_\lambda$	$\log \kappa_\lambda$	$\frac{\kappa_\lambda}{\kappa_0}$	$\log q'_\lambda$	$\log h'_\lambda$
0,001	1,223	3,46	9,42	2,50	7,88 [6]	8,13	0,788	9,98	1,49	8,23	9,96	1,47	1,35 [7]	8,36	1,35	9,88	1,38
0,002	1,211	3,62	9,59	2,51	1,58 [7]	8,27	0,789	9,98	1,34	8,38	9,96	1,32	2,70 [7]	8,51	1,35	9,87	1,23
0,004	1,191	3,79	9,75	2,63	3,15 [7]	8,40	0,789	9,98	1,21	8,51	9,95	1,18	5,41 [7]	8,64	1,35	9,86	1,09
0,006	1,172	3,88	9,85	2,82	4,73 [7]	8,47	0,789	9,97	1,14	8,57	9,94	1,11	8,11 [7]	8,71	1,35	9,85	1,01
0,008	1,161	3,96	9,92	2,90	6,31 [7]	8,52	0,788	9,97	1,08	8,63	9,94	1,05	1,08 [8]	8,76	1,35	9,84	0,95
0,01	1,151	4,01	9,98	3,00	7,89 [7]	8,56	0,788	9,97	1,04	8,66	9,94	1,01	1,25 [8]	8,79	1,35	9,83	0,91
0,02	1,115	4,18	0,15	3,35	1,58 [8]	8,68	0,788	9,96	0,92	8,78	9,92	0,88	2,70 [8]	8,91	1,35	9,80	0,76
0,04	1,072	4,36	0,33	3,79	3,15 [8]	8,78	0,788	9,94	0,80	8,89	9,89	0,75	5,41 [8]	9,02	1,35	9,76	0,61
0,06	1,039	4,47	0,44	4,16	4,73 [8]	8,84	0,787	9,93	0,72	8,94	9,87	0,67	8,12 [8]	9,07	1,35	9,72	0,51
0,08	1,016	4,55	0,53	4,42	6,30 [8]	8,88	0,787	9,91	0,67	8,98	9,85	0,60	1,08 [9]	9,12	1,36	9,68	0,44
0,1	1,000	4,61	0,59	4,59	7,88 [8]	8,92	0,787	9,90	0,62	9,02	9,83	0,55	1,35 [9]	9,15	1,36	9,66	0,37
0,2	0,944	4,80	0,82	5,19	1,57 [9]	9,04	0,787	9,85	0,44	9,15	9,76	0,35	2,71 [9]	9,28	1,36	9,54	0,13
0,4	0,880	4,97	1,14	5,82	3,15 [9]	9,24	0,786	9,75	0,15	9,35	9,63	0,02	5,43 [9]	9,48	1,36	9,35	9,74
0,6	0,836	5,06	1,41	6,20	4,72 [9]	9,42	0,786	9,65	9,86	9,53	9,49	9,70	8,16 [9]	9,67	1,37	9,16	9,37
0,8	0,806	5,10	1,61	6,44	6,29 [9]	9,57	0,785	9,55	9,62	9,67	9,36	9,43	1,09	9,81	1,38	8,98	9,05
1,0	0,783	5,14	1,78	6,62	7,86 [9]	9,69	0,786	9,45	9,39	9,80	9,24	9,18	1,37	9,94	1,39	8,80	8,75
1,4	0,747	5,18	2,05	6,89	1,10	9,89	0,784	9,23	8,98	9,99	8,96	8,71	1,93	0,14	1,41	8,43	7,18
1,8	0,723	5,20	2,23	7,07	1,41	0,02	0,781	9,01	8,62	0,13	8,69	8,30	2,50	0,29	1,43	8,06	7,67
2,2	0,707	5,22	2,36	7,19	1,72	0,12	0,778	8,81	8,32	0,22	8,44	7,95	3,08	0,39	1,45	7,70	7,22
2,6	0,695	5,24	2,45	7,27	2,04	0,18	0,776	8,62	8,06	0,30	8,20	7,64	3,66	0,46	1,47	7,36	6,89
3,0	0,686	5,25	2,53	7,33	2,34	0,24	0,774	8,43	7,82	0,35	7,97	7,35	4,25	0,52	1,48	7,00	6,39
3,5	0,676	5,26	2,60	7,40	2,73	0,30	0,772	8,22	7,55	0,41	7,69	7,02	4,99	0,59	1,50	6,55	5,88
4,0	0,668	5,28	2,67	7,46	3,12	0,35	0,770	7,99	7,27	0,46	7,40	6,68	5,74	0,64	1,51	5,96	5,24
4,5	0,661	5,29	2,73	7,51	3,50	0,39	0,768	7,74	6,98	0,51	7,08	6,31	6,50	0,69	1,53		
5,0	0,656	5,30	2,77	7,54	3,88	0,42	0,766	7,52	6,72	0,54	6,76	5,96	7,27	0,73	1,54		

TABLE VIII  
Average temperature distribution,  $A = 20\,000$ ,  $B = 0.4$

$\tau_0$	$\theta$	$\log p$	$\log p_e$	$\log \frac{N_{H^+}}{N_H}$	24000				25000				28000				
					$\tau_j$	$\log \kappa_j$	$\frac{\kappa_j}{\kappa_0}$	$\log g'_j$	$\log h'_j$	$\log \kappa_0$	$\log g'_0$	$\log h'_0$	$\tau_j$	$\log \kappa_j$	$\frac{\kappa_j}{\kappa_0}$	$\log g'_j$	$\log h'_j$
0.001	1.223	3.50	9.19	2.74	7.88 [6]	8.09	0.788	9.98	1.73	8.20	9.96	1.70	1.35 [7]	8.32	1.35	9.88	1.62
0.002	1.212	3.67	9.35	2.74	1.58 [7]	8.24	0.789	9.98	1.58	8.34	9.96	1.56	2.70 [7]	8.47	1.35	9.87	1.47
0.004	1.191	3.83	9.52	2.87	3.15 [7]	8.37	0.789	9.98	1.44	8.47	9.95	1.42	5.41 [7]	8.60	1.35	9.86	1.33
0.006	1.172	3.93	9.61	3.06	4.73 [7]	8.43	0.789	9.97	1.37	8.54	9.94	1.35	8.11 [7]	8.67	1.35	9.84	1.25
0.008	1.161	4.00	9.68	3.14	6.31 [7]	8.49	0.788	9.97	1.32	8.59	9.94	1.29	1.08 [8]	8.72	1.35	9.81	1.19
0.01	1.150	4.06	9.74	3.24	7.89 [7]	8.52	0.788	9.97	1.28	8.63	9.94	1.25	1.35 [8]	8.76	1.35	9.83	1.14
0.02	1.115	4.23	9.92	3.58	1.58 [8]	8.64	0.788	9.96	1.16	8.74	9.92	1.11	2.70 [8]	8.88	1.35	9.80	0.99
0.04	1.072	4.41	0.10	4.02	3.15 [8]	8.75	0.788	9.94	1.03	8.86	9.89	0.98	5.41 [8]	8.99	1.35	9.76	0.84
0.06	1.039	4.52	0.22	4.39	4.73 [8]	8.81	0.787	9.93	0.95	8.92	9.87	0.89	8.12 [8]	9.05	1.35	9.72	0.74
0.08	1.016	4.59	0.33	4.63	6.30 [8]	8.86	0.787	9.91	0.89	8.96	9.85	0.82	1.08 [9]	9.10	1.36	9.68	0.66
0.1	1.000	4.65	0.38	4.80	7.88 [8]	8.91	0.787	9.90	0.83	9.01	9.83	0.76	1.35 [9]	9.14	1.36	9.66	0.58
0.2	0.944	4.82	0.66	5.34	1.57 [9]	9.09	0.786	9.85	0.69	9.19	9.76	0.51	2.71 [9]	9.32	1.36	9.54	0.29
0.4	0.880	4.97	1.06	5.90	3.15 [9]	9.36	0.786	9.75	0.23	9.47	9.63	0.16	5.43 [9]	9.60	1.36	9.35	9.82
0.6	0.836	5.03	1.37	6.24	4.72 [9]	9.58	0.786	9.65	9.90	9.69	9.49	9.74	8.17 [9]	9.82	1.37	9.16	9.41
0.8	0.806	5.07	1.58	6.46	6.29 [9]	9.74	0.785	9.55	9.64	9.85	9.36	9.46	1.09	9.98	1.38	8.98	9.07
1.0	0.783	5.09	1.76	6.64	7.86 [9]	9.87	0.786	9.45	9.41	9.98	9.24	9.20	1.37	0.12	1.39	8.80	8.76
1.4	0.747	5.12	2.04	6.90	1.10	0.08	0.784	9.23	8.99	0.18	8.96	8.72	1.93	0.33	1.41	8.43	8.19
1.8	0.723	5.14	2.22	7.08	1.41	0.21	0.780	9.01	8.63	0.32	8.69	8.31	2.50	0.48	1.43	8.06	7.68
2.2	0.707	5.16	2.35	7.20	1.72	0.30	0.778	8.81	8.33	0.41	8.44	7.96	3.08	0.58	1.45	7.70	7.22
2.6	0.695	5.17	2.44	7.28	2.03	0.37	0.775	8.62	8.07	0.48	8.20	7.66	3.66	0.65	1.47	7.36	6.81
3.0	0.686	5.18	2.52	7.35	2.34	0.43	0.773	8.43	7.83	0.54	7.97	7.36	4.25	0.71	1.48	6.99	6.39
3.5	0.676	5.19	2.59	7.41	2.73	0.49	0.771	8.22	7.56	0.60	7.69	7.03	5.00	0.78	1.50	6.55	5.89
4.0	0.668	5.20	2.66	7.47	3.12	0.54	0.769	7.99	7.28	0.65	7.40	6.69	5.75	0.83	1.52	5.94	5.23
4.5	0.661	5.21	2.72	7.52	3.50	0.58	0.767	7.74	6.99	0.70	7.08	6.32	6.51	0.88	1.53		
5.0	0.656	5.21	2.76	7.56	3.88	0.61	0.766	7.52	6.73	0.73	6.76	5.97	7.28	0.92	1.54		

(9000, 0,2), (20 000, 0,04) (tables V-VIII<sup>1)</sup>). For comparison Claas' weighting functions ( $A=8000$ ,  $B=0$ ) are given in table I. In addition to the weighting functions some other quantities are tabulated; we believe that in this respect the tables are self-explanatory.

It is important to remind of the fact that for the formation of weak lines the layers between  $\tau_0$ -values 0,1 and 2 are the most important ones. After comparing the tables in this  $\tau_0$ -interval we can draw the following conclusions:

Tables I and V: Claas' model had a very high boundary temperature. By choosing a more probable model, but keeping to almost the same composition, maximum changes of 0,14 in the logarithm of the weighting functions are introduced.

Table II, III, IV and VI: In so far as the influence of temperature is concerned, the maximum scatter in the logarithm of the weighting functions for a number of recently derived models is 0,17.

Tables V, VI, VII and VIII: The maximum scatter introduced by different helium contents is 0,08 in the logarithm. The low metal content  $A=20\,000$  found by WEIDEMANN [10] gives rise to differences up to 0,15 for the low  $\tau_0$ -values. Very interesting is the fact that the functions  $g'_\lambda$  are practically independent of the composition. This means that for a given model the influence of a change in composition can be estimated very easily. For this purpose we correct  $\log p_e$  by means of the tables given by MINNAERT [4] and HUBENET [5].

From the equations (3) and (6) it can be seen that the change in  $\log h'_\lambda$  is the opposite of the change in  $\log (\kappa_H + \frac{Q_e}{m_H} k_{H-})_{25000}$ . Since  $\kappa_H$  and  $k_{H-}$  are independent of  $p_e$  the latter change can be estimated easily.

It has already been said that abundance determinations are not only influenced by changes in the weighting functions. The quantity  $N_1/N_H$  is important as well. At the present moment we will not deal with this problem. It will, however, be clear that the change of  $N_1/N_H$  is different from element to element and for each element depends on the state of excitation and ionization. We estimate that at least in some cases the change of  $N_1/N_H$  will be of greater importance than the change in the weighting functions. Calculations on this point are in progress.

<sup>1)</sup> For typographical reasons a not quite satisfactory notation for the negative numbers had to be chosen. A few examples from Table II may serve to explain the notation: For  $\tau_0 = 0,001$  we find in column 4 ( $\log p_e$ ) 9,38. This means  $\log p_e = 9,38-10$ . For  $\tau_0 = 0,02$  we find  $\log p_e = 0,07$ , here the table value has not to be supplemented with  $-10$ . By inspection both cases can generally be distinguished. In columns 5, 9, 12 and 17 all the tabulated numbers have to be supplemented with  $-10$ . The numbers in brackets are exponents (base 10), but since all the exponents are negative, they have to be supplemented with  $-10$ . E.g., for  $\tau_0 = 0,001$  the corresponding value of  $\tau_{4000}$  is  $7,89 \cdot 10^{-4}$ .

*Acknowledgement*

The author wants to express his gratitude towards Dr. FRANK K. EDMONDSON and Dr. MARSHAL H. WRUBEL for giving him the opportunity to work during a year at Indiana University. Mr. ARNOLD M. HEISER kindly spent many hours in operating the computer. To him the author is also greatly indebted.

*Utrecht, October 1956*

*Sterrenwacht "Sonnenborgh"*

## REFERENCES

1. CLAAS, W. J., The composition of the solar atmosphere (Thesis, Utrecht, 1951)  
— *Rech. Astr. Obs. Utrecht XII*, Part 1 (1951).
2. UNSÖLD, A., *Physik der Sternatmosphären*, p. 384 (2nd edition, Springer-Verlag, Berlin, Göttingen, Heidelberg, 1955).
3. PECKER, J. C., *Ann. Astroph.* **14**, 119 (1951) — *Contrib. Inst. Astroph. Paris*, Serie B, No. 65, 75 (1951).
4. MINNAERT, M., *The sun*, ed. G. P. Kuiper, p. 128 (Chicago, The University of Chicago Press, Chicago, 1953).
5. HUBENET, H., *Proc. Kon. Ned. Ak. Wetensch. Amsterdam*, Series B, **59**, 211 (1956) — *Overdruk Utrecht Quarto* No. 5.
6. JAGER, C. DE, *The hydrogen spectrum of the sun* (Thesis, Utrecht, 1952)  
*Rech. Astr. Obs. Utrecht XIII*, Part 1, p. 68 (1952).
7. PAGEL, B., *M.N.* (116?) in press.
8. VITENSE, E., *Zeitschr. Astroph.* **34**, 213 (1954).
9. VOIGT, H. H., *Zeitschr. Astroph.* **27**, 104 (1950).
10. WEIDEMANN, V., *Zeitschr. Astroph.* **36**, 101 (1955).
11. CHANDRASEKHAR, S. and F. H. BREEN, *Astroph. Jrn.* **104**, 430 (1946).



## AN X-RAY STUDY OF GLAUBERSALT

BY

P. N. MEULENDIJK

(Communicated by Prof. J. M. Bijvoet at the meeting of June 30, 1956)

After the introduction of an electrostatic model of the water molecule and the X-Ray structure determination of the water molecule in ice I [1], it has become possible to understand the structure of many hydrated salts. Bernal has adopted a classification of these salts on a purely geometrical basis and assumed that Glaubersalt belongs to the (ice-like) Tectohydrates, though the structure of this salt was unknown.

As few Tectohydrates have been investigated, it seemed worth while to attempt the structure determination of Glaubersalt.

This communication presents a survey of the results which have been attained up till now.

The crystals of  $\text{Na}_2\text{SO}_4 \cdot 10 \text{H}_2\text{O}$  are monoclinic, the cell dimensions are  $a = 11.43 \text{ \AA}$ ,  $b = 10.34 \text{ \AA}$ ,  $c = 12.90 \text{ \AA}$  and  $\beta = 107^\circ 45'$ ;  $U = 1451 \text{ \AA}^3$ ,  $D_m = 1.464 \text{ g/cm}^3$ ,  $Z = 4$ ,  $D_x = 1.479 \text{ g/cm}^3$ .

From the systematic absences the space group follows to be  $P2_1/C$ ; moreover the  $h00$  reflections for  $h$  odd are absent. From the latter it has been assumed that atoms of the same element occur in pairs with  $x$ -values differing by  $\frac{1}{2}a$ .

The intensities of the reflexions on Weissenberg photographs were visually estimated and corrected for Lorentz and polarisation factor.

The place of the Sulphur atom was found from Patterson projections along  $[010]$  and  $[001]$ .

Results, obtained from Patterson projections, using the "minimum function method" [2], looked unfavourable as a consequence of the high symmetry of these projections.

Next the method of isomorphous replacement was applied. From the isomorphous salts  $\text{Na}_2\text{CrO}_4 \cdot 10 \text{H}_2\text{O}$  and  $\text{Na}_2\text{SeO}_4 \cdot 10 \text{H}_2\text{O}$  the latter was chosen for this purpose.

The intensities were put on a absolute scale by finding the best fit of  $F_{\text{selenate}} - F_{\text{sulfate}}$  with  $f_{\text{se}} - f_{\text{s}}$ . At the same time this gave the signs of  $F_{\text{sulfate}}$  and the Fourier projections  $[010]$  and  $[001]$  were synthesized.

From the Fourier projections all atomic positions could be derived (fig. 1 and 2). After some refinement structure factors were calculated which gave a disagreement factor

$$R = \frac{\sum |F_{\text{calc.}} - F_{\text{obs.}}|}{\sum |F_{\text{obs.}}|} = 14 \%$$

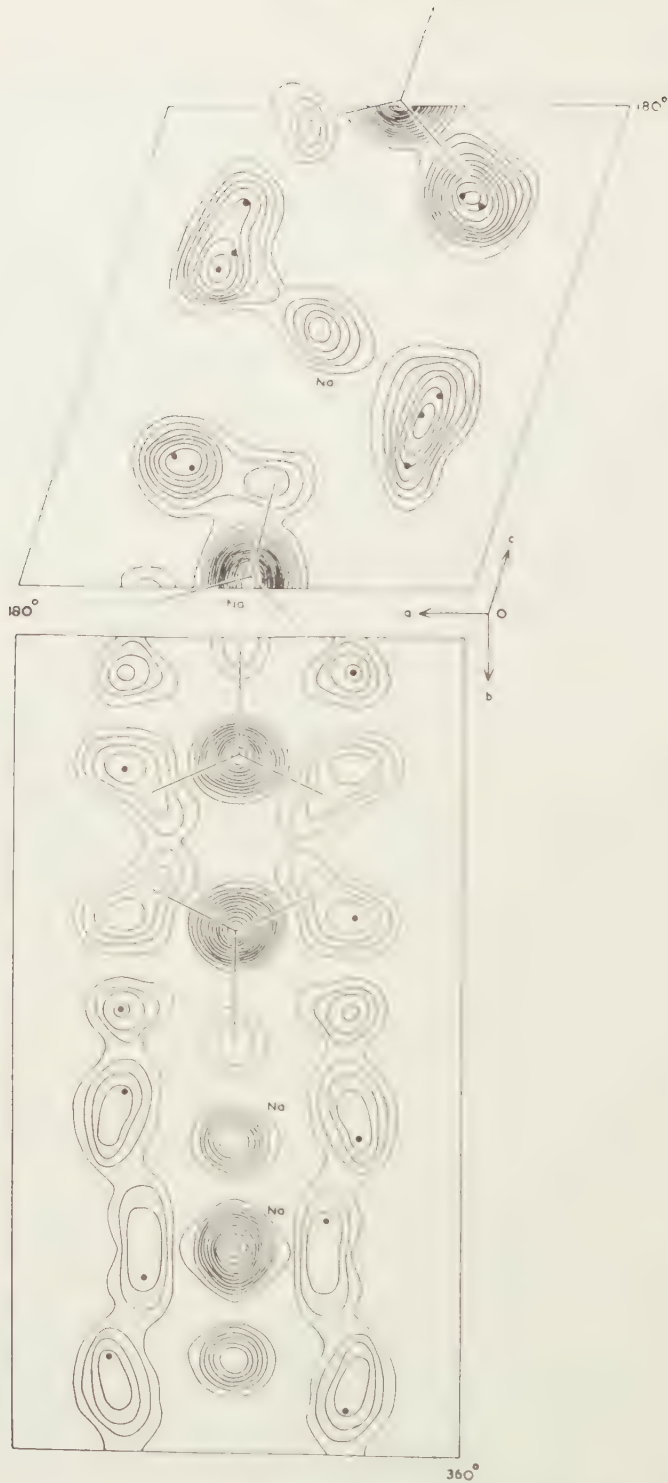


Fig. 1. Fourier projections along [001] and [010]. In the oxygen layers the positions of the atoms of the asymmetric unit have been indicated ( $0 < c < 180^\circ$ ), the other maxima are produced by the action of the glide symmetry.

The Glaubersalt structure consists of layers; one, at  $\frac{1}{4}a$ , contains the kations, the Sulfur atom and two Oxygens of the  $\text{SO}_4$  tetrahedron.

Two adjacent layers, at  $\frac{1}{8}$  and  $\frac{3}{8}a$ , contain crystal water and one of the  $\text{SO}_4$  oxygens.

The oxygen atoms in these layers are in deformed hexagonal close packing. The kations are surrounded octahedrally by water molecules.

The 10 molecules of crystalwater may be divided in the following five groups (see fig. 3):

- 2  $\text{H}_2\text{O}$  tetrahedrally surrounded by 2 Na and 2  $\text{H}_2\text{O}$ ,
- 2  $\text{H}_2\text{O}$  tetrahedrally surrounded by 2 Na and 1  $\text{H}_2\text{O}$  and 1  $\text{SO}_4$ -oxygen,
- 2  $\text{H}_2\text{O}$  tetrahedrally surrounded by 1 Na and 2  $\text{H}_2\text{O}$  and 1  $\text{SO}_4$ -oxygen,
- 2  $\text{H}_2\text{O}$  tetrahedrally surrounded by 1 Na and 1  $\text{H}_2\text{O}$  and 2  $\text{SO}_4$ -oxygen.
- 2  $\text{H}_2\text{O}$  tetrahedrally surrounded by - - - - - 2  $\text{H}_2\text{O}$  and 2  $\text{SO}_4$ -oxygen.

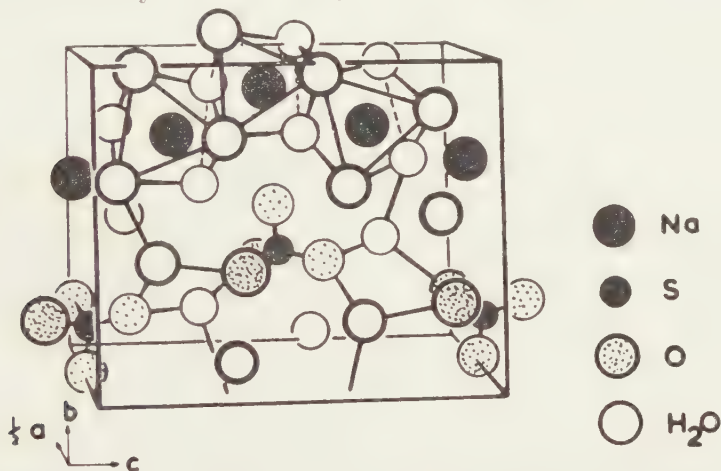


Fig. 2. Half a cell of  $\text{Na}_2\text{SO}_4 \cdot 10 \text{H}_2\text{O}$ ; one sees the  $\text{H}_2\text{O}$  octahedron around the Sodium-ion, two remaining water molecules are not attached to the kation.

The 8 first mentioned water molecules form the octahedron around the Na ions, the whole resembles the structure of  $\text{NiSO}_4 \cdot 7 \text{H}_2\text{O}$ .

Hydrogen atoms could not be found in this investigation. When placed on  $1.0 \text{ \AA}$  from the oxygen atoms, the bonds  $\text{H}_2\text{O} - \text{H}_2\text{O}$  and  $\text{H}_2\text{O} - \text{SO}_4$  could be effected in only one way by means of hydrogen bridges.

By inclusion of these H atoms in the structure factor calculation, the disagreement factor decreased another 2–3 %.

The investigation as to the positions of the Hydrogen atoms will perhaps be continued by three-dimensional Fourier analysis and by means of nuclear-resonance.

*Laboratorium voor Kristalchemie  
der Rijks-Universiteit Utrecht*

#### REFERENCES

1. BERNAL and FOWLER, *J. Chem. Soc.* **1**, 515 (1933); *Trans. Faraday Soc.* **148**, 29, part 9.
2. BUERGER, *Proc. Nat. Acad. Sci. Wash.* **36**, 738 (1950c); *Acta Cryst.* **4**, 531 (1954).





# INDEX

(Proceedings, Series B, Vol. LIX, 1956)

## Astronomy

- HAUG, S. G. M.: The effect of orientation on the thickness of prominences, p. 174.  
HOUTGAST, J.: Report of the Netherlands expedition to Ceylon, p. 335.  
HUBENET, H.: Note on the influence of the helium and metal content on the pressure in the solar atmosphere, p. 211.  
HUBENET, H.: Solar weighting functions. I, p. 480.  
ZANSTRA, H.: On the theory of emission lines in expanding nebulae, p. 389.

## Biochemistry

- BAAS BECKING, L. G. M. and I. R. KAPLAN: Biological processes in the estuarine environment. III, p. 85.  
BAAS BECKING, L. G. M. and I. R. KAPLAN: Biological processes in the estuarine environment. IV, p. 97.  
BAAS BECKING, L. G. M. and MARGARET MACKAY: Biological processes in the estuarine environment. VA, p. 109.  
BAAS BECKING, L. G. M. and MARGARET MACKAY: Biological processes in the estuarine environment. VB, p. 118.  
BAAS BECKING, L. G. M.: Biological processes in the estuarine environment. VI, p. 181.  
BAAS BECKING, L. G. M., E. J. FERGUSON WOOD and I. R. KAPLAN: Biological processes in the estuarine environment. VIII, p. 398.  
BAAS BECKING, L. G. M.: Biological processes in the estuarine environment. IX, p. 408.  
BLOEMENDAL, H.: Starch electrophoresis of the bovine eye lens proteins. *Summary*, p. 23.  
KÖGL, F. and I. MULDER: Over de invloed van hetero-auxine op biochemische processen in de kiemplant van *Avena sativa*, p. 231.

## Chemistry

- BEVERLOO, A., M. C. DIELEMAN, K. S. DE VRIES, P. E. VERKADE and B. M. WEBSTER: The reactions of organic halogen compounds with solutions of metals in non-aqueous solvents, p. 445.  
BOER, J. H. DE, J. J. STEGGERDA and P. ZWIETERING: The dehydration of alumina hydrates. III, p. 435.  
CORSMIT, A. F., A. SCHUYFF and D. FEIL: On the crystal structure of L-cystine hydrochloride, p. 470.  
DORST, W., W. PRINS and J. J. HERMANS: Effect of electrolyte mixtures on the critical micelle concentration in solutions of dodecyl-1 sulphate, p. 190.  
LABAW, LOUIS W. and RALPH W. G. WYCKOFF: The electron microscopy of protein crystals, p. 171.  
LABAW, LOUIS W. and RALPH W. G. WYCKOFF: The electron microscopy of minute crystalline detail, p. 449.  
MACGILLAVRY, D.: Electrochemical behaviour of ion-exchanging substances. XI, p. 73.

- MACGILLAVRY, D. and H. J. C. TENDELOO: Electrochemical behaviour of ion-exchanging substances, p. 343.
- MEULENDIJK, P. N.: An X-ray study of Glaubersalt, p. 493.
- PEERDEMAN, A. F. and J. M. BIJVOET: Phase determination in the heavy atom method in the case of non-centrosymmetric crystals, p. 312.
- PRINS, W. and J. J. HERMANS: Theory of light-scattering by detergent solutions, p. 162.
- SIXMA, F. L. J. and H. HENDRIKS: Investigations of the mechanism of the Friedel-Crafts reaction; the reaction of ethyl bromide and aluminium bromide, p. 61.
- SPAREBOOM, S.: The synthesis of *cis*, *cis*-9, 11- and *cis*, *cis*-10, 12-octadecadienoic acids, p. 472.
- SPRENGELS, A. J. J.: The crystal structure of lithium-ammonium-tartrate-monohydrate, p. 221.
- WIBAUT, J. P. and F. P. K. DE JONG: Ozonolysis of indan, 4,7-dimethylindan and 5,6-dimethylindan in connection with the so-called Mills-Nixon effect, p. 285.
- WIBAUT, J. P. and TH. J. DE BOER: The Ozonolysis of Phenanthrene, p. 421.
- WIBAUT, J. P. and U. HOLLSTEIN: Investigation of the Alkaloids of *Punica Granatum* L. (3rd. communication), p. 426.

### Chemistry, Physical

- BUNGENBERG DE JONG, H. G. and A. DE BAKKER: Contributions to the colloid chemistry of phosphatides. IIIA, p. 124.
- BUNGENBERG DE JONG, H. G. and A. DE BAKKER: Contributions to the colloid chemistry of phosphatides. IIIB, p. 136.
- BUNGENBERG DE JONG, H. G. and A. DE BAKKER: Contributions to the colloid chemistry of phosphatides. IV, p. 149.
- BURGERS, W. G., Miss C. L. D. KOOY and T. J. TIEDEMA: Thermal diffuse scattering by lead single crystals, p. 195.
- HAMEKA, H. F. and A. M. LIQUORI: Structure of heterocyclic molecules containing nitrogen. III, p. 242.
- KUO, KEHSIN and W. G. BURGERS: An X-ray investigation of the white to grey transformation of tin, p. 288.
- PRINS, W. and J. J. HERMANS: Light-scattering by solutions of some sodium alkyl-1-sulfates, p. 298.

### Geology

- EDELMAN, C. H. und K. J. ZANDSTRA: Niveo-äolische Sande im Saargebiet, p. 253.
- KUENEN, PH. H. and E. TEN HAAF: Graded bedding in limestones, p. 314.
- LOOMAN, H.: Observations about some differential equations concerning recession of mountain slopes. I, p. 259.
- LOOMAN, H.: Observations about some differential equations concerning recession of mountain slopes. II, p. 272.
- TEX, E. DEN: Studies in comparative petrofabric analysis. I, p. 11.
- VENING MEINESZ, F. A.: A phase-transition layer between 200 and 900 km depth in the earth?, p. 1.

### Mechanics

- KOITER, W. T.: A new general theorem on shake-down of elastic-plastic structures, p. 24.
- KOITER, W. T.: On the flexural rigidity of a beam, weakened by transverse saw cuts. I, p. 354.
- KOITER, W. T.: On the flexural rigidity of a beam, weakened by transverse saw cuts. II, p. 365.

**Meteorology**

VISSER, S. W.: The Novaya-Zemlya phenomenon, p. 375.

**Paleontology**

DROOGER, C. W.: *Miogypsina* at Puente Viejo, Spain, p. 68.

DROOGER, C. W.: Parallel evolutionary trends in larger foraminifera, p. 458.

KOENIGSWALD, G. H. R. VON: Remarks on the correlation of mammalian faunas of Java and India and the Plio-Pleistocene boundary, p. 204.

KOENIGSWALD, G. H. R. VON: Gebissreste von Menschenaffen aus dem Unterpliozän Rheinhessens. I, p. 318.

KOENIGSWALD, G. H. R. VON: Gebissreste von Menschenaffen aus dem Unterpliozän Rheinhessens. II, p. 330.

KOENIGSWALD, G. H. R. VON: The geological age of Wadjak Man from Java, p. 455.

WISSINK, A. J.: Heterostegines du miocène de l'Angola, p. 386.

**Physics**

BOKHOVEN, C. and H. H. J. THEEUWEN: Deuterium content of some natural organic substances, p. 78.

FOKKER, A. D.: Accelerated spherical light wave clocks in chronogeometry, p. 451.

KRAMERS, H. C.: Some properties of liquid helium below 1° K. IVA, p. 35.

KRAMERS, H. C.: Some properties of liquid helium below 1° K. IVB, p. 48.



# AUTHOR-INDEX

## B

- BAAS BECKING, L. G. M., 85, 97, 109,  
118, 181, 398, 408.  
BAKKER, A. DE, 124, 136, 149.  
BEVERLOO, A., 445.  
BLOEMENDAL, H., 23.  
BOER, J. H. DE, 435.  
BOER, TH. J. DE, 421.  
BOKHOVEN, C., 78.  
BUNGENBERG DE JONG, H. G., 124,  
136, 149.  
BURGERS, W. G., 195, 288.  
BIJVOET, J. M., 312.

## C

- CORSMIT, A. F., 470.

## D

- DIELEMAN, M. C., 445.  
DORST, W., 190.  
DROOGER, C. W., 68, 458.

## E

- EDELMAN, C. H., 253.

## F

- FEIL, D., 470.  
FERGUSON WOOD, E. J., 398.  
FOKKER, A. D., 451.

## H

- HAAF, E. TEN, 314.  
HAMEKA, H. F., 242.  
HAUG, S. G. M., 174.  
HENDRIKS, H., 61.  
HERMANS, J. J., 162, 190, 298.  
HOLLSTEIN, U., 426.  
HOUTGAST, J., 335.  
HUBENET, H., 211, 480.

## J

- JONG, F. P. K. DE, 285.

## K

- KAPLAN, I. R., 85, 97, 398.  
KOENIGSWALD, G. H. R. VON, 204, 318,  
330, 455.  
KÖGL, F., 231.  
KOITER, W. T., 24, 354, 365.

- KOOY, C. L. D., 195.  
KRAMERS, H. C., 35, 48.  
KUENEN, PH. H., 314.  
KUO, KEHSIN, 288.

## L

- LABAW, LOUIS W., 171, 449.  
LIQUORI, A. M., 242.  
LOOMAN, H., 259, 272.

## M

- MACGILLAVRY, D., 73, 343.  
MACKAY, MARGARET, 109, 118.  
MEULENDIJK, P. N., 493.  
MULDER, I., 231.

## P

- PEERDEMAN, A. F., 312.  
PRINS, W., 162, 190, 298.

## S

- SCHUYFF, A., 470.  
SIXMA, F. L. J., 61.  
SPARREBOOM, S., 472.  
SPRENKELS, A. J. J., 221.  
STEGGERDA, J. J., 435.

## T

- TENDELOO, H. J. C., 343.  
TEX, E. DEN, 11.  
THEEUWEN, H. H. J., 78.  
TIEDEMA, T. J., 195.

## V

- VENING MEINESZ, F. A., 1.  
VERKADE, P. E., 445.  
VISSER, S. W., 375.  
VRIES, K. S. DE, 445.

## W

- WEBSTER, B. M., 445.  
WIBAUT, J. P., 285, 421, 426.  
WISSINK, A. J., 386.  
WYCKOFF, RALPH W. G., 171, 449.

## Z

- ZANDSTRA, K. J., 253.  
ZANSTRA, H., 389.  
ZWIETERING, P., 435.